

UNIVERSITY OF CAMBRIDGE

# FRPRCS-5

## Fibre-reinforced plastics for reinforced concrete structures

**VOLUME 1**

Edited by C.J. Burgoyne

Proceedings of the fifth international conference on fibre-reinforced plastics for reinforced concrete structures, Cambridge, UK, 16–18 July 2001

*Sponsoring organizations:*



The Institution of Structural Engineers






THE INSTITUTION OF CIVIL ENGINEERS



Thomas Telford

Published for the Conference Organizers by Thomas Telford Publishing, 1 Heron Quay, London E14 4JD
http://www.thomastelford.com

Distributors for Thomas Telford books are
*USA:* ASCE Press, 1801 Alexander Bell Drive, Reston, VA 20191-4400, USA
*Japan:* Maruzen Co. Ltd, Book Department, 3–10 Nihonbashi 2-chome, Chuo-ku, Tokyo 103
*Australia:* DA Books and Journals, 648 Whitehorse Road, Mitcham 3132, Victoria

First published 2001

A catalogue record for this book is available from the British Library

ISBN: 0 7277 3029 0

© The Authors and Thomas Telford Limited, unless otherwise stated, 2001

All rights, including translation, reserved. Except as permitted by the Copyright, Designs and Patents Act 1988, no part of this publication may be reproduced, stored in a retrieval system or transmitted in any form or by any means, electronic, mechanical, photocopying or otherwise, without the prior written permission of the Publishing Director, Thomas Telford Publishing, Thomas Telford Ltd, 1 Heron Quay, London E14 4JD.

This book is published on the understanding that the authors are solely responsible for the statements made and opinions expressed in it and that its publication does not necessarily imply that such statements and/or opinions are or reflect the views or opinions of the organizers or publishers. While every effort has been made to ensure that the statements made and the opinions expressed in this publication provide a safe and accurate guide, no liability or responsibility can be accepted in this respect by the editor or publishers.

Printed and bound in Great Britain by MPG Books, Bodmin, Cornwall

# Preface

Fibre Reinforced Plastics, in various forms, offer us new ways to design or strengthen our structures. The potential has been around for many years, but the applications are still relatively few and far between. Glass fibres were proposed for use in prestressing tendons in the 1950s but were not used for fear of stress-rupture. Then in about 1980 several teams began work independently on the subject; in Switzerland on the use of carbon fibre for repair, in Germany on glass fibres for prestressing, in the UK and the Netherlands on the use of aramid fibres. This work expanded, and was taken up elsewhere, notably in Japan, the USA and Canada. The first major international conference on the subject took place in Vancouver in 1993 as a set of special sessions in the ACI fall convention. That was, effectively, FRPRCS-1. It was agreed that the conference had been a useful forum for exchange of views, and that the process should be repeated biennially, taking in Europe, Asia and North America in sequence. Subsequent conferences, in Ghent in 1995, Sapporo in 1997 and Baltimore in 1999 have now led to Cambridge in 2001.

What has changed over the years? In 1980 the three fibrous materials, glass, carbon and aramid, were seen as wonder materials. They had high strength, a stiffness that was at least comparable with steel, very little creep and, above all, good resistance to corrosion. They were thought of as being expensive but the expectation was that costs would be brought down by volume production. All that was needed was to demonstrate that they could be used as reinforcement or as prestressing tendons, and the world would beat a path to our door, making us rich in the process!

This has not happened, and it is worth considering why. There has been a failure to take a 'whole structure' view. FRP rods are not simply replacements for steel bars; they have different properties and structures will behave differently. We should be asking what the form of the structure should be that makes best use of the new materials. We should also spend far more time considering 'whole-life' costings. Lip service is paid to that at present, provided the structure that is adopted is also the cheapest to build in the first place.

It is also easy to knock new materials. Stress-rupture is often confused with chemical degradation, and we make matters worse ourselves by combining the study of the two effects. It is easy to criticise lack of bond, when in fact too much bond is a bad thing. FRPs are brittle, so the argument goes that brittle reinforcement in a brittle matrix gives us a brittle beam, ignoring the very high strain capacities of these materials which normally allow very high post-cracking rotations.

Cost remains an issue. We have to compare structures built with steel reinforcement that is produced by an extremely competitive industry. Margins are tight and production chains from steel maker to building contractor are very short. The composites industry makes small quantities, in batches, using specialist equipment. They want to recoup their research costs and the supply chains are rarely short. With structures that are not optimally designed for composites in the first place, the cost penalty is high. This problem must be addressed if the composites industry is to take off.

The one success of the composites industry, so far, is in the field of repair or strengthening, as is demonstrated by the large number of papers here dealing with the subject. Beams can be strengthened in both flexure and shear resistance, and several papers that deal with prestressing to take advantage of the high strain capacities of these materials. Columns can be strengthened to resist seismic or impact forces. In these applications the cost of the materials is relatively unimportant, since the economic benefit is reduced time on site. The clients' fear of new materials is removed, since the structure has been there for a long time already so is clearly capable of supporting its own weight. These uses will assist with the perception of fibres as sensible engineering materials.

Comparing the papers in these volumes with those published in the first conference, it is clear that we have moved away from the simple demonstration test. Many of the fundamental issues of behaviour are addressed here and there is a move towards codification to give support to practising engineers.

I remain confident that there is a long-term future for composites in the civil engineering industry. The materials do have good fundamental properties; we now must demonstrate to industry the economic benefits that would accrue.

***Chris Burgoyne***

Cambridge
July 2001

# FRPRCS-5 Organizing Committees

**University of Cambridge Organizing Committee**

Chris Burgoyne (*Chairman*)
Janet Lees
Rowena Baxter
Miguel Morais
Iannis Balafas
Gyamera Kesse
Nadun Alwis

**International Scientific Committee**

Dr Chris Burgoyne, University of Cambridge, UK (*Chairman*)
Dr Marco Arduini, Composite for Civil Engineering, Italy
Dr Baidar Bakht, Canada
Dr Charles Bakis, Pennsylvania State University, USA
Professor Lawrence Bank, University of Wisconsin-Madison, USA
Professor Francois Buyle-Bodin, EUDIL, Lille, France
Professor Alain Chabert, LCPC, Paris, France
Dr John Clarke, Concrete Society, UK
Professor Di Tommaso, University of Venice, Italy
Professor Charles Dolan, University of Wyoming, USA
Mr. Arie Gerritse, Netherlands
Dr Gowripalan, University of New South Wales, Australia
Professor Patrice Hamelin, University of Lyon
Professor Len Hollaway, University of Surrey, UK
Dr Tim Ibell, University of Bath, UK
Dr Janet Lees, University of Cambridge, UK
Professor Atsuhiko Machida, University of Saitama, Japan
Professor Gaetano Manfredi, University of Naples FedericoII, Italy
Mr. Stijn Matthys, University of Ghent, Belgium
Professor Urs Meier, EMPA Laboratories, Switzerland
Dr Toby Mottram, University of Warwick, UK
Professor Aftab Mufti, University of Manitoba, Canada
Professor Hiroshi Mutsuyoshi, University of Saitama, Japan
Professor Antoine E Naaman, University of Michigan, Ann Arbor, USA
Professor Antonio Nanni, University of Missouri-Rolla, USA
Professor Ken Neale, University of Sherbrooke, Canada
Dr Kypros Pilakoutas, University of Sheffield, UK
Professor Marco Pisani, Polytechnic of Milan, Italy
Professor Sami Rizkalla, North Carolina State University, USA
Professor Ferdinand Rostasy, University of Braunschweig, Germany
Professor Luc Taerwe, University of Ghent, Belgium
Dr Bjorn Taljsten, Luleå University of Technology, Sweden
Professor Vitauts Tamuzs, Institute of Polymer Mechanics, Riga, Latvia
Professor Kiang Hwee Tan, University of Singapore
Professor Ralejs Tepfers, University of Chalmers, Sweden
Professor Thanasis Triantafillou, University of Patras, Greece
Professor Tamon Ueda, University of Hokkaido, Japan
Professor Taketo Uomoto, University of Tokyo, Japan
Professor Peter Waldron, University of Sheffield, UK

# Contents: Volume 1


## INTRODUCTION

**European activities on the use of FRP reinforcement, fib Task Group 9.3 and the ConFibreCrete network**
L. Taerwe, S. Matthys, K. Pilakoutas and M. Guadagnini 3

**Durability considerations for FRP reinforcements**
T. Uomoto 17

## EXTERNALLY BONDED REINFORCEMENT FOR FLEXURE

**FRPs for the rehabilitation of concrete beams exhibiting alkali–aggregate reactions**
C. Lacasse, P. Labossière and K.W. Neale 35

**The role of composite materials in concrete durability. Case study of alkali–aggregate reaction**
M. Ibrahim, E. Ferrier, L. Curtil and P. Hamelin 45

**Performance of inorganic polymer-fiber composites for strengthening and rehabilitation of concrete beams**
R. Garon, P.N. Balaguru and H. Toutanji 53

**Evaluation for effect of strengthening method for opening on CFRP sheet**
T. Kage, Y. Masuda and T. Ina 63

**Flexural behaviour of over-reinforced FRP RC beams: effect of design parameters and material partial safety factors**
K. Neocleous, K. Pilakoutas and P. Waldron 71

**Concrete Beams Strengthened with Misaligned CFRP Laminate**
X. Yang and A. Nanni 79

**Failure behavior of flexural strengthened RC beams with AFRP sheet**
N. Kishi, H. Mikami, K.G.Matsuoka and Y. Kurihashi 87

**Strengthening of R.C. beams in flexure and shear using CFRP laminate**
I.A.E.M. Shehata, E.C. Cerqueira, C.T.M. Pinto and L.C.D. Shehata 97

**Concrete beams strengthened with near surface ounted CFRP laminates**
B. Täljsten and A. Carolin 107

**Parameters influencing the flexural response of RC beams strengthened using CFRP sheets**
A.E. Naaman, S.Y. Park, M.M. Lopez, and R.D. Till 117

**A study on tension stiffness of reinforced concrete members strengthened by carbon fiber sheet**
R. Yamaguchi, Y. Sato and T. Ueda 127

**Capacity assessment of a bridge rehabilitated using FRP composites**
C. Sikorsky, N. Stubbs, V. Karbhari and F. Seible 137

**Long-term behaviour of CFRP-laminate-strengthened concrete beams at elevated temperatures**
T. Ulaga and U. Meier 147

**Design of concrete members strengthened with externally bonded FRP reinforcement**
T. Triantafillou, S. Matthys and L. Taerwe 157

**Design guidelines for flexural strengthening of concrete members using FRP composites**
C. Arya and N. Farmer 167

**Simplified design guidelines for FRP reinforced concrete beams in flexure**
N. Pešći and K. Pilakoutas 177

**Guidelines for strengthening concrete structures with FRP laminates**
C. Arya, J.L. Clarke, E.A. Kay and D.P. O'Regan 187

## EXTERNALLY BONDED REINFORCEMENT FOR SHEAR

**Effect of corner radius on the performance of externally bonded FRP reinforcement**
X. Yang, A. Nanni and G. Chen 197

**A shear strength model for FRP-strengthened RC beams**
J.F. Chen and J.G. Teng 205

**The effect of stiffness of externally bonded FRP in RC beams subjected to shear**
T. Kanakubo, T. Furuta and H. Fukuyama 215

**Design and shear behaviour of FRP mesh reinforcement across cracks in concrete**
E. Makitani, A.R. Burden, T. Makitani and W. Qi 223

**CARBOSTRAP – An advanced composite tendon system**
A. Winistoerfer and U. Meier 231

**T beams strengthened in shear with carbon sheet laminates (CFRP)**
M. Salles Neto, G.S. Melo and Y. Nagato 239

**Shear strengthening of dapped beams using FRP systems**
K.H. Tan 249

## EXTERNALLY BONDED PRESTRESSED REINFORCEMENT

**Prestressed CFRP sheets for strengthening concrete beams at room and low temperatures: experimental and analytical investigations**
R. El-Hacha, G. Wight and M. Green 261

**Prestressed externally bonded FRP reinforcement for RC beams**
E. Ferrier, C. Ennaceur, D. Bigaud and P. Hamelin 271

**Non-linear finite element analysis of RC beams prestressed with CFRP straps**
G. Kesse, C. Chan and J..M. Lees 281

**Strengthening of concrete structures with prestressed and gradually anchored CFRP strips**
I. Stöcklin and U. Meier 291

## FRPs IN SEISMIC CONDITIONS

**Advanced wrapping system with CF-anchor – seismic strengthening of RC columns with wing walls**
K. Masuo, S. Morita, Y. Jinno and H. Watanabe 299

**Seismic rehabilitation of reinforced concrete building corner joints**
C.P. Pantelides, C. Clyde, C.P. Lau and L.D. Reaveley 309

**Seismic performance of hybrid RC columns with aramid fiber reinforced polymer square tube and steel reinforcement**
P. Zhong, T. Yamakawa, H. Satoh and K. Komesu 319

**Experimental investigation of FRP-strengthened RC beam–column joints**
C.P. Antonopoulos, T.C. Triantafillou and C.G. Papanicolaou 329

**Seismic upgrade of beam–column joints with FRP reinforcement**
A. Prota, A. Nanni, G. Manfredi and E. Cosenza 339

**Assessment of seismic rehabilitation and repair of RC bridges with CFRP composites**
C.P. Pantelides and L.D. Reaveley 349

## BOND

**Prediction of debonding failure load due to flexural cracks of concrete for FRP-strengthened structures**
H. Niu and Z. Wu 361

**Study on the bond between concrete and externally bonded CFRP sheet**
B.B. Adhikary and H. Mutsuyoshi 371

**Advanced wrapping system with CF-anchor – stress transfer mechanism of CF-anchor**
K. Kobayashi, S. Fujii, Y. Yabe, H. Tsukagoshi and T. Sugiyama 379

**Rapid flexural strengthening of RC beams using powder actuated fasteners and FRP strips**
A.J. Lamanna, L.C. Bank and D.W. Scott 389

**Bond analysis of curved structural concrete elements strengthened using FRP materials**
M.A. Aiello, N. Galati and A. La Tegola 399

**Anchoring method of carbon fiber sheet for strengthening of reinforced concrete beams**
Y. Sagawa, H. Matsushita and H. Tsuruta 409

**Strength models for plate end debonding in FRP-strengthened RC beams**
S.T. Smith and J.G. Teng 419

**Effect of test methods on plate-to-concrete bond strength**
J.F. Chen, Z.J. Yang, X.M. Pan and G.D. Holt 429

## CODES

**JSCE design recommendations for upgrading of RC members by FRP sheet**
K. Maruyama and T. Ueda 441

**Outline of the Japanese guidelines for seismic retrofitting of RC buildings using FRP materials**
H. Fukuyama, G. Tumialan and Y. Matsuzaki 447

**Japanese and North American guidelines for strengthening concrete structures with FRP: a comparative review**
G. Tumialan, K. Nakano, H. Fukuyama and A. Nanni 457

## DURABILITY OF FIBRE REINFORCED PLASTICS

**Durability of GFRP composites reinforcing rods in concrete environment**
B. Benmokrane, P. Wang, M.T. Ton-That and K. Laoubi 469

**Alkali resistance of fibers, FRP rods and epoxy resins**
H. Mutsuyoshi, A. Sumida and T. Uomoto 479

**Durability of FRP sheet used for concrete in sulphuric acid environment**
A. Hattori, Y. Ohnishi and T. Miyagawa 489

**Durability of FRP rebars after four years of exposure**
A. Katz, L.C. Bank and M. Puterman 497

**Durability and service life prediction of GFRP for concrete reinforcement**
V. Dejke and R. Tepfers 505

## CREEP AND LONG-TERM BEHAVIOUR

**Stress-rupture of FRP: state of the art**
K. Audenaert, L. Taerwe and D. Gazouli 517

**Long-term creep of hybrid FRP bars**
V. Tamuzs, R. Maksimovs and J. Modniks 527

**Analysis of time-dependent behaviour of concrete beams prestressed with FRP tendons**
X.W. Zou, R.I. Gilbert and N. Gowripalan 535

## THERMAL AND EXTERNAL EFFECTS

**Fire testing of concrete slabs strenghtened with fibre composite laminates**
H. Blontrock, L. Taerwe and P. Vandevelde 547

**Heat resistance of continuous fiber reinforced plastic rods**
A. Sumida, T. Fujisaki, K. Watanabe and T. Kato 557

**Measurement of electromagnetic transmission through structures reinforced with high strength fibers**
Y. Kurosaki, K. Ishibashi and Y. Murano 567

**Behaviour and design of structural concrete reinforced with CFRP rebars for temperature effects**
M. Elbadry and O. Elzaroug 573

**Author index**

# Introduction

# European activities on the use of FRP reinforcement, fib Task Group 9.3 and the ConFibreCrete network

L. TAERWE and S. MATTHYS, Magnel Laboratory for Concrete Research, Department of Structural Engineering, Ghent University, Belgium
K. PILAKOUTAS and M. GUADAGNINI, Dept. of Civil & Structural Engineering, University of Sheffield, UK

**ABSTRACT**
Since the introduction of fibre reinforced polymer (FRP) reinforcement in the construction industry, the use of non-ferrous reinforcement has been growing exponentially. Although much research has been done world-wide and many applications already exist in various countries, the development of codes of practice incorporating advanced materials is still seen as a barrier for its more extensive use. In 1996 the International Federation for Structural Concrete (*fib*) established Task Group 9.3, with the objective of developing guidelines for the design of concrete structures, reinforced, prestressed or strengthened with advanced composites. In December 1997 the EU TMR Network, ConFibreCrete, has been established and operates in support of the *fib* Task Group 9.3. Activities of these committees are reported here as well as other European activities on the use and design of constructions reinforced with FRP.

**INTRODUCTION**
The use of fibre reinforced polymers (FRP) as structural reinforcement gains more and more interest in construction practice world-wide. Continuing efforts in material development and research activities, with strong links to engineering practice, make FRP reinforcement where it stands today: a viable alternative to classical types of reinforcement, offering many potentials. Extensive research on the use of FRP in concrete structures started in Europe about 25 years ago and resulted, for example, in the world's first highway bridge using FRP post-tensioning cables in Germany in 1986. Clearly, a long way has been gone from these first applications and still much is to be done to stimulate the implementation and use of structural FRP reinforcement.

In the following the use of FRP reinforcement in Europe is discussed, as well as the research efforts conducted in Europe and the design guidelines currently developed with respect to standard material testing and the use of FRP for RC (reinforced concrete), PC (prestressed concrete) and EBR (externally bonded reinforcement). Furthermore, the paper will report on the established databases concerning research, FRP products and applications as well as on the efforts of taking into consideration the interests of industries, contractors and designers. It is demonstrated that a major part of the European activities focus on externally bonded FRP reinforcement (FRP EBR), along with the large commercial interest in this technique. Nevertheless, there is also considerable interest in the use of FRP for newly built structures.

*FRPRCS-5*, Thomas Telford, London, 2001.

## USE OF FRP REINFORCEMENT IN EUROPE

### General

Since many years there has been a great interest in FRP reinforcement in Europe [1,2] and to some extent pioneering work in this field has been done in Europe. As these early developments were commercially less successful than hoped for, today the commercial application of FRP reinforcement in Europe is less exploited than in North-America and Japan. Also, compared to Europe, the market for FRP (fibre reinforced polymer) reinforcement is larger in Japan and North America. Nevertheless, in various European countries, a considerable amount of research and application projects are available, several research projects were established and developments in the use of advanced composites for construction have been taken place. Given these efforts and interest, FRP reinforcement and its use is getting more generally known. A large number of types and shapes of FRP reinforcement have become available, as shown in Figure 1, and its use in construction is expanding rapidly. Mainly, with respect to the repair and strengthening of existing structures, FRP reinforcement is of considerable interest. The use of externally bonded FRP reinforcement (FRP EBR) can be regarded as well documented and is becoming a standard technique in a fast way, with the number of applications growing exponentially in several countries throughout Europe. Also, on the use of FRP reinforcement for RC and PC, recently increasing efforts are taken by certain companies. Hereby, the durability characteristics are one of the major advantages of these new types of reinforcement.

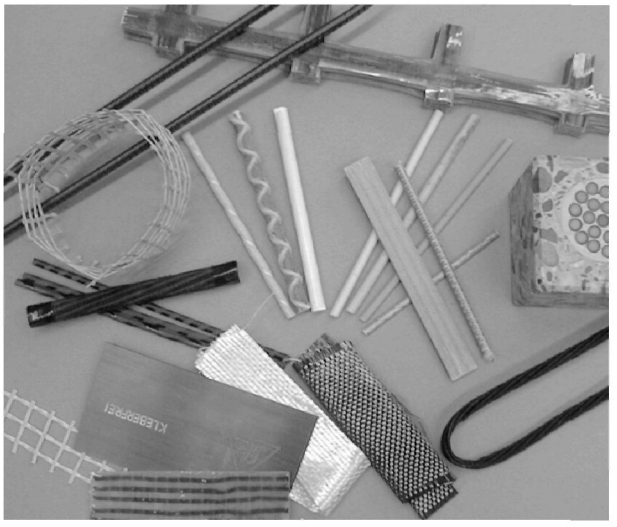


Figure 1. Examples of various FRP reinforcements

### Externally bonded FRP reinforcement

Although applications and demonstration projects have been taken place already in the late 1980's and early 1990's, commercial use of FRP EBR started mainly in Switzerland around 1993 and soon followed in other European countries. Whereas in the beginning it was expected that the use of FRP EBR would mainly apply to strengthening of bridges, it appears that a lot of the strengthening work with this technique is done in the building sector, among which the restoration of old buildings. The amount of FRP used per project varies from a few meters to some

kilometres. In Switzerland alone, the amount of FRP material applied for strengthening, has reached 30 to 50 km a year. Basically, the FRP EBR is used for RC as well as PC structures. To a lesser extent, yet various applications deal with FRP EBR on masonry, timber and metals.

Over the last years, the market for externally bonded FRP reinforcement is characterized by a clear dynamism. Different manufacturers and contractors are active in or enter this market segment, while researchers and commissions are trying to provide design guidelines on a short term basis. The type of applications range widely and different challenging projects have been executed, such as strengthening of silos in Sweden, tripling the bearing capacity of a floor slab in Belgium (Figure 2), seismic strengthening in Italy and Greece, etc. Furthermore, new types of products and techniques enter the market to extend the possibilities of the FRP EBR strengthening technique: L-shaped CFRP strips for shear strengthening, systems for increased anchorage capacity by means of mechanical devices, techniques to allow prestressed FRP EBR, modular systems consisting of prefab wood/CFRP beams to increase the stiffness and efficiency (due to the increased lever arm between the compression zone and the externally bonded FRP reinforcement) of the FRP EBR, cut-in FRP strips which are positioned inside (near the surface) the concrete or wood and have high anchorage capacity, etc.



Figure 2. Strengthening of floor slab-beam system with prefab wood/CFRP beams and bolted anchorage at the Zoological garden of Antwerp

**FRP reinforcement for RC and PC**

The use of FRP reinforcement for RC and PC is commercially much less established than that of externally bonded reinforcement. Nevertheless, FRP (prestressing) reinforcement is available in different European countries by local manufacturers or suppliers. Examples of recent initiatives are two prefabricated CFRP prestressed girders for a bridge over the high speed rail way line at Kortenberg (Belgium), CFRP PC poles in Switzerland (Figure 3), a cable stayed bridge at Herning (Denmark) with extensive use of CFRP reinforcement (both stay cables and (prestressing) reinforcement) and external post-tensioning with CFRP cables in the Dintelhaven bridge in Rotterdam (The Netherlands).



Figure 3. CFRP prestressed pole (left) versus conventional pole (right)

## FIB TASK GROUP 9.3 AND THE CONFIBRECRETE NETWORK

### General

Important research activities concerning the use of FRP reinforcement are performed at several universities and research institutes in Europe. A major part of this research deals with FRP EBR, along with the strong commercial interest in this technique. To a lesser extent research is conducted on the use of FRP for PC, RC and on FRP material properties. A considerable part of the current European research activities are linked by the ConFibreCrete Network, as discussed further in this section.

A major obstacle in adopting FRPs widely in construction is the lack of accepted standards for design and quality control. As this aspect is generally recognised, several initiatives to develop design guidelines are ongoing on a national and international level. An overview is given in the section on 'Design Guidelines'. To stimulate the development of unified guidelines for Europe, a *fib* (Fédération International du Béton) Task Group has been established [3]. The work started in a CEB (Comité Euro-International du Béton) Task Group (TG 3.10) in September 1996 which converted, with the merger of CEB and FIP in June 1998, into an *fib* Task Group (TG 9.3), under the supervision of Commission 9 "Reinforcing and Prestressing Materials and Systems". The title of TG 9.3 is "FRP Reinforcement for Concrete Structures". The task group consists of about 60 members, representing most European universities, research institutes and industrial companies working in the field of advanced composite reinforcement for concrete structures, as well as representing members from Canada, Japan and USA. Starting December 1997, the work of the *fib* TG 9.3 has been largely supported by the EU TMR (European Union Training and Mobility of Researchers) Network, ConFibreCrete that comprises of 11 teams from 9 European countries [4]:

1. University of Sheffield
2. University of Chalmers
3. Ghent University
4. Universita' degli Studi di Bologna
5. University of Patras
6. TU Braunschweig
7. Université d'Artois
8. University of Cambridge
9. SINTEF
10. Eurocrete Ltd
11. Institute of Polymer Mechanics




**Organization and Objectives**

Having the same objectives, *fib* TG 9.3 and the ConFibreCrete Network co-ordinate the research efforts in Europe and lead the development of guidelines for design of concrete structures reinforced, prestressed or strengthened with FRP. Before arriving at guidelines, fundamental research is undertaken to close gaps in knowledge and understanding. Both are involved in many tasks ranging from material testing and characterisation to internal and external reinforcement and industrial collaboration as specified below:

- Information Management and Dissemination
- Material Testing & Characterisation
- Reinforced Concrete (RC)
- Prestressed Concrete (PC)
- Externally Bonded Reinforcement (EBR)
- Industrial Collaboration

In the *fib* TG9.3 inaugural meeting on December 1996 the following basic objectives were set:

1. The elaboration of design guidelines in accordance with the design format of the CEB-FIP Model Code and Eurocode 2.
2. For the design guidance important input is needed concerning material characterization. This characterization should be related to standard testing methods to be developed.
3. Participation in initiatives to set-up international databases on research and applications in the field of advanced composite reinforcement.
4. Guidance on practical execution of concrete structures reinforced by FRP.
5. To publish *fib* Bulletins on design guidance and the work progress of TG9.3.

The main objectives of the ConFibreCrete research network are the following:

1. Gather and maintain a database of information on existing research in the field.
2. Bring together researchers in the field.
3. Identify gaps in understanding and knowledge.
4. Identify the needs of the construction industries for advanced composites in the various EU countries.
5. Enable young researchers through their training and mobility to "cross-pollinate" European research in this field.
6. Support the development of standard tests and models.
7. Determine an appropriate philosophy of design.

8. Help the European advanced composites industry identify improvements and new uses for their materials in the concrete construction field.
9. Produce guidelines for the design of concrete structures reinforced with advanced composites.
10. Disseminate the research findings and guidelines.

**Task Group Responsibilities and Progress**

*Information Management and Dissemination*

Information gathering and exchange being one of the objectives of the ConFibreCrete Network, an internet web site (http://www.shef.ac.uk/~tmrnet) [4] was established at the beginning of the contract period (Figure 4). This web site is proving very popular and offers useful information to students and researchers in the field of FRPs. Among the features available on line, the external visitor can find a searchable database of research publication in the field and a specific database on Case Studies. Information on the ConFibreCrete Network, including profiles of the teams, work plan and other organisational aspects are also available and links to important internet sites make the web site a good starting point for gathering information on FRPs. All the activities of ConFibreCrete can be found on line and the site is often used as a media for coordinating international activities. For instance, a specifically dedicated section has been developed to provide news and technical support on a round robin test project organized by ConFibreCrete research Network together with *fib* TG 9.3 and ISIS Canada. Also a *fib* TG9.3 web site (http://allserv.rug.ac.be/~smatthys/fibTG9.3) is available [3], which reports on the members, meetings and work progress of the task group. The restricted area of this web site is extensively used by the members to develop working documents and design guidelines.

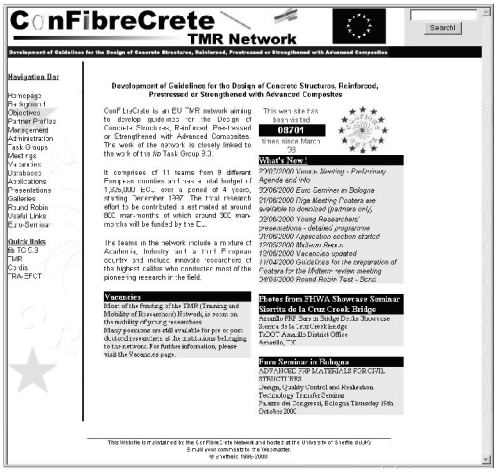



Figure 4. Homepage of the ConFibreCrete Network

*Material Testing and Characterization*

Material characterization and testing is always an obstacle in rapidly developing fields due to the different methods used by various manufacturers and researchers. Whilst various standards for the determination of the mechanical characteristics of advanced composites

exist in the aerospace field, they do not cover their use with concrete and the problem must be addressed in order to clarify the material advantages and disadvantages as well as the economics of these advanced materials as opposite to the more classic steel reinforcement. The work carried out by this task group includes tests on bond characteristics, tensile strength and durability of the materials in the concrete environment, performance of non-ferrous rebar at elevated temperature and work to assess the effectiveness of non-destructive techniques has also been carried out. To study the durability, mainly with respect to proper strength reduction factors for the design, a comprehensive literature study has been executed. Furthermore, together with the fib Task Group 9.3 and ISIS Canada ,an international round robin testing programme has been initiated by ConFibreCrete on the bond behaviour of FRP reinforcement to concrete [5].

*Reinforced Concrete*

Investigations carried out by this task group include shear and punching shear, deflections, deformation of crack widths and ductility (Figure 5). The issue of philosophy of design was also extensively investigated and the outcome proposals were discussed at network meetings and at various international conferences. A comprehensive state-of-the-art report on bond has been produced jointly with fib Task Group 4.2. State-of-the-art reports on shear, deflection and cracking have also been produced. An "Interim guidance on the design of reinforced concrete structures using fibre composite materials" has been published by the British Institution of Structural Engineers [6] and modifications to the Norwegian "Process code for bridges" [7] to include non-metallic reinforcement have been written by network participants.

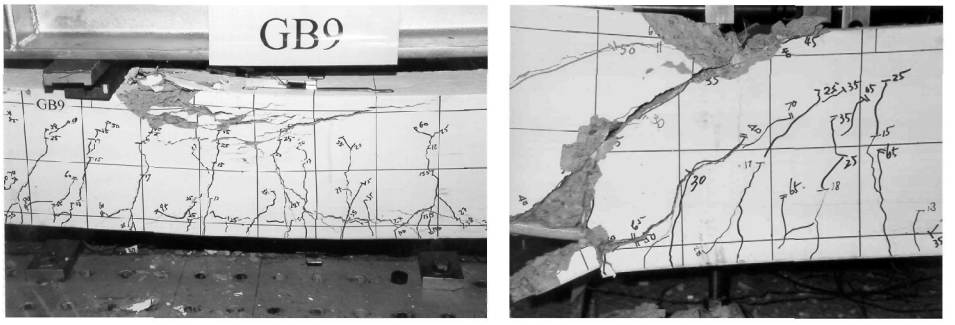



Figure 5. Flexural (left) and shear (right) failure in GFRP RC beams

*Prestressed Concrete*

Much of the initial developments in the field of FRPs started with prestressing. As with prestressing steel, the fundamental problem is anchoring the tendons in the transfer zone. Here, the anisotropic properties of FRP pose a real challenge since composites are weaker in the transverse direction. This and other issues, such as the stress-rupture of FRP prestressing elements, the transfer length of some FRP types, the long term behaviour of FRP prestressed concrete members (Figure 6) and the behaviour of concrete elements with partially bonded prestressing tendons have been investigated and work on these matters have been published.

*Externally Bonded Reinforcement*

Repairing and strengthening of concrete structures is a costly and disrupting exercise, where the cost of the projects is less sensitive to the price of the material used. Given the ease-of-

application and the advanced properties, the interest in FRP reinforcement for externally bonded reinforcement is considerable. Many applications have been conducted worldwide

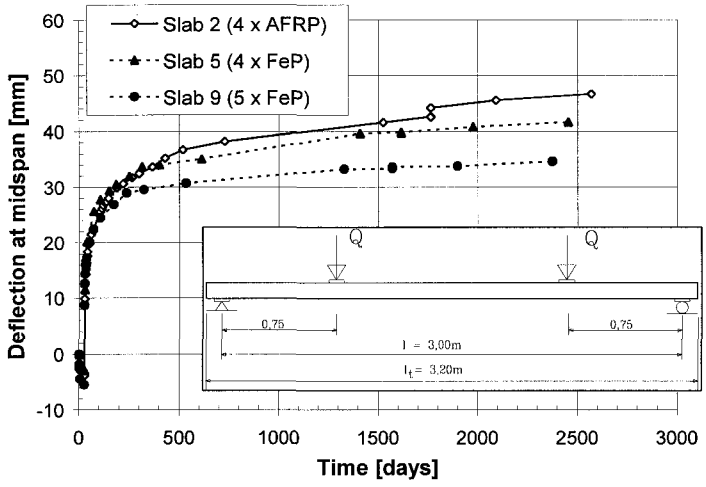



Figure 6. Long-term behaviour of prestressed slabs

and especially a considerable amount of work is done in seismic regions. Though these applications, which differ considerably in design approach and sometimes show lack of design rationale, there is an urgent need to develop design recommendations in this field. Work carried out by this task group addresses the issues of FRP confinement of axially loaded columns (Figure 7) and serviceability of concrete elements strengthened with bonded FRP. Different types of failure modes of externally reinforced beams were investigated and experimental work was done on the delamination fracture toughness of carbon fibre reinforced epoxy sheets. The issue of fire was also considered and an experimental program on EBR-RC elements started concerning the behaviour of these structures when subjected to high or low temperatures as well as decay of mechanical properties after a series of cycles on heating and cooling. In a comprehensive study [8] mechanical models were verified for the prediction of the structural behaviour of concrete beams strengthened in flexure or shear and of confined axially loaded columns. As part of this work much consideration was given to the design and safety concept of externally bonded reinforcement, as well as the quality control. Other research conducted aimed in extending the knowledge of specific aspects such as non-destructive testing of the bond quality of external reinforcement, shear strengthening of masonry walls and strengthening of beam-column joints (Figure 8).

*Industrial Collaboration*

A specific task group is in charge of establishing connections to industries and to identify their needs and help the European advanced composites industry identify improvements and new uses for their materials in the concrete construction field. For this purpose, papers have been presented in various international conferences and national meetings and a European seminar on "Advanced FRP materials for civil structures: design, quality control and realizations" took place in October 2000 mainly addressing FRP producers, contractors and professional engineers. The seminar focused on design rules and applications details in order to develop the confidence needed for a

broad acceptance of modern materials in concrete structures. Furthermore, research has been initiated on the economical viability of FRP reinforcement, so to demonstrate that often the cost effectiveness of concrete structures reinforced with FRP is larger than currently assumed.




Figure 7. Rectangular column strengthened with GFRP at failure

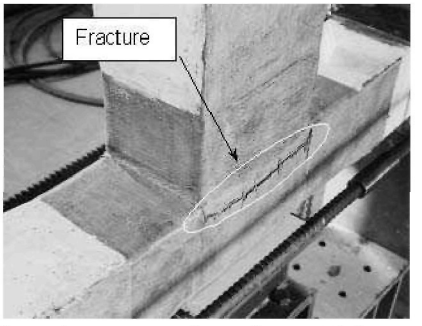



Figure 8. Fracture of FRP in a RC joint tested under cyclic loading

## CONFIBRECRETE AND THE TRAINING OF YOUNG RESEARCHERS

Being a TMR (Training and Mobility of Researchers) Network, great effort is put in encouraging mobility of young researchers. Their training takes place in the areas of the scientific task groups previously mentioned and according to the expertise they have and the one they are expecting to develop.

A progress meeting is held, in conjunction with the *fib* TG 9.3 meetings, approximately every six months for management purposes and the researchers are encouraged to present their work creating good opportunity for comments and interesting discussions. As part of the training, a seminar was also organized in January 1999 in Sintra, Portugal and a poster session was held in conjunction with the midterm meeting of the Network in June 2000 in Riga, Latvia.

## DATABASE OF RESEARCH AND APPLICATIONS

A searchable database of research publications in the field is available at the ConFibreCrete web site. The database is maintained jointly by ConFibreCrete and *fib* TG 9.3 members and a specific section on Case Studies on Externally Bonded Reinforcement (EBR) for Concrete Structures has also been established. Furthermore, examples of applications and products can be found on the same web site. These documents don't pretend to be an exhaustive collection of what is available world wide but try to be an easy-to-use tool for researchers and a gateway for industries and contractors who can look up at what has been done in the field and create a stronger link between pure research and its applicability.

## DESIGN GUIDELINES

### International context

The first research committee on Continuous Fiber Reinforcing Materials (CFRM) was established in 1989 by the Japan Society of Civil Engineers (JSCE). Its work was published in Japanese [9] in the form of a State-of-the-Art report in 1992 addressing various issues such as applications, design guidelines, durability and test methods. Part of this first publication, specially concerning design considerations, was translated into English and published in 1993 [10]. Since the need of design guidelines was seen as necessary to allow a major development in using CFRM the work of the Committee focused on this issue and design recommendations on RC and PC were firstly published in Japanese in 1996 and then in English in 1997 [11]. Parallel to JSCE, in Japan also committees by the Architectural Institute of Japan (AIJ) and the Building Research Institute (BRI) have been active, resulting in various publications [12,13].

A commission in Canada regarding FRP for concrete also began in 1989. The Canadian Society of Civil Engineers created a technical committee on the use of advanced composite materials in bridges and structures. The effort of this committee resulted in the publication of a State-of-the-Art Report in 1991 [14] and lead to design recommendations, with respect to the Canadian Highway Bridge Design Code, that were published in February 1996 [15]. In 1991 the American Concrete Institute (ACI) formed Committee 440 on Fiber Reinforced Polymer Reinforcement, whose effort lead to the publication of a State-of-the-Art report in 1996 [16] followed by provisional design recommendations last drafted in January 2000 [17].

In Europe coordinated activity started in November 1991, with a 5-years BRITE/EURAM Project "Fibre Composite Elements and Techniques as Non-Metallic Reinforcement of Concrete", financed by the commission of the European Communities. This project mainly focussed on the use of FRP as prestressing reinforcement. In December 1993, the EUROCRETE project started in Europe and ended in 1997. This pan-European research programme was established with the aim of developing FRP rebars for concrete and many areas of interest were examined. One of the task groups put its effort in the development of suitable design guidelines. More work on the development of design guidelines, according to the Eurocode format, started as already stated in September 1996, with *fib* Task Group 9.3 "FRP Reinforcement for Concrete Structures".

### Guidelines for FRP reinforcement in Europe

One of the early initiatives to develop guidelines followed from the work done by the EUROCRETE project, which has been included in interim guidelines published by the British Institution of Structural Engineers [6] and SINTEF Norway [7] in 1999. These documents provide recommendations on the use of FRP reinforcement for RC, with respect to the British and Norwegian standards respectively. Various other national initiatives on design guidelines have been taken or are ongoing. Most of them relate to the use of externally bonded reinforcement, among which the following:

- In Sweden a report has been established on 'Strengthening of existing concrete structures with carbon fibre fabrics or laminates - Dimensioning, materials and execution', which has been excepted as a Swedish National Railroad and Road Code in 1999 [18]. A report by the Swedish Concrete Association, called 'Possibilities of non-metallic (FRP) reinforcement to day and in the future' is currently under development.
- In Germany, different so-called expert opinions, which are product related, have been issued. These documents are commissioned by the manufacturer and assess the suitability and design of the FRP product for use as adhesive-bonded reinforcement to strengthen concrete members.

- End 2000, a technical report called 'Design guidance for strengthening concrete structures using fibre composite materials' has been published by the Concrete Society in the UK [19]
- In the Netherlands, a CUR working commission has reached its final stage in preparing recommendation on the use and design of externally bonded CFRP reinforcement for concrete members, to be published by the end of 2001.
- In Switzerland, a commission has been initiated which aims in the development of a SIA code on FRP EBR.
- In Greece, commissioned by the Seismic Planning and Protection Agency, a project has been started to develop design recommendations for seismic strengthening with FRP EBR.

On the European level, unified design guidelines are currently under development by *fib* TG9.3. Two reports are being produced, one regarding EBR and one on materials and internal reinforcement. The first bulletin, called "Design and use of Externally Bonded FRP Reinforcement for Reinforced Concrete Structures", is in its final review stage and will be published in the second half of 2001. It gives detailed design guidelines on the use of FRP EBR, the practical execution and the quality control, based on the current expertise and state-of-the-art knowledge of the task group members [20]. A second bulletin, called "FRP Reinforcement for Concrete Structures" is under development and deals with design aspects and state-of-the art knowledge on FRP materials, their properties and characterisation, as well as its use for RC and PC structure.

## CONCLUSIONS

The interest in FRP reinforcement in Europe is considerable and its use is getting more generally known, mainly with respect to externally bonded FRP reinforcement. A major part of the European activities (applications, research, development of guidelines) relate to the latter technique, in addition to FRP reinforcement for RC and PC.

In different European countries design guidance documents are available or under development. To develop unified European guidelines for the use of FRP reinforcement in concrete structures a *fib* (International Federation for Structural Concrete) Task Group 9.3 "FRP Reinforcement for Concrete Structures" has been established in 1996. On the research and dissemination of results level, *fib* TG9.3 is supported by a EU TMR Network "ConFibreCrete".

Two bulletins are being produced by *fib* TG9.3 on design guidelines for the use of FRP in concrete structures. A first bulletin, dealing with externally bonded FRP reinforcement, is in a final stage and will be published in the second half of 2001. A second bulletin on FRP materials and their use for RC and PC is under development.

A database of research and applications is available on line and an international round robin testing has been initiated by TMR ConFibreCrete, *fib* TG9.3 and ISIS Canada.

## ACKNOWLEDGMENTS

The authors wish to acknowledge the European Commission for funding the TMR Network "ConFibreCrete" and the ConFibreCrete and *fib* TG 9.3 members for their support and their continuous involvement in the activities. The authors also want to acknowledge the contribution of various individuals in sending useful information on the European activity.

**REFERENCES**


1. Taerwe L., Matthys S. (October 1999), "FRP For Concrete Construction: Activities In Europe", ACI - Concrete International, October 1999, Vol. 21, No. 10, pp.33-36.
2. Meier, U., Deuring, M., Meier, H., and Schwegler, G., "FRP Bonded Sheets", in Fiber-Reinforced-Plastic (FRP) Reinforcement for Concrete Structures: Properties and Applications, Elsevier, 1993, pp. 423-434.
3. *fib* Task Group 9.3, "FRP Reinforcement for Concrete Structures", International Federation for Structural Concrete, Commission 9, Task Group 9.3, http://allserv.rug.ac.be/~smatthys/fibTG9.3.
4. TMR, "Development of Guidelines for the Design of Concrete Structures, Reinforced, Prestressed or Strengthened with Advanced Composites (ConFibreCrete)", Training and Mobility of Researchers, Research Network TMR "ConFibreCrete", http://www.shef.ac.uk/~tmrnet.
5. TMR ConFibreCrete, fib TG9.3 and ISIS, "International Round Robin Tests for FRP Reinforcement", http://www.shef.ac.uk/~tmrnet/rrt.
6. Institution of Structural Engineers, "Interim guidance on the design of reinforced concrete structures using fibre composite reinforcement", Published by SETO Ltd, August 1999, 116 pp.
7. Thorenfeldt, E., "Modifications to NS3473 when using fibre reinforced plastic (FRP) reinforcement", SINTEF Report STF22 A98741, Trondheim, 1998.
8. S. Matthys, "Structural Behaviour and Design of Concrete Members Strengthened with Externally Bonded FRP Reinforcement", PhD-thesis, Ghent University, Faculty of Engineering, Department of Structural Engineering, Ghent, Belgium, November 2000, 345 pp.
9. JSCE, "Application of Continuous Fiber Reinforcing Materials to concrete Structures" (in Japanese), Concrete Library, No. 72, 1992.
10. JSCE, "State-of-the-Art Report on Continuous Fiber Reinforcing Materials", Concrete Engineering Series 3, October 1993.
11. JSCE, "Recommendation for Design and Construction of Concrete Structures using Continuous Fiber Reinforcing Materials", Concrete Engineering Series 23, 1997.
12. AIJ (1991), "Evaluation items and evaluation methods for new reinforcement materials and new reinforced concrete" (in Japanese), Report, Task Committee on Continuous Fibre Composite Materials, Architectural Institute of Japan, Tokyo, 1991.
13. Sonobe, Y., Fukuyama, H., Okamoto, T., Kani, N., Kimura, K., Kobayashi, K., Masuda, Y., Matsuzaki, Y., Mochizuki, S., Nagasaka, T., Shimizu, A., Tanano, H., Tanigaki, M., and Teshigawara, M., "Design guidelines of FRP reinforced concrete building structures", Journal of Composites for Construction, Vol. 1, No. 3, August 1997, ASCE, USA, August 1997, pp. 90-115.
14. Mufti, A. A., Erki, M. A., and Jaeger, L. G. (editors), "Advanced composite Materials with Application to Bridges". The Canadian Society for Civil Engineering, Montreal, Quebec, 1991, 297 pp.
15. CHBDC - Canadian Highway Bridge Design Code, "Section 16: Fibre Reinforced Structures", Final Draft, July 1996.
16. ACI Committee 440, "State-of-the-Art Report on fibre Reinforced Plastic Reinforcement for Concrete Structures", American Concrete Institute, U.S.A., February 1996.
17. ACI Committee 440, "Guide for the Design and Construction of Concrete Reinforced with FRP bars", American Concrete Institute, Revision January, 2000.

18. B. Täljsten, "Strengthening of existing concrete structures with carbon fibre fabrics or laminates - Dimensioning, materials and execution", An extract from Swedish National Railroad and Road Codes, Lülea University, Sweden, 1999.
19. Concrete Society, "Design guidance for strengthening concrete structures using fibre composite materials", Technical report 55, The Concrete Society, UK, 2000.
20. T. Triantafillou, S. Matthys and L. Taerwe, "Design of concrete members strengthned with externally bonded FRP reinforcement", Proc. of the 5th. Intern. Con. on Non-Metallic Reinforcement for Concrete Structures (FRPRCS-5), Cambridge, UK, 2001.

# Durability considerations for FRP reinforcements

TAKETO UOMOTO, International Center for Urban Safety Engineering
(ICUS/INCEDE), Institute of Industrial Science, The University of Tokyo, Japan

## INTRODUCTION

Many concrete structures have been made in Japan since the 1950's. In particular, just before 1964, when the Olympic games were held in Tokyo, not only the facilities for the Olympic games but also traffic facilities such as "Shinkansen" (rapid train railways), "Shuto Kousoku-doro" (metropolitan highways), and "Toumei Kousoku-doro"(highway connecting Tokyo and Nagoya) were made. Many projects have been proposed and numerous facilities have been constructed since then, using concrete. Recently, three huge bridges connecting Honshu Island and Shikoku Island (Honshu-Shikoku Renraku-kyo) have been made and people can travel to 4 main islands (Hokkaidou, Honshu, Shikoku and Kyusyu) by land.

Although there are still many structures to be made, one of the most important tasks to be carried out by the civil engineers today is to maintain these structures for use. The Shinkansen and highways have been in use for more than 35 years and without these important facilities, the economy of Japan cannot be maintained. To deal with the problem many attempts have been made 1) to maintain these existing structures and 2) construct more durable concrete structures that may be used for more than several hundred years. One of the main reasons for utilizing fiber-reinforced plastics (FRP) as reinforcements for concrete is to produce more durable concrete structures and also to repair existing structures using FRP reinforcements.

This paper briefly explains the present situation in Japan on durability aspects of concrete structures and explains why the civil engineers attempted to utilize FRP to reinforce concrete structures.

*FRPRCS-5*, Thomas Telford, London, 2001.

## NEEDS AND BACKGROUND OF FRP REINFORCEMENTS IN JAPAN

### Construction Works being done since 1950's

As shown in Fig.1, a tremendous amount of cement has been produced and used to construct structures in Japan since 1950. The figure shows that the production increased up to 1974, the year of "Oil Shock", and it stopped the growth gradually after that. To estimate the amount of concrete been produced, the total amount of concrete is estimated by assuming that the all cement was used to produce concrete, and 300kg of cement was used to produce $1m^3$ of concrete. The calculated result is shown in Fig.2. As shown in the figure, a large amount of concrete has been consumed since 1950. As seen in the figure, for instance, the concrete structures constructed up to 1970 can be estimated as only about 20% of the total amount of concrete structures that have been constructed up to 2000. We can easily understand how rapid the growth was until the year 2000, and as a result, a tremendous amount of concrete structures have been constructed in Japan.

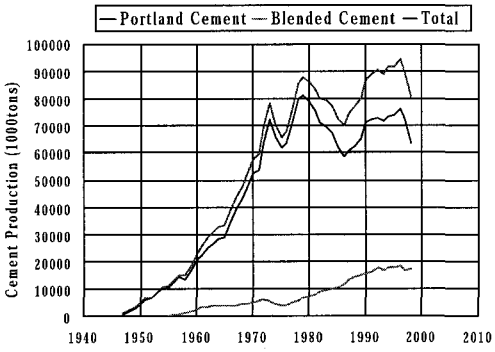



**Fig.1 Amount of Cement Production per year 1947-1998**

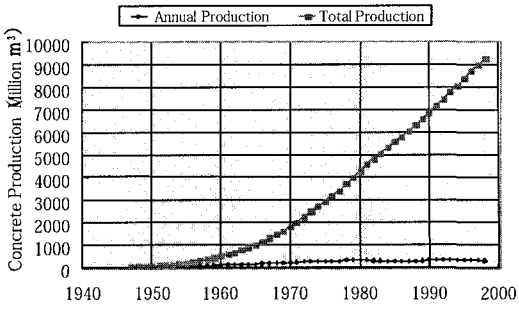



**Fig.2 Estimated amount of concrete production**

Fig.3 shows the relation between the years in service and the percentage of repaired number of bridges in Japan. The data clearly shows that as the years in service increases, the repaired number of bridges increases. When the bridges are used for more than 50

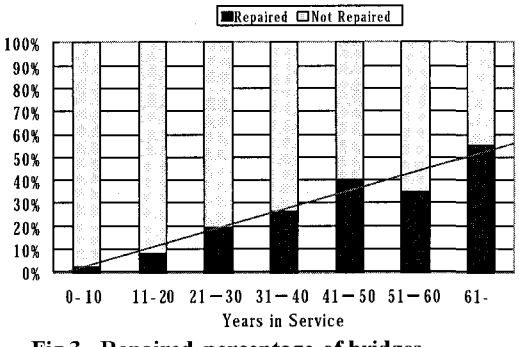



**Fig.3 Repaired percentage of bridges and years in service**

years, 40 to 50 percent of the bridges have to be repaired. This indicates that in order to utilize concrete structures for more than 100 years, maintenance works are essential for the concrete structures and we cannot expect concrete structures as maintenance-free structures.

**Change of Durability Problems of Concrete Structures**

Before 1970's, concrete structures are believed to possess high durability compared to steel structures. The main durability items considered in design and construction at that time were: fatigue, freeze-thaw deterioration, abrasion, permeability and chemical attack resistance. As can be easily estimated from these items, the concrete engineers were proud of using concrete as a construction material compared to steel. They did not have to consider corrosion of reinforcing steel bars, which was a big problem in the case of steel structures. The steel structure engineers have to consider the rate of corrosion in different environment even at the stage of design.

From 1965 to 1974, due to rapid growth of the Japanese economy, tremendous amount of structures has been constructed. The construction engineers were too busy to check the quality of materials to be used, design methods, construction procedures, etc., and also due to the lack of river sand and gravel, a large amount of sea sand and crushed stone was used as aggregates. Although there were regulations on chloride content, people did not realize the importance of the limitation. To facilitate the casting of concrete and to increase the strength of concrete, not only water content but also cement content was increased. At that time there were no special regulations on reactive aggregates or the amount of alkali content in cements. As a result, many newly constructed concrete structures deteriorated abruptly within 5 years, which was unusual up till then.

After the investigations of these deteriorated concrete structures, the following items were considered important from the durability point of view. Additionally to fatigue, freeze-thaw deterioration, abrasion, permeability and chemical attack, corrosion of reinforcing steel, alkali aggregate reaction, acidic rain, biological attack, etc., were decided important to increase the durability of structures. Not only JSCE (Japan Society of Civil Engineers), AIJ (Architectural Institute of Japan), and JCI (Japan Concrete Institute)

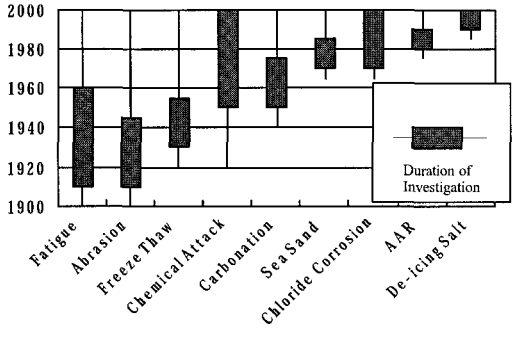



**Fig.4 Deterioration causes and development of countermeasures**

recommended many important aspects of the problems but also the relevant Ministries took prompt counter measures to cope with the situation. A large amount of research has related to the durability of concrete structures and countermeasures for each cause were proposed. Recently, the concrete committee of JSCE has published a new standard specification for construction considering durability-based design in January 2000 and for maintenance of concrete structures in January 2001.

The Fig.4 shows briefly how the problems on durability were investigated and overcome in Japan. As shown in the figure, the remaining problems are chloride induced steel corrosion (seawater attack and de-icing salt) and chemical attack to concrete structures (mostly due to acids in sewage facilities, etc.).

**Needs for countermeasures against chloride-induced corrosion**

Among these remaining problems, chloride-induced corrosion is the most important item to be overcome. Especially when chlorides are supplied continuously from seawater or de-icing salt, the countermeasures must resist against a tremendous amount of salt that will never end. In Japan, most of the people live close to the coast due to the locations of mountains at the center of our islands and many structures including railways and highways are located at the coast. Further, due to cancer problems from asphalt pavements, spike tires are limited in northern district of Japan, and de-icing salt became essential in these regions in the wintertime.

To deal with the problem, many attempts were performed, such as to use galvanized steel bars, epoxy-coated bars, catholic protection, etc. Among these attempts, utilization of FRP reinforcement was evaluated as a good method to deal with the problem, because it does not corrode even in a chloride environment. As mentioned by the JSCE research committee (1993), many researches were performed in Japan to utilize FRP as concrete reinforcement, especially for prestress tendons, since 1980's.

Today, a large amount of FRP has been applied to reinforce concrete structures not only to new structures but also to existing structures using recommendations by JSCE (1997), etc., but we must note that application of FRP in the field of concrete structures was little up till 1980. Types of FRP commonly used are rods embedded in concrete for new structures and sheets applied to the surfaces of existing structures to strengthen the structure, etc..

## DURABILITY OF FRP REINFORCEMENT

Concrete structures are normally used for more than 50 to 100 years, and the reinforcement

must be durable enough to reinforce the concrete for the same period of time. Although FRP does not corrode in a chloride environment, compared to steel, it must be clarified how it behaves in other environments. If FRP deteriorates in other environments, care must be taken when it is used as reinforcement for concrete structures.

Because most of the concrete structures using FRP as reinforcement were constructed within 20 years, it cannot be said whether the material has enough durability. In other words, one of the most important subjects that remains to be clarified in using FRP, as concrete reinforcement, is durability. Without the knowledge on durability of FRP in other environments than chlorides, engineers may easily make mistakes in using them.

**Main Causes of Deterioration of FRP**

FRP is a composite material, composed of millions of fibers and resin. The diameters of fibers are in the range of 6 (carbon fibers) to 15 microns (Aramid fibers and glass fibers). When tensile load is applied to FRP, fibers carry load and resin transfers stress to the neighboring fibers. The resin can also protect fibers from ingress of harmful ions from their environment. In this paper, carbon fiber reinforced plastics, Aramid fiber reinforced plastics and glass fiber reinforced plastics are abbreviated as CFRP, AFRP and GFRP.

Deterioration of both fibers and resin, and also the transition zone between fibers and resin govern the durability of FRP. This makes the deterioration mechanism of FRP complicated compared to steel. As most of the mechanical properties are governed by fibers, if the fibers are not deteriorated, FRP can resist against load in most cases. But when resin is attacked and deteriorated, the fibers fall off from the surface and the FRP strength reduces.

Considering the properties and usage of FRP, important items on deterioration to be considered are listed below. Items 1) to 3) are for reinforcements embedded in concrete (rods), and items 4) to 6) are for surface reinforcements (mainly sheets).

1) Static fatigue fracture
2) Fatigue fracture
3) Alkali resistance
4) Acidic resistance
5) Ultra-violet ray resistance
6) Freeze-thaw resistance
7) High temperature resistance and fire resistance

In the following paragraphs, explanations are given on each item.

**Basic Properties of FRP and Fibers Tested**

According to Uomoto et al (1998), the fibers tested in the following explanations are monofilament fibers of carbon, Aramid and glass, and FRP specimens tested are

**Table 1 Properties of fibers (monofilament) for FRP**

| | Type | Aramid | Glass | Carbon |
|---|---|---|---|---|
| Diameter | Average | 12.15 | 12.77 | 6.68 |
| | S.D. | 0.4141 | 0.6049 | 0.4441 |
| (μm) | C. of V. | 0.0341 | 0.0474 | 0.0664 |
| Strength | Average | 3890 | 2510 | 3350 |
| | S.D. | 360 | 870 | 520 |
| (MPa) | C. of V. | 0.092 | 0.347 | 0.155 |
| Elastic | Average | 83.55 | 85.51 | 227.3 |
| Modulus | S.D. | 10.81 | 16.29 | 21.52 |
| (GPa) | C. of V. | 0.129 | 0.191 | 0.095 |

**Table 2 Properties of resins for FRP**

| | Type | Ripoxy-R802 | Ripoxy-H600 |
|---|---|---|---|
| Tensile | Average | 84.9 | 67.00 |
| Strength | S.D. | 1.15 | 4.96 |
| (MPa) | C. of V. | 0.01 | 0.07 |
| Elastic | Average | 3110 | 4000 |
| Modulus | S.D. | 37 | 39 |
| (MPa) | C. of V. | 0.01 | 0.01 |
| Maximum | Average | 5.22 | 1.95 |
| Strain | S.D. | 0.11 | 0.27 |
| (%) | C. of V. | 0.02 | 0.14 |
| Notes | | AFRP, GFRP | CFRP |

**Table 3 Properties of FRP rods (Diameter: 6mm, round bar)**

| | Type | AFRP | GFRP | CFRP |
|---|---|---|---|---|
| Tensile | Average | 1690 | 1690 | 1340 |
| Strength | S.D. | 148 | 85.3 | 112 |
| (MPa) | C. of V. | 0.0876 | 0.0505 | 0.0836 |
| Elastic | Average | 45.70 | 52.11 | 135.30 |
| Modulus | S.D. | 1.946 | 0.476 | 23.63 |
| (GPa) | C. of V. | 0.0426 | 0.0091 | 0.0175 |

one-dimensionally reinforced FRP rods (diameter: 6mm) of CFRP, AFRP and GFRP with fiber content of 55%. The properties of fiber, resin and FRP rods are given on Tables 1 to 3. Numbers of test specimens for each case are 50 specimens for fibers and 20 for FRP rods.

**Static Fatigue Fracture**

One of the most important problems for the use of FRP as reinforcement for concrete is "static fatigue fracture" of FRP. When sustained tensile load is applied to FRP, due to uneven stress distribution to individual fibers, some of the fibers may fracture. Redistribution of load, carried by the remaining fibers, increases the stress of some of the fibers and this causes individual fracture of fibers one at a time.

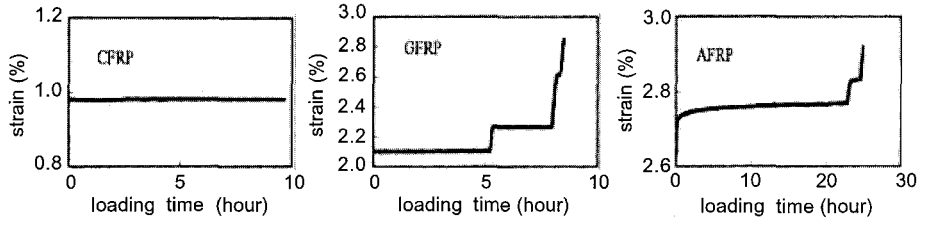



**Fig.5 Strain of FRP rod under sustained tensile load** **Uomoto et al (1996)**

Considering their evidences, much research was done to check the behavior of FRP under different sustained load. Fig.5 shows how the strain of FRP rod changes under sustained tensile load. As can be seen from the figure, although improvement is made, AFRP and GFRP rods may fracture partially depending on time and load till the final fracture of the whole rod. Fig.6 shows that when CFRP is used, static fatigue fracture does not occur within 1000 hours at 20 °C when the load is below 95% of the static strength. In the case of AFRP and GFRP, static fatigue fracture may occur when load is above 63% and 54%, respectively, within 1000 hours.

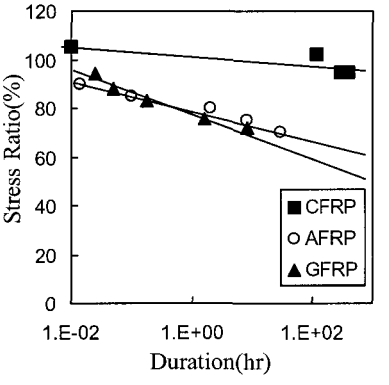



**Fig.6 Static fatigue fracture and duration time, Uomoto et al (1996), Yamaguchi (1998)**

The regression analysis by Yamaguchi (1998) proposed the relation between the applied stress ratio ($Fa/F_0$) and duration time (T) after 0.01 hours to 1000 hours are as follows:

[1] Fa/Fo(CFRP) = 102 - 1.91 logT

[2] Fa/Fo(AFRP) = 79.8 - 5.67 logT

[3] Fa/Fo(GFRP) = 79.2 - 8.29 logT

Where, Fa: applied stress

Fo: mean static strength

T: duration time (hours)

As mentioned in JSCE recommendation (1997), using equations [1], [2] and [3], estimated static fatigue fracture limits (Fa/Fo) after 1 million hours (about 100 years) are 91%, 46% and 30% for CFRP, AFRP and GFRP, respectively.

**Fatigue Fracture**

Fatigue behavior of FRP under cyclic load is another important problem. When fatigue load is applied, FRP may fracture as in the case of steel. Fig.7 shows the relation between applied mean stress and cycles of fatigue failure of CFRP, AFRP and GFRP rods. The tests were performed up to 2million cycles.

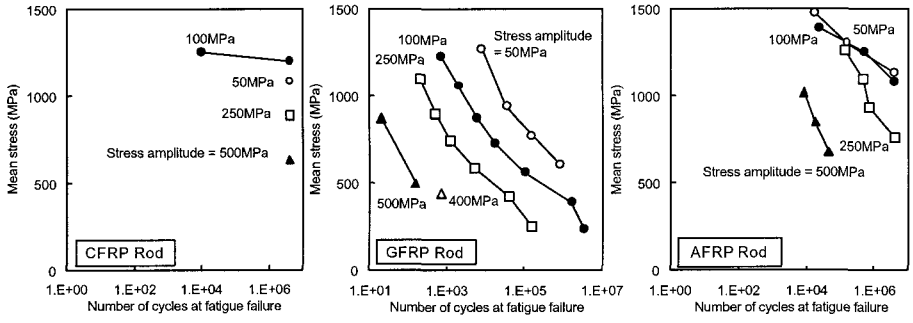



**Fig.7 Applied mean stress and number of cycles at dynamic fatigue failure Uomoto et al (1996,1998)**

In the case of GFRP, as mean stress or stress amplitude increases, the failure cycle reduces abruptly. From the figure, when mean stress is 845MPa (50% of the static strength of GFRP rod) and the stress amplitude is 100MPa, GFRP rod may fracture at 10,000 cycles. In the case of AFRP, the failure cycle reduces abruptly when stress amplitude becomes higher than 250MPa. If the stress amplitude is less than 100MPa, they do not fracture within 2 million cycles even when the mean stress is above 1180MPa (70% of the static strength of AFRP rod). In the case of CFRP, compared to GFRP and AFRP rods, they do not fracture within 2 million cycles. Uomoto et al (1996,1998) showed that if the stress amplitude is 100MPa, they do not fracture within 2 million cycles even when the mean stress is above 1100MPa (85% of the static strength of CFRP rod).

**Alkali Resistance**

When FRP is embedded in concrete and used as reinforcement, FRP must be durable enough against alkali, which comes from hydrated cement. Although the solution in the pores of concrete is not the same as in pure NaOH solution, alkali resistance of FRP can be estimated in accelerated test in NaOH solution.

Fig.8 shows the relation between the tensile strength of FRP rods and immersed period. The figure shows that in the case of CFRP and AFRP rods, there is no special change in strength even when they are immersed for 1000 hours. But in the case of GFRP rods, the strength reduces abruptly as temperature increases and concentration of NaOH increases. Uomoto et al (1996,1998) showed that the remaining strength of GFRP rod is less than 40% at 120 days in 40°C.

To estimate the strength reduction of GFRP, Katsuki (1996) proposed the following equation when the immersion period is short. Using the equations [4] and [5], the strength reduction of GFRP rod (diameter: 0.6cm) after 9 years in 20 °C is about 50% when concentration of alkali in concrete is 0.05N (pH=12.7),

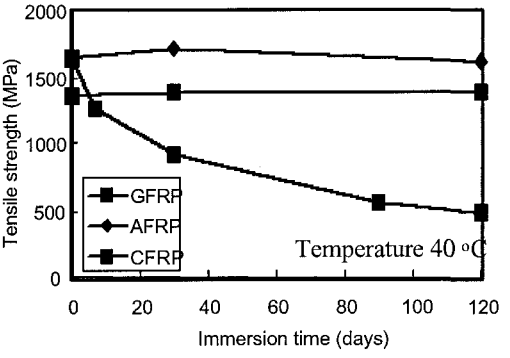



**Fig.8 Tensile strength of FRP rods immersed in NaOH solution (1mol/l) Katsuki (1996)**

[4] $F/F_0 = (\sqrt{1-2kCt}/R_0)^2$

[5] $\log k = -2.23(1000/T) + 1.57$

where, F : Strength of GFRP rod after immersion
Fo: Strength of GFRP rod without immersion
k : diffusion coefficient ($cm^2/hr$)
C : concentration of alkali (N)
t :time after immersion (hr)
Ro: radius of GFRP rod (cm)
T :surrounding temperature (°K)

**Acidic Resistance**

When FRP is embedded in concrete, no consideration is needed on acidic resistance. But when FRP is used as external reinforcement, such as external cables and sheet reinforcement, acids may attack FRP as in the case of acidic river, acidic rain etc.

To accelerate the test, fibers were immersed directly in acidic solution and strength tests were performed using 30 specimens for each case. Fig.9 shows the test results of tensile strength of fibers immersed in HCl solution. As shown in the figure, strength reduction is observed in all the fibers at 80 °C. In the case of carbon fibers and glass fibers, they do not deteriorate much up to 40 °C. But in the case of Aramid fibers, especially Kevler 49, strength reduction can be observed also in the case of 40 °C. To estimate the strength reduction of Kevler fibers, Nishimura et al (1999) applied Weibull's weakest-link theory. As a result, the following equation was obtained for HCl solution (1mol/l):

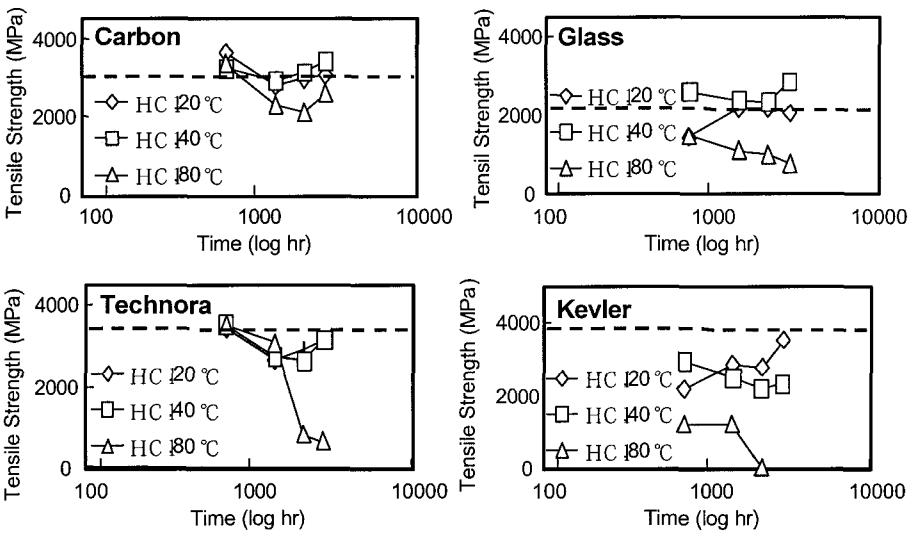



**Fig.9 Tensile strength of fibers immersed in HCl solution (1 mol/l)**

[6] $F = \alpha\,\Gamma(1+1/m),\ \alpha = \nu^{-(1/\mu)}Fo$

where, F : strength after immersion

Fo: strength before immersion

α, m: Weibull modulus

n : number of defects in the link

n=0.0076t+4.31 (20 °C), n=0.0742t+4.31(40 °C), n=0.684t+4.31(80 °C)

t : time after immersion (days)

Comparing the test results with the calculated result, this equation fits well with the experimental data and this shows that strength reduces several percent per year when immersed in HCl solution (1mol/l) at 20 °C. To estimate the actual situation, the effect of

HCl concentration must be considered.

**Ultra-Violet Ray Resistance**

When FRP is used as external reinforcement, as in the case of acidic resistance, the effect of ultra-violet rays must not be neglected. FRP is composed of fibers and resin, but resin can easily deteriorate by ultra-violet rays when they are exposed in sunlight. In the case of AFRP, the Aramid fiber may also deteriorate in the same manner.

Fig.10 shows the strength change of FRP rods exposed for 3 years at exposure sites both in marine environment and normal atmosphere in Japan. The figure shows that all FRP rods have reduced strength after 3 years; AFRP rod reduced 30-32%, GFRP rod reduced 1-19 % and CFRP reduced 9-17 %.

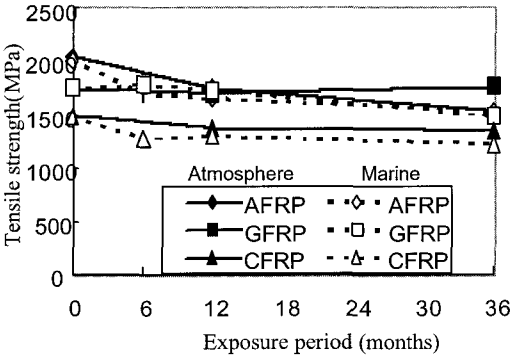



**Fig.10 Tensile strength of FRP rods exposed in marine and inland atmosphere Nishimura et al (1999)**

To verify the effect of ultra-violet rays, Uomoto et al (1998) performed accelerated tests using ultra-violet ray chamber (0.2 MJ/m$^2$/hr: average amount in Choshi in June) for both FRP rods and fibers. In the case of fibers, no special strength reduction was observed for carbon fibers and glass fibers. In the case of Aramid fibers, strength reduction was observed. For FRP rods, to consider the deterioration of resin under ultra-violet rays, it is assumed that strength reduction of CFRP rod was caused by the loss of deteriorated resin from the surface. Yamaguchi (1998) obtained the following equation from the data to calculate the thickness of the deteriorated layer.

$$\delta = 0.03\, t^{0.26}$$

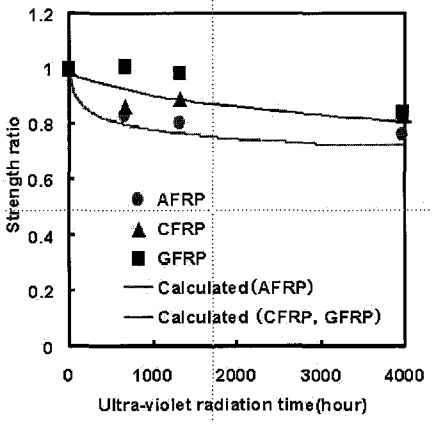



**Fig.11 Calculated strength of FRP rods exposed in ultra-violet rays (Rapid test) Yamaguchi (1999)**

where, δ:depth of deteriorated resin (mm)

t : time in ultra-violet rays chamber (hours)

Considering the thickness of deteriorated resin and the deterioration of fibers, the calculated strength coincide well with experimental results as shown in Fig.11. This evidence indicates that even in the case of CFRP and GFRP, deterioration depth of resin after 10 years of exposure in Choshi, Japan, will be about 0.6mm and special care must be taken to protect FRP from sunlight when used as external reinforcement

**Freeze-Thaw Resistance**

To check the durability of FRP in cold climates, freeze-thaw tests were performed. FRP rods were directly immersed in a freeze-thaw water chamber ( −20 °C to 15 °C) for 300 cycles. Test results are shown in Fig.12. The weight change was little and a few fibers appeared at the surface after 300 cycles. The strength reduction was observed only in the case of GFRP rod, but the reduction was only 8% after 300 cycles. Uomoto et al (1996,1998) showed that the effect of freeze-thaw is limited only on the surface of FRP.

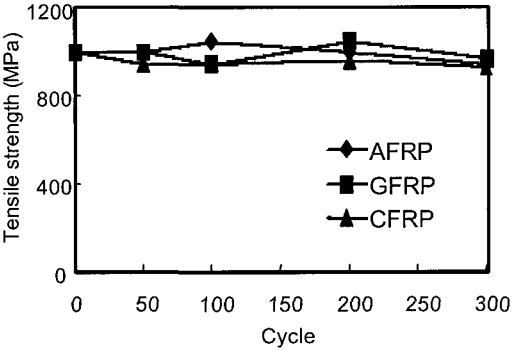



**Fig.12 Tensile strength of FRP rods after freeze-thaw cycles Uomoto et al**

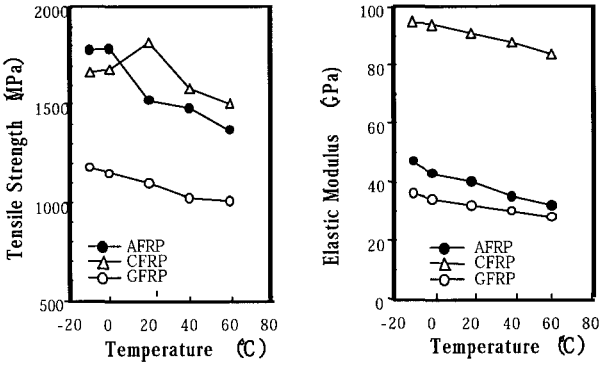



**Fig.13 Tensile strength of FRP rods in different temperatures Kobayashi et al (1988)**

**High Temperature Resistance and Fire Resistance**

High temperatures may affect properties of both fibers and FRP. Kobayashi et al (1988) performed tensile strength tests for FRP rods at different temperatures from −10 °C to 60 °C. The results are shown in Fig.13. As shown in the figure, both strength and elastic modulus reduce 20% to 30% as temperature rises from −10 °C to 60 °C. These results indicate that mechanical properties of both FRP and fiber itself are easily affected at high temperatures, and care has to be taken when applying FRP as reinforcement to concrete structures in high temperature environment.

Fig. 14 shows the test results by AIJ on fire resistance of both FRP and steel embedded in concrete. FRP is burnable and compared to steel, both strength and elasticity of FRP reduce more after the fire. For GFRP and CFRP, in the range of up to 350 °C, the reductions are within 25%, but in the case of AFRP there is a large reduction up to 35% in the range above 250 °C. The results show that care has to be taken when applying FRP reinforcements to structures that require fire resistance.

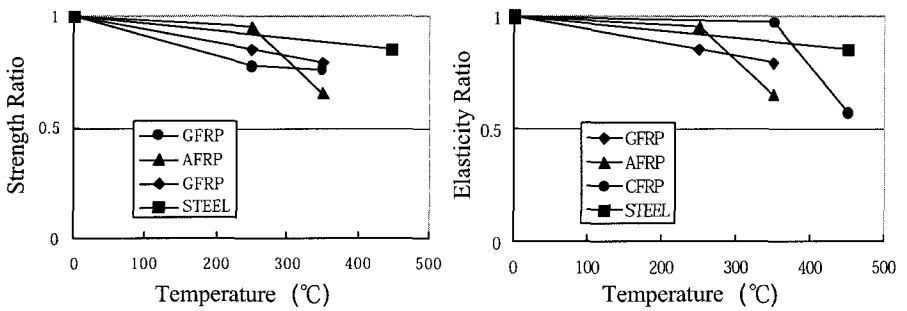



**Fig.14 Tensile strength and modulus of elasticity of FRP rods after fire**
**Architectural Institute of Japan (1998)**

## COMPARISON BETWEEN FRP AND STEEL REINFORCEMENT

As explained above, although FRP may not deteriorate by chlorides as in the case of steel, there are several important items to be considered when applying FRP as reinforcements for concrete structures. Table 4 summarizes the important items to be considered on durability of FRP reinforcement.

The items, such as static fatigue, cyclic fatigue and alkali resistance are the 3 important items to be considered in the case of FRP rods. As shown in the table, CFRP rods have little problem in the aspect of durability compared to other FRP reinforcements. In the case of GFRP, rods deteriorate tremendously in all the cases and the strength reduces. Even when the alkali resistance is improved by special technique (hybrid FRP with glass fiber and

Aramid fiber: ref.21), fatigue properties are poor compared to other FRP rods. It is better not to use GFRP for internal reinforcement. In the case of AFRP, although alkali resistance and cyclic fatigue properties are good, care must be taken on static fatigue. The simple method is to limit the tensile load applied to AFRP rod below 46% of the static strength at the time of designing if the structure is to be used for 100 years, or to replace the rod at certain period of time.

**Table 4 Durability of fibers and FRP (Strength ratio)**

| | Fiber | | | |
|---|---|---|---|---|
| | Carbon | Aramid | Glass | Notes |
| Static Fatigue | - | - | - | |
| Cyclic Fatigue | - | - | - | |
| Alkali Resistance | 95% | 92% | 15% | NaOH, 40 °C, 1000hr |
| Acidic Resistance | 100% | 60-85% | 100% | HCl, 40 °C, 120 days |
| Ultra-Violet Ray Resist. | 100% | 45% | 81% | 0.2MJ/m2/hr, 1000hr |
| Freeze-Thaw Resistance | - | - | - | |
| High Temperature Resist. | - | - | - | |
| Fire Resitance | - | - | - | |
| | FRP Rod | | | |
| | CFRP | AFRP | GFRP | Notes |
| Static Fatigue | 91% | 46% | 30% | 20°C, 100 years (Cal.) |
| Cyclic Fatigue | 85% | 70% | 23% | 100MPa Amp., 2 million cycles |
| Alkali Resistance | 100% | 98% | 29% | NaOH, 120days, 40 °C |
| Acidic Resistance | - | - | - | |
| Ultra-Violet Ray Resist. | 77% | 69% | 90% | 3 years exposure |
| Freeze-Thaw Resistance | 100% | 100% | 100% | -20 °C to+15 °C, 300 cycles |
| High Temperature Resist. | 80% | 75% | 80% | -10 °C to 60 °C |
| Fire Resistance | 75% | 65% | 75% | 350 °C |

The items, such as acidic resistance, ultra-violet ray resistance and freeze-thaw resistance are the 3 important items to be considered in the case of external reinforcement, such as external cables or sheet reinforcements. As shown in the table, carbon fibers and glass fibers have no special problem on durability except ultra-violet ray resistance. As explained above, resin may deteriorate under sunlight from the surface and this causes the deterioration of CFRP and GFRP. In any of the cases, measures must be taken to protect resin from deterioration or to replace FRP before deterioration exceeds a certain limit. In the case of Aramid fibers, the fiber deteriorates by ultra-violet rays and high concentrated acid,

especially in the case of Kevler 49. To deal with the problem, measures must be taken to prevent the deterioration from sunlight and acidic water or to replace FRP before deterioration exceeds a certain limit.

For high temperature resistance and fire resistance, FRP has poor properties compared to steel. To prevent deterioration, measures have to be taken to reduce the temperature around FRP and not to expose the reinforcements to fire directly. The increase of cover concrete may be a good way to prevent the deterioration.

## CONCLUSIONS

The following conclusions can be drawn from the test results.

1) Carbon fiber and CFRP have good durability properties for both internal and external reinforcements.
2) When CFRP of carbon sheets are used as external reinforcement, deterioration due to ultra-violet rays must be considered.
3) Aramid fiber and AFRP have good durability properties except static fatigue, ultra-violet rays and acidic environment.
4) In order to use AFRP as internal reinforcement, tensile load must be limited according to the duration time. When AFRP or Aramid sheet are used as external reinforcement, not only the sustained load but also deterioration due to ultra-violet rays and acidic environment must be considered.
5) Glass fiber and GFRP have poor durability except acidic resistance and freeze-thaw resistance.
6) GFRP is not recommendable for internal reinforcements. When glass fiber or GFRP is used as external reinforcements, care must be taken to the deterioration due to sustained load, fatigue load, alkali resistance and ultra-violet rays.
7) FRP has poor resistance against high temperature and fire. It is recommended to protect the FRP reinforcements by cover concrete, etc. to reduce the temperature around FRP reinforcements.

## REFERENCES

Research Committee on CFRM(1993), "State-of-the-Art Report on Continuous Fiber Reinforcing Materials", Concrete Engineering Series 3, JSCE

Research Committee on CFRM(1997), "Recommendation for Design and Construction of Concrete Structures Using Continuous Fiber Reinforcing Materials", Concrete Engineering Series 23, JSCE

Kobayashi, K., Uomoto, T. and Cho, R (1988), " Prestressed Concrete Structure using FRP Tendons (in Japanese), Prestressed Concrete, Vol.30, No.5, pp19-26

Uomoto, T. et al (1995) "Fatigue Strength of FRP Rods for Concrete Reinforcement", Building for the 21st Century, Edited by. Y.C.Loo, EASEC, pp.1659-1664

Uomoto, T.. and Katsuki, F (1996), "Deterioration Mechanism of Glass Fiber Reinforced Concrete and Prediction of Strength Reduction", Integrated Design and Environmental Issues in Concrete Technology, Edited by K.Sakai, FN & Spon, pp.137-146

Katsuki, F. (1996), "Evaluation of Alkali Resistance of FRP Rods for Concrete Reinforcement with Different Types of Fibers" (in Japanese), Doctoral Thesis, University of Tokyo

Uomoto, T. and Ohga, H. (1996), "Performance of Fiber Reinforced Plastics for Concrete Reinforcement", Advanced Composite Materials in Bridges and Structures, pp.125-132

Yamaguchi, T. (1998), "Study on deterioration of FRP Rods for Concrete Reinforcement on Ultra-Violet Rays and Creep Rupture" (in Japanese), Doctoral Thesis, University of Tokyo

Uomoto, T., et al. (1998), "Strength and Durability of FRP Rods for Prestressed Concrete Tendons" (in Japanese), Report of the Institute of Industrial Science, The University of Tokyo, Vol.39, No.2, No.244

Nishimura T., et al (1999), "Temperature Effect on Fiber Strength in Different solutions", JCI General Meeting, Vo.21, No.2, pp.288-293

# Externally bonded reinforcement for flexure

# FRPs for the rehabilitation of concrete beams exhibiting alkali-aggregate reactions

C. LACASSE, P. LABOSSIÈRE and K.W. NEALE
Université de Sherbrooke, Canada

**ABSTRACT**
A recently established technique for strengthening reinforced concrete structures is the external bonding of fibre reinforced polymers (FRPs). Indeed, this promising rehabilitation technology has the potential to be one of the most effective repair methods in the future. This paper deals with the use of FRPs as a rehabilitation method for concrete beams affected by alkali-aggregate reactions (AARs). Numerous corrective techniques have been developed to inhibit alkali-aggregate reactions in concrete structures. However, most of the existing techniques do not allow the structures to recover their initial mechanical properties.

In order to investigate the effectiveness of FRPs for beams exhibiting alkali-aggregate reactions, laboratory simulations are required. In this study, the effectiveness of FRPs as external reinforcement for reinforced concrete beams affected by AARs is investigated. The time schedule for the installation of the FRPs and for the flexural tests was determined in order to evaluate the composite's contribution in reducing AAR-related beam expansion and to assess the effect of FRP on flexural strength.

The effect of AARs on the behaviour of beams depends on the internal steel reinforcement, which reduces the concrete expansion and thus diminishes losses in mechanical properties. Futhermore, the development of AARs is inversely proportional to the size of the specimens. In our study we have used small-scale reinforced concrete beams (100 x 150 x 1220 mm) with two different longitudinal steel ratios (0.24 and 0.42% respectively). The concrete mix and the exposure conditions have been selected to rapidly develop the AARs. This investigation focuses on the measurements of strength variations. Also, experimental measurements of beam expansion with time will be discussed.

*FRPRCS-5*, Thomas Telford, London, 2001.

## INTRODUCTION

Alkali-aggregate reactions (AARs) are chemical reactions that occur between the concrete interstitial solution and reactive aggregates when the alkali content in the concrete and the relative moisture exposition are high. The commonly known symptoms of AARs are expansion, cracking, scaling, gel exudation, pop outs and early concrete degradation [1].

The loss of mechanical properties in reinforced-concrete structures, because of the unavoidable development of AARs in concrete, is a problem that must be faced all around the world, and Canada does not escape this problem. For instance, in Eastern Canada alone, over 1000 structures, most of them bridges, are known to be affected by this type of severe degradation [2].

The objective of the work presented here is to evaluate the efficiency of composite materials used as external reinforcement for RC-beams affected by AARs. Efficiency is determined by measuring the concrete expansion and the increase of flexural strength of the beams.

## EXPERIMENTAL PROGRAM

### Beam Specimens

For this research program, 38 small-scale beams (100 mm x 150 mm x 1220 mm) were fabricated, with the internal steel configuration shown in Figure 1. Since AARs are known to be affected by the amount of internal steel reinforcement, two different ratios of longitudinal steel reinforcement are being investigated here. Rebars with a 6 mm diameter were selected for 22 beams, and 16 beams were reinforced with 4 mm rebars. Steel ratios of 0.24% and 0.42% were achieved with the indicated dimensions. Shear failure of the beams under loading is prevented with internal stirrups made of 6 mm bars spaced at 75 mm c/c.

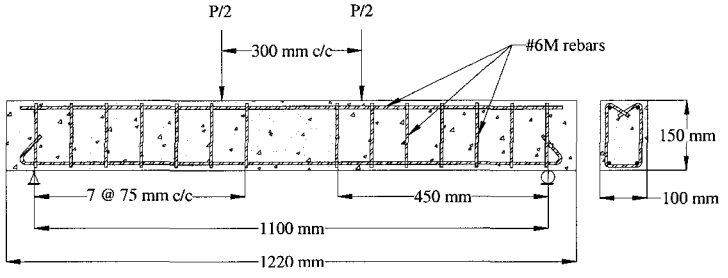



Figure 1. Beam details

Figure 2 shows the configuration of the 24 beams strengthened externally with two layers of MBrace CF-130, a carbon-fibre reinforced polymer (CFRP) material. At the extremities of the beams, U-shaped external stirrups are installed to improve the anchorage of the longitudinal reinforcement, and to prevent debonding of the CFRP when it is submitted to the four-point bending test. These stirrups are made of Fibrwrap SEH51-Tyfo, a glass-fibre reinforced polymer (GFRP) product. Since the only function of the stirrups is to prevent delamination, they are installed only shortly before testing.

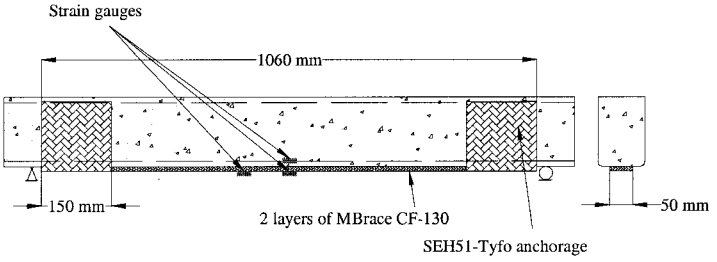



Figure 2. External reinforcement with composite materials

The CFRP schedule of installation is shown in Table 1. In the cases where the table shows that four specimens were tested, two beams with moderately reactive aggregates have been cast to compare their behaviour with that of similar beams with highly reactive aggregates.

Table 1. List of the beams for the research program

| | Longitudinal Steel | | | |
|---|---|---|---|---|
| | 4 mm (0.24%) | | 6 mm (0.42%) | |
| | Composite configurations | | Composite configurations | |
| Time schedule for the installation of the composite materials and for the flexural tests | None | 2 layers | None | 2 layers |
| Test after 28 days | 2 | - | 2 | - |
| Installation after curing, test after 6 months | 2 | 2 | 2 | 2 |
| Installation after curing, test after 12 months | 2 | 2 | 4 | 4 |
| Installation after 6 months, test after 6 months | - | 2 | - | 2 |
| Installation after 6 months, test after 12 months | - | 2 | - | 4 |
| Installation after 12 months, test after 12 months | - | 2 | - | 2 |

Total number of specimens: 38

**Concrete**

Two concrete mix designs were selected in order to develop AARs rapidly: one with reactive aggregates and another with moderately reactive aggregates. NaOH was added to both concrete designs to increase the alkali content to 1.25% of the cement weight. Table 2 shows the average compressive strength and elastic modulus evaluated at seven days, 28 days, six months and twelve months. These tests have been performed on standard concrete cylinders (100 mm diameter, 200 mm height).

Table 2. Concrete properties

Reactive concrete

| | 7 days | 28 days | 6 months | 12 months |
|---|---|---|---|---|
| f'c (MPa) | 30.1 | 34.2 | 43.9 | 42.2 |
| E (GPa) | 24.3 | 24.4 | 21.9 | 22.8 |

Moderately reactive concrete

| | 7 days | 28 days | 6 months | 12 months |
|---|---|---|---|---|
| f'c (MPa) | 28.0 | 32.9 | 42.8 | 45.4 |
| E (GPa) | 19.4 | 20.3 | 23.1 | 21.7 |

**Steel Reinforcement**
Five samples of 4 mm and 6 mm rebars were tested under uniaxial tension. The rebars exhibited an average yield stress of 600 MPa and an elastic modulus of 200 GPa.

**Composite Materials**
Mechanical properties for the two composite materials used in this research program are the following, according to the manufacturer's data sheets:

- Carbon-epoxy : MBrace CF-130, ultimate strength = 3550 MPa,
  elastic modulus = 235 GPa, ultimate strain = 0.015, thickness = 0.165 mm

- Glass-epoxy : Fibrwrap SEH51, ultimate strength = 552 MPa,
  elastic modulus = 27.6 GPa, ultimate strain = 0.020, thickness = 1.3 mm

We already know that the properties of CFRPs are not affected in a significant way by this kind of exposure conditions [3]. Uniaxial tests have been done on CFRP coupons (15 x 250 mm) with the ASTM D3039/D3039M-95a standard test method after six and twelve months of exposure to validate the manufacturers information.

**Exposure Conditions**
The exposure conditions for the beams were 38°C and 100% of relative moisture for a period of six months or one year, depending on the specimens. These conditions were selected in combination with the concrete properties in order to produce accelerated AARs at a significant rate.

**Test Setup**
During exposure, the expansion of 20 beams was measured on a monthly basis using Demec gauges. The location of these gauges are shown in Figure 3. There are four different positions for the expansion measurements (A = top, B = side up, C = side down and D = bottom of the beam).

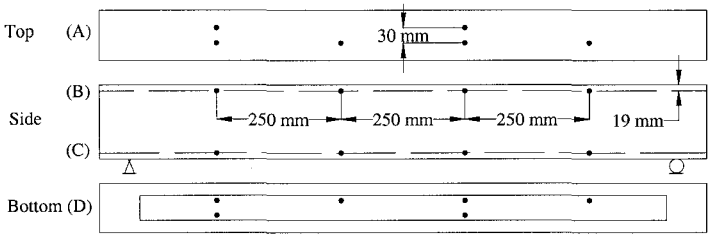



Figure 3. Positions of Demec gauges

Deformation of the steel rebars were measured using electric strain gauges on six beams on a monthly basis, to establish correlations with the expansion measurements taken with the Demec gauges at the same level on the concrete surface. Moreover, these strain gauge measurements were taken during the flexural tests of the beams.

After completion of the exposure periods, all beams were tested under a four-point bending static load up to failure as shown in Figure 1. In addition, electric strain gauges were used to measure strain on the external CFRP reinforcement for eight beams. Deflections of all 38 beams under loading were recorded with a Linear Variable Differential Transducer (LVDT) located at mid-span.

## PRELIMINARY RESULTS

### Expansion of the beams

After 12 months of exposure, general observations can be made for the overall expansions. Longitudinal expansions were measured between Demec gauges spaced at 250 mm as shown in Figure 3. Transversal expansions were measured between gauges spaced at 112 mm, on the side faces of the beams, and at 30 mm on the top and the bottom faces of the beams.

In view of the considerable number of expansion data, a statistical study is required to reach accurate conclusions. The statistical models used are the complete $2^3$ factorial designs, and designs with both nested and factorial factors [4]. With the complete $2^3$ factorial designs, we analyze results from an experiment with three different factors (composite reinforcement, expansion position and longitudinal steel ratio or type of concrete) and with two levels for each factor.

Preliminary results after five months of exposure were presented at the Third International Conference on Advanced Composite Materials in Bridges and Structures [5]. The most recent results, from the statistical analysis of the RC-beams submitted to 12 months of exposure, are presented here :

- The average expansion for the beams without CFRPs and with reactive concrete is about 0.098%;
- The expansion of beams without CFRPs is practically the same at the four measurement locations on the beam;
- The expansion of the RC-beams with 4 mm rebars is about 17.4% less than for the 6 mm rebars;

- The expansion of the RC-beams with 6 mm rebars and the one for the reactive concrete beams are not influenced in a very significant way by CFRPs;
- The expansion of the RC-beams with 4 mm and CFRPs is 17.1% less than that for the beams with 4 mm rebars only;
- The expansion on the top of the beams with CFRPs is 7.5% higher than for the beams without CFRPs;
- The expansion on the bottom of the beams with CFRPs is 9.6% less than for the beams without CFRPs;
- The beams with CFRPs tend to have an upward bending and beams without CFRPs tend to have either a downward or upward bending, in this case, much less important;
- The bending of the beams with moderately reactive concrete does not seem to be affected by CFRPs;
- For the same longitudinal steel ratio, the moderately reactive concrete RC-beams showed 31.4% less expansion than the reactive RC-beams;
- For the beams with moderately reactive concrete, the expansion of those with CFRPs is 13.8% less than for those without CFRPs.

**Bending tests**

The flexural strengths of the 38 beams tested are presented in Table 3. Figure 4 shows their theoretical resisting moment versus their experimental resisting moment. The theoretical resisting moment was calculated with the assumption that the failure will occur with steel yielding followed by tensile failure of CFRP. Moreover, the theoretical resisting moment was calculated with the composite material properties obtained from our laboratory tests on CFRP coupons.

We observe that the CFRP layers have increased the flexural strength of the beams by approximately 119%. The points which lie below the 45° line in Figure 4 correspond to debonding failure.

The duration of exposure of the CFRPs has a significant impact on the increase of flexural strength that can be reached by the beams. For instance, the average increase in flexural strength for all beams reaches 153% when the CFRPs are installed just prior to testing. However, when the testing is performed after a long contact between CFRPs and the AAR-affected beams, the increase in flexural strength is less important. After six-month exposure, it reaches 108%, and after twelve months, it attains 91%. While these values remain quite impressive, this is a clear indication that the AARs do affect the bond between the CFRPs and the concrete surface. Figure 5 illustrates typical load-deflexion curves of beams with 6 mm longitudinal steel.

Table 3. Flexural strengths of the 38 beams tested

| Rebars | Theoretical Mr (kN.m) 4 mm | Theoretical Mr (kN.m) 6 mm | Experimental Mr (kN.m) 4 mm | Experimental Mr (kN.m) 6 mm | Maximum deflexion (mm) 4 mm | Maximum deflexion (mm) 6 mm |
|---|---|---|---|---|---|---|
| Reactive concrete | | | | | | |
| Without CFRPs | | | | | | |
| Test after 28 days | 2.72 | 4.70 | 2.84 | 5.08 | 12.96 | 8.98 |
| | - | - | 2.83 | 4.97 | 8.96 | 9.75 |
| Without CFRPs | | | | | | |
| Test after 6 months | 2.74 | 4.75 | 3.45 | 6.21 | 30.38 | 29.95 |
| | - | - | 3.15 | 6.28 | 42.99 | 14.05 |
| Without CFRPs | | | | | | |
| Test after 12 months | 2.74 | 4.74 | 3.54 | 5.96 | 29.97 | 29.90 |
| | - | - | 3.46 | 6.22 | 25.53 | 28.20 |
| CFRPs installed after curing | | | | | | |
| Test after 6 months | 12.50 | 13.07 | 7.50 | 8.71 | 23.40 | 10.00 |
| | - | - | 9.33 | 11.05 | 25.70 | 22.88 |
| CFRPs installed after curing | | | | | | |
| Test after 12 months | 11.75 | 12.37 | 7.62 | 9.80 | 23.32 | 40.15 |
| | - | - | 8.08 | 10.92 | 25.01 | 26.58 |
| CFRPs installed after 6 months | | | | | | |
| Test after 6 months | 13.05 | 13.75 | 10.61 | 11.67 | 21.93 | 21.91 |
| | - | - | 10.77 | 13.26 | 21.14 | 25.00 |
| CFRPs installed after 6 months | | | | | | |
| Test after 12 months | 11.83 | 12.44 | 8.80 | 11.04 | 22.01 | 24.81 |
| | - | - | 9.06 | 11.50 | 31.63 | 35.38 |
| CFRPs installed after 12 months | | | | | | |
| Test after 12 months | 11.73 | 12.35 | 9.96 | 12.18 | 22.29 | 18.59 |
| | - | - | 10.12 | 12.36 | 21.32 | 19.98 |
| Moderately reactive concrete | | | | | | |
| Without CFRPs | | | | | | |
| Test after 12 months | - | 4.76 | - | 5.84 | - | 25.52 |
| | - | - | - | 5.84 | - | 37.21 |
| CFRPs installed after curing | | | | | | |
| Test after 12 months | - | 12.83 | - | 10.26 | - | 20.23 |
| | - | - | - | 10.48 | - | 25.43 |
| CFRPs installed after 6 months | | | | | | |
| Test after 12 months | - | 12.91 | - | 10.98 | - | 32.53 |
| | - | - | - | 11.00 | - | 30.30 |

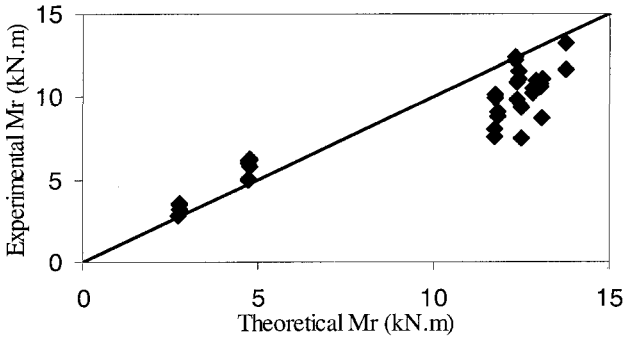



Figure 4. Flexural strength of the beams

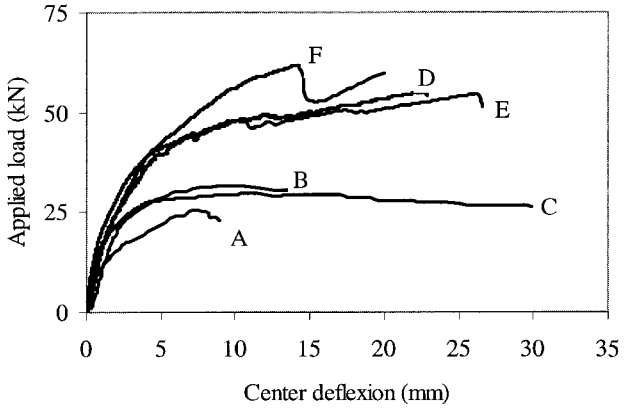



Figure 5. Typical load-deflexion curves of beams with 6 mm rebars

Legend:
A = Beam without CFRPs, tested after 28 days
B = Beam without CFRPs, tested after six months of exposure
C = Beam without CFRPs, tested after 12 months of exposure
D = Beam with CFRPs installed after the curing of the concrete, tested after six months of exposure
E = Beam with CFRPs installed after the curing of the concrete, tested after 12 months of exposure
F = Beam with CFRPs installed after 12 months, tested after 12 months of exposure

## CONCLUSION

The main purpose of this research was to evaluate the contribution of the FRPs in reducing the expansion of the beams due to AARs, and also to assess the increase in their flexural strength due to the FRP strengthening. The concrete mix design and the exposure conditions have been selected to rapidly develop AARs.

Even though Table 2 shows that the concrete properties had not changed significantly after 12 months of exposure, the results of the expansion measurements already indicated preliminary signs of AARs in the beams.

The moderately reactive concrete beams showed less expansion than the more reactive concrete beams. The tendency towards an upward bending for the beams with external composite reinforcement suggests that the composite contributes to limiting the expansion at the bottom face of the beams. These expansion results were obtained with only the bottom face of the beams reinforced with CFRPs. It could be interesting to study the behaviour of columns entirely confined with FRPs or beams with all sides wrapped with FRPs.

The CFRPs have increased the flexural strength of the beams by approximately 119%. As shown in Table 3 and Figure 4, debonding failure seems to be caused by the exposure conditions. More investigations need to be undertaken to understand this problem.

## ACKNOWLEDGEMENTS

This research project is funded by the Natural Sciences and Engineering Research Council of Canada (NSERC) through the Network of Centres of Excellence (NCE) on Intelligent Sensing for Innovative Structures (ISIS Canada), whose support is gratefully acknowledged. Composite materials were generously provided by Master Builders and Composite Retrofit International. The technical assistance of Claude Aubé, Marc Demers and Dany Toulouse was essential to the completion of the laboratory setup. In addition, the authors wish to acknowledge the fruitful discussions they had with Dr. Benoit Fournier, from CANMET, to establish the research procedures for this project.

## REFERENCES

1. Fournier, B. and Bérubé, M-A., 'Les produits de la réaction alcalis-silice dans le béton : étude de cas de la région de Québec', Canadian Mineralogist, 24 (1986) 271-288.

2. Rogers, C.A., 'Canadian standard for controlling alkali-aggregate reaction', CANMET/ACI International Workshop on alkali-aggregate reactions in concrete, Dartmouth, Nova Scotia, Canada (1995) 109-121.

3. Raîche, A., Beaudoin, Y. and Labossière, P., 'Durability of composite materials used as external reinforcement for RC-beams', Annual Conference of the Canadian Society for Civil Engineering, Regina, Saskatchewan, Canada (1999) 155-164.

4. Montgomery, D.C., 'Design and analysis of experiments', Fourth Edition, John Wiley & Sons, New York, United States (1996).

5. Lacasse, C., Labossière, P. and Neale, K.W., 'Composite materials used as external reinforcement for RC-beams affected by alkali-aggregate reactions', Third International Conference on Advanced Composite Materials in Bridges and Structures, Ottawa, Ontario, Canada (2000) 537-544.

# The role of composite materials in concrete durability. Case study of alkali-aggregate reaction

M. IBRAHIM, E. FERRIER, L. CURTIL and P. HAMELIN
Laboratoire Mécanique Matériaux, Université Lyon 1, France

## INTRODUCTION

The alkali-aggregate reaction (AAR) occurs in some concrete structures between alkali-hydroxide in the pore solution and some siliceous aggregates. AAR seriously damages the concrete, resulting in expansion, cracking and loss of strength. The figure 1 illustrates a 20-year-old structure affected by AAR. The best solution to limiting AAR damage is to prevent it by selecting aggregates and cement in new constructions. Once the structures are damaged by AAR (bridges, retaining walls, dams, breakwaters...), effective remedial measures need to be applied in order to repair and/or reduce the problem.

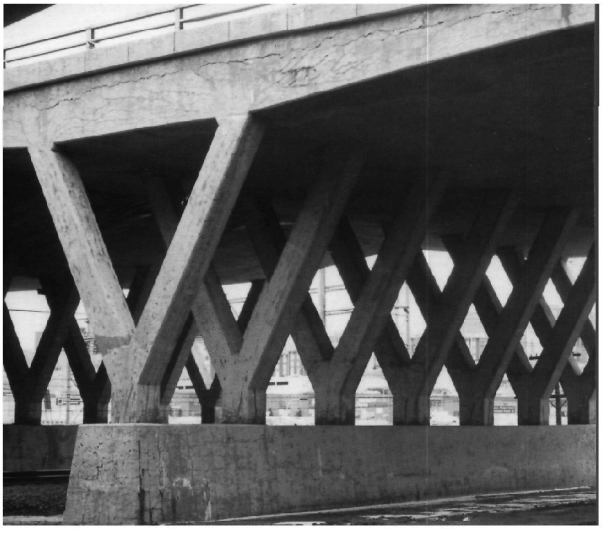


Fig. 1: Longitudinal cracks on the edge of the deck and in the column of a 20-year-old highway bridge affected by AAR [1].

Several authors have already described the remedial measures commonly used on concrete structures affected by AAR. We briefly sum them up below [1]:

- limiting moisture entry

The flexible moisture proof membranes can manage some volumetric changes. For example, the badly cracked concrete piers of the Hanshin Expressway in Japan were first repaired by filling the cracks with epoxy resin and then, by applying epoxy coating.

- physical restraint or strengthening

Strengthening with straps steel plates or composite materials (E. Ferrier, P. Hamelin [2]) and post tensioning can be effective for providing AAR in concrete structure elements. This strengthening provides AAR development.

- slot cutting

The slot cutting modifies the distribution of stresses in the concrete and reduces the internal restraint against expansion.

The main purpose of the present research is to evaluate the effectiveness of external bonded FRP in limiting AAR in civil engineering structures. We have carried out tests with mortar cylinders. Two mortar formulations are selected: reactive and not reactive mortars. The composite skins (FRP reinforcement) are placed before aging (composite 1) or after some expansions (composite 2) and a third category is not reinforced. Two accelerated mortar bar tests are used to develop detectable damage within a reasonable period of time. First, we will show the contribution of a composite skin on the linear expansion. Secondly, we will enhance its influence on the mechanical performances.

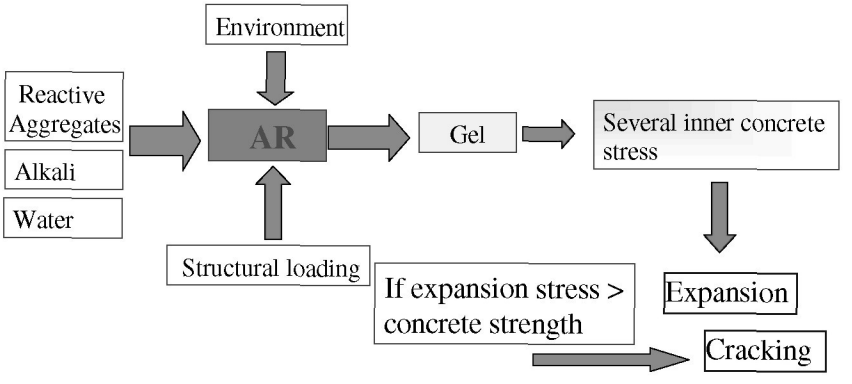



Fig. 2: Alkali-reaction in concrete

## EXPERIMENTAL CONDITIONS

### Materials and formulation

Two types of mortar are formulated (tables 1 and 2).

**Table 1: No Reactive Mortar composition (No AAR)**

| Materials | Weight |
|---|---|
| Normal sand | 1680 kg/m$^3$ |
| Cement CEM I 52.5 | 560 kg/m$^3$ |
| Water | 280 kg/m$^3$ |

**Table 2: Reactive Mortar composition (AAR)**

| Materials | Weight |
|---|---|
| Tourney limestone (0/5) | 1630 kg/m$^3$ |
| Opal sand (0.16/0.32) | 3 % per kg of aggregates |
| Cement CEM I 52.5 | 560 kg/m$^3$ |
| Water | 280 kg/m$^3$ |
| NaOH 1N | 0.55 % per kg of cement |

The Reactive mortar (AAR) is worked up with a French reference aggregate in the study of alkali-aggregate reaction. It is a siliceous limestone known for its reactivity (containing 20 % of reactive silica) [J.S. GUEDON-DUBIED and al, 3]. To accelerate the reaction, a second reactive aggregate, the French opal sand, finely crushed , is added to the mix. The cement used is a Portland cement in order to obtain very good mechanical performances. The alkali content of Portland cement is 0.7 % $Na_2O$ equivalent and we are adjusted to 1.25 % $Na_2O$ equivalent by adding sodium hydroxide to the mix water. Many reactive and no reactive mortar cylinders (16 cm high, 8 cm in diameter) are cast. Prepared samples are divided in two batches. After 24 hours, the cylinders are demoulded and then stored at 23°C and high humidity (100 % Relative Humidity) during 28 days.

**Reinforcement of cylinders**

Half of the samples is strengthened by composite reinforcement. This reinforcement is done at the beginning (after the cure period but before the maturing phase) or after some expansions (during the aging phase). The composites are provided by Replark®. The high strength carbon fibers are applied by a wet-lay-up method using epoxy resin. The table 3 gives all the mechanical properties of all the materials

**Table 3: Material characteristics**

| **Fibers** | **Carbon** |
|---|---|
| Young modulus (GPa) | 235 |
| Ultimate strength (MPa) | 3250 |
| **Polymer** | **Modified BPA epoxy** |
| Young modulus (GPa) | 3.2 |
| Ultimate strength (MPa) | 40 |
| Glass transition temperature Tg (°C) | 55 |
| **Composite** | **Carbon epoxy** |
| Young modulus (GPa) | 62.5 |
| Ultimate strength (MPa) | 500 |
| Elongation (%) | 1 |

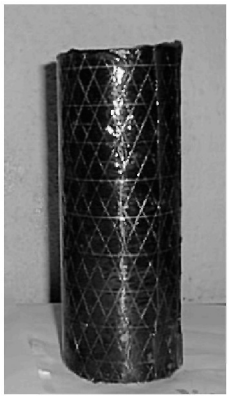
Several stages of worked up composite are as following:

* Dry mortar cylinders are scraped with a wire brush and a pneumatic tool eliminates the dust.
* The primer is applied to fill up the defects of cylinder surface.
* The epoxy resin is then applied. After that, the carbon is cut to size 16 cm x 40 cm. The cylinders are wrapped up by these carbon fibers with a second lay of epoxy resin.
* The epoxy resin is also applied at the top of samples to prevent water penetration (figures 3a and 3b)

The final thickness of the composite is 1.6 mm.




*(a) Samples without reinforcement*

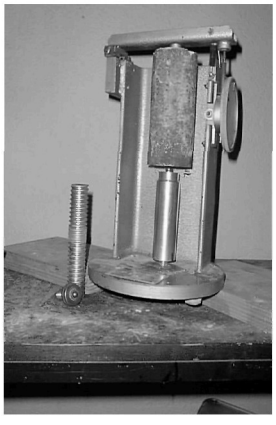


*(b) Samples with Replark® reinforcement*

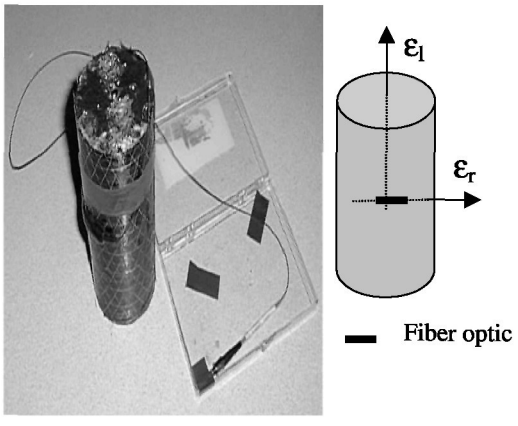
Fig. 3: Mortar cylinders

**Alkali-aggregate reaction measurement**

An extensometer device measures the linear expansion of mortar cylinders (fig. 4a). This measurement is completed by the composite strain evolution as a function of aging. On two reinforced cylinders (one reactive mortar, one non-reactive mortar), we have implemented a Fabry-Perot optic sensor (Type FOS of FISO technologies) to control the tension of the composite (fig 4b).



*(a) linear expansion measurement*




*(b) fiber optic sensors*

Fig. 4: Linear expansion measurement

**Aging methods**

The cylinders are aged either in NaCl solution [S. CHATTERJI and A. JENSEN, 4], or according to AFNOR P 18 585 Standard Procedure.

*NaCl Solution*

The samples are immersed in saturated NaCl solution at 50°C in a sealed container. The cylinders are arranged vertically and under solution. Each week, the cylinders are taken out of the solution. The samples are dried and cooled at 23°C and measured by an extensometer.

*AFNOR P 18 585 Standard Procedure*
The samples are immersed in water at 38°C into a sealed container and linear expansions are measured. This test is a French standard test procedure that gives results after six months.
Our samples are so reactive that we have measured linear expansion each week instead of each month like the standard instructions.

## INFLUENCE OF THE COMPOSITE ON THE LINEAR EXPANSION

### NaCl method

The linear expansions are measured each week (figure 5).

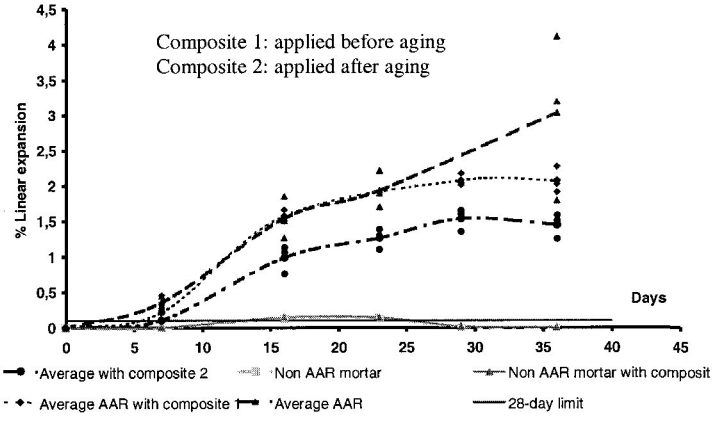



Fig 5: Linear expansion on cylinders with NaCl method

For non-reactive mortar samples no swelling occurs. It remains under 0.1% at 28 days that is the limit of expansion to determine alkali-aggregate reactive (AAR). Reinforced specimens seem to have a better behavior. These results should be confirmed with other tests.
Reactive and non-reinforced mortars have a very important expansion. Expansions as a function of time have a shape like an "S". It is probably due to a very important cracking at the beginning of the second week. The water diffusion in mortar is increased due to the cracking; therefore, the speed of the expansion increases. We observe an important dispersion after 25 days. The reason is essentially due to different patterns of cracking (figure 6).



Fig. 6: Patterns of cracking on AAR non-reinforced cylinders

After three weeks, the reactive samples swell less than non-protected AAR samples. The final expansion is reduced by 32 % in 2 weeks in comparison with reactive and non reinforced specimens. Moreover, we can see that the curve levels off. So, the composite skin seems to stop reaction not long after. The residual water reacts and the composite skin acts like a chemical barrier. The reactive specimens protected before AAR reaction beginning have a final linear expansion reduced by 52 %. The swelling is always above 0.1 % at 28 days. It may be explained by the fact that residual water reacts and allows swelling. A few changes in composite strain are measured by optical fibers sensor. On both alkali-aggregate reactive specimen (AAR) and non-alkali-aggregate reactive specimen (Non-AAR), composite wrapped up specimens, the range of strain goes from 40 μm/m to –40 μm/m. This small change in strain may be essentially due to the shrinkage of the composite consequence of the post cure. It proves that carbon fibers do not support any stress. The swelling composite skin acts like chemical barrier and not like a mechanical reinforcement (Fig. 7).

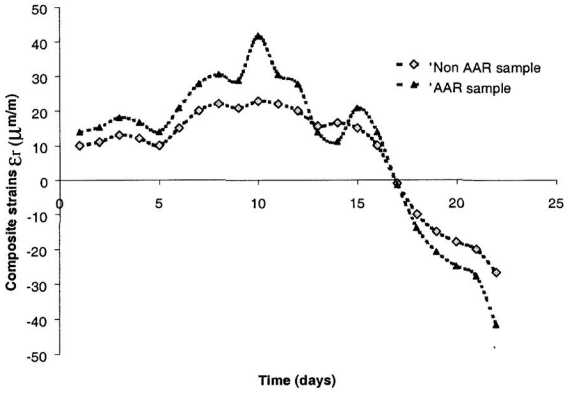



Fig. 7: Composite strain measured by fiber optic sensors on samples

**AFNOR NF P 18 585 Procedure**

This accelerated bar test lasts six months. In this study, the aging time is reduced to two months because our specimens are very reactive.

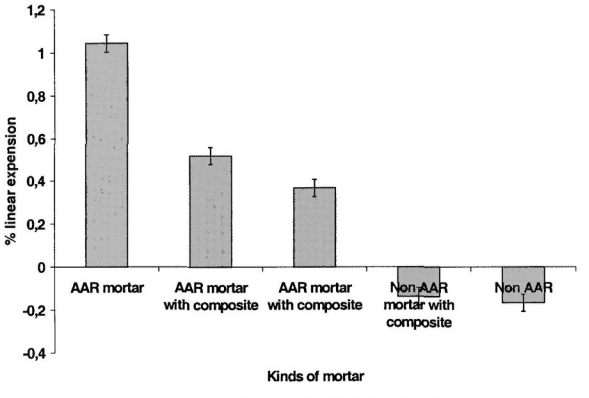



Fig. 8: Ultimate linear expansion on cylinders with NFP 18-585 procedure

The same observations as in NaCl method aging procedure are done with a less important expansion. This difference may be explained by the aggressiveness of the NaCl method.

## INFLUENCE OF THE COMPOSITE ON MORTAR MECHANICAL PERFORMANCES

In this part, we only consider samples aged with NaCl method. After 36 maturing days, the samples are taken out of the NaCl bath. We let them dry and let them get cold during one week. The composite reinforcement is completely removed by heat treatment (180°C during 2 hours). Then, compressive tests are done to failure. After cooling at 23°C, the samples are tested in compression.

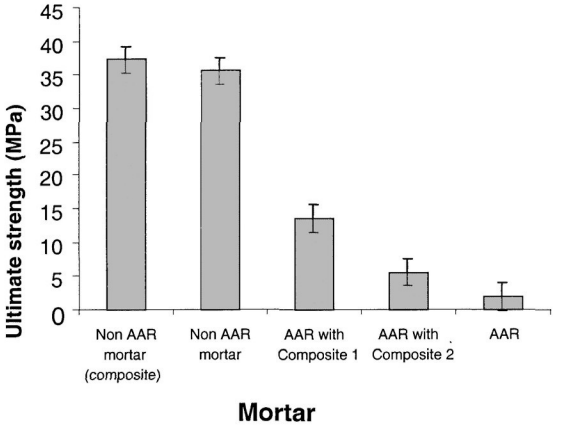



Fig. 9: Ultimate strength on test samples

The compression strengths for non-reactive specimens are 35 MPa. The concrete strengths of AAR specimen are 4 MPa. This is due to the over cracking of samples. For the specimen protected by composite before any aging, the mortar strength is reduced to 15 MPa. When the same reinforcement is applied during the aging, the mortar strength is reduced to 5 MPa.
The efficiency of the composite barrier depends on the specimen aging level. The earlier is the composite recovery, the lesser linear expansion is and the better the mechanical performances are.

## MECHANICAL TEST ON CONFINED CYLINDERS

All the samples aged with the NFP-18-585 procedure were tested in compression with a composite skin. The result enhances the efficiency of the composite (Fig. 10).

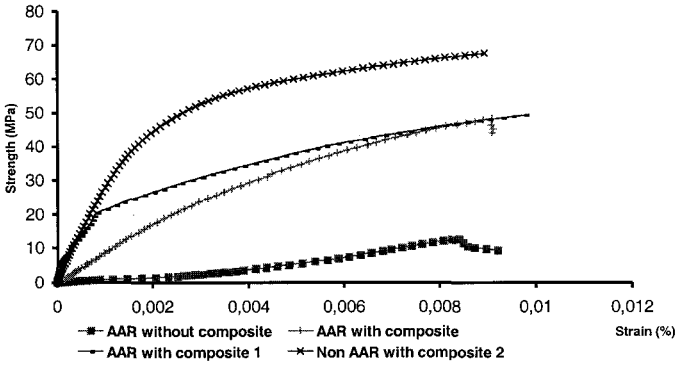



Fig. 10: Compressive test on composite confined cylinders

Even if carbon fibers do not directly act on the AAR concrete reduction, the use of composite allows increasing the mechanical properties of the confined specimen. Those results are encouraging for the development of this technique in the repair of AAR columns and so to secure AAR structures.

## CONCLUSION AND PERSPECTIVES

Alkali-aggregate reaction produces important damages in civil engineering structures. In this investigation, the effectiveness of external bonded FRP is evaluated. An improvement on linear expansion and mechanical performances are noticed.

An important point to outline is the fact that the earlier is the composite recovery, the lesser the linear expansion will be. The mechanical performances evolution of AAR specimen will also be reduced. However, complementary tests taking into account scale effects are useful to prove that the composite reinforcement acts only like a chemical barrier.

This technical procedure for structural reinforcement seems to be interesting to secure the structure and also to reduce the AAR development.

## REFERENCES

[1] B. Fournier and M-A Bérubé, Alkali-aggregate reaction in concrete: a review of basic concepts and engineering implications, Canadian Journal of Civil Engineering Vol. 27, N°2 April 2000, pp.167-191

[2] E. Ferrier, P. Hamelin, Durability of beams in reinforced concrete repaired by composites, CDCC'98, First International Conference on Durability of Composites for Construction, Sherbrooke, Québec, 5-7 août 1998, pp. 217-229

[3] Chatterji. S. And Jensen. A. D. A simple chemical test method for the detection of alkali-silica reactivity of aggregates. Cement and concrete research. 1988. Vol. 18, pp. 654-656.

[4] Guedon-Dubied J.S., Cadoret G., Durieux V., Martineau F., Fasseu P., Van Overbecke V. – Study on Tournai limestone in atoning cimes cast quarry petrological, chemical and alkali reactivity approach. 11th International Conference on Alkali Aggregate Reaction. Quebec City, Canada , June 2000, pp. 335-344.

[5] Le Roux A., Ouali. A Et Guedon-Dubier J.s. Importance de la connaissance pétrographique dans la démarche préventive. Bulletin du Laboratoire Central des Ponts et Chaussées. Septembre-octobre 1997, pp. 133-139.

[6] Curtil L. Comportement chimique de la silice vitreuse et de l'opale dans les milieux basiques. Application à l'étude de la réaction alcali-granulat dans les bétons hydrauliques. Thèse de doctorat à l'UCBL.1991. 254 pages.

# Performance of Inorganic Polymer-fiber Composites for Strengthening and Rehabilitation of Concrete Beams

RONALD GARON, P.N. BALAGURU, Rutgers University, Piscataway, NJ, USA, and
HOUSSAM TOUTANJI, University of Alabama in Huntsville, Huntsville, AL, USA

## ABSTRACT

High strength carbon fiber composites are being successfully used for various types of repair applications. Unreinforced concrete and brick walls have been strengthened with carbon and glass fabrics to improve their lateral resistance. Results reported in this paper deal with the behavior of unreinforced concrete strengthened with carbon tows and fabrics. The primary variables studied were adhesive and fiber types. In the case of adhesives, the performance of an inorganic matrix is compared with an organic matrix currently used for repairs. In the case of fiber types, the performance of unidirectional carbon fabrics, low cost fiber tows, and commercial fiber sheets are compared. Strength and stiffness increases, failure mechanisms, and analysis of strengthened prisms are presented. The results show that the inorganic matrix can be effectively used with economical carbon tows. The matrix bonded well to the concrete and strength increases of 200 percent can be achieved. The strength increases can be predicted using the classical bending theory and the properties of the constituent materials, namely: concrete and carbon fibers. Organic matrix provides a higher strength increase for unidirectional fabrics and fiber sheets.

## INTRODUCTION

Acceptance of high strength composites in the construction industry has grown at a rapid pace during the last decade. One of the areas where composites are preferable is strengthening of unreinforced walls. These walls, constructed using concrete or brick masonry or plain concrete, are very weak in the lateral direction. Carbon and glass fabrics can be very effectively used for strengthening these walls [1]. A number of studies have been conducted to evaluate beams made with clay bricks, concrete hollow core blocks, and carbon fabrics [2]. Walls reinforced with fabrics have also been tested [3]. All of these studies indicate that high strength composites have excellent potential for this application. They are easy to apply and occupy very little space and hence can be applied even in locations with very little clearance.

The research program reported in this paper was aimed at developing an inorganic adhesive that is fire proof and compatible with common construction materials, namely: concrete, clay bricks, wood, and steel. Commercially available, low cost, carbon reinforcement was also evaluated for strengthening. The current available systems are based on proprietary carbon sheets and compatible adhesive systems. The performance of the organic and inorganic matrices were evaluated and compared with an existing commercial system. The smaller scale model prisms were chosen for the basic understanding of the failure mechanism.

*FRPRCS-5*, Thomas Telford, London, 2001.

## PROPERTIES OF THE INORGANIC MATRIX

The matrix to be evaluated was developed for use in aircraft structures and modified for use as a coating material and adhesive for brick, concrete, wood, and steel [4-9]. The cementitious part is a potassium aluminosilicate, or polysialate-silox with the general chemical structure:

$$K_n \{-(SiO_2)_z - AlO_2\}_n \bullet wH_2O \quad (1)$$

where Z >>n. The resin hardens to an amorphous (glassy) structure at moderate temperatures of 80° to 150°C. Hardeners have been developed to obtain a room temperature cure in about a day. The research conducted so far has focussed on the mechanical, thermal, and durability properties of composites made with carbon, glass, and steel, and the properties of strengthened reinforced concrete beams [4-9]. The unique features of the matrix are as follows.

- The resin is prepared by mixing a liquid component with silica powder. Fillers and hardening agents can be added to the powder component. The two components can be mixed to a paint consistency. Since the matrix is water based, tools and spills can be cleaned with water. All of the components are nontoxic and no fumes are emitted during mixing or curing. The excess material or material removed from the old application can be discarded as general waste.
- The pot life varies from 30 minutes to 3 hours for compositions that cure at room temperature. Compositions that require heat for curing at 80° to 150° C can be stored for weeks.
- Common application procedures such as brushing and spraying can be used for the application. The product was successfully used to coat bridge substructures by brush and a sprayer in Rhode Island, USA.
- The matrix bonds well with carbon and glass fibers and these fibers can be used as reinforcements. Tows and fabrics made out of carbon and glass can also be attached to existing structures.
- The matrix can withstand temperatures up to 1000°C, and is not affected by UV radiation. Fire tests show that the flame-spread index is zero. Since the air permeability is low, the matrix also protects the material it is covering by reducing the amount of oxygen for combustion.

## EXPERIMENTAL PROGRAM

The reinforcement consisted of low cost carbon tows made of 48000 fibers with an average diameter of 7μm. Performance of tows and sheets made of 1000 fiber-tows is compared with the performance of carbon sheets made specifically for repairs. The experimental investigation consisted of testing prisms strengthened with 1, 2, and 3 tows, 1 and 2 carbon sheets utilizing both an organic and inorganic matrices and a proprietary system. The concrete prisms, measured 50 x 50 x 330 mm, were cast using steel molds and table vibrators and cured at 100% relative humidity for at least 28 days. The cured samples were prepared for strengthening using the standard procedures. This involves sand blasting and then cleaning with a wire brush. Sand blasting was performed using silica quartz sand at a pressure of 60 KPa. Once the surface was cleaned, a thin layer of the inorganic matrix was

applied to fill the small air voids and to create a smooth surface. Pre-cut carbon tows and sheets were impregnated with the matrix and placed on the prepared concrete surface and bonded using grooved rollers. A second layer of the matrix was applied as a protective coating. The samples were cured for 24 hours at room temperature followed by 24 hours at 80°C. The elevated temperature was used to ensure adequate curing in a two-day period. One day curing at 80°C is equivalent to about one week curing at room temperature.

For the organic matrix, the manufacturer's recommendations were followed. The cleaned surface was coated with primer and cured for three days. The matrix and the carbon were placed on the primed surface and bonded using rollers. After applying the top coat, the samples were left at room temperature for at least seven days before testing. A typical strengthened prism is shown in Figure 1. The prisms were tested using a center point load over a span of 300 mm. An MTS testing machine with computer controls was used to measure load and midspan deflections. The tests were run under displacement control at the rate of 0.1 mm/min. The loads and displacements were recording using the computer at intervals of 15 seconds.

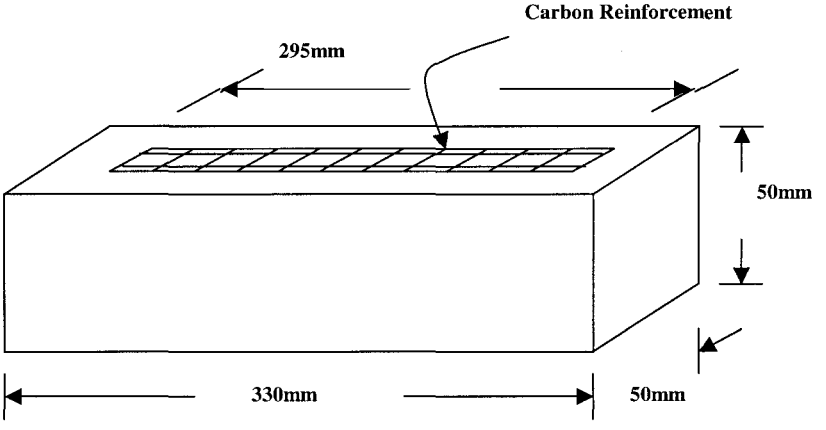



**Fig. 1.** Typical strengthened prism

## TEST RESULTS AND DISCUSSION

### Failure Pattern

As expected, the control beams behaved linearly elastic up to peak load, followed by brittle failure. The post-peak curve could be obtained if special loading methods such as crack mouth opening displacement controls were used. All of the strengthened beams had post-peak strength. Each of the strengthened beams carried considerable load after the development of the crack at the mid span. Only one crack developed which widened until failure of the specimen. The crack width at failure increased with an increase in reinforcement area. An increase in deflection at failure was also experienced as the crack width increased.

In the case of the organic matrix, the crack at midspan extended at the interface towards the supports. In each case, failure occurred because of debonding of the reinforcement. After the tests were completed, the debonded tows and fabrics could easily be peeled away from the sample. It can be hypothesized that a thin layer of concrete near the interface was weakened by the shear produced by the carbon fibers.

In the case of the inorganic matrix, the failure was always caused by fracture of the carbon fibers. It should be noted that the inorganic matrix is much more brittle than the organic matrix and hence microcracks occur within the matrix. Therefore, the fibers act individually rather than as a single plate reducing the possibility of delamination. The reinforcement was not easily peeled away from the prisms after failure as in the case of the organic matrix.

**Load-Deflection Behavior**

The load-deflection behavior of beams strengthened with inorganic and organic matrices is presented in Figures 2 and 3, respectively. In Figure 2, the behavior of beams strengthened with 1, 2, and 3 tows, 1 and 2 layers of fabric, and control beams are presented. In Figure 3, an additional curve for the unidirectional carbon sheet is also presented. A careful review of these curves leads to the following observations.

- The load-deflection behavior of these plain concrete beams is different from the curves corresponding to the strengthened reinforced concrete beams. The major difference could be due to the single crack that occurs in plain concrete beams. This difference in behavior should be considered when high strength composites are used to strengthen unreinforced concrete and masonry. The test results also provide an opportunity to understand the mechanism of load transfer near the crack.
- The beams strengthened with the organic matrix had larger deflections before failure. As mentioned earlier, the inorganic matrix cracks at strains of about 0.007mm/mm [8]. In addition, the silicate matrix bonds with the concrete chemically by transfer of CaOH and KOH between parent concrete and the adhesive, resulting in the absence of a well defined interlaminar layer. Therefore, when the concrete cracks, the cracks will go through the repair layer, transferring the forces to the carbon fibers. As a result, the debonding of the repair plate at the crack is much less in the inorganic matrix and the average strain in the plate at failure is also lower.

**Increase in Failure Loads**

Increase in the failure loads is compared in Figure 4. The increases are presented as a factor of control strength for easy comparison. In beams reinforced with carbon tows, the strength increase for the inorganic and organic matrices is not significantly different. In the case of the inorganic matrix, the beam reinforced with only one tow had a greater strength increase than the beam reinforced with two tows. Initially, this was assumed to be an experimental error. When inorganic matrix is used for repair, the amount of fibers and their distribution plays an important role near the crack and load transfer. In the case of one tow, the fibers are well spread out and are very close to the bonded surface. As soon as the crack forms in the parent concrete, it penetrates the repair matrix.

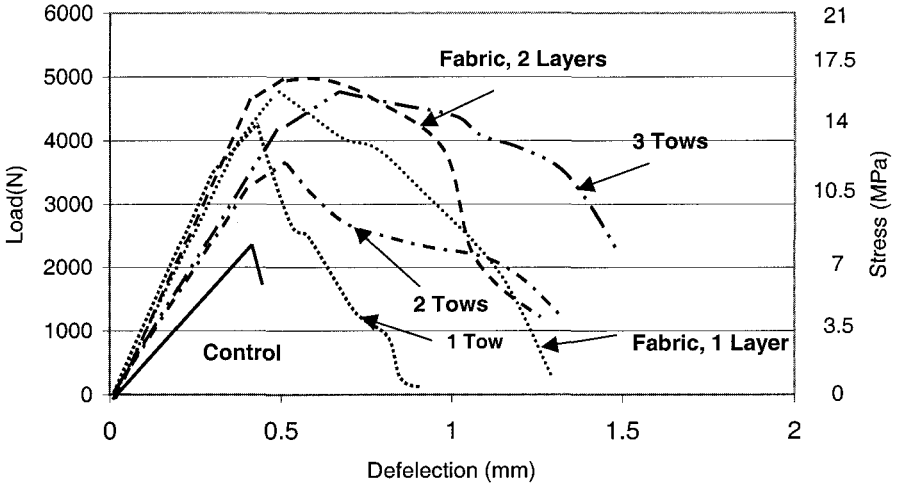



Fig. 2. Load-deflection Behavior, inorganic matrix

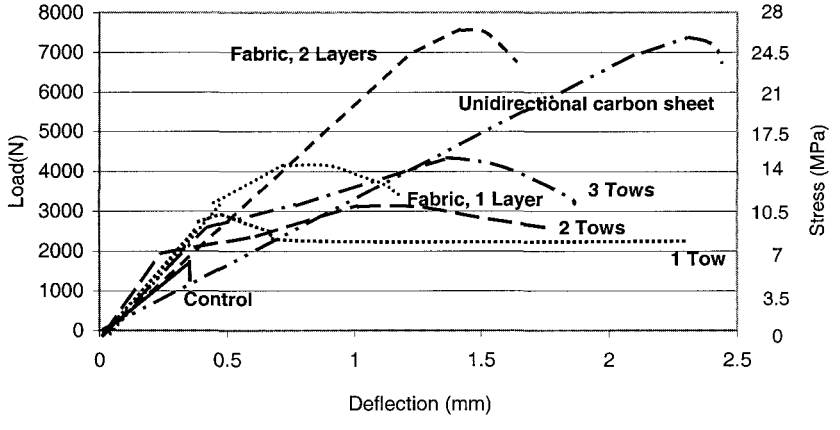



Fig. 3. Load-deflection behavior, organic matrix

## Analytical Investigation

The classical mechanics of materials approach was used to analyze the behavior of the beams. In addition to the standard assumptions such as plane sections remain plane and perpendicular to the neutral axis, the following additional assumptions were made.

- Since the amount of reinforcement is small, the concrete was assumed to behave linearly elastic up to failure. This was verified by computing the maximum stress in the concrete at failure.

- The behavior of the carbon fibers was assumed to be linearly elastic up to failure.
- As mentioned earlier, the carbon fiber contribution depends upon the amount of reinforcement. Even though the fracture strain of carbon is 1.5%, this strain is never achieved in the beams. Carbon plate with inorganic matrix fractures at a lower strain because of the non-uniform distribution of stress. Local stress concentrations result in partial delamination. In the case of organic fibers, a larger fiber volume promotes delamination before failure resulting in a lower average carbon strain. The experimental results were used to estimate the fracture strain using the procedure described in the next section.

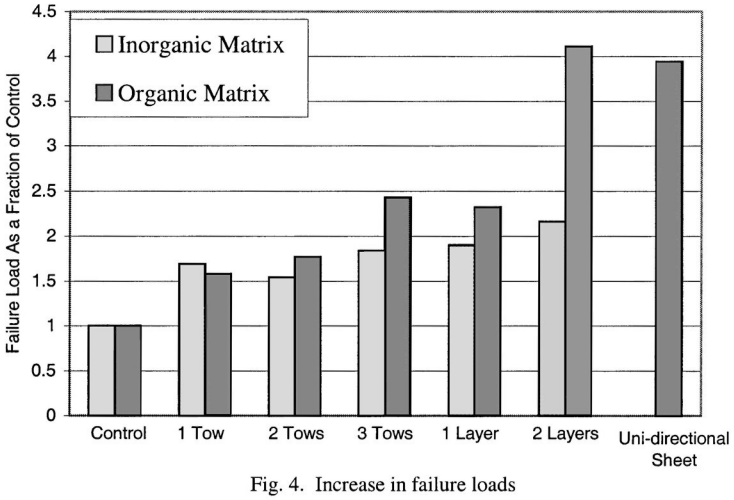



Fig. 4. Increase in failure loads

## Estimation of Carbon Fiber Strains at Failure

Carbon fiber strains were computed using the deflection at peak load. A transformed section, similar to the one used for reinforced concrete was used to develop a relationship between moment and maximum stress. The cross section, strain, and stress distributions are shown in Figure 5. The tension force contribution of concrete is neglected. Since the concrete behavior is assumed to be linearly elastic, the depth of the neutral axis, *kh*, can be computed using the following equation:

$$\frac{b(kh)^2}{2} = nA_f(h - kh) \tag{2}$$

where $b$ is the width of the beam, h is thickness of the beam, $A_f$ is area of the carbon fiber and $n$ is modular ratio(modulus of carbon/modulus of concrete).

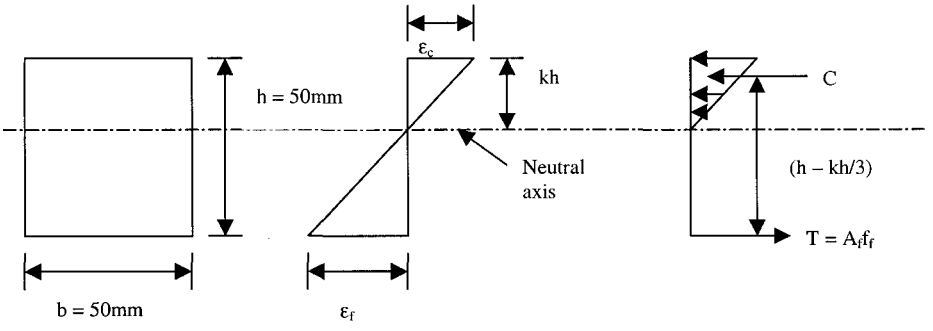



Fig. 5. Stress and strain distribution across beam depth: (a) beam cross section; (b) strains; (c) stress distribution

The moment capacity, $M$, can be computed as follows

$$M = bc\left(\frac{f'_c}{2}\right)\left(h - \frac{kh}{3}\right) \tag{3}$$

where $f'_c$ is the maximum concrete stress. For a given carbon fiber area, modulus and failure load are known. The only unknown in Equation (3) is $f'_c$. The strain in the extreme compressive fiber can be computed as

$$\varepsilon_c = \frac{f_c}{E_c} \tag{4}$$

where $E_c$ = modulus of elasticity of concrete. If $E_c$ is not given, it can be estimated using the ACI code equation

$$E_c = 4730\sqrt{f'_c} \qquad \text{N/mm}^2 \tag{5}$$

The carbon strain at failure can then be determined using similar triangles,

$$\varepsilon_f = \varepsilon_c\left(\frac{h - kh}{h}\right) \tag{6}$$

The failure strain computed using Eq. (6) was expressed as a function of the reinforcement ratio. The reinforcement ratio can be computed as $\rho$ = area of carbon reinforcement / $bh$. Exponential functions were found to accurately represent the variation in failure strains.

For organic matrix: $\varepsilon_f = 0.0084e^{-120.04\rho}$ (7)

For inorganic matrix: $\varepsilon_f = 0.125e^{-315.95\rho}$ (8)

**Computation of Moment Capacities**

Based on the discussion presented in the earlier sections of this paper, the following procedure can be used for the computation of moment capacity of the strengthened beams.

Given: section width, $b$; section thickness, $h$; type and area of carbon reinforcement, $A_f$; and modulus of elasticity of carbon, $E_f$. The modulus ratio $n = E_f / E_c$.

Compute depth of the neutral axis, $kh$, and moment capacity, $M$, using Equations (2) and (3), respectively. Equation (2) is based on the geometric properties of the specimens and the modular ratio of the reinforcement. In Equation (3), the maximum compressive stress, $f_c$, can be estimated using the following procedure.

- Compute carbon reinforcement ratio, $\rho$, ($\rho$ = area of carbon reinforcement / $bh$).
- Estimate carbon failure strain using Equation (7) or (8) for the organic and inorganic matrices, respectively.
- Estimate extreme fiber compressive strain, $\varepsilon_c$, using similar triangles.
- Then compressive stress, $f_c = E_c \varepsilon_c$

In most instances, the concrete will be under a certain stress due to the existing loads. The authors believe that this stress will be very low and hence can be neglected for the computation of the moment capacity.

**Evaluation of Analytical Model**

The experimental and predicted failure loads are presented in Tables 1 and 2. Since the failure strains of carbon were estimated using the experimental results, the prediction was accurate for the current set of data, Table 1. The model was also evaluated using the results of Huang [6] and Toutanji and Gomez.[10]. Huang tested concrete prisms reinforced with carbon tows and carbon fabrics using an inorganic polymer. He also used more carbon reinforcement as compared to the current investigation. The results are compared in Table 2. Moment capacities were predicted using 100 and 80 percent of the modulus of the carbon fiber. Typically, fiber tows and unidirectional fabrics tend to have a lower modulus because of undulations present in fiber bundles. The two sets of values can be used as lower and upper bounds for strength prediction.

The model was also used to predict the results of an analysis conducted using a different organic matrix. The investigation conducted by Toutanji and Gomez [10] studied the effectiveness of externally bonded carbon in repair and rehabilitation of concrete structures. The test variables in this experiment included the type and area of fiber, the type of epoxy system, and the environmental exposure condition. The 50 x 50 x 300mm samples were tested at room temperature and after exposure to 300 cycles in a wet/dry environment. Performance of the samples kept at room conditions and the predictions made by the failure strain model developed in this paper are shown in Table 2.

As seen in Table 2, the failure strain model developed in this paper provides reasonably accurate results for samples studied by Huang. Experimental values for samples reinforced with six tows as well as two, three, and four layers of carbon fell within the range predicted by the model. The observed data for the specimen reinforced with nine carbon tows was slightly greater than the prediction. In the case of the organic matrix, for sample C1, the experimental maximum load is within the range. For sample C2, the model over predicts the load by a small margin.

Table 1-Comparison of experimental and predicted max. loads, experimental results from current investigation

| Peak Load, kN | | |
|---|---|---|
| Beam | Experimental | Predicted |
| O-T2 | 11 | 11 |
| O-T3 | 15 | 15 |
| O-L1 | 14 | 14 |
| O-L2 | 25 | 25 |
| O-TONEN | 23 | 23 |
| I-T1 | 13 | 11 |
| I-T2 | 12 | 14 |
| I-T3 | 14 | 15 |
| I-L1 | 15 | 15 |
| I-L2 | 17 | 16 |

Table 2- Comparison of experimental and predicted maximum loads, experimental results from References 6 and 10

| Peak load, kN | | | |
|---|---|---|---|
| Beam | Experimental | Predicted | |
| | | Fiber modulus, 100% | Fiber modulus, 80% |
| I-T6 | 5.09 | 5.66 | 4.54 |
| I-T9 | 6.43 | 6.26 | 5.03 |
| I-L2 | 6.35 | 7.09 | 5.71 |
| I-L3 | 7.72 | 9.09 | 7.32 |
| I-L4 | 9.1 | 11.3 | 9.08 |
| C1 | 3.74 | 4.27 | 3.45 |
| C2 | 4.86 | 6.86 | 5.54 |

## CONCLUSIONS

Based on the experimental and analytical results presented in this paper and observations made during the testing, the following conclusions can be drawn.

- Both inorganic and organic matrices can be effectively used for strengthening unreinforced concrete. The organic matrix provides higher deformations at failure. The inorganic matrix is fire and UV resistant.

- The load transfer mechanisms are different for inorganic and organic matrices. The inorganic matrix composite develops micro cracks and failure occurs by fracture of the carbon. The load transfer from fiber to fiber within the composite plate is not very efficient, especially when fiber areas are large. The organic matrix plates fail by delamination.
- For both organic and inorganic matrices, the average fiber strain at failure reduces with an increase in fiber area.
- When carbon composites are used to strengthen unreinforced systems, load redistribution through a crack plays a major role in the failure mechanism. This aspect should be considered in repair design.
- Strength capacities of strengthened plain concrete beams can be predicted with reasonable accuracy.

## ACKNOWLEDGMENT

The authors would like to acknowledge the financial support of the National Science Foundation Grants CMS-9900431 and CMS-9909830.

## REFERENCES

1. Ehsani, M.R., and Saadatmanesh, H., "Seismic Retrofit of URM Walls with Fiber Composites," TMS Journal, The Masonry Society, V. 14, No. 2, December 1996.
2. Roko, K., Booithby, J.E., Bakis, C.E., "Failure Modes of Sheet Bonded Fiber Reinforced Polymer Applied to Brick Masonry," American Concrete Institute SP. 188-28, 1999, pp. 305-312.
3. Hamilton III, H.R., Holberg, A., Caspersen, J., and Dolan, E.W., "Strengthening Concrete Masonry with Fiber Reinforced Polymers," American Concrete Institute SP. 199-92, 1999, pp. 1103-1111.
4. Foden, A., Balaguru, P., and Lyon, R., "Mechanical Properties of Carbon Composites Made Using an Inorganic Polymer," ANTEC, 1996, pp. 3013-3018.
5. Foden, A., Lyon, R., and Balaguru, P., "A High Temperature Inorganic Resin for Use in Fiber Reinforced Composite," Proceedings, First International Conference on Composites in Infrastructure, Tucson, AZ, January 1996, pp. 166-177.
6. Huang, G.G., "An Inorganic Polymer for Use in Fiber Composites," Project Report Submitted to Rutgers, The State University, 1995, 73 pp.
7. Balaguru, P., "Use of Composites as a Protective Coating for Bridge Infrastructure," Progress Report, New England Transportation Consortium, Dec. 1999, 35 pp.
8. Lyon, R. E., Balaguru, P., et.al., "Fire Resistant Alumino Silicate Composites," Fire and Materials, V. 21, 1997, pp. 67-73.
9. Balaguru, P., Kurtz, S., "Use of Inorganic Polymer-Fiber Composites for Repair and Rehabilitation of Infrastructures," Proceedings on " Repair and Rehabilitation of Reinforced Concrete Structures: the State-of-the-Art," ASCE Publication, Maracaibo, Venezuela, 1997, pp. 155-168.
10. Toutanji, H., Gomez, W., "Durability Characteristics of Concrete Beams Externally Bonded with FRP Composite Sheets," *Cement and Concrete Composites*, V. 19, 1997, pp. 351-358.

# Evaluation for Effect of Strengthening Method for Opening on CFRP sheet

T. KAGE, Building Research Institute, Tsukuba, Japan,
Y. MASUDA and T. INA, Utsunomiya University, Utsunomiya, Japan

## INTRODUCTION

When strengthening reinforced concrete buildings with carbon fiber-reinforced plastic (CFRP) sheet, the portions to be strengthened by CFRP sheet normally have applied finishing materials. If a dry finishing process is adopted, then bolt holes should be drilled through the sheet. Receptacles and boxes embedded in the building body also require openings in the sheet. Since the strengthening effect of CFRP sheet is produced by its continuous adhesion onto the member, such openings, which cause discontinuity of the sheet, may reduce the strengthening effect. Because of the directional property of CFRP sheet, uncertainty remains about the method of strengthening around openings. Accordingly, the authors intend to evaluate CFRP sheeting's effect of strengthening artificial openings by experiments and FEM analysis.

## EXPERIMENT OVERVIEW

### Materials

Table 1 gives the mechanical properties of CFRP sheets used in the experiment.

Table 1. Mechanical properties of CFRP sheets (manufacturer's specification)

| | |
|---|---|
| Fiber content ($g/m^2$) | 200 |
| Unit width cross-sectional area ($cm^2/m$) | 1.11 |
| Tensile strength ($N/mm^2$) | 3,500 [4,101] * |
| Elastic modulus ($kN/mm^2$) | 240 [273] * |

*[ ] : measured values by tension test

### Factors and levels

A CFRP sheet (base sheet) with an opening was strengthened by other CFRP sheeting (strengthening sheets) bonded to the base sheet. The factors and levels of strengthening are given in Table 2. These were selected according to the following procedure:

A tension test was conducted on specimens, each strengthened by a strengthening sheet bonded in the same direction as the base sheet (model 1). As a result, the base sheets were split axially from the opening and ruptured at a point outside the strengthened area. Since this method was found insufficient, an additional transverse strengthening sheet was applied (model 3). Additionally, specimens with only transverse strengthening sheets (model 2) were also adopted for comparison. Their effects were investigated by varying the length of strengthening sheets.

Table 2. Factors and levels

| Model | Strengthening direction | Strengthening length (mm) |
|---|---|---|
| 1 | Longitudinal | 50, 100, 150, 200 |
| 2 | Transverse | 50, 100, 150, 200 |
| 3 | Longitudinal and transverse | 50, 100, 150, 200 |

**Specimens**

The sketches of specimens are shown in Figure 1. Each specimen consisted of a base sheet 500 mm in length and 25 mm in width having a circular hole with a diameter of 12.5 mm, or half the width, and one or two strengthening sheets having the same width as the base sheet and bonded to the base sheet. The strengthening length was set at 4 levels. Aluminum plates 2 mm in thickness was attached to both ends of specimens to form the tabs for gripping by the testing machine. 2 specimens were prepared for each set of parameters.

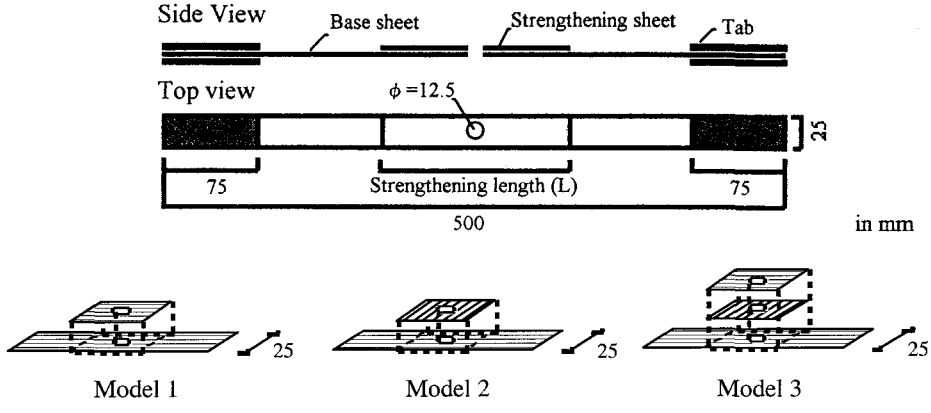



Figure 1. Specimen overview

**Preparation of specimens**

Specimens were fabricated on a releasable vinyl sheet in a room with a temperature of 20°C. Strengthening sheets were applied to the base sheets before the epoxy resin of the base sheet cured. The procedure for preparing specimens is described as follows:

An undercoat epoxy resin is applied to a vinyl sheet to a target spread of 0.4 kg/m$^2$. The base sheet is mounted on the undercoat and de-aerated. An overcoat epoxy resin is applied to a target spread of 0.2 kg/m$^2$ to the base sheet 30 min after mounting the base sheet. For specimens to be strengthened, an epoxy resin is applied to the area receiving the strengthening sheet with a spread of 0.4 kg/m$^2$, on which a strengthening sheet is mounted. An epoxy overcoat is then applied with a spread of 0.2 kg/m$^2$. The specimens are allowed to cure for 7 days or more at 20°C, and their sides are then trimmed. The openings are cut from above the strengthening sheets using a drilling press.

**Test method**

Simple tension tests were conducted with a rate of 1 mm/min in terms of the cross-head speed. The load was measured using a load cell, while the strain on the base sheet side was measured with 5-mm strain gages. Also the state of rupture was visually observed.

## TEST RESUITS AND DISCUSSION

### Tensile strength

Table 3 and Figure 2 show the relationship between the strengthening method and the tensile strength. The epoxy resin pickup given in Table 3 was calculated from the mass of specimens. The results of models 1 and 2 suggest that they produce no strengthening effect irrespective of the strengthening length. As for model 3, the tensile strength increased as the strengthening length increased, suggesting its strengthening effect. However, the effect is insufficient, as the values are much lower than CFRP sheets having the same width but no opening.

Table 3. Test results

| Model | Strengthening length (mm) | Epoxy resin pickup ($g/m^2$) | Tensile strength ($N/mm^2$) | Coefficient of variation (%) | Mode of failure* |
|---|---|---|---|---|---|
| Unstrength-ened | 0 | 881 | 1494.6 | 14.49 | I |
| 1 | 50 | 518 | 1187.4 | 12.23 | II |
| | 100 | 495 | 1720.3 | 14.78 | II |
| | 150 | 467 | 1634.7 | 11.18 | II |
| | 200 | 446 | 1875.7 | 6.79 | II |
| 2 | 50 | 687 | 1597.3 | 19.06 | I |
| | 100 | 804 | 1595.0 | 2.84 | I |
| | 150 | 565 | 1581.1 | 3.79 | I |
| | 200 | 541 | 1401.8 | 9.18 | I |
| 3 | 50 | 733 | 2641.1 | 1.37 | I |
| | 100 | 672 | 2502.6 | 15.72 | I |
| | 150 | 542 | 2978.6 | 8.54 | I |
| | 200 | 555 | 3028.1 | 1.12 | I |

*Failure mode I: Failure at the opening
II: Longitudinal splitting and failure in the unstrengthened area.

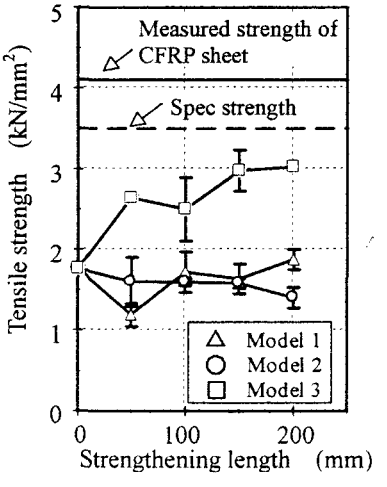



Figure 2. -Tensile strength-Strengthening length relationship

**State of rupture**

Rupture occurred at the opening in most cases, excluding model 1. One reason for the axial split in model 1 may be that the insufficient shear strength of epoxy resin caused insufficient stress transfer among fibers. The smaller epoxy resin pickup in model 1 may also be a cause of the mode of rupture. As a result, axial splits occurred in the direction parallel to fibers at the boundaries between uncut fibers and fibers cut by the opening.

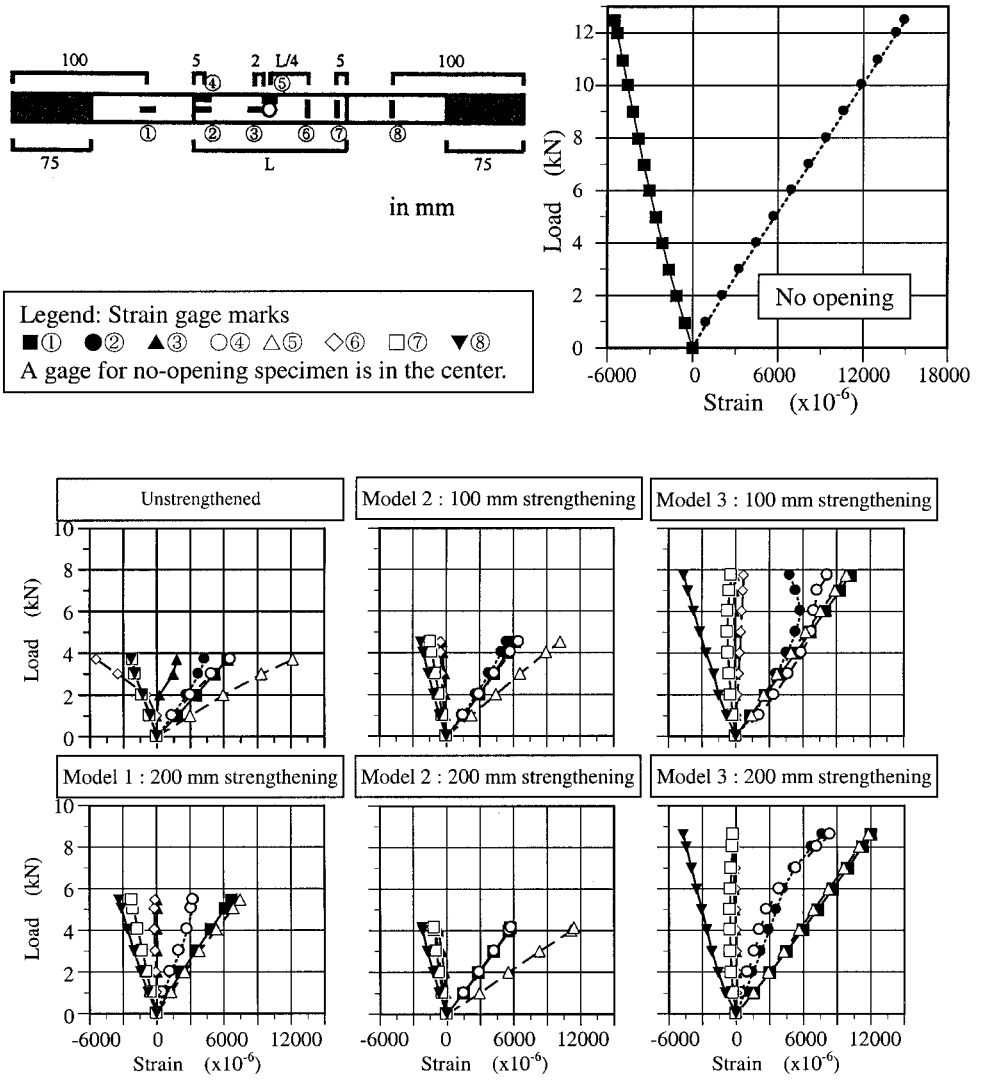



Figure 3. Load-Strain relationship

**Strain**

Figure 3 shows the load-strain relationship. For unstrengthened specimens, the strain at gage 4 is higher than at gage 2, suggesting that the stress in fibers cut by the opening is not sufficiently transferred to continuous fibers. Transverse strain is higher at locations closer to openings.

*(1) Model 1*

In model 1 specimens, the breaking strain at gage 5 is low in contrast to other models. This may be because splitting occurred in the direction of fibers and rupture occurred in the base outside the strengthened area.

*(2) Model 2*

In model 2 specimens, the strain of model 2 specimens with a strengthening length of 200 mm was nearly the same at gages 1, 2, and 4, whereas the strain of those with a strengthening length of 100 mm exhibited different values at these gages under near-peak loads. With a strengthening length of as long as 200 mm, the strain is distributed uniformly at a distance of 100 mm from the opening. It is found that transverse strain is lower than that in unstrengthened specimens. The breaking strain at the opening does not differ from that of unstrengthened specimens. Since this model is intended to confirm that strengthening sheets in the transverse direction can transfer the stress, no strengthening is applied in the axial direction. Therefore the strain at gage 5 is twice as high as at gage 1.

*(3) Model 3*

In model 3, the strains at gages 1 and 5 are the same at $12000 \times 10^{-6}$, which equals the breaking strain of CFRP sheet, suggesting sufficient stress transfer by transverse sheets. The strain at gage 5 is half that of model 2 under the same load, indicating that the axial strengthening sheet bears half the stress. The strains at gages 4 and 5 exhibit different tendencies depending on the strengthening length. Stress transfer is less effective at ends of strengthening sheets, requiring a sufficient anchorage length. A strengthening length of 100 mm is considered insufficient for the stress transfer. The reason for the insufficient strengthening effect of model 3 may be that the high stress on the inside edges of the cut portion causes the fibers to rupture from the inside edges.

## ANALYSIS

FEM analyses were carried out to explain rationally the experiment results and to investigate the strengthening effect of each model.

**Material tests**

Material tests were conducted to determine the values to be used for the FEM analysis. The results are given in Table 4. Figure 4 shows the stress-strain relationship of CFRP sheet. The CFRP sheet was assumed to be a two-dimensional elastic body, as it is very thin and scarcely exhibits a plastic zone, and underwent a two-dimensional elastic analysis using an existing program[1)] with modifications[2)] in consideration of its anisotropy.

Table 4. Material test results of CFRP sheet

| Direction | Longitudinal | Transverse |
|---|---|---|
| Epoxy resin pickup ($g/m^2$) | 858 | 942 |
| Elastic modulus (kN/mm)* | 29.8 | 3.93 |
| Poisson's ratio | 0.304 | - |
| Tensile strength (N/mm)* | 355.5 | 19.9 |
| Breaking strain ($x10^{-6}$) | 12,000 | 5,000 |

*The thickness of a CFRP sheet is assumed to be 1 mm and per unit width of CFRP sheet

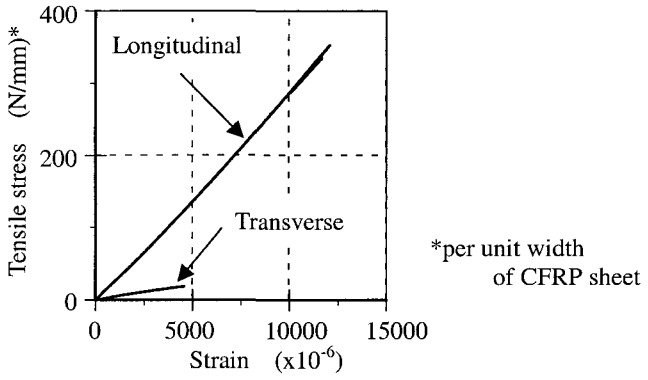



Figure 4. Tensile stress-Strain relationship of CFRP sheeting

**FEM analysis**

Since CFRP sheeting is an anisotropic material, its stress-strain matrix was assumed by equation (1) as follows:

$$[D]=\frac{1}{1-\nu_x\nu_y}\begin{pmatrix} E_x & \nu_y E_x & 0 \\ \nu_x E_y & E_y & 0 \\ 0 & 0 & (1-\nu_x\nu_y)G_{xy} \end{pmatrix} \quad (1)$$

where $E_x$ = Elastic modulus in Longitudinal direction
$E_y$ = Elastic modulus in Transverse direction
$\nu_x$ = Poisson's ratio in Longitudinal direction
$\nu_y$ = Poisson's ratio in Transverse direction
$G_{xy}$ = Modulus in shear

Also, according to Maxwell-Betty's reciprocal theorem, the following equation (2) holds:

$$\nu_y E_x = \nu_x E_y \quad (2)$$

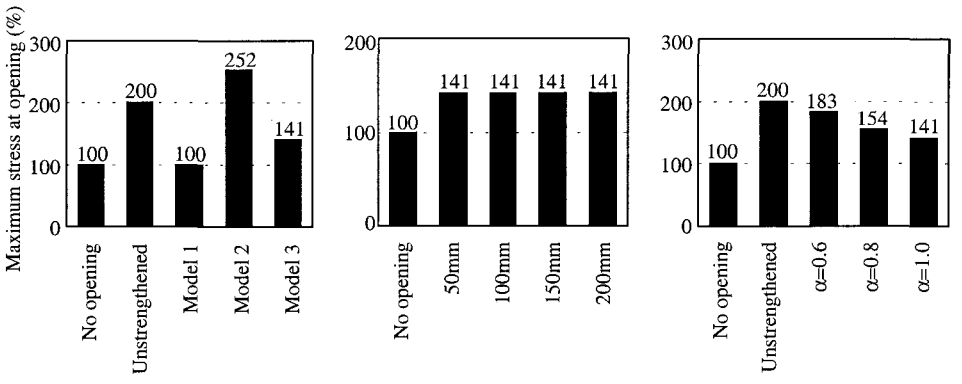
$G_{xy}$ was assumed by equation (3) as follows using the value for epoxy resin in consideration of the uniaxial stress condition:

$$G_{xy} = \frac{E_y}{2(1+\nu_y)} \quad (3)$$

**Analysis results and discussion**

The thickness of specimens was assumed to be the unit thickness. The elastic modulus of strengthened portions was assumed to be the total of the elastic modulus of each sheet in its direction. According to Table 4, element failure was assumed to occur when the stress in the transverse direction reaches 0.056 times that in the longitudinal direction axis for unstrengthened areas and areas strengthened only in the longitudinal direction. The elastic modulus of elements that failed was assumed to be zero for subsequent analysis steps. The maximum stresses of the three strengthened models (strengthening length: 200 mm) and an

unstrengthened model were compared under a unit load at the opening with respect to the stress of the base sheet with no opening. The result is shown in Figure 5(1).




(1)Strengthening methods (2)Strengthening length (3)Effectiveness coefficient

Figure 5. Maximum stresses at the opening

In the unstrengthened model, shear failure was found to occur from the opening in the direction of fibers before the peak load was reached. The fibers cut by the opening therefore cannot bear the load. The analysis revealed that the stress of the unstrengthened model was twice as high as the case with no opening, exhibiting the same ratio of the tensile strength to the measured strength in the experiment. Shear failure also occurred in model 1 as in the unstrengthened model. The stress of model 2 is 2.5 times that of the case with no opening, which agrees with the experiment result for the strengthening length of 200 mm. This may be because the transverse sheet restricted shear failure, while the stress concentration reduced the strength. The stress of model 3 is 1.4 times that of the no-opening case. The value for model 3 agrees with the ratio of the measurement of model 3 for a strengthening length of 200 mm to the measured tensile strength of CFRP sheet.

Figure 5(2) shows the maximum stress of model 3 at the opening with different strengthening lengths. In this FEM analysis, no difference is observed among the strengthening effects of the 4 strengthening lengths. This may be attributed to the fact that the bond between strengthening sheets and the base sheet gradually decreased as the stress increased, inhibiting the stress transfer from the base sheet to the strengthening sheets. Accordingly, an effectiveness coefficient of strengthening sheets ($\alpha$) was considered in the range of 50 mm, with which the changes in the stress concentration were compared. The method of calculating the elastic modulus of elements using the effectiveness coefficient $\alpha$ is the equation (4) as follows:

$$E = E_b + \alpha(E_{s1} + E_{s2}) \tag{4}$$

where E = Elastic modulus of elements
$E_b$ = Elastic modulus of base sheet
$E_{s1}$ = Elastic modulus of the first strengthening sheet
$E_{s2}$ = Elastic modulus of the second strengthening sheet
$\alpha$ = Effectiveness coefficient of strengthening sheet

Figure 5(3) shows the relationship between the effectiveness coefficient and the maximum stress at the opening. Stress concentration tends to decrease as the effectiveness coefficient of strengthening sheets increases. The effectiveness coefficient of strengthening sheets inversely calculated from this result is 0.78 when the strengthening length is 50 mm.

## 1. CONCLUSIONS

The effect of strengthening of CFRP sheets having an opening by applying other CFRP sheets was investigated by tests and analysis. In this study, the following results were found:

(1) No strengthening effect is observed when strengthening only in the direction parallel to the fibers.
(2) A strengthening effect is obtained by applying both longitudinal and transverse sheets on the base sheet. However, in consideration of the stress concentration, it is necessary that a longitudinal strengthening sheet be larger than needed just to compensate for the loss in the cross-sectional area of the base sheet.
(3) Insufficient strengthening lengths do not produce the intended strengthening effects.

## ACKNOWLEDGMENT

The authors express their gratitude to Mr. Tatsuo Ando of the Carbon Fiber Construction Materials Association and Mr. Tsutomu Oide of Dainippon Shikizai Co. for their assistance in the experiments.

## REFERENCES

1)T.Yyang : Handbook of FEM structural Analysis, Gihodo, pp.443-447, 1996.6.
2)H.Yoshida, T.Kobori : Structural Analysis program by Finite Element, pp.141-150, 1976.12

# Flexural behaviour of over-reinforced FRP RC beams: effect of design parameters and material partial safety factors

K. NEOCLEOUS, K. PILAKOUTAS and P. WALDRON
Centre for Cement and Concrete, Department of Civil & Structural Engineering, The University of Sheffield, Sheffield, United Kingdom

## ABSTRACT
The reported work aims at the development of recommendations for the flexural design of over-reinforced concrete beams, reinforced with fibre reinforced polymer reinforcement. The flexural structural reliability and probability of concrete crushing are determined for a number of beam configurations. The results indicate that the effect of various design parameters and material partial safety factors ($\gamma_m$) on the flexural behaviour of the beams is influenced by the type of failure assumed at the design stage. The outcome of this work is the recommendation of appropriate short-term $\gamma_{FRP}$ in conjunction with certain design provisions for the flexural design of concrete beams reinforced with FRP reinforcement.

## INTRODUCTION
The flexural design of concrete elements reinforced with fibre-reinforced polymers (FRP) is currently performed on the basis that a brittle failure would occur either due to concrete crushing or fracture of the FRP reinforcement. It is assumed that whichever is the desired mode of flexural failure, this will be attained primarily by the application of specific material partial safety factors for FRP reinforcement ($\gamma_{FRP}$). Furthermore, it is assumed that the target structural reliability level ($P_{ft}$) would be attained by the application of these $\gamma_{FRP}$. However, recent investigations showed that the application of specific $\gamma_{FRP}$ would neither lead to the desired mode of flexural failure nor would attain the target $P_{ft}$ [1].

The research reported in this paper examines the above issues further for over-reinforced beams designed to resist uniformly distributed loads in accordance to the preliminary design guidelines developed in Europe [2]. The work is carried out as part of the European Union sponsored TMR network "ConFibreCrete" and task group 9.3 of the International Federation of Concrete (*fib*) whose aim is the development of design guidelines for concrete structures reinforced, prestressed or strengthened with advanced composites

The probability of flexural failure occurring due to concrete crushing ($P_{fr}$) and the flexural notional structural reliability level ($P_f$) of 48 rectangular beam configurations, reinforced with Eurocrete FRP reinforcement [3], are determined for a number of $\gamma_{FRP}$. The investigation is carried out for two cases: a) simply supported beams reinforced with carbon FRP (CFRP) reinforcement and b) simply supported beams reinforced with glass FRP (GFRP) reinforcement.

*FRPRCS-5*, Thomas Telford, London, 2001.

## ASSESSMENT PROCEDURE

A numerical simulation approach is adopted to determine the $P_{fc}$ and flexural $P_f$; the simulations are performed using MATLAB [4]. The procedure followed in the assessment is illustrated in figure 1; this procedure is further elaborated in [5]. It is noted that the resistance-capacity models, adopted by the European design guidelines, are modified accordingly to account for flexural failure occurring either due to concrete crushing or reinforcement fracture.

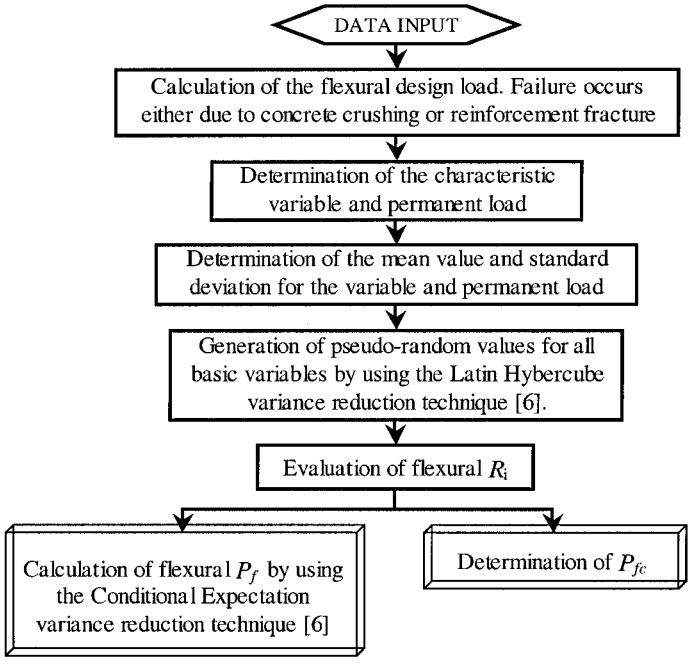



Figure 1. Assessment procedure

The flexural $P_f$ and $P_{fc}$ are evaluated by equations 1 and 3, respectively.

$$\overline{P}_f = \frac{\sum_{i=1}^{N} P_{f_i}}{N} \tag{1}$$

$$P_{fi} = P(Q > R_i - G_i) = 1 - F_Q(R_i - G_i) \tag{2}$$

$$P_{fc} = \frac{\sum_{i=1} \varepsilon_c \geq 0.0035}{N} \tag{3}$$

The statistical data used in earlier investigations by the authors are utilised for the statistical modelling of all random variables [1], [5]. Tables 1 and 2 summarise the statistical data used for the geometric and loading variables. In the case of the material strength of concrete and FRP reinforcement, the adopted statistical data are derived from the analysis of experimental results. A constant standard deviation of 6 N/mm$^2$ is used for the concrete compressive strength; the probability distribution is truncated at 3.16 standard deviations from the mean value. In the case of CFRP and GFRP reinforcement (table 3), the strength obtained

experimentally in RC beams was adopted, since existing direct tensile tests fail to simulate the in-service load-transfer mechanisms for FRP reinforcing bars.

Table 1 Statistical data for geometrical basic variables

| Dimension Description | Mean Value $\mu_i$ (mm) | Standard Deviation $\sigma_i$ (mm) | Probability Distribution |
|---|---|---|---|
| Width | Nominal + 2.4 | 4.8 | Normal |
| Overall Depth | Nominal – 3.2 | 6.4 | Normal |
| Concrete Cover | Nominal + 1.6 | 11.6 | Normal |
| Beam Spacing and Span | Nominal | 17.5 | Normal |

Table 2 Statistical data for loading

| Load Description | Coefficient of variation $cov_i$ | Characteristic $i_k$ | Probability Distribution |
|---|---|---|---|
| Permanent Load G | 0.05 | $\mu_G + 0.082$ | Normal |
| Variable Load Q | 0.4 | $\mu_Q \cdot 1.98$ | Gamma |

Table 3 Statistical data for CFRP and GFRP reinforcement

| | Tensile Strength (N/mm$^2$) | | Young's Modulus (N/mm$^2$) | |
|---|---|---|---|---|
| | CFRP | GFRP | CFRP | GFRP |
| Mean $\mu_i$ | 1380 | 810 | 115000 | 45000 |
| Standard Deviation $\sigma_i$ | 69 | 40.5 | 5750 | 2250 |
| Coefficient of Variation $cov_i$ | 0.05 | 0.05 | 0.05 | 0.05 |
| Minimum $i_{min}$ | 1235.1 | 725 | 105800 | 41400 |
| Maximum $i_{max}$ | 1524.9 | 895.1 | 124200 | 48600 |
| Characteristic $i_k$ | 1272.2 | 746.7 | 106012.8 | 41483.3 |
| Probability Distribution | Normal | Normal | Normal | Normal |

## ANALYSIS OF SIMULATIONS

The flexural design of CFRP RC beams was performed on the basis that a brittle failure would occur due to concrete crushing. However, in the case of beams with low reinforcement ratio ($\rho$) and high concrete compressive strength ($f_c$), the design was carried out based a brittle failure due to fracture of the reinforcement. This is because the actual tensile strain developed in the reinforcement at the design stage ($\varepsilon_{FRP}$) exceeded the design limit ($\varepsilon_{FRPd}$) imposed by the $\gamma_{FRP}$. It is noted that this is only observed for the CFRP RC beams designed using a $\gamma_{FRP}$ of 1.8 (figure 2).

In the case of the GFPR RC beams designed using a $\gamma_{FRP}$ of 3.6, the design of all beam configurations was carried out assuming that brittle failure would occur due to fracture of the longitudinal reinforcement, for the reasons explained above. Whereas, in the case of GFRP RC beams designed using a $\gamma_{FRP}$ of 1.3, the type of flexural failure is similar to the one observed for CFRP RC beams designed with a $\gamma_{FRP}$ of 1.8 (figure 3).

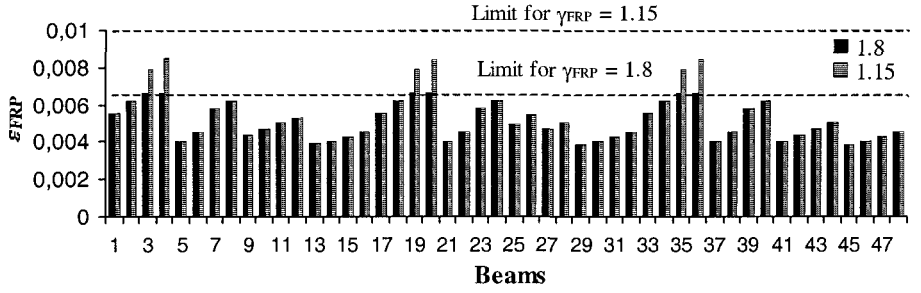



Figure 2. Actual tensile strain developed in the CFPR reinforcement at the design stage

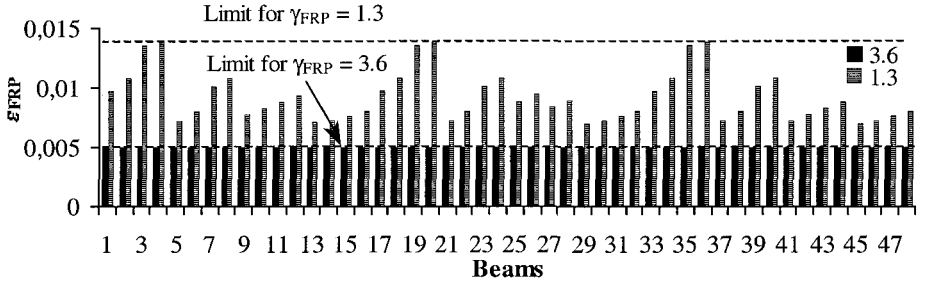



Figure 3. Actual tensile strain developed in the GFPR reinforcement at the design stage

The results obtained for $P_{fc}$ indicate that the majority of beams would actually fail due to concrete crushing, as assumed at the design stage. However, in some cases, there is a large probability (up to 0.2 for CFRP RC beams and 0.73 for GFRP RC beams) to fail due to fracture of the reinforcement. This was observed when: a) the design was carried out assuming failure due to fracture of the reinforcement, and b) the value of $\varepsilon_{FRP}$ was relatively close to $\varepsilon_{FRPd}$. In addition, it is observed that the $P_{fc}$ decreases as $f_c$ increases; this is because the tensile strength of FRP reinforcement is further utilised. For instance, in the case of the CFPR RC beams, $P_{fc}$ decreases from 0.97 to 0.27 as $f_c$ increases from 33 to 50 N/mm$^2$.

Figure 4 shows that the flexural $P_f$ is not affected by $\gamma_{FRP}$, as long as the type of failure assumed at the design stage is concrete crushing. In such cases, the flexural resistance capacity remains constant because the $\varepsilon_{FRP}$ does not change with $\gamma_{FRP}$. Thus, if concrete crushing is chosen as the desired mode of flexural failure, it may be possible to abolish the use of $\gamma_{FRP}$ and incorporate the uncertainties relevant to longitudinal reinforcement in the partial safety factor adopted for $f_c$. Figure 5 indicates that the $P_f$ is affected by $\gamma_{FRP}$ if flexural failure occurs due to reinforcement fracture.

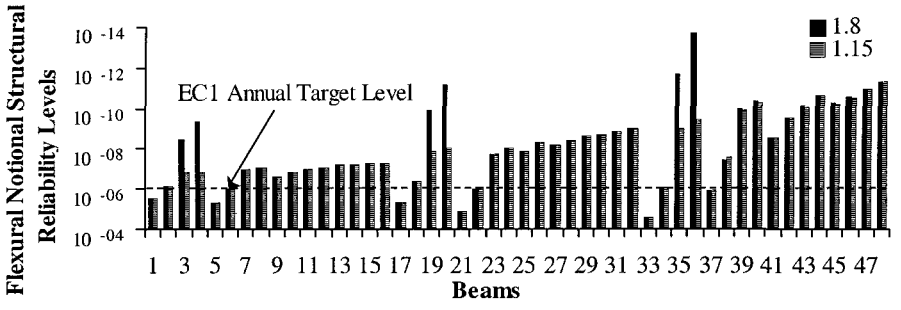



Figure 4. Effect of $\gamma_{FRP}$ on the flexural $P_f$ of CFRP RC beams

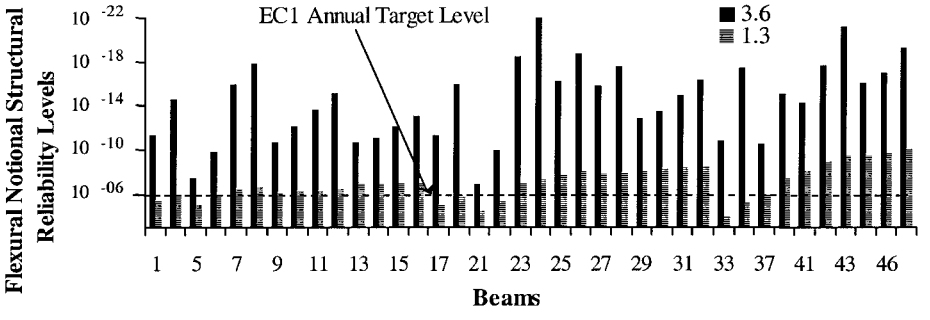



Figure 5. Effect of $\gamma_{FRP}$ on the flexural $P_f$ of GFRP RC beams

In figures 4 and 5, it is also observed that the structural reliability generally satisfies the target value of $10^{-06}$ adopted by Eurocode 1 [7]; however, the figures indicate that the calculated $P_f$ is greatly variable. This is due to the effect of various design parameters as illustrated in figures 6 and 7 for CFRP and GFRP RC beams, respectively. These figures suggest that the ratio of permanent to variable load greatly influences the flexural $P_f$. This implies that, for the same $\gamma_{FRP}$, the structural reliability varies for different types of structures and hence, in order to avoid reliability differentiation, it is recommended to use different $\gamma_{FRP}$ (or more appropriately load factors) for different types of structures. Figures 6 and 7 also indicate that the ratio of $\rho$ and $f_c$ influence the $P_f$ of both CFRP and GFPR RC beams. The results of the assessment show that the effect of these two parameters is greatly affected by the type of flexural failure assumed at the design stage. If flexural design is performed assuming reinforcement fracture, the $P_f$ is affected by both $f_c$ and $\rho$; it increases with $\rho$, while it decreases as $f_c$ increases (figure 7). Whereas, if flexural design is carried out assuming concrete crushing, the $P_f$ is only affected by $f_c$ (figure 6). It is noted that in this case the $P_f$ is more uniform across the range of beam configurations examined.

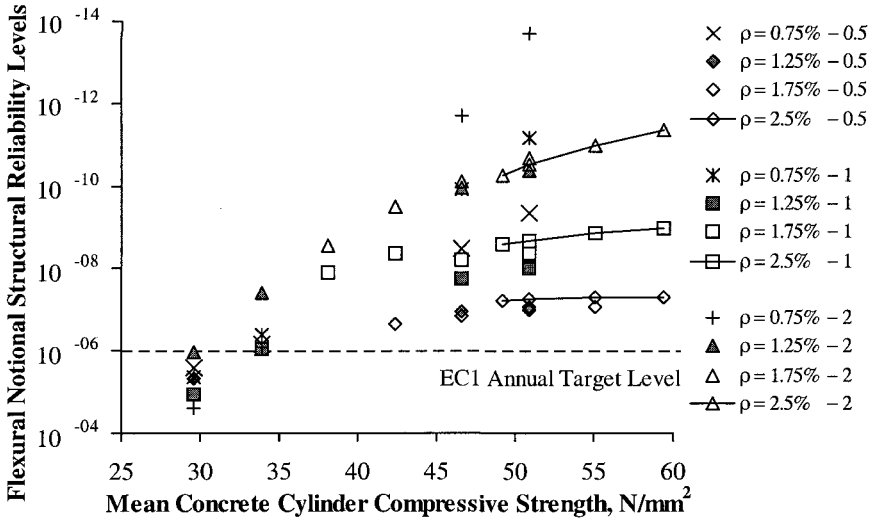



Figure 6. Effect of $f_c$, ρ and load ratio on the flexural $P_f$ (CFRP RC beams – $\gamma_{FRP} = 1.8$)

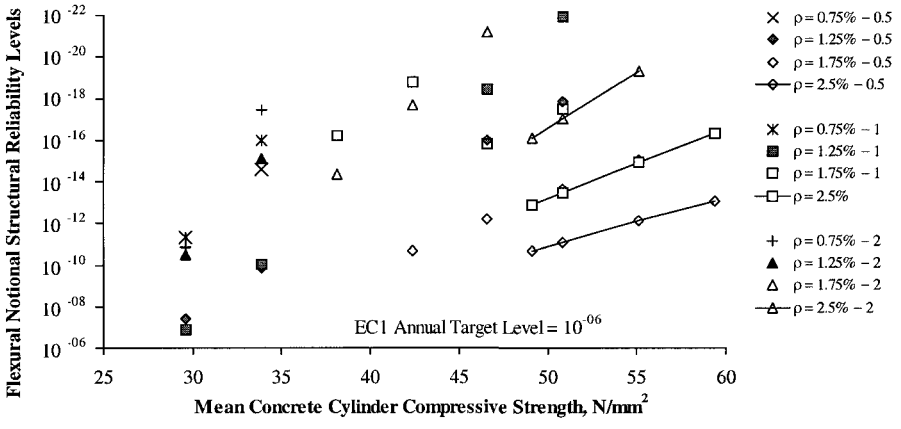



Figure 7. Effect of $f_c$, ρ and load ratio on the flexural $P_f$ (GFRP RC beams – $\gamma_{FRP} = 3.6$)

## DESIGN RECOMMENDATIONS

Based on the findings of the analysis, design recommendations are proposed for the flexural (short-term) design of over-reinforced FRP RC beams, reinforced with Eurocrete FPR reinforcement. Since the results showed that concrete crushing is the most probable type of flexural failure, it is recommended that flexural design is carried out to attain concrete crushing.

Provided that flexural failure occurs due to concrete crushing, it was determined from the analysis that the use of $\gamma_{FRP}$ for longitudinal reinforcement is not vital, since the flexural $P_f$ is not affected by $\gamma_{FRP}$. Based on this finding, it was proposed that the uncertainties relevant to

longitudinal reinforcement are incorporated into the $\gamma_m$ adopted for $f_c$. This would probably involve the modification of concrete $\gamma_m$, used currently in flexural limit state design. However, the mechanical behaviour of Eurocrete FRP reinforcement in flexure is not established thoroughly and therefore, it may not be prudent to abolish the use of $\gamma_{FPR}$ based on the existing knowledge of the reinforcement's mechanical characteristics. Consequently, to be conservative, it is recommended to use the smallest $\gamma_{FRP}$ examined in the assessment of the CFRP and GFRP RC beams. In the case of CFRP reinforcement, a value of 1.15 is recommended and a $\gamma_{FRP}$ of 1.3 is selected for GFRP reinforcement. It should be noted that the different $\gamma_{FRP}$ - recommended for Eurocrete CFRP and GFRP reinforcement - reflect the different material characteristics of the two reinforcements. In addition, it is noted that these $\gamma_{FRP}$ are recommended for the short-term design of FRP RC beams and hence, they do not take into account the long-term behaviour of FRP reinforcement. A limit is imposed on $\rho$, as shown in equation 4, in order to diminish the possibility of actual flexural failure occurring due to reinforcement fracture.

$$\rho_{min} = \frac{0.81(f_{ck}+8)\varepsilon_c}{f_{FPR\,k}\left(\frac{f_{FRPk}}{E_{FRPk}}+\varepsilon_c\right)} \tag{4}$$

## CONCLUSIONS

This study examined the effect of design parameters and $\gamma_{FRP}$, adopted for longitudinal reinforcement, on the flexural behaviour of over-reinforced FPR RC beams.

One of the main findings of the assessment is that the desired mode of flexural failure is not attained by the application of $\gamma_{FRP}$ alone. Thus, in order to attain the desired mode of failure, it is necessary to apply limits on the design parameters considered by the models adopted to predict the resistance-capacity. In addition, it is concluded that failure due to concrete crushing is the expected type of flexural failure.

The flexural structural reliability is not uniform due to the effect of various design parameters. The ratio of permanent to variable load is one of the most influencing parameters and hence, it is recommended to adopt different load factors for different types of structures.

The results also showed that the effect of $\gamma_{FRP}$ and design parameters on the flexural structural reliability is governed by the type of flexural failure, assumed at the design stage.

It is also concluded that the use of $\gamma_{FRP}$ for longitudinal reinforcement may not be necessary, if the design is performed to achieve flexural failure due to concrete crushing.

## ACKNOWLEDGEMENTS

The authors wish to acknowledge the European Commission sponsored TMR network "ConFibreCrete" and the Overseas Research Student (ORS) Award Scheme of the vice chancellor's committee of the United Kingdom's universities.

## REFERENCES

1. Neocleous K., Pilakoutas K. and Waldron P., "Structural Reliability Levels for FRP RC Structures", ACI SP-188, Proceedings of the Fourth International Symposium on Fiber

Reinforced Polymers for Reinforced Concrete Structures (FRPRCS-4), Baltimore USA, 31 October – 5 November 1999, pp 65 – 74.

2. IGDRCS, "Interim Guidance on the Design of Reinforced Concrete Structures Using Fibre Composite Reinforcement", The Institution of Structural Engineers, August 1999, 116 pp.

3. Eurocrete Project, "The Development of Non-ferrous Reinforcement for Concrete Structures – Final Report", Prepared by Euro-Projects (LTTC), 1997, 109 pp.

4. MATLAB, "The Language of Technical Computing", Version 5.3, Published in the Math Works Inc. Website: http://www.mathworks.com/products/matlab, 1999.

5. Neocleous K., "Design and Safety Philosophy for Concrete Structures Reinforced with Fibre Reinforced Polymers (FRP)", Ph.D. Thesis, The University of Sheffield, Department of Civil and Structural Engineering, Sheffield, 1999.

6. Avramidis A. N. and Wilson J. R., "Integrated Variance Reduction Strategies for Simulation", Operations Research, Vol. 44, No 2, March-April 1996, pp 327 – 346.

7. ENV 1991-1, "Eurocode 1 – Basis of Design and Actions on Structures – Part 1: Basis of Design", European Prestandard, European Committee for Standardisation, 1994, 85 pp.

## TERMINOLOGY

CFRP carbon fibre reinforced polymers,
FRP fibre reinforced polymers,
GFRP glass fibre reinforced polymers,
RC reinforced concrete.

## NOTATION

$\gamma_{FRP}$ material partial safety factor for FRP reinforcement,
$\varepsilon_c$ concrete strain,
$\varepsilon_{FRP}$ actual tensile strain developed in the FPR reinforcement at the design stage,
$\varepsilon_{FRPd}$ design limit imposed on the tensile strain of FRP reinforcement by $\gamma_{FRP}$,
$E_{FRPk}$ characteristic value of elastic modulus of FRP reinforcement,
$f_c$ concrete compressive strength
$f_{FRPk}$ characteristic value of tensile strength of FRP reinforcement,
$F_i()$ cumulative distribution function of a variable $i$,
$G_i$ permanent load evaluated at each simulation cycle, i,
N amount of simulation cycles performed,
$Q$ variable load,
$P_f$ notional structural reliability level,
$\overline{P}_f$ mean probability of failure, which corresponds to the notional $P_f$,
$P_{fc}$ probability of flexural failure occurring due to concrete crushing,
$P_{fi}$ probability of failure evaluated at each simulation cycle,
$P_{ft}$ target structural reliability level,
$R_i$ resistance-capacity evaluated at each simulation cycle.

# Concrete Beams Strengthened with Misaligned CFRP Laminates

XINBAO YANG and ANTONIO NANNI
Department of Civil Engineering, University of Missouri-Rolla, Rolla, MO 65409, USA.

## ABSTRACT
A unidirectional carbon fiber reinforced polymer (CFRP) laminate has its maximum strength and stiffness in the fiber direction. However, misalignment of fibers can be introduced intentionally or unintentionally during design or construction of structures. In this paper, the effect of fiber misalignment on the performance of concrete beams strengthened with CFRP laminates is experimentally investigated. Five unreinforced concrete Tee beams were cast and strengthened with CFRP laminates. The laminates had an off-axis angle of 0, 2, 5, 8, and 10°, respectively. The beams were tested under four-point loading to total failure. The objectives of this research were to investigate (1) strength and stiffness of beams, (2) strain distribution of CFRP laminates and, (3) failure modes. It was found that the variation of beam capacity with the severity of misalignment showed a different trend from that of midspan deflection and that failure by rupture of the CFRP laminate was experienced by all beams. A bond length of 127 mm was sufficient to develop the strength of the CFRP laminate.

## INTRODUCTION
Composite materials are generally applied in the optimal direction so their performance (stiffness and strength) can be well developed. However, it is unavoidable that FRP may not be applied in the exact direction as expected and some misalignment may exist. The misalignment can be introduced unintentionally by errors in design and construction or intentionally by the restriction in the structure's geometry. Because FRP laminates are orthotropic materials, the maximum stiffness and strength are exhibited along the fiber direction. Any deviation from this direction will cause strength and stiffness degradation. The influence of this degradation needs to be investigated to obtain an accurate evaluation of the performance of strengthened structures. The ultimate goal of this investigation is that the effect of misalignment on stiffness and strength degradation be implemented into design and analysis. M'Bazaa(1996) tested three RC beams strengthened with two symmetric misaligned CFRP plies and one CFRP ply in the direction of the longitudinal axis of the beam. The results indicated that the strength and deflection did not change significantly compared with the beams strengthened with three CFRP plies having fibers applied with the longitudinal beam axis. There is no other literature available on the subject.

In this paper, five 1.22 m plain concrete beams were constructed and strengthened with one ply of misaligned CFRP laminate. The beams had a saw-cut crack at the midspan of the tension face and a fixed hinge was installed at the midspan of the compression face. After cracking of concrete at the center, only the CFRP laminate sustained the tension force, which allowed to investigate the performance of the laminate, to determine the strain distribution, and to identify the effective bond length.

*FRPRCS-5*, Thomas Telford, London, 2001.

Before testing the concrete beams, CFRP laminate coupons consisting of one and two-plies were tested to investigate the strength and stiffness degradation with misalignment. All coupon specimens had an aspect ratio of 4 and a width of 38 mm. The specimens were tabbed at both ends and tested in an MTS 880 testing machine. For the two-ply laminates, one ply was oriented in the loading direction and the other ply was oriented at angles ranging from a minimum of 0-deg to a maximum of 90-deg. Coupon size effect on the strength and stiffness of misaligned CFRP laminates was addressed by making samples with the same width but different aspect ratios ranging from 2 to 8 until no through fibers existed between end tabs (Yang *et al.* 2000). This paper only reports part of the results of the entire project.

## EXPERIMENTAL PROGRAM

### Material Properties

The design properties of carbon fiber and saturant are listed in Tables 1 and 2 as provided by the manufacturer (MBrace, 1998).

The CFRP system was applied to the beam tension surface with a hand lay-up technique according to the procedure specified by the manufacturer. After the concrete surface was sandblasted and cleaned by pressure air, a thin layer of primer was applied to the surface using a roller. Following the application of the primer, putty was applied to the areas with small holes in order to smooth the concrete surface. Then the first layer of saturant and fiber ply were applied when the primer was still sticky. After smoothing the ply into the saturant with a nap roller, a second layer of saturant coat was applied to obtain thorough epoxy impregnation.

Table 1 Mechanical properties of CF130 tow sheet

| | |
|---|---|
| Ultimate strength | 4275 MPa (4525 MPa *) |
| Design strength | 3790 MPa |
| Yielding modulus | 228 GPa (264 GPa *) |
| Ultimate strain | 0.017 mm/mm |

* results from coupon tests (Yang *et al.* 2000)

Table 2 Mechanical properties of MBrace saturant

| | |
|---|---|
| Maximum stress | 55 MPa |
| Maximum strain | 0.03 mm/mm |
| Yielding strain | 0.025 mm/mm |
| Modulus of elasticity | 30 GPa |

Concrete cylinders were tested showing concrete strength of 24.96MPa to 38.24MPa. Miller(1999) indicated that concrete strength does not play a critical role on bond strength of CFRP laminates on concrete and only affects the cracking load. The ultimate load was controlled by the CFRP strength and bond strength. This conclusion was justified by the results of current research, where all beams experienced the same failure by rupture of the CFRP laminate regardless of concrete strength.

**Specimens and Test Setup**

Five plain concrete inverted Tee beams were constructed with dimensions as shown in Figure 1. A 51mm-deep artificial crack was cut at the center of the tension face. A steel hinge was installed into a 51mm-deep saw-cut groove at the center point of the top compression surface. After cracking of the beam, the force was sustained by the CFRP laminate only to facilitate the evaluation of the bond characteristics between CFRP laminate and concrete substrate. After cracking, a constant moment arm of 222 mm was produced from the center of steel hinge to the CFRP laminate.

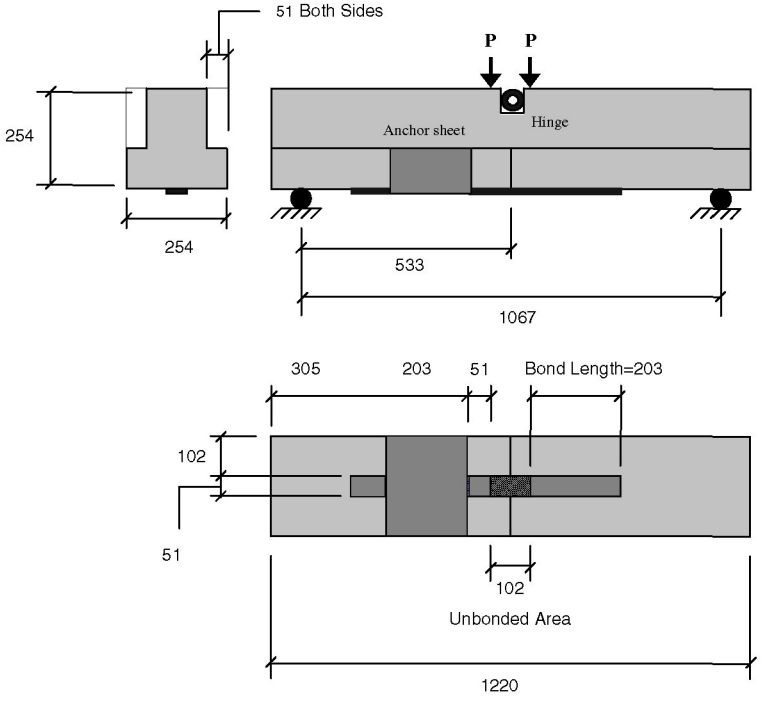



Fig. 1 Specimen and strengthening (Unit: mm)

The bond length of the CFRP laminate was 203 mm. There was an unbonded area of 51 mm at both sides of the artificial crack to prevent stress concentration at the center point. A 203 mm wide lateral anchor laminate was installed at one end of the beam to force failure of the opposite side.

The beam was tested under four-point loading. Midspan deflection and strains along the fiber directions were collected with LVDT and strain gauges, respectively. Strain gages were attached along the fiber direction (Figure 2).

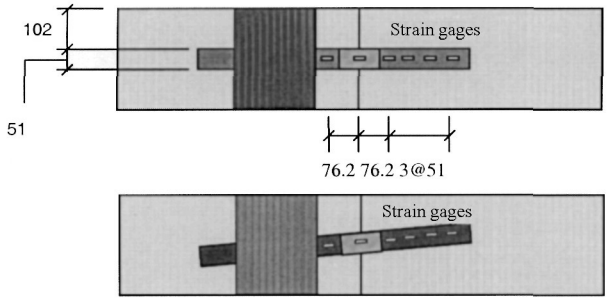



Fig. 2 Strain gage arrangement (Unit: mm)

## TEST RESULTS

### Strength and Deformation

Figure 3 shows the load versus midspan deflection for all five beams. Before cracking, beams had different stiffness and cracking loads due to the different concrete strength. At this stage, the contribution of CFRP is negligible. After cracking, the load decreased with different slopes but converged to a point with a load and deformation of 7.5 kN and 0.7 mm, respectively. The measured strain on the surface of the CFRP laminate within the central unbonded area was around 0.4%. After this point, the response of the beam entered the second stage, when only the CFRP laminate carried the tension force until failure and the compression force acted in the center of the steel hinge.

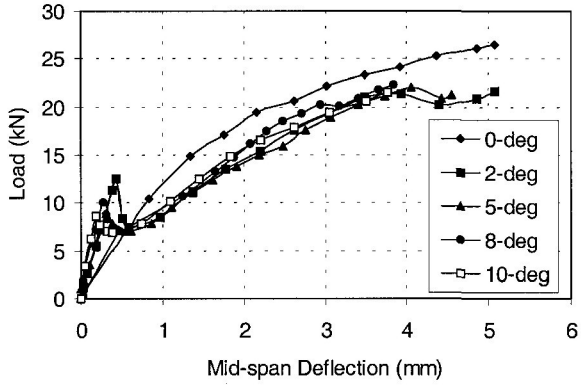



Fig. 3 Load-midspan deflection of all beams

Figure 3 shows that the beam with 0-deg CFRP laminate had a higher ultimate load from the beginning of the second stage while all other four beams did not show much difference in ultimate load and response. The individual ultimate load and midspan deflection are listed in Table 3 and plotted in Figures 4 and 5 versus the misalignment angle. Except for the ultimate load of the 2-deg beam that decreased by 18.2% compared with that of the 0-deg beam, all of the other four beams had a negligible difference in ultimate load. The change of midspan deflection shows a little difference from that of ultimate load. The 0-deg and 2-deg beams had the same maximum deflection. The deflection of the 5-deg beam was only 10.0% less

than that of the 0-deg beam. For misalignment angles larger than 5 degree, the midspan deflection decreased significantly. The deflection of 8-deg and 10-deg beams decreased 25.0% compared with the 0-deg beam.

The change of midspan deflection actually reflects the trend of the stiffness degradation of misaligned CFRP laminates from the tensile coupon tests (Yang *et al.* 2000). The modulus of elasticity of 0, 5, and 10-deg coupons and the normalized average modulus of laminates from these beam tests is depicted in Figure 6. When the misalignment angle is less than 5 degree, the modulus of elasticity does not degrade. After the angle exceeds 5 degree, the modulus degrades rapidly. The modulus degradation of CFRP laminates shows the same trend of the coupon tests.

Table 3 Ultimate load and deflection of all beams

| Angle (deg) | Ultimate load (kN) | Maximum midspan deflection (mm) |
|---|---|---|
| 0 | 26.43 | 5.10 |
| 2 | 21.62 | 5.10 |
| 5 | 21.23 | 4.55 |
| 8 | 22.27 | 3.84 |
| 10 | 21.48 | 3.76 |

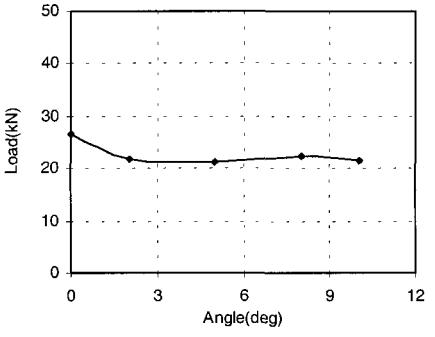



Fig. 4 Degradation of ultimate load

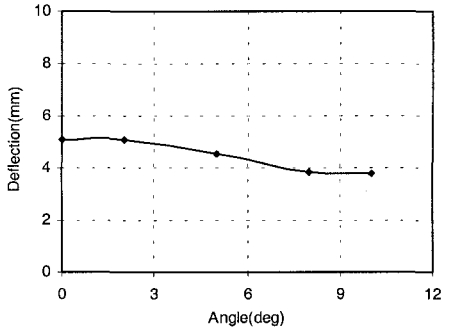



Fig. 5 Degradation of midspan deflection

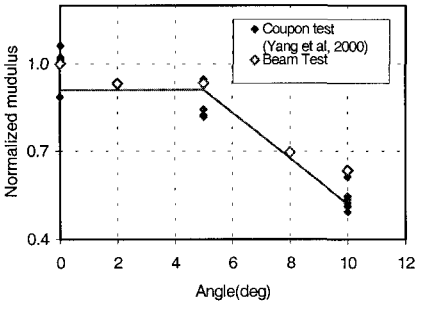



Fig. 6 Modulus degradation of tensile coupons and beams

**Strain Distribution and Failure Modes of CFRP Laminates**

Figure 7 shows the typical strain distribution for CFRP laminates along the fiber direction. The strain gage positions were measured from the center of the beam, which is also the center of the unbonded area. It is assumed that the strain in the laminates within the unbonded area is constant. Figure 7 also shows that the effective bond length of CFRP laminate when delamination first occurred is independent of other parameters such as concrete strength and surface condition. All five beams have an effective bond length of 127 mm.

All beams failed with rupture of CFRP laminate within the delaminated area. Figure 8 shows that the CFRP laminate of the 0-deg beam pulled off less concrete and had a smoother surface than that of the CFRP laminate of 10-deg beam.

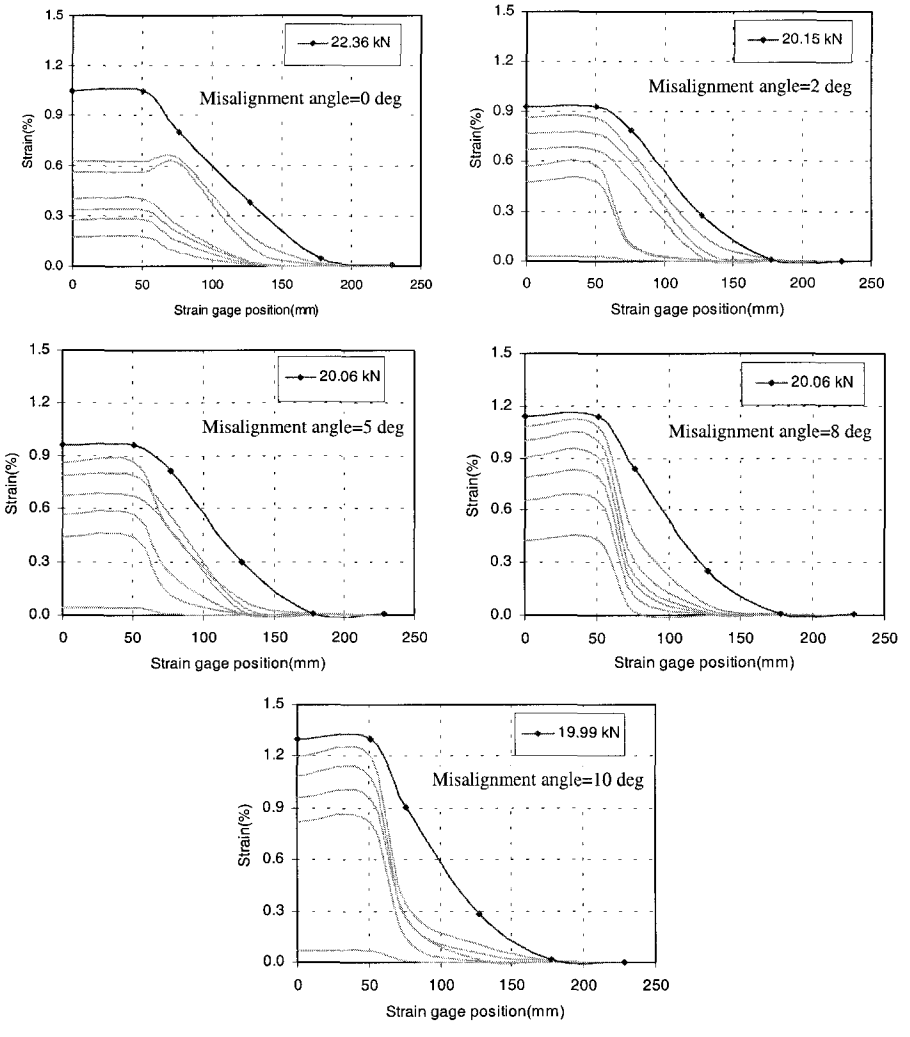
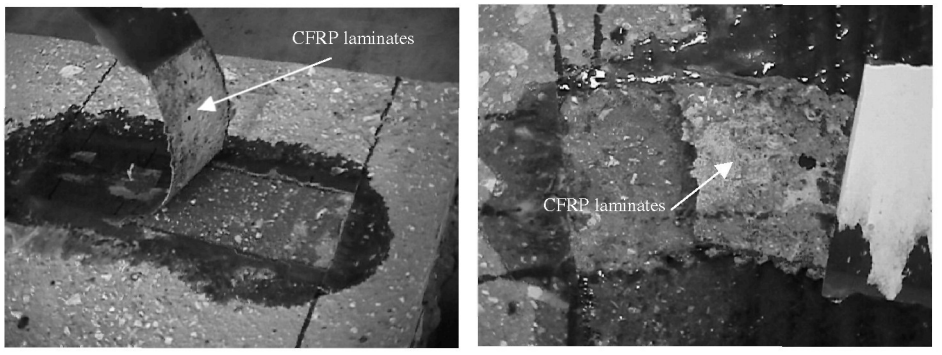



Fig. 7 Strain distribution of all beams




0-deg beam 10-deg beam

Fig. 8 Delamination of CFRP laminates

## CONCLUSIONS

Based on the experimental investigation of concrete beams strengthened with misaligned CFRP laminate, the following conclusions can be reached.

- The change of strength and deformation with misalignment shows different trends. When the misalignment angle is small (less than 5 degree), the strength of the beam is not affected. The deformation decreases very slowly at first, and then more rapidly with increasing misalignment, which agrees with the stiffness degradation of CFRP laminate with misalignment.
- Rupture of CFRP laminates is the controlling failure mode if the concrete surface is properly prepared. Delamination occurs in the CFRP laminates but it is not the controlling failure mode.

## ACKNOWLEDGEMENT

The Federal Highway Administration is gratefully acknowledged for financially supporting this research. The research was undertaken in the Center for Infrastructure Engineering Studies at University of Missouri-Rolla. The authors want to thank Jeff Bradshow and Steve Haug for their contributions to the experimental work.

## REFERENCES

1. M'Bazza, I., Missihoun, M. and Labossiere, P. (1996), "Strengthening of Reinforced Concrete Beams with CFRP Sheets". *Proc. 1st Conference on Composites in Infrastructure;* Ed., Saadatmanesh, H. and Ehsani, M . R., Tucson, AR, USA, pp 746-759.
2. MBrace ™ (1998), Composite Strengthening System, Engineering Design Guidelines, 2nd Edition, Master Builders, Inc., Cleveland, OH, pp 109.
3. Miller, B. D. (1999), Bond Between Carbon Fiber Reinforced Polymer Sheets and Concrete, MS thesis, Department of Civil Engineering, University of Missouri-Rolla.
4. Yang, X. B, Nanni, A., Haug, S. and Sun C. L. (2000), "Strength and Modulus Degradation of CFRP Laminates from Fiber Misalignment", *J. Mat. Civil Engrg*, ASCE.(accepted)

# Failure behavior of flexural strengthened RC beams with AFRP Sheet

N. KISHI, Muroran Inst. of Technology, Muroran, Japan
H. MIKAMI, TRI of Mitsui Construction Co., Ltd., Chiba, Japan
K. G. MATSUOKA, Muroran Inst. of Technology, Muroran, Japan
Y. KURIHASHI, Muroran Inst. of Technology, Muroran, Japan

## ABSTRACT
In this paper, in order to establish a rational flexural strengthening method for Reinforced Concrete (RC) members with Fiber Reinforced Plastic (FRP) sheet, static loading tests on RC beams strengthened with Aramid FRP (AFRP) sheet were conducted. Sixteen kinds of strengthened RC beams were used, in which following parameters were varied: rebar ratio (0.8, 1.2, and 1.8 %), shear span ratio (3.1, 4.0, 5.0, 6.0, and 6.9), and sheet volume ratio (1.0 and 2.0 ‰). The experiments revealed the following: 1) There are two failure modes (sheet debonding failure and flexural compressive failure), with the mode depending on the rebar yield length; 2) in both cases, the sheet finally debonds due to exfoliation of concrete on the lower cover concrete of the equi-shear span; and 3) strengthening design of flexural-failure-type RC beams can be performed within a margin of safety by using a fiber model.

## INTRODUCTION
Concrete and steel usually are the primary materials for structural members. Fiber Reinforced Plastic Sheet (FRPS) has the following advantages over these materials: light weight, flexibility, better workability, and high strength. Therefore, FRPS sometimes is used for raising the ultimate strength and/or increasing the ductility of Reinforced Concrete (RC) and Prestressed Concrete (PC) members as well as steel plates and concrete. There are two kinds of FRPS typically applied: Carbon FRPS (CFRPS) and Aramid FRPS (AFRPS). AFRPS is of lower E-modulus and strength, but it is more flexible than CFRPS.

Wrapping FRPS around an RC/PC member can increase the shear capacity, and bonding FRPS to the tension-side surface can increase the flexural capacity. To establish rational retrofit methods toward increasing these capacities for RC beam/plate, the plane-shear bonding properties of FRPS have been studied[1), 2), 3)]. However, bonding properties of FRPS for flexural strengthening are affected not only by plane-shear but also by flexural-shear.

To establish a rational design method for RC beams strengthened by bonding with FRP sheet on the tension-side surface, this study experimentally investigated the load carrying capacity and debonding mechanism of FRPS. Sixteen strengthened rectangular RC beams were prepared, in which parameters of rebar ratio, shear span ratio, and sheet volume ratio were varied. Because strengthening effect of FRPS is affected only by axial stiffness of FRPS, only AFRPS is addressed in this paper. Under four-point loading, measurements were made of

*FRPRCS-5*, Thomas Telford, London, 2001.

Table 1. RC beams

| Specimen | Main rebar (SD345) | Rebar ratio $p_t$ (%) | Clear span length (m) | Shear span ratio $r_s$ | Number of sheet layers | Sheet volume ratio $p_f$ (‰) |
|---|---|---|---|---|---|---|
| A1-R7-1 | D13 | 0.8 | 3.4 | 6.9 | 1 | 1.0 |
| A1-R5-1 | | | 2.6 | 5.0 | | |
| A1-R3-1 | | | 1.8 | 3.1 | | |
| A2-R7-1 | D16 | 1.2 | 3.4 | 6.9 | 1 | 1.0 |
| A2-R6-1 | | | 3.0 | 6.0 | | |
| A2-R5-1 | | | 2.6 | 5.0 | | |
| A2-R4-1 | | | 2.2 | 4.0 | | |
| A2-R3-1 | | | 1.8 | 3.1 | | |
| A2-R7-2 | | | 3.4 | 6.9 | 2 | 2.0 |
| A2-R6-2 | | | 3.0 | 6.0 | | |
| A2-R5-2 | | | 2.6 | 5.0 | | |
| A2-R4-2 | | | 2.2 | 4.0 | | |
| A2-R3-2 | | | 1.8 | 3.1 | | |
| A3-R7-1 | D19 | 1.8 | 3.4 | 6.9 | 1 | 1.0 |
| A3-R5-1 | | | 2.6 | 5.0 | | |
| A3-R3-1 | | | 1.8 | 3.1 | | |

surcharged load, mid-span displacement, and axial strain distribution of AFRPS. These experimental results were compared with calculated ones obtained using a fiber model.

## EXPERIMENTAL OVERVIEW

Sixteen RC beams were used (Table 1). Each specimen's three-part designation indicates rebar ratio (A1 (0.8%), A2 (1.2%), or A3 (1.8 %)), shear span ratio (R3 to R7, rounded to the nearest integer) and sheet volume ratio (1 or 2‰). The dimensions and rebar arrangement for each type of RC beam are shown in Fig. 1, in which all beams are 250 x 150 mm in cross section and SD345 D13, D16, and D19 rebars are used for main rebar and SD295 D10 rebars are used for stirrup. Because loading interval is fixed as 500 mm, the clear span is varied from 1,800 to 3,400 mm corresponding to shear span ratio.

Figure 2 shows an example of the area strengthened with AFRPS and the location of each glued strain gauge. The 130 mm-wide AFRPS is bonded to the central portion of the lower surface 100 mm inside the supporting points of each RC beam, and the concrete surface is chipped heavily where it is bonded with AFRPS[4].

The material properties of AFRPS used in this study are listed in Table 2. AFRPS with 0.415 kg/m$^2$ mass per unit area is used for all RC beams considered here.

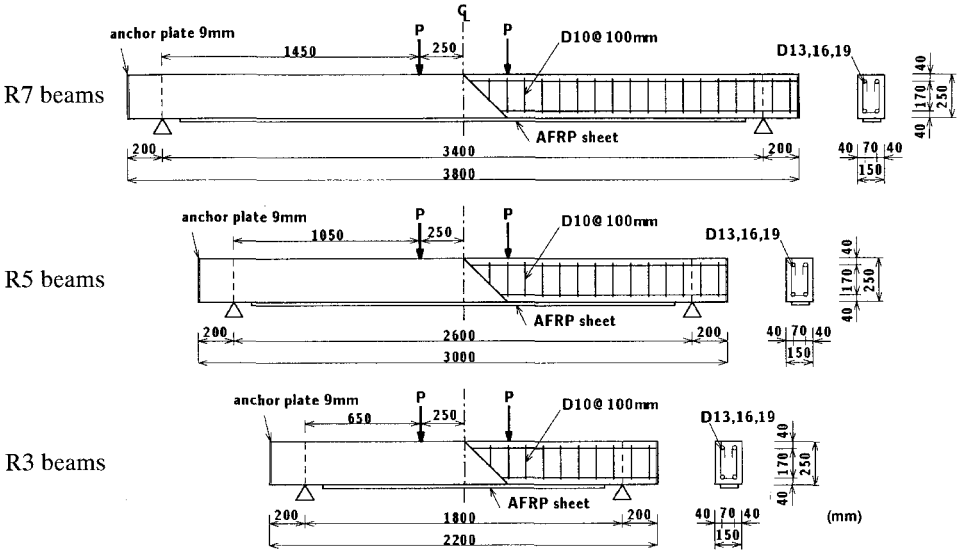



Figure 1. Dimensions of RC beams

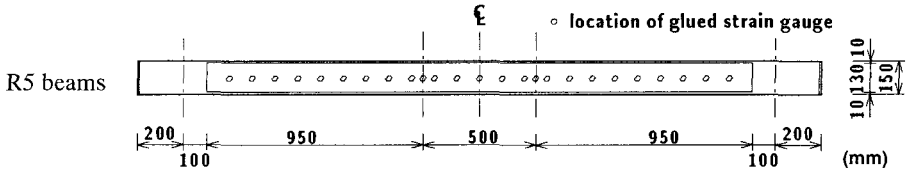



Figure 2. An example of area strengthened with AFRPS and location of glued strain gauge

Table 2. Material properties of AFRPS

| Mass per unit area ($kg/m^2$) | Thickness (mm) | E-modulus (GPa) | Tensile strength (GPa) | Strain limit (%) |
|---|---|---|---|---|
| 0.415 | 0.286 | 126.5 | 2.48 | 1.96 |

Estimating the bending and shear capacities of strengthened RC beam by using fiber model and modified truss theory[5], respectively, confirmed for all RC beams that the bending capacity was less than the shear capacity even after strengthening. At commencement of experiment, the average compressive strength of concrete was 28.2 MPa. The ultimate compressive strain of concrete for numerical analysis was assumed as 3,500 μ based on the specifications of Japan Concrete Standard[5].

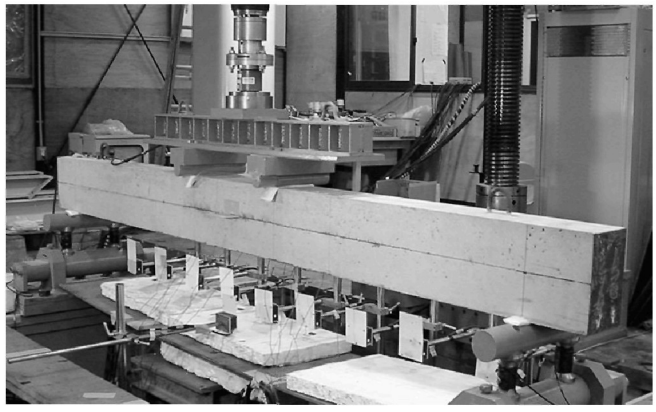


Photo 1. Experimental setup

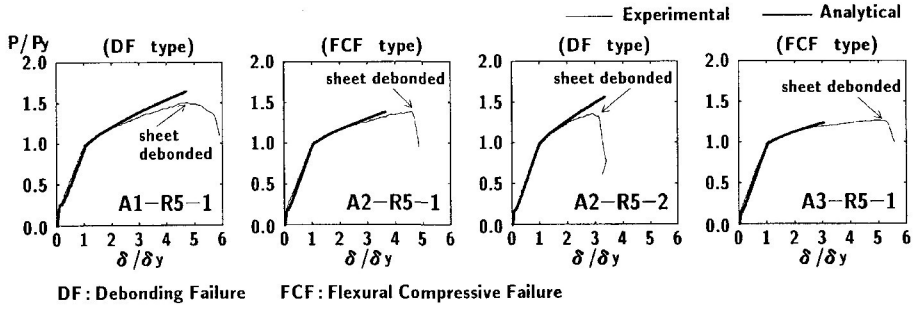


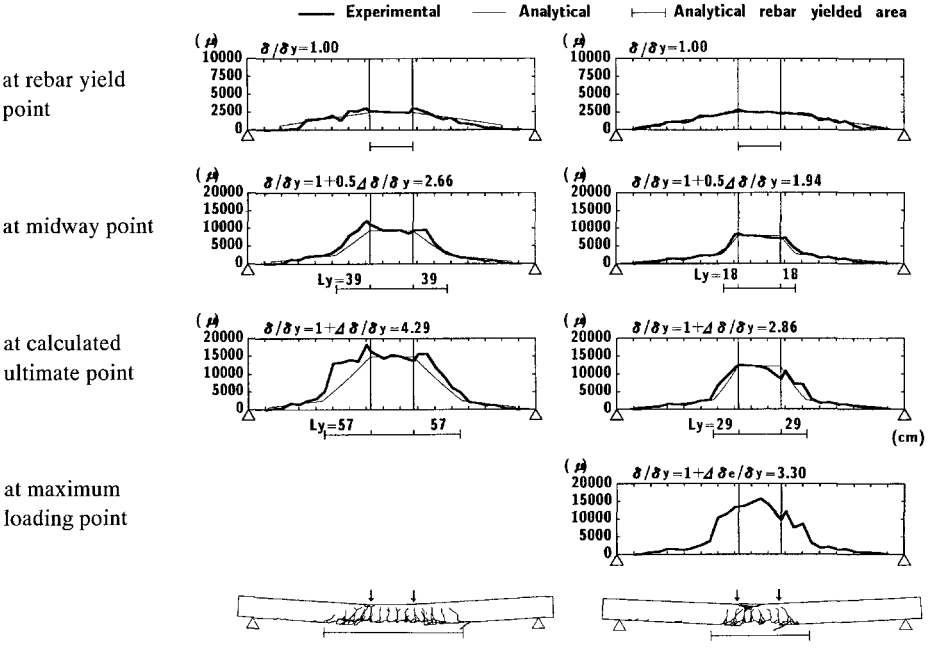

Figure 3. Comparison between experimental and calculated results on relationship between load and displacement

A surcharged load (hereinafter, load), the mid-span displacement (hereinafter, displacement), and axial strain distribution of AFRPS were measured and continuously were recorded by digital data-recorder to precisely investigate the debonding process of AFRPS. Photo 1 shows the experimental setup.

## EXPERIMENTAL RESULTS

### Relationship between load and displacement

Figure 3 compares the load-displacement curves of experimental results with those of calculation results. Each load $P$ and displacement $\delta$ is normalized with reference to the values of $P_y$ and $\delta_y$ at the main rebar yield, respectively. The figures reveal failure modes of two types: 1) After main rebar yielding, the load-displacement curve is lower than the calculated curve and RC beam failure is due to AFRPS debonding near the loading point at a value less than the calculated maximum one (A1-R5-1, A2-R5-2); 2) the load-displacement curve corresponds closely to the calculated values until displacement reaches the calculated ultimate point, after which the displacement increases while the load remains roughly




(a) A1-R7-1 beam (DF type) (b) A3-R7-1 beam (FCF type)

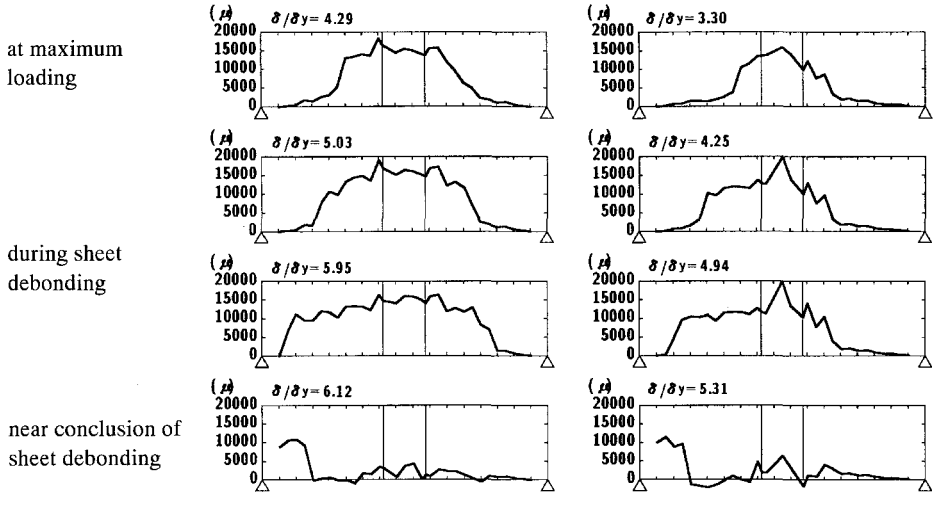
Figure 4. Comparison between experimental and calculation results of AFRPS strain distribution, and crack patterns

constant and the RC beam fails due to AFRPS debonding and crushing of the upper cover concrete (A2-R5-1, A3-R5-1). The failure modes are called Debonding Failure (DF) and Flexural Compressive Failure (FCF), respectively.

Failure classification showed A1-R*n*-1 (*n* = 3, 5, and 7) and A2-R*n*-2 (*n* = 3, 4, 5, 6, and 7) beams to be DF type, and A2-R*n*-1 (*n* = 3, 4, 5, 6, and 7) and A3-R*n*-1 (*n* = 3, 5, and 7) beams to be FCF type, irrespective of shear span ratio.

**Strain distribution of AFRPS and crack pattern**

Figure 4 compares typical experimental and calculation results of AFRPS strain distribution at each loading step for RC beams of each type. The results are indicated for DF type (A1-R7-1) and FCF type (A3-R7-1). These figures show the comparisons for three and four loading steps: 1) at rebar yield point; 2) at displacement midway between rebar yield point and calculated ultimate point (hereafter, midway point); 3) at calculated ultimate point; and 4) experimental maximum loading point only for FCF type (hereafter, maximum loading point). These figures specify calculated rebar yield area, in which the length, $L_y$ in both sides excluding equi-bending area is identified. Crack patterns for each type of RC beam also are shown.




(a) A1-R7-1 beam (DF type) (b) A3-R7-1 beam (FCF type)

Figure 5. AFRPS strain distribution at sheet debonding

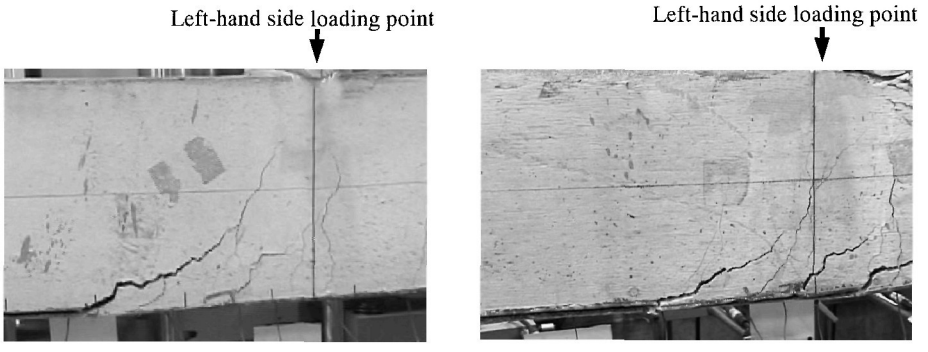
These figures reveal that at rebar yield point, AFRPS remains perfectly bonded to the concrete surface for beams of both failure types. We know this because experimental and calculated strain distributions are close.

Observing the calculated strain distributions at both midway and calculated ultimate points, calculated rebar yielded area is expanded from equi-bending area toward both supporting points and following then, a bigger strain distribution zone is also spread. It can be seen that the length of rebar yield area, $L_y$ in one-side equi-shear span of DF type is about twice the width of that for FCF type. In the case of DF-type beam, comparison of the strain distributions at calculated ultimate point shows the experimental strain distribution in rebar yield area to exceed the calculated values. This suggests that AFRPS debonding progresses locally due to exfoliation of the lower cover concrete in equi-shear span near the loading point. In contrast, in the case of FCF, it can be observed that AFRPS does not debond from concrete surface up to the calculated ultimate point. However, at maximum loading, debonding of AFRPS may progress because the strain at this step distributes similarly to that of DF type at calculated ultimate point.

The crack patterns of both RC beams reveal that the concrete exfoliates around the lower cover concrete of the equi-shear span due to interaction between bending and shear cracks, and that the area corresponds to the calculated rebar yield area in the equi-shear span.

**Strain distribution at AFRPS debonding**

Figure 5 shows AFRPS strain distribution during sheet debonding, from maximum loading to the conclusion of sheet debonding. The results are for DF type (A1-R7-1) and FCF type (A3-R7-1). Observing the left-hand side strain distribution in equi-shear span area for both beams, almost linear strain distribution in the rebar yielded area is gradually rising




(a) A2-R5-2 beam (DF type) (b) A3-R7-1 beam (FCF type)

Photo 2. Beginning of sheet debonding

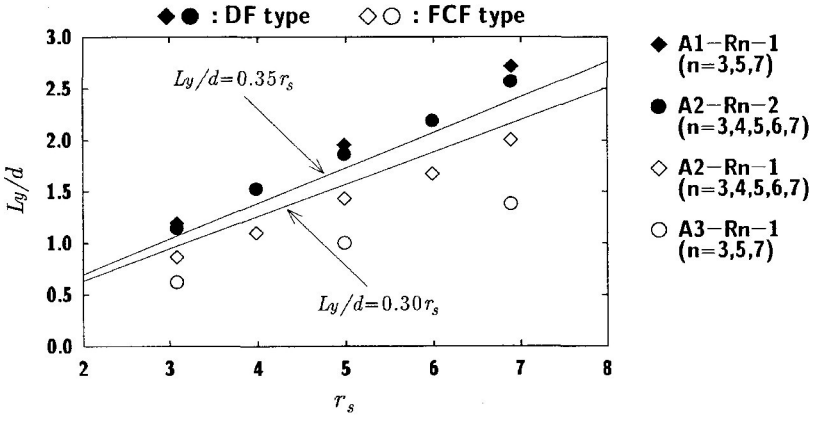



Figure 6. Experimental results on relationship between $L_y/d$ and failure type

corresponding to an increment of displacement, and finally these strains are released toward zero level. This suggests that 1) sheet debonding progresses outward from near the loading point of rebar yield area in equi-shear span; 2) the sheet finally debonds completely in the one-side equi-shear span area and bending tensile stress introduced in the sheet is released; and 3) RC beam will collapse. In both types of failure, sheet debonding results from the exfoliated concrete pushing on the sheet with shear force.

Photo 2 shows the beginning of sheet debonding for an RC beam of each failure type: A2-R5-2 for DF and A3-R7-1 for FCF. It can be seen that, irrespective of failure type, 1) concrete exfoliates at the lower cover concrete of the rebar yield area by interaction between bending and shear cracks; 2) the exfoliated concrete is pushed downward and out by shear force that results in a level difference that causes the sheet to peel; and 3) the sheet debonds outward from the point of the level difference. These photos confirm that the sheet debonds due to the concrete exfoliation.

## PREDICTION OF FAILURE TYPE

The former discussion shows that the length of rebar yield area, $L_y$ in equi-shear span for DF is larger than that for FCF. This suggests that the length, $L_y$ significantly affects the failure type and that it may be possible to predict the type by using the length. Here, normalizing $L_y$ with reference to the effective depth of cross section, $d$, the experimental results on failure type are plotted on an $L_y/d - r_s$ diagram (Fig. 6) in which $r_s$ is shear span ratio. In this figure, DF-type beams are black diamonds and circles, and the two lines passing the origin point are the upper and lower bounds for each failure type.

This figure clearly reveals two failure types:

$$L_y/d > 0.35\, r_s \qquad \text{for DF type} \qquad \ldots(1)$$

$$L_y/d < 0.30\, r_s \qquad \text{for FCF type} \qquad \ldots(2)$$

Using $r_s = a/d$ and the relationship between $L_y/d$ and $M_y/M_u$, in which $M_y$ and $M_u$ are bending moment capacity at rebar yield and ultimate moment capacity of strengthened RC beam, respectively, Eqs. (1) and (2) are converted as follows:

$$M_y / M_u < 0.65 \qquad \text{for DF} \qquad \ldots(3)$$

$$M_y / M_u > 0.70 \qquad \text{for FCF} \qquad \ldots(4)$$

Therefore, the failure type for RC beams strengthened with AFRPS may be predicted by using Eqs (3) and (4). Because experimental ultimate moment capacity for FCF exceeds that of calculated results, as mentioned in the former session, this confirms that design for strengthening of FCF-type RC beams can be rationally performed with a safety margin.

## CONCLUSIONS

Toward establishing a rational design method for RC beams strengthened by bonding with FRP Sheet (FRPS) on the tension-side surface, experiments investigated the load carrying capacity and debonding mechanism of FRPS. Sixteen RC beams strengthened with Aramid FRPS (AFRPS) were used, with the parameters of rebar ratio, shear span ratio, and sheet volume ratio as variables. Not only were surcharged load and mid-span displacement measured, axial strain distribution of AFRPS also was measured. The results follow.

1. Two failure modes were revealed: sheet Debonding Failure (DF) and Flexural Compression Failure (FCF). The mode can be predicted from the length of rebar yield area in equi-shear span.
2. Sheet debonds by concrete exfoliation at the lower cover concrete of equi-shear span due to interaction between bending and shear cracks.
3. Design for strengthening of FCF-type RC beams can be rationally performed with a safety margin.

## REFERENCES

1) Maeda T., Asano Y., Sato Y., Ueda T., and Kakuta Y.: A Study on Bond Mechanism of Carbon Fiber Sheet, Non-Metallic (FRP) Reinforcement for Concrete Structures, Proceedings of the Third International Symposium, Vol. 1, pp. 279-286, 1997.10.

2) Nanni, A., Bakis, C. E., and Boothby. T. E.: Externally Bonded FRP Composites for Repair of RC Structures, Non-Metallic (FRP) Reinforcement for Concrete Structures, Proceedings of the Third International Symposium, Vol. 1, pp. 303-310, 1997. 10.

3) Bizindavyi L., and Neale K. W.: Transfer Length and Bond Strength for Composites Bonded to Concrete, Journal of Composites for Construction, pp. 153-160, 1997. 11.

4) Kurihashi Y., Kishi N., Mikami H., Sato M., and Matsuoka K. G.: Experimental Study on Flexural Bonding Property of AFRP Sheet Glued on RC Beams, Proceedings of EASEC-7, Vol. 2, pp. 1271-1276, 1999.8.

5) JSCE: Japan Concrete Standard, 1996, in Japanese.

# Strengthening of R.C. beams in flexure and shear using CFRP laminate

I. A. E. M. SHEHATA, E. C. CERQUEIRA, C. T. M. PINTO, COPPE – Federal University of Rio de Janeiro, BR, and L. C. D. SHEHATA, COPPE/UFRJ and Fluminense Federal University

## ABSTRACT

This work presents an experimental program that aims to study the behaviour of reinforced concrete beams strengthened either in shear, in flexure or in both flexure and shear by applying externally glued carbon fibre reinforced plastic (CFRP) laminates. The fibre laminates used were of the SIKA CARBODUR S512 type and had an average modulus of elasticity of about 165 GPa and ultimate tensile strength of 2800 MPa.

From the test results obtained it was possible to establish failure criteria for the strengthened beams and to propose calculation models based on the flexure theory and the truss model. The models gave good results when compared to the experimental values.

## EXPERIMENTAL PROGRAM

### Description of Tested Models

Six beams with rectangular cross section of 150 mm x 450 mm and a total length of 4500 mm were simply supported and loaded, until their failure, under two equal point loads at one third and two thirds of the span (4000 mm). Except for one beam (reference beam VR), the beams were strengthened either in flexure (two beams V1, V3), or in shear (two beams V2, V4) or in both flexure and shear (one beam V5) by gluing CFRP laminates to the surface. The laminates were 50 mm wide and 1.20mm thick.

The beams were designed so that three of the beams had insufficient flexural strength (V1, V3 and V5) and another three had insufficient shear strength (V2, V4 and V5), when compared to the reference beam VR. The reference beam VR had approximately a balanced steel ratio and had sufficient stirrups to ensure that its shear strength was slightly higher than its flexural strength. The geometrical and strength characteristics of all beams, without strengthening, are summarised in tables 1 and 2.

Two beams (V1 and V3) were strengthened in flexure and another two (V2 and V4) were strengthened in shear while a single beam (V5) was strengthened in both flexure and shear. The difference between the beams strengthened in flexure was the number of CFRP laminates used, two in V1, three in V3 and five in V5. The difference between the beams strengthened in shear was the orientation of the CFRP laminate with respect to the beam axes, 45° or 90°, and the CFRP laminate end condition. The CFRP laminate end condition was either free

as in V2 or fixed as in V4 and V5 by gluing another cross CFRP laminate on the top of their ends (see figure 1). The strengthening of the beams was always carried out under sustained loads (40kN at each load point) and on previously cracked beams to simulate the realistic case that is usually faced in practice. Figure 1 shows schematically the strengthening details of beams V2, V4 and V5.

All beams were instrumented with strain gauges (on the flexural and shear reinforcement and on the CFRP laminate) and deflection transducers in order to monitor their behaviour during loading.

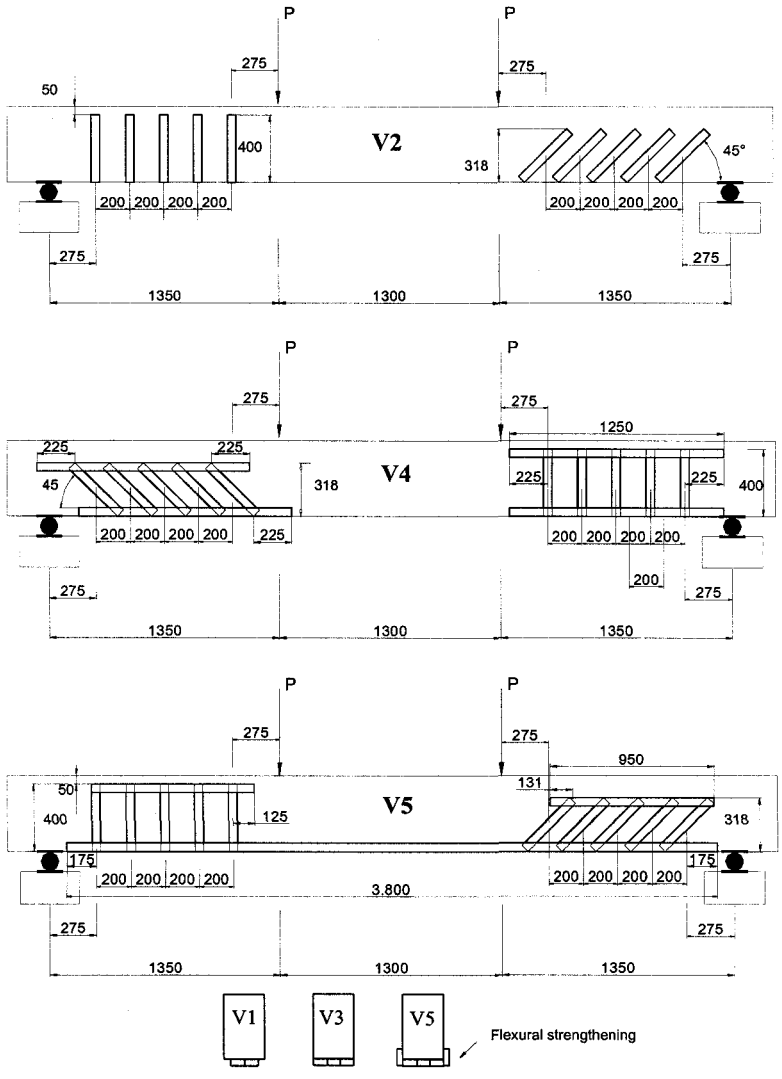



Figure 1. Strengthening details of beams V2, V4 and V5 in shear and V1, V3 and V5 in flexure (dimensions are in mm).

Table 1. Main flexure characteristics of tested beams (unstrengthened)

| Beam | $f_{cm}$ (MPa) | $A_s$ ($mm^2$) | $A'_s$ ($mm^2$) | ρ (%) | $b$ (mm) | $d$ (mm) | $d'$ (mm) | $f_y$ (MPa) | $P_u$* (kN) (1) | (2) |
|---|---|---|---|---|---|---|---|---|---|---|
| V1 | 33,3 | 603 | 100,5 | 0,96 | 150 | 420 | 27 | 630 | 87 | 108 |
| V2 | 36,6 | 1344 | 100,5 | 2,18 | 150 | 410 | 25 | 600<br>630 | 171 | 198 |
| V3 | 34,3 | 603 | 100,5 | 0,96 | 150 | 420 | 27 | 630 | 88 | 108 |
| V4 | 39,2 | 1344 | 100,5 | 2,18 | 150 | 410 | 25 | 579<br>634 | 173 | 202 |
| V5 | 34,7 | 603 | 100,5 | 0,95 | 150 | 422 | 24 | 579 | 88 | 101 |
| VR | 34,4 | 1344 | 100,5 | 2,18 | 150 | 410 | 25 | 511<br>545 | 169 | 180 |

**Values obtained from a non-linear analyses program (CONSEC95).*
*(1)Based on nominal values for $f_y$ = 500 MPa.*
*(2)Based on experimental values for $f_y$*

Table 2. Main shear characteristics of tested beams (unstrengthened)

| Beam | $f_{cm}$ (MPa) | $S$ (mm) | $A_{sw}$ ($mm^2$) | $f_{yw}$ (MPa) | $V_c$* (kN) | $V_s$ (kN) (1) | (2) | $V_s+V_c$ (kN) (1) | (2) |
|---|---|---|---|---|---|---|---|---|---|
| V1 | 33,3 | 100 | 100,5 | 590 | 42 | 184 | 216 | 226 | 258 |
| V2 | 36,6 | 200 | 39,2 | 688 | 52 | 42 | 48 | 94 | 100 |
| V3 | 34,3 | 100 | 100,5 | 590 | 42 | 184 | 216 | 226 | 258 |
| V4 | 39,2 | 200 | 39,2 | 688 | 54 | 42 | 48 | 96 | 102 |
| V5 | 34,7 | 200 | 39,2 | 688 | 43 | 46 | 52 | 89 | 95 |
| VR | 34,4 | 100 | 100,5 | 684 | 50 | 199 | 227 | 249 | 277 |

** Based on the Brazilian Code of Practice NBR-6118 (1980).*
*(1)Based on nominal values for $f_{yw}$ = 500 MPa (V1) or 600 MPa (V2, V4, V5, VR)*
*(2) Based on experimental values for $f_{yw}$*

**Test Procedure, Results and Failure Loads**

The beams were placed in a test rig and subjected to incremental load of equal load steps (10 kN) until a load that corresponded to an internal steel deformation of about 0.2% (in either the longitudinal reinforcement or the shear stirrups) and then unloaded and reloaded again with a similar load cycle. The beams were then subjected to a third load cycle that stopped at a load equal to 40 kN (at each load point) and the load was sustained during the execution of the beam strengthening and the curing process of the resin. This took one week to be completed.

The value of the sustained load (40 kN) was chosen so that the internal steel deformation (either longitudinal or shear stirrups) at the time of strengthening would be around one half its yield deformation ($\varepsilon_y$ = 2.5 °/₀₀ or 3.0 °/₀₀). This would represent an actual steel deformation in RC members in practice under service loading (counting for a global factor of safety equal to 2.0).

After the complete curing of the resin (SIKADUR30), the beams were then loaded in increments of 10 kN until their failure. During all load cycles measurements of the steel and CFRP laminate strains together with the beam deflection (at the centre and under the load) were taken at each load step. Figures 2 to 5 show examples of the test results obtained for the internal steel and external CFRP laminate deformations and the beam deflection (at the centre) while table 3 gives the failure load and the failure type for all beams.

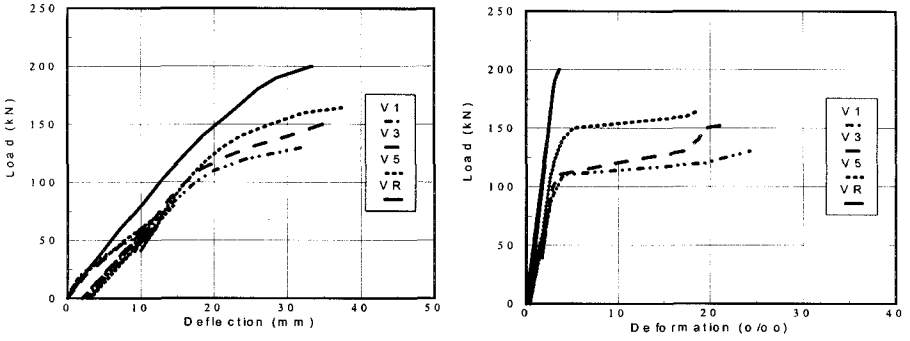



Figure 2. Experimental Load-Deflection and Load-Longitudinal steel deformation curves for beams V1, V3, V5 and VR

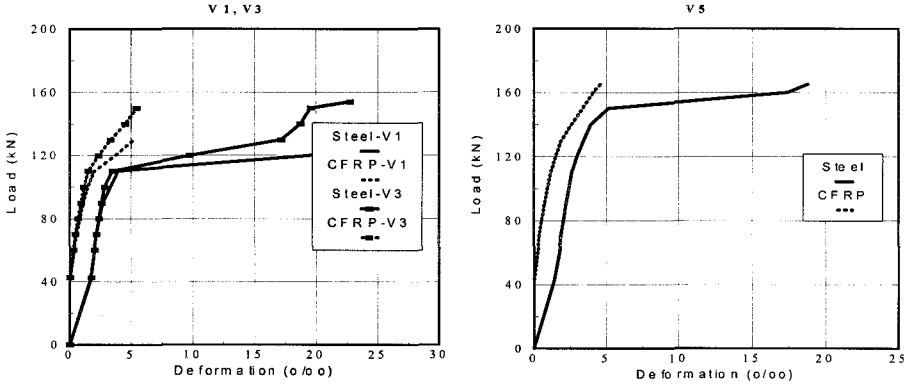



Figure 3. Experimental Load-Longitudinal steel deformation and Load-Flexural CFRP deformation curves for beams V1, V3 and V5 (strain of lower CFRP).

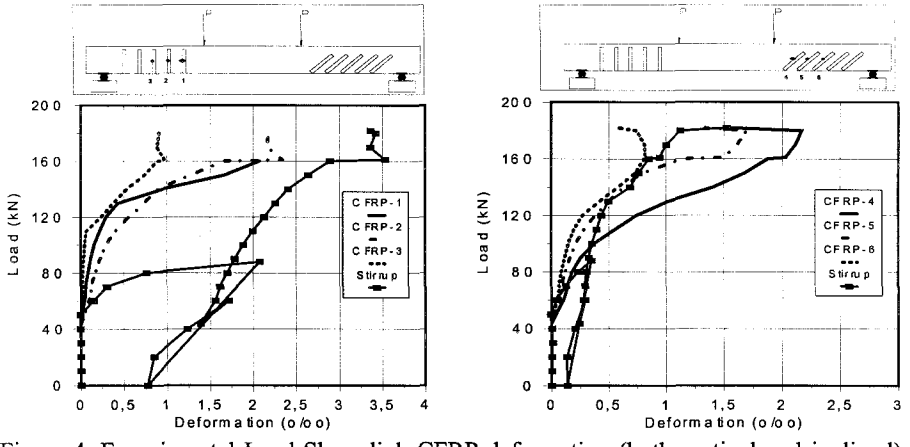



Figure 4. Experimental Load-Shear link CFRP deformation (both vertical and inclined) and Load-internal stirrup deformation curves for beam V2.

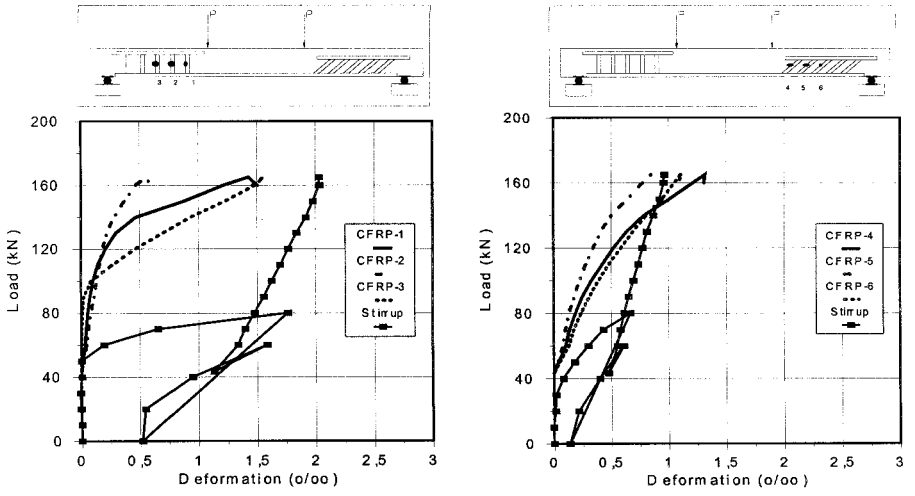



Figure 5. Experimental Load-Shear link CFRP deformation (both vertical and inclined) and Load-internal stirrup (2 and 5) deformation curves for beam V5.

The failure of both beams V1 and V3, that were strengthened in flexure with two and three CFRP laminates respectively, was of the brittle type. It occurred by debonding of the CFRP that started at the section of maximum moment (under the load) and extended towards the supports when the fibre deformation exceeded the value of 5‰ (see figure 3).

In the case of beam V5 that was strengthened in flexure with 5 CFRP laminates, the failure was ductile and mainly caused by crushing of concrete in compression above the neutral axis depth and yielding of the internal main steel. The registered deformation of CFRP in this beam at failure was less than 5‰ (see figure 3) and there was no sign of debonding noticed.

On the basis of the test results of beams V1, V3 and V5 it is suggested that, as a criterion for design at ultimate state, the failure by debonding of the CFRP laminate can be considered to take place when the CFRP deformation reaches the value of 5‰.

The failure of V2 occurred at first by tearing off the concrete cover that supported the vertical CFRP laminate shear links at a load of 161 kN. At this stage the test was, temporarily, interrupted to strengthen the shear span of the beam that had vertical CFRP laminate shear links by means of externally prestressed stirrups. The test was then continued until the final failure of the beam that took place at a load of 182 kN. The failure type was a combined flexure-shear one and occurred by crushing of concrete in compression above the neutral axis depth and yielding of the internal main steel (at a section of maximum moment) and by tearing off the concrete cover that supported the inclined CFRP laminate shear links.

From the registered deformation of the CFRP laminate at the instance of tearing off in V2 it was possible to estimate the value of the shear strength of the concrete cover (using equation 11). The strength was related to the concrete tensile strength, obtained from the standard split cylinder test, and found to be in the order of $\tau_{lim} = 0.45 f_t$. The measured deformation in the CFRP laminate at half height and near to the shear crack was much less than 5‰.

In the case of flexural strengthening, as this mode of failure did not occur in the beams tested in this research program, it is estimated that the shear strength of the concrete cover to flexural reinforcement should be slightly lesser than the previously obtained ($\tau_{lim}= 0.45f_t$ ). This is due to the fact that the cover beneath the flexural reinforcement suffers in addition to shear stresses, a reduction that is caused by the dowel effect of the main steel which weakens the region. A reasonable limit in the case flexural strengthening is here proposed as $\tau_{lim}= 0.3f_t$.

On the basis of the previous discussion, two values for the shear strength of the concrete cover associated with the tearing off failure criterion are proposed;

a) $\tau_{lim}= 0.45f_t$ for the concrete cover on the beam sides and;
b) $\tau_{lim}= 0.3f_t$ for the concrete cover to flexural reinforcement.

Both beams V4 and VR failed in flexure, as did V5, by crushing of the concrete in compression above the neutral axis depth and yielding of the main steel.

Table 3. Failure load and failure type for the tested beams

| Beam | $P_u$ (kN) | Type of Failure |
|---|---|---|
| V1 | 140 | Debonding of CFRP |
| V2 | 161/182 | Tearing off the concrete cover (vertical/inclined) |
| V3 | 150 | Debonding of CFRP |
| V4 | 181 | Flexural – concrete crushing |
| V5 | 165 | Flexural – concrete crushing |
| VR | 200 | Flexural – concrete crushing |

## FLEXURAL ANALYSIS OF THE STRENGTHENED BEAMS

Assuming that concrete sections remains plane after deformation and using the concrete stress block distribution shown in figure 6 at ultimate state, from the section equilibrium, the following expression can be easily deduced;

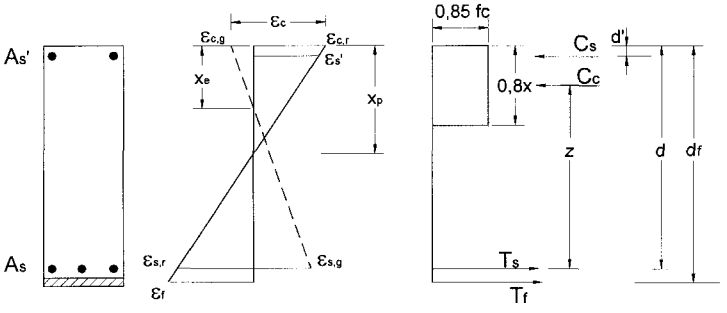



Figure 6. Section strains, stresses and forces at ultimate state.

$$M_u = \sum A_f \sigma_f (d_f - 0.4x_p) + A_s f_y (d - 0.4x_p) + A_s' \sigma_s' (0.4x_p - d') \quad (1)$$

$$x_p = \frac{A_s f_y - A_s' \sigma_s' + \sum A_f \sigma_f}{0.85 f_c 0.8b} \quad (2)$$

$$\sigma_s' = \varepsilon_s' E_s \quad (3)$$

$$\varepsilon_s' = \frac{\left(x_p - d'\right)}{x_p}\varepsilon_c \tag{4}$$

$$\varepsilon_s = \varepsilon_f \frac{\left(d - x_p\right)}{\left(d_f - x_p\right)} + \varepsilon_{s,g} \tag{5}$$

Where $A_f$ = the area of CFRP laminate added to the concrete section;
$A_s$ = the area of the tension steel;
$A_s'$ = the area of the compression steel;
$\sigma_f$ = the stress in the CFRP;
$d_f$ = the effective depth of the CFRP;
$\varepsilon_{s,g}$ = the internal steel strain at strengthening;
$\varepsilon_{c,g}$ = the concrete strain at strengthening;
$x_p$ = the plastic neutral axis depth;
$x_e$ = the neutral axis depth of the transformed cracked section.

From the two previously established failure criteria, the strengthened beam in flexure can fail either by debonding of CFRP laminate from the concrete cover or by tearing off the concrete cover that sustain the CFRP laminate. The CFRP laminate contribution to the beam flexural strength ($\sigma_f$) in equation (1) is then determined from the lesser of the following two limits;

a) From the limit of $\varepsilon_f \leq 5‰$ to the fibre deformation associated with debonding mode of failure,

$$\sigma_{f,\lim} = \varepsilon_f E_f = 0.005 E_f \tag{6a}$$

b) From the limit of $\tau_{lim} = 0.3 f_t$ to the shear stress at the concrete cover associated with tearing off mode of failure,

$$\sigma_{f,\lim} = \frac{\tau_{\lim} \cdot L_f \cdot b_f}{e_f \cdot b_f} = \frac{\tau_{\lim} \cdot L_f}{e_f} \tag{6b}$$

where $L_f$ = shear span, length in which shear stresses are transmitted between CFRP laminate and concrete cover (=1175 mm for the beams of this work)
$b_f$ = width of CFRP
$e_f$ = thickness of the CFRP
$E_f$ = modulus of elasticity of the CFRP
$\varepsilon_f$ = deformation of the CFRP.

Table 4 shows the calculated flexural strength according to the limits of equation (6) and the section analysis at ultimate state for the strengthened beams. In this table the ultimate load was determined from

$$P_u = \frac{M_u}{a} \qquad \text{where } a = 1350mm \text{ (shear span)}$$

From tables 3 and 4 the obtained ratio ($P_u/P_{u,exp}$) for beams V1, V3 and V5 were 0.96 , 0.99 and 0.98 , respectively, which shows the good agreement between the calculated and experimental results.

Table 4. Calculated flexural strength and sectional analysis of the strengthened beams

| Beam | $A_f$ (mm$^2$) | $d_f$ (mm) | $E_f$ (GPa) | $x_p$ (mm) | $\varepsilon'_s$ (‰) | $\varepsilon_{c,r}$ (‰) | $\varepsilon_{s,r}$ (‰) | $\varepsilon_f$ (‰) | $\varepsilon_c$ (‰) | $\varepsilon_s$ (‰) | $M_u$ (kN.m) | $P_u$ (kN) |
|---|---|---|---|---|---|---|---|---|---|---|---|---|
| V1 | 120 | 450.6 | 165 | 123 | 2.05 | 1.88 | 4.54 | 5.00 | 2.63 | 6.24 | 181.5 | 134.5 |
| V3 | 180 | 450.6 | 165 | 125 | 2.07 | 1.90 | 4.80 | 5.00 | 2.64 | 6.23 | 201.0 | 148.9 |
| V5 | 180<br>120 | 450.6<br>425.0 | 165 | 151 | 2.75 | 2.52 | 4.52 | 5.00<br>4.57 | 3.27 | 6.26 | 219.2 | 162.4 |

*Based on experimental steel yield strength*

## SHEAR ANALYSIS OF THE STRENGTHENED BEAMS

To calculate the shear strength of the strengthened beams, the general truss model was adopted with the concrete contribution to the shear strength $V_c$ included thus,

$$V_R = V_s + V_f + V_c \tag{7}$$

Considering the case of vertical internal stirrups, inclined external CFRP laminates glued at an angle $\alpha$ to the beam axis and a compressive strut angle of $45^0$, from the truss model analysis equation 7 takes the form

$$V_R = \frac{A_{sw} \cdot f_{yw}}{s} z + \frac{2A_f \cdot \sigma_{fw}}{s_f} z(1 + \cot\alpha) sin\alpha + V_c \tag{8}$$

For vertical CFRP laminates equation 8 reduces to

$$V_R = \frac{A_{sw} \cdot f_{ywr}}{s} z + \frac{2A_f \cdot \sigma_{fw}}{s_f} z + V_c \tag{9}$$

and for CFRP inclined at $45^0$ it becomes

$$V_R = \frac{A_{sw} \cdot f_{ywr}}{s} z + \frac{2A_f \cdot \sigma_{fw}}{s_f} z\sqrt{2} + V_c \tag{10}$$

where $V_s$ = shear resisted by the internal stirrups according to the truss model;

$V_f$ = is the shear resisted by the CFRP according to the truss model;

$A_f$ = area of the CFRP shear links;

$s_f$ = spacing of the CFRP shear links;

$\sigma_{fw}$ = stress in the CFRP shear links;

The value of the concrete contribution to the beam shear strength ($V_c$) used here is adopted in accordance with the Brazilian code of practice NBR 6118; $V_c$ is a function of the flexural steel ratio and the square root of the compressive cylinder strength of the concrete.

The CFRP laminate contribution to the shear strength ($\sigma_{fw}$) in the previous equations, as explained in the flexural analysis, is limited either by debonding of the CFRP laminate or tearing off the concrete cover that sustain the CFRP laminate, so

a) From the limit of $\varepsilon_f \leq 5‰$ to the fibre deformation associated with debonding mode of failure,

$$\sigma_{fw,\lim} = \varepsilon_f E_f = 0.005 E_f \tag{11a}$$

b) From the limit of $\tau_{lim} = 0.45 f_t$ to the shear stress at the concrete cover associated with tearing off mode of failure,

$$\sigma_{fw,\lim} = \frac{\tau_{\lim} \cdot h_f \cdot b_f}{2 \cdot e_f \cdot b_f} = \frac{\tau_{\lim} \cdot h_f}{2 \cdot e_f} \tag{11b}$$

In which $h_f$ is the height of the CFRP laminate.

When end fixings are present, it is assumed that the contact area which resists the tearing off shear is enhanced by a length on each side of the shear link equal to the cross laminate width ($b_f$) and, hence, equation 11b takes the form

$$\sigma_{fw,\lim} = \frac{\tau_{\lim} \cdot \left( \frac{h_f}{2} + 2 \cdot b_f \right) \cdot b_f}{e_f \cdot b_f} = \frac{\tau_{\lim} \cdot \left( h_f + 4 \cdot b_f \right)}{2 \cdot e_f} \tag{11c}$$

Table 5 gives the estimated shear strength of the strengthened beams based on the proposed procedure. From tables 3 and 5, for beam V2 that failed by tearing off the concrete cover the ratio ($P_u/P_{u,exp}$) was found to be 0.96, which also shows the good agreement between the calculated and experimental values.

Table 5. Calculated shear strengths of the strengthened beams

| Beam | Shear Strength (Vc) as in NBR 6118/80 | | | | | |
|---|---|---|---|---|---|---|
| | | | Vertical CFRP | | Inclined CFRP | |
| | $V_s$ (kN) | $V_c$ (kN) | $V_f$ (kN) | $V_R$ (kN) | $V_f$ (kN) | $V_R$ (kN) |
| V2 | 48 | 52 | 55 | 155 | 77 | 177 |
| V4 | 48 | 54 | 82 | 184 | 115 | 217 |
| V5 | 52 | 43 | 82 | 178 | 115 | 210 |

## CONCLUSIONS

From the results of the current test program, it was possible to detect two modes of failure for beams strengthened in flexure and in shear using CFRP laminates. In addition, calculation models were proposed to estimate the ultimate strengths of the strengthened beams.

The first mode of failure was by debonding of the CFRP laminate when the deformation attained a value of 5‰. The second mode was the tearing off the concrete cover that bonded the CFRP laminate when the shear stress in the concrete cover reached its strength value.

Two values for this strength were proposed depending on the region, i.e. the beam sides or beam bottom face.

The calculated strengths of the beams on the basis of the proposed procedure compared well with the test results and indicated the validity of the models used.

**ACKNOWLEDGEMENT**
The authors would like to thank SIKA S.A. (Brazilian branch) for the support given through out this research program, and the Brazilian Government Research Agencies CAPES and CNPq for financing this project.

**REFERENCES**

1. Brazilian Code of Practice for Project and Execution of RC Structures (1980) "ASSOCAÇÃO BRASILEIRA DE NORMAS TÉCNICAS (ABNT), NBR-6118 - *Projeto e Execução de Obras de Concerto Armado – Procedimento*", available only in Portuguese. Brazil, pp.76.
2. CERQUEIRA , ELIETE. DA CONCEIÇÃO (2000) – Shear strengthening of RC beams using CFRP - "*Reforço ao cisalhamento de Vigas de Concreto Armado com fibras de carbono.*" – M.Sc. thesis., only available in Portuguese, COPPE/UFRJ, Rio de Janeiro, Brazil, 2000.
3. PINTO , CRISTINA T.P. (2000) – Flexural strengthening of RC beams using CFRP - "*Reforço à flexão de Vigas de Concreto Armado com fibras de carbono.*" – M.Sc. thesis., only available in Portuguese, COPPE/UFRJ, Rio de Janeiro, Brazil, 2000.

# Concrete Beams Strengthened with Near Surface Mounted CFRP Laminates

BJÖRN TÄLJSTEN and ANDERS CAROLIN
Department of Civil Engineering, Luleå University of Technology, Sweden

**Abstract**

All over the world there are structures intended for living and transportation. The structures are of varying quality and function, but they are all ageing and deteriorating over time. Of the structures needed in 20 years from now about 85-90 % of these are already built. Some of these structures will need to be replaced since they are in such a bad condition. It is not only deterioration processes that make upgrading necessary, errors may have been made during the design or construction phase so that the structure needs to be strengthened before it can be used. New and increased demands from the transportation sector can be another reason for strengthening. If any of these situations should arise it needs to be determined whether it is more economical to strengthen the existing structure or to replace it. A strengthening method that has been increasingly used the last decade is Plate Bonding with FRP materials. This technique may be defined as one which a composite plate or sheet of relatively small thickness is bonded with an epoxy adhesive to in most cases a concrete structure to improve its structural behaviour and strength. The sheets or plates do not require much space and give a composite action between the adherents. Extensive research and laboratory testing have been carried out all over the world and at many different locations. These investigations show that the method is very effective and a considerably strengthening effect can be achieved.

However, plate bonding with laminates or fabrics placed on a structure outside has its drawbacks. One of these is that they are relatively unprotected against wear and impact loads. Another drawback is the environmental effect, i.e. moisture, temperature and freeze-thaw can affect the strengthening material in an unwanted way. Nevertheless, some of these drawbacks can be overcome if the laminates could be placed inside the structure or at least near the surface of it.

This paper presents laboratory tests and theory for strengthening concrete beams with near surface mounted CFRP laminates. Slots have been sawn up in the soffit of the beams and the laminates have been bonded with epoxy and cement grout in these slots. The results from these tests are very interesting and show that, compared to laminate bonding to the outside of the structure, better utilisation of the CFRP material. However, different failure modes between the epoxy bonded laminates and the cementisous bonded could be noticed with a better bond in the slot for the epoxy bonded.

*FRPRCS-5*, Thomas Telford, London, 2001.

## Introduction

Over the past decade, the issue of deteriorating infrastructure has become a topic of critical importance in Europe, and to an equal extent in the United States and Japan. The deterioration of decks, superstructure elements and columns can be traced to reasons ranging from ageing and environmentally induced degradation to poor initial construction and lack of maintenance. Added to the problems of deterioration, are the issues related to the needs for higher load ratings and increased the number of lanes to accommodate the ever-increasing traffic flow on the major arteries. As an overall result, a significant portion of our infrastructure is currently either structurally or functionally deficient. Beyond the costs and visible consequences associated with continuos retrofit and repair of such structural components, are the real consequences related to losses in production and overall economics related to time and resources caused by delays and detours. As we prepare for the twenty-first century, the renewal of our lifelines becomes a critical issue. To keep a structure at the same performance level it needs to be maintained at predestined time intervals. If the lack of maintenance has lowered the performance level of the structure need for repair up to the original performance level can be required. In cases when higher performance levels are needed upgrading may be necessary. With the performance level mean load carrying capacity, durability, function or aesthetic appearance. Upgrading refers to strengthening, increased durability, a change of function or improved aesthetic appearance. In this paper strengthening is discussed. The cheapest and the easiest way can be an administrative upgrading where refined calculation methods are used in connection with exact material parameters to show that the existing structure has a higher load-carrying capacity than what has earlier been assumed (Carolin 1999).

The introduction of fibre reinforced polymers (FRPs) in civil engineering structures has progressed at a very rapid rate in recent years. These high-performance materials have unique properties that make them extremely attractive for a wide range of structural applications. The basic ideas relative to the use of FRPs for structural strengthening, along with examples of application, have been presented by (Triantafillou, 1998). The past and potential future use of FRP strengthening and rehabilitation have also recently been documented in many conference proceedings (Meier and Betti, 1997), (Täljsten, 1997), (Benmokrane and Rahman, 1998), keynote lectures (Maruyama, 1997), (Neale and (Labossiére, 1997) and journal articles (Thomas, 1998), (Humar and Razaqpur, 2000) . The rapidly expanding body of literature in this area, along with the corresponding increase in level of activity, confirms that these new materials are progressively gaining wider acceptance by the civil engineering community.

At Luleå University of Technology, Division of Structural Engineering, research is taking place in the field of CFRP – Strengthening. The research work started in 1988, then with steel plates. Both comprehensive experimental and theoretical work has been undertaken in this field since then. Some of these works are reported in (Täljsten, 1994, 1996, 1997, 1998, 1999, 2000). The laboratory tests include strengthening for bending as well as for shear and torsion. In addition several full-scale tests have been undertaken. Sweden and the Swedish authorities have also accepted FRP strengthening and today Swedish code exists for these types of strengthening works.

There exists a number of methods to strengthen concrete structures. The three most common techniques are additional steel reinforcement covered by concrete, post-tensioning and plate bonding. All these methods have advantages and disadvantages that makes them more or less suitable for different strengthening applications. Plate bonding is the most novel method and has shown to be an effective and economic tool for strengthening concrete structures (Carolin, 1999).

One of the advantages with plate bonding is its possibilities of being used for many geometrical shapes. Another advantage of plate bonding is that the method can be applied on structures with dynamic loads during the work (Täljsten and Carolin, 1999) Further the method doesn't change the frequency or the architecture of the structure. A disadvantage with plate bonding is that it is sensitive to impacts, fire and other environmental effects since the laminate or fabric is placed outside and unprotected on the surface of the structure. Precluding this happening the composite can be inserted into the concrete cover in specially sawed slots or grooves, see figure 1. This method is called NSMR (Near Surface Mounted Reinforcement).

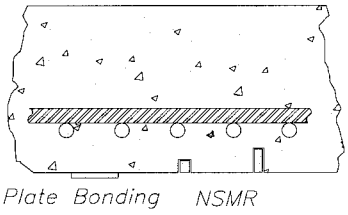



Figure 1 Plate bonding vs. NSMR (Near Surface Mounted Reinforcement)

For plate bonding the surface needs to be treated so that the aggregates will be exposed and all concrete latiance is removed. If the surface is plan enough sandblasting can be satisfactory, however, if the surface has bigger irregularities, from form work for instance, the surface then needs more powerful treatment, for example grinding. Whichever method chosen, the work will be time consuming and costly. For NSMR only slots need to be sawn up in the concrete cover of the surface. However, a drawback with this is that the placement of the NSMR is dependent on the concrete cover. For very thin concrete covers the method will unlikely be possible without damaging the existing steel reinforcement.

The idea of NSRM presented in this paper is to insert the added reinforcement into sawed slots in the concrete cover. By doing this the fragile composite will be protected from outer damage. Further, the pretreatment for this procedure is less time consuming compared to conventional plate bonding. The insertion of the laminates should also vouch for a better quality since it is not as dependent on the worker's skills. The bond surface will also increase compared to plate bonding which most likely gives a higher strengthening capacity. However, since the methods only have been used in limited extent for structures all benefits and drawbacks are not fully outlined yet. Another idea that came up during the planning of the tests was to investigate the possibility of replacing epoxy as the bond medium with mineral based adhesives such as cement grout. The reason for this is that an environmental argument has been going on for several of years regarding the harm of epoxy on man and that it would be beneficial if the epoxy had been replaced.

## Research significance

If NSMR could be used easier field applications would be possible. A higher strengthening effect also would be possible to achieve in comparison with traditional plate bonding. Furthermore better force transfer in the anchorage zone can be expected. It is important that this area is thoroughly investigated before it is applied in a full extent in field.

**Theoretical work**

For beams subjected to bending there exists models based on the Bernoulli's hypothesis. Similar equations have later been derived for beams strengthen with FRP's. The model derived by (Täljsten, 1999), do consider the anisotropy of the composite material. This model is also accepted by the Swedish Road Administration to be used for strengthening their bridges with FRP's. Without considering the anchorage, the equations for NSMR would be the same except that the internal level arm for the added reinforcement will be smaller than in the case with surface plate bonding. The principles for strengthening in bending are shown in Figure 2. It is important to notice that if there exists a strain field on the structure due to for example the dead load this must be considered in design for strengthening. In Figure 2b) this is shown schematically, where $\varepsilon_{u0}$ is the initial strain in the bottom face of the cross section. The influence of the creep in the concrete is taken care of with a reduced modulus of elasticity as in normal concrete design. A calculation is then made to control if the concrete is uncracked or not. The studied section can be consider uncracked if the tensile capacity of the concrete is not exceeded.

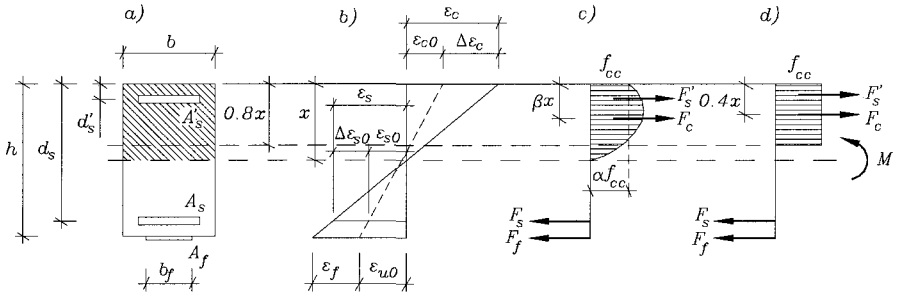



Figure 2 Principles for strengthening in bending

The next step is to calculate the stresses over the cross section. First are the stresses at the top and bottom of the studied cross section calculated, then in the steel reinforcement. The strains can easily be calculated from the stresses by Hooke's law. However, if the calculations show that the cross section is cracked new calculations are needed. A first estimation for the necessary area of the fibre composite material to increase the bending moment can be made with:

$$M = A_s' f_{st}'\left(0.4x - d_s'\right) + A_s f_{st}\left(d_s - 0.4x\right) + \mu\varepsilon_f E_f A_f\left(h - 0.4x\right) \qquad (1)$$

However, if the type of failure that can occur is assumed to be failure in the composite material without yielding in the compressive reinforcement, the bending capacity can then be expressed as, see also Täljsten, 2000:

$$M = \frac{x - d_s'}{h - x}\left(\varepsilon_{fu} + \varepsilon_{uo}\right)A_s' E_s\left(0.4x - d_s'\right) + A_s f_s\left(d_s - 0.4x\right) + \mu\varepsilon_{fu} E_f A_f\left(h - 0.4x\right) \qquad (2)$$

a horizontal equilibrium equation for the section in Figure 2d) gives:

$$0.8 f_{cc} bx + \frac{x - d_s'}{h - x}\left(\varepsilon_{fu} + \varepsilon_{u0}\right)A_s' E_s = A_s f_s + \mu\varepsilon_{fu} E_f A_f \qquad (3)$$

where $x$ can be solved with an equation of the second degree:

$$C_1 x^2 + C_2 x + C_3 = 0 \tag{4}$$

there

$$\left.\begin{aligned} C_1 &= 0.8 f_{cc} b \\ C_2 &= -0.8 f_{cc} bh - (\varepsilon_{fu} + \varepsilon_{u0}) A_s' E_s - A_s f_s - \mu \varepsilon_{fu} E_f A_f \\ C_3 &= (\varepsilon_{fu} + \varepsilon_{u0}) A_s' E_s d_s' + (A_s f_s + \mu \varepsilon_{fu} E_f A_f) h \end{aligned}\right\} \tag{5}$$

Anchorage is not covered in the above equations. However, the anchorage should be better for inserted reinforcement compared to surface bonded reinforcement, but will most likely be dependent on the geometry of the rod, see figure 3. Also if the rods are placed too close to each other failure can occur by interaction. No investigations regarding the anchorage are reported in this paper.

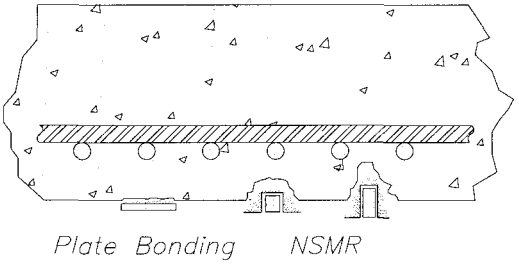



Figure 3 For NSMR the anchorage situation is likely to be dependent on rod geometry and differernt crack paths can be expected.

**Experimental work**

To investigate the strengthening effect for NSMR four beams were manufactured, three were strengthened and one served as a control beam. The geometry and loading conditions is shown in figure 4. Slots for the additional reinforcement were sawn on the tension side of the beams, see figure 5.

The beams were loaded in four point bending in deformation controlled mode. The load was applied with a head displacement of 0.6 mm/min. Applied load, deflections and strains were recorded for during the test. Also the crack distribution was recorded, this for every 10 kN step. The material data for the tests specimens can be found in table 1. The NSMR laminates were manufactured by vacuum infusion at SICOMP AB and measurement after test has shown a fibre content of 50 % in the laminates. For the laminates vinylester 411 C50 was used for the matrix and to bond the laminate to the concrete beam the epoxy adhesive BPE 417 manufactured by Nils Malmgren AB was used. The cement grout used for bonding Beam C3 was BEMIX High Tech 310. However, before these laminates were bonded to the beam the surface was pre-treated by gluing quarts sand to it. This to increase the bond properties for the laminate.

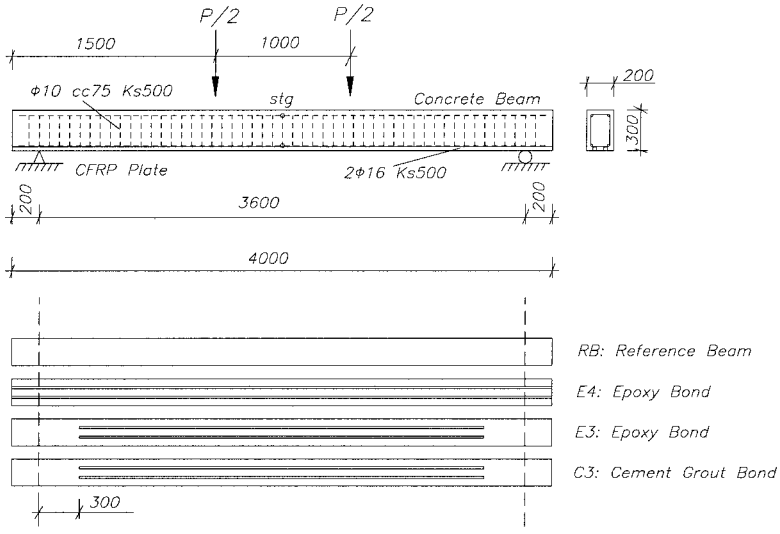



Figure 4 Test set up and dimensions of the test beams.

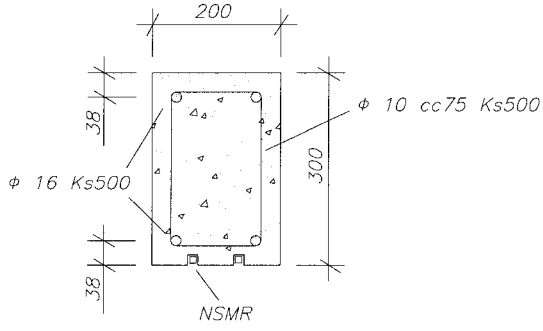



Figure 5 Cross-section of the beams

Table 1 Material data

| | $f_{cc}$ [MPa] | $f_{ct}$ [MPa] | $f_{st}$ [Mpa] | $E_s$ [GPa] | $f_{cu}$ [MPa] | $E_f$ [GPa] | $\varepsilon_{fu}$ [%] |
|---|---|---|---|---|---|---|---|
| Concrete | 60.7 | 3.6 | | | | | |
| Steel | | | 490 | 200 | | | |
| Carbon Fibre | | | | | 4140 | 230 | 1.8 |

**Results from tests**

The results from the tests are presented in figure 6 and in table 2. In figure 6 the load-deflection curves can be seen. Beam C3 is the beam where the carbon fibre laminate has been bonded with cement grout in the slot. For Beam E3 and E4 a low viscosity epoxy adhesive has been used as the bond medium. It can clearly be noticed in figure 6 that Beam B4, as expected, has the best failure envelope. Beam E3 and Beam C3 follows each other up to the level where an anchorage failure arises in the cement grout for Beam C3.

Cracks in parallel to the laminates appeared and while the load increased the mortar started to fall down from the beam. Also for Beam E3 an anchor failure occurred, however more ductile behaviour could be noticed compared to Beam C3 and the failure load was also somewhat higher. Finally Beam 4 reached failure due to failure in the laminate in the centre of the beam. The failure arose quite suddenly and in a brittle mode. In table 2 the ultimate load and deflections are given.

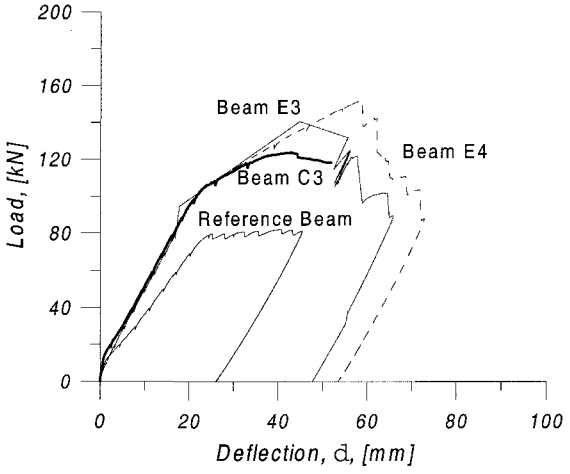



Figure 6 Load- deflection curves for the tested beams.

Table 2 Results from tests

| Beam | $P_{test}$ [kN] | $d_{test}$ [mm] | $\varepsilon_{fc}$ [%] |
|---|---|---|---|
| C3 | 123.5 | 43.0 | 0.74 |
| E3 | 140.0 | 51.5 | 1.12 |
| E4 | 152.0 | 58.5 | 1.15 |
| Reference | 79.0 | 24.0 | --- |

Theoretical calculations of the load capacity for the tests were also done, the results from these calculations are shown in table 3. In table 3 the measured strains at failure for the laminates have been used for calculating the theoretical failure loads.

Table 3 Theoretical calculation compared with load at failure

| Beam | $P_{test}$ [kN] | $P_{theory}$ [mm] | $P_{test}/P_{theory}$ |
|---|---|---|---|
| C3 | 123.5 | 149.3 | 0.83 |
| E3 | 140.0 | 167.7 | 0.83 |
| E4 | 152.0 | 196.3 | 0.77 |
| Reference | 79.0 | --- | --- |

It can be noticed in table 3 that the theory described earlier in this paper overestimates the failure load. The reasons for this can be numerous. For Beams C3 and E4 where we had anchorage failure, the theory described in this paper will not cover this. However, for beam E4, higher failure load was expected, but it is possible that the strain in the utmost fibres was unevenly distributed, exceeding the ultimate strain capacity and that a propagating failure arose for the tests beam not covered for in the measurements.

## Further work

The performed pilot study was considered successful. Good strengthening effects could be achieved both when cement grout and when epoxy was used as a bond medium. However, there are still many questions regarding this strengthening technique and a comprehensive study in this field is planned during 2001. In this study several different grades of carbon fibre laminates will be used. Furthermore the anchorage lengths will be varied and tests with different cement grout will be investigated.

## Conclusions

From the performed field test it is confirmed that it is fully possible to strengthen concrete structures with NSMR. From experience in field and laboratory it is many times much easier and faster to apply this method for strengthening compared with traditional plate bonding. The performed pilot tests in this test series showed that a considerably strengthening effect could be achieved together with quite ductile behaviour and large deformations at failure. The test with cement grout is of particular interest even though it did not perform best in the presented test series. However, if epoxy can be replaced with cement grout the work environment on site will be improved considerably.

A comparison between the theory and test gives that the theory somewhat overestimates the ultimate load at failure. There can be many reasons for this and deeper investigations in this area are planned.

Finally more tests are needed to clarify the force transfer from the concrete to the laminate and a deeper study should be put into the use of cement as a bond medium. Efforts also should be placed to theoretical studies.

## Acknowledgement

Financial support has been provided by the Swedish Building and Development Fund and Skanska AB. For help with the laboratory tests special attention should be given to Håkan Johansson and Georg Danielsson at TESTLAB, Luleå University of Technology. Last but not least the student Johannes Sichelschmidt from Germany should be thanked for his never ending energy working with this project.

**References**

Benmokrane B. And Rahman H. Eds., 1998, Durability of fibre reinforced polymer (FRP) composites for construction, Department of Civil Engineering, Université de Sherbrooke, 1998.

Carolin, A., 1999, *"Improvement of the Load-Bearing Capacity of Existing Bridges – a Review of Literature"*, Technical Report, Luleå: Luleå University of Technology, Division of Structural Engineering, 1999:19, ISSN 1402-1536, 1999, p. 21.

Humar J. and Razaqpur A.G., edt., 2000, *Advanced Composite Materials in Bridges and Structures*, Conference Proceedings ACMBS III, Ottowa Canada, 2000, p 876.

Maruyama K., 1997, *JCI activities on continuous fibre reinforced concrete, Non-Metallic (FRP) Reinforcement for Concrete Structures*, Japan Concrete Institute, pp 3-12, 1997.

Meier U. And Betti R. Eds., 1997, *Recent advances in bridge engineering – Advanced Rehabilitation, durable materials, non-destructive evaluation and management.* EMPA Switzerland, 1997.

Neale KW. And Labossiére P., 1997, *State-of-the-art report on retrofitting and strengthening by continous fibre in Canada*, Non-Metallic (FRP) Reinforcement for Concrete Structures, Japan Concrete Institute, 1997, pp 25-39.

Thomas J., 1998, *FRP strengthening – Experimental or mainstream technology?,* Concrete International, ACI, 1998, pp57-58.

Triantafillou T.C., 1998, *Strengthening of Structures with advanced FRPs. Progress in Structural Engineering and Materials*, No. 1, 1998, pp 126 – 134.

Täljsten B., 1994, *Plate Bonding, Strengthening of Existing Concrete Structurers with Epoxy Bonded Plates of Steel or Fibre reinforced Plastics*, Doctoral Thesis 1994:152D, Div. of Structural Engineering, Luleå University of Technology, ISSN 0348 – 8373, 1994, p 308.

Täljsten B., 1996, *Strengthening of concrete prisms using the plate-bonding technique*, International Journal of Fracture 82, Kluwer Academic Publishers, Printed in the Netherlands, 1996, pp 253-266..

Täljsten B., 1997, *Strengthen of Concrete Structures, From Steel Plates to Carbon Fibre Reinforced Plastic*, FIP 97, The Concrete Way to Development, International Conference, South Africa, Johannesburg, March 1997, p 12.

Täljsten B., 1997, *Strengthening of concrete structures for shear with bonded CFRP-fabrics*, Recent advances in bridge engineering, Advanced rehabilitation, durable materials, nondestructive evaluation and mangement, Eds. U. Meier and R. Bettid, Dubendorf July 1997, pp 57-64.

Täljsten B., 1997, *Strengthening of Beams by Plate Bonding,* Journal of Materials in Civil Engineering, November 1997, pp. 206-212.

Täljsten B., 1997, *Defining anchor lengths of steel and CFRP plates bonded to concrete*, Int. J. Adhesion and AdhesivesVolume 17, Number 4, 1997, pp 319-327.

Täljsten B., 1998, *Strengthening of Concrete Structures for Shear with CFRP-fabrics, Test and Theory*, Int. Conf: in Tromsö, Norway, Concrete under severe conditions, Edited by O.E. Gjörv, K. Sakai and N. Banthia, ISBN 0 419 23870 0, pp. 1298-1310.

Täljsten B. And carolin A., 1999, *"Strengthening of a Concrete Railway Bridge in Luleå with Carbon Fibre Reinforced Polymers – CFRP – Load bearing capacity before and after strengthening"*, Technical Report, Luleå University of Technology, Division of Structural Engineering, 1999:18, ISSN 1402-1536, 1999, p 60.

Täljsten B., 2000, *"Förstärkning av befintliga betongkonstruktioner med kolfiberväv eller kolfiberlaminat, Dimensionering, material och utförande"*, Teknisk Rapport, Luleå tekniska universitet, Avdelningen för Konstruktionsteknik, 1999:12, ISSN 1402-1536, 1999, p 122 (In Swedish).

## Notations and symbols

Roman Capital Letters

| | | |
|---|---|---|
| $A_f$ | cross section area for composite | [m$^2$] |
| $A_s$ | cross section area for tensile steel reinforcement | [m$^2$] |
| $A_s'$ | cross section area for compressive steel reinforcement | [m$^2$] |
| $C_1$ | constant | [N/m] |
| $C_2$ | constant | [N] |
| $C_3$ | constant | [Nm] |
| $E_f$ | modulus of elasticity, fibre | [Pa] |
| $E_s$ | modulus of elasticity, steel | [Pa] |
| $E_{sk}$ | modulus of elasticity, steel | [Pa] |
| $F_c$ | compressive force in concrete | [N] |
| $F_f$ | tensile force in composite | [N] |
| $F_s$ | tensile force in the tensile steel reinforcement | [N] |
| $F_s'$ | compressive force in the compressive steel reinforcement | [N] |
| $M$ | bending moment | [Nm] |
| $P$ | Load | [N] |

Roman Lower Case Letters

| | | |
|---|---|---|
| $b$ | width | [m] |
| $b_f$ | width of composite laminate | [m] |
| $d_s$ | effective depth to tensile reinforcement | [m] |
| $d_s'$ | effective depth to compressive reinforcement | [m] |
| $f_{cc}$ | compressive strength, concrete | [Pa] |
| $f_{cc}$ | tensile strength, concrete | [Pa] |
| $f_s$ | yield strength, steel reinforcement | [Pa] |
| $f_{st}$ | yield strength, steel reinforcement | [Pa] |
| $f_{yk}$ | yield strength, steel reinforcement, characteristic | [Pa] |
| $h$ | height | [m] |
| $x$ | inner lever | [m] |

Greek Lower Case Letters

| | | |
|---|---|---|
| $\beta$ | proportional factor for concrete | [--] |
| $\varepsilon_c$ | strain in concrete | [--] |
| $\Delta\varepsilon_c$ | additional strain in concrete | [--] |
| $\varepsilon_{c0}$ | compressive strain in concrete due to e.g. dead load | [--] |
| $\varepsilon_f$ | strain in fibre | [--] |
| $\varepsilon_{fc}$ | strain in composite | [--] |
| $\varepsilon_{fu}$ | ultimate strain in fibre | [--] |
| $\varepsilon_s$ | tensile strain in reinforcement | [--] |
| $\varepsilon_{s0}$ | tensile strain in reinforcement due to e.g. dead load | [--] |
| $\Delta\varepsilon_{s0}$ | additional strain in reinforcement | [--] |
| $\varepsilon_{u0}$ | strain in the bottom face due to e.g. dead load | [--] |
| $\mu$ | reduction factor | [--] |

Abbreviations

FRP: Fibre Reinforced Polymer, CFRP: Carbon Fibre Reinforced Polymer, NSMR: Near Surface Mounted Reinforcement

# Parameters Influencing the Flexural Response of RC Beams Strengthened using CFRP Sheets

A.E. NAAMAN, University of Michigan, Ann Arbor, USA
S.Y. PARK, Cheju University, Cheju, South Korea
M.M. LOPEZ, Clarkson University, Potsdam, New York, USA
R.D. TILL, Michigan Department of Transportation, Lansing, Michigan, USA

## ABSTRACT

Repair and strengthening techniques using bonded fiber reinforced polymeric (FRP) laminates (also called plates, sheets, and tow-sheets) form the basis of a new technology being increasingly used for bridges and highway superstructures.

The study described in this paper is part of a larger investigation on the use of carbon fiber reinforced polymeric (CFRP) sheets for repair and strengthening of reinforced and prestressed concrete beams. The experimental program includes four main parts: 1) tests of RC beams strengthened in bending; 2) tests of RC beams strengthened in shear; 3) freeze-thaw tests of strengthened beams followed by their test in bending; and 4) tests in bending and shear of strengthened beams under low temperature (-29° C) and high amplitude cyclic loading.

The part of the investigation dealing with reinforced concrete beams strengthened in bending is described in this paper, where the results are also analyzed and discussed. The experimental program comprised fourteen reinforced concrete T-beams. The test parameters included two levels of steel reinforcement ratio before strengthening, and up to four strengthening levels. Two commercially available strengthening systems were tested, the Sika CFRP plate system (CarboDur), and the Tonen CFRP sheet system (MBrace). Other selective parameters investigated included two different concrete covers; two conditions of cover preparation, three different end anchorage systems of the bonded sheets, and pre-loading pre-yielding of the beam prior to strengthening. Conclusions are drawn and some recommendations for design are suggested.

## MAIN OBJECTIVES

The primary objectives of this comprehensive 3-years project were: 1) to ascertain the applicability of Carbon Fiber Reinforced Plastic (CFRP) bonded laminates for repair and strengthening of reinforced concrete beams; 2) to synthesize existing knowledge and develop procedures for implementation in the field; 3) to identify key parameters to insure successful performance; and 4) to adapt this technique to the specific environmental conditions encountered in the state of Michigan. Detailed results of this investigation are described in Ref. 11 which is divided in seven volumes to reflect the various tasks of the project. It can be observed that the project included an extensive review of existing literature, strengthening in bending, strengthening in shear, freeze-thaw testing of strengthened beams, very low temperature (-29°C) testing under monotonic and fatigue loading, field specifications and designrecommendations.

*FRPRCS-5*, Thomas Telford, London, 2001.

This paper describes the key experimental results related to the parameters affecting strengthening in bending. Some of the references consulted for similar work are listed in Refs. 3 to 10, and 12 to 19.

## TEST PARAMETERS

The experimental program comprised fourteen reinforced concrete T-beams. Typical cross-section and test conditions are shown in Fig. 1. The main test parameters are summarized in Table 1. They included the existing steel reinforcement ratio before strengthening, and the strengthening level. For each steel reinforcement ratio, a control beam was tested and compared with CFRP bonded beams having different strengthening levels. The steel reinforcement ratios of the control beams were respectively $0.27\rho_{max}$ and $0.54\rho_{max}$, where the maximum reinforcement ratio, $\rho_{max}$, is defined as per the AASHTO or ACI Code [Ref. 1, 2] to represent 75% of the balanced ratio. The strengthening level (that corresponds to the number of CFRP sheets) was determined assuming the total reinforcement of steel and CFRP will not exceed the maximum reinforcement ratio allowed for the beam by the AASHTO LRFD Code, based on the assumption that the CFRP sheet will fail in tension.

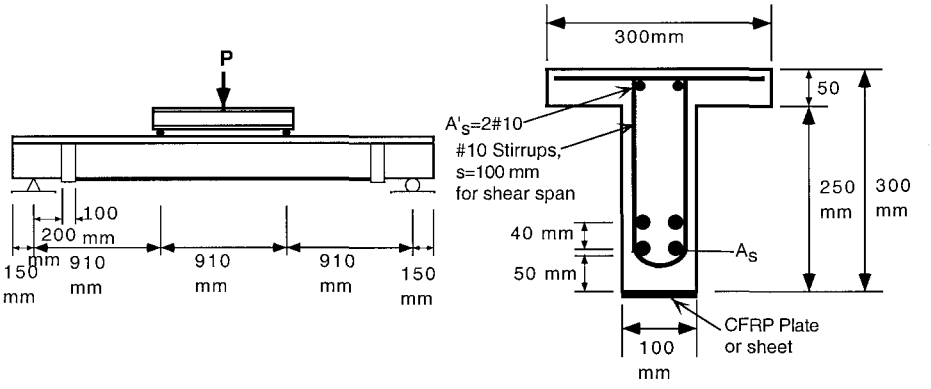



**Figure 1. Typical cross-section of beam and testing set-up**

Two strengthening systems were tested: 1) the Sika CFRP plate system (trade name CarboDur), and 2) the Tonen CFRP sheet system (trade name Mbrace Forca Tow). The Sika plate was about 1.2 mm thick and quite rigid, while the Tonen sheet was 0.11 mm thick and flexible like wall paper. The Tonen system was used for 12 beams and the Sika system for 2 beams. For Beam No. 8, the glued-on Sika CFRP plate had a width of 40 mm, which is equivalent in tensile strength to 2 layers of Tonen CFRP sheets (Mbrace sheet). Following testing, Beam No. 8 (Table 1) was in very good shape even after the interfacial shear failure of concrete. There was no spalling of concrete cover even though the reinforcing bars had yielded and the 40 mm wide CFRP plate was completely delaminated. Beam No. 8 was later re-used as Beam No. 8-1, this time with a CFRP plate 100 mm wide to evaluate a different bond width and strengthening level.

For one selected set of parameters, two different concrete covers and cover conditions were investigated to study the influence of concrete cover on strengthening effect and mode of failure. The normal clear cover of concrete was taken as 50 mm. For one beam (Beam No. 12) a concrete clear cover of 25 mm was used. Another beam (Beam No. 9) was cast with an initial 25 mm clear concrete cover; however an additional 25 mm repair mortar cover was added prior to strengthening to simulate damaged concrete in real beams.

To evaluate different anchorage systems, three different anchorage conditions were provided for beams using the Tonen system. One beam (Beam No. 10) had extended end anchorage which means that the glued-on CFRP sheets were extended up to about 50 mm from the

supports, without adding the U-shaped wrapped-around end anchorage. Another beam (Beam No. 14) had neither a U-shaped wrapped-around end anchorage nor an extended end anchorage. All other beams strengthened with Tonen sheets had, at both ends, a 100 mm wide U-shaped wrapped-around end anchorage perpendicular to the longitudinal CFRP sheets. The beams strengthened with the Sika system did not have a wrapped end anchorage.

**Table 1 Summary of test parameters of bending tests and failure mode**

| Beam No. | Test parameter | Reinforce-Ment ratio | No. of CFRP layer | Failure mode[1] |
|---|---|---|---|---|
| 1 | Steel reinforcement ratio & strengthening level (Tonen) | $0.27\rho_{max}$ | 0 | Steel yielding |
| 2 | | | 1 | CFRP rupture |
| 3 | | | 2 | Interface failure |
| 4 | | | 4 | Interface failure |
| 5 | | $0.54\rho_{max}$ | 0 | Steel yielding |
| 6 | | | 1 | Interface failure |
| 7 | | | 2 | Interface failure |
| 8 | Different system (Sika) | $0.54\rho_{max}$ | 40mm | Interface failure |
| 8-1 | | | 100 mm | Interface failure |
| 9 | Repaired concrete cover | | 2 | Interface bond failure |
| 10 | Extended end anchorage | | | Interface failure |
| 11 | Pre-loading | | | Inter-laminar failure |
| 12 | Concrete cover depth | | | Interface failure |
| 13 | Cleaned surface | | | Interface failure |
| 14 | No anchorage | | | Interface failure |

1: Steel yielding: Compression failure of top concrete long after reinforcement yielding
CFRP rupture: Tensile failure of CFRP sheet
Interface failure: Interfacial shear failure of concrete just above the epoxy adhesive.
Interface bond failure: Interfacial bond failure between the repair mortar and the existing concrete
Inter-laminar failure: Inter-laminar shear failure between glued-on CFRP sheets

One beam (Beam No. 11) was pre-loaded slightly beyond yielding of steel reinforcing bars to investigate the influence of loading history before the application of CFRP plate. The permanent deflection and maximum crack width at unloading in the pre-cracked beam were 25 mm and 0.9 mm, respectively. The beam was then strengthened with CFRP and tested.

For all beams except one (Beam No. 13), the concrete surface to be glued on was prepared, for better bond, by grinding with a disk grinder according to the recommendations of the supplier of the strengthening system used. For Beam No. 13, the surface of concrete was simply cleaned with a vacuum cleaner and wiped with a clean cloth to remove any dust. It was left to dry prior to CFRP application.

**Strengthening Level and Strengthening Ratio**

For the Tonen thin sheet system, the term "different strengthening level" refers to a different number of CFRP sheets used, such as one, two, or four. For the Sika system (thicker plate laminate), a "different strengthening level" implied different widths of the CFRP plate used.

The strengthening ratio of a beam is defined as the increment of nominal bending resistance induced by strengthening to the nominal bending resistance of the control beam. The ratio can be based on analysis or experimental observation and is defined accordingly when used.

## EXPERIMENTAL OBSERVATIONS

1. Reinforced concrete beams strengthened in bending with CFRP laminates generally fail by interfacial shear failure (delamination) that occurs within the concrete, instead of by tensile failure of the CFRP sheet or plate (Table 1). Most often, after failure of the CFRP, the beam retains its capacity based on conventional reinforced concrete behavior; however, it is likely to loose the integrity of its concrete cover to the first layer of reinforcement and will suffer related consequences (Fig. 2).

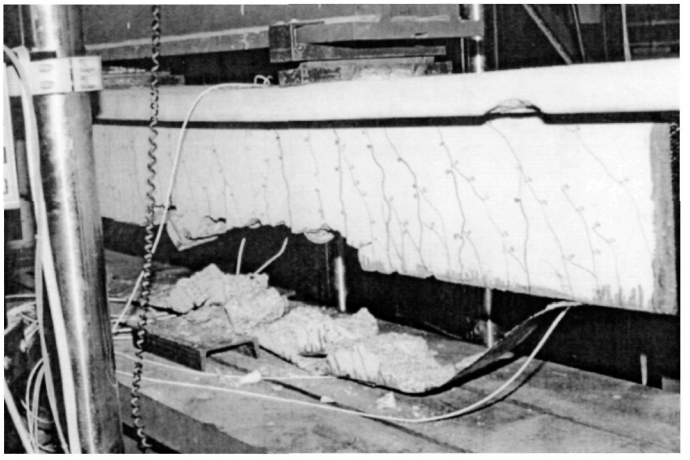


**Figure 2. Interfacial shear failure of concrete and spalling of concrete cover (tooth type failure) in Beam No. 3**

2. For a given reinforcement ratio, the ultimate load capacity increases with the strengthening level, or the number of CFRP sheets, while the ultimate deflection decreases implying smaller ductility (Figs. 3-5). However, the strengthened beams had, after failure or delamination of the CFRP sheets, a minimum loading capacity and ductility which were almost same as those of the control beam.

3. The lower the reinforcement ratio, the higher the strengthening effect in terms of percent increase in ultimate load capacity (Fig. 6).

4. Figure 7 illustrates the predicted strengthening ratio using strain compatibility analysis and equilibrium similarly to a conventional reinforced concrete beam, assuming that failure does not occur by interlaminar shear but instead by failure of the concrete in compression or CFRP reinforcement in tension. It can be observed that predicted values can be significantly larger than experimental values implying that additional failure criteria (such as interface shear failure, or cover tooth failure) should be considered in the design of these structural systems.

5. Beams using the strengthening system with CFRP plate (Sika system) showed similar load versus deflection response as beams using the strengthening system with CFRP sheet (Tonen system), even though the tensile modulus of the CFRP plate was two thirds that of the CFRP sheet (Fig. 8). In this investigation where non-trained personnel (students) was involved, it was found that the system using CFRP plate is easier and more convenient to apply for flexural strengthening than that using the CFRP sheet.

6. The strengthened beam with a smaller concrete cover had similar ultimate load and slightly larger ultimate deflection than its similar sister beam but with normal concrete cover (Fig. 9).

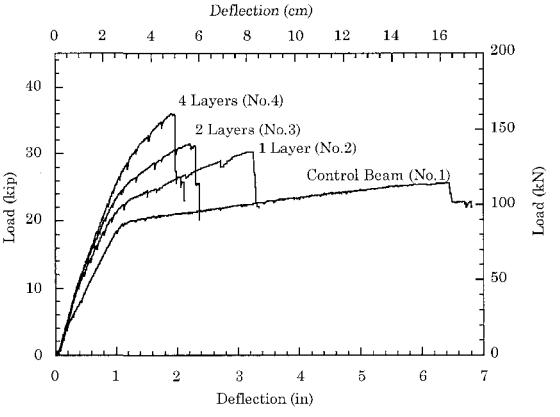



**Figure 3. Load-deflection curves of RC beams with reinforcement ratio, $0.27\rho_{max}$, at three different strengthening levels (MBrace system)**

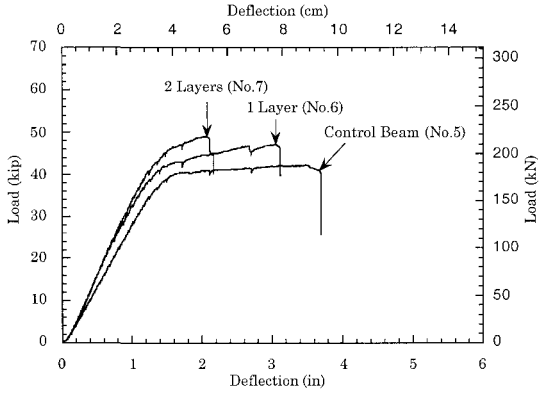



**Figure 4. Load-deflection curves of RC beams with reinforcement ratio, $0.54\rho_{max}$, at two different strengthening levels (MBrace system)**

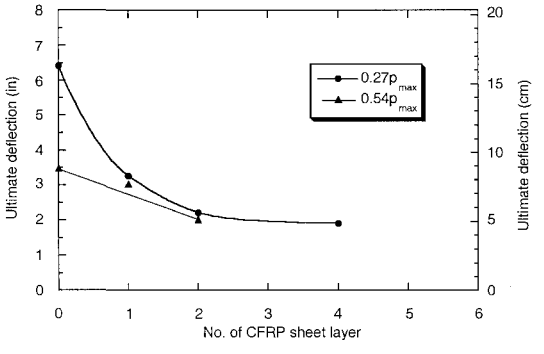



**Figure 5. Ultimate deflection versus strengthening level**

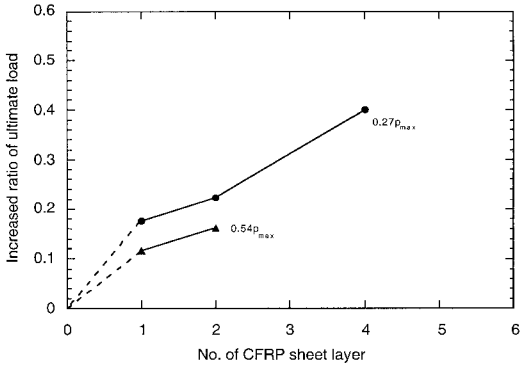



**Figure 6. Increase in ratio of ultimate load versus strengthening level, at two different reinforcement ratios**

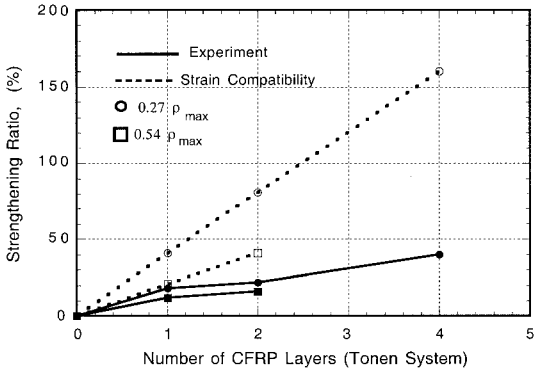



**Figure 7. Comparison of experimental and predicted increase in strengthening ratio as a percent of ultimate load of control beam, versus strengthening level or number of bonded CFRP sheets**

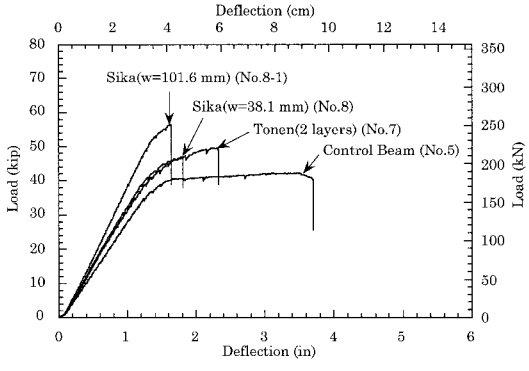



**Figure 8. Load-deflection curves of beams with two different strengthening systems**

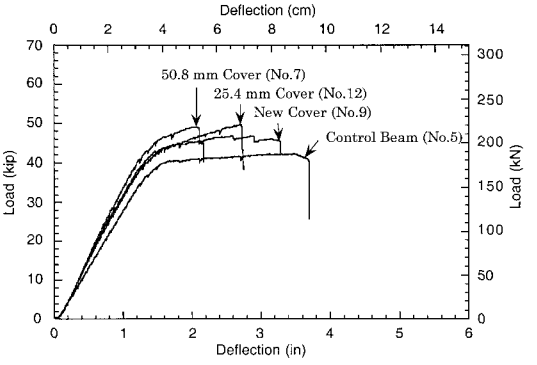



**Figure 9. Load-deflection curves of beams with different concrete cover**

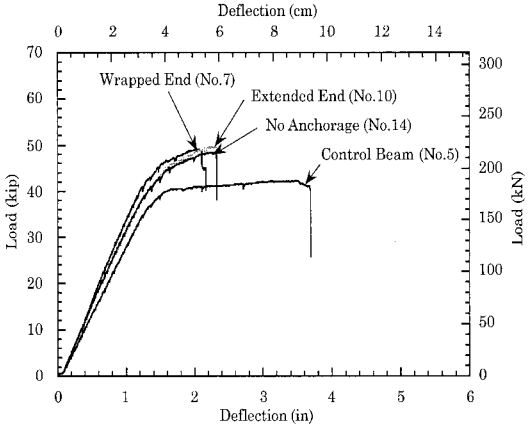



**Figure 10. Load-deflection curves of beams with different CFRP end anchorage**

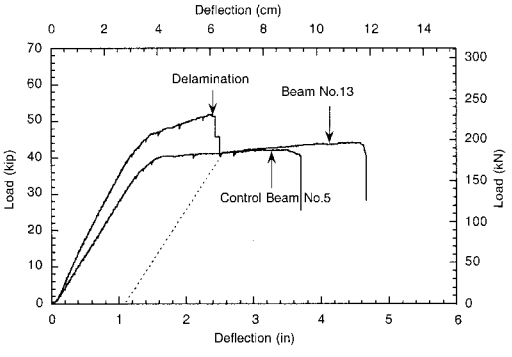



**Figure 11. Load-deflection curves of Beam No. 13 compared to that of the control beam**

7. The beam strengthened after having a repaired concrete cover, failed by gradual interlaminar debonding at the interface between existing concrete and repair mortar; it led to a ductile behavior, but did not achieve an adequate level of strengthening (Fig. 9).

8. Using a U-shaped end anchorage of the CFRP sheet did not help attain higher ultimate loads or deflections, in comparison to having no anchorage beyond the design required development length (Fig. 10). Extending the sheet up to the supports led to a very slightly higher ultimate deflection. Therefore, it seems from these limited tests, that neither a U-shaped anchorage nor an extended end anchorage justify the additional expense. Further tests are recommended to ascertain this conclusion.

9. There was no evidence that preparing the concrete surface by grinding prior to the application of CFRP sheets, was more effective than simply vacuum cleaning and wiping the surface. However this conclusion should be further confirmed in real beams with deteriorated concrete surfaces.

10. Pre-loading and pre-cracking a beam beyond reinforcement yielding had no serious influence on the strengthening effect. Therefore, the CFRP bonded strengthening technique can be applied even to severely damaged beams. Strengthening with CFRP also inhibits the growth of large cracks by helping distribute a larger number of smaller cracks; it further protects the main steel reinforcement from ingress of corrosive agents.

11. The beam that failed by CFRP sheet delamination and was damaged due to severe concrete cover spalling had, upon reloading, the same ultimate load as, and slightly larger deflection than the control beam, even though the damage to the cover was severe (Fig. 11). This fact can insure some minimum safety level for beams strengthened using CFRP sheets, should failure by delamination or tension of the sheet occur.

## CONCLUDING REMARKS

A number of design parameters were investigated in this project. However, in many cases only one specimen was tested and results with only one specimen are not definitely conclusive. The design guidelines suggested next are based on the observed results as well as the experience gained from the project.

Although numerous factors can affect the extent to which a reinforced concrete beam can be strengthened for bending using adhesively bonded CFRP laminates, it seems safe to design for increments of bending strength not exceeding about 20% of the nominal bending resistance of the beam calculated assuming a reinforcement ratio equal to $\rho_{max}$, where $\rho_{max}$ is the maximum reinforcement ratio defined in the ACI Building Code. This limitation arises from the concern that should failure occur at the interface, it will not significantly damage the concrete cover (tooth failure). A smaller concrete cover is generally better and there is no need for special anchorages beyond extending the laminate to close to the support or point of zero moment. Also, in order to comply with the code, it is necessary to keep the total reinforcement ratio or index below the maximum value recommended in the code.

In analyzing or designing a strengthened RC. beam, the design criteria should include not only equilibrium, strain compatibility and stress-strain relations of component materials, but also criteria related to the interlaminar shear resistance of the concrete both in the direction of bending and shear.

## REFERENCES

1. AASHTO LRFD Specification for Highway Bridge Design, *American Association of State Highway and Transportation Officials,* Washington, D.C., 1995.
2. ACI Committee 318, Building Code Requirements for Reinforced Concrete and Commentary, ACI 318R-95, American Concrete Institute, Farmington Hills, 1995.
3. ACI Committee 440, "State-of-the-art Report on Fiber Reinforced Plastic (FRP) Reinforcement for Concrete Structures". ACI Committee 440, 1996.

4. Arduini, M., and Nanni, A.,(1997). "Behavior of Pre-Cracked RC Beams Strengthened with Carbon FRP Sheets," Journal of Composites for Construction, Vol. 1, No. 2, ASCE, May 1997.
5. Chajes, M., Thomson, T.A., and Tarantino, B., (1995), "Reinforcement of Concrete Structures Using Externally Bonded Composite Materials," in Non-Metallic Reinforcement for Concrete Structures, L. Taerwe, Editor, RILEM, published by E. & FN Spon.
6. Chajes M.J., Thomson T.A., Januszka T.F., Finch W.W., "Flexural Strengthening Of Concrete Beams Using Externally Bonded Composite Materials". 1994.
7. Ganga Rao, H.V.S., and Vijay, P.V., (1998). "Bending Behavior of Concrete Beams Wrapped with Carbon Fabrics," Journal of Structural Engineering, Vol. 124, No. 1, 1998.
8. Kobayashi A., Ohori N., Kuroda H., "Repair and Reinforcement of Concrete Structure With Carbon Fiber Tow Sheet", International Symposium on Non-metallic (FRP) Reinforcements for Concrete Structures, FRPCS-2, 23-25 August 1995, Ghent, Belgium.
9. Lopez, M.M., Naaman, A.E., and Till, R., "Bending Behavior of RC Beams Strengthened with CFRP Laminates and Subjected to Freeze-Thaw Cycles" Proceedings ACI 4th International Symposium on FRP Reinforcements in Reinforced Concrete Structures, FRPRCS 4, ACI October 1999, pp. 559-576.
10. Meier U., "Strengthening of Structures Using Carbon Fiber/Epoxy Composites", Construction and Building materials, Vol.9, No.6, pp.341-351, 1995.
11. Naaman, A.E., Park, S.Y., Lopez, M.M., Pinkerton, L., Stankiewicz, P., and Till, R.D., "Repair and Strengthening of Reinforced Concrete Beams Using Adhesive Bonded CFRP Laminates: Vol. 1: Summary Report; Vol. 2: Literature Review; Vol. 3: Behavior of Beams Strengthened for Bending; Vol. 4: Behavior of Beams Strengthened for Shear; Vol. 5: Behavior of Beams under Cyclic Loading at Low Temperature; Vol. 6: Behavior of Beams Subjected to Freeze-Thaw Tests; Vol. 7: Technical Specifications" University of Michigan, Department of Civil and Environmental Engineering, Report No. UMCEE 99-04, and Michigan Department of Transportation, Research Project No. RC-1372, April 1999, 310 pages.
12. Nakamura M., Sakai H., Yagi K., Tanaka T., "Experimental Studies On The Flexural Reinforcing Effect Of Carbon Fiber Sheet Bonded To Reinforced Concrete Beam", pp760-773.
13. Norris, T., Saadatmanesh H., and Ehsani M.R., (1997). "Shear and Flexural Strengthening of RC Beams with Carbon Fiber Sheets," Journal of Structural Engineering, ASCE, Vol. 123, No. 7, July 1997.
14. Ritchie Philip A., Thomas David A., Lu Le-Wu, and Connelly Guy M., "External Reinforcement of concrete Beams using Fiber Reinforced Plastics," ACI Structural journal, vol. 88, July-August 1991, pp. 490-500.
15. Saadatmanesh H., Ehsani M.R., "Fiber Composite Plates can Strengthen Beams," Concrete International, ACI, Vol. 12, No. 3, pp. 65-71.
16. Saadatmanesh H., Ehsani M.R., "RC Beams Strengthened with GFRP Plates. I: Experimental Study", Journal of Structural Engineering, Vol.117, No.11, Nov, 1991, pp.3417-3433.
17. Sharif A., Baluch M.H., "External FRP Plates to Strengthen Reinforced Concrete Beams", 1st International Conference Composites in Infrastructure, ICCI, Tucson, Arizona, January 1996, pp.814-828.
18. Taljsten, B. , 1997, "Strengthening of Beams by Plate Bonding," Journal of Materials in Civil Engineering, ASCE, November 1997, pp. 206-212.
19. Yoshizawa H., Myojo T., Okoshi M., Mizukoshi M., Kliger H.S., "Effect Of Sheet Bonding Condition On Concrete Members Having Externally Bonded Carbon Fiber Sheet", Materials for the New Millennium. Proceedings of the Fourth Materials Engineering Conference. Washington D.C. Nov. 10-14, 1996, pp.1608-1616.

# A study on tension stiffness of reinforced concrete members strengthened by carbon fiber sheet

RYUICHI YAMAGUCHI, YASUHIKO SATO and TAMON UEDA
Hokkaido University, Sapporo, Japan

## INTRODUCTION

Recently, there have been many reports concerning structures damaged by earthquakes. Reinforced concrete (RC) structures are no exception. The strengthening of RC structures against earthquakes is currently an important issue in seismic regions.

There are many methods of strengthening RC. Strengthening by Carbon Fiber Sheet (CFS) is one effective method and many studies on the shear strength and ductility of RC strengthened using CFS have been carried out. However, none of the studies pay attention to the correct prediction of the tension stiffness of RC strengthened by CFS.

The purpose of this study is to clarify the tension stiffness of RC strengthened by CFS experimentally and analytically, considering the bond properties of both CFS and steel reinforcement.

## OUTLINE OF EXPERIMENT

Two types of specimen, Type A and Type B, were prepared in this study. In order to obtain the average stress – average strain relationship of the strengthened specimens, type A specimens were used. Type B specimens were prepared to investigate the plastic length of steel around crack where no bond stress is developed ($\tau_s$ =0). The differences between the 2 types of specimens were the strain gage interval, length of test area, and strength of concrete (see Figs.1 and 2).

For both types of specimens, the cross sectional area of the concrete is 150×150 ($mm^2$). At the center of the concrete cross section, one steel bar was embedded. At the ends of the steel bar, a steel bar with a larger diameter was welded to prevent the bar from yielding at its end. CFS was attached to two opposite sides of the concrete prism. The mechanical properties of steel and CFS are shown in Tables 1 and 2 respectively.

Experiments were carried out with 8 specimens; 3 specimens of type A whose reinforcement ratio of steel was 1.27%, and 5 specimens of type B whose reinforcement ratio of steel was 0.32% or 1.72%. The details of the specimens are shown in Table 3.

*FRPRCS-5*, Thomas Telford, London, 2001.

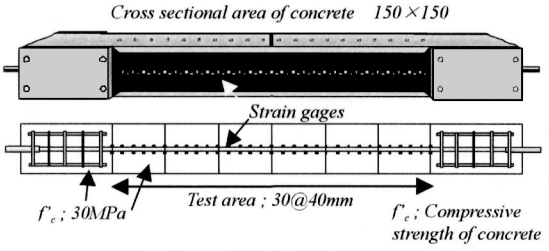



Fig.1 Type A Specimen

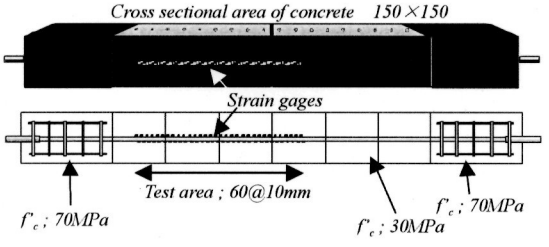



Fig.2 Type B Specimen Unit; mm

Table 1 Mechanical Properties of Steel

| Diameter of Steel | $E_s$ (GPa) | $\varepsilon_y$ (%) | $f_y$(MPa) |
|---|---|---|---|
| D10 | 188 | 0.178 | 335 |
| D19 | 172 | 0.230 | 396 |
| D22 | 178 | 0.220 | 392 |

$E_s$; Young's Modulus of Steel
$\varepsilon_y$; Yielding Strain $f_y$; Yielding Stress

Table 2 Mechanical Properties of CFS

| t (mm) | $\rho$ (g/m$^2$) | $f_t$ (Mpa) | $E_{CFS}$ (GPa) | $\varepsilon_u$(%) |
|---|---|---|---|---|
| 0.11 | 200 | 3479 | 230 | 1.50 |

t; Thickness $\rho$; Fiber Density
$f_t$; Tensile Strength
$E_{CFS}$; Young's Modulus of CFS
$\varepsilon_u$; Ultimate Strain

Table 3 Specimen Parameters

| Specimens*) | $f'_c$(MPa) | Diameter of Steel (mm) | $p_s$(%) | N | B(mm) | $P_{CFS}$(%) | Specimen Type |
|---|---|---|---|---|---|---|---|
| S-3-0 | 29.0 | 19 | 1.27 | 0 | 0 | 0 | A |
| S-3-1 | 30.6 | 19 | 1.27 | 1 | 120 | 0.12 | A |
| S-3-2 | 32.2 | 19 | 1.27 | 2 | 120 | 0.23 | A |
| S-4-1' | 31.5 | 10 | 0.32 | 1 | 150 | 0.15 | B |
| S-4-2' | 31.8 | 10 | 0.32 | 2 | 150 | 0.29 | B |
| S-4-3' | 38.2 | 10 | 0.32 | 3 | 150 | 0.44 | B |
| S-5-0 | 33.5 | 22 | 1.72 | 0 | 0 | 0 | B |
| S-5-2' | 37.8 | 22 | 1.72 | 2 | 150 | 0.29 | B |

*) S-3-1

0 ; RC 1; $p_{CFS}$=0.117% 1' ; $p_{CFS}$=0.147% 2; $p_{CFS}$=0.234% 2' ; $p_{CFS}$=0.293%
3'; $p_{CFS}$=0.440%

3 ; $p_S$=1.27% 4 ; $p_S$=0.32% 5 ; $p_S$=1.72%

$f'_c$ ; Compressive Strength of Concrete $p_s$ ; Reinforcement Ratio of Steel N ; Number of CFS Layers
B ; Bond Width of CFS $p_{CFS}$ ; Reinforcement Ratio of CFS

## OUTLINE OF ANALYSIS

The flow chart for the program used for analysis is shown in Fig.3. The stresses in the RC member strengthened by CFS, which are calculated in the analysis, are shown in Fig.2. The flow chart in Fig.3 is for the pre-yielding stage. For the post-yielding stage, additional assumptions are necessary (see next section). The analysis procedure in the pre-yielding stage is as follows:

1. Give a strain in the steel at the crack ($\varepsilon_{STEEL,0}$).
2. Assume the slip of the steel at the crack ($S_{STEEL,0}$).
3. Using the Shima Model[1], calculate the bond stress of steel ($\tau_{STEEL,0}$).
4. Using force equilibrium, calculate the stress in the steel of the next element ($\sigma_{STEEL,0}$).
   $\left(\sigma_{STEEL,1} = \sigma_{STEEL,0} - \pi \cdot D \cdot dx \cdot \tau_{STEEL,0} / A_s\right)$
   where, $D$ ; diameter of steel bar, $dx$ ; length of micro element, $A_s$ ; cross sectional area of steel bar.
5. Using the stress-strain relationship, calculate the strain in the steel of the next element ($\varepsilon_{STEEL,1}$).
6. Integrating the strain, calculate the slip of the steel in the next element ($S_{STEEL,1}$).
   $\left(S_{STEEL,1} = S_{STEEL,0} - \left(\varepsilon_{STEEL,0} + \varepsilon_{STEEL,1}\right)dx / 2\right)$
7. Steps 3 to 6 are repeated for elements to the center of concrete prism.
8. Compare the slip calculated by integrating the calculated strain ($\int \varepsilon_s dx$) with the assumed slip ($S_{STEEL,0}$). In case the two slips are not in agreement, go back to step 2 and assume the slip ($S_{STEEL,0}$) again.

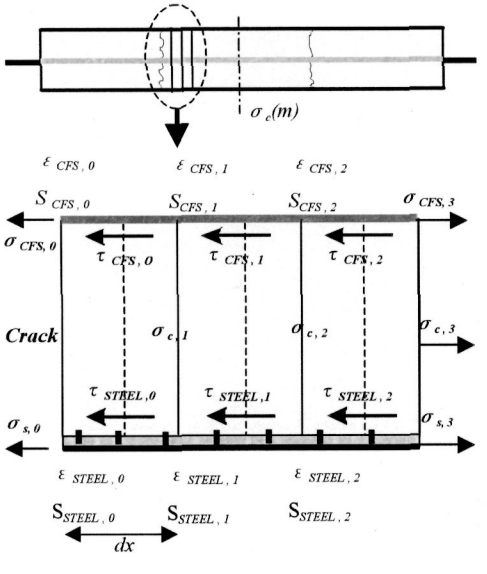



*Fig.2 Microscopic RC Member Strengthened by CFS*

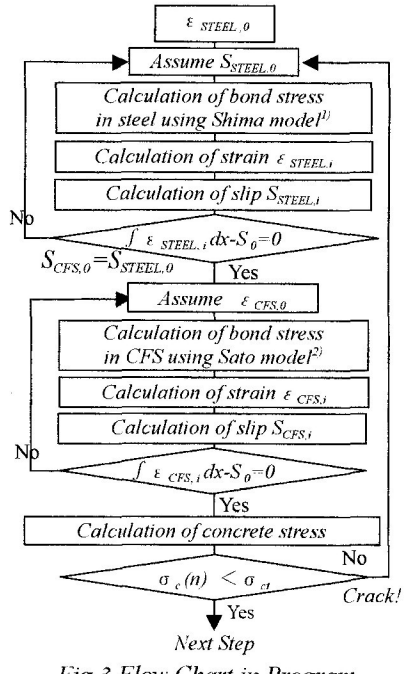



*Fig.3 Flow Chart in Program*

9. Give the slip at the crack of CFS ($S_{CFS,0}$) that is the same as the slip of the steel at the crack and assume the strain at the crack in the CFS ($\varepsilon_{CFS,0}$).
10. Using the Sato Model[2)], calculate the bond stress of CFS ($\tau_{CFS,0}$).
11. Using force equilibrium, calculate the stress in the CFS of the next element ($\sigma_{CFS,1}$). $\left(\sigma_{CFS,1} = \sigma_{CFS,0} - \tau_{CFS,0} \cdot dx / t\right)$
12. Using the stress-strain relationship, calculate the strain in the CFS of the next element ($\varepsilon_{CFS,1}$).
13. Integrating the strain in the CFS, calculate the slip of the CFS of the next element ($S_{CFS,1}$).
14. Steps 10 to 13 are repeated for elements to the center of concrete prism.
15. Compare the slip calculated by integrating the calculated strain distribution ($\int \varepsilon_{CFS} dx$) with the given slip ($S_{CFS,0}$). In case the two slips are not in agreement, go back to step 9 and assume the strain ($\varepsilon_{CFS,0}$) again.
16. Using force equilibrium, calculate the stress in the concrete of each element ($\sigma_{c,1}, \sigma_{c,2}$ ...).
17. If the stress in the concrete at the center of the prism is greater than the concrete tensile strength, the concrete is assumed to crack, then go back to step 2 (decrease in crack spacing). Otherwise go back to step1 (increase the strain in the steel at the crack).

In the analysis, two bond models are used. The Shima model, used for calculation of the bond stress in steel, is as follows:

$$\tau_s / f_c' = 0.73 \cdot [\ln(1+5s)]^3 / (1+\varepsilon \times 10^6) \quad (1)$$

in which, $\tau_s$ ; bond stress, $f_c'$ ; compressive strength of concrete, $s = 1000\, S/D$, $S$ ; slip, $D$ ; diameter of steel, $\varepsilon$ ; strain

On the other hand, the Sato model for bond between concrete and CFS is as follows:

$$\begin{aligned} &\tau_{CFS} / f'^{\,a}_c = \alpha S / (1+\beta\varepsilon) \\ &\tau_{\max} = 9.1 \cdot f'^{\,0.2}_c \cdot tE_{CFS} \cdot 10^{-5} \cdots\cdots (\tau_{\max} \le 3.49 f_c'^{0.2} MPa) \\ &\tau_{\max-i} = \tau_{\max}(1 - x/60) \cdots\cdots\cdots\cdots (\tau_{\max-i} \ge 0.5\tau_u) \\ &\tau = \tau_{\max-i} \cdot e^{-10(S-S_0)} \end{aligned} \quad (2)$$

where, $\tau_{CFS}$; bond stress, $f_c'$; compressive strength of concrete, $S$ ; slip, $\varepsilon$ ; strain, $a$ =0.2, $\alpha$ =148, $\beta$ =1000, $tE_{CFS}$ ; stiffness of CFS in unit width, $\tau_{max}$ ; maximum bond stress at the starting point of peeling-off, $\tau_{max-i}$ ; maximum bond stress at the point except starting point of peeling-off, $x$ ; distance from the starting point of peeling-off, $S_0$ ; slip when bond stress is maximum.

## MODEL FOR BOND DETERIORATION OF STEEL IN POST-YIELDING STAGE

In the post-yielding stage, the stress in the steel at the crack is assumed to be equal to the yield stress ($\sigma_{STEEL,0} = \sigma_y$). Then the slip of the steel at the crack ($S_{STEEL,0}$) is assumed. Then, from Eq.(2), the bond stress ($\tau_{STEEL,0}$) can be obtained. If a bond stress exists, the stress in the next element ($\sigma_{STEEL,1}$) should be smaller than the yielding stress ($\sigma_{STEEL,1} < \sigma_y$). This means that the yielding stress in steel can be found only at crack. However, the actual yielding zone extends from the cracked section.

To solve this contradiction, it is necessary to assume a plastic zone ( $L_p$ ) where no bond stress of steel exists and the steel stress is the yield stress. Factors influencing the length of the plastic zone at one side of the crack ( $L_p$ at one side and $2L_p$ at both sides) and other parameters were investigated in this study. The relationship between $L_p / D$ and the strain in the steel at the crack of S-4-1', S-4-2' and S-4-3' with deformed bar of 10mm diameter are shown in Figs.4-(a), (b) and (c).

In Fig.4-(a), the ratio, $L_p / D$ at each crack approaches a value of 3 to 5 as the steel strain increases. The values greater than 4 are found at cracks where secondary slanting cracks induced by the bond stress of the CFS occurred. From Figs.4-(b) and (c), it can be seen that $L_p / D$ mostly approaches a value of 3 to 4. These facts imply that reinforcement ratio of CFS has only a few effects on the final value of $L_p / D$.

Relationships between $L_p / D$ and the steel strain at the crack for specimens S-5-0 and S-5-2' are shown in Figs.4-(d) and (e). In those cases the steel bar is a deformed bar with diameter of 22 mm (D22). From Fig.4-(d) (specimen S-5-0), $L_p / D$ again approaches a value of 3 to 4 as well. It means that the final value of $L_p / D$ is hardly affected by the

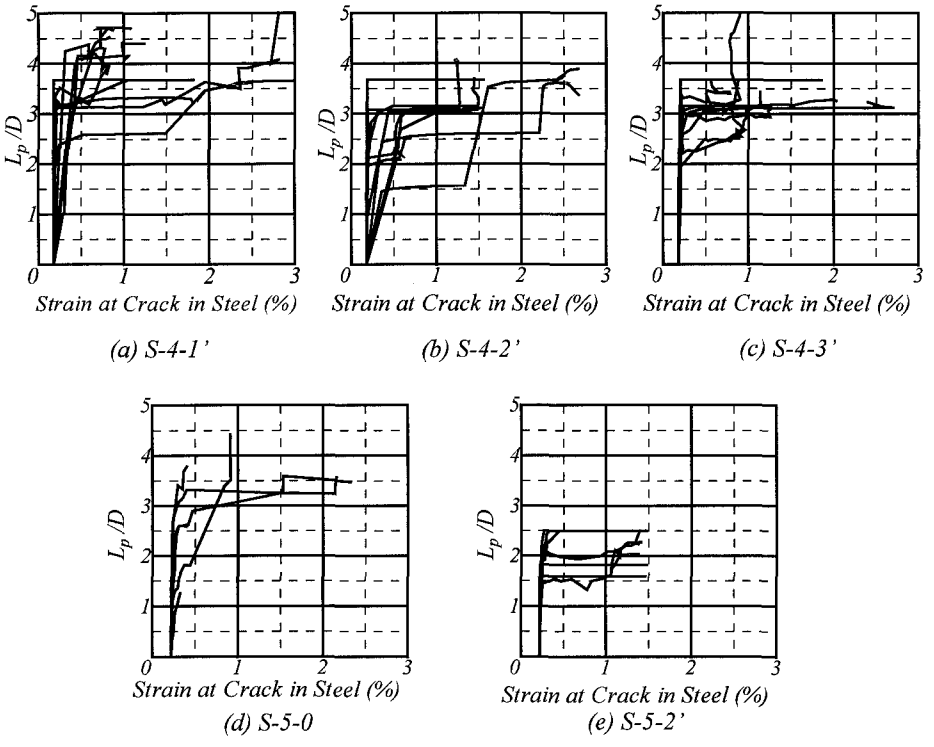



*Fig.4 Variation of plastic length*

reinforcement ratio of steel. In specimen S-5-2', the crack spacing decreased, so that all the strain gages indicated yielding in the steel. As a result, $L_p / D$ approaches one half of the crack spacing.

Considering the observed facts, for simplicity, $L_p / D$ is assumed to be 3.5 in the analysis.

## MODEL OF BOND DETERIORATION IN CFS

As shown in the previous section, there is bond deterioration in the steel bar near the crack. In the same way, it is natural that there is bond deterioration in the CFS near the crack. In this study the deterioration mechanism is considered as follows. When a crack occurs, concrete near the crack moves suddenly due to the opening at the crack. This movement causes some slip between the concrete and the CFS. The sudden introduction of slip may damage the bond near the crack. If there is a bond-damaged zone, the concrete near the crack may be deformed as shown in Fig.5. Based on the experimental results in a previous study[2] and this study, Eq.(3) is assumed to represent the bond deterioration. Equation (3) indicates how much of a reduction in maximum bond stress takes place near a crack (see Fig.6.).

$$\begin{aligned} \tau_{\max-i} &= \tau_{\max} \times (x/60) \cdots\cdots\cdots\cdots\cdots (x \le 60) \\ \tau_{\max-i} &= \tau_{\max} \times [1-(x-60)/60] \cdots\cdots (60 \le x \le 90) \\ \tau_{\max-i} &= 0.5 \times \tau_{\max} \cdots\cdots\cdots\cdots\cdots\cdots (90 \le x) \end{aligned} \quad (3)$$

in which, $\tau_{max}, \tau_{max-i}$ ; same as in Eq.(2). $x$ ; distance from crack. A comparison of the analytical results using Eq.(3) with the experimental results is shown in the next section.

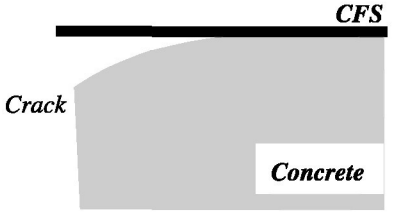



*Fig.5 Mechanism of Bond Deterioration*

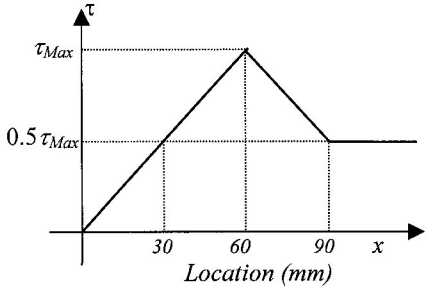


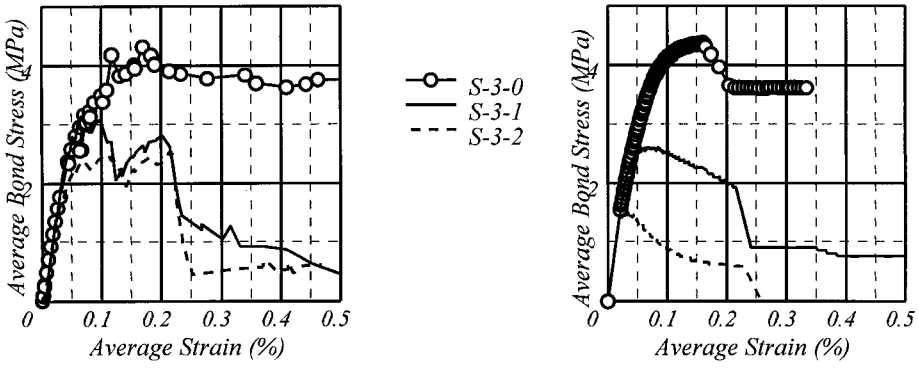

*Fig.6 Bond Deterioration Model*

## COMPARISON OF ANALYTICAL AND EXPERIMENTAL RESULTS

### Average Strain – Average Bond Stress Relation of Steel Bar

Experimental and analytical results for the average bond stress – average strain relationships of steel are shown in Figs.7-(a) and (b) respectively.

The relationships for the specimen without strengthening (S-3-0) and the specimen with one layer of CFS (S-3-1) indicate good agreement. However, the specimen with two layers of CFS shows a difference between the experimental and analytical results. The average bond stress in the experiment is greater than that in the analysis. The difference may be due to a larger scatter of measured bond stresses induced possibly by the larger spacing of strain



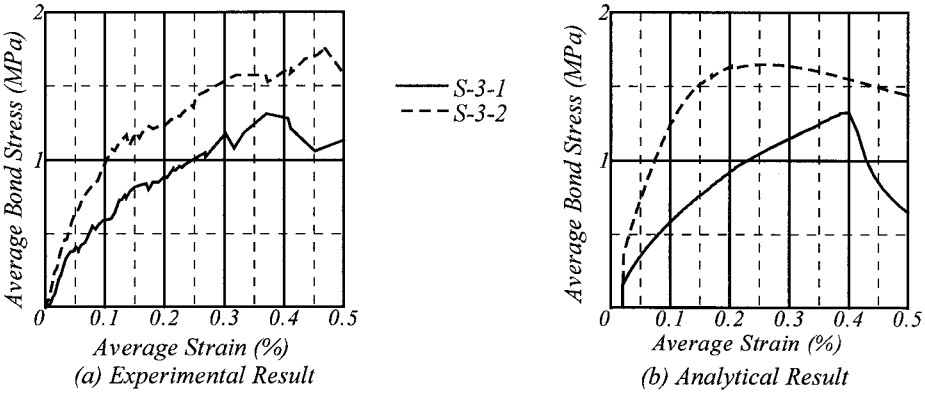

*(a) Experimental Result* *(b) Analytical Result*

*Fig.7 Average Bond Stress in Steel*

**Average Strain – Average Bond Stress Relationship of CFS**

Experimental and analytical results of average bond stress – average strain relationships for CFS are shown in Figs.8-(a) and (b) respectively.

Although there is some discrepancy in the average bond stress – average strain relationship, the analytical results can predict the general tendency in the experimental results. In order to achieve a more precise prediction, further study on the deterioration model is necessary.




*(a) Experimental Result* *(b) Analytical Result*

*Fig.8 Average Bond Stress in CFS*

**Tension Stiffening**

Both experimental and analytical relationships between the average concrete stress normalized by its tensile strength and average strain in the specimen without strengthening (S-3-0) are shown in Fig.9-(a). Figures 9-(b) and (c) show the relationships for specimens with one and two layers of CFS (S-3-1 and S-3-2). In specimen S-3-0, some cracks appeared before the average strain reaches 0.01% because of an unexpected bending moment during

the test. The last crack appeared when the average strain was around 0.1%. Then, tension softening started. The softening curve rather follows the curve predicted by Eq.(4).

$$\sigma_c / f_t = \left( \frac{\varepsilon_{tu}}{\bar{\varepsilon}} \right)^c \qquad (4)^{1)}$$

where, $\sigma_c$ ; average stress in concrete, $f_t$ ; tensile strength in concrete,

$\varepsilon_{tu}$ ; strain at crack, $\bar{\varepsilon}$ ; average strain, $c$ =0.4

For the full cracking stage, where no new cracking takes place and the crack spacing is narrow, the experimental and analytical results indicate good agreement in specimen S-3-0.

In specimen S-3-1 with one layer of CFS, the concrete stress in the experiment is slightly bigger than that in the analysis. However, it can be said that the analytical result can predict the experimental values with reasonable accuracy.

In specimen S-3-2 with two layers of CFS, the experimental and analytical results show some discrepancy. It is caused by the discrepancy in the average bond stresses of the steel bar and CFS. The tensile stress in specimen S-3-1 with one layer of CFS is greater than that in specimen S-3-0 without CFS. However, the tensile stress in specimen S-3-2 with two layers of CFS becomes less than that in the case of one layer in both the experiment and analysis. It was clarified that the tensile stress of the concrete in a RC member with CFS does not increase as the amount of CFS increases.

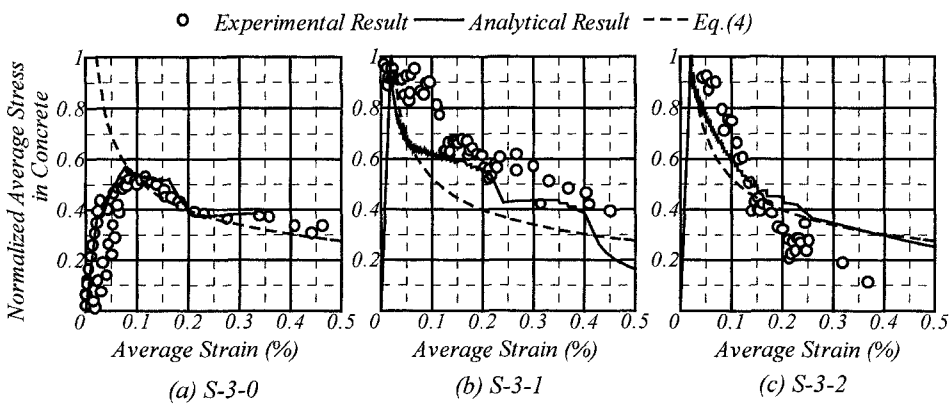
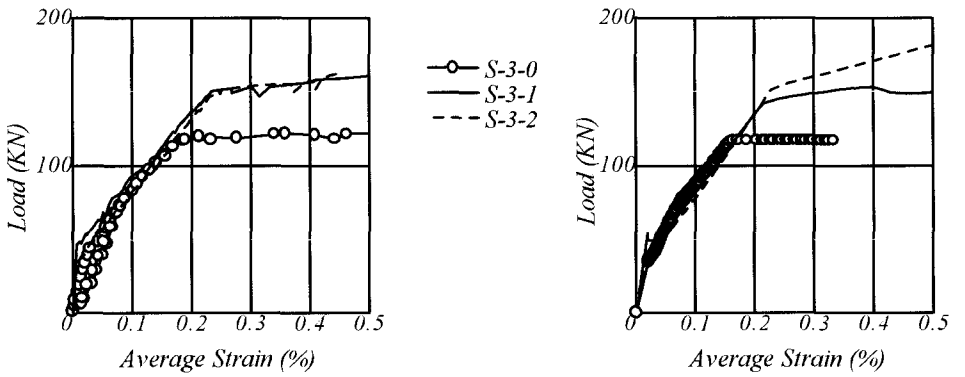



*Fig.9 Average stress – Average strain curves*

**Load - Average Strain Relation**

Figures 10-(a) and (b) show the experimental and analytical relationships between load and average strain. The experimental and analytical results show good agreement except for the case of specimen S-3-2. Loading for specimen S-3-2 was stopped when the average strain was around 0.4% because of concrete failure outside the test zone. For this reason, the observed average strain near 0.4% may not be correct.




*(a) Experimental Result* *(b) Analytical Result*

*Fig.10 Load - Average Strain Relation*

## CONCLUSIONS

From the experimental and analytical studies on the behavior in tension of reinforced concrete members strengthened by carbon fiber sheet (CFS), the following conclusions were obtained:

The tension stiffness of a reinforced concrete member strengthened by CFS can be evaluated with an analysis using bond models for steel bar reinforcement (Shima model [1]) and for CFS (Sato model[2]).

For the post-yielding stage of the steel bar reinforcement, the plastic zone near the crack where no bond of the steel bar reinforcement exists should be considered for the evaluation of the tension stiffness.The size of the plastic zone, $L_p$ at ultimate is approximately 3 to 4 times the bar size.

In the case of one layer of CFS, bond deterioration of the CFS near the crack can be represented by a reduction of its maximum bond stress and modeled by Eq.(3).

Considering the bond deterioration of the steel bar and CFS near the crack, a relationship between average bond stresses and average strain for steel bar and CFS can be predicted.

The average concrete stress in tension (concrete tension stiffness) as well as the relationship between load and average strain (tension stiffness of member) can also be predicted, considering the bond deterioration near the crack.

Further study is necessary to predict the behavior in tension of a strengthened member with a better accuracy.

## ACKNOWLEDGMENTS

The authors would like to express their gratitude to Prof KAKUTA Yoshio of Hokkaido University for his valuable advice, and Mr KIMURA Tsutomu of Hokkaido University and Mr SHOJI Kazuteru of Japan Engineering Consultants for their assistance with the experimental work.

**REFERENCES**

1. Shima, H., Micro and Macro Models for B ond in Reinforced Concrete, Journal of the Faculty of Engineering, The University of Tokyo (B), Vol. XXXIX, No.2, 1987.
2. Sato, Y., Asano, Y., Ueda, T., Fundamental Study on Bond Mechanism of Carbon Fiber Sheet, Concrete Library International of JSCE, No.37, June 2001.
3. Hamed Salem, Maekawa K. Spatially Averaged Tension Mechanics for Cracked Concrete and Reinforcement under Highly Inelastic Range, J. Materials, Conc. Struct., Pavements, JSCE, No.613/V-42, 277-293, 1999 February.

# Capacity Assessment of a Bridge Rehabilitated Using FRP Composites

CHARLES SIKORSKY, California Department of Transportation, Sacramento, CA, USA
NORRIS STUBBS, Texas A&M University, College Station, TX, USA
VISTASP KARBHARI and FRIEDER SEIBLE
University of California San Diego, La Jolla, CA, USA

## BACKGROUND

Polymer matrix composite (PMC) materials, or fiber reinforced polymer (FRP) composites, are widely recognized as an effective material for strengthening structures subjected to seismic events. These materials are also being investigated as a possible means of bridge rehabilitation to increase live-load capacity. PMC's consist of strong and stiff fibers embedded in a polymeric resin. They provide structural advantages due to their lightweight, high strength-to-weight ratio, high stiffness-to-weight ratio and corrosion resistance. While there are benefits to the use of these advanced materials, there are limitations as well. One such limitation is the lack of data to evaluate the long-term performance of bridges rehabilitated with these materials. For example, the long-term durability of carbon/vinylester composites subjected to environmental effects, as well as heavy truck traffic, is relatively unknown (Karbhari et al., 2000). Performance is taken here to include requirements important to a bridge manager such as functionality, reliability and durability. The functionality of the bridge is defined by the load carrying capacity of the bridge. Reliability describes the probability these elements will survive the specified loading condition(s), and durability is taken here as the length of time these components can continue to support their design loads.

While the application of advanced composite materials in civil infrastructure rehabilitation is not new, most applications in the United States at least, have not been planned with the objective of evaluating long-term performance. Therefore, to compare the application of advanced composites with conventional materials for bridge rehabilitation requires the following. First, a performance measurement system would have to be defined. Second, a technique to quantify the target values identified in the performance measuring system is needed. As a minimum this should include the ability to locate, quantify and evaluate changes (or damage) to the structure. For this work, damage is defined in terms of a loss of element stiffness. The objective of this paper is to summarize ongoing work to evaluate the performance of a bridge rehabilitated using advanced composite materials. To accomplish this, a performance measuring system will first be developed. Performance measures to evaluate load capacity (functionality), probability of failure (reliability) and estimated remaining service life (durability) will be identified, as well as measurable target values. Next, a system identification and damage detection algorithm will be selected to quantify the required target values. In order to demonstrate this technique, a rehabilitation technique for a bridge will be formulated and implemented. Finally, after the rehabilitation work is completed, the results will be evaluated to determine if any change in bridge performance was achieved.

*FRPRCS-5*, Thomas Telford, London, 2001.

## PERFORMANCE MEASURES

As part of a separate study, the California Department of Transportation (Caltrans) has begun to investigate the integration of performance measures useful to upper management with non-destructive damage detection methods. The purpose for establishing these measures is to monitor the health of the state transportation system (Sikorsky, 1999). In that work, quality management techniques were used to develop system performance measures (SPM), which the Department can use to improve the productivity of its various transportation systems. System performance measures were developed at the corporate, program and operational levels. Corporate performance measures (CPM) monitor the health of a transportation system. Program measures are required to monitor the planning, design, construction, operations and maintenance phases of the state transportation system. Operational or basic performance measures in turn were developed to monitor delivery of materials and services, which ensure the success of each program. For this research project, basic performance measures describe the quality of the material, while program performance measures describe the quality of the structure during its lifetime.

### Program Performance Measures

Normally, program performance measures (PPM) should be developed to monitor program cost ($\mathbf{C_{ij}}$) and determine expected losses ($\mathbf{L_{ij}}$), during the planning, design, construction, and maintenance phases of a bridge. Planning performance measures are developed to transform the customer's requirement's through design and construction to ensure the transportation system satisfies the customer's needs and expectations. Figure 1 shows the development of PPM at the operational or maintenance phase. This is the phase where the structure is already in service and opened to traffic.

A major obstacle to developing such performance measures has been the inability to quantify the condition of the bridge in-service. For example, during the life of the structure, it is subjected to hazards such as earthquakes, floods and excessive vehicle traffic. The structure will deteriorate as a result of these hazards. Periodically, and after extreme events, the structure must be evaluated to determine its ability to safety resist those hazards. That is, has the stiffness of key structural elements ($\square_j$ ) changed? In this case however, it also gives management an indicator as to when to either reduce traffic loads or close the bridge completely. Evaluation of this indicator is now possible due to recent advances in non-destructive damage detection methods.

## NON-DESTRUCTIVE DAMAGE EVALUATION

On a national scale, the seriously deteriorating condition of the transportation infrastructure has stimulated great interest in the development of non-destructive damage detection methods using modal parameters. In response to these concerns, many techniques in nondestructive damage detection and the evaluation of structural safety have been developed in recent years. Caltrans has supported the development of a Level IV nondestructive damage evaluation method (Stubbs et al., 1999). The method combined an independently verified Level III Method of nondestructive damage evaluation with systems reliability and fatigue analysis (Park et al., 1998). According to Rytter (1993), a Level IV method locates and estimates the magnitude of the damage, as well as evaluates the impact of damage on the structure. For the sake of continuity, a summary of the non-destructive damage evaluation method is provided. A more detailed explanation of the method can be found in the references.

**System Identification Scheme for the Baseline Structure**

Suppose a flawed (i.e., damaged) structure is given with field-measured mode shapes $\Phi_i^*$ and eigenfrequencies $\omega_i^*$. Assume that the magnitude of the flaw is small in comparison to a flawless (i.e., baseline) structure. Suppose that an estimate of the flawless structure can be identified using only the frequency information from the flawed structure. Then the identified baseline model will have the same eigenfrequencies $\omega_i^*$ (in the least square sense) of the flawed model but the mode shapes of the two structures will be different in the neighborhood of the flaw. This difference in the mode shapes of the identified baseline structure and the measured mode shapes of the existing structure will be exploited to localize the flaw.

Here, a system identification methodology to identify baseline modal responses of a structure is outlined (Stubbs and Kim 1996). Consider a linear skeletal structure with *NE* members and *N* nodes. Suppose $\mathbf{k}_j^*$ is the unknown stiffness of the $j^{th}$ member of the structure for which *M* eigenvalues are known. Also, suppose $\mathbf{k}_j$ is a known stiffness of the $j^{th}$ member of a finite element (FE) model for which the corresponding set of *M* eigenvalues are known. Then, relative to the FE model, the fractional stiffness change of the $j^{th}$ member of the structure, $\alpha_j$, and the stiffnesses are related according to the following equation.

$$\mathbf{k}_j^* = \mathbf{k}_j (1 + \alpha_j) \tag{1}$$

Similarly the fractional mass change of the $j^{th}$ member of the structure, $\beta_j$, and the masses are related according to the following equation.

$$\mathbf{m}_j^* = \mathbf{m}_j (1 + \beta_j) \tag{2}$$

The fractional stiffness change and the fractional mass change of *NE* members may be obtained using the following equation (Stubbs and Osegueda 1990):

$$\mathbf{Z} = \mathbf{F}\alpha - \mathbf{G}\beta \tag{3}$$

where $\alpha$ is a *NE* x 1 matrix containing the fractional changes in stiffness between the FE model and the structure, $\beta$ is a *NE* x 1 matrix containing the fractional changes in mass between the FE model and the structure, **Z** is a *M* x 1 matrix containing the fractional changes in eigenvalues between the two systems, **F** is a *M* x *NE* stiffness sensitivity matrix relating the fractional changes in stiffnesses to the fractional changes in eigenvalues, and **G** is a *M* x *NE* mass sensitivity matrix relating the fractional changes in masses to the fractional changes in eigenvalues.

**Damage Localization Theory (Damage Index Method)**

The damage index method utilizes the change in mode shapes of the pre-damage and post-damage structure to detect and locate damage in a structure. Consider a linear, undamaged, skeletal structure with NE elements and N nodes. After writing the equations of motion for the structure and solving the eigenvalue problem, the $i^{th}$ modal stiffness, $K_i$, of the arbitrary structure is given by

$$K_i = \Phi_i^T C \Phi_i \tag{4}$$

where $\Phi_i$ is the $i^{th}$ modal vector and C is the system stiffness matrix. From matrix structural analysis, the contribution of the $j^{th}$ member to the $i^{th}$ modal stiffness, $K_{ij}$, is given by

$$K_{ij} = \Phi_i^T C_j \Phi_i \tag{5}$$

where $C_j$ is the contribution of the $j^{th}$ member to the system stiffness matrix. The fraction of modal energy for the $i^{th}$ mode that is concentrated in the $j^{th}$ member (i.e., the element sensitivity of the $j^{th}$ member to the $i^{th}$ mode) is given by

$$F_{ij} = K_{ij}/K_i \tag{6}$$

Let the corresponding modal parameters in Equations (4) to (6) associated with a subsequently damaged structure be characterized by asterisks. Then for the damaged structure,

$$F_{ij}^* = K_{ij}^* / K_i^* \tag{7}$$

where $K_{ij}^*$ and $K_i^*$ are given by, respectively

$$K_{ij}^* = \Phi_i^{*T} C_j^* \Phi_i^* \tag{8}$$

and

$$K_i^* = \Phi_i^{*T} C^* \Phi_i^* \tag{9}$$

The quantities $F_{ij}$ and $F_{ij}^*$ are related by the equation:

$$F_{ij}^* = F_{ij} + dF_{ij} \tag{10}$$

where $dF_{ij}$ is related to the change in the fraction of modal energy of the $j^{th}$ member in the $i^{th}$ mode. The quantity $dF_{ij}$ can be obtained from the expression:

$$dF_{ij} = \frac{K_{ij}}{K_i}\left[\frac{dK_{ij}}{K_{ij}} - \frac{dK_i}{K_i}\right] \tag{11}$$

This quantity $dF_{ij}$ is then exploited to develop an expression for the damage index where $DI_{ij}$ is the indicator of damage in the $j^{th}$ member using the $i^{th}$ mode.

$$DI_{ij} = \frac{k_j}{k_j^*} = \frac{f_{ij}^*/f_{ij}+1}{2} \tag{12}$$

If $DI_{ij} > 1$, damage may exist.

The final step in damage localization is classification. While several approaches are available to classify these damage indices, the authors are currently utilizing techniques primarily from hypothesis testing. The criteria for damage localization is established based on statistical reasoning. The values, $DI_1$, $DI_2$, $DI_3$, ..... , $DI_{NE}$ for each element, are considered the realization of a random variable. The normalized damage indicator is given by

$$z_j = \frac{DI_j - \mu_{DI}}{\sigma_{DI}} \tag{13}$$

where $\mu_{DI}$ and $\sigma_{DI}$ represent mean and standard deviation of the damage index, $DI_j$, respectively. Let $H_o$ be the hypothesis that structure is not damaged at member j, and let $H_1$ be the hypothesis that structure is damaged at member j. The following decision rules may be used to assign damage to member j: (1) choose $H_1$ if $z_j \geq \lambda$ and (2) choose $H_o$ if $z_j < \lambda$ where $\lambda$ is a threshold which assigns a level of significance.

**Damage Severity Estimation**

Note that in Equation (12) the indicator of damage is the ratio of the undamaged stiffness to the damaged stiffness. Such a number exists for each potentially damaged member. For example, in the case of a truss there is a $DI_j$ associated with every member j. Here the damage is expressed as the fractional change in stiffness of an element:

$$\alpha_j = \frac{k_j^* - k_j}{k_j} = \frac{1}{DI_j} - 1 \tag{14}$$

Thus if there is no damage, $\alpha_j = 0$; if there is damage, $\alpha_j < 0$. Note that if $\alpha_j = -1$, all stiffness capacity is completely lost.

**Identification of Stiffness of Existing Structure**

Having stiffness parameters for the baseline structure, location of damage, and the severity of damage, the stiffness properties of the existing structure can be obtained from the equation:

$$k_j^{(\text{existing})} = k_j^{(\text{baseline})}\left[1 + \alpha_j\right] \tag{15}$$

Note that if there is no damage at location j, the stiffness properties of the baseline and the existing structures are the same.

## REHABILITATION PHILOSOPY AND DESCRIPTION

The Byron Road Bridge was designed and built in 1964. The bridge is a 103 m (340 ft) long, 5 span, two-lane highway bridge, across the California Aqueduct Canal in northern California. The superstructure consists of a cast in-place reinforced concrete T-girder, continuous and monolithically connected to the bents. The 5 spans have lengths of 17.5, 22.7, 22.7, 22.7 and 17.5 m (58, 75, 75, 75, and 58 ft.), respectively. The 0.16 m (6-1/4 inch) thick reinforced concrete deck spans transversely between the 2.2 m (7.25-ft) center-to-center spaced girders. Expansion joints are provided at the abutments and within the center span. It should also be noted that the bridge was seismically retrofitted in the past decade. At that time, the top two inches of the concrete deck was removed and replaced with a polymer concrete overlay of equal thickness. Unfortunately, cores taken from the bridge deck show the deck was not cleaned properly prior to the application of the polymer concrete resulting in poor overall adhesion between the layers.

**Failure Assessment**

In the spring of 1998, the bridge experienced punching shear failures at two locations on the bridge superstructure (Figure 1). At several other locations in the same region, punching failure was imminent. Punching failures were concentrated in deck regions where evenly spaced cracks in both directions were visible on the bridge soffit. These cracks showed large amounts of efflorescence indicating water penetration through the deck. The punching failures occurred approximately three feet from the bridge centerline, which locates them under the left wheel load of the southbound traffic lane, a strong indicator that local wheel loads contribute to the observed failure conditions. The punching shear cone is approximately fifteen inches in diameter and features very steep, close to vertical failure planes, which is not the typically observed inclination of 45° or less. This is more indicative of the punching shear failure plane forming along existing transverse and longitudinal flexure cracks, which seem to be on a 130 – 150 mm grid pattern corresponding to the 0.14 m (5.5 inch) reinforcement spacing of the #5 deck reinforcement along the bottom soffit in the transverse direction

(Figure 2). In the longitudinal direction, only bottom reinforcement exists in the deck slab with six #5 bars evenly spaced over the center 1.2 m of the deck between girders. This results in a longitudinal bottom deck reinforcement spacing of approximately 0.24 m (9.6 inches) or longitudinal bottom deck reinforcement which is approximately 57% more than the transverse bottom deck reinforcement.

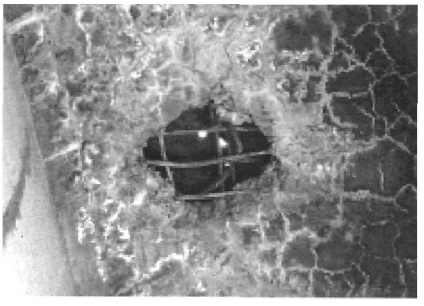


Figure 1: Punching shear in deck



Figure 2: Typical cracking and damage visible on deck soffit

Detailed analytical investigations showed the transverse spanning decks first cracked in longitudinal bending along the transverse soffit reinforcement since longitudinally very little flexural capacity exists and transverse cracks can open widely. Subsequently, the effective width in the transverse direction is limited to the spacing between the transverse cracks resulting in significant flexure and shear overloads. As a consequence, longitudinal cracks develop which spread along the entire deck length due to the moving nature of the wheel loads. Finally, the local shear capacity is exceeded over a shear area limited by the existing flexural cracks in both directions.

**Rehabilitation Criteria**

Based on the analytical damage assessment, the following rehabilitation criteria were formulated.

(a) To avoid sequential crack openings, first in the transverse and subsequently in the longitudinal deck slab directions, the longitudinal deck reinforcement should equal the transverse reinforcement.
(b) To maintain soffit crack widths of 1 mm (0.039 inch) or less for sufficient aggregate interlock, bottom soffit strains should be limited to 0.75%. This strain limit allows a nominal shear capacity of more than $2\sqrt{f'c}$.
(c) To prevent the formation of punching shear cones 0.4m (15 inches) in diameter, a clear spacing between added reinforcement strips should not exceed 300 mm (12 inches) to provide added reinforcement at intervals less than the observed punching shear diameter.

Therefore, the rehabilitation design can be performed by adding longitudinal soffit reinforcement equivalent to at least 2.75 #5 bars with less than 300 mm (12 inches) spacing and specified soffit strain limits of $\varepsilon \leq 0.75\%$.

**Proposed Rehabilitation Measure**

The deck strengthening measure assumes advanced composite carbon reinforcement bonded directly to the bottom soffit with an epoxy adhesive. Two rehabilitation systems used

extensively in Europe and Japan are investigated here. These systems, including the number of strips equivalent to 2.75 #5 bars are summarized in Table 1.

Table1: Description of Composite Systems

| Description | Material Properties | | | Steel Equivalent |
|---|---|---|---|---|
| | Dimension* mm (inches) | Modulus GPa (msi) | Ult. Stress MPa (ksi) | |
| Sika Carbodur 50 Pultruded carbon laminates | 51 x 1.2 (2.0 x 0.047) | 150 (21.7) | 3000 (348.0) | 4 |
| SCCI C2-06 12k tow carbon fabric | 152 x 1.1 (6.0 x 0.042) | 75 (10.9) | 930 (135.0) | 3 |

*Width x thickness

Both systems were applied to different spans within the bridge. The Sika system was bonded to the concrete bridge surface using the Sikadur 30 adhesive system. The SCCI C2-06 system comprised a 68 gm/sq m (20 oz / sq yd) unidirectional carbon fabric impregnated on site using an appropriate epoxy. Examples of placement in bays are shown in Figures 3 and 4.



Figure 3: Placement of unidirectional fabric in both directions in a bay

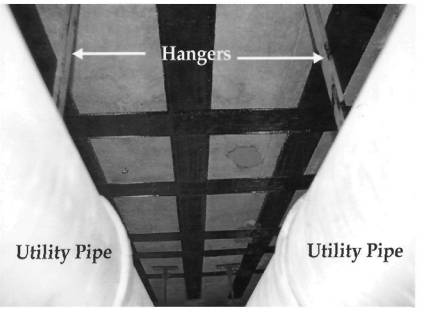



Figure 4: Ease of placement around utility pipes

## APPLICATION

Evaluation of the performance of the rehabilitated bridge requires both an analytical model, as well as experimental results. First a finite element model was developed and updated using a systems identification technique. The systems identification technique relies on the frequencies of the bridge to update the finite element model and provides the baseline from which future measurements will be compared. After the repairs were completed, a second modal test was performed and the model evaluated for increased stiffness changes. The stiffness changes were then used to quantify the performance measures.

### Modal Analysis and System Identification

Field modal tests were performed on the bridge 3 December 1999 and 12 May 2000. The modal analysis results from the field data for December 1999 and May 2000 are summarized in Table 2. The initial values for the parameters of the finite element model are listed in Table 3. Table 4 shows the rate of convergence of the iteration scheme as the initial finite element

model is updated. The identified material properties of the structure using the May 2000 data are shown in Table 5.

Table 2: Measured Frequencies

| Mode | Frequency (Hz) – 1999 | Frequency (Hz) - 2000 |
|---|---|---|
| 1 | 3.950 | 4.030 |
| 2 | 4.428 | 4.440 |
| 3 | 6.007 | 6.144 |
| 4 | 6.788 | 6.895 |

Table 3: Initial Values of Material Properties of FE Model (1999)

| | Deck and Piers | Springs for Soil-Structure Interaction | |
|---|---|---|---|
| | | Pier | Abutment |
| E - GPa ($lb/ft^2$) | 17.2 ($360 \times 10^6$) | - | - |
| $\rho$ ($lb \cdot s^2/ft^4$) | 4.7 | - | - |
| k<br>kg/m (lb/ft) | | $48.28 \times 10^6$<br>($32.40 \times 10^6$) | $21.11 \times 10^6$<br>($14.17 \times 10^6$) |

Table 4: System Identification (1999)

| Mode | Frequency of Initial FE model | Updated Frequencies (Hz) | | | Frequency of Target Structure | Error (%) | |
|---|---|---|---|---|---|---|---|
| | | Iter. 1 | Iter. 3 | Iter. 5 | | Initial | Final |
| 1 | 5.707 | 4.194 | 4.196 | 4.197 | 3.950 | 44.5 | 6.2 |
| 2 | 5.889 | 4.428 | 4.442 | 4.445 | 4.428 | 33.0 | 0.4 |
| 3 | 8.376 | 6.154 | 6.156 | 6.157 | 6.007 | 39.4 | 2.5 |
| 4 | 8.520 | 6.269 | 6.272 | 6.273 | 6.788 | 25.5 | 7.6 |

Table 5: Identified Material Properties of FE Model (2000)

| | Deck and Piers | Springs for Soil-Structure Interaction | |
|---|---|---|---|
| | | Pier | Abutment |
| E - GPa ($lb/ft^2$) | 9.81 ($200.78 \times 10^6$) | - | - |
| $\rho$ ($lb \cdot s^2/ft^4$) | 4.68 | - | - |
| k<br>kg/m (lb/ft) | | $32.01 \times 10^6$<br>($21.48 \times 10^6$) | $13.99 \times 10^6$<br>($9.394 \times 10^6$) |

**Damage Identification**

The damage identification results are listed in Table 6. The results from 1999 indicate a decrease in stiffness from the theoretical as-built condition, whereas the results from 2000 indicate an increase due to the composite rehabilitation. Also, the results of the pull-off tension tests are compared with the results from the sensitivity approach in Table 6 (Karbhari,

2000). These results show the span in which the highest tensile force was recorded, is also where the largest increase in stiffness was detected (i.e., Span 2).

Table 6: Comparison of Damage Identification Results with Pull-Off Test Results

| SPAN | AVERAGE STIFFNESS CHANGE (%) | | TENSILE FORCE * |
|---|---|---|---|
| | 1999 | 2000 | kN (kips) |
| 1 | -21.0 | 2.5 | 4.9/3.1 (1.1/0.7) |
| 2 | -12.0 | 22.6 | 7.6/5.3 (1.7/1.2) |
| 3 | -34.0 | 6.4 | -/0.9, 4.5/2.7 (-/0.2, 1.0/0.6) |
| 4 | -14.0 | 3.5 | 7.1/3.6 (1.6/0.8) |
| 5 | -12.0 | 0.3 | -/5.3 (-/1.2) |

* disk applied to composite material / disk applied to concrete,
- indicates disk not attached properly and failed prematurely

## DISCUSSION OF RESULTS

The field data indicated that the frequencies of the structure increased between December 1999 and May 2000. Both the systems identification as well as non-destructuve damage evaluation results indicate an increase in the stiffness of the structure in the time period spanning 3 December 1999 and 12 May 2000. The first method accounts for any changes in boundary conditions such as changes in soil-structure interaction properties, but does not

localize the changes. It only indicates a change has occurred and in which direction the change occurred. The second method localizes the stiffness changes and attempts to quantify the change.

## SUMMARY AND CONCLUSIONS

This paper summarized ongoing work to evaluate the performance of a bridge rehabilitated using advanced composite materials. First, a performance measuring system was developed. Next, a systems identification and damage detection algorithm were selected to identify the target values needed for the performance measuring system. To demonstrate this technique, a rehabilitation technique was formulated and applied to a bridge. Finally, after the rehabilitation work was completed, the results were evaluated to determine if any change in performance of the bridge was achieved. The method indicates an increase in the stiffness of the structure in the time period spanning 3 December 1999 and 12 May 2000.

**REFERENCES**

Karbhari, V.M. (2000). "Pull-Off Test Results Pertaining to the Byron Road Bridge Rehabilitation Project." Structural Systems Research Project Report No. TR-2000/17, University of California – San Diego, July.

Karbhari, V.M., Chin J. W., and D. Reynaud (2000). "Critical Gaps in Durability Data for FRP Composites in Civil Infrastructure." *Proceedings, 45th International SAMPE Symposium,* SAMPE, Long Beach, May 21-25.

Park, S., Stubbs, N. and R. Bolton (1998). "Damage detection on a steel frame using simulated modal data." *Proceeding, 16th International Modal Analysis Conference*, SEM, Santa Barbara, February 2-4.

Rytter, A. (1993). Vibrational Based Inspection of Civil Engineering Structures. Ph.D. Thesis, University of Aalborg, Aalborg, Denmark.

Sikorsky, C. (1999). "Development of a Health Monitoring System for Civil Structures Using a Level IV Non-Destructive Damage Evaluation Method." *Proceeding, 2nd International Workshop on Structural Health Monitoring*, Stanford University, Stanford, CA September 8-10.

Stubbs, N. and Osegueda, R. (1990). "Global Non-destructive Damage Evaluation in Solids." *The International Journal of Analytical and Experimental Modal Analysis*, Vol. 5 (2), 1990, pp. 67-79

Stubbs, N., and Kim, J.T. (1996). "Damage Localization in Structures without Baseline Modal Parameters.", *AIAA J.*, 34(8), 1644-1649.

Stubbs, N., S. Park, S. Choi, R. Bolton and C. Sikorsky (1999). "Point-in-Time Systems Identification of Structural Properties of Lavic Road Bridge." Technical Report submitted to State of California, Department of Transportation, Sacramento, California. Texas Engineering Experimental Station, Texas A&M University, College Station, Texas.

# Long-term Behaviour of CFRP-laminate-strengthened Concrete Beams at Elevated Temperatures

T. ULAGA and U. MEIER
EMPA Duebendorf, Switzerland

## ABSTRACT
To investigate the long-term behaviour of CFRP-laminate-strengthened concrete at elevated temperatures and high humidities, two post-strengthened, steel-reinforced concrete beams with a span of 2.3 m were exposed to sustained flexural loads in a climate chamber. The temperature and humidity were increased over a period of several months. A comprehensive measurement system was employed to record strain and displacement. The test data allowed conclusions to be drawn about the deformational behaviour and limiting climatic conditions for CFRP strengthening systems. One laminate was based on an epoxy, the other on a thermoplastic matrix system.

## INTRODUCTION
Today, carbon-fibre-reinforced plastic (CFRP) laminates are widely used for strengthening concrete structures. Of the many facility types to which these systems are applied, probably the most common are bridges [1] and residential, office and industrial buildings, where climatic conditions tend to remain moderate. Laboratory investigations have proved the efficiency and durability of CFRP laminates for such applications [2,3], and these results have formed the basis for dimensioning and detailing the strengthening works [4,5].
Climatic conditions in tropical regions or in buildings housing industrial plant may impose exceptional demands (e.g. temperatures permanently above 40°C coupled with high humidity) that cast doubt on the suitability of CFRP laminate in such situations. At the same time, CFRP strengthening systems may represent the most or even the only appropriate rehabilitation method in such cases.
The individual components of a strengthened structure (concrete body, steel bars, CFRP laminate, adhesive) react differently to fluctuations in temperature and humidity. Although these characteristics are known, it is difficult to predict the behaviour of combined systems and define the limiting conditions.
To investigate these issues, a long-term experiment was carried out in a climate chamber.

## BACKGROUND
### Test specimens
The aim was to test standard concrete beams reinforced with steel bars and strengthened with CFRP laminates.
Real structures tend to require strengthening only after reaching a certain age, and old concrete is much less susceptible to creep than young concrete. To make allowance for this, 15-year-old beams provided by the Institute of Structural Engineering (IBK) at the Swiss

*FRPRCS-5*, Thomas Telford, London, 2001.

Federal Institute of Technology (ETH) in Zurich were used for the tests. The geometry is shown in Figure 3.

**Characterization of materials**

*Concrete*

The concrete body serves to form the flexural compression zone and transfer internal shear stresses.

Overall, the concrete deformation consists of four strain components [6]. The stresses caused by loading the concrete element produce an initial strain. Loads and stresses sustained over a longer period result in creep – this strain component may be particularly significant if the concrete is loaded at an early age. Shrinkage strains develop during hardening. Thermal strains occur where the concrete body (regardless of its age) is heated or cooled and may be determined using the coefficient of thermal expansion $\alpha_T = 10^{-5}\ K^{-1}$.

Concrete mix

| | | |
|---|---|---|
| Max. aggregate size | Ø | 16 mm |
| Cement content | | 325 kg/m$^3$ |
| Water-cement ratio | | 0.45 |

*Steel*

Deformation of steel reinforcing bars in standard concrete structures is generally caused by stress, with thermal strain generally playing a minor role.

Reinforcing bar properties

| | | |
|---|---|---|
| Diameter | $Ø_s$ | 14 mm |
| Young's modulus | $E_s$ | 210 GPa |
| Yield stress | $f_y$ | 520 MPa |

*CFRP laminates*

CFRP laminates may be bonded to the relevant beam surface as additional tension chord reinforcement where the expected flexural tensile stresses exceed the capacity of the steel bars.

The greater part of the strain is caused by flexural tension. Though thermal strain may also occur, this is very modest compared to thermal movement in steel or concrete [7]. The laminate matrix may absorb water when exposed to high humidity, and this, in turn, may affect the material strength and strain.

Two different laminates were investigated in the tests: beam *CaDu* was strengthened with the commercial product "Sika CarboDur S512", while a recently developed laminate was tested on beam *THELA*. The latter comprises carbon fibre embedded in a thermoplastic matrix system (unlike traditional laminates such as Sika CarboDur S512, which generally use an epoxy-resin matrix).

Laminate properties

| | | Sika Carbo-Dur S512 | Thermoplastic laminate |
|---|---|---|---|
| Width | $b_l$ | 50 mm | 50 mm |
| Thickness | $t_l$ | 1.2 mm | 1.15 mm |
| Young's modulus | $E_l$ | approx. 161 GPa | approx. 130 GPa |
| Strength | $f_{lu}$ | min. 2800 MPa | min. 2300 MPa |

*Adhesive*

The adhesive transmits shear stresses from the concrete to the CFRP laminate, i.e. the adhesive must exhibit a high shear modulus and creep resistance. The commonly used epoxy adhesives are therefore mixed with an inorganic filler. Thermal performance is a key factor: the mechanical properties change radically once the glass transition temperature of the epoxy resin has been exceeded.

The epoxy adhesive "Sikadur 30" was used to bond the laminate. A torsion pendulum test [8] was carried out to investigate temperature performance [3]. Figure 1 shows the changes in shear modulus: this remains high up to a temperature of approx. 42°C, before the material softens and deformation increases. The glass transition temperature $T_g$ is defined as the temperature corresponding to the mid-point in the steep section of the shear modulus curve (55°C); however, this is of limited relevance here as the adhesive starts to soften at 42°C. As stiffness and strength diminish, the adhesive is no longer able to transmit the shear stresses. Structural failure may then occur due to peeling off of the laminate.

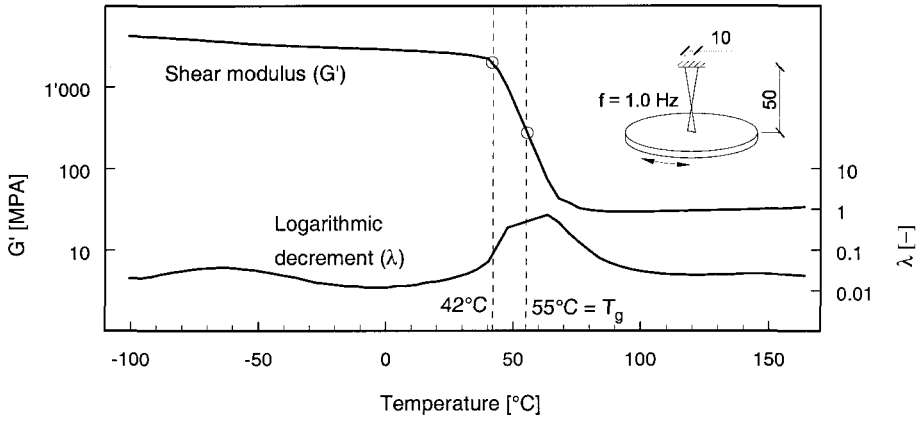



Figure 1: Torsion pendulum test: temperature dependence of shear modulus

**Overall performance of cross-section**

The deformation mechanisms of the individual cross-section components have been briefly outlined above. Comprehensive literature is available showing how these strains are estimated (e.g. [6]).

When the components are combined to form a single cross-section, interactions occur that considerably complicate prediction of deformation.

## LABORATORY TESTS

**Test set-up**

The experiments were carried out in a climate chamber. The limited space and high test loads required construction of an appropriate testing facility (Figure 2).

The specimens were supported in the middle and loaded with concrete cubes at the ends in order to realize four-point bending (Figure 3). This arrangement allowed a bending moment of 17.6 kNm to be achieved at midspan. This level corresponds to the maximum serviceability limit state with the steel remaining just below its yield strain (Figure 5).



Figure 2: Testing facility

**Test programme**

The experiment was designed to test heavily loaded CFRP-strengthened concrete beams under elevated long-term climatic conditions. The limiting components with regard to temperature are the synthetic materials. As described above, the adhesive starts to soften at approx. 42°C. When exposed to humidity, the polymers absorb water which may affect their mechanical properties. Hence, the thermoplastic matrix of the newly developed laminate in particular was viewed as potentially problematic.

The test was set up at room temperature. After loading, the temperature was raised to 40°C and relative humidity adjusted to 30%. These atmospheric conditions were maintained for several weeks until deformations stabilized. Conditions were subsequently adjusted and again maintained until growth in deformation almost ceased.

**Measurement programme**

The aim of the comprehensive measurement programme (Figure 3) was to collect detailed information on the process of deformation in the test specimens.

A series of Demec gauge segments with a length of 200 mm were applied to the top and side faces of the specimens. Monitoring of these segments allowed the corresponding strains to be determined. The creep behaviour of the (adhesive) interface was investigated by measuring the relative displacement, $\Delta$, between laminate and concrete surface at the end of the laminate. Global deformation was recorded by deflection measurements at the ends of the specimens.

A combined temperature/humidity measurement device installed in the middle of the chamber was used to monitor atmospheric conditions.

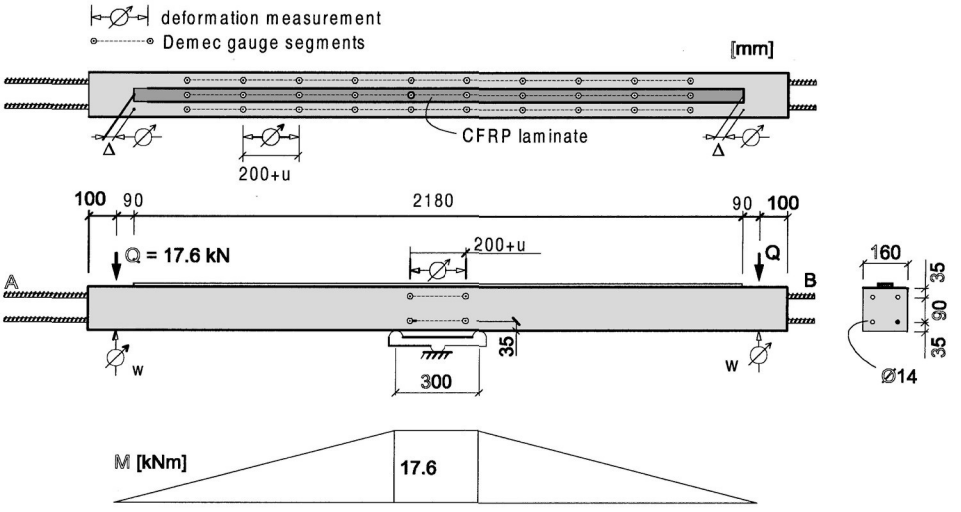



Figure 3: Load arrangement, geometry and measurement programme

## RESULTS

### Progress of the experiment

As mentioned above, regulation of the atmospheric conditions in the chamber was dictated by the deformation behaviour of the test specimens. The progress of the test between 2 February and 21 September 2000 is detailed below. The temperature and humidity measurements are shown in Figure 4.

| Climatic conditions | Beginning – end | Duration |
|---|---|---|
| | 29 February 2000 | |
| Period 1: approx. 40°C, 30% r.h. | | 48 days |
| | 17 April 2000 | |
| Period 2: approx. 40°C, 80% r.h. | | 79 days |
| | 5 July 2000 | |
| Period 3: approx. 45°C, 80% r.h. | | 78 days |
| | 21 September 2000 | |
| | | 205 days (total time) |

### Deformation

The midspan deflection is shown in Figure 4. The dots relate to measurements made at intervals of between one and seven days. Figure 4 also shows the relative displacement, Δ, of the laminate ends.

Seven Demec gauge segments were monitored in the middle part of the beams: two on either side face, two on the top face and one on the laminate (Figure 5). Linear regression of the corresponding strains yielded the average deformation of the cross-section. The lines in Figure 5 show the state of the cross-section at the end of each climate period. The inclination of these lines is equal to the curvature of the beam.

Table 1 gives the deformations measured at the end of each climate period.

Table 1: Characteristic deformation at the end of each climate period

| | THELA | | | | | CaDu | | | | |
|---|---|---|---|---|---|---|---|---|---|---|
| Date | w [mm] | $\Delta_A$ [mm] | $\Delta_B$ [mm] | $\chi$ [$m^{-1}$] | $\varepsilon_l$ [%] | w [mm] | $\Delta_A$ [mm] | $\Delta_B$ [mm] | $\chi$ [$m^{-1}$] | $\varepsilon_l$ [%] |
| 29.2. | 12.30 | -0.002 | 0.001 | 0.0305 | 0.34 | 11.10 | 0.000 | -0.002 | 0.0247 | 0.30 |
| 17.4. | 14.12 | 0.006 | 0.014 | 0.0334 | 0.37 | 12.23 | 0.010 | 0.009 | 0.0263 | 0.32 |
| 5.7. | 14.61 | 0.016 | 0.028 | 0.0340 | 0.37 | 12.68 | 0.019 | 0.021 | 0.0268 | 0.32 |
| 21.9. | 14.88 | 0.052 | 0.065 | 0.0360 | 0.39 | 13.19 | 0.051 | 0.057 | 0.0293 | 0.35 |

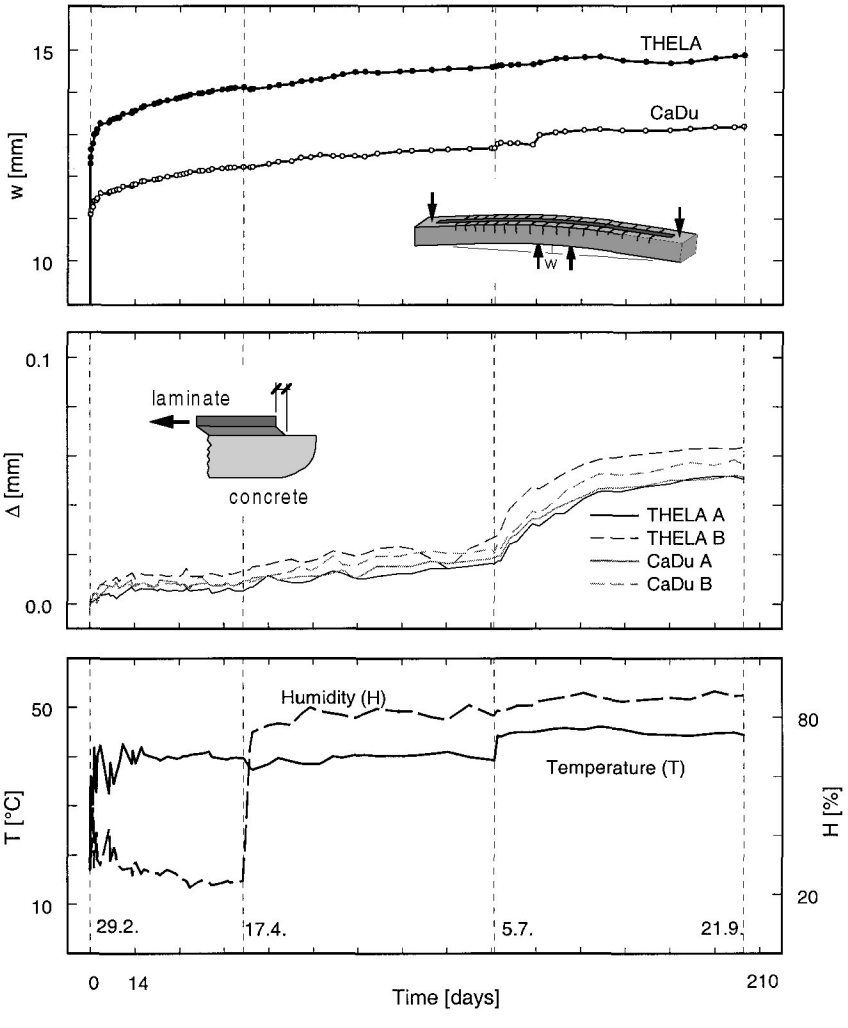



Figure 4: Deflection w, relative displacement Δ and changes in climatic conditions

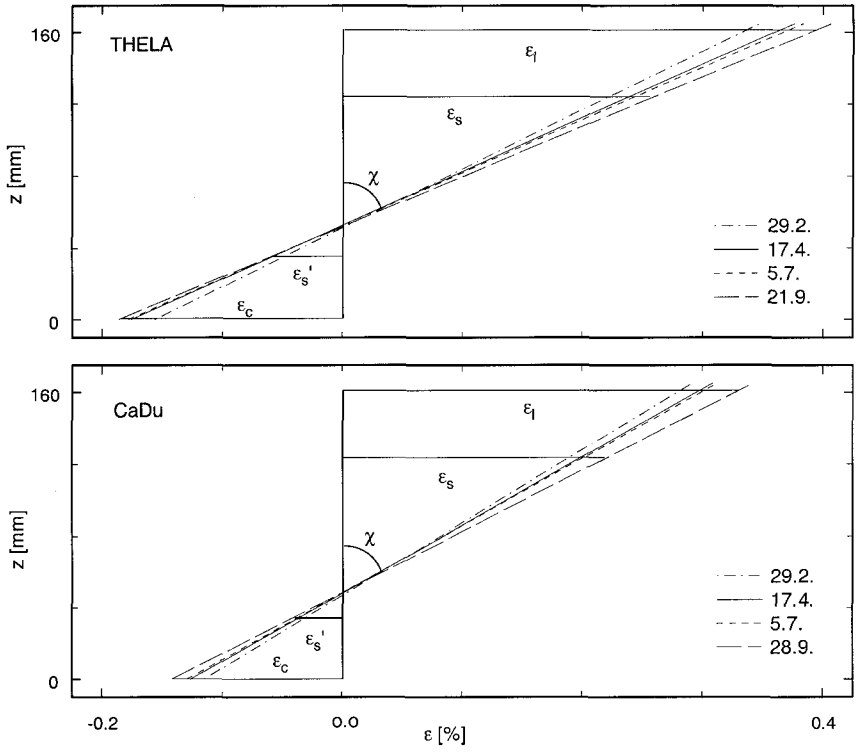



Figure 5: Average deformation of the cross-section at the end of each climate period

## DISCUSSION

Loading of the specimens caused an initial midspan deflection of approx. $^1/_{200}$ of the span (the deflection of THELA is slightly greater due to the softer laminate; see Figure 4). An increase in these deformations was recorded at the beginning of the first climate period, but creep largely ceased after some weeks. The transition between the first and second climate periods appears very smooth, with only a slight discontinuity in the deflection line. In climate period 3, the temperature at which the epoxy adhesive starts to soften (Figure 1) was exceeded. The relative displacement, $\Delta$, thus rose sharply at the beginning of this period. All deformations again levelled off after a few weeks.

The variations in curvature shown in Figure 5 may be used to assess the impact of the individual causes of deformation. During the first climate period, the specimens were exposed to constant stress and constant atmospheric conditions. The increase in curvature may thus be interpreted as creep deformation. The changes in concrete strain, $\varepsilon_c$, may be construed as creep deformation in the material, whereas the strain variations in the tension zone probably stem from creep at the steel–concrete and CFRP–concrete interfaces. The compression zone depth remained constant due to the equilibrium between these strain variations.

As Figure 4 shows, creep deformation ceased towards the end of climate period 1. In period 2, curvature remained more or less constant. The high humidity hardly affected deformation, and the slow creep process at the end of period 1 continued.
The temperature was raised by 5°C in climate period 3. The resulting thermal strains of steel and concrete were in the order of 0.005% and thus had only a minor impact on the overall deformation of the specimens. Thermal deformation of the CFRP laminate was even smaller. By contrast, the rise in temperature had a significant impact on the epoxy adhesive, which started to soften, and substantial creep deformations were recorded (Figure 4). As a result, the curvature increased further.

## CONCLUSIONS

The values and limits derived from the experimental results are only valid for the tested CFRP strengthening systems. Further tests are required for other systems. Nevertheless, a number of general statements can be made:

Commonly used CFRP strengthening systems tend to be more sensitive to elevated temperatures and humidities than steel or concrete. To establish the limiting conditions for application, the limiting component of the cross-section must be investigated. In the described tests, initial softening of the epoxy adhesive was expected at a temperature of 42°C. This was confirmed by the experimental results: the CFRP-concrete bond started to soften when the temperature was increased from 40°C to 45°C. One positive finding is that the deformations stabilized under sustained loading after a couple of weeks and no structural failure occurred. This may be viewed as an additional safety reserve in case the softening temperature is exceeded.
The glass transition temperature, $T_g$, is frequently used in defining the limiting thermal conditions for synthetic components. However, this parameter is of limited relevance as the mechanical properties of the epoxy adhesive actually start to change at a lower temperature.
Overall, creep deformation appears to be very limited. This may be due to the use of old concrete beams with relatively high creep resistance.
The precise impact of humidity remains unclear. Although it can generally affect the strength of polymers, it is unlikely to affect the materials in the climatic and stress ranges of the present experiment.

The above results relate to the test period ending 21 September 2000. The experiment is not yet concluded and ongoing monitoring is planned.

## ACKNOWLEDGEMENTS

The tests were performed as part of a joint-venture project with Sulzer Innotec AG (Winterthur, Switzerland) and Sika AG (Zurich, Switzerland). The financial support of the Swiss Commission for Technology and Innovation (KTI) is gratefully acknowledged.
The valuable assistance of H. Altorfer, J. Regnault, F. Stenger, I. Stoecklin, W. Trindler and A. Winistoerfer is highly appreciated.

## NOTATION

| | | | |
|---|---|---|---|
| A | at location A | $\chi$ | curvature |
| B | at location B | $\varepsilon$ | strain |
| E | Young's modulus | $\lambda$ | logarithmic decrement |
| G | shear modulus | | |
| H | Humidity | Subscripts | |
| M | bending moment | T | thermal |
| T | Temperature | l | laminate |
| | | s | steel |
| b | Width | u | ultimate |
| f | Strength | y | yield |
| u | Displacement | | |
| w | Deflection | Superscripts | |
| z | beam depth coordinate | ' | at compression |
| | | | |
| $\Delta$ | relative displacement | Symbol | |
| $\alpha$ | Coefficient | Ø | diameter |

## REFERENCES


[1] Meier, U., Betti, R. (Eds.): Recent Advances in Bridge Engineering. First edition, EMPA Duebendorf (Switzerland), 1997.

[2] Kaiser, H.: Bewehren von Stahlbeton mit kohlenstoffaserverstärkten Epoxidharzen. Diss. ETH Nr. 8918, Zurich (Switzerland), 1989, 224 p.

[3] Deuring, M.: Verstärken von Stahlbeton mit gespannten Faserverbundwerkstoffen. EMPA report no. 224, Duebendorf (Switzerland), 1993, 279 p.

[4] Ulaga, T.: Analytical Analysis of Simply Supported and Continuous Beams Strengthened with CFRP Laminates. PhD Symposium in Civil Engineering, Vienna (Austria), October 2000, 9 p.

[5] FIB TG 9.3: Externally Bonded Reinforcement. 2nd Draft, January 2000.

[6] CEB-FIP Model Code for Concrete Structures, Comité Euro-International du Béton, Lausanne (Switzerland), 1990, 437 p.

[7] Terrasi, G.P.: Mit Kohlenstoffasern vorgespannte Schleuderbetonrohre. EMPA report no. 240, Duebendorf (Switzerland), 1998, 306 p.

[8] DIN 53 445: Prüfen von Kunststoffen, Torsionsschwingversuch. Deutsches Institut für Normung, Berlin (Germany), 1965.

# Design of concrete members strengthened with externally bonded FRP reinforcement

T. TRIANTAFILLOU, University of Patras, Greece
S. MATTHYS, Magnel Laboratory for Concrete Research, Department of Structural Engineering, Ghent University, Belgium
L. TAERWE, Magnel Laboratory for Concrete Research, Department of Structural Engineering, Ghent University, Belgium

## ABSTRACT

Nowadays, there is a considerable interest in FRP (fibre reinforced polymer) reinforcement for building construction. Especially, the use of FRP for externally bonded reinforcement (EBR) to repair and strengthen existing structures is becoming more and more established worldwide. Since first applications in the late 1980s, the commercial use of externally bonded FRP reinforcement (FRP EBR) is currently increasing exponentially in many countries. Nevertheless, there is still a lack of design guidelines concerning this technique. Activities to develop design guidelines by the EBR working group of *fib* (International Federation for Structural Concrete) Task Group 9.3 are reported here. A *fib* Bulletin on this subject is scheduled for the summer of 2001.

## INTRODUCTION

Each year, considerable investments in construction engineering are related to maintenance, repair and strengthening (including seismic retrofit) of structures, following the social and economical needs for reliable and functional infrastructure. The need for repair and strengthening follows from several reasons, such as changes in the use and the functionality of structures, damage due to mechanical actions or environmental effects, more stringent design requirements, poor detailing, design and construction errors. Basically, the aim is to extend the service life of a structure, while minimising costs, environmental impact and disrupt in economical activity.

Several techniques for repair and strengthening are available, among which the use of externally bonded reinforcement (EBR). In this effective and frequently applied method, developed in the late 1960's, steel plates were originally used. A state-of-the-art overview on steel plate bonding is given in [1]. Alternatively, the application of steel plates can be extended to FRP reinforcement, as the latter shows advanced properties and considerable flexibility and ease-of-application. Pioneering work on the use of FRP for EBR has been performed at the EMPA [2]. This research resulted in more than a thousand applications in Switzerland alone. Internationally, many research projects and applications have been conducted and several FRP systems for strengthening have become commercially available. However, design guidelines are yet scarce, as a result of which the design approach of applications conducted so far differs considerably and is sometimes characterized by lack of design rationale. Hence, there is an urgent need to develop design recommendations in this field. The work with this respect by *fib* TG9.3 is discussed in the following.

## FIB TG 9.3 WORKING GROUP ON EBR

In December 1996, a CEB (Comité Euro-International du Béton) task group (TG 3.10) was established with the main objective to elaborate design guidelines for the use of FRP reinforcement in accordance with the design format of the CEB-FIP Model Code [3] and Eurocode2 [4]. With the merger of CEB and FIP in June 1998 into *fib* (Fédération International du Béton), CEB TG 3.10 became *fib* TG 9.3 "FRP Reinforcement for concrete structures" [5], resorting under Commission 9 "Reinforcing and Prestressing Materials and Systems". The task group consists of about 60 members, representing most European universities, research institutes and industrial companies working in the field of advanced composite reinforcement for concrete structures, as well as corresponding members from Canada, Japan and USA. Meetings are held twice a year and on the research level its work is supported by the EU TMR (European Union Training and Mobility of Researchers) Network "ConFibreCrete" [6]. The work by *fib* TG 9.3 is performed by five sub-groups:

- Material testing and characterization (MT&C)
- Reinforced concrete (RC)
- Prestressed concrete (PC)
- ***Externally bonded reinforcement (EBR)***
- Marketing and applications (M&A)

Within *fib* TG 9.3, the working group on externally bonded reinforcement (EBR) comprises about 25 active members. The involvement of this group has been considerable and resulted in the preparation of a first *fib* Bulletin in this field, called "Design and Use of Externally Bonded FRP Reinforcement (FRP EBR) for Reinforced Concrete Structures – Progress Report". This bulletin is in its final review stage and will be published in the summer of 2001. It gives detailed design guidelines on the use of FRP EBR, the practical execution and the quality control, based on the current expertise and state-of-the-art knowledge of the task group members. The content of the bulletin is discussed in the following section.

## FIB BULLETIN ON DESIGN GUIDELINES FOR THE USE OF FRP EBR

### General

In this bulletin it is aimed to give design guidance on the use of externally bonded FRP reinforcement (FRP EBR) for the repair and strengthening of concrete structures. The bulletin is regarded as a progress report because:

- it is not the aim of this report to cover all aspects of RC strengthening with composites,
- several of the topics presented are subjects of ongoing research and development, and the details of various modelling approaches may be subjected to future revisions.

Nevertheless, a considerable effort has been made to present material which is state-of-the-art in the area of composites as strengthening material for concrete structures, as well as to offer detailed design guidelines on those aspects which form the majority of the design problems. Also, much consideration is given to the practical execution aspects and quality control.

In the following the content of the bulletin chapters is briefly discussed.

### Chapter 1 - Introduction

This chapter gives an introduction to the repair (retrofit) and strengthening (upgrading) of civil infrastructure and introduces the FRP EBR strengthening technique and its benefits. The various application possibilities are briefly discussed and reference is made to internet databases and

literature on practical applications, demonstrating this technique from a practical point of view for potential users. The aim and concept of the bulletin are also given in this chapter.

**Chapter 2 - FRP Strengthening Materials and Techniques**

The selection of materials for the different strengthening systems is a critical process. Every system is unique in the sense that the fibres and the resin components are designed to work together. This implies that a resin system for one strengthening system will not automatically work properly for another. Furthermore, a resin system for the fibres will not necessarily provide a good bond to concrete. This implies that only systems that have been tested and applied in full scale on reinforced concrete structures shall be used in FRP strengthening. The chapter discusses the constituent materials for FRP strengthening, the FRP EBR systems and the techniques for FRP strengthening. With respect to the latter, reference is made to the so-called "basic technique" and to some special techniques. The basic FRP strengthening technique (Table 1), which is most widely applied, involves the manual application of either wet lay-up (so-called hand lay-up) or prefabricated systems by means of cold cured adhesive bonding. Examples of special techniques are automated wrapping, prestressing, in-situ fast curing using heating device, etc.

Table 1. Main characteristics and typical application aspects of FRP EBR (basic technique)

| | **PRE-CURED (PREFAB)** | **CURED IN SITU (WET LAY-UP)** |
|---|---|---|
| Shape | Strips or laminates | Sheets or fabrics |
| Thickness | About 1.0 to 1.5 mm | About 0.1 to 0.5 mm |
| Use | Simple bonding of the factory made elements with adhesive | Bonding and impregnation of the sheets or fabrics with resin (shaped and cured in-situ) |
| Typical application aspects | If not pre-shaped only for flat surfaces | Regardless of the shape, sharp corners should be rounded |
| | Thixotropic adhesive for bonding | Low viscosity resin for bonding and impregnation |
| | Normally 1 layer, multiple layers possible | Often multiple layers |
| | Stiffness of strip and use of thixotropic adhesive allow for certain surface unevenness | Often a putty is needed to prevent debonding due to unevenness |
| | Simple in use, higher quality guarantee (prefab system) | Very flexible in use, needs rigorous quality control |
| | Quality control (wrong application and bad workmanship = loss of composite action between FRP EBR and substrate/structure, lack of long term integrity of the system, etc.) | |

**Chapter 3 - Basis of Design and Safety Concept**

*Design Process and General Concept*

Compared to new structures, the design process for concrete structures strengthened with FRP EBR is more extensive. To start with, the existing state and load bearing capacity of the element to be strengthened should be evaluated and verified. Reasons of defects should be known (e.g. steel corrosion will generally not be arrested by the EBR) and all necessary repair actions should be taken. Next, the status and initial stress state of the member prior to strengthening should be

evaluated. With this data generated, the actual design of the EBR can be performed, according to the relevant limit states. In addition, special design considerations (bond stresses due to differences in coefficient of thermal expansion, fire resistance, etc.) and accidental situation design may apply. In the latter case, accidental loss of the EBR (e.g. due to impact, fire, etc.) is assumed, corresponding to an unstrengthened beam subjected to the loads of a strengthened beam. This situation is verified in ultimate limit state with no or reduced safety factors [4].

*Basis of Design*

The chapter discusses the basis of design according to the ultimate (ULS) and serviceability limit state (SLS). It is stated that often the latter is governing. Indeed, as FRP materials have high strength, small cross-sectional areas of FRP are needed for satisfying the ULS requirements. In order to meet the serviceability criteria, this cross-section may be insufficient, especially given the relative low modulus of elasticity of some FRP's. In the ultimate limit state (ULS), the modelling will be related to the different failure modes which may occur. Design should be such that brittle failure modes, such as shear are not governing. For the same reason, it should be guaranteed that the internal steel is sufficiently yielding in ULS (see section on Ductility), so that the strengthened member will fail in a ductile manner, despite the brittle nature of concrete crushing, FRP rupture or bond failure.

For the design stress-strain behaviour of the FRP a linear elastic behaviour is assumed. In the SLS, reference is made to the characteristic value of the secant modulus of elasticity (determined between 10 % and 50 % of the FRP ultimate strength). In the ULS, the modulus of elasticity at ultimate is used $E_{fu} = f_{fk} / \varepsilon_{fuk}$, based on the characteristic values of the FRP tensile strength and ultimate strain. The design value of the FRP strength is defined as:

$$f_{fd} = \frac{f_{fk}}{\gamma_f} \frac{\varepsilon_{fue}}{\varepsilon_{fum}}$$

where, $\gamma_f$ is the FRP material safety factor as suggested in Table 2 (boxed values stand for indicative values). The ratio $\varepsilon_{fue}/\varepsilon_{fum}$ normally equals 1, as the effective ultimate FRP strain $\varepsilon_{fue}$ expected in-situ will not significantly differ from the mean strain $\varepsilon_{fum}$ obtained through uniaxial tensile testing, and as small variations are accounted for in the FRP material safety factor $\gamma_f$. However in particular cases, the effective failure strain $\varepsilon_{fue}$ may be significantly lower, as a result of wrapping of FRP around sharp corners, application of a large number of layers, multi-axial state of stress, etc. A reduced value of the FRP failure strain may also be considered as a simplified design alternative.

Table 2. FRP material safety factors $\gamma_f$

| FRP type | Application type A[(1)] | Application type B[(2)] |
|---|---|---|
| CFRP | 1.20 | 1.35 |
| AFRP | 1.25 | 1.45 |
| GFRP | 1.30 | 1.50 |

(1) Application of prefab FRP EBR systems under normal quality control conditions. Application of wet lay-up systems if all necessary provisions are taken to obtain a high degree of quality control on both the application conditions and the application process.

(2) Application of wet lay-up systems under normal quality control conditions. Application of any system under difficult on-site working conditions.

*Accidental Situation*

The strength increase of properly designed strengthened members will be limited by ductility, ultimate and serviceability limit state requirements. Nevertheless, it is sometimes suggested that

the FRP EBR should serve as secondary reinforcement, so that in case of accidental loss of the FRP strengthening, the existing structure does not (totally) collapse. If the accidental design situation is fulfilled, structural safety is maximized with respect to loss of the externally bonded reinforcement. In this case, special design considerations such as vandalism, impact or fire are generally no longer of concern, or they are of minor importance. On the other hand, it can be argued that the accidental design situation restricts the maximum strength increase, while sufficient evidence is available to rely on the externally bonded FRP reinforcement not only as secondary reinforcement.

*Ductility*

To guarantee a minimum ductility of strengthened flexural (or tensile) members, the internal steel should sufficiently yield at failure, i.e. the curvature at ultimate should be large enough. With respect to this issue, EC2, Section 2.5.3.4.2 (5) [5] is followed. However, if the design is governed by e.g. the SLS, the amount of FRP provided to the structure may be considerably higher than what is needed for the ULS. In this case, it may be difficult to fulfil the ductility condition while yet high safety factors between the acting ($S_d$) and the resisting ($R_d$) design load in ULS are obtained (hence also a high safety factor between the service load and the resisting design load). In case $R_d \geq \boxed{1.2} S_d$, the ductility condition may no longer be fulfilled.

**Chapter 4 - Flexural Strengthening**

In this chapter calculation models for both the ultimate limit state and serviceability behaviour are proposed, concerning flexural strengthening of concrete members. These can be summarized as follows.

For the ULS, classical calculation methods for RC elements still apply as long as full composite action between the FRP and the concrete may be assumed (Fig. 1). The initial strain distribution during strengthening should be taken into account. In addition, bond failure modes should be verified, which forms a rather complex aspect of the calculation. Given the various possibilities for debonding, this verification may include several aspects.

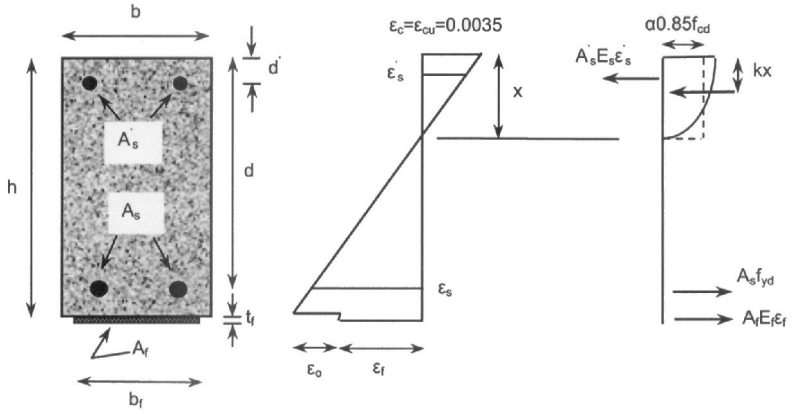



Figure 1. Analysis of cross section for the ultimate limit state of bending

Regarding bond failure, three different approaches are suggested in the bulletin (the final approach is still subject to further study and discussion). A first approach deals with an overall strain limitation in addition to the verification of the anchorage length. Although very simple with

respect to the design, it is felt that the strain limitation is a very crude simplification which may be very uneconomical. In a more complicated approach (too complex to be a practical engineering model), the FRP strain distribution of the cracked member is assessed and, in addition to anchorage failure, debonding at flexural cracks is verified. In a third approach, it is argued that local debonding at cracks in the ULS can be allowed. In addition to anchorage failure, this approach focuses on vertical crack displacements, defining the critical failure mode, and on shear stresses due to the overall variation of the FRP force along the member length. For the anchorage zone, reference is made to fracture mechanics based models for the determination of the anchorage length. In addition, anchorage failure by means of concrete rip-off (failure at the level of the internal steel) is verified.

Concerning the SLS, verification of stresses and deflections can be based on to classical methods. Compared to steel RC members the calculation becomes somewhat more complicated as the initial strain distribution during strengthening should be considered. To predict the crack width of RC elements strengthened in flexure, the influence of both the internal and external reinforcement, which have a different bond behaviour, should be taken into account. Hereby, a model along the lines of the MC90 [4] is proposed. Providing proper restriction of crack widths, no bond interface cracking is to be expected in the SLS.

In Chapter 4 of the bulletin, also some special cases are mentioned: strengthening of post- or pre-tensioned concrete members, EBR in compression and strengthening with prestressed FRP.

**Chapter 5 - Strengthening in Shear and Torsion**

The external FRP reinforcement may be treated in analogy to the internal steel (accepting that the FRP carries only normal stresses in the principal FRP material direction, Fig. 2), assuming that at the ultimate limit state in shear (concrete diagonal tension) the FRP develops an effective strain in the principal material direction, $\varepsilon_{f,e}$ (note: this is not the principal tensile strain, which may be assumed perpendicular to the crack), which is, in general, less than the tensile failure strain, $\varepsilon_{fu}$. Qualitative arguments lead to the conclusion that the effective strain is related to the quantity $E_{fu}\rho_f/f_{cm}^{2/3}$, where $\rho_f$ is the area fraction of FRP. This relationship depends also on the type of shear reinforcement (closed wraps versus open jackets). The expressions adopted in this chapter for the effective FRP strain are those derived in [7] based on best fit analysis of over 75 test results.

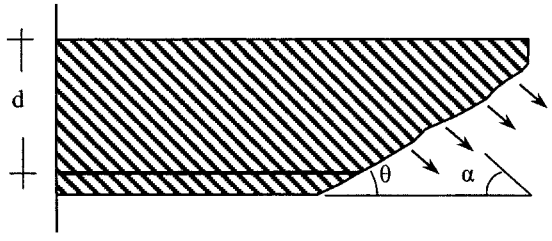



Figure 2. Modelling of FRP shear contribution

Strengthening for increased torsional capacity may be required sometimes in conventional beams and columns, as well as in bridge box girders. The principles applied to strengthening in shear are also valid in the case of torsion, with a few minor differences, which are also highlighted in this chapter.

**Chapter 6 - Confinement**

Unlike the modelling of RC elements in flexure or shear, classical calculation models are no longer suitable in case of FRP confined concrete members. This is because the increasing confining action of the FRP (Fig. 3) should be taken into account (for steel confinement a constant confining action is generally assumed). For the modelling of the constitutive stress-strain relationship of FRP confined concrete, reference is made to specific models, of which one (which is believed to be currently most accurate) is presented in detail in the chapter. This model [8], dealing with the increasing confining action, proposes an incremental-iterative calculation and combines the often applied steel confinement model of Mander et al [9] with a model linking the axial and the circumferential strain. In addition, a more practical engineering model for the maximum strength and ultimate state of the FRP confined concrete is described.

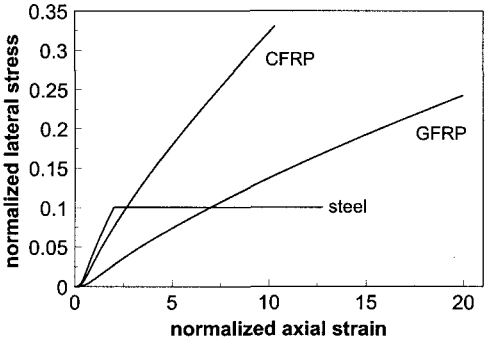



Figure 3. Comparison of confinement actions of steel and FRP materials

The FRP being a linear elastic material, the design value of the maximum lateral confining pressure $\sigma_{\ell ud}$ exerted by the FRP wrapping reinforcement is obtained when reaching the design value $\eta_e f_{fd}$ of the effective FRP strength. The reduction factor $\eta_e$ follows from the fact that the mean ultimate strain of the FRP wrapping reinforcement is lower than that obtained from tensile test coupons. This is due to local stress concentrations in the FRP near ultimate, the multiaxial state of stress of the FRP, size effects when using multiple layers, etc. Appropriate factors for $\eta_e$ should be based on experimental evidence. In addition, factors are given concerning the confinement effectiveness, taking into account partial wrapping, fibre orientation and column shape (Fig. 4).

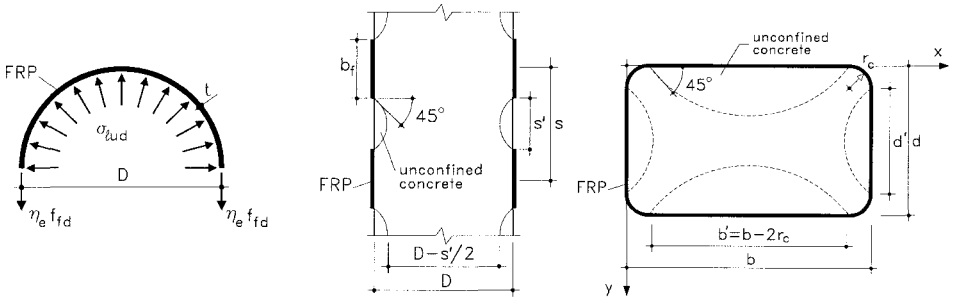



Figure 4. Effectiveness of the lateral confining stress

Besides the stress-strain behaviour of the FRP confined concrete and the influence of the wrapping configuration and column shape, the chapter also deals with aspects related to seismic strengthening for ductility increase and FRP encasings which act both as formwork and confining reinforcement.

**Chapter 7 - Detailing Rules**
Detailing rules give practical information on the location, arrangement and limitations of the FRP reinforcement required by considerations such as minimum ductility, functional requirements, adequate anchorage, applicability of calculation models, practical durability measures, friendliness of execution, etc. With respect to this issue limited information or research data are available and future work on this subject is needed. Nevertheless, in Chapter 7 of the bulletin some detailing rules are provided with respect to the strengthening lay-out and anchorage of FRP EBR, depending on its use (flexural and shear strengthening, as well as confinement).

**Chapter 8 - Practical Execution and Quality Control**
In Chapter 8 of the bulletin provisions and requirements are given concerning the practical execution of the basic technique (Fig. 5). These deal with preceding repair and concrete soundness, application conditions and procedures, limitation of unevenness, etc. The application of the FRP EBR should be performed by qualified and trained workers (preferably, the FRP EBR system and the applicators are certified by an independent certification body). This chapter also deals with the quality control aspects and gives detailed provisions (including test methods) with respect to characterization and quality control of the strengthening materials, qualification of workers, quality control on the practical execution, bond quality control after the practical execution and in-service inspection and maintenance.

**Chapter 9 - Special Design Considerations and Environmental Effects**
Depending on the use of the strengthened structure and the environmental conditions, specific aspects with respect to the FRP EBR may apply and call for additional design verifications. These special design considerations are often of a considerable importance to guarantee the structural safety of the strengthened structure. Hereby, it is of concern to evaluate the behaviour of the strengthened member rather than the FRP itself. With respect to this issue, Chapter 9 deals with design considerations such as long-term loading (creep, stress rupture and stress corrosion), cyclic loading and impact. Furthermore, the influence of environmental effects with respect to the design are considered: temperature effects, fire, chemical resistance, moisture, UV light, lightning and galvanic corrosion.

## CONTINUED WORK BY FIB TG 9.3 WORKING GROUP ON EBR

The "Design of Externally Bonded FRP Reinforcement for Reinforced Concrete Structures – Progress Report" provides state-of-the-art information on the use and especially on the design of concrete members strengthened with FRP EBR. Moreover, it is expected that this document will form the basis for further discussions on the design approach and models, on an international level. Hence, the FRP EBR working group of *fib* TG 9.3 aims to continue its work to develop design guidelines for FRP EBR, taking into account the following aspects:

- further verification and refinement of models provided in the bulletin
- more detailed work on the assessment of safety factors
- development of practical engineering models for bond behaviour, incorporating models which take into account the use of mechanical anchorages
- broaden the range of models to the less common design problems, e.g. strengthening of connections (e.g. beam-column joints)

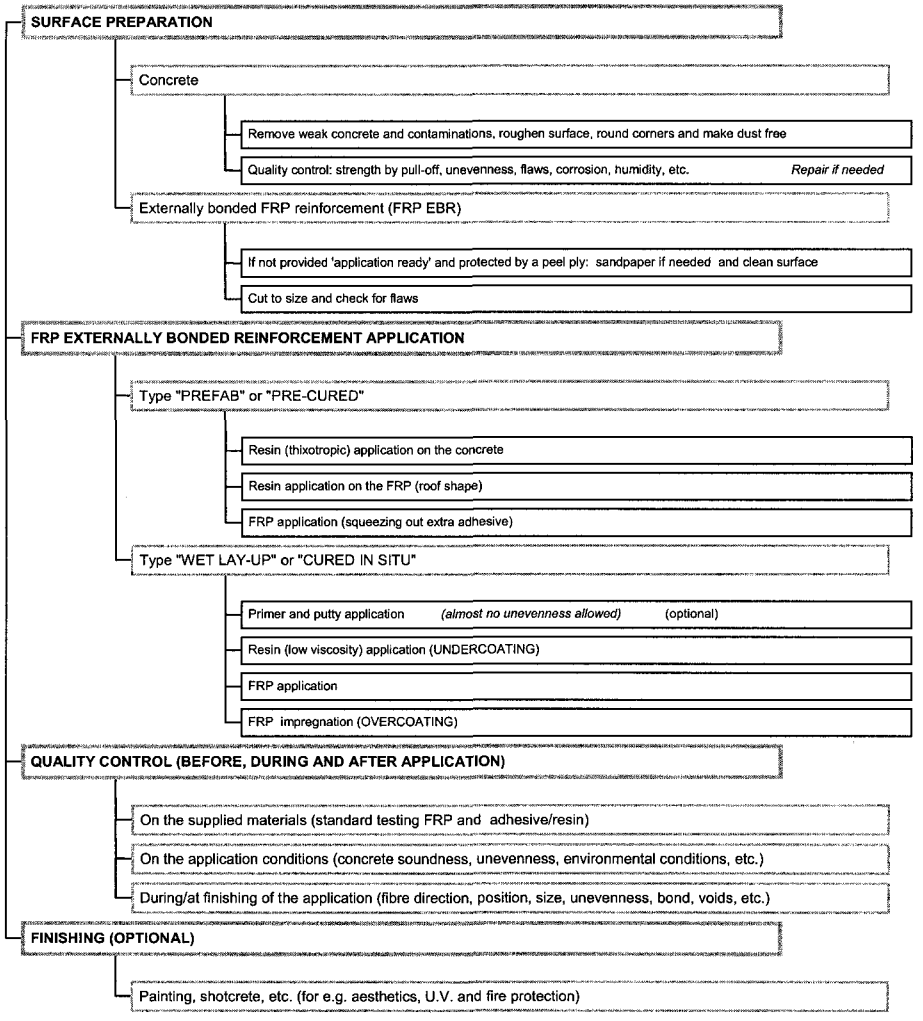



Figure 5. General scheme for the practical execution and quality control

- more emphasis on detailing aspects
- participation in the development or agreement on standard test methods
- contribution on round robin testing, with respect to tensile and bond testing of FRP EBR
- contribution or stimulation initiatives promoting the use of FRP EBR

Based on this work a new bulletin will be generated in a couple of years.

## CONCLUSIONS

A *fib* Bulletin, called "Design and Use of Externally Bonded FRP Reinforcement for Reinforced Concrete Structures – Progress Report", is in its final review stage and will be published in the summer of 2001. It gives detailed design guidelines on the use of FRP EBR,

the practical execution and the quality control, based on the current expertise and state-of-the-art knowledge of the task group members. Mainly those aspects are covered which form the majority of the design problems. In some cases they are subject of ongoing research and development, so that the details of various modelling approaches may be subjected to future revisions. As a result the bulletin is published as a progress report and the work by fib TG 9.3, working group on FRP EBR, to develop design guidelines will be continued.

**ACKNOWLEDGMENTS**

The authors wish to acknowledge the *fib* TG 9.3 members of working group "EBR" for their support and their continuous involvement in the activities.

**REFERENCES**

1. Swamy R.N, Gaul R., Eds. (1996), "Repair and Strengthening of Concrete Members with Adhesive Bonded Plates", ACI SP-165, American Concrete Institute, Michigan, 264pp.
2. Meier U., Deuring M., Meier H., and Schwegler G. (1993), "FRP Bonded Sheets", in Fiber-Reinforced-Plastic (FRP) Reinforcement for Concrete Structures: Properties and Applications, Elsevier, pp. 423-434.
3. CEB (1993), "CEB-FIP Model Code 1990, Design Code", Comité Euro-International du Béton, Lausanne, Switzerland, Thomas Telford, 437 pp.
4. CEN (1991), "Eurocode 2: Design of concrete structures – Part 1-1: General rules and rules for buildings", ENV 1992-1-1, Comité Européen de Normalisation (CEN), Brussels, Belgium, 263 pp.
5. *fib* Task Group 9.3, "FRP Reinforcement for Concrete Structures", International Federation for Structural Concrete, Commission 9, Task Group 9.3, http://allserv.rug.ac.be/~smatthys/fibTG9.3.
6. TMR, "Development of Guidelines for the Design of Concrete Structures, Reinforced, Prestressed or Strengthened with Advanced Composites (ConFibreCrete)", Training and Mobility of Researchers, Research Network TMR "ConFibreCrete", http://www.shef.ac.uk/~tmrnet.
7. Triantafillou T.C., Antonopoulos, C.P. (2000), "Design Approach for Concrete Flexural Elements Strengthened in Shear With FRP", ASCE Journal of Composites for Construction, Vol. 4, No. 4, pp. 198-205.
8. Spoelstra M.R., Monti G. (1999), "FRP-Confined Concrete Model", ASCE, Journal of Composites for Construction, Vol. 3, No. 3, pp. 143-150.
9. Mander J.B., Priestley M.J.N., Park R. (1988), "Theoretical stress-strain model for confined concrete", Journal of Structural Engineering, ASCE, Vol. 114(8), pp. 1804-1826.

# Design guidelines for flexural strengthening of concrete members using FRP composites

C. ARYA, University College, London, UK
N. FARMER, Tony Gee & Partners, Surrey, UK

## ABSTRACT
This paper provides design guidance on the use of fibre reinforced polymer (FRP) composites for flexural strengthening of reinforced concrete beams. The design guidance is based on the recommendations contained in Concrete Society Technical Report 55 and is compatible with British Standard BS:8110. The paper identifies limit states relevant to this method of construction and also discusses the partial safety factors that should be used in design. Design procedures are introduced that can be used to evaluate the moment capacity of strengthened sections. Finally, a worked example of a beam strengthened with bonded FRP reinforcement is presented in order to illustrate the design procedure.

## INTRODUCTION
Over recent years many concrete structures have been strengthened using externally bonded FRP plates and fabrics in the UK. Specialist consulting engineers have generally designed these schemes. However, apart from a draft Interim Advice Note that deals with strengthening bridge piers produced by the Highways Agency[1], currently there are no national standards or codes of practice on this method of strengthening available in the UK. Work is in hand by several non-UK bodies including the American Concrete Institute and The Federation Internationale du Beton to develop suitable guidelines, but these are either incomplete or not directly compatible with British practice. This lack of guidance is believed to be responsible for limited use of FRP materials by some designers, specifiers and owners of infrastructure.

To address this problem, the UK Concrete Society established a committee in 1999 to produce a Report[2] on strengthening with FRP composites. Using limit state principles and set in the context of BS 8110[3] for buildings and BS 5400:Part 4[4] for bridges, the Report provides guidance on this method of strengthening concrete structures, based on UK experience and practice.

In its present form, the guide does not contain any worked examples that illustrate the procedures outlined. This need is addressed in the present paper. Due to space limitations the paper focuses on flexural strengthening of concrete beams with FRP reinforcement, this representing the majority of applications.

## LIMIT STATES
In line with standard British practice, the design of FRP strengthening schemes should be based on limit state principles. Table 1 lists ultimate and serviceability limit states relevant to the design of reinforced concrete beams strengthened with bonded FRP.

*FRPRCS-5*, Thomas Telford, London, 2001.

Table 1. Limit States

| Ultimate | Serviceability |
|---|---|
| Strength<br>bending<br>shear<br>plate separation | Deflection<br>Cracking |

For buildings, fire should also be included in the above limit states as it will influence the properties of both the FRP and the adhesive used to attach the FRP to the concrete. Other relevant limit states are fatigue, creep rupture and durability. Structures that cannot resist working loads without collapsing should not normally be considered suitable for strengthening.

Since the design of FRP strengthening systems is normally concentrated on the ultimate limit state of strength, this paper focuses on bending and plate separation. However checks are also made on stresses induced under working loads in order to avoid excessive deformation.

## MATERIAL MODELS

The analytical expressions that have been developed are based on the idealised material models for concrete and reinforcing steel recommended in BS8110. FRPs used as structural reinforcement are assumed to have a linear elastic response to failure.

## FACTORS OF SAFETY

For structures constructed before 1997, the partial safety factors for concrete (in flexure), $\gamma_{mc}$, and steel reinforcement, $\gamma_{ms}$, should be taken as 1.5 and 1.15 respectively. The partial safety factors applied to the characteristic mechanical properties of FRPs, however, should be taken as a function of the type of fibre and the manufacturing route. Assuming a partial safety factor on carbon fibre, $\gamma_{mf}$, of 1.4 and the pultrusion process, $\gamma_{mm}$, of 1.1, an overall factor of safety on carbon pultruded plate, $\gamma_{mF}$, of (1.4 x1.1=) 1.54 is indicated. It is further suggested that a partial safety factor should be applied to the mean modulus of elasticity of FRP materials, $\gamma_{mE}$. A value of 1.1 is recommended for use with carbon FRP reinforcement.

## MOMENT CAPACITY

The area of FRP, $A_f$, required for strengthening can be determined iteratively using a computer programme by finding the internal equilibrium of forces acting on the concrete cross-section. The compressive force in the concrete and the tensile forces in the steel and FRP reinforcement can be calculated using the following assumptions:

- plane sections before loading remain plane after loading;
- the stresses in the concrete in compression and the steel reinforcement are calculated using idealised stress strain models for concrete and steel contained in national codes and standards;
- FRP has a linear elastic response to failure;
- the tensile strength of concrete is ignored;
- no slip occurs at the concrete/FRP interface.

An alternative approach which involves calculating the balanced moment of resistance of the section, $M_{r,b}$, and comparing with the design ultimate moment, M, can also be used[5]. The design ultimate moment is normally calculated using elastic principles. The balanced condition is assumed to occur when the concrete and the FRP reach their ultimate strains simultaneously as shown in Fig. 1. An expression for $M_{r,b}$ is obtained by taking moments about the bottom face (see Equation 1).

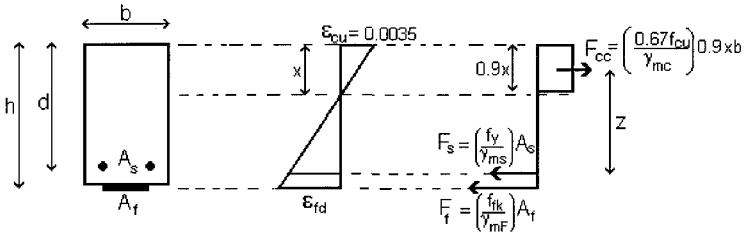



Figure 1. Stress and strain distributions at balanced condition

$$M_{r,b} = (0.67/\gamma_{mc})f_{cu}0.9bx\,[z + (h - d)] - (f_y/\gamma_{ms})A_s(h - d) \quad (1)$$

If M is less than $M_{r,b}$, failure theoretically occurs as a result of FRP rupture. However, in practice, FRP rupture is a rare event and FRP debonding is more likely (see below). By assuming that the strain in the FRP is the lesser of the design FRP strain and the strain limit for debonding, the area of FRP required to sustain the design moment can be estimated by dividing the additional moment capacity by the product of the FRP design stress and the steel lever arm. A check is subsequently required to ensure that the strain in the reinforcement can be mobilised for the calculated neutral axis depth.

If M is greater than $M_{r,b}$, failure occurs due to concrete crushing. As both the stress in the FRP and the tensile force in the FRP are unknown in this case, the design procedure is more complex. The stress in the FRP, $f_f$, can be obtained using the following:

$$f_f = E_{fd}(\varepsilon_{cft} - \varepsilon_{cit}) \quad (2)$$

where

$E_{fd}$ elastic modulus of FRP = $E_{fk}/\gamma_{mE}$ (3)

$\varepsilon_{cft}$ final tensile strain in the concrete at the FRP/concrete interface (see below)

$\varepsilon_{cit}$ initial tensile strain in the concrete at the FRP/concrete interface calculated on the basis of an elastic analysis of the cracked section using the following:

$$\varepsilon_{cic} = M_s x_o/E_c I_{ce} \quad (4)$$

$$\varepsilon_{cit} = \varepsilon_c (h - x_o)/ x_o \quad (5)$$

where

$\varepsilon_{cic}$ = initial compressive strain in concrete

$M_s$ = service moment based on unfactored permanent loads acting on the unstrengthened member

$x_o$ = depth of neutral axis of existing section

$E_c$ = modulus of elasticity of concrete
$I_{ce}$ = second moment of area of concrete equivalent transformed cracked section
h = overall depth of member

The final strain in the concrete at the FRP/concrete interface is a function of the compressive strain in the concrete and the depth of the neutral axis. Since the design moment causes compressive failure of the concrete, the strain in the concrete, $\varepsilon_{cu}$, will be 0.0035. The depth of the neutral axis is calculated using the design moment and section properties. For example, Fig. 2 shows the stress and strain distributions in a singly reinforced beam strengthened with bonded FRP.

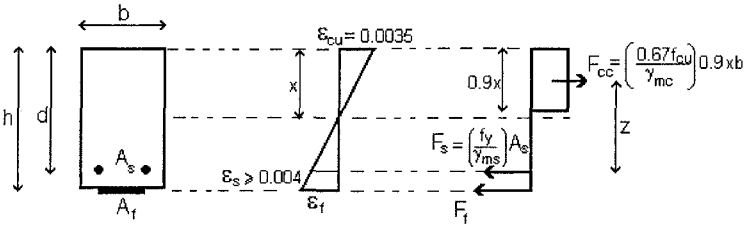



Figure 2. Strain and stress distributions when $M_{r,b} < M$

Taking moments about the bottom face of the beam and assuming $x = (d - z)/0.45$, the flexural strength of the beam is given by

$$M_r = (8/9)f_{cu}b(d - z)[z + (h - d)] - (f_y/\gamma_{ms})A_s(h - d) \quad (6)$$

By putting $M_r = M$, the depth of the lever arm, z, can be determined. The depth of the neutral axis is then obtained by back substituting into the expression for $x$ above. Knowing the ultimate strain in the concrete, the depth of the neutral axis and the overall depth of the section, the final strain in the concrete at the level of the FRP, $\varepsilon_{cft}$, can be estimated

The force in the FRP is a function of the design moment acting on the member. It is estimated using an alternative expression obtained by taking moments about the compressive force in the concrete as follows

$$M_r = F_s z + F_f[z + (h - d)] \quad (7)$$

Again by putting $M_r = M$ and $F_s = (f_y/\gamma_{ms})A_s$ the tensile force in the FRP, $F_f$, can be obtained. Finally the area of FRP required for flexural strengthening can be evaluated using the following:

$$A_f = F_f/f_f \quad (8)$$

## PLATE SEPARATION

Members strengthened with external FRP can fail prematurely as a result of local FRP separation. This can arise due to two different mechanisms: end peel and debonding. These mechanisms are not totally understood and are difficult to model theoretically. Therefore, semi-empirical methods of design have been suggested for dealing with these modes of failure.

### End peel

End plate separation failure can be avoided by:

- anchoring the FRP by extending beyond the point at which it is theoretically no longer required;
- limiting the longitudinal shear stress between the FRP and the substrate to 0.8 N/mm$^2$.

The anchorage length can be estimated using the model proposed by Neubauer and Rostasy[6]. According to their model the maximum ultimate bond force, $T_{k,max}$, that can be developed by the FRP at a discontinuity in the bonded surface is given by

$$T_{k,max} = 0.5 k_b b_f \sqrt{(E_f t_f f_{ctm})} \quad (9)$$

$T_{k,max}$ can be used to estimate the theoretical cut-off point of the FRP. Extending the FRP the greater of $\ell_{t,max}$ and 500 mm past this point obtains the actual cut-off point. $\ell_{t,max}$ is given by the following expression

$$\ell_{t,max} = 0.7\sqrt{(E_f t_f / f_{ctm})} \geq 500 \text{ mm} \quad (10)$$

where

$k_b$ = $1.06\sqrt{[(2 - b_f/b)/(1 + b_f/400)]} \geq 1.0$

$b_f$ = plate (mm)

$b_w$ = beam width (mm)

$t_f$ = plate thickness (mm)

$E_{fd}$ = elastic modulus of the FRP

$f_{ctm}$ = tensile strength of concrete = $0.18(f_{cu})^{2/3}$

The longitudinal shear stress, $\tau$, can be calculated using the following expression:

$$\tau = VA_f\alpha_f(h-x)/I_{cs}b_a \quad (11)$$

where

V = ultimate shear force at the FRP end

$\alpha_f$ = short term modular ratio of FRP to concrete

$A_f$ = area of FRP

x = depth of neutral axis of strengthened section

h = overall depth of section

$I_{cs}$ = second moment of area of strengthened concrete equivalent cracked section

$b_a$ = width of adhesive layer

The longitudinal shear stress should be checked at the plate ends, where the shear force acting on the strengthened member will be at its greatest. Additionally, the longitudinal shear stress should be checked at locations in the span where the steel reinforcement has yielded. At these locations any steel reinforcement does not contribute towards the second moment of area of the transformed section post yielding, as its modulus of elasticity is zero.

**Debonding**

The risk of bedonding is exacerbated by the formation of wide flexural and shear cracks. A direct way of avoiding this potential failure mode is simply to limit the strain in the concrete at the interface with the FRP. For steel reinforcement the ultimate strain should not exceed $5\varepsilon_y$. The strain in the concrete at the FRP interface should not exceed 0.8% when the applied loading is uniformly distributed or 0.6% if combined high shear forces and bending moments are present, such as where the applied loads are concentrated at a point and at hogging regions close to supports.

## EXAMPLE OF DESIGN CALCULATIONS FOR BEAM STRENGTHENED WITH FRP BONDED REINFORCEMENT

A singly reinforced concrete beam 350 mm wide and 700 mm deep is required to span 9 m between the centres of supports. The longitudinal reinforcement in the beam consists of 2T25 +

2T32 and the shear reinforcement of 8mm diameter links. Nominal cover to the reinforcement is 40mm.

The beam was originally designed to support characteristic dead and imposed loads of 15 kN/m and 21 kN/m respectively but is now required to carry additional characteristic dead and imposed loads of 5 kN/m and 7 kN/m respectively. To achieve this, externally bonded CFRP plate is to be attached to the beam soffit.

*Material Properties and Partial Safety Factors*

| *Concrete* | | *Steel reinforcement* | | *CFRP* | |
|---|---|---|---|---|---|
| $f_{cu}$ | $= 40$ N/mm$^2$ | $f_y$ | $= 460$ N/mm$^2$ | $f_{fk}$ | $= 2500$ N/mm$^2$ |
| $E_c$ | $= 31$ kN/mm$^2$ | $E_s$ | $= 200$ kN/mm$^2$ | $E_{fk}$ | $= 200$ kN/mm$^2$ |
| $\varepsilon_{cu}$ | $= 0.0035$ | $\varepsilon_y$ | $= 0.002\,3$ | $\varepsilon_{fk}$ | $= 0.013$ |
| $\gamma_{mc}$ | $= 1.5$ | $\gamma_{ms}$ | $= 1.15$ | $\gamma_{mf}$ | $= 1.4$ |
| | | | | $\gamma_{mm}$ | $= 1.1$ |
| | | | | $\gamma_{mE}$ | $= 1.1$ |

**1. Design ultimate moment, M**

$$g_{new} = g_{initial} + g_{add} = 15 + 5 = 20 \text{ kN/m}$$

$$q_{new} = q_{initial} + q_{add} = 21 + 7 = 28 \text{ kN/m}$$

$$M = \frac{(1.4g_{new} + 1.6q_{new})\ell^2}{8} = \frac{(1.4\times20 + 1.6\times28)\,9^2}{8} = 737 \text{ kNm}$$

**2. Moment of resistance for balanced failure, $M_{r,b}$**

$$\gamma_{mF} = \gamma_{mf}\gamma_{mm} = 1.4\times1.1 = 1.54 \qquad \varepsilon_{fu} = \varepsilon_{fk}/\gamma_{mF} = 0.013/1.54 = 0.0084$$

$$x = \frac{h}{\varepsilon_{fu}/\varepsilon_{cu} + 1} = \frac{700}{0.0084/0.0035 + 1} = 206 \text{ mm} \qquad z = d - \frac{0.9x}{2} = 636 - \frac{0.9\times206}{2} = 543 \text{ mm}$$

$$M_{r,b} = \left(\frac{0.67f_{cu}}{\gamma_{mc}}\right)b\,0.9x[z + (h-d)] - \frac{f_y}{\gamma_{ms}}A_s(h-d)$$

$$= \left(\frac{0.67\times40}{1.5}\right)350\times0.9\times206\,[543 + (700-636)] - \frac{460}{1.15}2592(700-636)$$

$$= 637\times10^6 \text{ Nmm}$$

Since $M > M_{r,b}$, failure will be due to concrete crushing.

**3. Area of FRP, $A_f$**

*(i) Second moment of area of existing section*

$$\alpha_e = \frac{E_s}{0.5E_c} = \frac{200\times10^3}{0.5\times31\times10^3} = 12.9 \qquad \text{(Note: long-term elastic modulus to account for creep)}$$

$$\sum Ax_o = 0 \qquad \frac{bx_o^2}{2} = \alpha_e A_s\,(d - x_o) \qquad \frac{350x_o^2}{2} = 12.9\times2592\,(636 - x_o) \quad \Rightarrow x_o = 266 \text{ mm}$$

$$I_{ce} = \frac{bx_o^3}{3} + \alpha_e A_s\,(d - x_o)^2 = \frac{350\times266^3}{3} + 12.9\times2592\,(636-266)^2 = 6.77\times10^9 \text{ mm}^4$$

*(ii) Initial strain in concrete*

Assume loading at time of strengthening = $g_{initial} + 25\%q_{initial} = 20.3$ kN/m

$\Rightarrow M_s = 20.3\times9^2/8 = 206$ kNm

$$\varepsilon_{cic} = \frac{M_s x_o}{E_c I_{ce}} = \frac{206\times10^6\times266}{(0.5\times31\times10^3)6.77\times10^9} = 5.22\times10^{-4}$$

$$\varepsilon_{cit} = \varepsilon_{cic}\frac{(h-x_o)}{x_o} = 5.22\times10^{-4}\frac{(700-266)}{266} = 8.52\times10^{-4}$$

*(iii) Final strain in concrete*

$$M_r = \frac{8}{9}f_{cu}b\,(d-z)\,[z+(h-d)] - \frac{f_y}{\gamma_{ms}}A_s(h-d)$$

$$737\times10^6 = \frac{8}{9}\times40\times350\,(636-z)\,[z+(700-636)] - \frac{460}{1.15}\times2592\,(700-636)$$

$\Rightarrow z = 527$mm

$$z = d - \frac{0.9x}{2}$$

$$527 = 636 - \frac{0.9x}{2}$$

$\Rightarrow x = 243$ mm $< 0.45d = 286$ mm $\quad\therefore$ steel will yield before failure of FRP or concrete

$$\varepsilon_{cft} = \varepsilon_{cu}\frac{(h-x)}{x} = 0.0035\frac{(700-243)}{243} = 6.58\times10^{-3} < 0.008 \qquad \text{O.K.}$$

*(iv) Stress in FRP*

$$f_f = E_{fd}(\varepsilon_{cft}-\varepsilon_{cit}) = \frac{200\times10^3}{1.1}(6.58\times10^{-3}-8.52\times10^{-4}) = 1041\ \text{N/mm}^2\ (E_{fd} = E_{fk}/\gamma_{mE})$$

*(v) Force in FRP*

$$M_r = F_f[z+(h-d)] + F_s z$$

$$737\times10^6 = F_f[527+(700-636)] + \frac{460}{1.15}2592\times527$$

$\Rightarrow F_f = 322{,}515$ N

*(vi) Area of FRP*

$$A_f = \frac{F_f}{f_f} = \frac{322515}{1041} = 310\ \text{mm}^2$$

Try 2 No. 1.4 mm thick and 120 mm wide carbon plates. Area of plate, $A_{f,prov} = 336$ mm$^2$.

**4. Anchorage length**

*(i) Second moment of area of strengthened section*

$$\alpha_f = \frac{E_{fd}}{E_c} = \frac{(200\times10^3/1.1)}{0.5\times31\times10^3} = 11.73$$

$$\sum Ax = 0$$

$$\frac{bx^2}{2} = \alpha_e A_s (d-x) + \alpha_f A_f (h-x)$$

$$\frac{350x^2}{2} = 12.9\times2592(636-x) + 11.73\times336(700-x)$$

$$\Rightarrow x = 279 \text{ mm}$$

$$I_{ce} = \frac{bx^3}{3} + \alpha_e A_s (d-x)^2 + \alpha_f A_f (h-x)^2$$

$$= \frac{350\times279^3}{3} + 12.9\times2592(636-279)^2 + 11.73\times336(700-279)^2 = 7.49\times10^9 \text{ mm}^4$$

*(ii) Maximum tensile force developed in FRP*

$$k_b = 1.06\sqrt{\frac{2-\frac{b_f}{b_w}}{1+\frac{b_f}{400}}} \geq 1.0$$

$$k_b = 1.06\sqrt{\frac{2-\frac{240}{350}}{1+\frac{240}{400}}} = 0.96$$

$$\therefore k_b = 1.0$$

$$f_{ctm} = 0.18 f_{cu}^{2/3} = 0.18\times40^{2/3} = 2.1 \text{ N/mm}^2$$

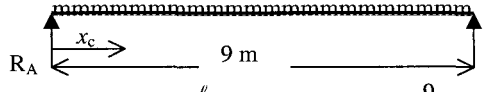
$$T_{k,max} = 0.5 k_b b_f \sqrt{E_{fd} t_f f_{ctm}} = 0.5\times1\times240\sqrt{(200\times10^3/1.1)1.4\times2.1} = 87{,}735 \text{ N}$$

*(iii) Theoretical cut-off point, $x_c$*

Tensile force in FRP plate, T, due to applied ultimate moment, M, is given by

$$T = \frac{M\alpha_f A_f (h-x)}{I_{cs}} \qquad 87{,}735 = \frac{M\times11.73\times336(700-279)}{7.49\times10^9}$$

$$\Rightarrow M = 396\times10^6 \text{ Nmm}$$




$$R_A = (1.4g_k + 1.6q_k)\frac{\ell}{2} = (1.4\times20+1.6\times28)\frac{9}{2} = 327.6 \text{ kN}$$

$$M_x = R_A x_c - (1.4g_{new} + 1.6q_{new})\frac{x_c^2}{2} = 327.6x_c - (1.4\times20+1.6\times28)\frac{x_c^2}{2}$$

$$= 327.6x_c - 36.4x_c^2$$

$396 = 327.6x_c - 36.4x_c^2 \qquad \Rightarrow x_c = 1.439\text{ m} \quad \text{say } 1.4\text{ m}$

*(iv) Anchorage length*

$\ell_{t,max} = 0.7\sqrt{E_{fd}t_f / f_{ctm}} \geq 500\text{ mm} \qquad \ell_{t,max} = 0.7\sqrt{(200\times10^3/1.1)1.4/2.1} = 244\text{ mm}$

$\therefore \ell_{t,max} = 500\text{ mm}$

Required plate length = 9 – (2 x 1.4) + 2 x 0.5 = 7.2 m

**5. Longitudinal shear stress**

*(i) At plate ends*

From 3(i), x = 266 mm and second moment of area of section ignoring FRP = $6.77\text{x}10^9$ $\text{mm}^4$

Ultimate moment at plate end i.e. $x_e = 0.9$ m obtained via 4(iii)

$$M_{x_e=0.9} = 327.6x_e - 36.4x_e^2 = 327.6\times0.9 - 36.4\times0.9^2 = 265.4\text{ kNm}$$

$$\sigma_s = \frac{M\alpha_e(d-x)}{I_{ce}} = \frac{265.4\times10^6\times12.9\,(636-266)}{6.77\times10^9} = 187\text{ N/mm}^2 < 0.87f_y = 400\text{ N/mm}^2$$

Since steel has not yielded, allow for longitudinal steel reinforcement in determining x and $I_{cs}$.

From 4(i) x = 279 mm and $I_{cs} = 7.49\text{ x}10^9$ $\text{mm}^4$, and longitudinal shear stress at plate ends is given by

$$\tau = \frac{V\alpha_f A_f(h-x)}{I_{cs}b_a} = \frac{262.1\times10^3\times11.73\times336\,(700-279)}{7.49\times10^9\times240} = 0.24\text{ N/mm}^2 < 0.8\text{ N/mm}^2\text{ O.K.}$$

(where $V = R_A - 72.8x_e = 327.6 - 72.8\times0.9 = 262.1$ kN)

*(ii) At the point of maximum shear where the steel yields*

It is conservative to assume that the point of maximum shear at which the steel yields occurs where the applied moment can be resisted by the steel reinforcement alone, $x_y$. This point can be estimated via the moment capacity of the unstrengthened beam, $M_o$.

$$\frac{100A_s}{bd} = \frac{100\times2592}{350\times636} = 1.16 \quad \text{From Chart No. 2, BS8110 : Part3} \quad \frac{M}{bd^2} = 4 \quad \therefore M_o = 566\text{ kNm}$$

From 5(i) it follows, $M_o = 327.6x_y - 36.4x_y^2 = 566\text{ kNm} \quad \Rightarrow x_y = 2.332\text{ m from support}$

The shear force acting on the beam is due to the difference between the ultimate load and the load at the time of strengthening, assumed to be equal to $g_k + 25\%q_k$. The additional load on the beam after strengthening is then given by

[(0.4x15 + 1.4x5 + 0.6(0.25x21) + 1.6(0.75x21) + 1.6x7)9 = 52.55 x 9 = ] 472.95 kN

Hence, shear force at yield point, $V_y = R_{A,y} - 52.55x_y = 236.475 - 52.55\times2.332 = 114$ kN

Second moment of area of section ignoring steel reinforcement is

$$\sum Ax = 0 \qquad \frac{bx^2}{2} = \alpha_f A_{f,prov}\,(h-x)$$

$$\frac{350x^2}{2} = 11.73\times336\,(700-x) \qquad \Rightarrow x = 115 \text{ mm}$$

$$I_{ce} = \frac{bx^3}{3} + \alpha_f A_{f,prov}(h-x)^2 = \frac{350\times115^3}{3} + 11.73\times336\,(700-115)^2 = 1.53\times10^9 \text{ mm}^4$$

Longitudinal shear stress at the point of maximum shear where the steel yields, is given by

$$\tau_y = \frac{V_y \alpha_f A_f (h-x)}{I_{cs} b_a} = \frac{114\times10^3\times11.73\times336\,(700-115)}{1.53\times10^9\times240} = 0.72 \text{ N/mm}^2 < 0.8 \text{ N/mm}^2 \text{ O.K.}$$

**6. Material stresses at service loads**

*(i) Before strengthening*

From 3(i), $x_o$= 266 mm, $I_{ce} = 6.77 \times 10^9$ and $M_{s,bs}$ = 205 kNm (= [15 + 0.25x21]$9^2$/8)

$$\therefore \text{Concrete stress, } f_{c,bs} = \frac{M_{s,bs} x_o}{I_{ce}} = \frac{205\times10^6\times266}{6.77\times10^9} = 8.1 \text{ N/mm}^2 \quad \text{and}$$

$$\text{Steel stress, } f_{s,bs} = \frac{M_{s,bs}\alpha_e (d-x_o)}{I_{ce}} = \frac{205\times10^6\times12.9\times(636-266)}{6.77\times10^9} = 144.5 \text{ N/mm}^2$$

*(ii) After strengthening*

From 4(i), x = 279 mm, $I_{ce} = 7.49 \times 10^9$ and $M_{s,as}$ = 281 kNm (= [5 + 0.75x21 + 7]$9^2$/8) after strengthening. Therefore, concrete and steel stresses are respectively

$$f_{c,as} = \frac{281\times10^6\times279}{7.49\times10^9} = 10.5 \text{ N/mm}^2 \text{ and } f_{s,as} = \frac{281\times10^6\times12.9(636-279)}{7.49\times10^9} = 172.8 \text{ N/mm}^2$$

*(iii) Total material stresses*

Concrete stress $f_{c,TOTAL}$ = 8.1 + 10.5 = 18.6 N/mm$^2$ < allowable = $0.6f_{cu}$ = 24 N/mm$^2$ O.K.
Steel stress $f_{s,TOTAL}$ = 144.5+ 172.8 = 317.3 N/mm$^2$ < allowable = $0.8f_y$ = 368 N/mm$^2$ O.K.

**REFERENCES**


1. Strengthening concrete bridge supports using fibre reinforced plastic, Interim Advice Note, The Highways Agency, London, 1999 Draft.
2. Concrete Society Technical Report 55, Design guidance for strengthening concrete structures using fibre composite materials, The Concrete Society, Crowthorne, UK, 2000.
3. BS8110: Structural use of concrete. Part 1, Code of practice for design and construction, Part 2, Code of practice for special circumstances, British Standards Institute, London, 1997.
4. BS5400: Part 4, Code of practice for design of concrete bridges, British Standards Institute, London, 1990.
5. Vijay, P.V., Kumar, S. and GangaRao, H.V.S., Design of carbon sheet wrapped concrete beams, West Virginia University, 1996.
6. Neubauer, U. and Rostasy, F.S. (1997), Design aspects of concrete structures strengthened with externally bonded CFRP-plates. Proceedings 7th International Conference on Structural Faults and Repairs, Vol 2, 109-118, 1997.

# Simplified design guidelines for FRP reinforced concrete beams in flexure

NINOSLAV PEŠIĆ and KYPROS PILAKOUTAS
Reader, Department of Civil & Structural Engineering, University of Sheffield, UK

**ABSTRACT**
This paper presents simplified design equations for FRP reinforced concrete (RC) beams in flexure in a form suitable for design practice. The design is based on the assumption that concrete crushing in compression is the desired mode of failure. An overview of the current recommendations for bending, shear and verification of the serviceability limit states is also given. The existing and newly proposed design guidelines are then demonstrated through a design example with additional comparisons between Eurocode 2 and the latest ACI-440 code provisions.

## Introduction

The successful replacement of conventional steel with FRP reinforcement requires investigation on many design aspects and in particular on likely modes of failure of FRP RC members. It is therefore necessary to assess a suitable design approach which will avoid the occurrence of non-desired modes of failure.

Several design codes and recommendations for FRP RC members have already been prepared in Canada [1], Japan [2] and the United States [3], mainly as modifications to the existing (steel) RC codes of practice. Modification principles are directly influenced by the unconventional mechanical properties of FRP reinforcement and empirical equations based on limited experimental work on FRP RC elements. At the moment, there is little information on the long-term behaviour of FRP RC elements and the impact of FRP material durability on safety.

In Europe, the design recommendations for FRP RC elements, derived as modifications to BS 8110 [4], the Norwegian standard NS3473 [5] and Eurocode 2 [6] codes of practice, are based on research undertaken within the Eurocrete programme [7].

Further work towards developing a more detailed design code of practice for FRP RC elements is being carried out by Task Group 9.3 of *fib* supported by the EU ConFibreCrete research network. A need for simple design equations in the forthcoming European code covering flexure of FRP RC beams is being addressed here. A simplified design equations and chart for rectangular FRP RC sections are presented next and then applied to an example of a simply supported GFRP RC beam.

The results from the Eurocode 2 serviceability limit state verification (deflections and crack widths) are also compared to the ACI-440 solutions.

*FRPRCS-5*, Thomas Telford, London, 2001.

**Bending**

New values of material safety factors have been proposed for design of FRP RC elements by Neocleous and Pilakoutas [8] as part of an alternative design philosophy in which the desired hierarchy of failure is predicted. In this case, a sudden failure of tensile FRP reinforcement is to be avoided. Due to the general absence of ductility of FRP reinforced elements in flexure, the most favourable mode of failure is chosen to be through concrete crushing in compression followed by shear failure due to fracture of the FRP stirrups. If the desired mode of concrete compression failure is to be achieved, over-reinforced FRP elements in structural applications are inevitable. For this reason, the partial safety factors for tensile strength of FRP reinforcement are less important when compared to steel RC design since they do not necessarily influence the structural safety.

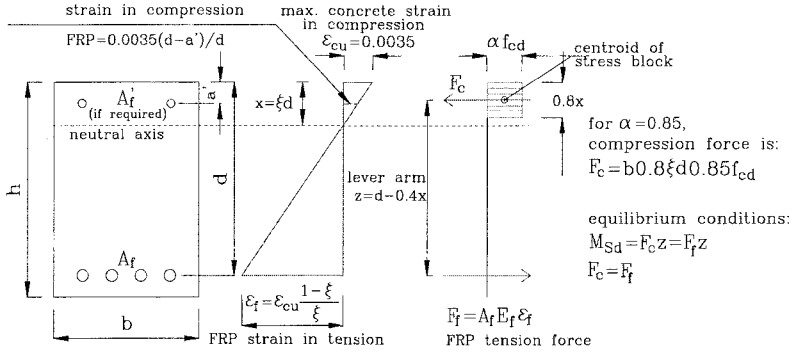



**Figure 1:** FRP reinforced concrete section and associated stress-strain diagrams

Considering the rectangular cross-section subjected to bending, as shown in Figure 1, the approximate value of the design (factored) bending moment resistance is:

$$M_{Sd} \approx 0.68bd^2 f_{cd}\xi(1-0.4\xi) \tag{1}$$

where $f_{cd}$ is the design value of concrete compressive strength.

By using a non-dimensional normalised bending moment coefficient:

$$m = \frac{M_{Sd}}{f_{cd}bd^2} \tag{2}$$

the neutral axis ratio '$\xi = x/d$' can be obtained from equation 1 by:

$$\xi \approx 1.25 - 0.5\sqrt{6.25 - 14.706m} \tag{3}$$

When the neutral axis depth coefficient $\xi$ is determined, the required FRP reinforcement ratio $\rho_f = A_f/(b \cdot d)$ can be calculated by using section equilibrium as:

$$\rho_{f,req} \approx \frac{0.68\xi^2}{1-\xi}\frac{f_{cd}}{E_f \cdot \varepsilon_{cu}} \tag{4}$$

A universal design chart for the determination of the required FRP reinforcement ratio (through its product with the tensile modulus of elasticity of the FRP reinforcement, $E_f$) is given in Figure 2 for different values of the normalised bending moment $m$ (eq.2) and design concrete compressive strength $f_{cd}$. The use of higher concrete grades in FRP RC structures is obviously beneficial because of the direct increase of the sectional bending resistance and much better utilisation of the relatively high tensile strength of the FRP reinforcement.

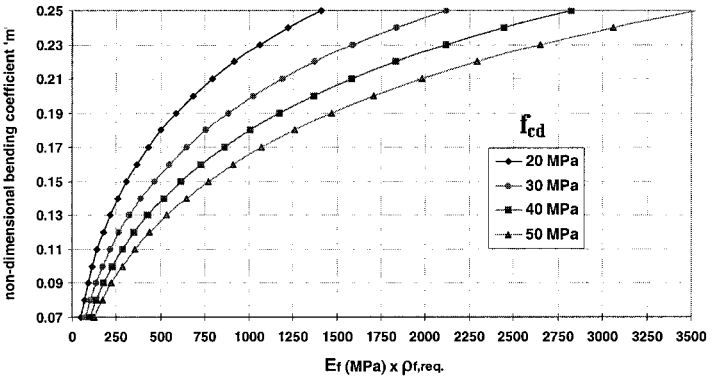



**Figure 2:** Determination of the required FRP reinforcement ratio ($E_f\rho_{f,req.}$)

At this stage, the minimum value of the required FRP reinforcement ratio is not affected by the actual design value of the reinforcement tensile strength, defined as $f_{fd}=f_{fk}/\gamma_{FRP}$, but rather with the concrete compression strength. If the value of the adopted FRP reinforcement ratio is greater than the one obtained from equation 4, the section can be considered to be over-reinforced and its expected mode of failure would be through concrete crushing in compression.

Additionally, the adopted area of tensile FRP reinforcement needs to be checked against the minimum area required to prevent the beam from failure without warning when first cracks develop. As for the minimum FRP reinforcement ratio, the authors would propose the following modified expression to the one provided in sub-clause 5.4.2.1 of Eurocode 2 [6] referring to steel RC elements:

$$\rho_{f,\min.} = \frac{0.6}{\alpha_E f_{fk}} \geq \frac{0.0015}{\alpha_E} \tag{5}$$

where $\alpha_E = E_f / E_s$ is the ratio of FRP over steel reinforcement modulus of elasticity.

After adjustments made to conform with SI units, the expression for the minimum FRP reinforcement ratio given in ACI-440 [3] has the following form:

$$\rho_{f,\min.} = \frac{0.45\sqrt{f_{ck}}}{f_{fk}} \geq \frac{2.5}{f_{fk}} \tag{6}$$

with the characteristic strengths of concrete, $f_{ck}$, and FRP reinforcement, $f_{fk}$, in MPa.

Finally, when the area of tensile FRP reinforcement is determined, the stress in FRP bars should be checked against the design tensile strength of the FRP reinforcement:

$$\sigma_f \approx \frac{M_{Sd}}{A_f d(1-0.4\xi)} < f_{fd} = \frac{f_{fk}}{\gamma_{FRP}} \tag{7}$$

where $\gamma_{FRP}$ is the partial safety factor applied to the tensile strength of the FRP material.

**Shear Design**

In its simplest form, the shear resistance of a RC member $V_{Rd}$ is evaluated as the sum of the shear capacities of plain concrete, $V_{Rd,1}$, and provided shear reinforcement $V_{wd}$. Codes of practice provide equations for shear capacity of plain concrete elements but there are different approaches for estimation of shear resistance provided by FRP links.

Modification to the existing formulae for the contribution of steel shear reinforcement such as the one given by Eurocode 2 [6], $V_{wd}=0.9f_{yd}A_{sw}d/s_w$, is the introduction of a tensile strain limitation for FRP shear links of $\varepsilon_{fv}=0.0020\div0.0025$ (the strain level at which steel bars would yield). The approach was initially proposed by Nagasaka at al. [9] and it results with the following expression for shear resistance of vertical FRP stirrups:

$$V_{fv} \approx \frac{0.0025E_f\, 0.9dA_{fv,1}}{s_w} \tag{8}$$

where $A_{fv,1}$ is the area of a single shear link, $s_w$ is the spacing between individual links and $E_f$ is the modulus of elasticity of FRP material.

The strain limitation approach might provide a convenient basis for future code developments but with the working strains in FRP shear links limited to the values of 0.0020÷0.0025, the tensile strength of FRP bars can not be fully utilised.

This point was addressed experimentally during the Eurocrete project [7] and it was observed [10] that shear failures took place at much higher loads than predicted by equation 8. Based on this work, the new lower bound strain limit for FRP shear links was found to be approximately 0.0045. Hence, a new strain correction factor $\phi_\varepsilon=0.0045/0.0025=1.8$ was proposed.

The design shear resistance provided by FRP vertical stirrups may then be conservatively taken as the smaller of two values:

$$V_{fv,d} = \min\left\{\frac{A_{fv}0.9d}{s_w}\phi_\varepsilon\, 0.0025E_f, \frac{A_{fv}0.9d}{s_w}\frac{f_{fk}}{\gamma_f}\right\} \tag{9}$$

**Serviceability Limit States**

Due to significantly lower stiffness properties, especially when compared to the steel reinforced members, FRP RC elements in flexure may exhibit excessive deformations and cracking affecting the appearance and performance of structures in service. It is accepted that, for most design situations, allowable crack widths for FRP RC elements can be larger than values adopted in codes for steel RC members aimed at preventing problems with corrosion. Crack width limiting values for FRP RC members recommended in Eurocrete project [7] are given in Table 1. In some special cases (where problems with the water-resistance or extreme aggressive environment may occur), values provided in Table 1 may not be adequate and, in the absence of more information in this field, the limitations suggested for steel RC elements can be applied.

**Table 1:** Crack width limitations for FRP reinforced concrete members (Eurocrete [7])

| Tightness | Aesthetic reasons | Structural integrity |
|---|---|---|
| 0.2 mm | 0.3 ÷ 0.5 mm | 0.5 ÷ 1.0 mm |

The application of Eurocode 2 strain-based approach, developed for steel reinforced RC elements in flexure for prediction of deflections, crack widths and spacing (as given in sub-clause 5.4) is demonstrated through a design example in the next section.

At the moment, the ACI-440 [3] document provides the most detailed approach specific to the evaluation of the short- and long-term deflections of FRP RC beams.

The instantaneous deflections under service loads can be obtained using standard linear analysis approach. The effective second moment of area of a cracked FRP RC beam should be estimated using the following expression recommended by Gao at al. [11]:

$$I_{cr,e} \approx \left(\frac{M_{cr}}{M}\right)^3 \beta_d I_g + \left[1 - \left(\frac{M_{cr}}{M}\right)^3\right] I_{cr} \le I_g \tag{10}$$

where $M$ is the bending moment under service loads, $M_{cr}$ is the bending moment corresponding to the first concrete sectional crack, $I_g$ and $I_{cr}$ are the second moments of area for un-cracked and cracked concrete section, respectively.

The parameter $\beta_d = \alpha_b (1 + E_f / E_s)$ takes into account bond properties of FRP bars with $\alpha_b = 0.5$ for GFRP bars which is the same as for steel bars. For bars with better bond properties than that of steel, values for $\alpha_b$ greater than 0.5 may be used but until more data become available, value of 0.5 can also be adopted for other types of FRP bars.

The deflections of FRP RC beams increase in time due to creep and shrinkage in a manner similar to that of steel RC beams. As found by Kage at al. [12], FRP RC beams under sustained load over a period of one year exhibited, depending on the type of FRP bars, the final deflections around 1.2 ÷ 1.8 times that of the equivalent steel RC beams.

The ACI-440 [3] prediction for long-term deflections of FRP RC beams can be written as:

$$f_{(cp+sh)} \approx \delta \xi f_{in,sus} \tag{11}$$

where $f_{in,sus}$ is the initial deflection and the time dependent coefficient $\xi$ takes values of 1.74 and 2.0 for loading duration periods of 12 months and 10 years, respectively. Parameter $\delta$ varies between 0.46 for AFRP and GFRP bars and 0.53 for CFRP bars and, for design considerations, can be conservatively taken as 0.6 [3].

In the following section, the application of ACI-440 [3] method for verification of serviceability limit states of a GFRP RC beam is demonstrated and compared to the method adopted by Eurocode 2 [6] (clauses 4.4.2 and 4.4.3).

**Design Example**

A simply supported GFRP RC beam with an effective span of 6m, as shown in Figure 3, is subjected to a uniformly distributed permanent and live loading of 5.0 and 18.3 kN/m.

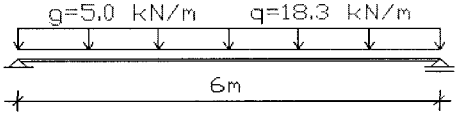



**Figure 3:** Load arrangement for a simply supported GFRP RC beam

The design process consists of the following steps:

a) defining the appropriate dimensions for the cross-section of the beam;
b) calculation of the required amount of tensile GFRP reinforcement;
c) stress verification for the GFRP reinforcement in tension and concrete in compression for un-factored loading;
d) shear design - calculation of required vertical GFRP shear links;
e) calculation of short- and long-term deflections;
f) calculation of average crack widths.

*Concrete properties (C25/35):*

design compressive strength $f_{cd} = 16.7$ MPa;
modulus of elasticity $E_{cm} = 28$ GPa;
design shear strength $\tau_{Rd} = 0.30$ MPa;
characteristic tensile strength $f_{ct} = 2.5$ MPa;

creep coefficient $\varphi_\infty = 1.5$.

*GFRP reinforcement:* modulus of elasticity $E_f = 48\,\text{GPa}$.

characteristic tensile strength $f_{fk} = 620$ MPa;

(partial safety factors) $\gamma_{FRP} = 1.3$ (long. bars), $\gamma_{FRP} = 2.0$ (shear links);

*Partial safety factors for loading:* $\gamma_G = 1.35$ (dead load), $\gamma_Q = 1.50$ (live load).

*(a) section dimensions*

Assuming the typical span to depth ratio for GFRP RC beams to be around L/d≈10÷12, adopted cross-section dimensions in this example are **b/d/h=300/550/600mm**.

*(b) required area of tensile GFRP reinforcement*

Design (factored) loading: $S_D = \gamma_G \cdot g + \gamma_Q \cdot q = 34.2$ kN/m.

Design value of bending moment: $M_{Sd} = S_D \cdot L^2/8 = 153.9 \approx 154.0$ kNm.

Normalised bending moment: $m_{Sd} = \dfrac{154.0 \cdot 10^6}{16.7 \cdot 300 \cdot 550^2} = 0.102 \Rightarrow m_{Sd} \approx 0.1$.

Neutral axis depth coefficient: $\xi_{Sd} = 1.25 - 0.5 \cdot \sqrt{6.25 - 14.706 \cdot m_{Sd}} = 0.157 \approx 0.16$.

Required reinforcement ratio: $\rho_{f,req} \approx \dfrac{0.68\xi^2}{1-\xi} \dfrac{f_{cd}}{E_f \cdot \varepsilon_{cu}} = 0.22\%$.

The minimum ratio (mod.EC2):

$$\rho_{f,\min.} = \max\left\{\frac{0.6}{620} \cdot \frac{205}{48}; 0.0015 \cdot \frac{205}{48}\right\} \Rightarrow \rho_{f,\min.} = 0.64\%$$

(ACI-440 [3]): $\rho_{f,\min.} = \max\left\{\dfrac{0.45 \cdot \sqrt{25}}{620}; \dfrac{2.5}{620}\right\} \Rightarrow \rho_{f,\min.} = 0.40\%$

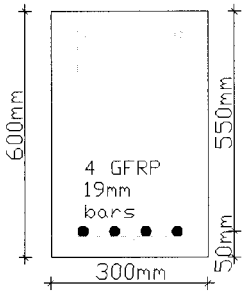



**Figure 4:** Cross-section geometry

Adopted reinforcing bars:
4 ∅19mm GFRP bars.

The area of tensile reinforcement:
$A_f = 1134.1\,\text{mm}^2$.

GFRP reinforcement ratio:
$\rho_f = 0.68\%$ (over-reinforced section).

(the same section considered by Eshani [13])

*(c) stress verification under service loads:*

Bending moment (un-factored): $M = (g+q) \cdot L^2/8 = 104.85 \approx 105.0$ kNm.

Average stress in concrete: $\sigma_c \approx \dfrac{M}{b \cdot \xi \cdot d^2 \cdot (1-\xi)} = 12.85$ MPa $< f_{cd} = 16.7$ MPa.

Normalised un-factored bending moment and the neutral axis coefficient:
$m \approx 0.0643$ and $\xi \approx 0.1$.

Tensile strength of GFRP bars: $f_{fd} = f_{fk}/\gamma_{FRP} = 620/1.3 \approx 476$ MPa.

Tensile stress in GFRP bars: $\sigma_f \approx \dfrac{M}{A_f \cdot d \cdot (1-\xi)} = 175.3 \text{ MPa} < f_{fd}$.

(the value computed in [13] is: $\sigma_f = 176$ MPa).

*(d) shear design – required vertical GFRP links*

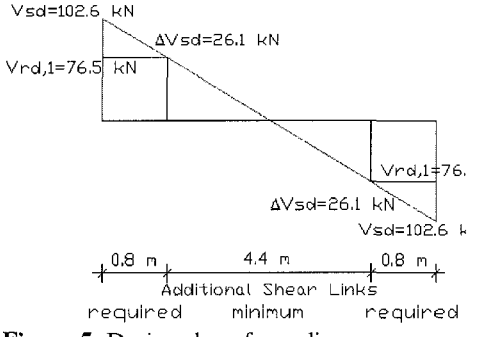



**Figure 5:** Design shear force diagram

Design (factored) shear force: $V_{Sd} = S_d \cdot L/2 = 102.6\,\text{kN}$.

Shear resistance of plain concrete:

$$V_{Rd,1} = \left[\tau_{Rd} \cdot k \cdot (1.2 + 40 \cdot \rho_f) + 0.15 \cdot \sigma_p\right] \cdot b \cdot d$$

*(Eurocode 2 [5]):* $V_{Rd,1} = [0.30 \cdot 1.05 \cdot (1.2 + 40 \cdot 0.0068) + 0] \cdot 300 \cdot 550 \cdot 10^{-3}$

Shear reinforcement required: $V_{Rd,1} = 76.5kN < V_{Sd} \Rightarrow \Delta V_{Sd} \approx 26.1\,\text{kN}$.

Trying ∅6mm GFRP stirrups: $A_{fv,1} = (\pi/4) \cdot 6.0^2 \approx 28.2\ \text{mm}^2$.

Maximum spacing: $s_{w,\max} = \dfrac{A_{fv,1} \cdot 0.9 \cdot d}{\Delta V_{Sd}} \cdot \phi \cdot 0.0025 \cdot E_f$;

$$s_{w,\max} = \frac{28.2 \cdot 0.9 \cdot 550}{26.1 \cdot 10^3} \cdot 1.8 \cdot 0.0025 \cdot 48 \cdot 10^3 = 115\,\text{mm}.$$

Adopted GFRP shear links: ∅6mm @ 10cm where $V_{Rd,1} < V_{Sd}$ (otherwise @20cm)

Shear resistance of GFRP links: $V_{Rd,2} = \dfrac{28.2 \cdot 0.9 \cdot 550}{100} \cdot 0.0045 \cdot 48 = 30.1\,\text{kN} > \Delta V_{Sd}$ ∴

*(e) serviceability limit state of deflections under service loading*

***Eurocode 2 approach***

The total long-term deflection: $f_{tot.} = f_I \cdot \xi + f_{II} \cdot (1-\xi)$

The distribution coefficient: $\xi = 1 - \beta_1 \cdot \beta_2 \cdot \left(\dfrac{M_{cr.}}{M}\right)^2$

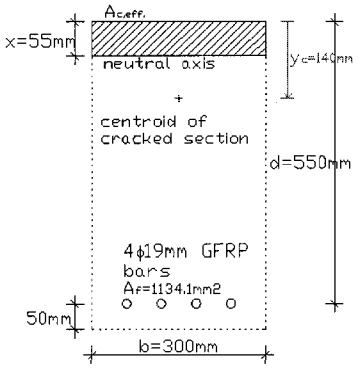
The coefficients $\beta_1$ and $\beta_2$: $\beta_1 = 1.0$ and $\beta_2 = 1.0$ (for bond and loading).

First moment of area for concrete: $W_g \approx \dfrac{300 \cdot 600^2}{4} = 18 \cdot 10^6\ \text{mm}^3$.

The bending moment corresponding to the appearance of the first crack:

$M_{cr} \approx W_g \cdot f_{ct} \quad \Rightarrow \quad M_{cr} \approx 18 \cdot 10^6 \cdot 2.5 \cdot 10^{-6} = 45.0\,\text{kNm}.$

The distribution coefficient is now: $\xi = 1 - 1.0 \cdot 1.0 \cdot \left(\dfrac{45.0}{105.0}\right)^2 = 0.816$.




A nominal deflection (un-cr. sec.):

$$f_I = \frac{5}{384}\cdot\frac{(g+q)\cdot L^4}{E_c \cdot I_g}$$

with $I_g \approx b\cdot h^3/12 = 5.4\cdot 10^{-3}\,\text{m}^4 \Rightarrow f_I = 2.6\,\text{mm}$.

The second moment of area for cracked section shown in Figure 6:

$$I_{cr} \approx \frac{b\cdot x^3}{12} + b\cdot x\cdot(y_c - \frac{x}{2})^2 + \frac{E_f}{E_{c,\varphi}}\cdot A_f\cdot(d-y_c)^2$$

$x = 0.1\cdot 550 = 55\,\text{mm}$ (neutral axis depth).

$E_{c,\varphi} = E_c/(1+\varphi) = 11.2\,\text{GPa}$.

$I_{cr} \approx 1.03\cdot 10^{-3}\,\text{m}^4$

**Figure 6:** Geometry of the cracked cross-section.

A nominal deflection on the basis of the cracked section:

$$f_{II} = \frac{5}{384}\cdot\frac{(g+q)\cdot L^4}{E_{c,\varphi}\cdot I_{cr}} \quad \Rightarrow \quad f_{II} = 34\,\text{mm}.$$

The final long-term deflection: $f_{tot.} = 2.6\cdot(1-0.816) + 34\cdot 0.816$

$f_{tot.} = 28.2\,\text{mm} > L/250 = 24\,\text{mm}$.

The limiting value for the final mid-span deflection is exceeded!

***ACI-440 (2000) approach***

The effective moment of inertia for the cracked beam:

$$I_{cr,e} = \left(\frac{M_{cr}}{M}\right)^3\cdot\beta_d\cdot I_g + \left[1-\left(\frac{M_{cr}}{M}\right)^3\right]\cdot I_{cr}$$

$$\beta_d = \alpha_b\cdot\left[\frac{E_s}{E_f}+1\right] = 0.5\cdot\left(\frac{205}{48}+1\right) \approx 0.62$$

$$I_{cr} = \frac{b\cdot d^3}{3}\cdot k^3 + n_f\cdot A_f\cdot d^2\cdot(1-k)^2$$

$n_f = E_f/E_c = 48/28 \approx 1.714$; $\rho_f = A_f/(b\cdot d) \approx 0.0068$;

$k = \sqrt{2\cdot\rho_f\cdot n_f + (\rho_f\cdot n_f)^2} - \rho_f\cdot n_f \approx 0.14$

$\Rightarrow \quad I_{cr} \approx 0.48\cdot 10^{-3}\,\text{m}^4$.

$$I_{cr,e} = \left(\frac{45}{105}\right)^3\cdot 0.62\cdot 5.4\cdot 10^{-3} + \left[1-\left(\frac{45}{105}\right)^3\right]\cdot 0.48\cdot 10^{-3}$$

$I_{cr,e} \approx 0.705\cdot 10^{-3}\,\text{m}^4$.

The instantaneous deflections: (dead load) $f_{i,DL} = \frac{5}{384}\cdot\frac{5.0\cdot 6.0^4}{28\cdot 10^6\cdot 0.705\cdot 10^{-3}} \approx 4.3\,\text{mm}$

(live load)

$$f_{i,LL} = \frac{5}{384} \cdot \frac{18.3 \cdot 6.0^4}{28 \cdot 10^6 \cdot 0.705 \cdot 10^{-3}} \approx 15.6\,\text{mm}$$

(total DL+LL) $f_{i,DL+LL} = 4.3 + 15.6 = 19.9\,\text{mm}$

The additional deflection due to creep and shrinkage is obtained as:

$$f_{(cr+sh)} = \delta \cdot \xi \cdot f_i$$

With the parameter for bond properties of FRP bars $\delta$=*0.5* and $\xi$=2.0 for duration period of 10 years, the total deflection of a beam after 10 years for 50% sustained live load is:

$$f_{tot.} \approx 0.5 \cdot f_{i,LL} + \delta \cdot \xi \cdot (f_{i,DL} + 0.5 \cdot f_{i,LL})$$

$$f_{tot.} \approx 0.5 \cdot 15.6 + 0.6 \cdot 2.0 \cdot (4.3 + 0.5 \cdot 15.6)$$

$$f_{tot.} \approx 22.3\,\text{mm} < L/250 = 24\,\text{mm} \quad \therefore$$

*(f) serviceability limit state of cracking*

***Eurocode 2** design crack width* $w_k \approx 1.5 \cdot \varepsilon_{fm} \cdot s_{rm}$

The main strain in FRP bars: $\varepsilon_{fm} \approx \xi \cdot \sigma_f / E_f = 0.816 \cdot 175.3 / (48 \cdot 10^3) \approx 3.0 \cdot 10^{-3}$

The average crack spacing: $s_{rm} = 50 + 0.25 \cdot k_1 \cdot k_2 \cdot \varnothing_f / \rho_{f,eff.}$

$\rho_{f,eff.} = A_f / [b \cdot 2.5 \cdot (h-d)] \approx 0.03$; $\varnothing_f = 19mm$; $k_1 = 0.8$ (for bond); $k_2 = 0.5$ (for bending)

$$\Rightarrow \quad s_{rm} = 50 + 0.25 \cdot 0.8 \cdot 0.5 \cdot 19 / [1134.1 / (2.5 \cdot 300 \cdot 50)] = 113.3\,\text{mm}.$$

The final (factored) crack width: $w_k \approx 1.5 \cdot 3 \cdot 10^{-3} \cdot 113.3 = 0.51\,\text{mm} \cong 0.50\,\text{mm} \quad \therefore$

***ACI-440 (2000)** design crack width:* $w \approx \frac{2.2}{E_f} \cdot \beta \cdot k_b \cdot \sigma_f \cdot \sqrt[3]{d_c \cdot A}$

$d_c \approx 50mm$; $\rho_{f,adopt.} = 0.0068$; $\sigma_f = 175.3\,\text{MPa}$; $k_b = 1.0$.

with $k = 0.14 \Rightarrow \beta = (h - k \cdot d) / (d - k \cdot d) \approx 1.106$;

The effective area of concrete in tension per one FRP bar:

$$A = 2 \cdot b \cdot d_c / n_{bars} = 2 \cdot 300 \cdot 50 / 4 = 7500mm^2.$$

The final crack width is: $w = \frac{2.2}{48 \cdot 10^{-3}} \cdot 1.106 \cdot 1.0 \cdot 175.3 \cdot \sqrt[3]{50 \cdot 7500}$

$$w \approx 0.64\,\text{mm} > 0.50\text{mm}.$$

**Concluding Remarks**

Based on the assumptions of sectional concrete compression failure, simplified design equations and chart for FRP RC beams were derived and demonstrated through a design example. The paper has also summarised the latest recommendations and guidelines on the shear design of FRP RC beams. The Eurocode 2 and ACI-440 (2000) approach in the verification of the serviceability limit states were also demonstrated and compared through a design example of a GFRP RC beam.

The long-term deflection obtained by applying the Eurocode 2 equations has exceeded the usual limitation of L/250, while the value obtained by using the ACI-440 equations has not. The ACI-440 approach (modified Branson's method) seems to be superior over the one given by Eurocode 2 as it takes into consideration the duration, type and distribution of loads in more detail. On the other side, the final crack width computed by Eurocode 2 was within the allowable limit of 0.50 while the one obtained by ACI-440 method was not (the latter code, however, allows the maximum value of crack width to be 0.71mm).

It was observed that both codes have some drawbacks and that significant differences exist between the two codes in the domain of serviceability limit state verification. In contrast to ACI-440, the Eurocode 2 still does not address specifically the use of FRP reinforcement and the equations derived for steel bars, which may well be inappropriate in FRP RC design, were used in the design example. It became apparent that the values adopted for the EC 2 coefficients taking into account bond properties of the steel reinforcing bars are not appropriate for the FRP reinforcement.

The ACI-440 equation (10) for effective moment of inertia $I_{cr,e}$ includes modification parameter $\beta_d$ which takes into account bond properties of the FRP bars. However, the implied relation between the bond properties of the FRP reinforcement and their Young's modulus of elasticity $E_f$ is not so obvious. The authors believe that the differences in results between the two codes of practice emerged mainly due to different considerations of bond properties of the FRP bars and any further code of practice should address this issue in a more consistent way.

***Acknowledgements***

*The authors wish to express their gratitude for financial support received from the EU Commission to the TMR network "ConFibreCrete" and ORS award scheme of the Vice-Chancellor's Committee of the British Universities.*

## References

1. CHBDC, "Canadian Highway Bridge Design Code, Section 16: Fibre Reinforced Structures", Final Draft, p.25, July 1996.
2. JSCE, "Recommendation for Design and Construction of Concrete Structures Using Continuous Fiber Reinforcing Materials", Japan Society of Civil Engineers, October 1997.
3. ACI Committee 440, "Guide for the Design and Construction of Concrete Reinforced with FRP Bars", American Concrete Institute, October 2000.
4. BS 8110, "Structural use of concrete, Part 1 - Code of Practice for Design and Construction", British Standards Institution, p.132, 1997.
5. Thorenfeldt, E., "Modifications to NS3473 when using Fibre Reinforced Plastic (FRP) reinforcement", SINTEF Report STF22 A98741, Trondheim 1998.
6. Eurocode 2, Part 1 - "Design of Concrete Structures: General Rules and Rules for Buildings", European Committee for Standardisation, 1992.
7. Eurocrete Project, "The Development of Non-ferrous Reinforcement for Concrete Structures - Final Report", Euro-Projects (LTTC) Ltd, 1997.
8. Neocleous, K. and Pilakoutas, K., "Safety Philosophy for FRP RC Structures", European Conference on Composite Materials, ECCM-98, Naples, Vol. 2 (pp.211–218), June 1997.
9. Nagasaka T., Fukuyama H. and Tanigaki M., "Shear Performance of Concrete Beams Reinforced with FRP Stirrups", Proceedings of the Int. Symposium on FRP reinforcement for Concrete Structures, pp.789-811., Nanni A. and Dolan C.W., (Ed.), ACI SP-138, 1993.
10. Djuranovic N., Pilakoutas K. and Waldron P., "FRP Reinforcement for Concrete Structures: Design Considerations", Non-metallic (FRP) Reinforcement for Concrete Structures, ", Proceedings of the Third International Symposium (JCI), Vol. 2 (pp.527-534), October 1997.
11. Gao, D, Benmokrane, B. and Masmudi, R., "A Calculating Method of Flexural Properties of FRP-Reinforced Concrete Beam: Part 1 – Crack Width and Deflection", Technical Report (p.24), Dept. of Civil Engineering, Uni. of Sherbrooke, Quebec, Canada, 1998.
12. Kage, T., Masuda, Y. and Tanano, Y., "Long-Term Deflection of Continued Fiber Reinforced Concrete Beams", Non-metallic (FRP) Reinforcement for Concrete Structures, Proceedings of the Second International Symposium (RILEM) pp.251-258, August 1995.
13. R.H.Ehsani, "Glass-Fiber Reinforcing Bars", in "Alternative Materials for the Reinforcement and Prestressing of Concrete" (Ed. by J.L. Clarke), pp.34-54, Chapman & Hall, London, 1993.

# Guidelines for strengthening concrete structures with FRP laminates

C. ARYA, University College, London, UK
J.L.CLARKE, The Concrete Society, Crowthorne, UK
E.A. KAY and D.P. O'REGAN, Halcrow Group, London, UK

## ABSTRACT
This paper reviews the contents of a recent Concrete Society Technical Report on strengthening concrete structures using externally bonded fibre composite materials. The paper describes the background, nature and mechanics of producing the Report. Set in the context of limit state philosophy, the Report provides design guidance on flexural strengthening of beams and slabs, shear strengthening of beams and columns, and flexural and compressive strengthening of columns. These procedures are briefly explained. Other aspects of the Report, which deal with material types and properties, field applications, workmanship and installation, and long-term monitoring, are summarised. The paper concludes by outlining The Concrete Society's future activities in this field.

## INTRODUCTION
There is a worldwide need for methods of strengthening and repairing concrete structures. This need may arise due to a variety of reasons, including non-compliance with revised loading requirements, material deterioration, proposed change of usage or alterations to the structure. Methods such as section enlargement, span shortening and external post-tensioning exist and are well established. However, all require considerable resources to implement. A more cost-effective solution is simply to bond plates to the external surfaces of beams and slabs or to enclose columns with collars. These plates and collars have traditionally been made of steel and a large number of structures have been strengthened in flexure and compression using this approach.

A recent development of this technique, which avoids the problems with steel, such as the heavy weight and lack of long-term durability, is the use of composite materials based on carbon, glass and aramid fibres. The research that has been carried out has shown that bonding composite plates to the tension face of the member can increase the flexural strength of beams and columns. Wrapping columns with FRP materials has been shown to increase compressive strength, flexural strength and ductility. Field experience has revealed that despite the high cost of these materials, there is an overall reduction in cost compared with traditional approaches when other factors such as labour and plant are included.

Further uptake of this technology is currently being hampered by the fact that there is little independent guidance on how the design of strengthening work should be carried out. Some FRP suppliers provide limited advice but this tends to be system specific. Also, this advice may not be compatible with national design codes. Because of this lack of design guidance, the UK Concrete Society set out in 1999 to produce a report on strengthening structures with externally

*FRPRCS-5*, Thomas Telford, London, 2001.

bonded FRP, which would be applicable to all types of FRP and all strengthening systems, and set in the context of British codes and standards. The resulting design guidance, Technical Report No. 55[1], was published in December 2000. The aim of this paper is to briefly describe the mechanics of producing the report and summarise its scope and salient features.

## WHO PRODUCED THE REPORT

Responsibility for drafting the report was undertaken jointly by Halcrow Group, The Concrete Society and University College London. A Steering Group consisting of representatives of client organisations, composite material suppliers, design consultants, contractors and research organisations reviewed the work.

## SCOPE OF REPORT

The overall aim of the Report is to provide design and construction guidelines on strengthening concrete structures strengthened with fibre composite materials, set in the context of British design codes and standards. A key feature is the design procedures, which are applicable to all FRP material and all strengthening techniques. The procedures are based on generally accepted principles and are in line with the approaches developed elsewhere, such as in the USA and Canada. The properties of FRP materials and manufacturing methods are discussed in so far as they have a direct effect on the design and performance of the strengthened structures. Some information on the properties of commercially available FRP materials is included, along with a list of composite suppliers with contact addresses. Some examples of field applications where composites have been employed to strengthen concrete structures in the UK are discussed. Workmanship and installation are vital aspects and have therefore been covered in some detail. Since this is a relatively new technique, some guidance on inspection and monitoring are included. A specification was felt to be inappropriate but a list of some significant points on quality control of the FRP and the method of installation was considered to be useful and has been included.

Prestressed FRP strengthening systems are not covered in detail in the Report. Also the discussion on retrofitting of concrete structures for enhanced seismic resistance is limited since this is not a major loading case for most UK structures. The emphasis in writing this Report, particularly those sections dealing with detailed design, was on providing guidance on design and construction and not necessarily a state-of-the-art report on strengthening.

## MATERIAL PROPERTIES

Indicative properties of some proprietary FRP sheet and plate materials are included in the Report as are the properties of some epoxy adhesives and laminating resins. The manufacture of FRP materials is outlined and some general guidance on the selection of FRP material for particular strengthening applications given. This section also briefly discusses other aspects related to selection such as durability, electrical resistance, fire, health and safety and environmental impact.

The properties of typical adhesives used to bond FRP composites to concrete surfaces are discussed. Common methods of application and ways of preventing degradation are described. To ensure compatibility, it is recommended that the composite materials and the adhesive, along with any paint or additional protective materials, should be obtained from a single supplier.

## FIELD APPLICATIONS

To help convince clients of the merits of this technique, brief summaries of projects where externally bonded FRP has been used to strengthen existing structures has been included. The

list is by no means exhaustive and mainly covers examples of strengthening works to buildings and bridges, mainly in the UK. Where possible, references to published articles are included. It was felt that these might provide a source of further information and also help the reader to identify individuals and organisations with experience of this technique.

## DESIGN GUIDANCE

In common with most British Codes of practice for structural design, the methods contained in the Report are based on limit state philosophy. This ensures that a structure will not become unfit for its intended use, that is, it will not reach a limit state during its design life. In assessing the effect of a particular limit state on the structure, the designer will need to assume certain values for the loading and the strength of the materials.

The Report identifies and discusses limit states relevant to the use of FRP for strengthening. In general, these are similar to those encountered in conventional reinforced concrete design but they also include checks for plate separation failure, which is peculiar to this method of construction. In limit state design, the variability of material properties is taken into account by assuming a characteristic strength. Usually, characteristic strength is taken as the value below which not more that 5% of test results lie. A similar approach is used to define characteristic strength of FRP in the Report but the acceptable failure rate has been reduced to 1%. Thus characteristic strength of FRP is defined as:

$$f_{fk} = f_{fm} - 2\text{s.d.}$$

where

$f_{fk}$ characteristic strength
$f_{fm}$ mean strength of FRP
s.d. standard deviation

The design strength is obtained by dividing the characteristic strength by a partial safety factor, which is a function of the type of fibre and the manufacturing route. In addition, a partial safety factor is also applied to the Young's modulus of the FRP, which is a departure from conventional concrete design.

The Report contains procedures for the following:

- Flexural strengthening of beams and slabs
- Shear strengthening of beams and columns
- Flexural and compressive strengthening of columns.

The following sub-sections briefly review the recommended design procedures.

### Flexural strengthening

Bonding FRP to the tension face increases the flexural strength of beams and slabs. Failure of the element may then occur as a result of either the concrete reaching its ultimate compressive strain or the FRP reaching its ultimate tensile strain. Laboratory tests have consistently shown, however, that the latter rarely occurs in practice. The element generally fails prematurely as a result of plate separation. This is undesirable since the failure load is difficult to predict. In design, anchoring the FRP and limiting the design strain in the FRP below its ultimate value normally avoids this condition.

The design procedure is a function of the failure mode. Calculating the design ultimate

moment and comparing with the balanced moment of resistance of the section can predict the failure mode. Balanced failure in a strengthened beam is said to occur when the concrete and the FRP reach their ultimate design strains simultaneously. When the design moment is less than the balance moment, the FRP will reach its design tensile strain before the concrete crushes whereas when the design moment exceed the balance moment, the concrete will crush before the FRP reaches its design tensile strain.

The steps involved in the design of members with enhanced flexural capacity are summarized in the flow chart shown in Fig 1. The procedure is discussed in more detail in a companion paper[2], which also includes a worked example to illustrate the design methodology.

**Shear strengthening**

Externally bonded FRP laminates and fabrics can be used to increase the shear strength of reinforced concrete beams and columns. Figure 2 shows examples of possible configurations.

It can be seen that the shear strength of columns can be easily improved by wrapping with a continuous sheet of FRP to form a complete ring around the member. Shear strengthening of beams, however, is likely to be more problematic since they are normally cast monolithically with slabs. This increases the difficulty of anchoring the FRP at the beam/slab junction and exacerbates the risk of debonding failure. Nevertheless, bonding FRP on either the side faces, or the side faces and soffit, will provide some shear strengthening for such members. In both cases, it is recommended that the FRP be placed such that the principal fibre orientation, $\beta$, is either $45^{o}$ or $90^{o}$ to the longitudinal axis of the member.

The design of shear strengthening systems made from FRP follows the same procedure used in conventional reinforced concrete. It involves calculating the design shear force due to ultimate loads and comparing with the shear capacity of the concrete and any steel shear reinforcement present. Where a deficiency exists, FRP shear reinforcement will be needed. The amount of FRP required can be calculated using the same principles adopted in conventional reinforced concrete design, that is assuming a crack pattern and multiplying the area of the FRP reinforcement intersecting the potential crack by the failure stress.

To calculate the shear resistance of the FRP, the design strain in the FRP must be evaluated. Its value depends on the failure mode of the strengthened member. Basically, failure can arise due to one of three possible mechanisms, namely:

(a) loss of aggregate interlock
(b) FRP rupture
(c) delamination of the FRP from the concrete surface.

Design involves calculating the design strain and hence for a given strengthening scheme determining the shear capacity of the member. Provided this exceeds the required shear capacity, the strengthening scheme is acceptable.

**Strengthening of columns**

Concrete columns may require upgrading to enhance some or all of the following properties:

- flexural capacity
- axial load capacity
- shear capacity.

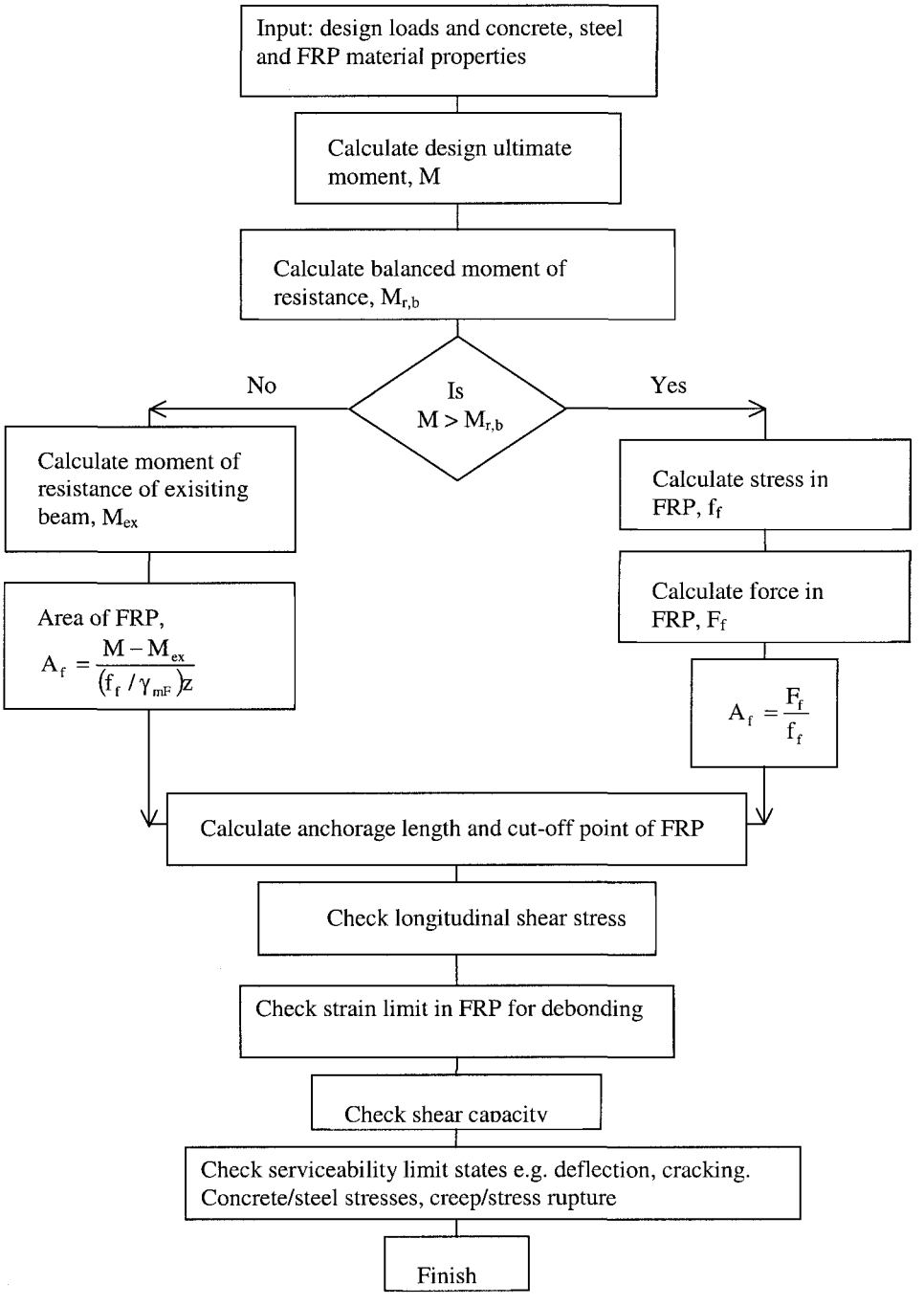



Figure 1. Design procedure for flexural strengthening with FRP

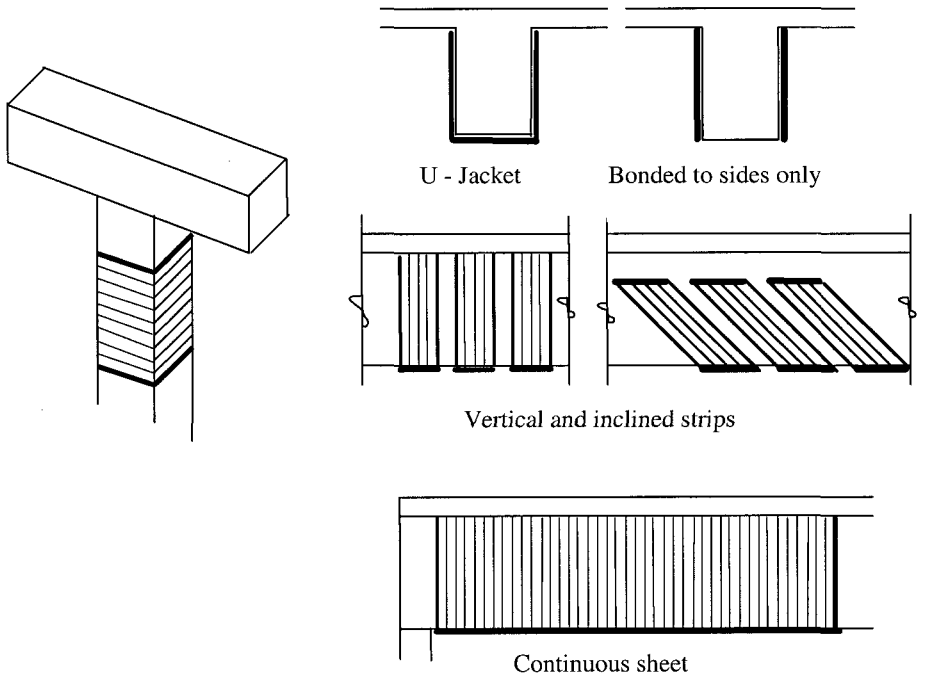



Figure 2. Beam and column shear reinforcement configurations

Generally, bonding axial FRP to the column surface enhances the flexural strength of the member. Hoop wrapping will also be necessary and should be placed over the axial FRP. The hoop wrapping increases the concrete strain capacity, which can significantly improve the efficiency of the strengthening design. It also improves buckling of the axial fibres, potentially enabling them to contribute in compression. However, this contribution will be small since FRP materials are weaker in compression than tension.

To calculate the thickness of axial FRP, the effect of hoop wrapping on compressive strength and strain to failure of the concrete must be known. Tests by Cuninghame et al[3] on wrapped circular columns have shown that provided the effective hoop stiffness of the FRP is greater than 320 N/mm$^2$, irrespective of the type of fibre and resin system used, the compressive strength of concrete may be assumed to vary linearly with strain from $f_{cu}$ at a strain of 0.0035 to $1.5f_{cu}$ at a strain of 0.01. This relationship enables the confined concrete stress block to be modeled, which is fundamental to flexural design of wrapped columns.

Bonding hoop FRP to the column surface enhances axial load capacity, shear capacity and ductility of columns. The hoop FRP resists lateral deformations due to the axial loading, resulting in a confining stress to the concrete core. This confinement delays rupture of the concrete, thereby enhancing both the ultimate compressive strength and the ultimate compressive strain of the concrete. This process is reported to be significantly more efficient with circular rather than square or rectangular columns: with the latter, the confinement action is mostly concentrated at the corners. Current estimates suggest that the confinement efficiency of

square columns may be around 30-70% of circular columns and is believed to decrease still further with columns of rectangular cross-section and/or large side dimensions.

Critical to compressive strength enhancement of columns is the behaviour of the strengthened member at service loads. The maximum compressive strain in the concrete should not be excessive otherwise loss of confining pressure due to accidental damage, fire, vandalism, etc may result in brittle collapse because the concrete is fissured. To prevent the possibility of this problem arising, it is recommended that the axial compressive strain in the concrete should not exceed 0.0035 under working loads.

## WORKMANSHIP AND INSTALLATION

Clearly, the design guidance is only valid if the installation of the fibre composite materials is carried out correctly. It is vital therefore that an experienced contractor is appointed to carry out the work. The chosen contractor must provide a Method Statement and Risk Assessment for his work, which complies with the installation procedures recommended by the FRP material supplier and current health and safety legislation.

If the FRP installation is to remain effective a survey of the structure focusing on the condition of the existing substrate and probable causes of deterioration is an essential requirement. Prior to installation, the surface of the concrete must be cleaned so that it is free of laitance and other material that are likely to affect the bond strength between the FRP and the concrete. Also, any sharp edges that are likely to damage the FRP should be removed. The surface of the fibre composite material may also require light abrasion prior to the application of the adhesive. It is generally necessary to control the environment in the work area during the preparation of the surface, the application of the adhesive and the subsequent curing period. For example, this may involve maintaining the temperature in the adhesive at an appropriate value and within specified limits. Also, the work site should be protected from moisture and humidity. The bonding adhesive should be applied evenly and the FRP material wrapped tightly over, avoiding any wrinkles, and rolled to expel any air.

Test should be carried out on samples obtained from each batch of adhesive and the composite materials in accordance with standard tests. Various non-destructive tests are available that may be used to inspect a completed and cured bond. Finally, where possible, identification/warning plates giving details of the installation should be provided in a prominent position to avoid accidental damage to the installation during future repair /renovation work. If over-coatings are applied to the surface of the fibre composite material, the warning plate should be placed above the coating.

## LONG-TERM INSPECTION AND MONITORING

As with all structural elements there will be a need to check the fibre composite strengthening system as part of the regular inspection and monitoring of the structure. This may be difficult if the fibre composite material has been covered with a protective coating. It is possible that this may have deteriorated in which case it will need to be replaced. The surface of the fibre composite should also be inspected visually for signs of crazing, cracking or delamination. De-bonding of the material from the concrete may be determined by tapping or thermography. Any identification/warning labels should also be checked. Where repairs are required, it is important that the material has similar characteristics to the material in place.

## STATUS

It should be noted that the Report has no official status.

Some notes of caution need to be observed with regards to ductility of the strengthened structure. Also attention needs to be paid to the fact that some of the design guidance is semi-empirical and based on small-scale laboratory tests. Therefore, the extrapolation of the recommendations to significantly larger elements needs to be undertaken with caution. It is essential that robust monitoring procedures be put in to monitor the installation until more experience is available.

## FUTURE ACTIVITIES

The Steering Group has identified that long-term inspection and monitoring is a key concern to the owners of structures. It is hoped that a subsequent project will look at the long-term performance of the adhesive and the fibres used and develop suitable inspection techniques. In addition, as experience of strengthening grows, it may be possible to modify some of the conservative assumptions made in the design recommendations.

## ACKNOWLEDGEMENTS

The work of preparing Technical Report 55 was supported by the following oraganisations whose help is gratefully acknowledged: London Underground Ltd, Railtrack, The UK Highways Agency, DJW Associates, DML Composites, Du Pont de Nemours International, Exchem Mining and Construction, Feb MBT, SBD Weber & Broutin, Sika, Sumitomo Corporation (Europe) Ltd., Toray Europe Ltd., Arup Research & Development, Buro Happold, Cornwall County Council, Curtins, Glamorgan Engineering Consultancy, Maunsells, Mott MacDonalds, Mouchells, PB Kennedy and Donkin, Tony Gee and Partners, Balvac Whitley Moran, Concrete Repairs Ltd., Makers Industrial Ltd., Taywood, Building Research Establishment, Glamorgan University and Surrey University.

## REFERENCES

1. Technical Report No. 55, *Design guidance for strengthening concrete structures using fibre composite materials*, The Concrete Society, Crowthorne, UK, December 2000, 71p.
2. Arya, C. and Farmer, N., *Design guidelines for flexural strengthening of concrete members using FRP composites. Fibre Reinforced Plastics for Reinforced Concrete Structures – 5*, ed. C.J. Burgoyne, Thomas Telford, London, 2001.
3. Cuninghame, J.R., Jordan, R.W. and Assejev, A., *Fibre reinforced plastic strengthening of bridge supports to resist vehicle impact*, Transport Research Laboratory, Crowthorne, 1999, Unpublished Project Report.

# Externally bonded reinforcement for shear

# Effect of Corner Radius on the Performance of Externally Bonded FRP Reinforcement

XINBAO YANG, ANTONIO NANNI and GENDA CHEN
Department of Civil Engineering, University of Missouri-Rolla, Rolla, USA.

## ABSTRACT
Externally bonded FRP reinforcement is wrapped around concrete members in order to provide confinement and/or shear strengthening. The need for bending the fibers over the member corners affects the performance of the FRP laminate and the efficiency of its confining/strengthening action. This paper presents an experimental study focusing on the effects of corner radius on FRP mechanical properties. A unique re-usable test device was designed and used for this purpose such that plies of FRP could be applied over interchangeable corner inserts. The radius of the inserts ranged from a minimum of 0 to a maximum of 50.8 mm, and one or two plies of carbon FRP were used. The monitored parameters were strain distribution in the FRP laminate and load. It was found that only a portion of the CFRP laminate capacity was developed when failure occurred at the corner. Increasing the number of plies from one to two slightly improved the efficiency of the laminate.

## INTRODUCTION
Advanced composite materials have been extensively used in the rehabilitation of concrete structural members. One practice is to externally wrap beams and columns with fibers impregnated with a resin-based matrix to increase the strength and deformation performance of the member. For example, FRP jackets may be used to wrap the potential plastic hinge of bridge columns in seismically active regions, where fibers can be regarded as continuously distributed transverse reinforcement. The ultimate strain of concrete and its pseudo-ductility can be significantly increased with negligible cumulative damage to the composite jacket under cyclic loading.

Externally bonded laminates have to be bent when wrapped around columns and beams. Bending affects performance of the FRP laminate and the corresponding confinement action depending on the curvature radius of the corners (Rochettee et al. 2000, Restrepo et al. 2000). In this paper, an experimental investigation was conducted to study the effects of corner radius on the FRP performance. A unique reusable test device was designed for this purpose, around which FRP laminates can be wrapped. By changing its corner inserts, different curvatures in the laminate can be simulated. A tension test was then performed until failure of the FRP laminate.

*FRPRCS-5*, Thomas Telford, London, 2001.

## EXPERIMENTAL PROGRAM

### Material Properties

High tensile strength carbon fiber tow sheets (MBrace, 1998) were used and impregnated using a two-part epoxy polymer saturant provided by the manufacturer. The low bound mechanical properties of the resulting CFRP laminate according to manufacturer's literature are listed in Table 1. These properties are determined and the experimental results of this project are analyzed based on the fiber cross section area rather than the composite area. This is due to the following reasons: (a) the laminate is fabricated using the manual lay-up technique and it is rather difficult to control the amount of resin; (b) small variations in the amount of resin, provided that the fibers are fully impregnated, do not affect the composite mechanical performance, and (c) mechanical properties of the resin are significantly lower than those of fibers.

Table 1: Manufacturer provided CFRP properties

| | |
|---|---|
| Ultimate strength (MPa) | 4275 |
| Design strength (MPa) | 3790 |
| Tensile modulus (GPa) | 228 |
| Ultimate strain (mm/mm) | 0.017 |

### Design of Test Specimen

In order to simulate the force transfer mechanism of FRP wrapping a cross section via running tension test, a unique reusable test device is designed and manufactured based on the following considerations: (a) the mechanical interaction between FRP laminate and device should be similar to that of wrapped concrete members for a meaningful correlation; (b) the device should be suitable for different corner radii; and (c) failure should occur in the test zone. A detailed drawing of the two-part steel device is illustrated in Figure 1.

The upper part is designed as the test zone with two interchangeable aluminum corner inserts separated by a 51 mm wide steel. It has a uniform thickness of 51 mm while the overall width and height are 254 mm and 292 mm, respectively.

The corner inserts are made of aluminum and have overall dimensions of 102 x102 mm. The corner radii investigated in this research include: 0.00, 6.35, 12.70, 19.05, 25.40, 38.10, and 50.80 mm. The largest radius of 50.80 mm corresponding to half of the width of the corner insert can be used to simulate a circular cross section. The corner inserts are glued to the steel part to prevent any movement during testing.

The lower part of the device is designed to anchor the FRP laminate. The semi-circular bottom steel block has a radius of 127 mm under which the FRP laminate is terminated with a lap splice length of 152 mm. Because the radius of the semi-circle is considerably larger than that of all corner inserts, no failure would be expected within the anchor zone.

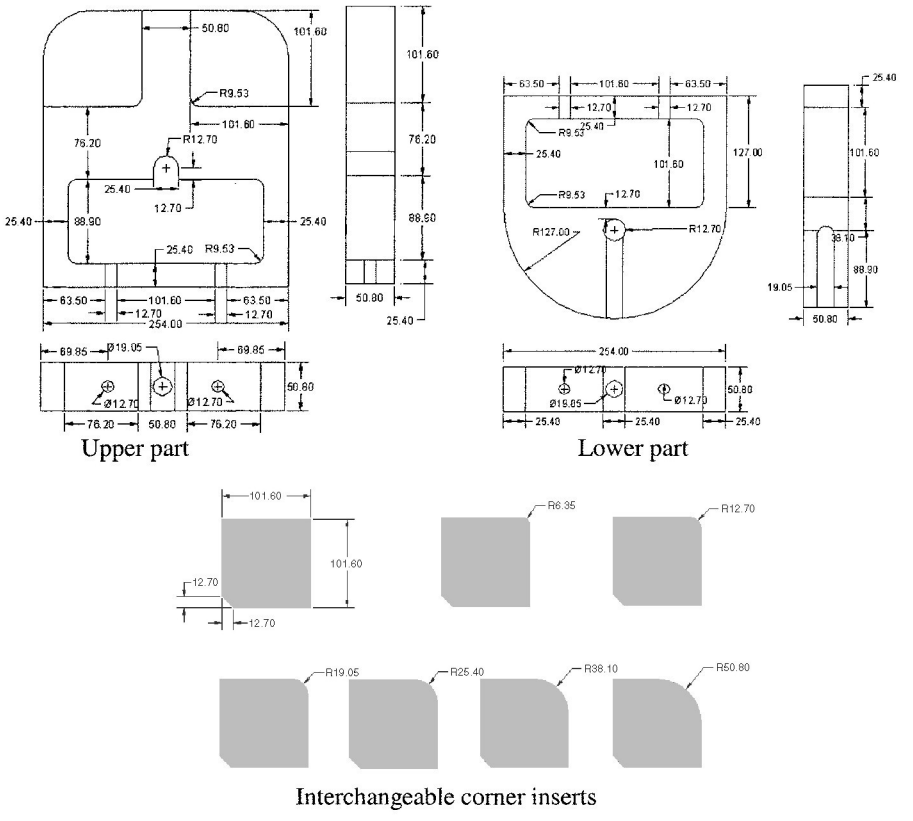



Fig. 1 Test apparatus (Unit: mm)

Prior to the installation of the FRP laminate, these two parts are joined using two through bolts. After the device is installed on the testing machine, the nuts on these bolts are loosened so that the tensile load is transferred to the FRP laminate. The loose bolts were also used as safety feature to hold the device after rupture of the laminate.

**Installation of Laminate**

After placing two identical aluminum corner inserts, the side surface of the device was covered with polyethylene tapes. The polyethylene tape was used as the release film to facilitate detaching of the FRP laminate from the steel surface after completion of the test. A strip of FRP laminate was 38.1 mm wide and 1.68 m long. The laminate was applied by the manual lay-up procedure. The two-part saturant was thoroughly mixed and a thin layer was applied on both the polyethylene tape and the carbon fiber sheet using a sponge brush. Through careful handling, the carbon fiber ply was wrapped around the specimen and lap-spliced at the bottom. Then, the backing paper was removed after application of gentle pressure. A plastic roller was used to remove the air entrapped between fiber ply and saturant. After approximately 30 minutes, a second layer of saturant was applied and the plastic roller was used again to work the resin into the fibers. The wet laminate was left to

cure for three days and then strain gages were attached. Two or three identical specimens were manufactured for each set of corner inserts.

**Instrumentation**

Strain gages were used to measure the strains at multiple points around each corner. The first gage was placed 38.10 mm away from the root of the corner on the flat part of the upper and side surfaces. Another two gages were positioned with one end exactly at the curvature changing point of the upper and side surfaces, respectively. For those laminates with corner radius larger than 19.05 mm, a fifth strain gage was attached at the center of the corner arc. Load was monitored by the built-in load cell in the testing machine. The strain gage arrangements for laminates with different corner radius are shown in Figure 2 and an instrumented specimen ready for testing is shown in Figure 3.

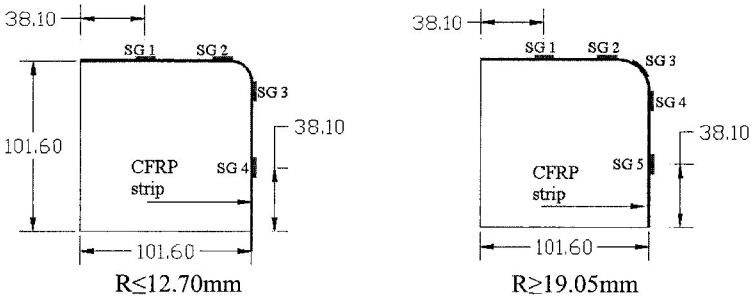



Fig. 2 Strain gage arrangement

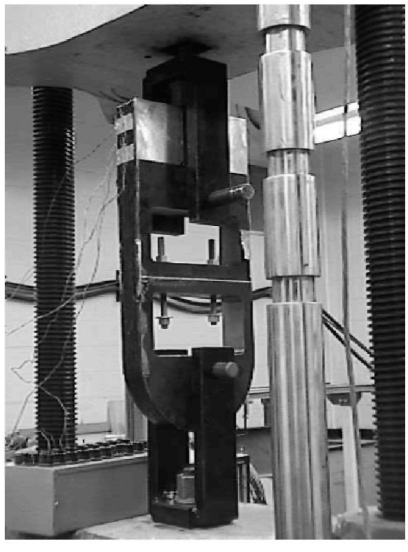


Fig. 3 Test setup

## TEST RESULTS

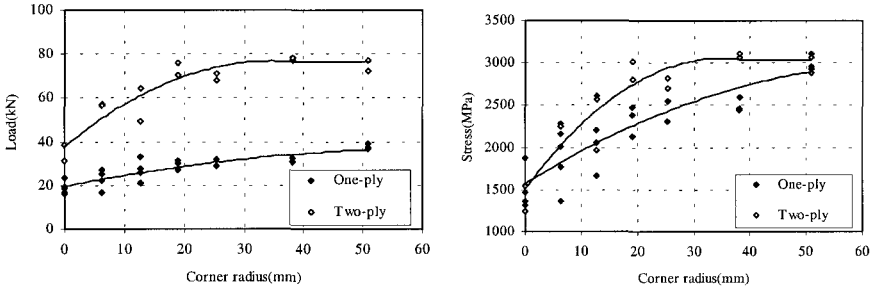
### Strength of CFRP laminates

The average ultimate load carried by CFRP laminates for different corner radii is shown in Table 2. The individual data points of load and stress versus corner radius are depicted in Figures 4(a) and (b). The average ultimate load increases with corner radius for both one and two-ply laminates. The ultimate load capacity of two-ply specimens is more than twice that of the corresponding one-ply specimen with two exceptions: corner radii of 0 and 50.80 mm, which represent the square and circular section, respectively.

Table 2 Average ultimate results

| One-ply | | | | | | | |
|---|---|---|---|---|---|---|---|
| R (mm) | 0 | 6.35 | 12.70 | 19.05 | 25.4 | 38.10 | 50.80 |
| Load (kN) | 19.03 | 22.92 | 26.86 | 29.39 | 30.56 | 31.46 | 37.72 |
| Stress (MPa) | 1513 | 1822 | 2135 | 2336 | 2429 | 2501 | 2999 |
| Percentage of reference strength* | 33 | 40 | 47 | 52 | 54 | 55 | 66 |
| Strain(%)** | 0.65 | 0.96 | 1.05 | 1.01 | 1.00 | 0.98 | 1.10 |
| Elastic Modulus (GPa) | 233 | 188 | 203 | 234 | 243 | 255 | 273 |
| Failure mode*** | I | I | I | I or II | II | II | II |
| Two-ply | | | | | | | |
| R (mm) | 0 | 6.35 | 12.70 | 19.05 | 25.4 | 38.10 | 50.80 |
| Load kN) | 34.92 | 57.00 | 56.94 | 73.24 | 69.62 | 77.62 | 74.73 |
| Stress (MPa) | 1388 | 2266 | 2263 | 2911 | 2767 | 3086 | 2970 |
| Percentage of reference strength* | 31 | 50 | 50 | 64 | 61 | 68 | 66 |
| Strain(%)** | 0.50 | 0.96 | 0.92 | 1.12 | 1.18 | 1.25 | 1.25 |
| Elastic Modulus (GPa) | 278 | 236 | 246 | 260 | 234 | 247 | 238 |
| Failure Mode*** | I | I | I | I | II | II | II |

* 4525MPa, ** average from all gages, *** I: at corner, II: at flat portion




(a) Ultimate load (b)Stress

Fig. 4 Ultimate load and stress vs. corner radius

The performance of the laminate is analyzed by comparing the stress-strain relationships with the reference one obtained through direct tension testing of CFRP coupons (Yang et al. 2000). The strain values reported in Figure 5 are those measured on the flat part of the side surface. It can be seen that even though the diagrams (with the exception of two-ply R = 50.80 mm) are almost the same for all specimens, only 67% of the reference strength (or strain) can be attained. When R is equal to 6.35 mm, only half the strength was developed,

corresponding to a strain of less than 1%. The laminate stiffness (modulus of elasticity) when wrapped is less than that of the straight form.

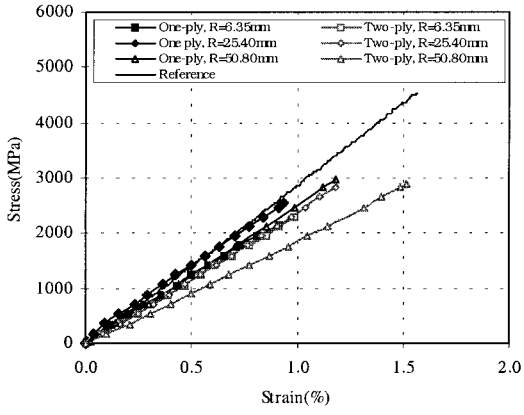
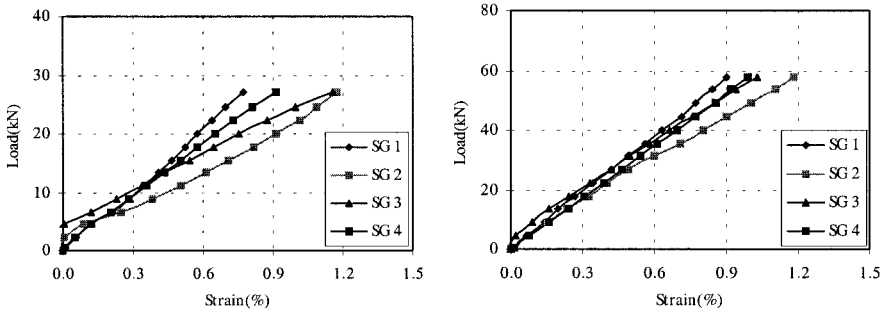



Fig. 5 Stress-strain curves of CFRP laminates

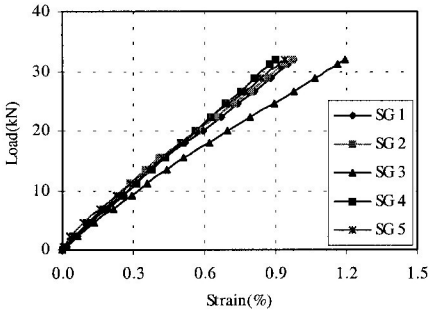
**Strain Distribution**

The strain at various locations around the corner is presented in Figure 6 for different corner radii of 6.35, 25.4, and 50.80 mm and different numbers of plies. Generally, the difference in strain values is insignificant and the ultimate strains are between 0.9% and 1.2%, which is smaller than the design value of 1.7% (MBrace 1998). For the small corner radius (R=6.35 mm), the largest strain occurs at the corner indicating the occurrence of stress concentration. As radius of the corner inserts increases, the location of the maximum strain shifts from the center of the corner (R=25.4 mm) to the flat portion of the side surface (R=50.80 mm). The strain difference at various locations is smaller for larger corner radii. One possible reason for this phenomenon is the presence of the release agent, which made the friction between CFRP laminates and the steel surface small and created a relatively smooth force transfer.

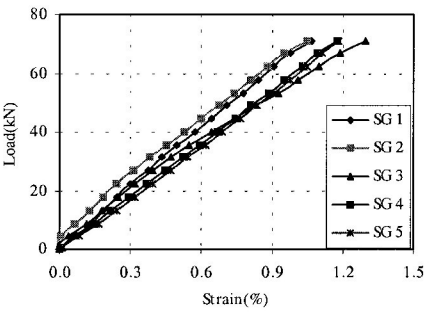



One-ply, R=6.35mm Two-ply, R=6.35mm

Fig. 6 (a)

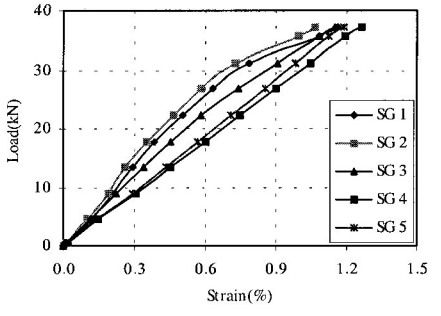



One-ply R=25.40mm

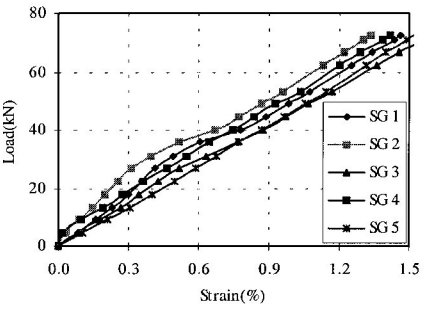



Two-ply R=25.40mm

(b)




One-ply R=50.80mm




Two-ply R=50.80mm

(c)

Fig. 6 Strain distribution around a corner

**Failure Modes**

One- and two-ply CFRP strips failed in a brittle manner. Three different failure modes were identified: fracture at one corner; simultaneous fracture at both corners; and fracture at the flat portion of the surface. The first failure mode mainly happened in cases of small corner radius. The other modes were typical in laminates bent around larger radii. The fractured laminates for different corner radius are illustrated in Figure 7.



R=0.0 mm




R=6.35 mm




R=19.05 mm

Fig. 7 (a)




R=25.4 mm R=38.10 mm R=50.80 mm

(b)

Fig. 7 Failure modes of CFRP laminates

## CONCLUSIONS

The experimental investigation on the effect of corner radius on the performance of CFRP laminates yielded the following conclusions:

- Corner radius plays an important role on the mechanical properties of CFRP laminates. Test results indicate that at best only 67% of the ultimate laminate strength can be developed when wrapped around a circular section. As the corner radius decreases, the efficiency of FRP wrapping further reduces.
- Multiple placement of FRP plies can slightly increase the strength of bent CFRP laminates and improve the overall strengthening performance except for the square or rectangular sections.

## ACKNOWLEDGEMENT

Financial supports from the Federal Highway Administration (FHWA) and the University Transportation Center based at UMR are gratefully acknowledged. The authors wish to thank J. Bradshaw and S. Haug for their generous help during lab testing.

## REFERENCES

MBrace ™ (1998), "Composite Strengthening System, Engineering Design Guideline", 2nd Ed., Master Builders Technologies, Inc., Cleveland, OH.

Restrepo, J. I, Wang, Y. C., Wymer, P. A. and Irwin, R. W. (2000), "Recent Developments in the Use of Advanced Composite Materials for Seismic Retrofitting", *Proc. 12th WCEE*, Paper number 1593(CD-ROM).

Rochettee, P. and Labossiere, P. (2000), "Axial Testing of Rectangular Column Models Confined with Composites", *Journal of Composites for Construction*, ASCE, 4(3), pp.129-136.

Yang, X. B, Nanni, A., Haug, S. and Sun, C. L. (2000), "Strength and Modulus Degradation of CFRP Laminates from Fiber Misalignment", Submitted to *J. Mat. Civil Engrg*, ASCE.

# A Shear Strength Model for FRP-Strengthened RC Beams

J.F. CHEN, School of the Built Environment, Nottingham University, UK and
J.G. TENG, Dept of Civil and Structural Engineering, Hong Kong Polytechnic University, Hong Kong, China.

**ABSTRACT**
Shear strengthening is often needed for reinforced concrete (RC) beams due to various reasons such as design and construction errors, environmental attacks and functional changes. The need for shear strengthening can also arise as a result of flexural strengthening. An attractive method for shear strengthening of RC beams is to externally bond fibre-reinforced polymer (FRP) composites to the sides of the beam. This paper is concerned with the development of a rational strength model for such shear-strengthened beams. Existing strength models are first reviewed and compared and their weaknesses discussed. A new model for the shear strength of RC beams bonded with FRP composites is then proposed, based on a careful interpretation of existing test results. The validity of this new model is demonstrated by a comparison of results from this new model and available test results.

**KEYWORDS**
Reinforced concrete beams, shear strengthening, shear strength, FRP, FRP rupture.

**INTRODUCTION**
Shear strengthening is often needed for reinforced concrete (RC) beams due to various reasons such as design and construction errors, environmental attacks and functional changes. The need for shear strengthening can also arise as a result of flexural strengthening. An attractive method for strengthening RC beams in shear is to externally bond fibre-reinforced polymer (FRP) composites to the sides or around the perimeters of them.

Many studies have been undertaken on the shear strengthening of RC beams using externally bonded FRPs in the last decade (e.g. Uji 1992; Al-Sulaimani et al.; 1994, Arduini et al. 1994; Chajes et al. 1995; Alexander 1996; Sato et al. 1996, 1997; Araki et al., 1997; Funakawa *et al.* 1997; Triantafillou 1997, 1998a, b; Chaallal et al. 1998; Malek and Saadatmanesh 1998; Mitsui *et al.* 1998; Kachlakev and Barnes 1999; Mutsuyoshi *et al.* 1999; Khalifa *et al.* 1998, 1999; Fanning and Kelly 1999; Hutchinson and Rizkalla 1999; Khalifa and Nanni 2000). Various strengthening schemes, including wrapping, U jacketing and side bonding have been used. Both FRP sheets/plates and strips have been employed. A detailed discussion on strengthening schemes is given in Chen and Teng (2001a) and Teng et al. (2000).

FRP rupture and FRP debonding have been the two main failure modes reported for these beams when failing in shear. Although the mechanisms of failure for these two modes are clearly different, they have not been properly distinguished from each other in previous shear strength models (e.g. Chaallal et al. 1998; Triantafillou 1998a) except the one developed by Khalifa et al. (1998).

This paper first presents a brief review of the existing research on the strength of shear strengthened RC beams. A clear distinction is made between the failure mode due to FRP rupture and that due to FRP debonding. A new rational strength model is then developed, which recognises the fundamental characteristics of FRP properties for the failure mode due to FRP rupture. The model is validated against experimental data collected from the literature. Finally, a design strength model is proposed. A separate strength model for the failure mode due to FRP debonding has also been developed recently and is presented elsewhere (Chen and Teng 2001b).

## PREVIOUS RESEARCH ON SHEAR STRENGTH MODELS

RC beams strengthened in shear using externally bonded FRPs show complex behaviour. Both the failure mode and the shear strength are affected by many factors such as the size and geometry of the beam, the properties of the concrete, internal shear and flexural reinforcements, loading conditions, the method of strengthening, and the properties of the bonded FRP. Shear strengthening using bonded FRPs is also much less investigated compared to flexural strengthening (Teng et al. 2000). The complexity of the problem, combined with the limited research available, makes it difficult to develop robust predictive strength models suitable for practical design. Nevertheless, several attempts have been made in developing such models as detailed below.

All existing models use the following expression to calculate the shear strength of a strengthened RC beam, $V_n$

$$V_n = V_c + V_s + V_f \tag{1}$$

where $V_c$ is the contribution of the concrete, $V_s$ is the contribution of the steel stirrups and bent-up bars and $V_f$ is the contribution of the FRP. $V_c$ and $V_s$ may be calculated according to provisions in existing design codes, so the main differences between available models lie in the evaluation of the FRP contribution $V_f$. They are briefly discussed as follows.

Chaallal et al. (1998) proposed the following equation (in the ACI format)

$$V_f = \phi_f A_f f_{fu} \frac{(\sin\beta + \cos\beta)\, d}{s_f} \tag{2}$$

where $\phi_f$=0.8 is the material reduction factor for the FRP; $A_f$ is the cross-sectional area of a pair of FRP strips; $f_{fu}$ is the ultimate strength of FRP; $\beta$ is the angle of the fibre orientation from the horizontal direction; d is the effective depth of the beam and $s_f$ is the spacing of FRP strips measured along the longitudinal axis. The design average shear stress between the FRP strips and the concrete is required to not exceed half the maximum debonding stress.

This model was proposed for inclined strips, vertical strips, side plates (wings) and U jackets. The basic assumption behind this design proposal is that the bonded FRP contributes to the shear resistance in the same way as that of internal steel stirrups and that all the FRP intersected by the shear crack reaches its full tensile strength at beam failure unless otherwise limited by insufficient bond lengths.

This model suffers from two major drawbacks. First, the assumption that all the FRP intersected by the shear crack reaches its full tensile strength at beam failure is over optimistic. There is clear experimental evidence that the strain distribution in the FRP along a shear crack is non-uniform (Sato et al. 1996; Kamiharako et al. 1997; Funakawa et al. 1997; Araki et al 1997). This combined with the brittle behaviour of FRPs means that at any instant

in the failure process, only the most highly stressed part of the FRP is at its full tensile capacity. Second, their bond strength model used for limiting the stress level in the FRP likely to debond does not fit well with experimental data (Chen and Teng 2001c). Furthermore, their bond strength model is given in terms of the average shear stress between the FRP and the concrete. This is dangerously misleading, because it implies that the tensile strength of the FRP can always be fully utilised if there is a sufficiently long bond length (e.g. the beam depth is large enough), while in reality the stress level in the FRP at debonding does not increase with bond length if the bond length is already sufficiently long (i.e. longer than the effective bond length, see Chen and Teng 2001c).

Triantafillou (1998a) argued that to accurately predict the contribution of FRP to shear resistance is rather difficult, because it depends on the failure mechanism which in turn depends on various factors. He thus used a semi-quantitative approach, leading to a design equation (in the Eurocode format) of

$$V_f = \frac{0.9}{\gamma_f}\rho_f E_f \varepsilon_{fe} b_w d(1 + \cot\beta)\sin\beta \tag{3}$$

where $E_f$ is the Young's modulus of the FRP; $\rho_f=2t_f/b_w$ is the FRP area fraction (for continuous sheets/plates); $t_f$ is the thickness of the FRP; $b_w$ is the width of the RC beam; $\gamma_f$ is the partial safety factor for the FRP in uni-axial tension which was proposed to be about 1.15, 1.20 and 1.25 for CFRP, AFRP and GFRP respectively (Triantafillou and Fardis 1997); and $\varepsilon_{fe}$ is the effective strain of FRP at failure which was obtained based on regression of experimental data:

$$\varepsilon_{fe} = 0.0119 - 0.0205\rho_f E_f + 0.0104(\rho_f E_f)^2 \quad \text{for } 0 \le \rho_f E_f < 1 \tag{4a}$$

$$\varepsilon_{fe} = -0.00065\rho_f E_f + 0.00245 \quad \text{for } 0 \le \rho_f E_f < 1 \tag{4b}$$

Khalifa et al. (1998) proposed a modification to Triantafillou's (1998) effective strain model. They used the ratio of effective stress (strain) in the FRP to its ultimate strength (strain), R, instead of $\varepsilon_{fe}$ ($=R\varepsilon_{fu}$). Regression of experimental data led to the following expression for the effective stress ratio R

$$R = 0.5622(\rho_f E_f)^2 - 1.2188\rho_f E_f + 0.778 \le 0.50 \tag{5}$$

Following the initial submission of this paper, Triantafillou and Antonopoulos (2000) published an extension of the above work in which different effective strain expressions were proposed for different types of FRP based on a regression analysis of a larger database. A close examination of the data presented in their paper shows that the average ratio of the observed to the predicted FRP strain by their model is 1.07 with a standard deviation of 0.4. This is statistically not satisfactory for safe practical design.

Khalifa et al. (1998) argued that the effective strain model is only applicable when failure is governed by FRP sheet rupture. They thus developed a bond mechanism design approach based on a bond strength model proposed by Maeda *et al.* (1997), leading to another expression for R. However, the bond strength model proposed by Maeda *et al.* (1997) is invalid because it cannot correctly predict the effective bond length (Chen and Teng 2001c). Furthermore, no satisfactory explanation is available for the small strain ratio R (which has an upper limit of 0.5) obtained based on regression of experimental data.

The deficiencies of the existing models necessitate the development of new shear strength models. Because of the distinct difference between the failure mode due to FRP rupture and that due to FRP debonding, a separate treatment is essential for each of them. A rational model for the FRP rupture failure mode is developed as follows. A model for the FRP debonding mode is given in Chen and Teng (2001b). Further details for both models can be found in Teng *et al.* (2000).

## A RATIONAL SHEAR STRENGTH MODEL

### *Shear Failure Controlled By FRP Rupture*

Available experimental data show that almost all beams strengthened with wrapping failed due to FRP rupture. Some beams strengthened using U jackets (e.g. Chajes et al. 1995) also failed in this mode, but most U jacketed beams and almost all side bonded beams failed due to FRP debonding.

Shear failure controlled by FRP rupture occurs most often with a diagonal-tension shear crack (Fig. 1). In such cases, vertical flexural cracks originating from the tension face usually occur first. One of the cracks near the support may propagate towards to the loading point and become an inclined critical crack. In some cases, a diagonal crack may be abruptly formed. As the width of the diagonal crack increases, the maximum strain in the FRP which is often at the lower end of the crack eventually reaches its ultimate strain. The FRP is immediately torn when its ultimate strength is reached. Rupture of FRP then propagates along the diagonal shear crack in the concrete leading to collapse of the beam. The failure is brittle because FRPs are linear elastic up to rupture.

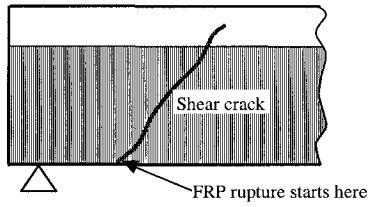



Figure 1. Shear tension with FRP rupture

The new shear strength model presented below is therefore applicable to both wrapping and U jacketing. Obviously, the shear strength of U jacketed beams shall also be examined for the FRP debonding mode, which is discussed in Chen and Teng (2001b) and Teng et al. (2000). However, if proper mechanical anchors are provided at the free ends of FRPs for U jackets and sides strips, the shear strength of the strengthened RC beams is likely to be governed by FRP rupture and the model presented below can be relevant even for side bonded RC beams.

### *Stress Distribution in FRP Along a Shear Crack*

Experimental evidence shows that the strain distribution in the FRP along a shear crack is non-uniform (Sato et al. 1996; Kamiharako et al. 1997; Funakawa et al. 1997; Araki et al 1997). This phenomenon can be attributed to the fact that the width of the critical shear crack changes from the lower end to the upper crack tip. This leads to a non-uniform strain distribution in the FRP because the strain anywhere in the FRP intersected by the crack is closely related to the width of the crack there. As FRPs are linear elastic until rupture failure, the stress in the FRP is also non-uniform along the shear crack.

This is the fundamental difference in behaviour between steel stirrups and external FRP shear reinforcement in RC beams. As steel stirrups can undergo large plastic deformation before rupture, it is reasonable to assume that all steel stirrups intersected by a shear crack reach their yield strength for shear design. For the FRP shear reinforcement, the non-uniformity of stress distribution means that the failure process will start when the most highly stressed point in the FRP intersected by the shear crack reaches the ultimate tensile strength of the FRP. Rupture of adjacent parts of the FRP then follows quickly, as the intact parts of the FRP need to take over the forces released by the ruptured parts. Rupture of the FRP, once started, will thus propagate rapidly along the shear crack, leading to catastrophic failure of the beam. The FRP intersected by the shear crack is, therefore, not stressed to the same ultimate tensile strength at any instant of the failure process.

Therefore, the assumption used for steel stirrups that all stirrups intersected by a shear crack reach their yield strength at beam failure cannot be extended to the FRP shear reinforcement with the rupture strength of the FRP treated as the equivalent of the yield strength of steel. Otherwise, rather un-conservative predictions are obtained for the shear strength of FRP-strengthened RC beams. The effective or average stress in the FRP intersected by a shear crack at the ultimate limit state, $f_{fe}$, is thus a fraction of its tensile strength $f_f$:

$$f_{fe} = D_f f_f \tag{6}$$

in which $D_f$ is termed the stress distribution factor here.

Little information is available about the actual strain distribution in the FRP along a shear crack in the literature. This distribution is likely to be affected by many factors. For a general wrapping or U jacketing scheme for a T beam (with $B=b_w$ being rectangular) as shown in Fig. 2, it may be assumed that the normalised strain distribution in the FRP intersected by the critical shear crack has a parabolic form:

$$\bar{\varepsilon}_{\bar{z}} = \begin{cases} \dfrac{1-C\bar{z}}{1-C}\bar{z} & 0 \le C < \dfrac{1}{2} \\ 4C\bar{z}(1-C\bar{z}) & \dfrac{1}{2} \le C \le 1 \end{cases} \tag{7}$$

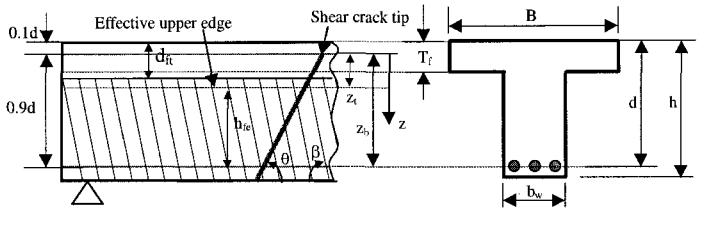



Figure 2. Notation for a general shear strengthening scheme

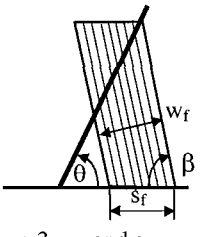



Figure 3. $w_f$ and $s_f$

where $\bar{z} = z / z_b$ = normalised vertical coordinate, $z_b = 0.9d$ = lower end of the effective FRP which is taken to be at the centre of the flexural steel reinforcement; and d = effective depth of the beam measured from the compression face to the centre of the flexural reinforcement. A downward coordinate z originating from the upper tip of the shear crack is used here (Fig. 2). The crack tip is assumed to be at 0.1d from the compression face. The shape of the strain distribution is dependent on the value of coefficient C, with C=0 being linear.

The strain distribution factor, being the ratio of the average strain to the maximum strain in the effective height of FRP $h_{fe}$, can be obtained by integrating Eq. 7:

$$D_f = \begin{cases} \dfrac{1+\zeta}{2(1-C)} - \dfrac{C}{3(1-C)}(1+\zeta+\zeta^2) & 0 \le C < \dfrac{1}{2} \\ 2C(1+\zeta) - \dfrac{4}{3}C^2(1+\zeta+\zeta^2) & \dfrac{1}{2} \le C \le 1 \end{cases} \tag{8}$$

where $\zeta=z_t/z_b$ is the coordinate ratio of the upper edge to the lower edge of the effective FRP. This upper edge is taken to be

$$z_t = \min(0.1d, d_{ft}) - 0.1d \tag{9}$$

in which $d_{ft}$ is the distance from the concrete compression face to the actual upper edge of the FRP ($d_{ft}=0$ so $z_t=0$ for wrapping).

Equation 9 means that the upper end of the effective FRP is taken to be at a small distance below the actual upper end of the FRP if the FRP is not bonded on the full height of the beam for U jacketing. This treatment is to maintain consistency for all cases, because there is a 0.1d extra bond length above z=0 if the FRP is bonded in full height.

For beams strengthened by wrapping, it is likely that the FRP has debonded along the full height of the beam across most part of the critical shear crack before rupture. The strain anywhere in the FRP covering the shear crack may thus be approximately proportional to the width of the shear crack. Furthermore, the shear crack may be closely represented by a linear function increasing from zero at the crack tip for most shear failures. Therefore, a linear strain distribution model (C=0 in Eq. 7), where the normalised FRP strain increases linearly from zero at the crack tip to unity at the lower end, may be a close and simple approximation for the actual strain distribution. In this case, the strain distribution factor (Eq. 8) becomes

$$D_f = (1+\zeta)/2 \tag{10}$$

For wrapping and U jacketing with FRP bonded over the full height of the beam, $\zeta = 0$ and Eq. 10 reduces to $D_f = 0.5$. This can be compared with the upper limit of the effective stress ratio R=0.5 as given by Khalifa et al. (1998) (Eq. 5).

The explicit inclusion of the effect of non-uniform strain distribution in the FRP along a shear crack can thus satisfactorily explain the phenomenon that the contribution of the FRP to the shear capacity of an RC beam is less than its ultimate tensile strength.

***FRP contribution to shear capacity***

If the critical shear crack has an angle of $\theta$ to the longitudinal direction of the beam (Fig. 2), the contribution of FRP to the shear capacity can now be expressed as

$$V_f = 2f_{fe}t_f w_f \frac{h_{fe}(\cot\theta + \cot\beta)\sin\beta}{s_f} \tag{11}$$

in which $t_f$ = thickness of FRP; $w_f$ = width of FRP strips (perpendicular to main fibre orientation); $\beta$ = angle of main fibres measured from the longitudinal axis of the beam; and the effective height of FRP on the sides of the beam $h_{fe} = z_b - z_t$.

It may be noted that for continuous FRP plates/sheets (Fig. 3),

$$s_f = w_f / \sin\beta \tag{12}$$

Therefore, $s_f = w_f$ only if $\beta = 90°$ (fibres vertically oriented). This is worth noting because some researchers have mistakenly used $s_f = w_f$ without giving due consideration to the fibre orientation.

## COMPARISON WITH EXPERIMENTAL OBSERVATIONS

An extensive literature review has been carried out to collect test data for shear strengthened RC beams. Available data include 56 RC beams which failed due to FRP rupture. Details of these beams are given in Chen and Teng (2001a). Tests that were not sufficiently well documented are excluded here from the comparison.

Tests on un-strengthened RC beams with similar geometrical and material parameters to the strengthened ones are available for all these test data. These un-strengthened beams were used as the reference beams for the strengthened ones. The contribution of FRP to the shear capacity for the strengthened RC beams was obtained using the test results of appropriate reference beams with due consideration of the material and geometrical differences between the reference and test beams if there was any.

An important factor affecting the contribution of FRP to shear capacity is the shear crack angle $\theta$ as shown in Eq. 11. Because this angle is usually not reported in the literature, it was estimated by the authors according to relevant reported details such as photographs, sketches of failure modes and textual descriptions (Chen and Teng 2001a).

Figure 4 shows that the predictions of the new model are in very close agreement with the available test data. Estimated shear crack angles have been used here. The average value of the observed to predicted strength ratio is 1.05 with a coefficient of variation of 21.4% after treating 4 data points as statistical outliers.

## SHEAR STRENGTHENING DESIGN

For practical design, it can be assumed that $\theta$=45°. The contribution of FRP to the design shear capacity is thus

$$V_f = 2\frac{f_{fe}}{\gamma_f} t_f w_f \frac{h_{fe}(\sin\beta + \cos\beta)}{s_f} \tag{13}$$

The effective stress $f_{fe}$ in FRP can be obtained by

$$f_{fe} = \begin{cases} 0.8 D_f f_f & \text{if } f_f/E_f \leq \varepsilon_{max} \\ 0.8 D_f \varepsilon_{max} E_f & \text{if } f_f/E_f > \varepsilon_{max} \end{cases} \tag{14}$$

in which $\gamma_f$ is the partial safety factor for FRP. A reduction factor of 0.8 is also introduced in Eq. 14, to account for detrimental factors associated with FRP shear strengthening not yet accounted for and to reduce the un-conservativeness of Eq. 13 as a design equation, before

the partial safety factor is included. One important issue in FRP shear strengthening is the detrimental effect a sharp corner may have on the ultimate tensile strength of the FRP. If a corner is not treated with care to form a round one with a sufficiently large radius, the wrapped FRP can rupture there at a stress much lower than its ultimate tensile strength.

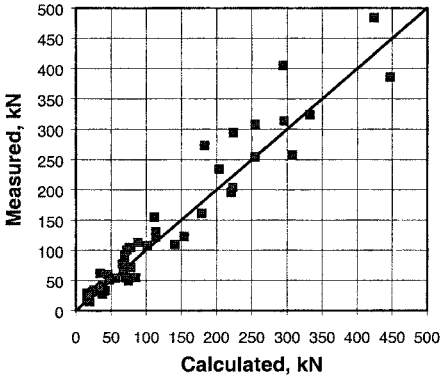



Figure 4. Theoretical predictions versus experimental observations

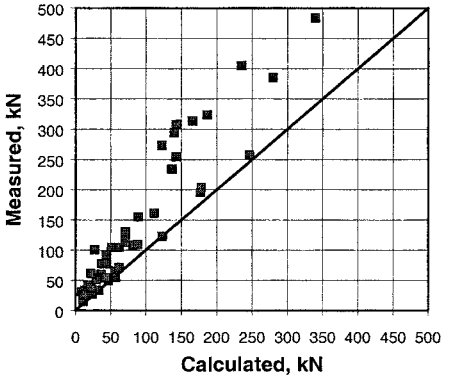



Figure 5. Predictions of design proposal versus experimental observations

It is also proposed in Eq. 14 to control the maximum strain of the FRP $\varepsilon_{max}$ so that the width of shear cracks can be controlled. The chief reason for this is that the shear capacity contributed by the concrete may be lost before the capacity of FRP is exhausted if the shear crack is too wide. There is insufficient information to date to determine this maximum strain quantitatively so further research is needed. A value of $\varepsilon_{max} = 1.5\%$ may be used before a proposal with confidence can be made.

Figure 5 compares the design proposal with experimental observations. The partial safety factor $\gamma_f$ was set to 1 for the purpose of this comparison. All data points excluding the statistical outliers have predicted values smaller than the experimental observations. The design proposal is thus suitable for practical use.

## CONCLUSIONS

FRP rupture and FRP debonding are the two main modes of shear failure for RC beams shear strengthened with externally bonded FRPs. The different failure mechanisms of the two modes make it necessary to develop separate shear strength models for them. This paper has presented a review of existing research on the shear strength and then developed a new shear strength model for beams failing by FRP rupture. The new model explicitly recognises the linear elastic and brittle behaviour of FRPs and the non-uniform strain distribution in FRPs along a shear crack. It has been validated against experimental data collected from the literature based on an extensive review. A design proposal has also been made based on this new shear strength model.

## ACKNOWLEDGEMENTS

The work presented here is the result of collaborative research between the Department of Civil and Structural Engineering, The Hong Kong Polytechnic University and the School of Engineering and the Built Environment, The University of Wolverhampton. The authors gratefully acknowledge the financial support provided by The Hong Kong Polytechnic

University through the Area of Strategic Development (ASD) in Advanced Building Technology in a Dense Urban Environment.

## REFERENCES

Alexander, J.G.S. (1996) "Shear Strengthening of Small Scale Concrete Beams with Carbon Fibre Reinforced Plastic Sheets", *Proceedings of Annual Conference, Canadian Society for Civil Eng*ineering, Vol. 2, No. A, pp. 167-178.

Al-Sulaimani, G.J., Sharif, A.M., Basunbul, I.A., Baluch, M.H. and Ghaleb, B.N. (1994) "Shear repair for reinforced concrete by fibreglass plate bonding", *ACI Structural Journal*, Vol. 91, No. 3, pp. 458-464.

Araki, N., Matsuzaki, Y., Nakano, K., Kataka, T. and Fukuyama, H. (1997) "Shear capacity of retrofitted RC members with continuous fibre sheets", *Non-Metallic (FRP) Reinforcement for Concrete Structures, Proceedings of the Third Symposium*, Vol. 1, Japan, pp. 512-522.

Arduini, M.; D'Ambrisi, A.; Di Tommaso, A. (1994) "Shear failure of concrete beams reinforced with FRP plates", *Infrastructure: New Materials and Methods of Repair Proceedings of the Materials Engineering Conference 804*, Oct 1994. ASCE, New York, pp123-130.

Chaallal, O., Nollet, M.J., Perraton, D. (1998) "Strengthening of reinforced concrete beams with externally bonded fibre-reinforced-plastic plates: design guidelines for shear and flexure", *Canadian Journal of Civil Engineering*, Vol. 25, No. 4, 692-704.

Chajes, M.J., Januszka, T.F., Mertz, D.R., Thomson, T.A. Jr. and Finch, W.W. Jr. (1995) "Shear strengthening of reinforced concrete beams using externally applied composite fabrics", *ACI Structural Journal*, Vol. 92, No. 3, 295-303.

Chen, J.F. and Teng, J.G. (2001a) "Shear capacity of FRP strengthened RC beams: FRP rupture", submitted for publication.

Chen, J.F. and Teng, J.G. (2001b) "Shear capacity of FRP strengthened RC beams: FRP debonding", To be published.

Chen, J.F. and Teng, J.G. (2001c) "Anchorage strength models for FRP and steel plates bonded to concrete", accepted by *ASCE Journal of Structural Engineering*.

Fanning, P. and Kelly, O. (1999) "Shear strengthening of reinforced concrete beams: an experimental study using CFRP plates", *8th International Conference on Advanced Composites for Concrete Repair (part 1)*, London, U.K., 7pp.

Funakawa, I., Shimono, K., Watanabe, T., Asada, S. and Ushijima, S. (1997) "Experimental study on shear strengthening with continuous fibre reinforcement sheet and methyl methacrylate resin", *Non-Metallic (FRP) Reinforcement for Concrete Structures, Proceedings of the Third International Symposium*, Japan, Vol. 1, pp. 475-482.

Hutchinson, R.L. and Rizkalla, S.H. (1999) "Shear strengthening of AASHTO bridge girders using carbon fibre reinforced polymer sheets", *Proceedings of the Fourth International Symposium on Fibre Reinforced Polymer Reinforcement for Reinforcement Concrete Structures*, ACI publications SP-188, pp945-956.

Kachlakev, D.I. and Barnes, W.A. (1999) "Flexural and shear performance of concrete beams strengthened with fibre reinforced polymer laminates", *Proceedings of the Fourth International Symposium on Fibre Reinforced Polymer Reinforcement for Reinforced Concrete Structures*, ACI SP-188, pp. 959-971.

Khalifa, A., Gold, W.J., Nanni, A. and Aziz, A. (1998), "Contribution of externally bonded FRP to shear capacity of RC flexural members", *ASCE Journal of Composites for Construction*, Vol. 2, No. 4, 195-203.

Khalifa, A., Tumialan, G., Nanni, A. and Belarbi, A. (1999) "Shear strengthening of continuous reinforced concrete beams using externally bonded carbon fibre reinforced

polymer sheets", *Proceedings of the Fourth International Symposium on Fibre Reinforced Polymer Reinforcement for Reinforcement Concrete Structures*, ACI publications SP-188, pp. 995-1008.

Khallifa, A. and Nanni, A. (2000) "Improving shear capacity of existing RC T-section beams using CFRP composites", *Cement and Concrete Composites*, Vol. 22, pp. 165-174.

Maeda, T., Asano, Y., Sato, Y., Ueda, T. and Kakuta, Y. (1997) "A study on bond mechanism of carbon fiber sheet", *Non-Metallic (FRP) Reinforcement for Concrete Structures, Proceedings Third International Symposium*, Vol. 1, pp. 279-285.

Malek, A.M. and Saadatmanesh, H. (1998) "Analytical study of reinforced concrete beams strengthened with web-bonded fibre reinforced plates or fabrics", *ACI Structural Journal*, vol. 95, No. 3, pp. 343-351.

Mitsui, Y., Murakami, K., Takeda, K. and Sakai, H. (1998) "A study on shear reinforcement of reinforced concrete beams externally bonded with carbon fibre sheets", *Composite Interfaces*, Vol. 5, No. 4, pp. 285-295.

Mutsuyoshi, H., Ishibashi, T., Okano, M. and Katsuki, F. (1999) "New design method for seismic retrofit of bridge columns with continuous fiber sheet – performance-based design", *Proceedings of the Fourth International Symposium on Fibre Reinforced Polymer Reinforcement for Reinforcement Concrete Structures*, ACI publications SP-188, pp229-241.

Sato, Y., Ueda, T., Kakuta, Y. and Ono, S. (1997) "Ultimate shear capacity of reinforced concrete beams with carbon fibre sheet", *Non-Metallic (FRP) Reinforcement for Concrete Structures, Proceedings of the Third Symposium*, Vol. 1, Japan, pp. 499-505.

Sato, Y., Ueda, T., Kakuta, Y. and Tanaka, T. (1996) "Shear reinforcing effect of carbon fibre sheet attached to side of reinforced concrete beams", *Advanced Composite Materials in Bridges and Structures*, Ed. M.M. El-Badry, pp. 621-627.

Swamy, R.N. and Mukhopadhyaya, P. (1995) "Role and effectiveness of non-metallic plates in strengthening concrete structures", *Non-Metallic (FRP) Reinforcement for Concrete Structures*, Edited by L.Taerwe, E&FN Spon, London, U.K., pp. 473-482.

Teng, J.G., Chen, J.F., Smith, S.T. and Lam, L. (2000) *RC Structures Strengthened with FRP Composites*, The Hong Kong Polytechnic University, Hong Kong, China, 134pp.

Triantafillou, T.C. (1997) "Shear strengthening of concrete members using composites", *Non-Metallic (FRP) Reinforcement for Concrete Structures, Proceedings of the Third Symposium*, Vol. 1, Japan, pp. 523-530.

Triantafillou, T.C. (1998a) "Shear strengthening of reinforced concrete beams using epoxy-bonded FRP composites", *ACI Structural Journal*, Vol. 95, No. 2, pp. 107-115.

Triantafillou, T.C. (1998b) "Composites: a new possibility for the shear strengthening of concrete, masonry and wood", Composites Science and Technology, Vol.58, No.8, pp.1285-1295.

Triantafillou, T.C. and Fardis, M.N. (1997) "Strengthening of historic masonry structures with composite materials." *Materials and Structures*, Vol. 30, pp. 486-496.

Triantafillou, T.C. and Antonopoulos, C.P. (2000) "Design of concrete flexural members strengthened in shear with FRP", *ASCE Journal of Composites for Construction*, Vol.4, No.4, pp.198-205.

Uji, K. (1992) "Improving shear capacity of existing reinforced concrete members by applying carbon fibre sheets", *Transactions of the Japan Concrete Institute*, Vol. 14, pp. 253-266.

# The effect of stiffness of externally bonded FRP in RC beams subjected to shear

T. KANAKUBO, University of Tsukuba, Japan, T. FURUTA, Akashi National College of Technology, Japan, and H. FUKUYAMA, Building Research Institute, Ministry of Construction, Japan

## INTRODUCTION

Nowadays, strengthening methods where continuous fiber laminates such as carbon, aramid, and glass are used as external seismic reinforcement for reinforced concrete (RC) structures are widely utilized. Recently, many experiments on these methods have been reported and the results of these experiments have provided some insight. However, the strength and deformation behaviour of the RC members have been predicted using existing design equations for steel rebars and by substituting the strength of the steel with that of the FRP (lateral reinforcement). Equations clarifying the actual failure mechanisms have not been reported. Most existing design equations for RC members are based on the yield strength of steel rebars and are not appropriate for elastic materials such as FRP. In addition, the failure of FRP is "fiber rupture failure" and thus brittle failures need to be considered when evaluating fiber RC members.

The final objective of study is to find an evaluation method for the ultimate strength and the deformation capacity of strengthened RC members, based on failure mechanisms. The members are reinforced using materials such as carbon or aramid fiber as externally bonded reinforcement for RC structures in seismic regions. In order to identify an appropriate analysis method, shear tests on RC members were conducted. These members were reinforced using several different types of continuous fibers (carbon, aramid, glass, and polyester). The effect of the FRP stiffness on the behavior of RC beams subjected to shear forces is thus investigated. The stiffness of FRP laminates is defined as elastic modulus ($_fE$) × fiber thickness ($_ft$).

## OUTLINE OF EXPERIMENTS

### Specimens and Materials

The specimen details are shown in Table 1 and Figure 1. The specimens are 160mm wide, 250mm high, and 750mm long, with a shear span ratio of 1.5 and a concrete strength between 30.3 and 44.2 MPa. The main steel bars are 8-D13 ($p_t$ =1.27%, yield strength grade 800MPa) and the lateral reinforcement, D4@90 ($_sp_w$ =0.17%, yield strength grade 295MPa). The main parameter in this study is the fiber material. As shown in Table 1, five different fibers were tested; normal carbon fiber (NCF), high elastic carbon fiber (HCF), aramid fiber (ARF), glass fiber (GLF), and polyester fiber (PAF). The elastic modulii ($_fE$) of NCF and HCF were 240GPa and 390GPa, respectively. The reinforcing amount of FRP for all specimens was set so that the elastic modulus ($_fE$) × fiber thickness ($_ft$) = 20.0. Since the cross section of the specimens is constant in this study, the ratio of FRP to unit cross section ($_fp_w$) is proportional

*FRPRCS-5*, Thomas Telford, London, 2001.

to the fiber thickness. Namely, ${}_fE{\cdot}_ft$ can be used for ${}_fE{\cdot}_fp_w$. The control specimen (No.1) had no FRP reinforcement, with ${}_sp_w$ =0.17%. Specimen No.2 had 150g/m$^2$ of NCF, No.3 93g/m$^2$ of HCF, No.4 242g/m$^2$ of ARF, No.5 698g/m$^2$ of GLF and No.6 727g/m$^2$ of PAF. The calculated bending strength for each specimen (${}_{cal}Q_{mu}$) was 167kN. All specimens were designed to obtain a shear failure at ultimate. Hence in the FRP strengthened specimens, a shear failure by fiber rupture is expected.

Table 1 List of Specimens

| No. | Identification | Fiber | ${}_ft$ (mm) | Layer | ${}_fE$ (GPa) | ${}_f\sigma_u$ (MPa) | ${}_ft{\cdot}_fE$ (kN/mm) | ${}_fp_w$ (%) | ${}_fE{\cdot}_fp_w$ (MPa) | ${}_f\sigma_u{\cdot}_fp_w$ (MPa) |
|---|---|---|---|---|---|---|---|---|---|---|
| 1 | N-0 | - | - | - | - | - | - | - | - | - |
| 2 | NCF-150 | Carbon | 0.084 | 1 | 240 | 3400 | 20.0 | 0.104 | 250.5 | 3.55 |
| 3 | HCF-93 | High elastic carbon | 0.051 | 62.5@162.5 | 390 | 2900 | 20.0 | 0.056 | 250.3 | 1.61 |
| 4 | ARF-242 | Aramid | 0.167 | 150@173 | 120 | 2100 | 20.0 | 0.209 | 250.5 | 4.38 |
| 5 | GLF-698 | Glass | 0.275 | 2+61.3@162 | 73 | 1470 | 20.0 | 0.344 | 250.9 | 5.05 |
| 6 | PAF-727 | PAF | 0.501 | 1+(50@58.3) | 40 | 1300 | 20.0 | 0.626 | 250.5 | 8.14 |

${}_f\sigma_u$ : tensile strength of fiber (nominal value), ${}_fp_w$ : ratio of FRP to unit cross section

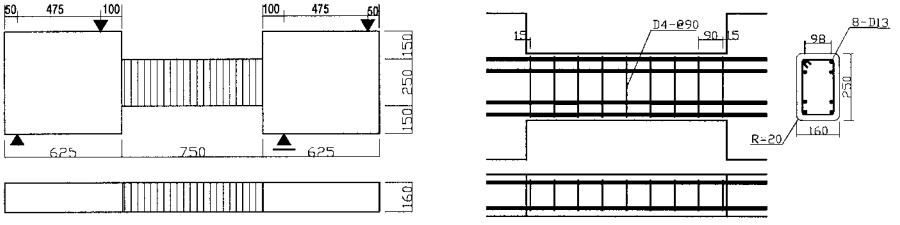



Figure 1 Specimen details (units : mm)

**Loading Method and Measurements**

The test apparatus and the positions of the displacement transducers are illustrated in Figure 2. The anti-symmetrical moment loading system was applied. Specimens were subjected to one way loading. The relative displacement was defined by two displacement transducers placed at the center of the beam (Figure 2). The locations of the strain gauges on the FRP and the rebars are illustrated in Figure 3.

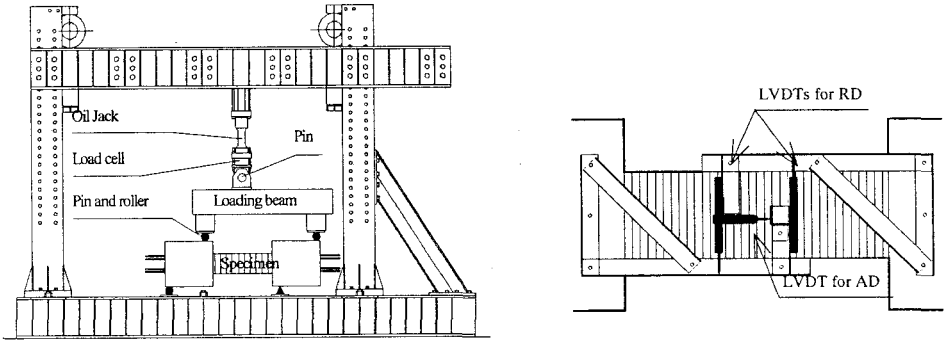



Figure 2 Loading Method

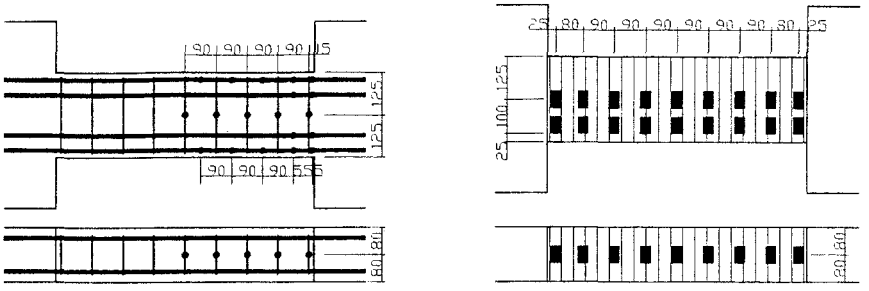


Figure 3 Locations of strain gauges (units : mm)

## EXPERIMENTAL RESULTS

### Failure Patterns

Figure 4 shows a diagram of the shear force ($Q$) versus relative displacement ($\delta$) and typical ultimate failure patterns are indicated in Photo 1. Table 2 shows the relationship between the drift angle ($R$) and shear force ($Q$). In beam No.1, shear cracks at both ends of the beam had developed at a drift angle of ($R$)=1/125rad, and the lateral reinforcement had yielded. At $R$=1/111rad, the specimen reached the ultimate strength ($Q_{max}$)=61.9kN. At this drift angle, the shear cracks opened widely. Simultaneously, the specimen exhibited a typical shear failure, with a sharp decrease in strength after the ultimate strength had been reached.

Except for beam No.3, the strengthened specimens were fully covered with FRP on the surface, and thus the crack patterns for these specimens were not observed. Specimens No.2, No.4, and No.5 reached $Q_{max}$ =127.4kN ($R$=1/30rad), $Q_{max}$ =124.0kN ($R$=1/24rad), and $Q_{max}$ =127.1kN ($R$=1/22rad), respectively. After these specimens reached the ultimate strength, the FRP reinforcement ruptured, and the expected shear cracks developed rapidly. Simultaneously, the strength of the specimens decreased radically. No.3 (HCF) reached $Q_{max}$=127.4kN at $R$=1/60rad. After that, the FRP reinforcement ruptured when the shear cracks opened widely, and the strength of the specimen decreased suddenly. No.6 (PAF) reached $Q_{max}$ =112.6kN at $R$=1/30rad. This specimen sustained a fairly constant load with no rupture even at the final drift angle ($R$=1/12rad). For specimens No.4, No.5 and No.6 it was observed that the main bars yielded after reaching the maximum strength.

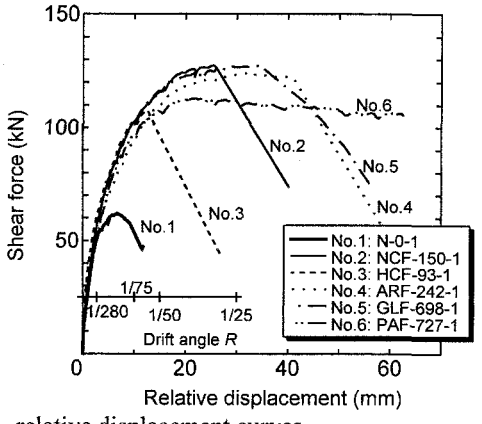
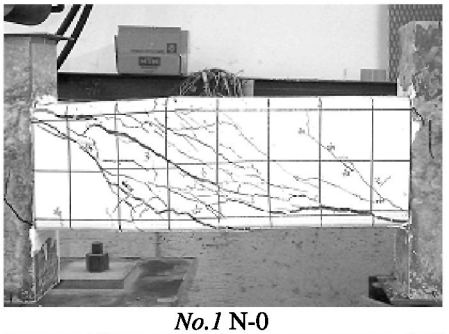
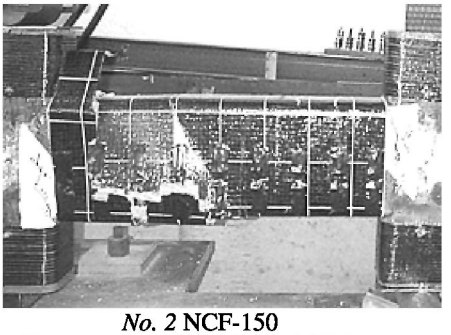


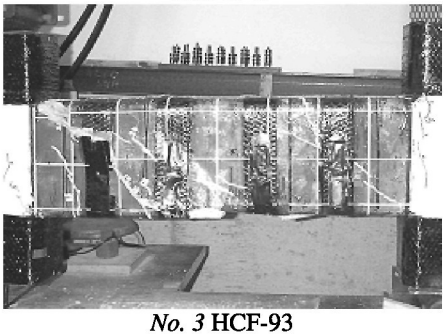

Figure 4 Shear force – relative displacement curves



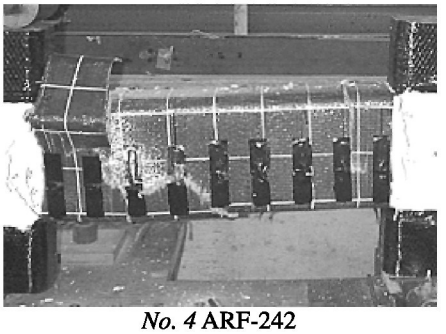
*No.1* N-0



*No. 2* NCF-150



*No. 3* HCF-93



*No. 4* ARF-242

Photo 1 Ultimate failure pattern

Table 2 Shear force vs drift angle

| No | Identification | Max shear force $Q_{max}$ (kN) | Drift angle at $Q_{max}$ (rad) | Drift angle at yielding of main bars (rad) | Shear force (kN) | | | | | | |
|---|---|---|---|---|---|---|---|---|---|---|---|
| | | | | | 1/280 | 1/200 | 1/150 | 1/100 | 1/75 | 1/60 | 1/30 |
| 1 | N-0 | 61.9 | 1/111 | — | 50.5 | 54.6 | 59.6 | — | — | — | — |
| 2 | NCF-150 | 127.4 | 1/30 | — | 55.9 | 66.9 | 76.7 | 91.5 | 102.5 | 116.0 | 126.9 |
| 3 | HCF-93 | 107.6 | 1/60 | — | 60.2 | 60.8 | 78.0 | 93.7 | 103.0 | 107.5 | — |
| 4 | ARF-242 | 124.0 | 1/24 | 1/22 | 50.7 | 61.4 | 69.2 | 83.4 | 94.3 | 110.0 | 123.2 |
| 5 | GLF-698 | 127.1 | 1/22 | 1/17 | 56.1 | 66.2 | 77.3 | 91.6 | 102.9 | 115.6 | 126.6 |
| 6 | PAF-727 | 112.6 | 1/30 | 1/20 | 50.6 | 62.0 | 72.6 | 87.7 | 96.5 | 106.9 | 111.5 |

The location where the FRP reinforcement ruptured was the same for all strengthened specimens. The rupture occurred because the shear cracks in the concrete inside the FRP opened significantly, and the concrete was pushed out toward the FRP. In particular, the fibers were damaged and cut due to the stress concentration at a certain point in the FRP. As shown in Figure 4 and Table 2, the $Q$-$\delta$ relationship is similar for all specimens until around $R$=1/280rad, when shear cracks started to occur in beam No.1. The $Q$-$\delta$ relationship of the strengthened specimens is similar until around $R$=1/60rad, the stage when specimen No.3 reached the ultimate strength. After $R$=1/60rad, the $Q$-$\delta$ relationships of specimens No.2, No.4 and No.5 were similar and the strength increased as the deformation increased.

However, in the case of Specimen No.6 the strength was maintained after $R$=1/60rad and only the deformation increased.

**Relationship between Shear Forces and Elastic Modulus of Fibers**

Plots of the relationship between the shear force ($Q$) and the elastic modulus ($_fE$) and between the shear force and the FRP strength times reinforcing amount ($_f\sigma_u \cdot {}_fp_w$) at $R$=1/200rad, 1/100rad, 1/60rad and at the ultimate strength are illustrated in Figure 5. Both diagrams show that, at each drift angle, a similar behavior for each specimen is observed. The shear forces sustained by specimens ARF and PAF were relatively lower than those of the other specimens. In particular, the shear force increment for PAF tended to decrease with increasing deformation, when compared to the other specimens. In the case of HCF, the ultimate strength was already reached at $R$=1/60rad, and the ultimate strength of HCF was the lowest amongst all the strengthened specimens.

When the reinforcing stiffness of FRP ($_fE \cdot {}_fp_w$) was identical, $Q_{max}$ for NCF, GLF and ARF were nearly the same. Considering that $Q_{max}$ of the lower elasticity PAF and higher elasticity HCF were lower than those of NCF, GLF and ARF, it is observed that $Q_{max}$ did not increase for a constant $_fE \cdot {}_fp_w$, when the factor $_f\sigma_u \cdot {}_fp_w$ increased.

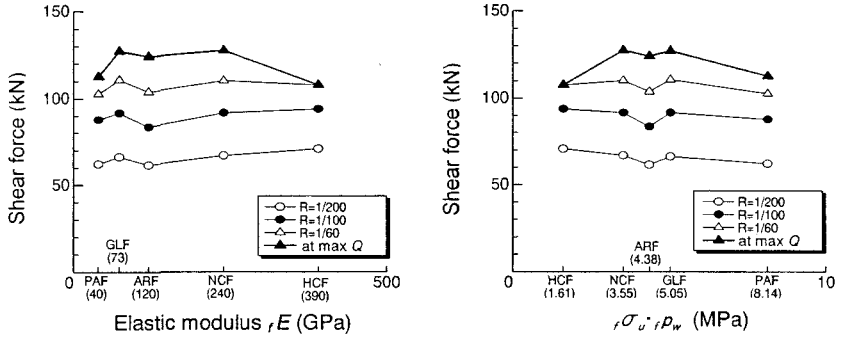



Figure 5 Shear force vs elastic modulus and strength of FRP

**Strain Distributions of FRP**

Figure 6 illustrates the FRP strain distribution at $R$=1/200rad, 1/100rad, 1/60rad, and at the ultimate load. The data points for the strain distribution are the average of two strain gauge readings at the same location along the fiber direction on the surface of each specimen (as shown in Figure 3).

The strains at $R$=1/200rad were very small, with an average value of approximately 220μ. The strains at $R$=1/100rad are more varied. The strains around 200mm from both ends of specimens at this drift angle tended to be large, with an average of about 2700μ. The average of all strains was approximately 1100μ. There was no marked difference between the different fiber types at $R$=1/60rad, when No.3 (HCF) had fiber rupture. All specimens showed generally the same strain distributions. The average of the strains around 200mm from both ends at $R$=1/60rad was about 4800μ. The global average strain was approximately 2500μ. At the ultimate load, specimen No.5 (GLF) showed the highest strain followed by, in descending

order, specimens No.4 (ARF), No.2 (NCF), No.3 (HCF) and No.6 (PAF). This order corresponded to the order of the ultimate strength. The average strain around 200mm from both ends was approximately 8200μ. The global average strain was about 6000μ.

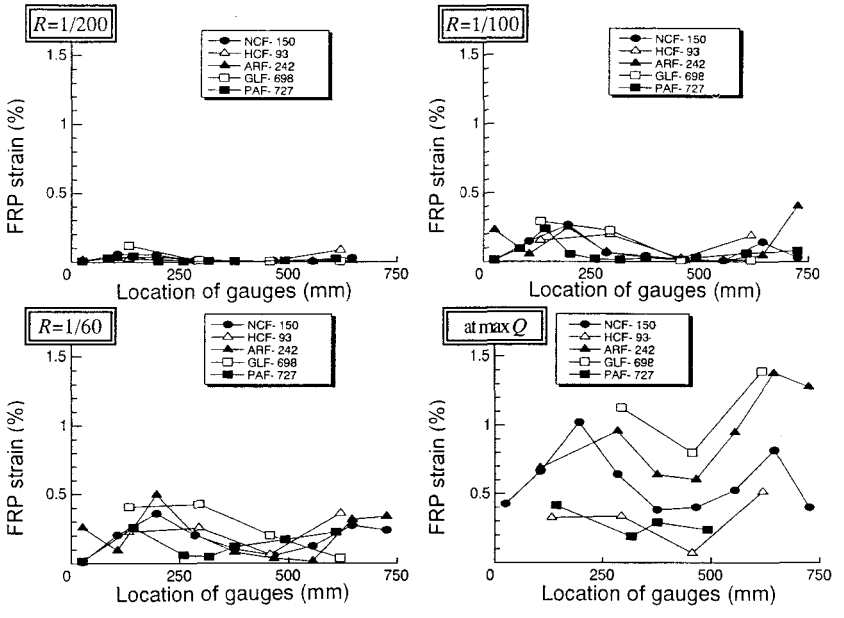



Figure 6 FRP Strain distribution

**Stress of FRP**

Figure 7 shows a diagram of the actual stress ($_f\sigma_s = \varepsilon \times {}_fE$) versus drift angle ($R$=1/200rad, 1/100rad, 1/60rad, and 1/30rad). The maximum values of the strains in Figure 6 are used in calculating $_f\sigma_s$. It was observed that generally the FRP in each specimen carried the same stress until $R$=1/60rad. The stress of specimen No.5 (GLF) at $R$=1/30rad (approximately when the specimen reached the ultimate strength) was the largest. The stresses of specimens No.4 (ARF), No.2 (NCF) and No.6 (PAF) were smaller in this order. In particular, the stress of No.6 was less than half that of the other specimens.

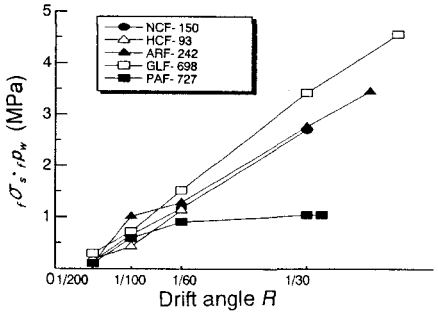



Figure 7 Actual stress of FRP vs drift angle

It was confirmed that the FRP stresses up until $R$=1/60rad were generally the same when the reinforcing amount of FRP was identified for a constant value of the elastic modulus (${}_fE$) × fiber thickness (${}_ft$). However, it appears that around $R$=1/30rad, there were different characteristics depending on the fiber type. It is supposed that not only the modulus of elasticity of the fiber but also parameters such as the thickness and shear capacity of the fiber caused the differences in the FRP stress in each specimen.

**Shear Strength Evaluations**

Table 3 compares the shear strength calculated by the Truss - Arch Method (Method A of AIJ[1]) with the experimental ultimate strength for each specimen. The following two methods of calculating the shear strengths were adopted; using the actual stress of FRP (${}_f\sigma_s$: the stress calculated from the maximum strain in Figure 6), and utilizing an effectiveness coefficient, ${}_f\nu$=0.3, for ${}_f\sigma_u$.

In case of using ${}_f\sigma_s$, the ratio, $Q_{max}$ / ${}_{cal}Q_{su}$, varied from 0.67 to 0.98. In all specimens except for No.6 (PAF), which had a low elasticity, the calculated shear strengths were noticeably higher than the actual ultimate strengths. It is supposed that the strain gauges at the location where fiber rupture occurred were significantly stressed due to the concrete cracks. When ${}_f\nu$ =0.3 is used, the ratio, $Q_{max}$ / ${}_{cal}Q_{su}$, varied from 0.71 to 1.20, because the strengths of all different types of fiber were multiplied by the same effectiveness coefficient (${}_f\nu$ =0.3). It is obvious that specific effectiveness coefficients for each different type of fiber should be proposed.

Table 3 Shear strength evaluation

| No. | Identification | $Q_{max}$ (kN) | ${}_{cal}Q_{f\sigma s}$ (kN) | $Q_{max}$/ ${}_{cal}Q_{f\sigma s}$ | Effectiveness coefficient ${}_f\nu$ | ${}_{cal}Q_{su}$ (kN) | $Q_{max}$/ ${}_{cal}Q_{su}$ |
|---|---|---|---|---|---|---|---|
| 2 | NCF-150 | 127.4 | 136.2 | 0.94. | 0.3 | 106.6 | 1.20 |
| 3 | HCF-93 | 107.6 | 120.9 | 0.89 | | 101.6 | 1.06 |
| 4 | ARF-242 | 124.0 | 194.4 | 0.64 | | 128.0 | 0.97 |
| 5 | GLF-698 | 127.1 | 190.4 | 0.67 | | 130.9 | 0.97 |
| 6 | PAF-727 | 112.6 | 115.4 | 0.98 | | 159.1 | 0.71 |

## CONCLUSIONS

On the basis of this study, the following conclusions can be drawn:

1. When the reinforcing amount of FRP for each fiber type was chosen to obtain a constant stiffness (elastic modulus (${}_fE$) × fiber thickness (${}_ft$) ) the shear force versus relative displacement curve and the relationship between the shear force and FRP stress for each specimen were generally the same, regardless of fiber type.
2. Fiber rupture occurred because the fibers became damaged and ruptured at a certain point due to stress concentrations at the location of the concrete cracks.
3. A specific effectiveness coefficient (${}_f\nu$) for each different type of fiber is required to evaluate the shear strengths of RC members.

**ACKNOWLEDGEMENTS**

This study was conducted under the University of Tsukuba Research Project. The authors also acknowledge Chikara Iihoshi from Asahi Chemical Industry Co., Keisuke Takahashi from Mitsubishi Chemical Functional Products Inc., and Masaharu Tanigaki from Mitsui Construction Co.

**NOTATION**

$_fE$ : elastic modulus of fiber
$p_t$ : main bar ratio
$_fp_w$ : reinforcement ratio for fiber
$_sp_w$ : lateral reinforcement ratio for steel rebar
$Q$ : shear force
$_{cal}Q_{f\sigma s}$ : calculated shear strength using $_f\sigma_s$
$Q_{max}$ : maximum shear force
$_{cal}Q_{mu}$ : calculated bending strength (in shear force)
$_{cal}Q_{su}$ : calculated shear strength using $_f\nu$
$R$ : drift angle
$_ft$ : thickness of fiber
$_f\nu$ : effectiveness coefficient for FRP
$_f\sigma_s$ : experimental obtained stress of FRP
$_f\sigma_u$ : tensile strength of fiber

**REFERENCES**

1) Architectural Institute of Japan : Design Guidelines for Earthquake Resistant Reinforced Concrete Buildings Based on Ultimate Strength Concept, pp.106 – 116, 1990

# Design and shear behaviour of FRP mesh reinforcement across cracks in concrete

EIJI MAKITANI, ALAN R. BURDEN, TAKAMITSU MAKITANI and WEI QI,
Kanto-Gaguin University ,Yokohama,Japan

## INTRODUCTION

It is important from a safety viewpoint in shear design to evaluate the shear transfer capacity of FRP mesh reinforcement across cracks generated in concrete structures subjected to high shear force, because the effective cross section of FRP mesh reinforcement is very small. However there is little experimental data related with shear behavior of FRP mesh reinforcement in concrete.

In the present study, a direct shear test was conducted for the purpose of investigating the shear behavior of FRP mesh reinforcement across a crack in a concrete element. An equation for shear design of FRP mesh reinforcement is proposed on the basis of these test results.

## TEST SPECIMEN

The test specimens had dimensions of effective thickness × width × height = 80 and 110 × 500 × 560mm, and had a stub for stiffness at both ends . They were reinforced by either single or double layer mesh FRP reinforcement at a pitch of 50 or 100mm, as shown in Fig.1. The FRP mesh reinforcement was made from continuous carbon fiber and epoxy resin. A crack had been formed previously in the center of the concrete specimens, with the CFRP mesh

Table 1 CFRP mesh reinforcement in test spcimen

| Test specimen | Arrangement of CFRP mesh | Pitch of CFRP mesh reinforcement (mm) | Angle of CFRP mesh to crack | numder of CFRP bars or nodes(*) across crack |
|---|---|---|---|---|
| SR-10 | single layer | 100 | right | 4 |
| SR-5 | | 50 | | 7 |
| SI-10 | | 100 | forty-five degrees | *4 |
| SI-5 | | 50 | | *7 |
| DR-10 | double layer | 100 | right | 8 |
| DR-5 | | 50 | | 14 |
| DI-10 | | 100 | forty-five degrees | *8 |
| DI-5 | | 50 | | *14 |

Table 2 Mechanical properties of CFRP mesh reinforcement

| Pitch of CFRP mesh (mm) | Area of cross section (mm2) | Strength of failure (N/mm2) | Young's Modulus (GN/mm2) | Strain at failure (%) |
|---|---|---|---|---|
| 100 | 18.2 | 1090 | 91.0 | 1.16 |
| 50 | | 1170 | 92.2 | 1.26 |

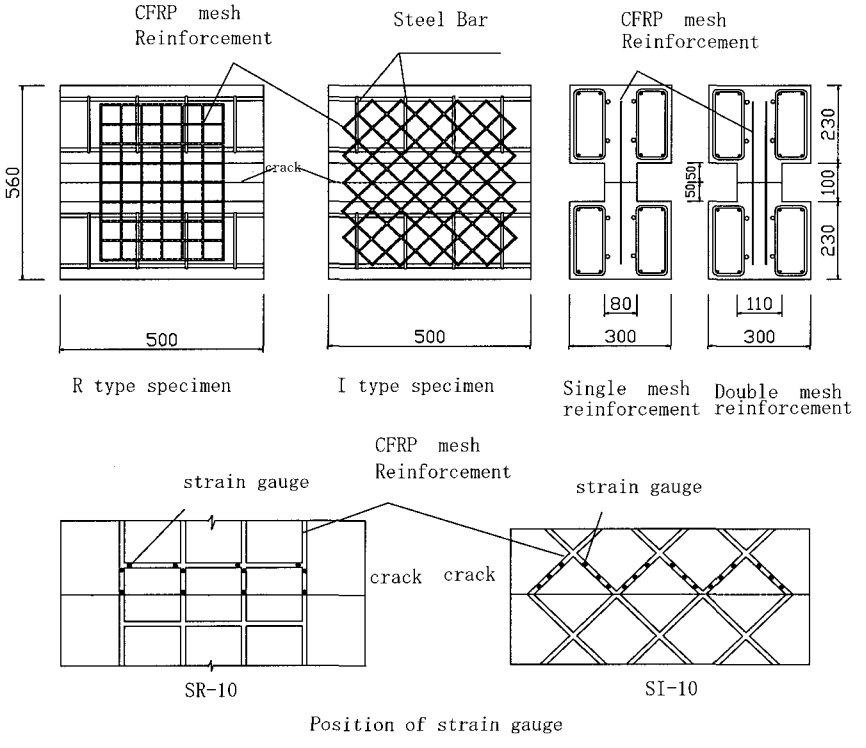



Fig.1 Details of test specimen and position of gauge

reinforcement arranged at inclinations of ninety and forty-five degrees to the crack. Eight test specimens were constructed. Their details are indicated in Table 1. The mechanical properties of CFRP mesh reinforcement are shown in Table 2. A compressive strength of concrete, $\sigma_B$=32 N/mm$^2$, was used for the test specimens.

## METHODS FOR LOADING AND MEASUREMENT

Direct shear force was applied as non-cyclic loading to the surface of the crack in the test specimens by a hydraulic jack having a capacity of 1000 kN through steel beams connected with PC steel bars to both sides of specimen, as shown in Fig. 2.

The load for direct shear was measured by a load cell with capacity of 1000 kN. The slip displacement caused by shear force along the surface of a crack was measured by displacement meters with high sensitivity. The strain in the CFRC mesh reinforcement was also measured by strain gauges which were attached close to a crack, as shown in Fig. 1.

## FAILURE OF CFRP MESH REINFORCEMENT

When the CFRP mesh reinforcements across a crack are subjected to direct shear force on its surface, composite axial and shear stresses act on it. Therefore, at final failure they fail by shear. A representative state of failure for a test specimen with normal and double arrangements is shown in Photo 1.

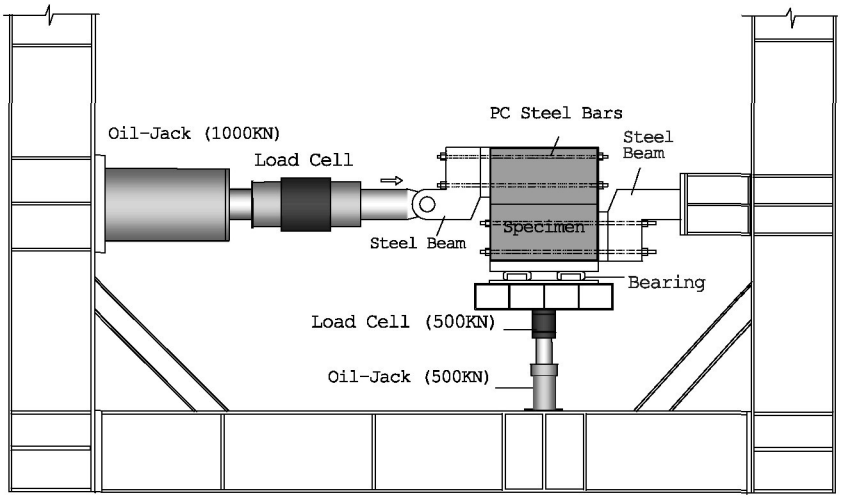



Fig.2 Loading Apparatus




Photo.1 State of failure (DR-5)

## RELATIONSHIP BETWEEN SHEAR FORCE AND DISPLACEMENT

The curves of shear force and slip displacement along the surface of a crack, in all test specimens for the normal and inclined arrangements of CFRP mesh reinforcement, are shown in Fig.3 and Fig.4 respectively. On the basis of these test results, the ratio of maximum shear stress $\tau_{fu}$ to tensile strength $\sigma_{fu}$ and number of CFRP mesh reinforcements across a crack is plotted in Fig.5.

It is found from Fig. 3 and Fig. 4 that the slip displacements at maximum shear force for the test specimens with normal arrangement of CFRP mesh reinforcement are significantly smaller than those of the inclined arrangements, because arching action occurs on the former test specimens by means of the inclined CFRP mesh reinforcement. It is also

apparent from Fig. 5 that the shear resistance of CFRP mesh reinforcement across a crack possesses a tendency to decrease when the number of bars increases and that the lower bound of the ratio ( $\tau_{fu}/\sigma_{fu}$) of shear stress to tensile strength is 0.2.

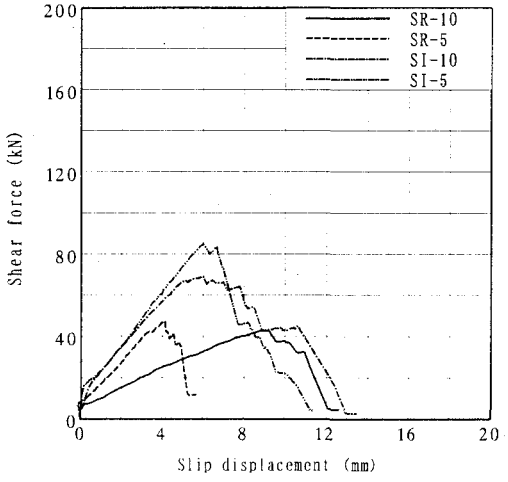



Fig.3 Shear force-slip displacement curves for the test Specimens with normal arrangement

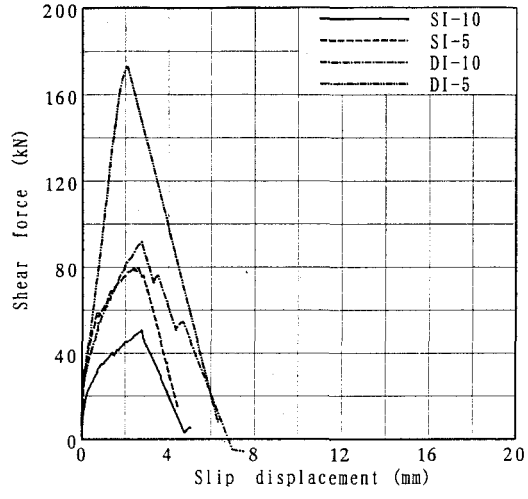



Fig.4 Shear force-slip displacement curves for the test specimens with inclined arrangement

## BEHAVIOUR UNDER AXIAL STRESS AND SHEAR

The relationship between shear resistance of CFRP mesh reinforcement and tensile stress acting on it close to a crack is demonstrated for test specimens DR-5 and DI-5 in Fig.6. It is found from this figure that the shear resistance for test specimens DI-5 is greater than that of the specimen DR-5 because in the former the number of mesh reinforcements across a crack is greater.

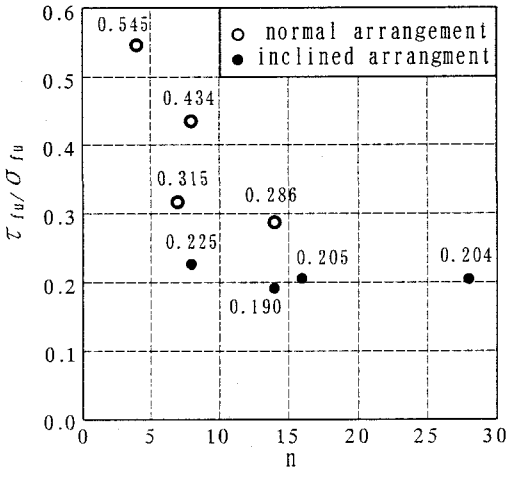



Fig.5 Relationship between shear strength $\tau_{fu}$ and number n of CFRP bars in normal and inclined arrangement across a crack

The distribution of tensile stress at failure which acts on CFRP mesh reinforcements at the position of a crack is plotted for test specimens DR-5 and DI-5 in Fig. 7, where the tensile stresses acting on CFRP mesh reinforcement of specimen DI-5 are greater than those of specimen DR-5. This is due to the truss action in the CFRP mesh reinforcement with an inclined arrangement. It is observed that compressive stress is caused in the alternative CFRP mesh reinforcements. It is believed that the tensile stress acting in the CFRP mesh reinforcement orthogonal to a crack in the specimen DR-5 was caused by dowel action.

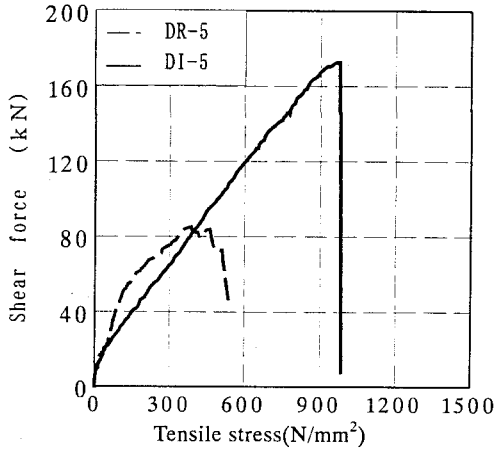



Fig.6 Relationship between shear force and tensile force acting on CFRP mesh reinforcement

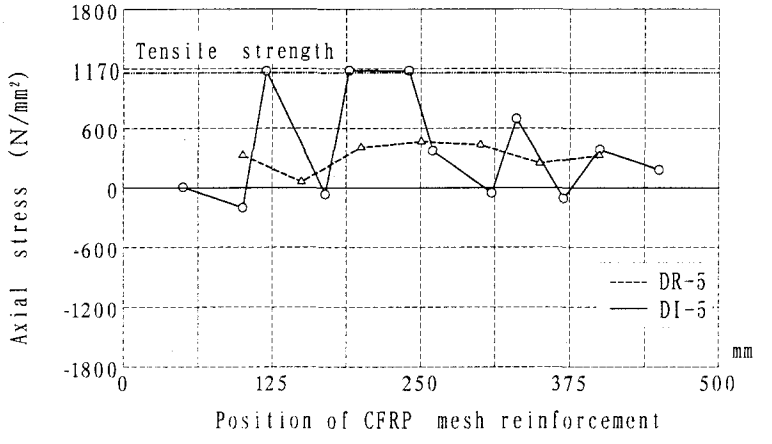



Fig.7 Distribution of axial force of CFRP mesh reinforcement at the location of a crack

## EVALUATION OF SHEAR STRENGTH OF CFRP MESH REINFORCEMENT

For CFRP mesh reinforcement across a crack under direct shear, a stress state of combined axial stress $\sigma_f$ and shear stress acts. Therefore, the criteria for failure of CFRC mesh reinforcement under axial stress and shear stress can be represented by the following equation:

$$\sigma_f^2 + (\alpha\tau_f)^2 \leq \sigma_{fu} \qquad (1)$$

where $\sigma_{fu}$ indicates the tensile strength of CFRP mesh reinforcement.

The criteria (1) associated with $\sigma_f/\sigma_{fu}$ and $\alpha\tau_f/\sigma_{fu}$ is depicted in Fig. 8, where the test results for eight test specimens are plotted under the assumption of $\alpha = 5$.

It is observed from Fig. 8 that the test results satisfy the criteria for failure of CFRP mesh reinforcement. Hence, the shear strength of CFRP mesh reinforcement $\tau_{fu}$ may be evaluated by the following equation:

$$\tau_{fu} = 0.2\sigma_{fu} \qquad (2)$$

where this relation is confirmed from Fig. 5.

The shear strength obtained from equation (2) is small compared with ordinary steel bar. Accordingly, it is very important in design to check the shear transfer of FRP mesh reinforcement in concrete structures.

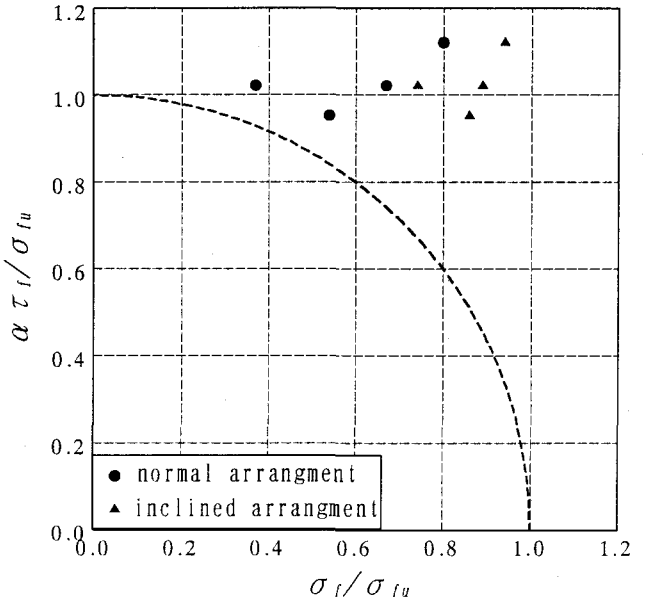



Fig.8 Failure criterion for CFRP mesh reinforcement( $\alpha$ =5)

## CONCLUSIONS

It was observed from the direct shear test of FRP mesh reinforcement across a crack in a concrete element that its shear strength was very small, because the effective cross section was extremely small. In the design for shear in structural concrete members with FRP mesh reinforcement, and especially for those having thin cross sections such as walls under high shear from seismic or wind forces, it is necessary to check shear transfer.

### References

(1) Makitani.E,Irisawa.J and Nishiura,N(1993). "Investigation of bond in concrete members with fiber reinforced plastic bars". Fiber-Reinforced Plastic Reinforcement for concrete Structures-International Symposium, American Concrete Institute sp-138, pp315-331.

(2) Makitani.E,Shindo.K,Wang.W, and Ishibashi,K (1995) "Structural Design and Behavior of concrete Members with two and three-dimensional FRP Reinforcements", Proceedings of the Second International RILEM Symposium (FRPRCS-2),PP314-321.

(3) Makitani .E,Wakamada.H,Shindo.K AND Ehang.Y(1999), "Flexural Behavior of concrete Member with Two and Three Dimensional FRP. Reinforcements ", Proceedings of the Third International Symposium on Non-Metallic (FRP) Reinforcement for Concrete Structures, Vol.2,pp,615-622

(4) Matsuzaki,Y.Nakano,K,Nakazawa.H and Fujisaki.T(1987), "Application of New Fiber Reinforced Composite Material(NFM) To Concrete Structures. (part2. Test for shear strength of NEM),Summaries of Technical Papers of Annual Meeting, Architectural Institute of Japan,pp.133-134.

# CARBOSTRAP – An advanced composite tendon system

A. WINISTOERFER and U. MEIER
EMPA, Swiss Federal Labs for Materials Testing and Research, Duebendorf, Switzerland

## SUMMARY
A novel load transfer concept for a carbon fibre tendon system for the strengthening and rehabilitation of existing civil engineering structures is introduced using non-laminated pin-loaded straps. The tendon is comprised of a maximum of seventy layers formed from a single, continuous carbon fibre tape with thermoplastic matrix material. The brittle behaviour of carbon fibres and the implications of this on the reliability of the tendon are discussed. The system is generally applied in a prestressed condition, externally to the structure. Hence, the long-term performance under sustained loading conditions is presented. It is concluded that the use of these novel tendon elements could represent a viable and durable means of strengthening existing concrete infrastructure.

## INTRODUCTION
Throughout the world there is a large number of existing structures, which need to be replaced or retrofitted. This may be due to a change of social needs, upgrading of design standards, increased safety requirements or deterioration [1, 2]. The problems are particularly severe in the case of reinforced concrete bridges where chloride induced deterioration is responsible for the need of rehabilitation methods [3]. Strengthening requirements for existing structures may demand either, or both, an increase in flexural or shear resistance.

Carbon Fibre Reinforced Plastic (CFRP) for externally bonded flexural strengthening, as described by Meier [4], has been used successfully in recent years. The strengthening method is experiencing an economical breakthrough in Switzerland with about 12 tons of CFRP used for retrofitting purposes in 1996. Meier [5] is predicting a worldwide usage of 850 tons per annum for such applications in about twenty years. Similar systems based on externally bonded fabrics or sheets for post shear strengthening purposes have been developed in the US by Chajes et al. [6] and in Canada by Hutchinson et al. [7], Drimoussis and Cheng [8].

The focus of previous research by Lees, Winistoerfer and Meier [9, 10] was the development of tensioned non-laminated CFRP straps as active (prestressed) external shear reinforcement for concrete. The use of an active system has several advantages compared with a passive (unstressed) reinforcement system. In particular, the prestressed CFRP straps provide confinement and enhance the performance of the concrete.

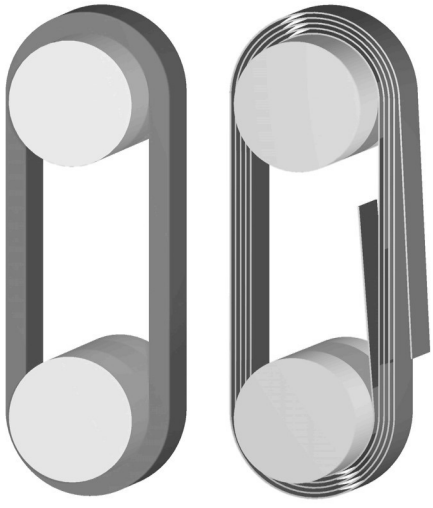
The current work seeks to discuss reliability aspects of this novel tendon system which is based on a brittle material and therefore subject to a large variability of strength properties. Experimental results of static short-term tensile tests and creep tests under severe loading conditions are presented.

*FRPRCS-5*, Thomas Telford, London, 2001.

## PIN-LOADED STRAP ELEMENTS

A carbon fibre reinforced laminated pin-loaded strap, as shown in Figure 1(a), might provide a practical tension element for the shear enhancement of concrete. Such an element can consist of a unidirectional fibre reinforced plastic, having a fibre volume fraction of about 60%, wound around two cylindrical steel pins in a racetrack shape. The maximum number of layers will, however, be limited by technical considerations in the manufacturing process [11]. No machining of holes is required to make a strap. The two pins transfer tensile load between the structure, and the fully consolidated strap.

Laminated straps have desirable characteristics of high tensile strength, low weight, low thermal conductivity, and, crucial, high durability. The US-Army has therefore investigated laminated CFRP tendons for temporary bridge deployment [12].



*(a)* *(b)*

*Fig.1 Conceptual design of pin-loaded strap elements.*

Laboratory experiments and analytical modelling by Winistörfer [11] has shown that there are severe stress concentrations in the region where the strap and the pin meet. The tensile resistance of the strap is therefore limited to about 60 % of the material's expected unidirectional strength. This is attributed to stress concentrations, which lead to premature failure. Furthermore, the production process for multi-layered laminated straps is not straightforward, if fibre misalignment is to be eliminated where the stress concentrations occur.

A novel design approach which diminishes the undesirable stress concentrations, overcomes the manufacturing difficulties and reduces cost is the use of a non-laminated strap system. The concept which has been patented by Meier and Winistoerfer [13] is shown in Figure 1(b).

The CFRP strap now comprises a number of unidirectionally reinforced layers, formed from a single, continuous, thermoplastic tape of about 0.13 mm thickness. The tape is wound around the two pins and only the end of the outermost layer is fusion bonded to the next outermost layer to form a closed loop.

The non-laminated strap element enables the individual layers to move relative to each other which allows an equalisation of forces in the layers as the strap is tensioned [11]. The stress concentrations are reduced since the new structural form is more compliant than the laminated equivalent. Control of the initial tensioning process reduces interlaminar shear stresses so that a more uniform strain distribution in all layers can be achieved. The approach allows greater flexibility in terms of the geometry of the tendon, and it can be manufactured on site. Moreover, the concept is going to be less expensive because there is no consolidation

## RELIABILITY OF NON-LAMINATED PIN LOADED STRAPS

An important aspect of non-laminated pin-loaded straps is the brittle nature of the carbon fibres. The stress at which brittle fibres fail usually depends on the presence of flaws, which may occur randomly along the length of a fibre. A statistical approach of this situation involves conceptually dividing a length of fibre into a number of incremental lengths. The fibre fractures when it has at least one incremental element containing a flaw sufficient to cause failure under a given stress. This analysis is known as the Weakest Link Theory (WLT) [14].

The Weibull modulus, $m$, is an important parameter for characterising the strength distribution of brittle solids. A low value of $m$ (e. g. < 10) implies considerable uncertainty about the strength of a specimen. In practice, many ceramic materials exhibit Weibull moduli in the range 2-15. Sommer et al. [15] reported values of $m$ = 5.25 for strength properties of single carbon fibre filaments (Sigrafil C).

### Experimental study

Fifty-three straps were produced from 12 mm wide carbon fibre tape with Nylon matrix (Toray T700 / PA 12). Various configurations in terms of number of layers, $N$, length, $L$, and pin diameter, $D$, were investigated. The tensile tests for the smaller pin diameters, summarised in Table 1, were performed on an Instron 1251 testing machine. The larger pin diameter straps were tested on an Instron 1346. The pin diameter had to be increased for the straps consisting of forty or more layers to prevent failure of the steel pin due to extensive bending and shear stresses. Load carrying capacities, $F_{ult}$ , are given instead of stresses because of large variations in the tape dimensions, hence inaccurate measurements of the cross-sectional area.

The Weibull plots of the experimentally determined $F_{ult}$ and the corresponding linear curve fits to resolve the gradients (Weibull moduli, $m$) are presented in Figure 2. The capacities are normalised with the total number of tapes present in each strap.

The highest mean strength was attained with a single layer containing a fusion bonded joint. Failure occurred in the joint, where minor fibre misalignment was introduced in the joining process. This may be the reason for the increased variability compared to other data sets. Only minor differences in the capacity per tape were observed for straps consisting of ten up to fifty layers. Furthermore, the variability of these sets was considerably reduced.

*Table 1: Summary of experimental investigation on non-laminated pin-loaded straps.*

| Number of layers, $N$ | 1 | 10 | 20 | 30 | 40 | 40 | 40 | 50 | 60 | 70 |
|---|---|---|---|---|---|---|---|---|---|---|
| Specimens tested, $n$ | 6 | 6 | 6 | 6 | 7 | 6 | 3 | 7 | 4 | 2 |
| Pin diameter, $D$ | 30 | 30 | 30 | 30 | 50 | 50 | 50 | 50 | 50 | 50 |
| Length, $L$ | 700 | 700 | 700 | 700 | 700 | 350 | 1500 | 700 | 700 | 700 |
| $F_{ult}$ [kN] | 6.2 | 50.0 | 101.2 | 157.8 | 207.4 | 173.8 | 204.0 | 249.0 | 269.8 | 278.0 |
| $s$ [kN] | 0.3 | 1.2 | 2.8 | 3.4 | 3.8 | 12.0 | 3.6 | 4.9 | 10.2 | 14.1 |
| $C.\ O.\ V$ [%] | 5.5 | 2.5 | 2.8 | 2.1 | 1.8 | 6.9 | 1.8 | 2.0 | 3.8 | 5.1 |
| Weibull modulus, $m$ | 16.0 | 33.6 | 32.0 | 40.9 | 49.2 | 12.5 | 43.7 | 47.2 | 21.6 | 13.8 |

Specimens consisting of less than thirty layers failed in a brittle manner, whereas those with thirty or more layers started to fail with localised fractures in the pin region starting with the innermost layer. Substantial, clearly visible, damage was accumulated in the pin region before the final failure occurred. This experimental observation is also reflected by the increase of the Weibull moduli, $m$, given in Table 1. A considerable reduction of the capacity per tape was observed in specimens consisting of sixty and more layers. It suggests that failure of such straps is dominated by excessive through-thickness stress components.

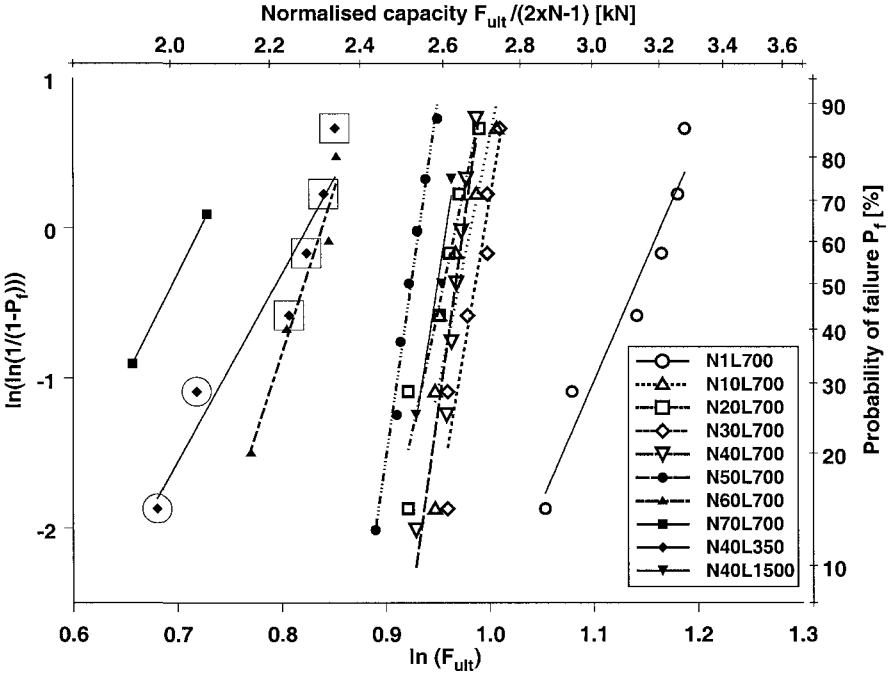



*Fig. 2 Weibull plots of load carrying capacities of non-laminated pin-loaded straps with different numbers of layers and lengths.*

Similarly, the short specimens ($L$ = 350) exhibited a considerable reduction of the load carrying capacity. This is attributed to an uneven strain distribution between individual layers because a reduced length requires increased relative displacement to attain an even strain distribution. The large variability in the set N40L350 indicates a difference in the tape qualities since the specimens marked in Figure 3 with large circles and square boxes are made from different production batches.

## DURABILITY OF NON-LAMINATED PIN LOADED STRAPS

Ongoing creep tests are being carried out on specimens consisting of five layers at 76 % of the average static load carrying capacity of such straps. Two test rigs are located in an air-conditioned laboratory with a constant temperature of 23 °C and 50 % relative humidity. Two different pin diameters ($D$ = 30 and 150 mm) are used since the through-thickness stress components are determined mainly by the pin diameter. It should therefore be possible to isolate different contributions to the overall creep deformation. The creep strain presented in

Figure 3 is monitored using mechanical dial gauges with a resolution of 0.01 mm. The gauges are attached to the cantilever beam of the test rig thus resulting in a magnification factor of 8.4 compared to the specimen extension. The creep strain is based on the extension of the specimen with an original distance of 209 mm between the pins. The initial elastic deformation is neglected to enhance resolution of the graph. The two horizontal lines represent the strain range derived from the gauge resolution. The length variations between two consecutive measurements is often within the resolution of the gauge. This may be a reason for the discontinuities in the graph in Figure 3.

A creep failure in the fusion bonded joint was observed in the specimen with the 150 mm diameter pins after about 400 days. The failure of the strap may have been a typical creep rupture type which appeared after primary, secondary and tertiary creep took place. The occurrence of a creep failure questioned the durability of the fusion bonded anchorage system of the final layer, although the circumstances were such that the result is not conclusive.

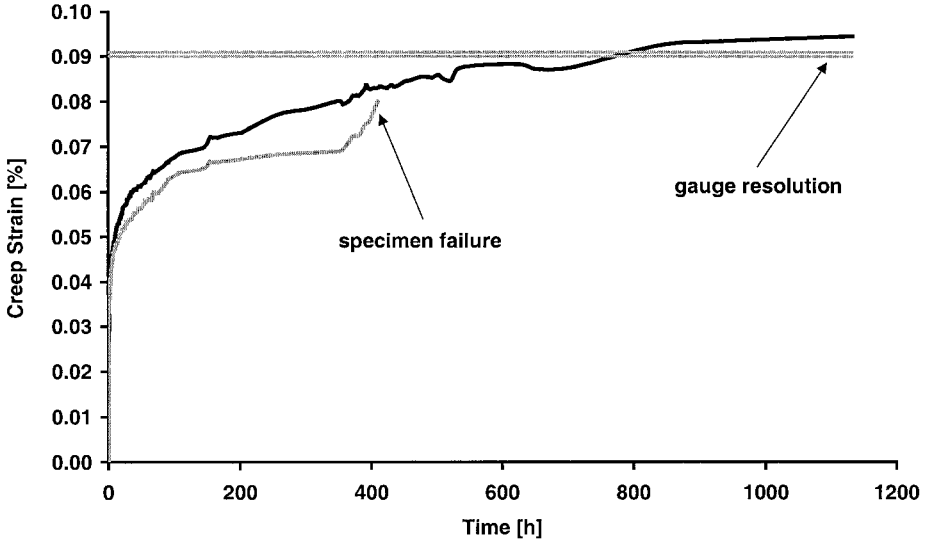



*Fig. 3 Creep strain based on the distance between the centres of the two pins.*

The welding technique for the anchorage of the final layer was improved as a consequence of these initial creep tests. Ongoing outdoor creep tests are being carried out on 500 mm long specimens consisting of twenty-seven layers using purposely made test rigs shown schematically in Figure 4. The specimens are loaded to about 90 % of the average static load carrying capacity of equivalent straps using concrete blocks fixed to the cantilever beams. The test rigs have been calibrated prior to the test fixing a load cell in between the pins instead of a strap specimen. The creep strain is not measured since no measurement system that would provide sufficient accuracy in outdoor conditions could be found Two specimens are being tested since fourteen months under these severe loading conditions without failure.

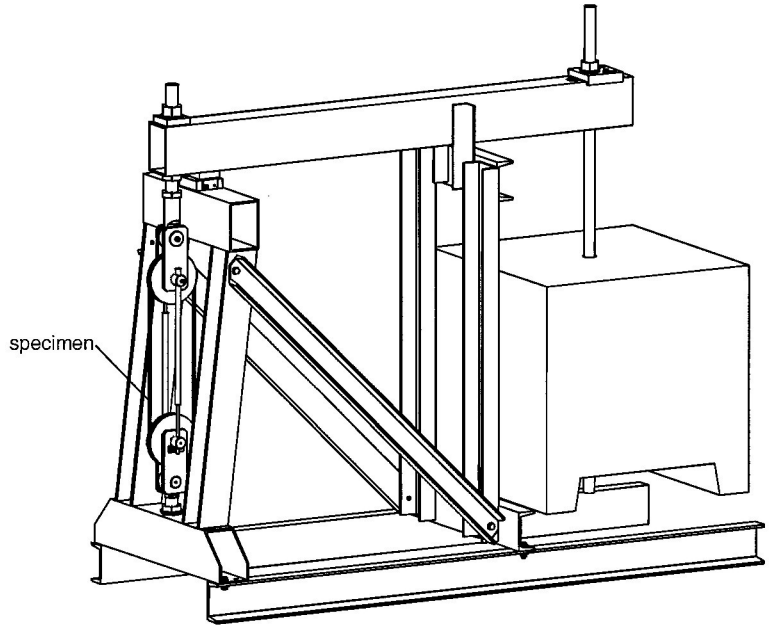



*Fig. 4 Creep test rig for outdoor weathering tests.*

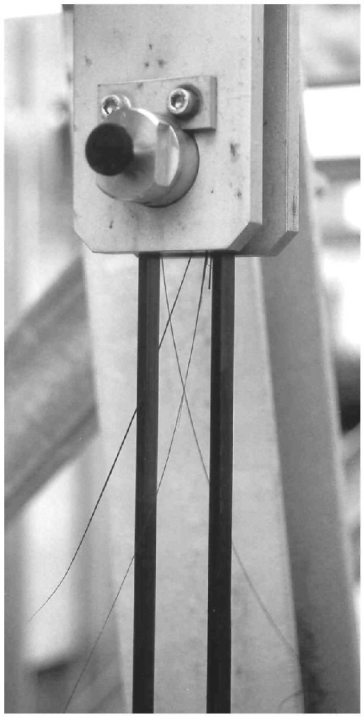


*Fig. 5 Damaged creep specimen.*

One of the two specimens under consideration exhibited some minor damage as shown in Figure 5 immediately after the initial loading. The amount of such delaminated fibre bundles has increased insignificantly. The photograph in Figure 5 was taken after about eight months under sustained loading. Consecutive photographs are taken from similar locations to monitor the accumulated damage. The damage after fourteen months is not considered to be critical compared to the level of damage observed in static short-term tests prior to failure.

There is no evidence of any damage in the second specimen. It is therefore assumed that the observed damage in the first specimen is not a long-term degradation of the tendon. It is attributed to inherent defects in the tape material. Such defects may have been introduced in the manufacturing process of the tape or in the wrapping procedure of the strap

## DISCUSSION AND CONCLUSIONS

The dramatic increase of the Weibull moduli presented in Table 1 compared to the values mentioned above for single fibres is attributed to the large number of filaments present in the composite and the ability of the matrix to transfer load into the fibres across the interface, thus resulting in load redistribution effects in the vicinity of cracks. The consequence is a much more reliable material than expected from tensile strength properties of single fibres.

Despite the only marginal increase of the strain with time in the creep test, the occurrence of a failure resulted in some concern about durability of the anchorage system for the final layer in non-laminated pin-loaded straps. Hence the outdoor creep tests were initiated under even higher loading conditions and furthermore, with the combination of climatic influences. The results obtained until the present time indicate that non-laminated pin-loaded straps are reliable and creep resistant tensile members which are very suitable for the shear enhancement of concrete.

Further investigations concerning durability are ongoing to develop the confidence needed for a broad acceptance of non-laminated pin-loaded straps and CFRP as a material for structural applications in general. Examples of such ongoing experiments are fatigue tests and further outdoor creep tests with eight additional test rigs.

## REFERENCES

[1] Dunker K. F. and Rabbat B. G., Why America's Bridges Are Crumbling, Scientific American, March 1993, pp. 18.

[2] Hamilton H. R., Breen J. E. and Al-Rashid N. I., Stay Cable Survey, Phil M. Ferguson Structural Engineering Laboratory, Department of Civil Engineering, Bureau of Engineering Research, The University of Texas at Austin, USA, February 15 1995.

[3] Clarke J., The need for durable reinforcement. in J. L. Clarke (Ed), Alternative Materials for the Reinforcement and Prestressing of Concrete, Blackie Academic and Professional, 1993, pp.1-33.

[4] Meier U., Brückensanierungen mit Hochleistungs-Faserverbund-Werkstoffen, Material und Technik, No. 4, 1987, pp. 125-128.

[5] Meier U., Repair Using Advanced Composites, in Composite Construction - Conventional and Innovative, Proceedings International IABSE Conference, Innsbruck, Austria, September 16-18 1997. pp. 113-124.

[6] Chajes M. J., Januszka T. F., Mertz D. R., Thomson T. A- and Finch W. W., RC Beams with Externally Applied Composite Fabrics, American Concrete Institute Structural Journal, Vol. 92 No. 3, May-June 1995, pp. 295-303.

[7] Hutchinson R., Abdelrahman A. and Rizkalla S., Shear Strengthening Using CFRP Sheets for a Prestressed Concrete Highway Bridge in Manitoba, Canada, in U. Meier and R. Betti (Eds), Recent Advances in Bridge Engineering, US-Canada-Europe Workshop on Bridge Engineering, Zürich, Switzerland, July 11-15 1997, pp. 99-106.

[8] Drimoussis E. and Cheng R., Shear Strengthening of Concrete Girders using Carbon Fiber Reinforced Plastic Sheets. Structural Engineering Report No. 205, University of Alberta, Canada, October 1994.

[9] Lees J. M.,Winistoerfer A. and Meier U., Non-laminated Pin-Loaded CFRP Straps for the Shear Enhancement of Concrete, Fiber Reinforced Polymer Reinforcement for Reinforced Concrete Structures. Dolan C. W., Rizkalla S. H. and Nanni A. (Ed.), ACI SP-188, Baltimore, 1999, pp. 985-993.

[10] Lees J. M.,Winistoerfer A. and Meier U., Behaviour of Concrete Beams Confined with Prestressed Carbon Fibre Reinforced Plastic Straps, Advanced Composite Materials in Bridges and Structures, ACMBS III, Ottawa, August 2000.

[11] Winistoerfer A., Development of non-laminated advanced composite straps for civil engineering applications, Ph.D. Thesis, University of Warwick, May 20 1999.

[12] Bauersfeld D. W., Composite graphite/epoxy tensile element, Report 2404, United States Army, Belvoir Research & Development Center, Fort Belvoir, Virginia 22060, USA, May 1984, pp. 1-62.

[13] Meier U. and Winistoerfer A., Multilayer Traction Element in the Form of a Loop, European Patent 0 815 329, January 7 1998.

[14] Hull D. and Clyne T. W., An introduction to composite materials, Second Edition, Cambridge solid state science series, Cambridge University Press, 1996.

[15] Sommer U., Kainer K. U., Böhm E. and Krüger G., Charakterisierung von Hochleistungsfasern für die Verstärkung von Metallmatrix-Verbundwerkstoffen, in Ziegler G. (Ed), Verbundwerkstoffe und Werkstoffverbunde, DGM Informationsgesellschaft 1996, pp. 375-378.

# T beams strengthened in shear with carbon sheet laminates (CFRP)

M. SALLES NETO, G. S. MELO and Y. NAGATO
Department of Civil and Environmental Engineering, University of Brasília, Brazil

## ABSTRACT

The shear resistance of eight "T" reinforced concrete simply supported beams, submitted to two top point loads using concrete strength of 30 MPa were investigated. Six of the beams were strengthened in shear with CFRP unidirectional layers, and the main variables investigated were the direction of the CFRP layer adopted, vertical (three beams) or inclined at $45^0$ (three beams), and the number and width of the layers. Four of the beams were loaded previously until service load before being strengthened. The beams were 4400 mm (overall length) x 400 mm (overall height) x 150 mm (web width), with 4000 mm clear span, 550 mm flange width and 100 mm flange thickness. The CFRP sheets in all strengthened beams went only up to the bottom of the slab, encapsulating the web of the beams. Results of ultimate loads, failure types, cracking, deflections, concrete and reinforcement strains are presented, together with comparisons with estimates by the laminates design method and by others authors.

Just before the ultimate load, below that was expected from the calculations, the CFRP laminates ends close to the flange were peeling off, being separated from the beams together with a thin layer of concrete, not allowing the laminates to be stretched up to failure. The ultimate loads of the reference beams (without strengthening), were better estimated by Zsutty formulations [1, 2]. In terms of stress reached at failure load (ultimate load $P_u$ divided by the applied carbon laminate area), the vertical strengthening for one layer of CFRP laminate was 32.9% more efficient than the inclined at $45^0$. The peeling off of the laminates was mainly due to insufficient anchorage at the beam and slab (flange) corner region. Unless special caution is taken a less efficient anchorage at this region should be expected anyway, as the roughening and cleaning of the substrate, and gluing of the laminates is much more difficult at the beam and slab (flange) corner region.

## TEST PROGRAMME

Tests were made on eight "T" reinforced concrete beams, simply supported, with 4400 mm (overall length); 4000 mm (clear span); 150 mm (width of the web); 400 mm (overall height); 550 mm (flange width) and 100 mm (flange thickness). The shear span was 1070 mm and the shear span / effective depth (*d*) was 3.01. Details of the beams are given in Table 1 and in Figures 1 to 3. All beams have the same flexural reinforcement, 3 bars of 20 mm ($f_y$ = 568 MPa; $f_r$ = 648 MPa; $\varepsilon_y$ = 4.71 $^o/_{oo}$) at the first layer and 3 bars of 16 mm ($f_y$ = 619 MPa; $f_r$ = 755 MPa; $\varepsilon_y$ = 5.00 $^o/_{oo}$) at the second. Beams 1 to 3 (type 1 reinforcement) did not have stirrups at the shear span and had seven 4.2 mm ($f_y$ = 773 MPa; $f_r$ = 812 MPa; $\varepsilon_y$ = 5.72 $^o/_{oo}$) stirrups between loads. Beams 4 to 8 (type 2 reinforcement) had nine 4.2 mm ($f_y$ = 568 MPa) stirrups

at each shear span and the same 7 (seven) 4.2 mm stirrups between loads. The anchorage of the longitudinal bars were assured by welded steel 12.5 mm thick plates, positioned outside the beam.

The strengthening arrangements of the beams are shown in Table 2. Beams 2, 3 and 5 to 8 were strengthened in shear with CFRP unidirectional layers, in the vertical direction (beams 2, 5 and 6), or 45° inclined directions (beams 3, 7 and 8). The strengthening of beams 2 and 3 was designed to increase in 40% the failure load of reference beam 1, without stirrups at the shear span, but keeping the shear failure, as the objective was to obtain the limit of the CFRP patch used. Strengthening of beams 5 (vertical) and 7 (45° inclined) were designed to increase in 20% the failure load of reference beam 4 while the strengthening of beams 6 (vertical) and 8 (45° inclined) was designed to increase in 40% the failure load of the reference beam 4, but also keeping shear failure. Design computations were based on assuming that shear failure should be combined with the CFRP rupture for all strengthened beams (2, 3 and 5 to 8).

Table 1– Test programme

| Beam | Reinf. Type | Pre-cracked | Strengthening |
|---|---|---|---|
| 1 | 1 | No | Reference beam (type 1 reinforcement), no strengthening |
| 2 | 1 | No | Strengthening with CFRP vertical strips |
| 3 | 1 | No | Strengthening with CFRP 45° inclined strips |
| 4 | 2 | No | Reference beam (type 2 reinforcement), no strengthening |
| 5 | 2 | Yes | Strengthening with 5 (five) CFRP vertical strips |
| 6 | 2 | Yes | Strengthening with 6 (six) two layers CFRP vertical strips |
| 7 | 2 | Yes | Strengthening with 4 (four) CFRP 45° inclined strips |
| 8 | 2 | Yes | Strengthening with 5 (five) CFRP 45° inclined strips |

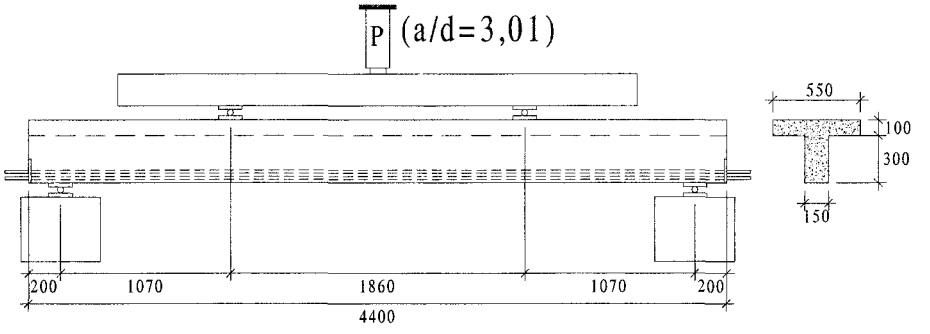



Figure 1 – Experimental setup (dimensions in mm)

The investigation was basically done in four steps: Beam 4 (reinforcement type 2 reference) was tested until rupture (1st step). It was adopted after this first test that 200 kN (about 50% of the ultimate load) was the load that beams 5 to 8 would be loaded before being strengthened. At this stage the shear crack widths of beam 4 was 0.3 mm and the strain at the stressed stirrup was 2.4‰. Beams 5 to 8 were then tested up to 200 kN, when they were unloaded (2nd step). Beams 2, 3 and 5 to 8 were then strengthened (3rd step). These beams and beam 1 (reinforcement type 1 reference) were then tested up to failure (4th step). Figure 4

show the loading arrangements for testing the beams and rupture of beam 4. Loading was applied in steps, and at the end of which readings were taken. The behaviour of the beams tested was analysed through the strains of the shear and flexural reinforcement, and of the concrete, the vertical and horizontal deflections, the developing and widths of the cracks, and by the ultimate load and mechanism of rupture.

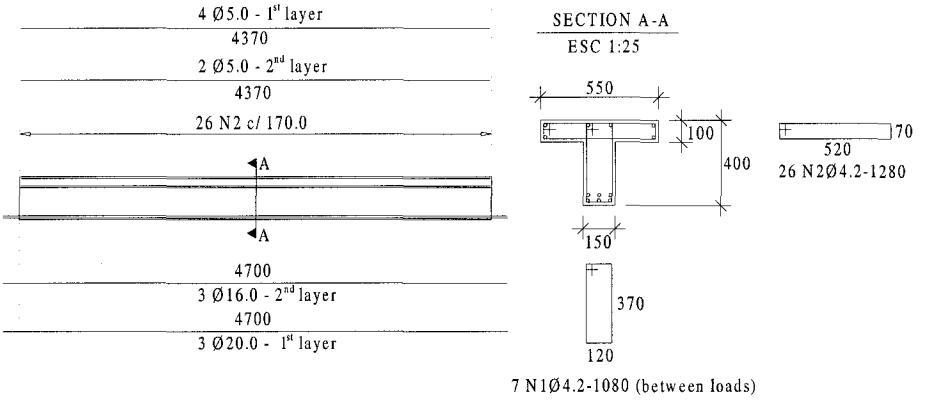



Figure 2 – Detailing of beams 1, 2 and 3 – "Type 1" (dimensions in mm)

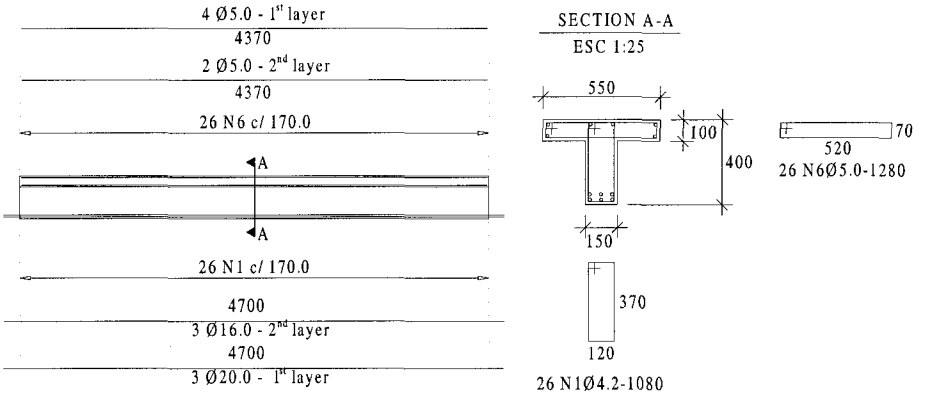
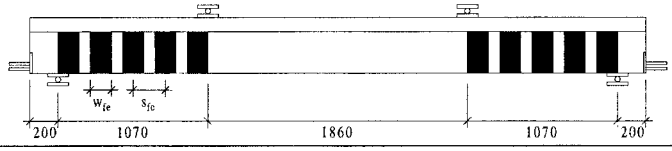
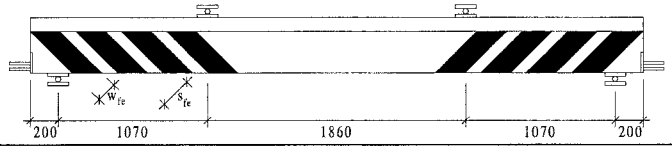
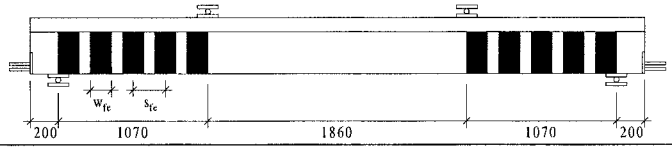
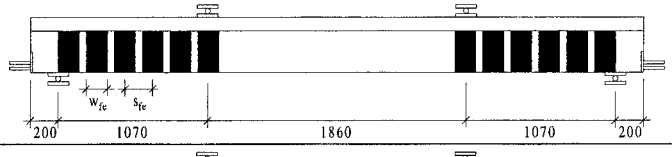
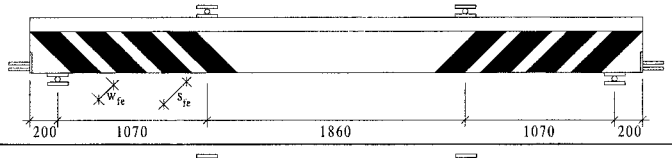
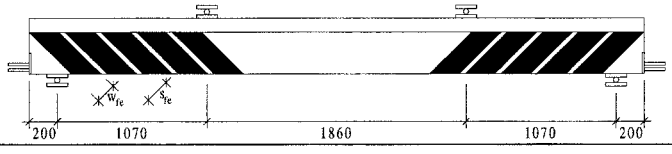



Figure 3 – Detailing of beams 4, 5, 6, 7 and 8 – "Type 2" (dimensions in mm)

Table 3 presents, for each beam, the strengthening adopted, the strength of the concrete, the estimated flexural ultimate load ($P_{flex}$), the shear ultimate load ($P_{shear}$), according to Zsutty [1, 2] for beams 1 and 4 (without strengthening), and according to the design method for the strengthened beams (2, 3, 5 to 8), and the experimental ultimate load ($P_u$). All beams failed in shear. The beams without strengthening (1 and 4) failed at loads respectively 59% and 47.8% higher than the estimated ones.

Table 2 – Strengthening arrangements – Beams 2, 3 and 5 to 8

| Beam | Strengthening Arrangements | |
|---|---|---|
| 2 |  | $w_{fe}$ = 150 mm<br>$s_{fe}$ = 230 mm<br>1 layer |
| 3 |  | $w_{fe}$ = 150 mm<br>$s_{fe}$ = 230 mm<br>1 layer / 45° |
| 5 |  | $w_{fe}$ = 150 mm<br>$s_{fe}$ = 230 mm<br>1 layer |
| 6 |  | $w_{fe}$ = 150 mm<br>$s_{fe}$ = 200 mm<br>2 layers |
| 7 |  | $w_{fe}$ = 150 mm<br>$s_{fe}$ = 230 mm<br>1 layer / 45° |
| 8 |  | $w_{fe}$ = 150 mm<br>$s_{fe}$ = 180 mm<br>1 layer / 45° |

All strengthened beams failed at loads below that was expected, due to peeling off of the CFRP laminates ends close to the flange, being separated from the beams together with a thin layer of concrete, and then not allowing the laminates to be stretched up to failure. Ultimate loads were from 17.1% (beam 5) to 31.3% (beam 8) below estimated (average of 24.3%). The vertical strengthening was a little more efficient, reaching a load average of 22% below estimated, while the inclined reached a load average 26.6% below estimated. There was practically no difference in efficiency between the beams with (5 to 8 - 25.5% below), and without (2 and 3 - 21.9%) original stirrups. Beam 6, with two layers of laminates was a little less efficient (29.2% below estimated) than the others with one layer of laminate (23.3% below estimated).

Figures 5 and 6 show Load vs. Flexural reinforcement strain curves, respectively for beams 1 and 8. Beam 1, without shear reinforcement in the shear span show close to rupture almost an arch type behaviour as the strains along the flexural reinforcement is almost the same. In

beam 8 strains are much bigger at the central point, as the shear reinforcement, stirrups and CFRP laminates worked together, and it assumed more a beam type behaviour.

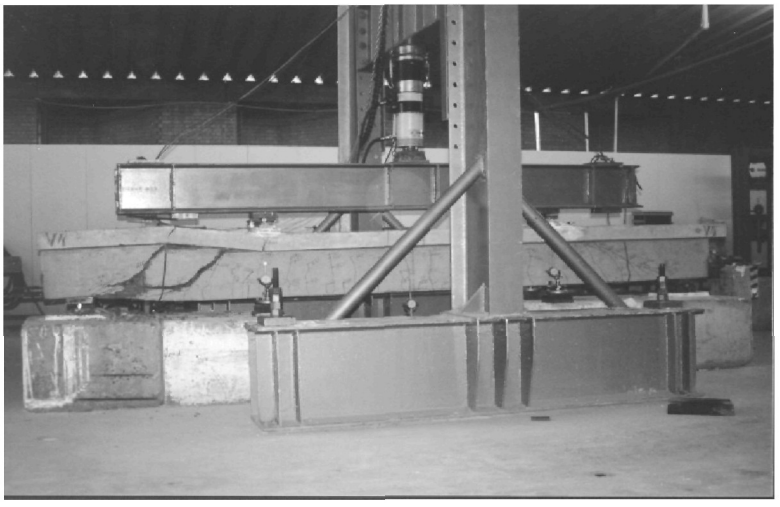


Figure 4 – Rupture of beam 4 and loading arrangements

Table 3 – Shear ultimate load, estimated and obtained experimentally

| Beam | Streng-thening | $f_c'$ (MPa) | $f_t$ (MPa) | Pflex (estimated) (kN) | Pshear (estimated) (kN) | Pu (test) (kN) | Pu / Pshear |
|---|---|---|---|---|---|---|---|
| 1 | ---- | 31,0 | 3,7 | 543 | 158 (z) | 251,0 | 1.591 |
| 2 | 5V1L | 44,6 | 3,5 | 558 | 343 | 275,6 | 0.803 |
| 3 | 4I1L | 44,6 | 3,5 | 558 | 422 | 320,5 | 0.759 |
| 4 | ---- | 31,0 | 3,7 | 543 | 249 (z) | 368,4 | 1.478 |
| 5 | 5V1L | 40,0 | 4,0 | 554 | 486 | 403,0 | 0.829 |
| 6 | 6V2L | 40,0 | 4,0 | 554 | 569 | 402,8 | 0.708 |
| 7 | 4I1L | 40,0 | 4,0 | 554 | 532 | 402,6 | 0.757 |
| 8 | 5I1L | 40,0 | 4,0 | 554 | 575 | 395,3 | 0.687 |

z – according to Zsutty estimations [1, 2]

The load versus shear reinforcement strains of beam 5 are shown in Figure 7. Steel (S1A/S1B, S2A/S2B and S3A/S3B) and CFRP laminates (C1 and C2) strains are shown in the graph. It can be seen that one of the CFRP laminates strain gauges registered maximum strain of 3.5 $^{o}/_{oo}$
at failure (C2) while the other (C1) practically did not register big variation in strains, apart from at the ultimate load. The steel strain gauges data show that two of the monitored stirrups yielded (S1 and S3).
Figure 8 show curves Load versus Displacements at middle of the span for beams 4, 5, 6, 7 and 8. It can be seen that from about 225 kN the beams strengthened with CFRP laminates

behaved a bit more stiff, with beam 6 (six two layers vertical strengthening) presenting lesser displacements until failure.

Figures 9 to 12 show details of the peeling off of CFRP laminates of beams 5 to 8 after rupture. In Figure 9 (beam 5) can be seen the main shear failure crack, and the third and the fourth strip from the middle of the beam separated from the beam. In this case there was not so much concrete glued to the laminate. In the case of beam 6 (Figure 10) can be seen that quite a lot of concrete was glued to the fourth strip from the middle of the beam, the fifth strip was easily taken off of the beam with the same quantity of concrete. It can also be seen the more smeared failure cracks for this beam, and two broken stirrups. For beam 7 (Figure 11) it can be seen the main failure crack across the beam flange, the "bend" it does to "avoid" the top of the second strip from the middle of the beam, the peeling off of the CFRP third laminate strip, a broken stirrup and the last CFRP laminate strip tore up at the bottom of the beam. In Figure 12 can be seen that the third and the fourth CFRP laminate strip from the middle of beam 8 peeled off of the beam with some concrete glued to it either. In this case also the main shear failure crack ran horizontally at the flange for some time, "avoiding" the second strip and going across the third and fourth.

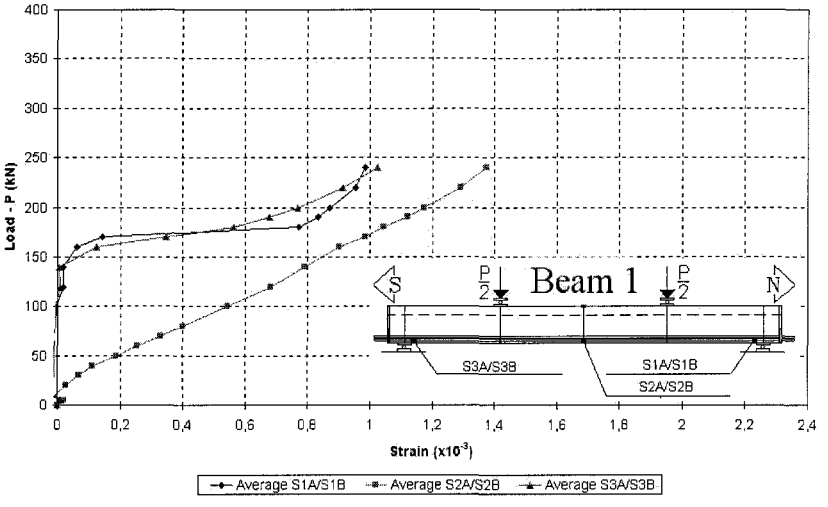



Figure 5 – Load versus strain – Flexural reinforcement - Beam 1

## CONCLUSIONS

The ultimate loads of the reference beams (without strengthening), were better estimated by Zsutty formulations [1, 2]. Beam 1, without shear reinforcement in the shear span, reached an ultimate load 59% higher than estimated, while beam 4, with shear reinforcement in the shear span, reached an ultimate load 48% higher than estimated.

The beams tested presented a brittle behaviour, typical of shear failure, and the limiting factor was the end anchorage of the CFRP laminates close to the ultimate load. Just before the ultimate load, below that was expected, the laminate ends close to the flange were peeling off, being separated from the beams together with a thin layer of concrete, not allowing the laminates to be stretched up to failure.

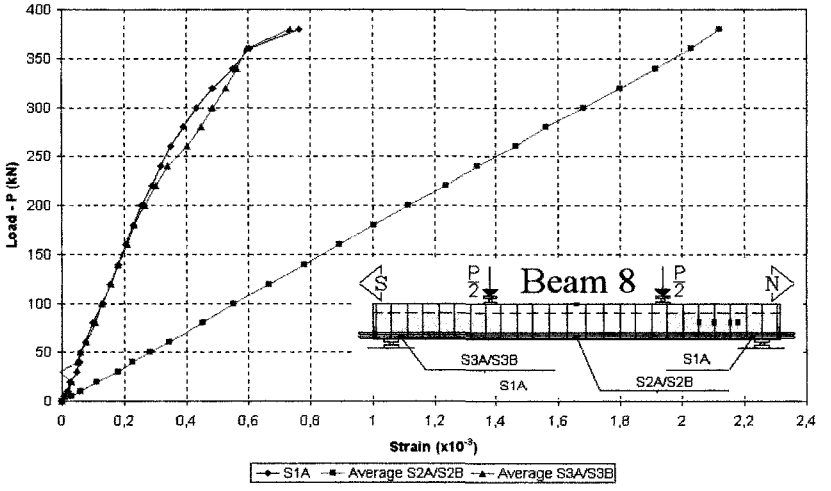



Figure 6 – Load versus strain – Flexural reinforcement - Beam 8

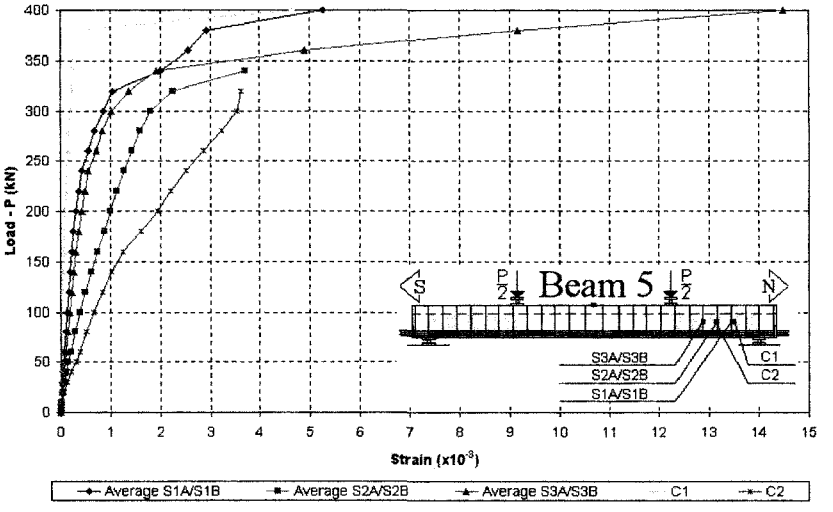



Figure 7 – Load versus strain – Shear reinforcement - Beam 5

It was not possible to verify the precision of the CFRP laminates strengthening design methods because of the anchorage premature failure of the strengthened tested beams. The vertical strengthening layout of CFRP laminates was just a little more effective than the inclined at $45^0$. The vertical (beams 2, 5 and 6) reached in average 78% of the expected load while the inclined at $45^0$ reached in average 73.4% of the expected load. The execution of the laminates at $45^0$ is more laborious and need more material than the vertical one, also due to the splicing needed at the bottom and the side of the beam corner.

In terms of stress reached at failure load (ultimate experimental load $P_u$ divided by the applied carbon laminate area), the vertical strengthening for one layer of CFRP laminate was 32.9% more efficient than the inclined at $45^0$ (beams 2 and 5 in relation of beams 3, 7 and 8).
The peeling off of the laminates strips were mainly due to insufficient anchorage at the beam and slab (flange) corner region. Unless special caution is taken a less efficient anchorage at this region should be expected anyway, as the roughening and cleaning of the substrate, and gluing of the laminates is much more difficult.

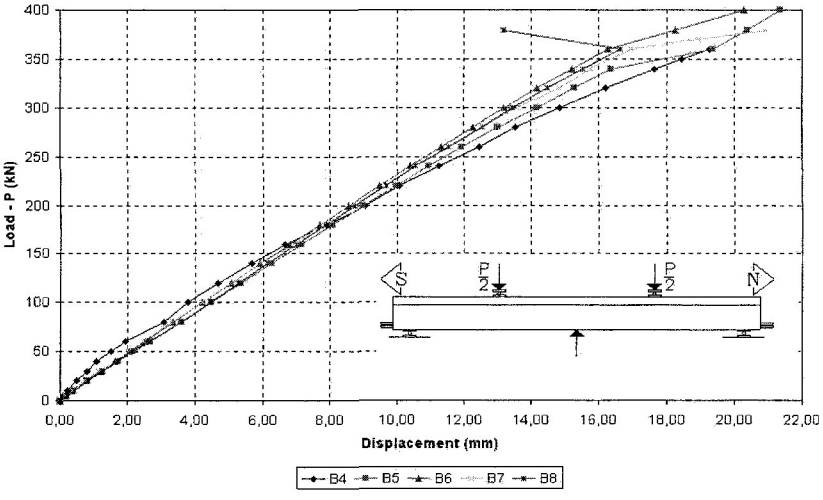



Figure 8 – Load versus Displacements – Middle of span – Beams 4, 5, 6, 7 and 8



Figure 9 – Peeling off of CFRP laminate – Beam 5

The tests reported in this paper were part of the M.Sc. Thesis of the first [3] author under the supervision of the others two authors. A second series of eight "T" beams of the same size and basically the same CFRP strengthening is being tested [4], aimed to prevent the peeling off anchorage failure of the laminate. In half of the strengthened beams the suggestions by Khalifa and others [5,6] were followed, as shown in Figure 13, and for the remaining beams the CFRP sheets enveloped all the web and flange trough holes drilled in the flanges.




Figure 10 – Peeling off of CFRP laminate – Beam 6




Figure 11 – Peeling off of CFRP laminate and rupture of beam 7



Figure 12 – Peeling off of CFRP laminate - Beam 8

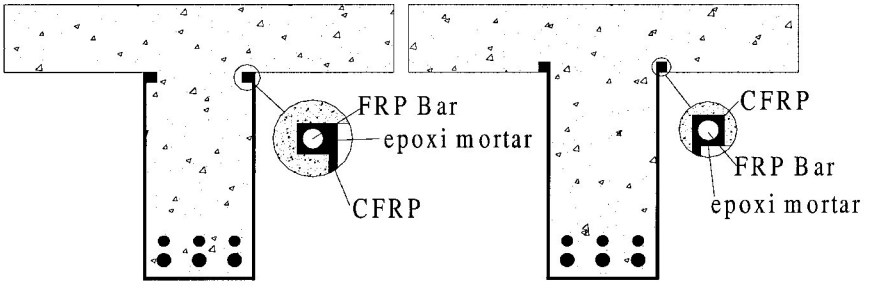



Figure 13 – Suggestion of improved anchorage by Khalifa and others [5,6]

**REFERENCES**

1. ZSUTTY, T. C., "Beam shear strength prediction by analysis of existing data". American Concrete Institute Structural Journal, Vol. 65 No 8, November, 1968.
2. ZSUTTY, T. C., "Shear strength prediction for separate categories of simple beam tests". American Concrete Institute Structural Journal, Vol. 68 No 2, February, 1971.
3. SALLES NETO, M., "Behaviour of "T" beams strengthened in shear with carbon sheet laminates (CFRP)", M.Sc. Thesis, Department of Civil and Environmental Engineering, University of Brasília, 2000 (in portuguese)
4. NERES J., "Additional tests in "T" beams strengthened in shear with CFRP laminates", M.Sc. Thesis, Depart. of Civil and Environ. Engin., University Brasília, 2001 (in portug.)
5. KHALIFA, A.; ALKHRDAJI, T. NANNI, A.; LANSBURG, S., "Anchorage of surface mounted FRP reinforcement". Concrete International / October 1999, p. 49-54.
6. KHALIFA, A.; TUMIALAN, G.; NANNI, A.; BELARBI, A., "Shear strengthening of continuous reinforced concrete beams using externally bonded carbon fiber reinforced polymer sheets". Fiber Reinforced Polymer Reinforcement for Reinforced Concrete Structures – Fourth Internat. Symposium, ACI International SP 188, 1999, p. 995-1008.

# Shear Strengthening of Dapped Beams Using FRP Systems

KIANG HWEE TAN, National University of Singapore, Singapore

## ABSTRACT

Dapped beams are commonly used in precast building construction and road bridges. In this study, several schemes for the strengthening of dapped beams in shear to cater for increased imposed loads were investigated. In all, seven single-load tests using four 2.25 metre long beams were carried out. One beam was un-strengthened while the other three beams were strengthened with carbon FRP plates (CP), carbon fibre sheets (CS), or glass fibre fabrics (GS). For each of the strengthened beams, the FRP system was installed with different anchorage systems on two ends. After failing the beam on the weaker side, the failed section was enlarged with additional reinforcement and the beam was re-tested to evaluate the effectiveness of the FRP system at the other end. Results indicated an increase in ultimate load of 43, 75 and 80 percent for the CP, CS and GS systems respectively. The use of an anchorage bolt in the CP system at the critical location further enhanced the strength by 16 percent, while the use of bonded transverse fabric led to further strength increase of 33 and 41 percent respectively for the CS and GS systems respectively. A strut-and-tie model is found suitable for the evaluation of the increased shear capacity due to the FRP system.

## INTRODUCTION

Dapped ends or half-joints are commonly used in precast building construction and bridge construction, by which simple-span beams are supported on ledger beams, columns or piers. There are five potential failure modes at the dapped ends due to (a) flexure (cantilever bending) and axial tension in the extended end; (b) direct shear at the junction between the dapped and the undapped portions of the member; (c) diagonal tension emanating from the re-entrant corner; (d) diagonal tension in the extended end; and (e) diagonal tension in the undapped portion. The Precast/Prestressed Concrete Institute (PCI 1999) provides guidelines on the design of reinforcement to avert such failures. Huang et al. (2000) have investigated two basic strengthening schemes based on PCI guidelines and concluded that externally bonded FRP strengthening systems provide a viable solution for the retrofit of dapped beams.

The strengthening of dapped beams in bridges and buildings may arise due to design faults, changes in usage or increase in design loads, and deterioration of structures, and the use of strut-and-tie models in the design of externally bonded FRP systems in such strengthening works forms the objective of study in this paper.

For this purpose, a test programme on simply supported dapped beams under mid-span loading, strengthened with three types of externally bonded FRP systems in six different configurations, was carried out. The effect of anchors was examined and strut-and-tie models were proposed to evaluate the load-carrying capacity of the strengthened beams.

*FRPRCS-5*, Thomas Telford, London, 2001.

## STRUT-AND-TIE MODELS

The proposed model for dapped beams, consisting the superposition of two sub-models shown in Figures 1(a) and (b), is shown in Figure 1(c). In the model, the concrete forms the strut members while the reinforcement forms the tie members, and these are connected at the nodes. All reinforcements are assumed fully anchored so that there is no bond-slip failure.

For a given load on the beam, the forces in the strut and tie members can be calculated from statics by considering equilibrium of forces at the nodes. The required width of each strut is obtained by considering an effective compressive strength for the concrete, typically between 0.3 to 0.5 times the cube compressive strength (MacGregor, 1997). Such a width should be made available in the member; otherwise, compressive reinforcement would be needed as supplement. The required reinforcement at the location of tie members is obtained by assuming the reinforcement to be at their design (yield) strength.

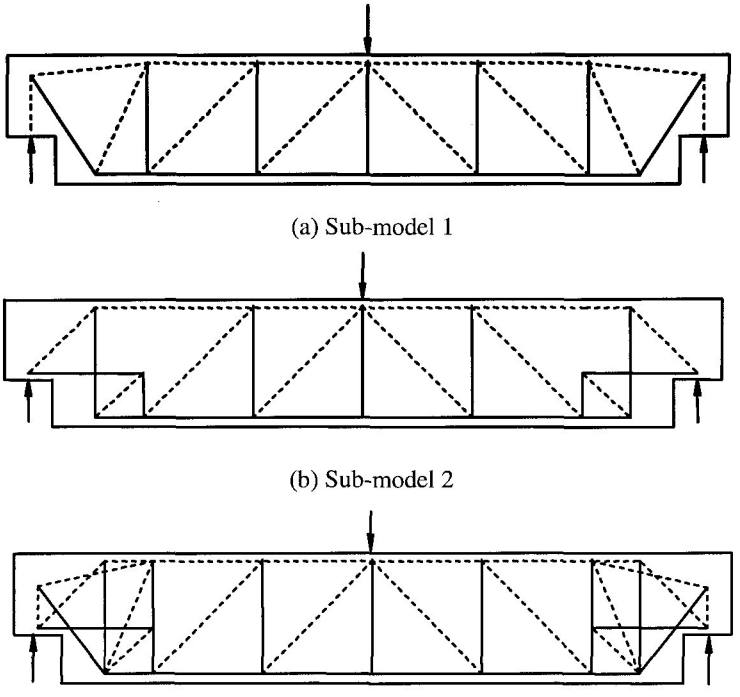
The models could be applied readily to externally bonded FRP reinforcement. Figure 2 shows the way by which diagonal and vertical FRP plates and fabrics/sheets are replaced by tie members. The required area of FRP reinforcement to carry an additional load is obtained by dividing the induced force by an effective tensile strength of the reinforcement.

## TEST PROGRAMME

Four dapped T-beams with the same dimensions and internal steel reinforcement were prepared (see Figure 3). As the focus was on the shear strengthening of the dapped ends, these beams were over-reinforced in flexure and provided with additional stirrups (closed links) at the middle length. The concrete mix proportion was 1 : 2 : 4 : 0.8 by weight of ordinary Portland Cement, natural river sand, 10 mm crushed granite and water.

One beam served as unstrengthened (control) beam (designated TB0) and three others were bonded externally with three different FRP systems using carbon FRP plates (CP1), glass fibre fabrics (GS1) and carbon fibre sheets (CS1). The CFRP plates were 50 mm in width and 1.2 mm in thickness. They were bonded onto the concrete surface using an epoxy mortar and further anchored down at intersections using 9 mm diameter, 40 mm long metal bolts with a square washer (50mm x 50mm) made of carbon FRP plates acting as a cushion. The glass and carbon fibre sheets were 320 mm width for the vertical ply, and 220 mm for the diagonal ply. They were bonded to the concrete surface using epoxy resins and further anchored down with 6 mm diameter, 50 mm long fibre bolts at the top of the beam just below the flange at a spacing of 100mm. The glass FRP fabric has a laminated thickness of 1 mm while the carbon fibre sheet had a thickness of 0.11 mm. The material properties of the FRP systems are shown in Table 1.

For each strengthened beam, the FRP system was installed with different anchorage systems on two ends (see Figure 4). In beam CP1, a through-hole bolt was installed on one end to further anchor the FRP plates at the dapped section. For beams GS1 and CS1, a horizontal 175 mm wide U-strip was bonded on one end to confine the FRP sheets beneath. After failing the beam on the weaker end, the failed end was strengthened by enlarging the web section using cement grout by 60 mm on three sides with additional longitudinal steel reinforcement and vertical stirrups going through and anchored in the flanges, topped with galvanized welded mesh of 1.22 mm wire diameter and 12.5mm square mesh. The beam was then re-tested to failure on the other end. The re-tested beams were designated CP1-R, GS1-R and CS1-R respectively.



(a) Sub-model 1

(b) Sub-model 2

(c) Combined model

Figure 1. Strut-and-tie model

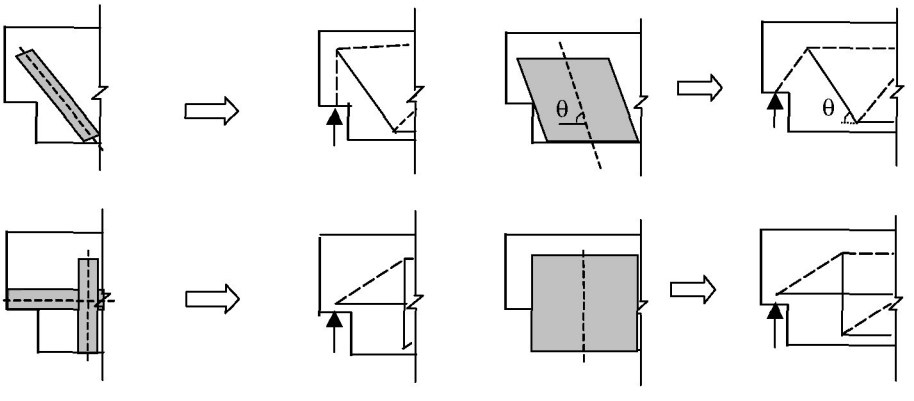



Figure 2. Modelling for FRP reinforcement.

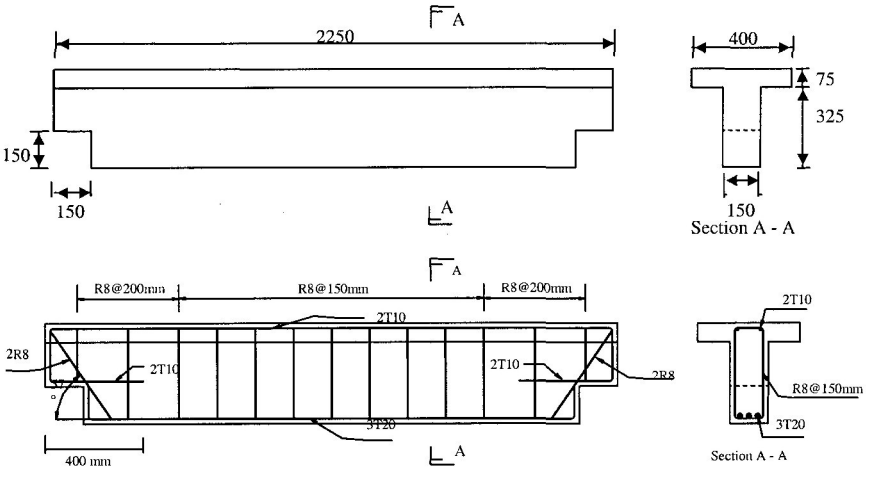



Figure 3. Internal steel reinforcement in test beams (all dimensions in mm)

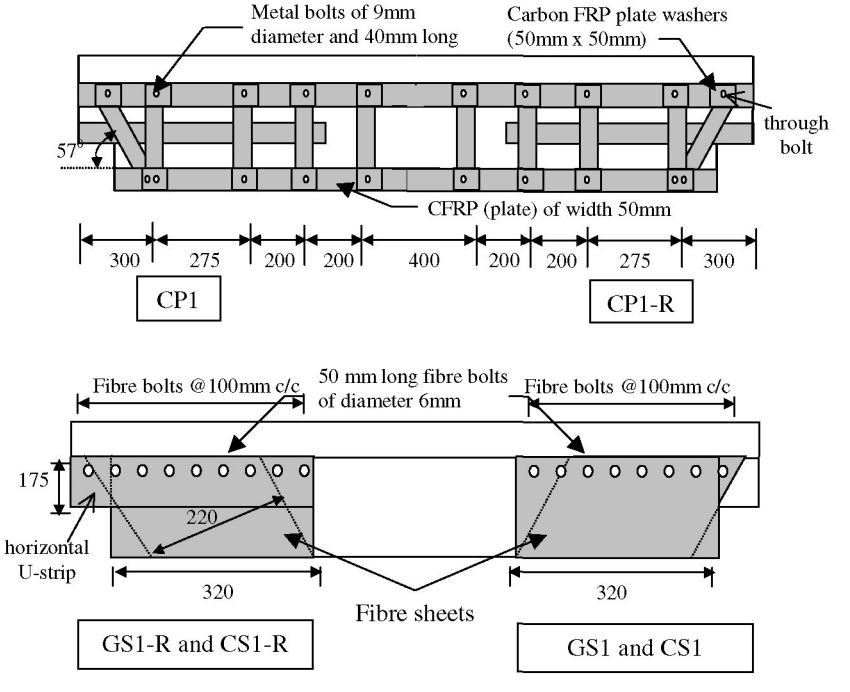



Figure 4. Test beams bonded with FRP systems (all dimensions in mm)

All beams were simply supported at the dapped ends over a span of 2.1 m and tested to failure under a single load at mid-span, as shown in Figure 5. The strains in the internal reinforcement, external FRP reinforcement and concrete surface were monitored using electrical resistance strain gauges. Deflections at mid-span were measured using linear variable displacement transducers. Crack widths were measured using a hand-held microscope with a resolution of 0.02 mm.

## FAILURE CHARACTERISTICS AND ULTIMATE STRENGTH

Control beam TB0 failed in shear at a load of 145kN with diagonal cracks propagating from the re-entrant corner to the flange [see Figure 5]. Beam CP1 failed in shear with detachment of the horizontal CFRP plate at the dapped ends at a load of 207 kN. A "bang" was heard and a slight drop in load and large increase in deflection was observed. Diagonal cracks widened and propagated upward till they reached the top of the flange, with the metal bolt pulled out from the concrete surface. The external CFRP plate resulted in an increase of 42.8% in ultimate strength over the un-strengthened beam TB0.

In beam GS1, the glass fibre fabric first de-bonded from the concrete surface near the bottom of the dapped end at a load of 250 kN. At the ultimate load of 261 kN, that is 80% more than the ultimate strength of beam TB0, the top edge of the diagonal sheet also detached from the concrete and diagonal cracks were seen propagating into the flange. For beam CS1, the carbon fibre sheet first detached at the location of the fibre bolts in the dapped end. The beam failed under a load of 253 kN or 74.5% more than for the control beam, with diagonal cracks propagating into the flange where the concrete crushed. There was a large sudden drop in load and large increase in deflection. Rupture of carbon fibre sheet was observed around the fibre bolts near the dapped end.

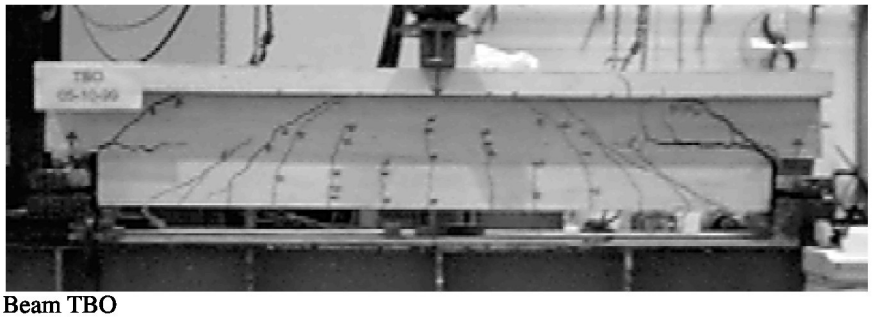
The failure characteristics of beam CP1-R was similar to that of beam CP1 with diagonal cracks propagating to the flange at an ultimate load of 240 kN, or an increase of 15.9% in strength compared to CP1. The CFRP plate was split into two at the location of the through bolt. Beam GS1-R failed in shear at a load of 369 kN or 41.4% more than beam GS1. The beam failed with diagonal cracks that appeared in the un-bonded region and propagated to the flange. Beam CS1-R failed at a load of 338kN, an increase of 33.6% over that of beam CS1. Like beam CS1, beam CS1-R failed with diagonal cracks propagating to the flange; in addition, rupture of the carbon fibre sheet was observed at the bottom of the web.

The test results showed that beams wrapped with glass or carbon fibre sheets exhibited higher ultimate loads than those bonded with CFRP plates. However, due to the rupture of the sheets, beams bonded with carbon fibre sheets tend to fail suddenly. On the other hand, beams bonded externally with CFRP plates were found to carry the ultimate load with rapidly increasing deflection. The additional through bolt in CP1-R and horizontal strip in beams GS1-R and CS1-R were effective in confining the FRP reinforcement.

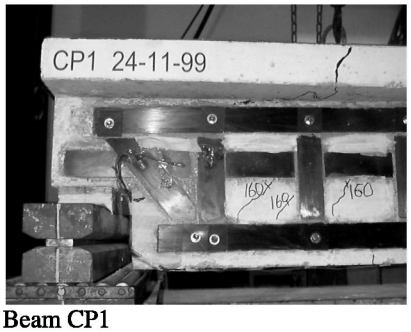
## DEFLECTION AND CRACKING CHARACTERISTICS

The load-deflection curves of all beams are shown in Figure 6. Beams bonded externally with FRP reinforcement are stiffer than the control beam. The additional anchoring elements further enhance the beam stiffness. All beams failed in a ductile manner.

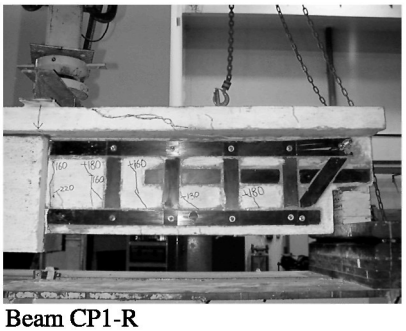
In all beams, cracks first appeared as vertical flexural cracks. As the load was increased, diagonal cracks started to appear at the re-entrant corner at the dapped end. Horizontal cracks



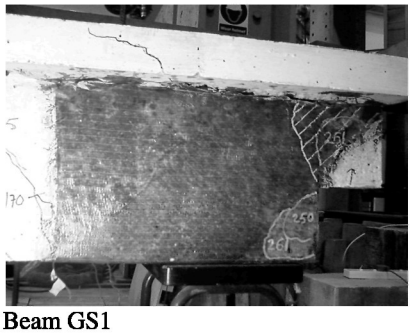

Beam TBO




Beam CP1



Beam CP1-R



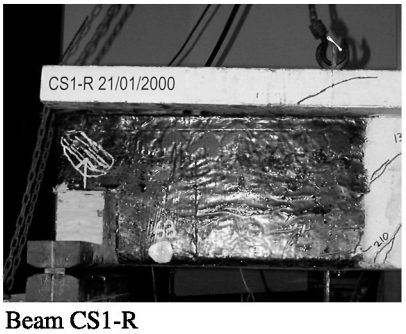
Beam GS1




Beam GS1-R




Beam CS1




Beam CS1-R

Figure 5. Appearance of test beams at failure

were also observed to emerge from the re-entrant corner in beam TB0, probably due to insufficient development length and hence slippage of the internal longitudinal reinforcement.

The loads at first flexural and diagonal cracking were higher for all strengthened beams than for the un-strengthened beam TB0. The delay was more significant in diagonal cracking than in flexural cracking, due to the externally bonded FRP reinforcement at the dapped ends. Beam CP1 had the highest flexural cracking load and smaller crack widths due to the horizontal FRP plates provided at the bottom of the web.

The development of flexural crack widths in beams TB0, CP1, GS1 and CS1 are shown in Figure 8(a) and of diagonal cracks widths in TB0 and CP1 in Figure 8(b). Except for beam GS1, the maximum crack widths were substantially reduced due to the FRP systems.

## STRAINS IN REINFORCEMENT

The internal diagonal steel bars in all beams except CP1 and the horizontal bars in the dapped ends in beams TB0 and CS1 yielded at incipient failure. For the same beam, the diagonal bars yielded at a lower load than the horizontal bars.

The average strain in the FRP reinforcement at incipient failure varied with orientation of the fibres. For the beam bonded with CFRP plates, strains of up to 0.24% were recorded in the diagonal plates whereas the strains in the vertical and horizontal plates next to the re-entrant corner were minimal. For beams bonded with fibre sheets or fabrics, the strains were about 0.15% to 0.18% in both the diagonal and vertical plies when the horizontal U-strip was not provided (that is, in beam GS1 and CS1) and they exceeded 0.4% when the U-strip was provided (in beams GS1-R and CS1-R).

## EFFECTIVENESS OF FRP REINFORCEMENT

Since the strains in the FRP reinforcement are in general lower than its ultimate tensile strain, $\varepsilon_{pu}$, an effectiveness factor to quantify the contribution of FRP reinforcement to load carrying capacity may be determined as $\alpha = \varepsilon_{fs}/\varepsilon_{pu}$ where $\varepsilon_{fs}$ is the observed strains in FRP reinforcement at incipient failure. The values of $\alpha$ for the FRP reinforcement are tabulated in Table 2.

Using the proposed strut-and-tie model shown in Figure 1, the ultimate strength of the beam can be predicted. In sub-model 1, the diagonal tie member is assumed to govern the load-carrying capacity of the truss. In sub-model 2, either the horizontal or the vertical tie member near the dapped end is assumed to govern, depending on which member result in a smaller load. Other strut and tie members are assumed to have the capacity to resist the force acting on them.

The calculation for the ultimate strength is carried out in two parts. The first determines the load carried by the internal steel reinforcement, and the second determines the load taken by the external FRP reinforcement. The contributions are then added together. The predictions are based on observed strains in the reinforcement.

Table 2 compares the predicted loads with the observed ultimate load of each beam. The predictions are close to the observed values, and the ratio of test to predicted ultimate loads has a mean of 1.06 with a coefficient of variation of 0.09. Further works however are

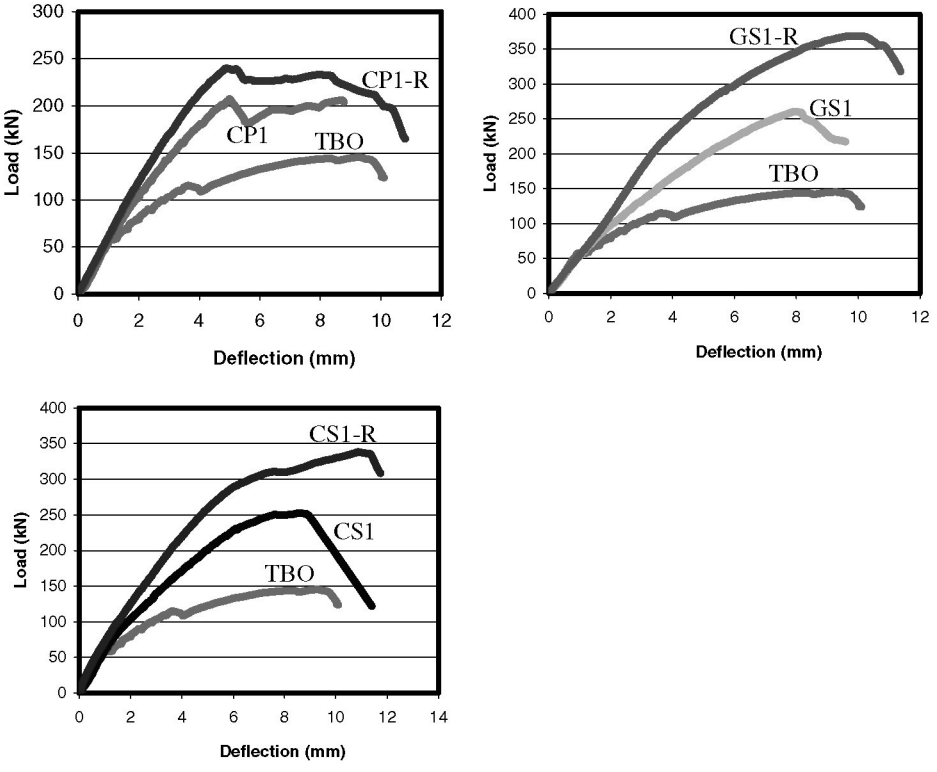



Figure 6. Load-deflection characteristics

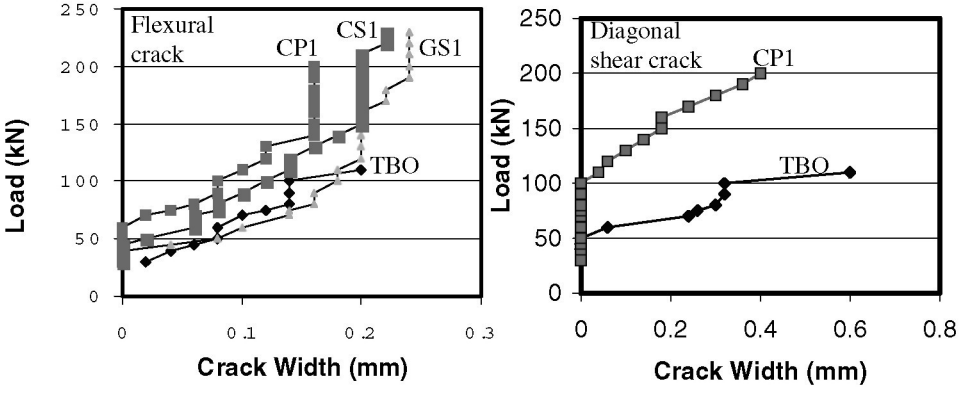



Figure 7. Maximum crack widths

Table 1. Properties of FRP systems

| | CP System | | GS System | | CS System | |
|---|---|---|---|---|---|---|
| | Plate | Epoxy mortar | Laminate | Epoxy Resin | Sheet | Epoxy Resin |
| Tensile strength (MPa) | 2400 | 24.8 | 600 | 72.4 | 3400 | 29.4 |
| Modulus of elasticity (GPa) | 150 | 4.5 | 26 | 3.2 | 230 | n.a. |
| Elongation at Break (%) | 1.4 | 1.0 | 2.2 | 4.8 | 1.5 | n.a. |
| Bond strength on concrete (MPa) | - | > 2 | - | n.a. | - | > 1.5 |

n.a. – not available

Table 2. Test results

| | $f_{cu}$ (MPa) | $P_u$ (kN) | % inc. over TB0 | % inc. due to anchor | Effectiveness factor, $\varepsilon_{fs}/\varepsilon_{pu}$ | | | $P_{u,pred}$ | $P_{u,test}/P_{u,pred}$ |
|---|---|---|---|---|---|---|---|---|---|
| | | | | | Diag. | Vert. | Hori. | | |
| Tb0 | 22.7 | 145 | n.a. | n.a. | n.a. | n.a. | n.a. | 148 | 0.99 |
| CP1 | 20.1 | 207 | 42.8 | n.a. | 0.156 | 0.043 | 0.055 | 195 | 1.06 |
| GS1 | 23.9 | 261 | 80.0 | n.a. | 0.062 | 0.071 | n.a. | 226 | 1.06 |
| CS1 | 21.8 | 253 | 74.5 | n.a. | 0.095 | 0.120 | n.a. | 243 | 0.98 |
| CP1-R | 20.1 | 240 | 65.5 | 15.9 | 0.171 | 0.022 | 0.038 | 286 | 1.18 |
| GS1-R | 23.9 | 369 | 154.5 | 41.4 | 0.176 | 0.185 | 0.011 | 239 | 0.90 |
| CS1-R | 21.8 | 338 | 133.1 | 33.6 | 0.264 | 0.171 | 0.020 | 414 | 1.16 |

n.a. – not applicable

required before strain values can be recommended for the evaluation of the load-carrying capacity of the dapped beam.

## CONCLUSIONS

The study was carried out to examine the use of strut-and-tie models in the evaluation of the ultimate strength of RC dapped beams strengthened with externally bonded FRP systems. A total of seven tests were carried out on simply supported dapped-ended beams under mid-span loading. All the beams failed in shear, with diagonal cracks propagating from the re-entrant corner to the flange of the beam in most cases. Beams strengthened with FRP systems exhibited a delay in diagonal cracking, increase in stiffness and an increase in ultimate load compared to the un-strengthened beam.

Debonding of the FPP reinforcement from the concrete surface was observed at the dapped ends at failure. In one case, rupture of carbon fibre sheets was also observed. Beams bonded with FRP plates failed in a slightly more ductile manner compared to those bonded with sheets or fabrics. The additional anchoring materials in the form of a through bolt for the CFRP plate system and a horizontal U-strip over the end face of the dapped beam for fibre fabric or sheet system helped to preserve the integrity of the FRP system, leading to further increase in ultimate shear capacity of the beam.

The proposed strut-and-tie model, consisting of two sub-models to evaluate the increased shear capacities due to vertical and diagonal reinforcement, was found to predict the ultimate strength of the dapped beams with good accuracy. Further studies are needed, however, to establish the design strains in the FRP reinforcement for the purpose of evaluating the design shear strength of the dapped beams.

## ACKNOWLEDGEMENT

The research work was partly supported by the research grant RP3981608 provided by the National University of Singapore.

## REFERENCES

Huang, P.C., Myers, J.J. and Nanni, A. (2000), "Dapped-End Strengthening of Precast Prestressed Concrete Double Tee Beams with FRP Composites", Advanced Composite Materials in Bridges and Structures, 3rd International Conference, Ottawa, Canada, pp. 545-552.

MacGregor, J.G. (1997), "Reinforced Concrete: Mechanics and Design", 3rd Edition, Upper Saddle River, N.J., Prentice Hall, pp. 753-812.

Precast/Prestressed Concrete Institute (1999), "PCI Design Handbook: Precast and Prestressed Concrete", 5th Edition, Chicago, USA, pp. 4/59–63.

# Externally bonded prestressed reinforcement

# Prestressed CFRP Sheets for Strengthening Concrete Beams at Room and Low Temperatures: Experimental and Analytical Investigations

Dr. Raafat EL-HACHA, NSERC Postdoctoral Fellow, Queen's University, Department of Civil Engineering, Kingston, Ontario, Canada.
Dr. Gordon WIGHT, Assistant Professor, Royal Military College of Canada, Department of Civil Engineering, Kingston, Ontario, Canada.
Dr. Mark GREEN, Associate Professor, Queen's University, Department of Civil Engineering, Kingston, Ontario, Canada.

## ABSTRACT

This paper presents results of experimental and analytical investigations that examine the feasibility of using prestressed carbon fiber reinforced polymer (CFRP) sheets to strengthen precracked and severely damaged concrete beams. The experimental program consisted of testing seven 4.5m simply supported post-tensioned concrete T-girders. Four beams were tested at room temperature (+22°C) and the other three at low temperature (−28°C). Tests were conducted to evaluate the effectiveness of bonded prestressed CFRP sheets on the short and long-term behaviour of precracked post-strengthened concrete beams. Materials and prestress changes due to temperature variations that would affect flexural behaviour were studied. A mechanical anchorage system developed as part of this study was used to directly prestress the CFRP sheets by jacking against the concrete beam. A non-linear numerical model based on principles of equilibrium, strain compatibility, and representative material properties was used to predict the overall behaviour of the strengthened beams during prestressing of the CFRP sheets and external loading. The analytical model was verified by comparing the predicted load-deflection curves to those measured in the tests. Comparison of room and low temperature test results indicates that the flexural behaviour of the strengthened beams is not adversely affected by reduced temperature, and that prestressed CFRP sheets could be used to increase and restore the original strength and serviceability of severely damaged concrete beams under extreme environmental conditions.

## INTRODUCTION

A large number of bridges and civil engineering structures have reached the end of their service life, either due to deterioration of the concrete and reinforcement or an increase in applied loads, thereby becoming structurally deficient or functionally obsolete. Strengthening can be used as a cost-effective alternative to the replacement of these structures and is often the only feasible solution. Fiber reinforced polymer (FRP) sheets, bonded to the tension face of concrete girders is an effective solution for the rehabilitation and strengthening of damaged structures, and the use of this material has been growing rapidly in recent years. In addition to their high-strength-to-weight ratios, FRP sheets bonded to the tensile face of an under-strength or damaged concrete beam increases flexural strength, thus providing an efficient, lightweight, non-corrosive alternative to other rehabilitation and strengthening methods. Because they are quickly and easily applied, their use minimizes traffic disruption and labour costs and can lead to significant savings in the overall costs of a project.

*FRPRCS-5*, Thomas Telford, London, 2001.

When non-prestressed FRP sheets are bonded to a concrete beam, they only support additional live load applied to a structure and are unable to carry the dead load. To improve the efficiency of this strengthening technique, FRP sheets may be prestressed using a suitable anchorage system prior to bonding them to the concrete beam. An initial prestress is induced in the member that can be used to balance applied dead and live loads as in conventional prestressed structures. When the FRP sheets are prestressed, the material may be used more efficiently since a greater portion of their tensile capacity is employed. Prestressed FRP sheets improve the serviceability of a beam by delaying cracking, and may further increase the ultimate strength by preventing premature failure modes. The benefit of prestressed FRP sheets in delaying cracking and closing existing cracks may help to restore durability of the structure since the cracks provide additional access for moisture into the concrete and the adhesive layer.

## LITERATURE REVIEW

Very limited research of concrete girders strengthened with epoxy-bonded prestressed FRP laminated sheets or plates have been reported in the literature. Saadatmanesh and Ehsani (1991) indirectly prestressed the glass FRP plates by cambering a beam upward using hydraulic jacks at midspan, holding the beam in the deflected position, bonding the GFRP plates to the tensile face and removing the jacks when the epoxy was cured. Only a low level of prestress was induced into the plates. However, using this method it is difficult to control the amount of prestress induced into the plates. A different technique to induce prestress into the carbon FRP sheets was used by Triantafillou et al. (1992), Garden et al. (1998), and Wu et al. (1999). The CFRP sheets were bonded to steel plates and were tensioned by jacking against an external reaction steel frame, independent of the strengthened beam. Once the sheets were tensioned, the lower face of the beam and the upper surface of the sheet on the stressing bed were brought into contact with one another and bonded together with epoxy adhesive. Once the epoxy was fully cured, both ends of the sheets were cut, and the prestress was transferred to the concrete beam. This method is only suitable for small beams tested in the laboratory or specialized equipment is required for long scale applications. Only a few studies of concrete beams strengthened with prestressed FRP sheets directly tensioned by reacting against the strengthened beams are reported in the literature (Wight et al. 1995; Izumo et al. 1997; Andrä et al. 1999; Garden and Mays 1999). Different anchorage systems were used. In general the systems consisted of FRP sheets bonded to anchors that were designed for the prestressing application. At one end, the anchors were fixed to the beam, and at the other end, the anchors were stressed using hydraulic jacks by reacting against a permanent anchorage system mounted on the concrete beam. This method of prestressing is suitable for use on real bridges or structures in site. A similar prestressing and anchorage system was used in this study.

## OBJECTIVES

The use of Carbon Fibre Reinforced Polymer (CFRP) composite sheets in civil engineering applications is growing, but one of the areas that has not been widely covered and where knowledge is limited is the low temperature exposure and the long-term behaviour of concrete beams strengthened with prestressed CFRP sheets. To address this deficiency, flexural tests were conducted to evaluate the effectiveness of bonded unidirectional prestressed CFRP sheets. These tests involved the short and long-term behaviour of precracked and severely damaged post-strengthened concrete beams subjected to room (22°C) and low (−28°C) temperatures. Material and prestress changes due to temperature variations that would affect and cause a change in flexural behaviour were studied. A non-linear numerical model was developed and used to predict the overall behaviour of the strengthened beams during prestressing of the CFRP sheets and under external loading. The predicted load-deflection curves were compared to those measured in the tests.

## EXPERIMENTAL PROGRAM

### Beam Details

The experimental program consisted of nine tests on seven 4.5m T-section concrete beams. The beams were one-third scale unbonded prestressed concrete T-girders, typical of a 12.0m long, simply supported short span highway bridge girder, internally post-tensioned with conventional prestressing steel strands. Figure 1 shows a typical elevation, cross-sections, and reinforcement layout of the T-beams. The internal prestressing steel strands were post-tensioned to 70% of their ultimate strength. The deck slab was cast after post-tensioning of the beams. The 28-day compressive strength of concrete was 40MPa.

### Test Set-up and Instrumentation

The 4.5m long beams were simply supported over a 4.0m span and subjected to quasi-static monotonic load up to failure. The beams were loaded in four-point bending, as shown in Figure 1, using a 500kN capacity MTS testing machine operating under displacement-control mode at a constant loading rate of 1mm/min. The room temperature tests were conducted at +22°C, while the low temperature tests were performed inside a cold room that was capable of maintaining constant temperature as a low as –28°C±1°C. All beams were fully instrumented to measure the applied load, deflections, and strain in the reinforcements and the CFRP sheets and in the concrete through the depth of the beam. Readings of all the LVDT's, strain gauges and load cells were recorded by a data acquisition system at every load increment during prestressing and loading operations. Details can be found in El-Hacha (2000).

### Test Procedure

The beams were divided into two groups to investigate their short and long-term behaviour at both room and low temperatures, as shown in Table 1. Precracking and testing up to failure was at room temperature for beams R1, R1r, R2, R3, and Q4, and at low temperature for beams Q1, Q1r, Q2 and R5. Strengthening of all beams was performed at room temperature.

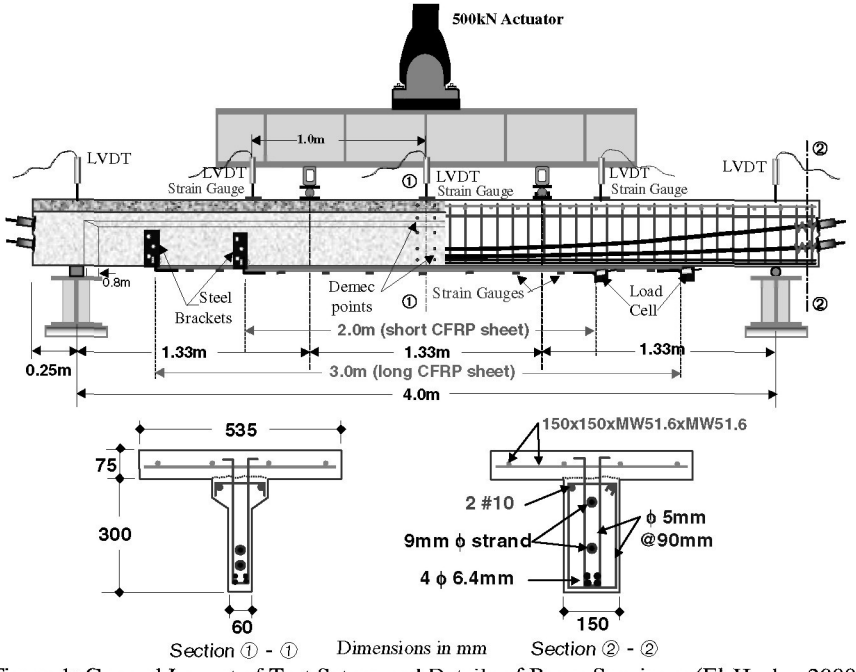



Figure 1: General Layout of Test Set-up and Details of Beam Specimen (El-Hacha, 2000)

Table 1: Concrete T-Beams Experimental Program (El-Hacha, 2000)

| *Temperature Exposure* | *Test Name* | *Beam No.* | *Beam Condition, Strengthening, and Exposure Test* |
|---|---|---|---|
| +22°C | R1 | R1 | Control Unstrengthened |
| | R1r | R1 | Damaged → Retrofitted → Short-Term |
| | R3 | R3 | Precracked → Strengthened → Short-Term |
| | R2 | R2 | Precracked → Strengthened → Long-Term: Own-Weight |
| | Q4 | Q4 | Under-Strength → Precracked → Strengthened → Short Term |
| −28°C | Q1 | Q1 | Control Unstrengthened |
| | Q1r | Q1 | Damaged → Retrofitted (+22°C) → Short-Term |
| | Q2 | Q2 | Precracked → Strengthened (+22°C) → Short-Term |
| | R5 | R5 | Precracked → Strengthened (+22°C) → Long Term: Own-Weight |

Two control unstrengthened beams, R1 at room temperature and Q1 at low temperature, were first precracked and unloaded. They were reloaded and tested to failure up until their ultimate capacity was reached, then unloaded. Thereafter, these two completely damaged beams R1r and Q1r were both retrofitted at room temperature with prestressed CFRP sheets. Five days after retrofitting, beam R1r was tested at room temperature, while beam Q1r was subjected to low temperature for 7 days, and was tested under this temperature.

Beam R3 and R2 were both precracked at room temperature before the prestressed CFRP sheets were applied. Beam R3 was tested 7 days after being strengthened, while the long-term beam R2 was kept under its own weight and tested to failure 398 days after being strengthened. Beam Q4 was under-strengthened with only one internal unbonded prestressing steel strand, representing a beam that suffered loss in internal prestressed reinforcement. The beam was precracked, unloaded, strengthened with prestressed CFRP sheets, and subsequently tested to failure at room temperature.

Beam Q2 and R5 were both precracked at low temperature before the prestressed CFRP sheets were applied at room temperature. Five days after strengthening, both beams were subjected to low temperature. Beam Q2 was tested after 7 days, while the long-term beam R5 was kept under its own weight and tested to failure after 327 days.

**Composite Materials**

The composite material used for strengthening was a unidirectional Carbon-Fibre-Reinforced-Polymer (CFRP) prepreg sheet type Replark™ 20 developed by Mitsubishi Chemical Corporation. The sheets were bonded to the lower face of the concrete beam with a two-part epoxy resin. The ultimate tensile strength and the modulus of elasticity of the sheet, determined from tension tests, were 1480MPa and 144GPa, respectively.

**Anchorage System and Application of Prestressed CFRP Sheets**

A new, practical, mechanical anchorage system developed as part of this study was used to directly prestress the CFRP sheets by jacking and reacting against the strengthened concrete beam itself (El-Hacha, 2000). The bottom width of the precracked beams and the severely damaged beams was strengthened over lengths of 3.0m and 2.0m using two sets of prestressed CFRP sheets tensioned individually. The long set was applied first. Each set consisted of three layers of CFRP sheet cut to the proper lengths with a width equal to that of the beam. The sheets were bonded at both ends to anchors designed for the prestressing application. The CFRP sheets with their anchorages at both ends were placed in position on the brackets mounted on the sides of the beam web. The sheets were tensioned using a hydraulic jack that reacted on the beam's brackets. Once tensioned, the sheets were bonded to the bottom face of the beam, and the anchorage system held the tensioned sheets until the

epoxy cured and the sheets were fully bonded to the bottom face of the beam. The anchorage system was left in place after prestressing to avoid peeling failure associated with the high shear stresses present at the ends of the CFRP sheets. After the prestressing was applied, to ensure full bond with concrete, the sheets were pushed upward by clamps and wires mounted on the beam, and the epoxy was cured for one week. The CFRP sheets were monitored during prestressing and the application of external load by strain gauges installed on the sheets at different locations and by load cells mounted at the jacking ends of the stressing apparatus.

**Experimental Results**

***CFRP Prestressing Results and Effectiveness of the Prestressing System***

The developed prestressing system achieved an initial prestress level approximately 50% of the ultimate tensile strength of the sheet. The level of prestress in the long and short CFRP sheets (L.S. and S.S.) was monitored until the strengthened beams were tested to failure. Both, the initial prestress applied to the sheets by jacking, and the remaining after transfer and until testing are reported in Table 2 and Table 3. These tables show the prestress levels in the sheets as percentage of the ultimate tensile strength of the sheets. After the removal of the jacking apparatus and transferring the prestress to the permanent anchorage system mounted on the beam, a portion of the prestress force was lost. The prestress level was stabilized 5 hours after transfer. Thereafter, if the temperature was unchanged the stresses remained almost constant until the beams were tested. There was a loss of prestressing in the CFRP sheets associated with the exposure to low temperature. The effect of this loss of prestress on the flexural behaviour of the strengthened concrete beams may have been offset by the increased strength of the concrete in the beams at low temperatures that is related to the freezing of capillary pore water in the concrete, and the increase of the mechanical properties of the reinforcement.

Table 2: Prestress Level in the Sheets for Beams Tested at +22°C (% of the Ultimate Stress)

| Condition | Beam R1r | | Beam R3 | | Beam Q4 | | Beam R2 | |
|---|---|---|---|---|---|---|---|---|
| | S.S. | L.S. | S.S. | L.S. | S.S. | L.S. | S.S. | L.S. |
| Initial Prestress | 45.0% | 51.2% | 44.2% | 49.2% | 50.6% | 51.0% | 52.0% | 52.2% |
| After 5 hours | 32.3% | 28.8% | 37.0% | 33.0% | 39.0% | 32.0% | 36.8% | 36.1% |
| After 7 days | 30.6% | 27.4% | 36.5% | 32.5% | 38.5% | 31.1% | 34.4% | 36.0% |
| After 50 days | — | — | — | — | — | — | 34.0% | 35.1% |
| After 398 days | — | — | — | — | — | — | 33.6% | 34.7% |

Table 3: Prestress Level in the Sheets for Beams Tested at −28°C (% of the Ultimate Stress)

| Condition | Beam Q1r | | Beam Q2 | | Beam R5 | |
|---|---|---|---|---|---|---|
| | S.S. | L.S. | S.S. | L.S. | S.S. | L.S. |
| Initial Prestress (+22°C) | 38.6% | 45.0% | 47.0% | 45.0% | 49.0% | 45.5% |
| After 5 hours (+22°C) | 26.5% | 33.3% | 36.0% | 32.0% | 37.1% | 26.0% |
| After 5 days (+22°C) | 23.0% | 32.0% | 33.0% | 31.0% | 34.4% | 24.6% |
| After 15 days (−28°C) | 21.5% | 31.5% | 27.0% | 28.0% | 31.0% | 23.0% |
| After 50 days (−28°C) | — | — | — | — | 30.8% | 22.7% |
| After 327 days (−28°C) | — | — | — | — | 29.5% | 21.5% |

**Flexural Behaviour of Beams Tested at Room and Low Temperatures**

The flexural response, at both room and low temperatures, of the unstrengthened control beams, the short and long-term behaviour of the strengthened beams is represented by their load midspan deflection curves as shown in Figure 2 and Figure 3. A summary of significant values describing the behaviour of the tested beams at +22°C and −28°C is given in Table 4 and Table 5 respectively. The beams were initially loaded to cause considerable damage, and

then unloaded to zero. Residual deflections were observed after unloading. The unstrengthened control beams failed in flexural mode due to tensile rupture of the bottom nonprestressed tension steel. The cracking and the ultimate loads for the unstrengthened control beam tested at low temperature were less than the one tested at room temperature, which can be attributed due to a slight difference in the details of the secondary steel.

During the application of the external prestressing in the CFRP sheets, the residual midspan deflections were reduced by 2.0mm because of the prestressing camber. The load-deflection response of the retrofitted and the strengthened concrete beams was improved as indicated by the increase in the stiffness and the ultimate capacity of the beams after strengthening and reloading as compared to the unstrengthened control beams. Displacement for any load in the strengthened beams was significantly decreased with the addition of the prestressed CFRP sheets due to the initial camber induced in the beams by the prestress and the ability of the prestressed CFRP sheets to delay and control cracking in the beams. It was observed that the external prestressing closed the cracks completely, and reduced the crack widths under further increase in the applied load. At the load when the steel yielded in the control beam, the displacement in the strengthened beams tested at both room and low temperatures decreased significantly when compared to the displacement of the control beams. The prestressed CFRP sheets contributed to the load carrying capacity of the beams, and a significant redistribution of the stresses from the steel reinforcement to the CFRP, delayed yielding of the steel so that it occurred at a higher load than was observed in the control beams. Although a similar maximum load was attained for the beams tested over the short and long term, the displacement at ultimate was larger for the beam tested over the long-term. This difference may be accounted for by the additional prestress losses in the CFRP sheets that occurred over the long-term and the effects of creep and shrinkage of concrete and relaxation of prestressing steel. The strengthened beams failed by tensile rupture of the prestressed CFRP sheets after yielding of the internal flexural steel reinforcement and the debonding of the sheets from the concrete. At failure, the stress in the prestressed CFRP sheets ranged between 1275 and 1400MPa. For the retrofitted beams (R1r and Q1r), in comparison with the control-unstrengthened (R1 and Q1) and the strengthened (R3 and Q2) beams, the prestressed CFRP sheets not only restored the original strength of the control-unstrengthened beams but an increase in the ultimate strength was obtained and approached the maximum load carrying capacity attained in the precracked undamaged strengthened beams (R3 and Q2). For the under-strengthened beam (Q4), the maximum load was 20.4% greater than the theoretical ultimate design load of similar beam internally post-tensioned with one steel strand. The addition of the prestressed CFRP sheets to the under-strengthened beam (Q4) recovered 78% of the strength of a similar beam internally post-tensioned with two prestressing steel strands (beam R1).

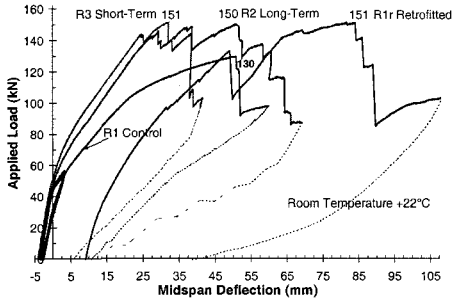



Figure 2: Load-Midspan Deflection at +22°C.

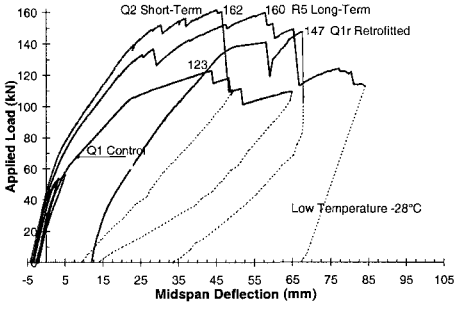



Figure 3: Load-Midspan Deflection at −28°C.

Table 4: Summary of Significant Test Results of Beams Tested at Room Temperature +22°C

| Load and corresponding Displacement | Control Unstrengthened R1 | Short-Term Retrofitted R1r | Short-Term Strengthened Q4* | Short-Term Strengthened R3 | Long-Term Strengthened R2 |
|---|---|---|---|---|---|
| First Visible Crack Load (kN) | 48 | — | 32 | 49** | 46** |
| Displacement at First Crack (mm) | 1.2 | — | 1 | 0.8 | 0.5 |
| Yield Load (kN) | 102.14 | — | — | 143.64 | 136.46 |
| Displacement at Yielding (mm) | 20.8 | — | — | 24.6 | 25.4 |
| Displacement at Yielding of Steel in Control Beam (mm) | 20.8 | — | — | 11.15 | 14.4 |
| % Decrease in this Displacement | — | — | — | 53.6 | 69.2 |
| Ultimate Load (kN) | 129.7 | 151.2 | 102 | 151.2 | 150.14 |
| Displacement at Ultimate (mm) | 51 | 81.54 | 28.65 | 32 | 50.67 |
| % Increase in the Ultimate Load | — | 16.6 | 20.4* | 16.5 | 15.7 |

Note:Q4*: % increase over the theoretical ultimate load of similar beam internally post-tensioned with one steel strand
** : This is the cracking load before strengthening those beams

Table 5: Summary of Significant Test Results of Beams Tested at Low Temperature –28°C

| Load and corresponding Displacement | Control Unstrengthened Q1 | Short-Term Retrofitted Q1r | Short-Term Strengthened Q2 | Long-Term Strengthened R5 |
|---|---|---|---|---|
| First Visible Crack Load (kN) | 46 | — | 47** | 49** |
| Displacement at First Crack (mm) | 1.18 | — | 1.7 | 2.3 |
| Yield Load (kN) | 105.57 | — | 138.41 | 126.08 |
| Displacement at Yielding (mm) | 22.73 | — | 22.68 | 21.7 |
| Displacement at Yielding of Steel in Control Beam (mm) | 22.73 | — | 12.65 | 14.7 |
| % Decrease in this Displacement | — | — | 55.63 | 64.67 |
| Ultimate Load (kN) | 122.97 | 147.32 | 161.67 | 159.97 |
| Displacement at Ultimate (mm) | 44 | 67 | 45 | 58 |
| Increase in the Ultimate Load (%) | — | 19.5 | 31.7 | 30.1 |

Note: ** : This is the cracking load before strengthening those beams

## ANALYTICAL STUDY

An iterative analytical model has been developed for predicting the flexural behaviour of the beams that can be compared with experimental results. The analytical model is based on principles of equilibrium and strain compatibility approach and representative material properties. The model considers the actual constitutive characteristics of the concrete, steel and CFRP sheet composite to predict flexural behaviour under room and low temperature effects. Data obtained from material testing was used for the models. The model is used to analyze the flexural behaviour of the strengthened beams when subjected to external flexural loading at serviceability and ultimate states at both room and low temperatures.

### Layer-by-Layer Approach

The developed model was based on the layer-by-layer approach to evaluate the sectional forces corresponding to a given strain distribution at a specific section. The load-midspan deflection was determined from the predicted moment-curvature responses at different sections of the beam by integrating the curvature along the beam. For the strengthened beams, the CFRP sheets at the bottom face of the beam are considered as a layer of tension reinforcement with linear stress-strain relationship up to failure. The tested beams were internally post-tensioned with unbonded prestressing steel tendons, and the strain compatibility at any section was not maintained. The stresses in the unbonded prestressing

steel at any load level, depends on the total change in length of the concrete at the level of the steel between end anchorages. Modifications were made to the model to account for this.

**Assumption**

The analysis of the prestressed concrete beams was performed using simple plane section analysis. The main assumptions used in the compatibility approach for the analysis and the computation of the flexural strengths of the concrete beams are the following:

1. Plane sections before bending remain plane after bending.
2. No slip between the nonprestressed reinforcing steel and the surrounding concrete.
3. No shear deformations and the section is subjected to pure bending.
4. After cracking, the tensile stresses in the concrete are neglected.
5. The internal prestressing steel is assumed to be bonded to the concrete using Naaman's methodology (Naaman and Alkhairi, 1991) by applying a bond reduction coefficient that relates the strain change in the unbonded tendon to the strain change in the concrete at the level of the tendon at any section along the beam length.
6. No premature sheet separation or shear failure is accounted for; full composite action is maintained up to failure. Perfect bonding of the sheets and the concrete beam exists.

**Discussion of the Analytical Results**

According to the prediction from the developed model, the addition of the prestressed CFRP sheets to the bottom face of the concrete beams delayed the yielding of the internal reinforcing steel, improved the serviceability of the strengthened beams by delaying cracking and controlling deflection, and increased their ultimate strength. The ultimate strength and the failure of the strengthened beams was governed by tensile rupture of the CFRP sheet. A summary of significant predicted results obtained from the developed model of the strengthened and unstrengthened concrete beam tested at room temperature is given in Table 6.

Table 6: Summary of Significant Predicted Results at Room and Low Temperatures

| Load and corresponding Displacement | Room Temperature +22°C | | Low Temperature −28°C | |
|---|---|---|---|---|
| | Unstrengthened | Strengthened | Unstrengthened | Strengthened |
| Cracking Load (kN) | 51.21 | 72.47* | 51.32 | 71.26* |
| Displacement at Cracking (mm) | 0.54 | 0.59 | 0.56 | 0.44 |
| Yield Load (kN) | 96.31 | 135.11 | 101.33 | 140.41 |
| Displacement at Yielding (mm) | 18.43 | 18.15 | 18.12 | 18.41 |
| Displacement at Yielding of Steel in Unstrengthened Beam (mm) | 18.43 | 6.61 | 18.12 | 7.53 |
| % Decrease in this Displacement | — | 35.6 | — | 41.56 |
| Ultimate Load (kN) | 125.31 | 154.36 | 130.86 | 159.01 |
| Displacement at Ultimate (mm) | 44.03 | 24.44 | 46.81 | 24.31 |
| Displacement at Ultimate Load of Unstrengthened Beam (mm) | 44.03 | 15.13 | 46.81 | 15.88 |
| Increase in the Ultimate Load (%) | — | 23.18 | — | 21.15 |

Note: *: This is the cracking load after strengthening those beams

## COMPARISON OF EXPERIMENTAL AND ANALYTICAL RESULTS

Figure 4 shows curves of the experimental and theoretical total applied load versus midspan deflection for the unstrengthened and the short term strengthened beams tested at room and low temperatures. The changes in slope of the curves in both graphs indicate the loads at which concrete cracking and internal rebar yield occurred. These loads were significantly higher for the strengthened beams. Also, the prestressed sheets were most effective at reducing crack widths, delaying cracking and, as a result, the strengthened beams have

smaller deflections and curvatures at failure. It can be seen that there is very good agreement between the experimental and analytical predictions. The slight difference between both curves can be due to the assumption, made in the analysis, of perfect bonding of the sheet and the concrete and ignoring the slipping of the sheet in the immediate vicinity of the crack. The model validates the observations from the experimental program. The analysis for beams tested under low temperature was performed by changing the material properties. Where it was not possible to determine the component's low temperature properties through ancillary tests, inputs for the model were based on the results of previous research.

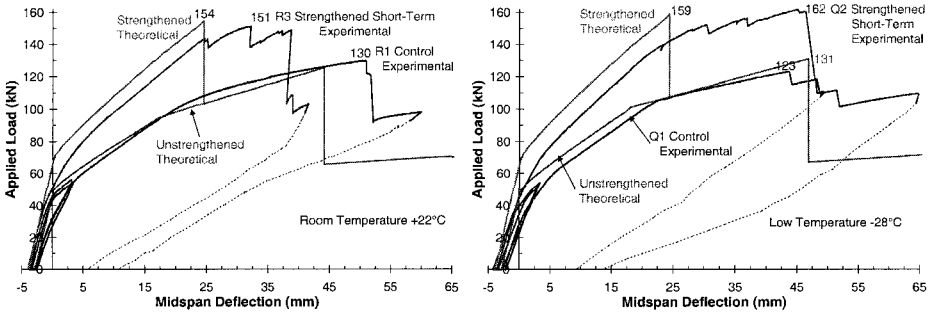



Figure 4: Theoretical and Experimental Load-Deflection Relationship for Unstrengthened and Short-Term Strengthened Beams Tested at Both Room and Low Temperatures

## SUMMARY AND CONCLUSIONS

Based on the test results and the analytical investigation, the following conclusions were drawn from this study:

- Strengthening with prestressed CFRP sheets improved the load deflection response of the precracked and severely damaged concrete beams, reduced the crack widths, decreased the level of stress in the prestressed and nonprestressed steel and delayed yielding of the reinforcement. Prestressed CFRP sheets increased the flexural stiffness and ultimate capacity of the strengthened beams.
- Due to prestress losses in the CFRP sheets over time, and long-term behaviour of the beam materials the deflections at any load level were greater and the deformations at ultimate were greater for the strengthened long-term beams. These prestress losses did not affect the ultimate strength of the beams.
- The flexural behaviour of the strengthened beams is not adversely affected by reduced temperature, and prestressed CFRP sheets could be used to increase and restore the original strength of damaged concrete beams under extreme environmental conditions.
- Failure of the strengthened beams was by tensile rupture of the CFRP sheets.
- No damage in the bond between the sheets and the concrete was observed at low temperature under short and long-term exposure.
- The behaviour of room and low temperature tests were similar with the exception of the difference in the ultimate loads. This indicates that the load-deflection behaviour is relatively insensitive to temperature change over the range tested (+22°C to −28°C).
- Overall, the load-deflection graphs at low temperature followed the same trend as the room temperature tests with a higher observed ultimate load.
- The analytical model accurately predicted the behaviour of concrete beams strengthened with prestressed CFRP sheets. The load-deflection behaviour of beams subjected at low temperature can be reasonably predicted by a simple model that takes into account the change in the beam's constituent properties with temperature.

## WORK IN PROGRESS

The experimental investigation is currently ongoing and it includes study of the long-term behaviour, at room and low temperatures, of concrete beams strengthened with prestressed CFRP sheets and loaded with a sustained dead load. The beams will be tested to ensure that prestressing levels in the sheets are sufficiently maintained when subjected to temperature variation and long-term exposure under sustained dead load. It is anticipated that the long-term prestress losses will be primarily due to creep and shrinkage of the concrete beam.

## ACKNOWLEDGEMENT

The authors wish to acknowledge the support of the Department of National Defense (DND) of Canada through the Military Engineering Research Group (MERG) at the Royal Military College of Canada, and Queen's University. The authors are members of the Intelligent Sensing for Innovative Structures Network (ISIS Canada) and wish to acknowledge the support of the Networks of Centres of Excellence Program of the Government of Canada and the Natural Sciences and Engineering Research Council (NSERC).

## REFERENCES

Andrä, H.-P., and Maier, M., (1999). "Post Strengthening of Reinforced Concrete Structures by Prestressed Externally Bonded Carbon Fibre Reinforced Polymer (CFRP) Strips," Proceedings of the Structural Faults + Repair 99, London, England, July 13–15, 1999, 7 p.

El-Hacha, R., (2000). "Prestressed CFRP Sheets for Strengthening Concrete Beams at Room and Low Temperatures." Queen's University, Department of Civil Engineering, Kingston, Ontario, Canada, December 2000, 525 pp.

Garden, H.N., Hollaway, L.C., and Thorne, A.M., (1998). "The Strengthening and Deformation Behaviour of Reinforced Concrete Beams Upgraded Using Prestressed Composite Plates," Materials and Structures, Vol. 31, No. 208, May 1998, pp. 247-258.

Garden, H.N., and Mays, G.C., (1999). "Structural Strengthening of Concrete Beams using Prestressed Plates," Strengthening of Reinforced Concrete Structures, Hollaway, L.C. and Leeming, M.B., (Editors), M.B. Woodhead Publishing, Cambridge, U.K.,

Izumo, K, M., Saeki, N., Asamizu, T., and Shimura, K., (1997). "Strengthening Reinforced Concrete Beams by Using Prestressed Fiber Sheets," Proceedings of the FRPRCS-3, Sapporo, Japan, October 14–16, 1997, Vol.1, pp. 379-386.

Naaman, A.E., and Alkhairi, F.M., (1991), "Stress at Ultimate Unbonded Prestressing Tendons. Part 2: Proposed Methodology," ACI Structural Journal, Vol.88, No.5, September-October 1991, pp. 652-692.

Saadatmanesh H., and Ehsani M., (1991). "RC Beams Strengthened with GFRP Plates: Part I: Experimental Study," Journal of Structural Engineering ASCE, Vol. 117, No. 11, November 1991, pp. 3417-3433.

Triantafillou, T.C., Deskovic, N. and Deuring, M., (1992). "Strengthening of Concrete Structures with Prestressed Fiber Reinforced Plastic Reinforced Plastic Sheets," ACI Structural Journal, Vol. 89, No. 3, May–June 1992, pp. 235-244.

Wight, R.G., Green, M.F., and Erki, M.-A., (1995). "Post-Strengthening Concrete Beams with Prestressed FRP Sheets," Proceedings of the FRPRCS-2, Ghent, Belgium, August 1995, pp. 568-575.

Wu, Z., Matsuzaki, T., Yokoyama, K., and Kanda, T., (1999). "Retrofitting Method for Reinforced Concrete Structures with Externally Prestressed Carbon Fiber Sheets," Proceedings of the FRPRCS-4, Baltimore, Maryland, US, October 31–November 5, 1999, pp. 751-765.

# Prestressed externally bonded FRP reinforcement for RC beams

E. FERRIER C. ENNACEUR, D. BIGAUD and P. HAMELIN
Laboratoire Mécanique Matériaux, Université LYON 1, Villeurbanne FRANCE

## INTRODUCTION

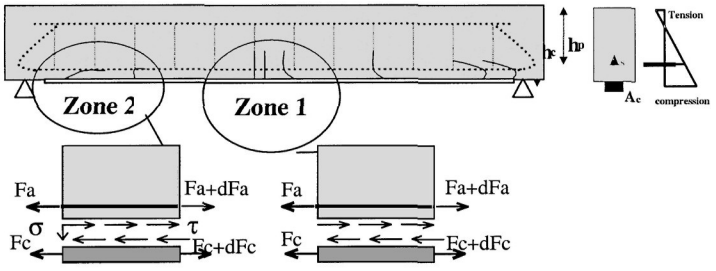
A bibliographical study of engineering structure pathologies allows the distinction of four main disorders in steel reinforced concrete structures: physico-chemical damage (alkali-reaction, carbonatation), mechanical damages due to overloading, poor strength calculation or accidental damage. We can define several technological techniques like post-stress, shotcrete (Resse [1]), steel plate bonded (L'Hermite [2]) to reinforce or repair damaged structure.

More recently external bonded carbon-epoxy composite is used to restore or to increase the beam capacity (Mieir [3], Triantafillou [4], Hamelin [5]). Composite materials reinforcement combined high strength unidirectional fibres and epoxy matrix working-up in normal temperature and moisture conditions. It is necessary to point out that those repair techniques are developed in the industrial field (Freyssinet [6], Replark [7], Sika Hexcel [8]).

The use of composite reinforcement in civil engineering structure is limited by the steel yielding. Actually this parameter reduces by five the ultimate efficiency of the composite (2000 μm/m in strain) in serviceability conditions. In accordance with several authors, the prestress of the composite before bonding improves the mechanical behaviour of a strengthened RC beam. The ultimate load is then increased by 200 % and the external load leading to steel yielding is increased by 40% (for a prestress level of 25 % of the composite strength [9, 10]). Saadatmasmesh and Ehsani [11] have conducted an experimental study of the strengthening of precracked RC beams. The plate prestress close some of the cracks indicating the benefit of prestressing from a serviceability point of view. The benefit of external prestressing using polymeric composite materials need further work in order to understand the behaviour of RC beams prestressing.

We propose in this paper to study the mechanical behaviour of a RC element strengthened with external prestress composite plate. The structural equilibrium depends essentially on two structural hypotheses. First the mechanical equilibrium of the strengthened RC beam, in common sections depends on the material properties and on the composite prestress level. The evolution of this equilibrium as a function of time essentially depends on the adhesive layer ability to insure the stress transfer (fig.1 zone 1). Secondly, we have to consider a zone that is located in the bonding limit of the composite plate. This interface zone is submitted to high shear stress. Usually in case of unanchored prestressed composite plate, the failure occurs in the interface (fig.1 zone 2).

This paper will first give more information about the interface behaviour and it effect on the structure and then, with a short experimental work, we propose to verify the hypothesis and remark initially taken.




*Fa, dFa: effort in steel; Fc, dFc: composite stress, Ac: composite area, Aa : steel area*

Figure1. Mechanical behaviour of a strengthened beam with external bonded prestressed composite

## PREVIOUS WORK ON CONCRETE/INTERFACE STRESS BEHAVIOUR

### Interface hear stress distribution

Täljsten [12] has already studied the shear stress distribution in the bonding adhesive layer in case of lap joint loaded in shear. In our study the behaviour of the bonding joint should be considered in case of flexural members. Täljsten [12] has already proposed an analytical solution of the strain and stress distribution in the adhesive joint. Applying the same approach, we propose to consider the problem of the interface in case of external prestress composite. Following hypothesis of mechanical shear behaviour of an adhesive joint illustrated by figure 2, we derive the relation 1. This relation gives the evolution of the stress as a function of x (bonding zone position), of the beam loading level and of the adhesive properties.

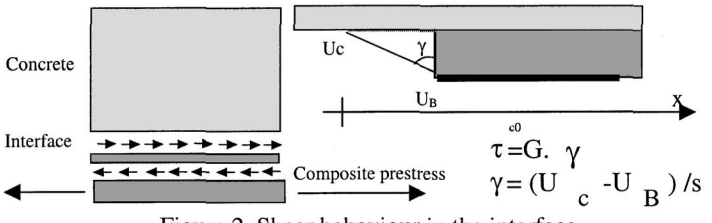



Figure 2. Shear behaviour in the interface

$$\tau(x)=\frac{G}{s}\cdot[U_C(x)-U_B(x)]$$

$$\varepsilon_B(x)=\frac{dU_B(x)}{dx}=\frac{M_B(x)}{E_B\cdot W_b}-\frac{N_B(x)}{E_B\cdot A_B}\ \text{and}\ \varepsilon_C(x)=\frac{dU_C(x)}{dx}=\frac{N_C(x)}{E_C\cdot A_C}+\varepsilon_{cp} \qquad (1)$$

$$\frac{d^2\tau(x)}{dx^2}=\frac{G}{s}\cdot\left[\frac{d^2U_C(x)}{dx^2}-\frac{d^2U_B(x)}{dx^2}\right]\ \text{so}\ \frac{d^2\tau(x)}{dx^2}=\frac{G}{s}\left[\frac{dN_C(x)}{E_C\cdot A_C\cdot dx}-\frac{dM_B(x)}{E_B\cdot W_b\cdot dx}+\frac{dN_B(x)}{E_B\cdot A_B\cdot dx}\right]$$

$$\tau_1(x)=\frac{G\cdot P}{2\cdot s\cdot E_B\cdot W_B}\cdot\left[\left[\left(\frac{a}{\lambda}\cdot tanh(\lambda\cdot b)\right)-\frac{1}{cosh(\lambda\cdot b)}\right]\cdot cosh(\lambda\cdot x)-\frac{a}{\lambda}\cdot sinh(\lambda\cdot x)+1\right]-\frac{G\cdot\varepsilon_{cp}}{s\cdot\lambda}\cdot tanh(\lambda\cdot b) \qquad (2)$$

with :

s: thickness of the adhesive layer, τ(x) : shear strain distribution, εb, εc: strain in concrete and composite, Ub, Uc: displacement in concrete and in composite, N: load (N), Eb: concrete modulus (MPa), Ec: composite modulus, L: anchorage length, Ac: composite area, Ab: concrete area

The evolution of stress along the bonding zone is given on figure 3. Two parameters allow identifying this evolution. First the value of shear stress in the current bonding length and then the high shear stress localised in the bonding limit.

**Influence of the prestress level on the average shear stress**

The external prestress of composite increases the shear stress in the adhesive bonding length. The value of the shear stress along the bonding length is given as a function of the prestress level. Firstly high shear stress are localised in the bonding limit (0-50 mm). Secondly the shear stresses reach an average value. Important point to outline is that this value of shear stress depends on the composite prestress. That will increases the creep in the adhesive and the loss in the adhesive and the loss of stress within the composite.

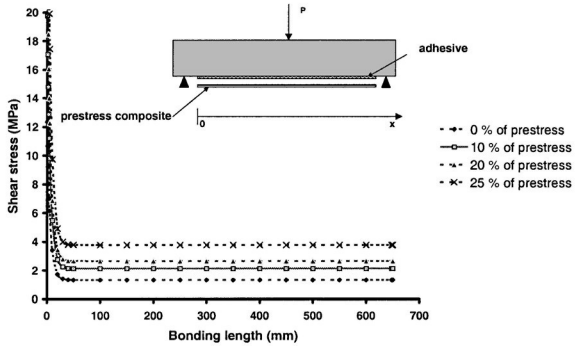



Figure 3. Evolution of stress in the bonding length (zone 1)

**Influence of the prestress level on the maximum shear stress**

The figure 4 illustrates the variation of maximal shear stress (in the bonding limit) as a function of anchorage length and composite prestress level. Locally the analytical result shows an important increase in stress on the last few centimetres of the bonding area (figure 3). Those high shear stress combined with peeling stress [Täljsten, 12] contribute to the interface split and delamination [9, 10, 11]. During the beam loading this local high stress increase and reach a critical value. Then the failure is propagated nearby bonding length. The level of high shear stress depends on the level of composite prestress (Nc) and the composite anchorage length.

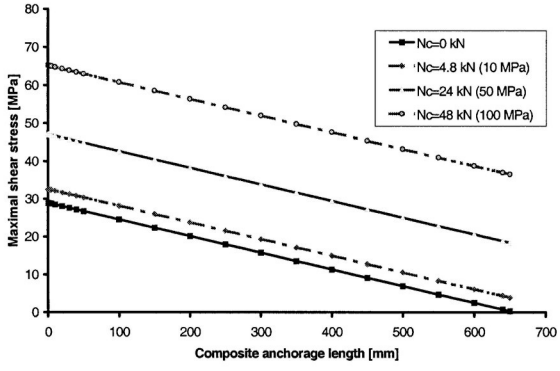



Figure 4. Evolution of shear stress in zone 2 bonding length

Those results explain the importance of anchorage of such prestress reinforcement. On the basis of this study, we describe an experimental work to verify first the loss in stress due to interface creep behaviour and then to evaluate the influence of anchorage length on the failure mode.

## EXPERIMENTAL WORK

Due to high shear stress level and to the increase adhesive creep, the loss of stress in the reinforcement increases as a function of time. During this experimental work, we have experimentally measured this loss of stress and tested up to failure beams in order to evaluate the high shear stress effect on the failure.

### Material characterization

*Concrete and steel*

The concrete used in this study has a nominal 28-day strength of 35 MPa, and a Young modulus of 35 GPa. The diameter of the tensile steel rebars is 4 mm, with usual properties (yield stress 550 MPa).

*Composites*

The CFRP plates bonded to the beam were made of from high strength carbon fibres fabrics manufactured by Replark. The fibres are applied by a wet-lay-up method using epoxy resin. Before application, a surface treatment is done by sand blasting, then epoxy putty is used to improve the adhesion on the concrete. The mechanical properties of all the materials are given in table1. The dimensions of the composite are 1.6 mm x 50 mm for all the beams.

Table 1: Material characteristics

| **Fibres** | **Carbon** |
|---|---|
| Young modulus (GPa) | 235 |
| Ultimate strength (MPa) | 3250 |
| **Polymer** | **Modified BPA epoxy** |
| Young modulus (GPa) | 3.2 |
| Ultimate strength (MPa) | 40 |
| Glass transition temperature Tg (°C) | 55 |
| **Composite** | **Carbon-epoxy** |
| Young modulus (GPa) | 62.5 |
| Ultimate strength (MPa) | 500 |
| Elongation (%) | 1 |

*Beam description and composite application*

The figure 5 shows the internal and external reinforcements of beams. Three beams of 1000 mm x 100 mm x 170 mm are considered. The first beam (beam 0) is reinforced with non-prestressed composite. The two others are reinforced with prestressed composite. The prestressed level is expressed as the ratio between the applied stress and the ultimate composite strength. This ratio is 0.30 corresponding to an initial concrete compressive stress of 4 MPa. The figure 6 shows the frame used for the application of the prestress on the composite fibres. For each configuration, the plate was initially positioned with its bonding surface and a small amount of prestress was applied so that the adhesive could be spread into the fabric.

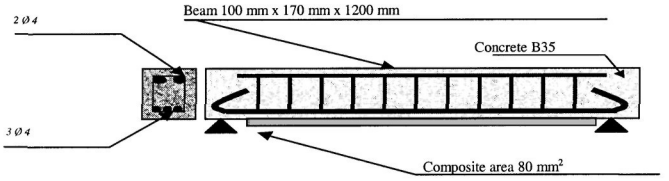



Figure 5. Internal and external reinforcement of beams

Electrical strain gauges were bonded on the bottom face of the composite. After a complete cure of the composite (7 days), the prestress was transferred into the concrete by releasing the jack. The length of composite material extending beyond the bond surface was removed from the prestressing frame.

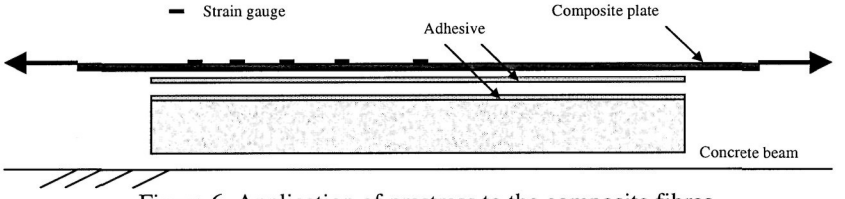



Figure 6. Application of prestress to the composite fibres

The instrumentation of the beams was complete with displacement transducer placed in the mid-span of the beam. Midspan deflections and plates strains were recorded by a Vishay micromesure datalogger. During the two first weeks after the prestress application, the stress levels is measured in both plates. After these two weeks the beams are tested to failure.

*Plate end anchorage systems used*

The figure7 describes the systems of plate end anchorage. On beams 0 and 2, no specific anchorage is applied. The composite is applied on bottom and lateral sides. On beam 1, the lateral composite completely wraps the beam section up. This last way of anchorage avoids slipping and peeling of the composite plate.




Figure 7. Plate anchorage system

**Evolution of composite prestress before loading**

*Influence of the anchorage on the loss of force*

During two weeks after the composite prestress, we have measured the strain level in the composite. The beam is unloaded all along this period. Three zones are observed. In a first zone, the high level of shear stress in the interface contributes to the immediate decrease of the composite stress (Fig.8 zone 1).

Then, the composite relaxation occurs due to the interface creep (figure 8 zone 2). Finally, the stress within the composite becomes stable (Fig.8 zone 3) because the interface shear stress is very low. The figure 8 shows the beams 1 and 2 on zones II and III of the relaxation. The loss in strain is more important when the reinforcement is non-anchored (15 % for 11 %). The loss in force on the beam 1 (11 %) may be explained by an unperfected anchorage system (lateral bonded plates).

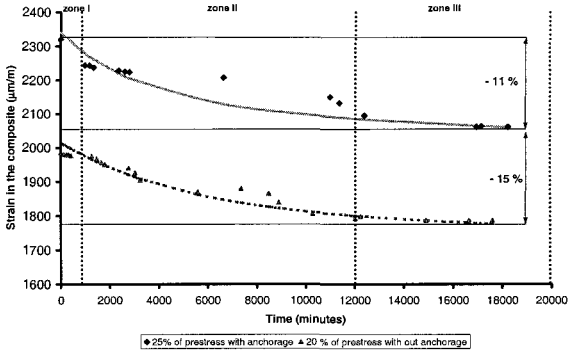



Figure 8. Evolution of the composite strain

*Influence of local high shear stress*

The figure 9 shows the evolution of loss in strain along the composite on beam 1. Four strains gauges have been bonded as described on figure 9. The variations of result given by the measurement may be explained by the shear stress distribution in the adhesive. Nearby the bonded limit, the shear stress is very high, the loss in strain is so very important (gauge 1 figure 9). In the current part of the bonded area, the strain loss is similar for the three gauges. These results prove that the loss in strain may be considered equal in the entire bonded zone, even if locally the loss of force nearby the plate end is important.

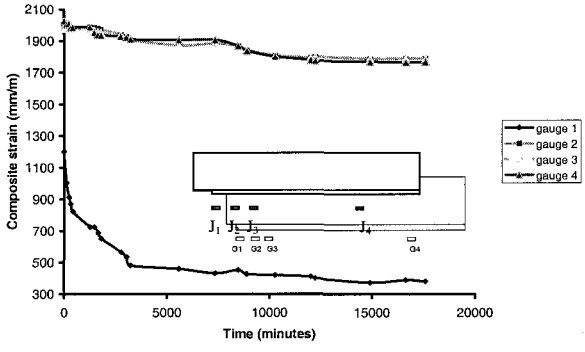



Figure 9. Evolution of composite strain for several positions on beam 2

*Evaluation of composite relaxation*

In order to calculate the level of prestress as a function of lifetime of the reinforcement, we use rheological model on zone II and III. We propose to estimate the loss of force for several levels of initial composite prestressing. The rheological model is described in figure 10. The parameters of this model are fitted with experimental relaxation data (on beams 1 and 2). This may be used in a design method to evaluate the level of composite stress as a function of time.

$$\varepsilon(t) = \varepsilon_e + \varepsilon_1 \cdot \exp(\frac{-t}{\tau_1}) + \varepsilon_2 \cdot \exp(\frac{-t}{\tau_2}) \quad (1)$$

$\varepsilon_e$ (μm/m): infinite relaxation strain, $\varepsilon_1$ (μm/m): relaxation strain of first mechanism, $\varepsilon_2$ (μm/m): relaxation strain of second mechanism, ,$\tau_1$ (mm): Time relaxation of first mechanism, $\tau_2$ (mm): Time relaxation of second mechanism

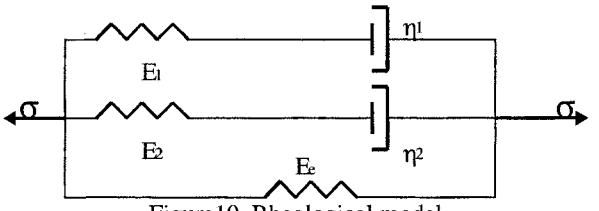



Figure10. Rheological model

Table 2. Rheological parameters

| | Beam 1 | Beam 2 |
|---|---|---|
| Infinite relaxation strain, $\varepsilon_e$ (μm/m) | 2000 | 1700 |
| Relaxation strain of first mechanism, $\varepsilon_1$ (μm/m) | 190 | 205 |
| Relaxation strain of second mechanism, $\varepsilon_2$ (μm/m) | 150 | 110 |
| Time relaxation of first mechanism,$\tau_1$ (mm) | $5\times10^3$ | $5\times10^3$ |
| Time relaxation of second mechanism,$\tau_2$ (mm) | $2\times10^4$ | $4\times10^4$ |

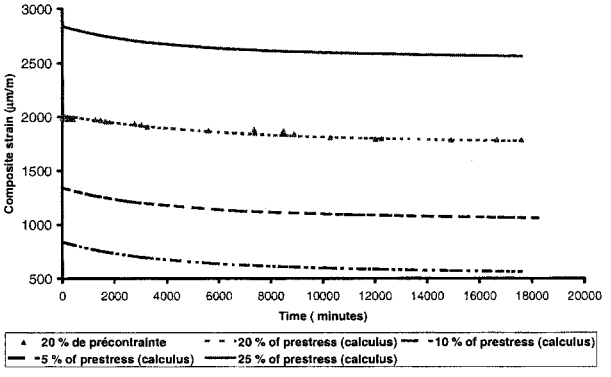



Figure 11. Relaxation in the externally bonded prestressed composite beam 2

Table 3. Relaxation of prestressed composite plate

| | Initial level of composite strain (μm/m) | Composite strain after 10 years (μm/m) | % of loss |
|---|---|---|---|
| Anchored composite | 2500 | 2000 | 20 % |
| Unanchored composite | 2500 | 1700 | 32 % |

For the design of RC beam with externally bonded prestressed composite, a reduction factor should be taken into account on the initial composite stress (for example 0.7 for a non-anchored reinforcement see table 3).

**Destructive bending tests**

Once we have verified that the interface creep behaviour cannot be neglected, destructive four-point-bending tests have been carried out. The load spacing in constant moment region is 300 mm. The prestress magnitudes of the beams are shown in fig 12. We have completed our comparison by using the software developed by Varastehpour and Hamelin [10]. This software is detailed in the following referenced paper [11]. We use the software to compare the behaviour of non-strengthened beam, prestress strengthened beam (beams 1 and 2) and strengthened beam without prestress (beam 0).

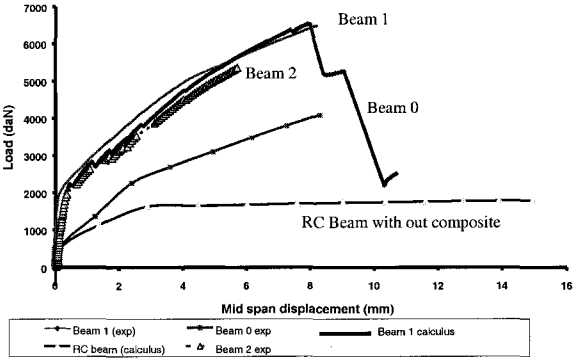



Figure 12. Load displacement curve (mix up of beam)

The table 4 gives information about the failure mode and the increase of ultimate load as a function of the reinforcement. This table proves the efficiency of the prestressing.

The figure 13 gives the evolution of composite strain during the loading. When the failure occurs on beam 2, the composite strain is 3000 μm/m. This small level may be explained by the composite debonding. In case of beam 1, the full composite capacity is reached (8500 μm/m).

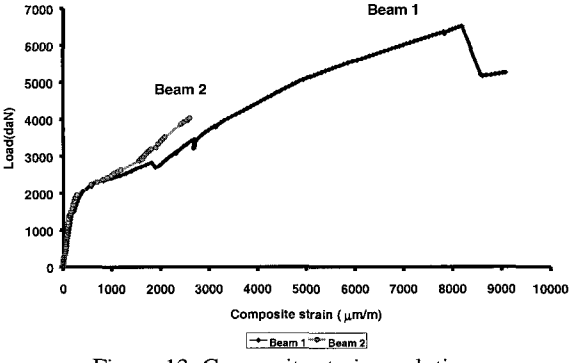



Figure 13. Composite strain evolution

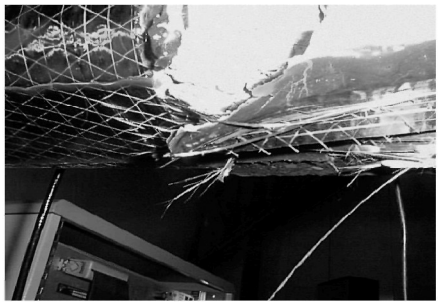
Table 4. Destructive test results

| | Beam 0 | Beam 1 | Beam 2 | Beam 3 (RC beam) |
|---|---|---|---|---|
| Ultimate load (kN) | 40 | 65 | 50 | 18 |
| Gain (%) | 122 | 261 | 177 | 0 |
| Failure mode | Composite | Composite | Debonding | Concrete crush |

**Failure mode analysis**

In case of failure by peeling-off, failure occurs when the bonded composite plate becomes separate from the concrete beam with a layer of concrete still bonded to the plate. Beam 1 failed by plate fracture before compressive concrete damage could occur (Fig. 14b). The fracture initiated was at mid span, followed by several local fibres failure in the same zone. The failure mode is considerably influenced by the shear stress developing in the interface. This observation has been already done by Triantafillou. Our analytical model shows that in case of beam 2, the failure occurs for a local high stress of 25 MPa and for a total load of 4000 daN. When this limit is reached the debonding appears.

This result shows the importance of the composite anchorage in order to significantly increase the ultimate beam capacity, the end plate should be anchored.



(a) failure beam 1

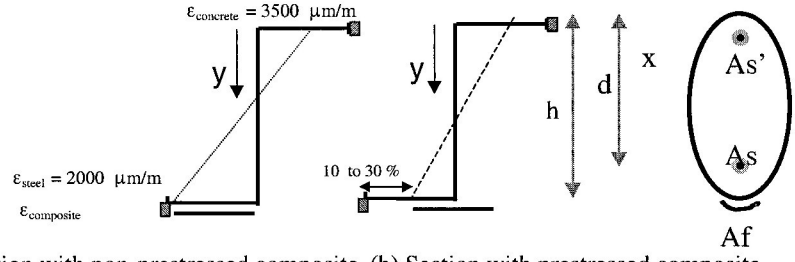


(b) failure beam 2

Figure 14. Failure mode

## CONCLUSION

The development of external bonded composite for structural reinforcement is limited by the structure serviceability conditions. The use of prestressed externally bonded composite is an effective method to increase the efficiency of external reinforcement. This reinforcement technique allows increasing the composite strain levels under structure loading. It also contributes to reduce the strain level in steel rebars. This effect is beneficial for structure serviceability conditions (Fig. 15).




(a) Section with non-prestressed composite (b) Section with prestressed composite

Figure 15. Strain distribution

The limit of this last reinforcement technique has been shortly described in this paper: the structural effect of interface shear stress with the loss in stress in the composite plate and the premature debonding of the plate. These researches enhance the importance of an appropriate adhesive selection and developing composite plate anchorage to reduce these effects.

## REFERENCES

[1] C. Resse et M. Venuat, 1981, *Projection des mortiers bétons et plâtres*, Techniques et applications bâtiment et TP

[2] R.L. L'Hermite, J. Bresson, 1967, *Concrete reinforced with glued plates*, RILEM, International Symposium on synthetic resins in building constructions, p. 175-203, 4–6 sept., Paris.

[3] U. Meier et al., 1992, Strenthening of structures with CFRP laminates : research and applications in Switzerland, ACMBS'1, Sherbrooke, Québec,Canada, p. 243-251.

[4] T. Triantafillou, 1998, *Shear strengthening of reinforced concrete beams using epoxy-bonded FRP*, Composites ACI structural Journal, Vol.95, March-April 1998

[5] H. Varastehpour, P. Hamelin, *Structural behaviour of reinforced concrete beams strengthened by epoxy bonded FRP plate*, Second international symposium on non metallic (FRP reinforcement of concrete structures), Ghent (Belgique), p 559-567, 23 august 1995.

[6] Mitsubishi chemical corporation, *Design guidelines of FRP for concrete structures*, Japanese standard association, 1986

[7] J.-L. Clément, Etude expérimentale et numérique du renforcement de poutres béton armé par collage de tissus à fibres de carbone TFC, XVIèmes rencontres universitaires de génie civil, Reims, p.164-171, 1998

[8] Sika, renforcement par le procédé SIKA CARBODUR Cahier des clauses techniques, CCT 37, 1998

[9] Triantafillou, T.C. and Deskovic, N. *Innovative prestressing with FRP sheets :mechanics of short-term behavior*, J. Eng. Mech., 1991, 117 (7), 1652-1672

[10] Wight, R.G. and al, Post-strengthening concrete beams with prestressed FRP sheets, Proceedings of the second international Rilem symposium on non-metallic reinforcement for concrete structures (FRPRCS-2), 1995, pp 568-575

[11] Saadatmanesh, H/ and Ehsani, *RC beams strengthened with GFRP plates. 1: experimental study*. J structur. Eng. 1991,117 (11), 3417-3433

[12] B. Täljsten, 1997, *Strengthening of beams by plates bonding*, Journal of materials in civil engineering, vol. 9, n°4, p. 206-212.

[13] H. Varastehpour, P. Hamelin, *Analysis and study of failure mechanism of RC beam strengthened with FRP plates*, second international conference on composite material for bridge and structure, Montreal (Canada), 11-15 august 1996.

[14] Bigaud D. and al, *Beam compo design: computer aided software for the design of reinforced and pre-stressed concrete beams strengthened by composite materials,* Advanced Composite Material in bridges and structures 3, Ed. Jagmohan Humar, A. Ghani Razaqpur 2000, pp. 405-412

# Non-linear Finite Element Analysis of RC Beams Prestressed with CFRP Straps.

GYAMERA KESSE, CATHERINE CHAN and JANET LEES
Department of Engineering, University of Cambridge, UK

## ABSTRACT
This paper reports on the finite element analysis of a reinforced concrete beam failing in shear. The analysis considers two beams: a control beam and a beam strengthened with CFRP straps. Experimental and FE results are compared. The results confirm the experimentally observed shear enhancement of concrete beams transversely prestressed with CFRP straps.

## INTRODUCTION
The current work investigates a finite element (FE) analysis of a concrete beam failing in shear. In particular, the effect of transversely pre-stressing a beam with external carbon fibre reinforced plastic (CFRP) straps is considered. The straps are located at discrete points along the shear span.

In the analysis of concrete with the finite element method, the first task is the selection of the right concrete model. Unfortunately, most existing models were developed to work on specific problems hence there is no single, general concrete model that can be implemented into an FE analysis. As a result, a preliminary study was carried out to aid in the choice of a robust model for the problem under consideration.

After the fundamental governing variables had been established, a control beam failing in shear was modelled. The model predicted peak load and deformations very well. The beam with pre-stressed CFRP straps was subsequently analysed. The results obtained from the FE analysis compared favourably well with the observed experimental results thus confirming the model reliability.

## PROBLEM BACKGROUND
The behaviour of reinforced concrete in shear is a challenging area. This is due to the many factors that influence the shear behaviour including the span to depth ratio, nature of loading (point load or uniformly distributed loading), proportion of steel and section dimensions. As a result, different theories have been developed to explain the mechanisms of shear failure. Three main factors have been proposed to account for the shear resistance of reinforced concrete beams:

- Dowel action
- Aggregate interlock
- Concrete in compression

*FRPRCS-5*, Thomas Telford, London, 2001.

However, the relative contribution of each of these factors is disputed. Thus, shear analysis becomes quite complicated since the factors being considered might not be relevant to a particular problem.

Consider an element of concrete subjected to pure shear. A crack will form perpendicular to the direction of the principal tensile stress and break the element into pieces. The load carrying capacity is thus reduced since the two pieces subsequently act independently. Any mechanism that can either reduce the tensile stress, or keep the two parts together, will have a profound effect on the load carrying capacity of this element.

## CARBON FIBRE REINFORCED PLASTIC STRAPS

The external CFRP straps act in two ways to improve the shear capacity. Because the strap is pre-stressed it puts the region where the major crack would form into compression. As a result, the shear stresses must overcome these compressive forces before inducing tensile forces which will lead to shear failure. Furthermore, after the crack forms, the strap keeps the elements together thus ensuring that the element carries shearing forces. However the CFRP straps are brittle materials and may snap if their breaking load is reached. This thus limits the level of pre-stress that can be induced.

## EXPERIMENTAL INVESTIGATION

Two T-beams were tested to investigate the proposed shear and strap behaviour. The first was a control beam which was designed to fail in shear. The second was a beam strengthened with CFRP straps. A summary of the testing and results is given below. (Full details can be found in [1].)

Both beams had the same cross-section dimensions but there were a few differences in the material properties of the two beams i.e. $f_c$, the concrete compressive strength, of the strengthened beam was 37.5 N/mm$^2$ and the bottom longitudinal reinforcement had a yield stress of 490 N/mm$^2$ whilst that of the control beam were 40.5 N/mm$^2$ and 400 N/mm$^2$ respectively (see Table 1). The beams were tested two weeks after casting.

The layout of the strengthened beam is shown in Fig. 1. The beam is symmetric so for clarity only half the beam is shown. Note that the control beam is similar to the strengthened beam except that there were no external CFRP straps.

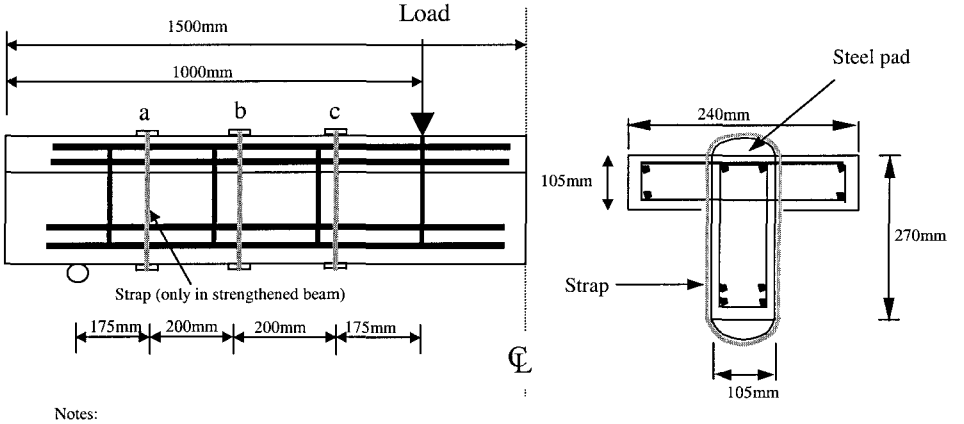
The straps were formed using a CFRP tape manufactured by Sulzer. The tape thickness is about 0.16 mm and has a width of 12 mm (see Winistoerfer [2] for full details). Ten layers of tape were wound around the interface steel pads that were placed on top and bottom of the beam. As the tape resin is thermoplastic, a closed loop was formed by fusion bonding the outer two tape layers over a length of approximately 60mm.

Strain gauges were placed on the outer layer of the straps and a hydraulic jack used to prestress the straps. Readings from the strain gauges were used to determine the level of prestress induced.

Metal shims were inserted underneath the interface steel pads, the jack released and the prestress force was transferred to the concrete. Three straps were applied to each shear span and each strap was pre-stressed to a force of about 30 kN (60% of its breaking load).

Table 1: Properties of control and strengthened beam

| | Control beam | Strengthened beam | Remarks |
|---|---|---|---|
| Concrete | | | |
| $f_c$ (14 days) | 40.5 N/mm$^2$ | 37.5 N/mm$^2$ | |
| $f_t$ (14days) | 3.6 N/mm$^2$ | 3.6 N/mm$^2$ | |
| Max aggregate size | 10 mm | 10 mm | |
| Reinforcement | | | |
| Bottom layer 1 | Fy=400 N/mm$^2$ | Fy=490 N/mm$^2$ | 20 mm Dia |
| Bottom layer 2 | Fy=490 N/mm$^2$ | Fy=490 N/mm$^2$ | 16 mm Dia |
| Links | Fy=380 N/mm$^2$ | Fy=380 N/mm$^2$ | 8 mm Dia<br>250 mm spacing |
| Top reinforcement | Fy=380 N/mm$^2$ | Fy=380 N/mm$^2$ | 8 mm Dia |
| CFRP strap | n/a | E=130,000 N/mm$^2$<br>Fult=50 kN | 10 layers |




Notes:
Straps d, e and f are symmetric about centreline and are not shown.
All dimensions are in mm

Section through pre-stressed beam

Fig 1: Schematic sketch of control and strengthened beam

## FINITE ELEMENT MODELLING

Although finite element analysis of concrete has been around for quite some time, there is no a single comprehensive model for concrete analysis. Most often, the parameters derived for a model tend to apply to that specific model and extrapolation to other models leads to numerous numerical problems. As a result, a parametric study is normally required to determine the necessary parameters for a particular problem. Parametric studies were performed on

- Softening curve: linear softening or non-linear Hordyk softening curve
- Failure criteria in compression: von-Mises or Drucker Prager
- Element type: 4 noded elements or 8-noded elements
- Criteria for cracking: combined tension and compression or tension only

Full details can be found in [3].

The parametric study showed that for the proposed 2-D model, the following input parameters gave good results

- Mesh sizing – 3 x aggregate size
- Crack band, $h_b$, is equivalent to mesh width
- Fracture energy, $G_f$ =100 N/m
- Linear softening curve with ultimate strain of $(2*G_f)/(f_t*h_b)$
- 4-noded elements with 4-point integration rule
- von-Mises yield criterion
- Criteria for cracking dependent on both tensile and compressive stresses
- Reinforcement is modelled with bar elements with 2 -point integration rules
- Support and load pads modelled using three-noded triangular elements

All the analyses were carried out using DIANA [4], a non-linear FE program. It should be noted that the parameters selected were chosen to ensure convergence at all stages of the analysis and also to ensure that the mode of failure was self-evident.

**Analysis**

A convergence criterion of $10^{-3}$ N(out of balance force at nodes) was used. The arc length method was combined with the constant stiffness method. This seemed to be the most effective solution technique. All the loading steps of the analysis converged. The FE mesh for the control beam and the FE mesh for the strengthened beam are shown in Figs 2 and 3 respectively.

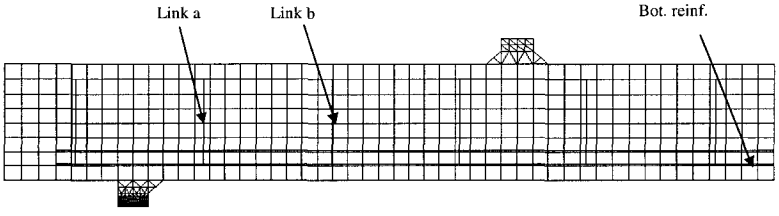
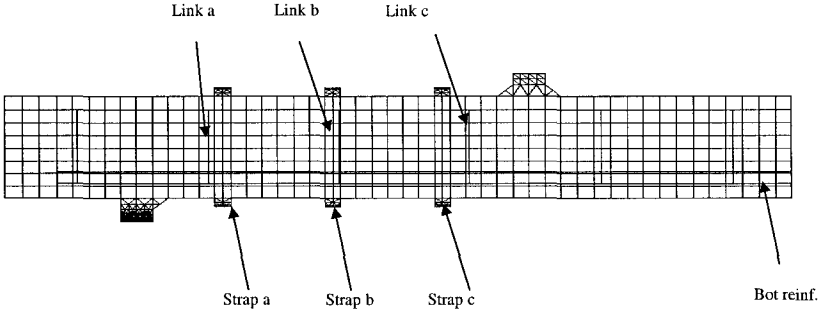



Fig 2: FE mesh for control beam



## CONTROL BEAM

### Load-deflection curve

Figure 4 shows the load deflection curve of the control beam predicted using the finite element model. The experimental results at midspan have been included in Fig. 4 for comparison purposes. The predicted results compare very well with the experimental results. However the FE model predicted a failure load of 113 kN and a final displacement of 15 mm whilst the experimental beam failed at 100 kN and 17 mm displacement.

### Failure Modes

An analysis of the crack pattern gave insight into the mode of failure (see Table 2). The sequence shown thus illustrates a classical shear failure. At the midspan, the maximum compressive strength of concrete was not attained at the top fibre.

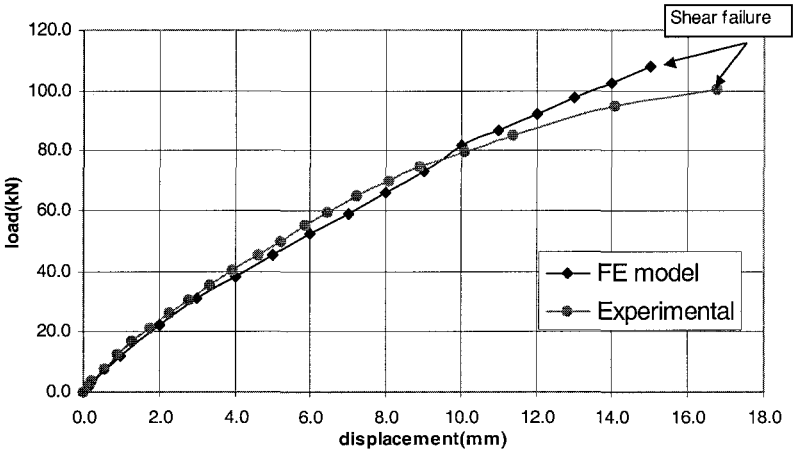



Fig 4: FE results of Control beam

### Stresses in the reinforcement predicted by FE model

Figure 5 shows the stress increase in selected reinforcement bars. The internal steel reinforcement layout is shown in Fig. 2. Initially the stresses in the bottom reinforcement increased steadily whilst the stresses in the vertical links were virtually zero. At a load of 46 kN the behaviour changed and the stresses in the links increased drastically. From 46 to 75 kN the link at position b had a stress increase from zero to the yield stress. Link a also yielded but this event occurred almost at the same time as the yielding of the bottom reinforcement.

The results showed that the model was able to capture all the relevant aspects of a beam failing in shear and the predictions appear to be reliable. The next stage was to incorporate the external CFRP straps in the analysis.

Table 2: - Results compiled from crack patterns

| Load (kN) | Experimental observation | FE inferences | FE remarks |
|---|---|---|---|
| 12 | Flexural and web shear cracks are visible. First web shear crack appeared at 11 kN. | Flexural cracks are the only visible cracks. | The closest web shear crack is under the loading point. |
| 37.7 | | Flexural and web cracking. | The web cracks continue to form in the shear spans. The flexural cracks propagate upwards and a well-defined crack spacing is achieved. |
| 40.8 | Cracks continued to appear at the bottom of the web extending upwards and turning towards the load point. | Web shear cracks have started to branch. Flexural cracks propagate vertically. | The web crack closest to loading point seems to be most active. |
| 51.5 | | Web shear cracks are spreading underneath the flange of the beam. | More cracks appear in the region close to the support. |
| 64.2 | | Extensive web cracks are noted underneath the flange and the cracks are spreading towards the support. | |
| 78 | A large shear crack was observed at 70 kN. Crack width approximately 1 mm. | Web cracks seem to start in the flange. Cracks are very close to the support. | |
| 84.6 | Biggest crack originating from the support extends from support to load point. | Cracks penetrate flange slightly. | |
| 113 | Experimental beam failed at 100 kN. | The closest element to the loading point cracks joining the already cracked flange elements. | This implies a continuous crack from load to support. Pending failure of FE beam. |
| 112.8 | | | The load drops and the solution fail to converge. Attempt to restart wasn't possible. |

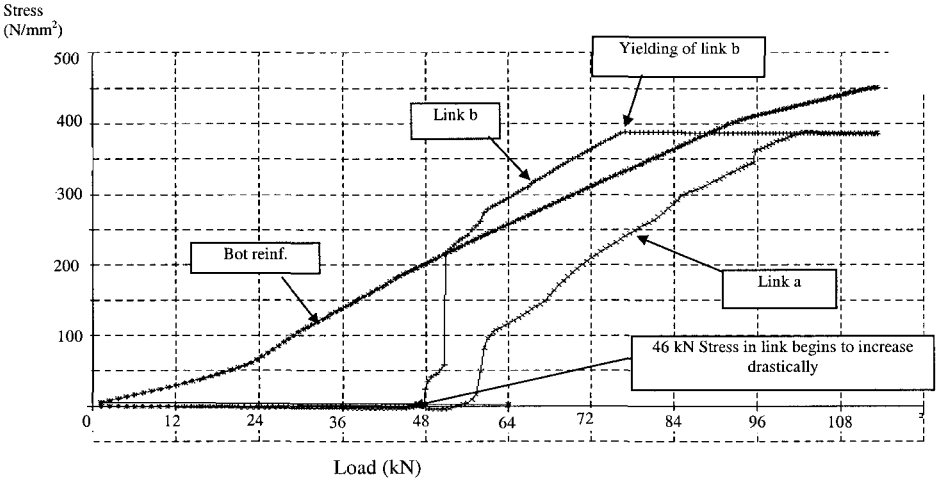



Fig 5: Stress in selected reinforcement bars predicted by FE model

## PRE-STRESSED BEAM

The FE model developed for the control beam was utilised with some modifications. The straps were introduced by modelling the steel interface pads and using a bar reinforcement to connect the top platen to the bottom platen.

### Pre-stressing

Figure 6 shows the cross section of the beam with an external CFRP strap. Although the problem is three-dimensional in nature, in the current work, a two-dimensional finite element model was used. It was therefore necessary to check how the pre-stress would be transferred from the strap to the web and flange of the beam.

For the actual beam the pre-stressing force compresses the rectangular region as shown in Fig. 6a. Figure 6b shows the equivalent FE model. In this case, a uniform pre-stress was applied to the strap. This results in forces $F_w$ and $F_f$ on the web and flange respectively. However, because the flange width is bigger than that of the web, the pressure on the flange is smaller. Hence the pressure $P_f$ is less than $P_w$. However, this effect seems to have negligible effect on the overall analysis hence it was implemented.

The pre-stressing forces were applied in 10 load steps. Checks were made on the regions of the corners of the interface pads to see if there was any cracking. No such cracking was observed in the experiment or in the model.

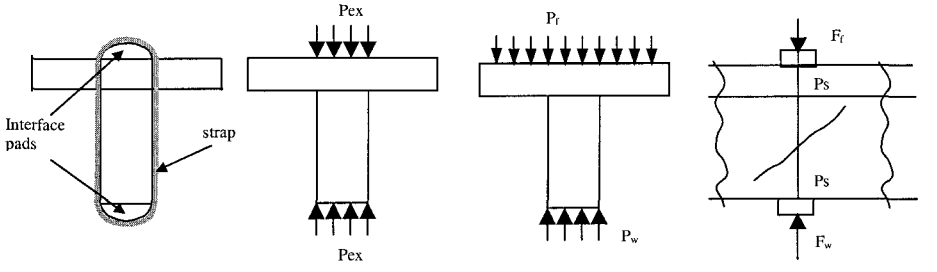



Fig 6: Comparison of Experimental and FE model for pre-stressing

### Load-deflection curve

Figure 7 shows the predicted and experimental load deflection curves for the strengthened beam. The model predicted a peak load of 135 kN and a deflection of 17.7 mm whilst the experimental beam failed at 148 kN and deflected by 22 mm. The accurate prediction of the stiffness was impressive.

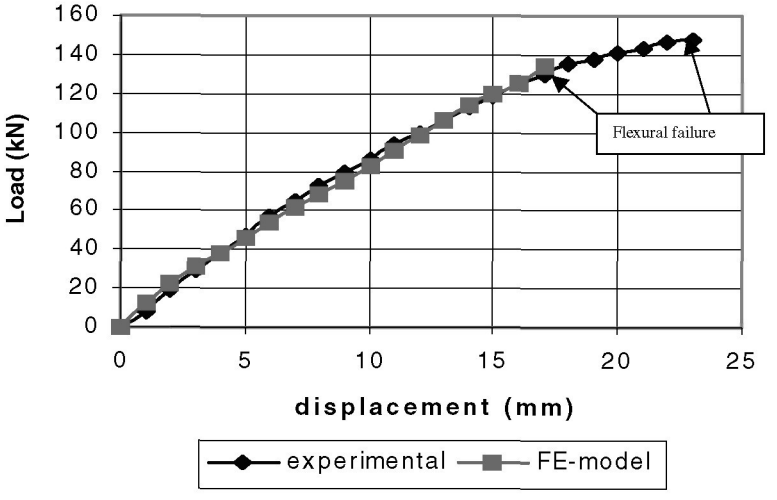



Fig 7: Load displacement curve of FE model and experimental beams

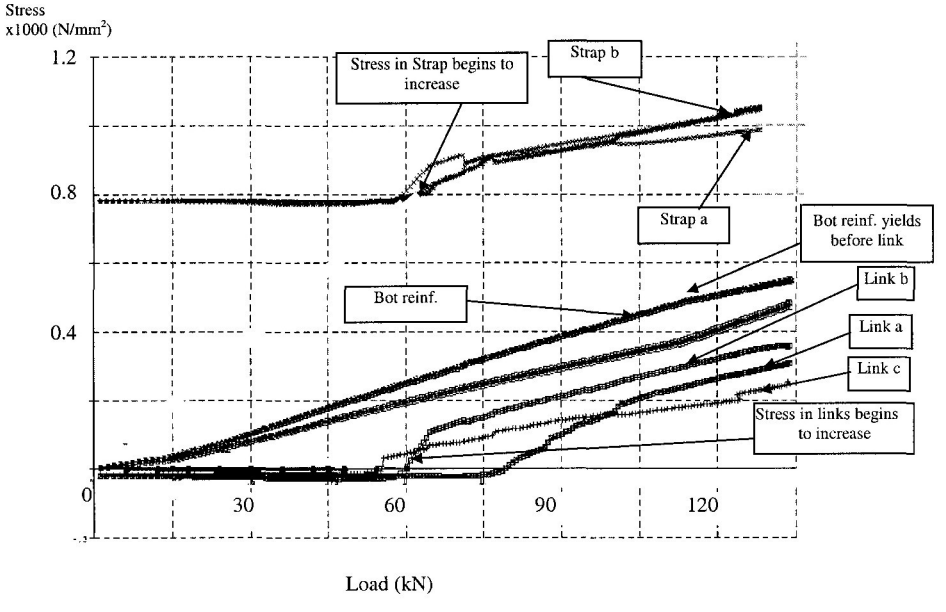



Fig 8: Stress in selected reinforcements and straps

**Failure modes**

In contrast to the control beam which exhibited a brittle shear failure, the strengthened beam failed due to yielding of the longitudinal reinforcement. The strength enhancement was approximately 50%. A comparison of the experimental and FE observations can be found in Table 3.

Table 3-Results from pre-stressed crack pattern

| Load (kN) | Experimental observation | FE inferences | FE remarks |
|---|---|---|---|
| 13.1 | First flexural crack appeared at 7 kN whilst a shear crack appeared at 11 kN. | Flexural cracks are the only visible cracks. | |
| 17.6 | | Flexural cracks in between straps b and c. | Web cracks occurred at 16kN. |
| 25.8 | Flexural cracks propagate upwards. | Flexural cracks propagate upwards. Web cracks attempt to cross strap. | Flexural cracks extend upwards. |
| 32.4 | | Flexural cracks extend vertically upwards. | |
| 46.5 | | Web cracks extending in web and some cracks crossing strap b. | |
| 53.1 | | Web cracks start to branch. | |
| 78.6 | Cracks are near support. Cracks begin to cross strap at 80 kN. | Web cracks spread between straps and flexural cracks continue their upward growth. | Cracks start to cross straps. |
| 92.4 | A big crack crosses strap e at 105 kN. | Web cracks spreading towards the support. | |
| 127.8 | | Intense cracking in the web. | |
| 133.2 | | Spalling of concrete on the right hand side of load pad. FE model fails. | |
| 148 | Crushing of compression flange. Load drops. Beam fails in flexure. | | Experimental beam failed at 148kN. |

**Stresses in the reinforcement**

The effect of the straps can be seen in Fig. 8. There was virtually no increase in the strap stresses until a load of about 63 kN. This compares very well with a value of 65 kN inferred from the strap strain readings measured during the experiment. The selected reinforcing elements chosen for discussion are shown in Fig. 3.

The stress increase in the links was gradual and commenced at a load of about 65 kN. The bottom reinforcement yielded before the links which is in contrast to the behaviour of the control beam. When the beam failed in flexure, the force in the straps was about 45 kN. This was quite close to the strap breaking force of approximately 50 kN.

**Results and discussion**

From the results discussed so far, the FE model predicted the beam behaviour well and has given insight into the problem. The differences in the ultimate load and deformation may be due to unintended influences of the loading plate. The plate seems to initiate stress localisation in the regions close to it. However, this also happens in experiments.

## CONCLUSION

The use of external CFRP straps proved to be an effective means of increasing the shear capacity of a reinforced concrete beam. The failure load of the strengthened beam was approximately 50% higher than that of the control specimen.

The beam behaviour was accurately predicted using the proposed FE model. In particular, the model was able to detect the brittle shear failure of the control specimen and the ductile flexural failure of the strengthened beam. Nevertheless it was found that the careful selection of the FE input parameters was crucial in the development of reliable model.

It is envisaged that the FE model will be a valuable tool in determining the optimum strengthening parameters such as the level of prestress, number of straps and strap spacing.

## REFERENCES

1. Chan, C. K. M., 2000, Prestressed Non-laminated Carbon Fibre Reinforced Plastic Straps, Fourth Year Project, Group A, Department of Engineering, University of Cambridge, UK.
2. Winistoerfer, A. W., 1999, Development of Non-laminated Advanced Composite Straps for Civil Engineering Applications, PhD Thesis, University of Warwick, UK.
3. Kesse, G., 2000, Finite Element Analysis of Concrete with Intermittent Prestress, MPhil Thesis, University of Cambridge, UK.
4. DIANA User's manual, 1998, Release 7, Nonlinear Reference Manual, TNO Building and Research.

# Strengthening of concrete structures with prestressed and gradually anchored CFRP strips

I. STÖCKLIN and U. MEIER, EMPA, Dübendorf, Switzerland

## ABSTRACT

Today post-strengthening of structures with externally bonded CFRP strips is state of the art. To take full advantage of this expensive material, it is beneficial to apply the strips in a prestressed state. This relieves the stresses in the internal steel reinforcement and reduces crack widths and deflections. Due to the limited shear strength of concrete, the high shear stresses at the ends of the strips cannot be transferred into the structure. To prevent premature failure of the system, the strips have to be anchored with special devices. Those are expensive, difficult to install and often subject to corrosion. These are the major reasons why prestressed, externally bonded CFRP strips have not yet been used in practice.

To overcome these anchorage problems, the prestressing force can be reduced gradually towards both ends of the strip. The result is an increased development length of the prestressing force such that the occurring shear stresses remain within the limitations of concrete. This can be achieved by using a purposely developed pretensioning device which allows the CFRP strips to be bonded to the concrete structure using a stepwise approach.

## INTRODUCTION

Post-strengthening of a structure is necessary when its safety under the specified loads is no longer guaranteed. For example poor workmanship, an increased payload or deterioration of the structure due to corrosion or mechanical influences, may require a strengthening of the structure.

Construction companies all over the world are looking for an easy, cost-effective and reliable way to enable these works. In case of bridges it is important not to interrupt the traffic or at least to reduce the interruption to a minimum. Therefore, the application has to be highly automated.

## EXTERNAL REINFORCEMENT WITH CFRP STRIPS

In 1969 the first structures have been strengthened with externally bonded steel plates. But these steel plates are heavy, have limited length and are subject to corrosion.

To overcome the disadvantages with these steel plates, non-prestressed carbon fibre reinforced plastic (CFRP) strips can be used. For about four years this technology is state of the art and is used by many companies throughout the world. These CFRP strips with a width of 50 mm to 150 mm and a thickness of approx. 1 mm are bonded with an epoxy-based adhesive to the pretreated concrete surface. The CFRP strips are lightweight, can be transported and stored rolled up and are produced in almost unlimited length. To take full advantage of this very expensive material, the CFRP strips should be prestressed. This relieves the stresses in the steel reinforcement and reduces crack widths and deflection. Furthermore, it results a better fatigue behaviour of the structure [1].

*FRPRCS-5*, Thomas Telford, London, 2001.

## ANCHORAGE OF PRESTRESSED CFRP STRIPS

### Premature failure

The major drawback is the occurrence of very high shear stresses at the ends of the strips (Fig. 1). Hence, the prestressing force cannot be transferred into the structure due to the limited shear strength of concrete. To prevent premature failure of the system as shown in Fig. 2 the strips have to be anchored at their ends for example by the use of pressing plates. These anchorages are a key element of the system. They are expensive and difficult to install. A failure of the anchorage would cause a total failure of the strengthening system due to peeling off of the CFRP strip. These are the major reasons why prestressed, externally bonded CFRP strips have not yet been used in practice.

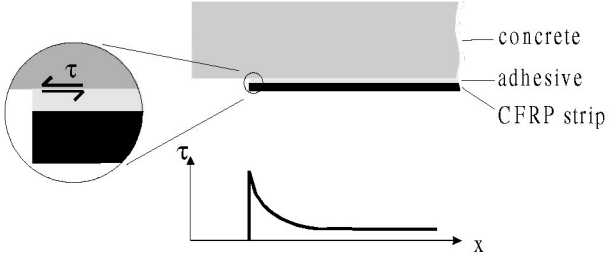



Fig. 1: Shear stress peak at the end of prestressed a CFRP strip [2].

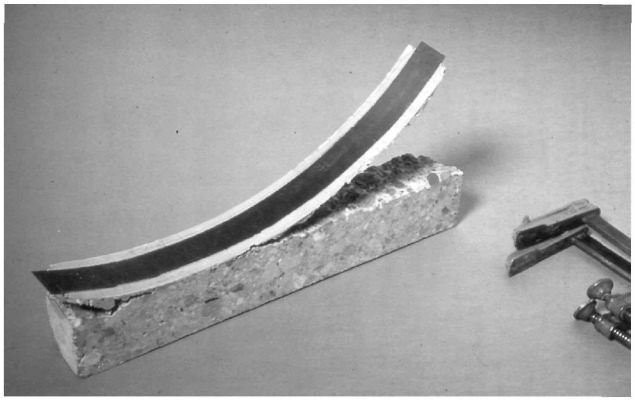


Fig 2: Premature failure of a prestressed CFRP strip without anchorage immediately after the prestressing force has been relieved. The shear strength of concrete is not sufficient to transfer the very high shear stresses into the structure. The CFRP strip starts to peel off from its ends due to premature failure in the concrete. To prevent such failure, the ends of the strip have to be anchored, e.g. by pressing plates.

**Gradually anchored CFRP strips**

To overcome these anchorage problems, the prestressing force, $F$, can be reduced gradually towards both ends of the strips. The result is an increased development length of the prestressing force such that the occurring shear stresses are within the limitations of the shear strength of concrete.

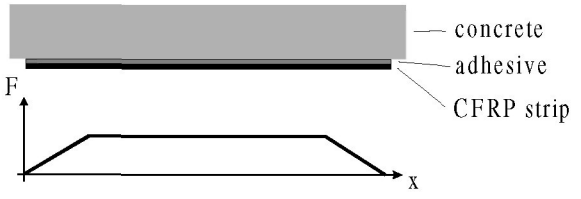



Fig. 3: Gradual anchorage of prestressed CFRP strips

**PRESTRESSING DEVICE**

To prestress a CFRP strip and to generate this gradient in the prestressing force, a new type of prestressing device was designed (Fig. 4 and 8). It enables to prestress a CFRP without the need of a preliminary anchorage device on the CFRP strip (e.g. bonding of brackets).

The developed prestressing device consists of two revolving cylinders which are connected to a beam of the required length (Fig. 4). The CFRP strip (1) is wrapped around the cylinders (2) and clamped at its ends (3). By rotating (4) the cylinders, the strip can be prestressed.

The prestressing device with the prestressed CFRP strip is temporarilly mounted to the structure. By using an air-cushion (5) between the strip and the beam, the CFRP strip can be pressed against the structure with a constant pressure. The pressure in the air-cushion is between 100 mbar and 200 mbar.

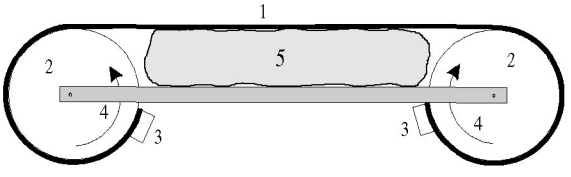
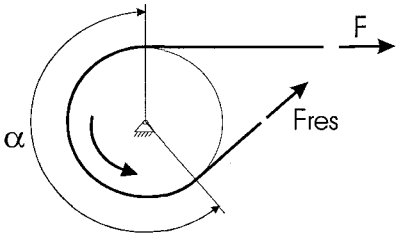



Fig. 4: Prestressing a CFRP strip. The CFRP strip is on the very top of the device and can be applied directly to the pretreated structure without any additional work at the structure itself.

By wrapping the CFRP strip around the cylinder, the remaining prestressing force, $F_{res}$, in the clamp on the cylinder is reduced by the friction of the CFRP strip on the cylinder (Fig. 5). It is desirable to have a high coefficient of friction, $\mu$. The higher the friction, the lower is the remaining force in the clamps (3). The coefficient of friction is approx. 0.29 between a CFRP strip and steel. To increase the coefficient of friction between the cylinder and the CFRP strip, a strip of a special film can be placed between them. The resulting coefficient of friction is about 0.57.

The decline of the prestressing force due to the friction on the cylinder can be calculated with equation (1).




$$F_{res} = F \cdot \frac{1}{e^{(\mu \cdot \alpha)}} \qquad (1)$$

Fig. 5: Reduction of prestressing force due to friction on the cylinder.

The theoretical results have been verified with experimental data (Fig. 6). For this purpose, a CFRP strip has been equipped with a number of strain gauges in the wrap area.

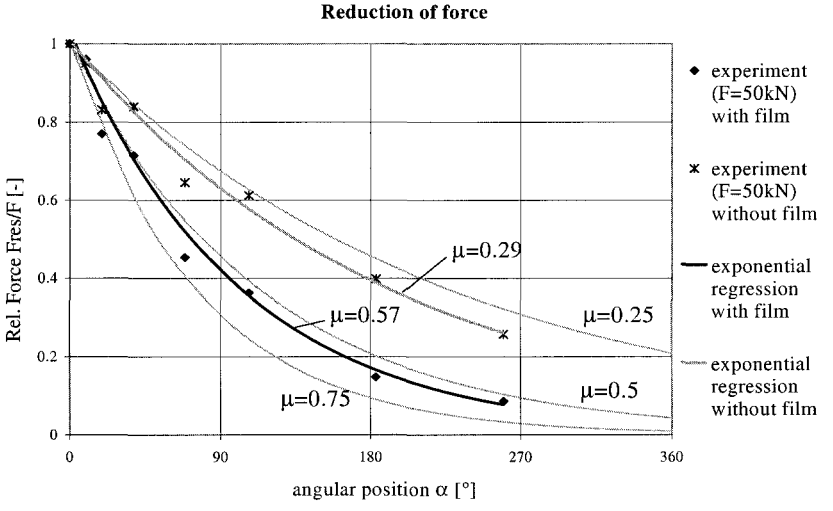



Fig. 6: Decrease of the prestressing force in the CFRP strip as a function of the angular position on the cylinder. By using a film, the remaining prestressing force at the clamp of the strip is about a tenth of the initial force. A simple pressing plate can be used to temporarily clamp the CFRP strip to the cylinder.

The stresses in the strip caused by prestressing are superimposed by stresses caused by bending the strip around the cylinder. This fact has to be considered for determining the diameter of the cylinder.

## GENERATE GRADUAL ANCHORING

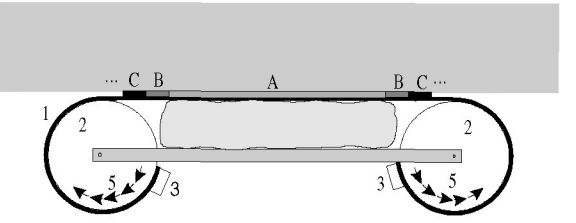



Fig. 7: Generating gradual anchoring using a stepwise approach

To generate a gradually anchored CFRP strip, as shown in Fig. 3, a stepwise approach is used. The CFRP strip (1) is clamped and prestressed on the prestressing device and covered with adhesive. The device is temporarily mounted to the structure. The middle part of the strip (Fig. 7) is bonded (A). Then, the force is marginally reduced (5), and the following areas (B) are bonded. The force is reduced further (5) and the adjacent areas (C) are bonded. This procedure is repeated until there is no remaining prestressing force at the ends of the strip. After that, the prestressing device can be removed immediately. The adhesive is completely cured.

For a stepwise bonding of the adhesives, each section is equipped with an electrical heating device. By using a heating device, the curing-time of the epoxy-based adhesive can be reduced considerably. This way, it is possible to control the curing process in the various sections. The used adhesive in the experiment is the commonly used Sikadur-30.

## RESULTS

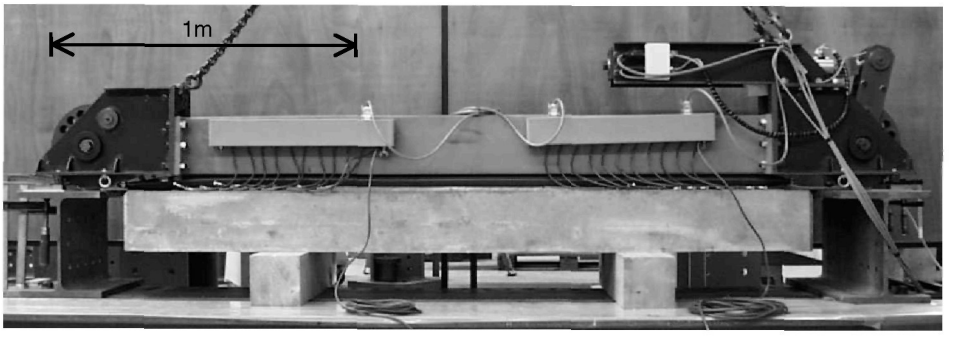



Fig 8: Prestressing device in use. A CFRP strip is bonded to a concrete specimen for a laboratory experiment. Max. length 10 m. Max. prestressing force 60 kN.

A prototype of the prestressing device has been built (Fig. 8). The prestressing force is generated by a electrical spindle drive. The speed at which the CFRP strip is prestressed can be varied between 0.05 mm/s and 0.5 mm/s. The maximal Force is 60 kN. The maximal length can be varied by changing the length of the beam, which is restricted to 10 m due to buckling problems. The prestressing device is completely automated. The force in the strip, the heating of the different sections and the temperature of the curing adhesive are controlled by a computer.

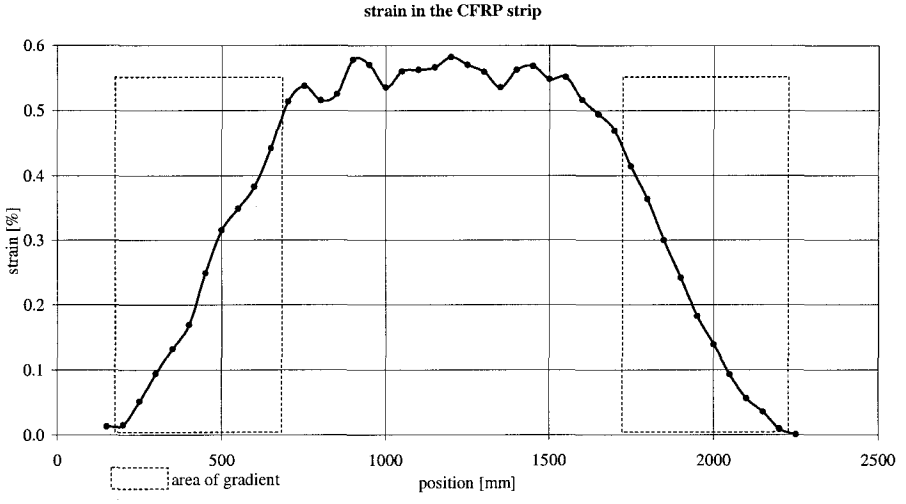



Fig. 9: Strain curve of a bonded prestressed CFRP strip (thickness: 1.15 mm, width: 50 mm, Young's-modulus: 160 GPa) on a concrete specimen. The prestressing force in the middle part is approx. 50 kN.

The prestressed strip shown in Fig. 9 has been observed over a period of 125 days. There was no measurable loss of prestressing force in the CFRP strip.

## CONCLUSIONS

Strengthening of concrete structures with CFRP strips is state of the art. By prestressing these strips, the effectiveness of the reinforcement can be improved considerably. However, it has not yet been used in practice due to anchorage problems at the end of the strips. To overcome this problem the strips can be bonded with a decreasing prestressing force towards their ends. To generate this gradient a prestressing device was designed at which the strip is wrapped partly around a cylinder. This way, the prestressing force at the clamp of the strip can be reduced considerably, depending on the coefficient of friction between the strip and the prestressing device. This coefficient can be increased by using a special film between the two friction partners. The use of an air-cushion provides an easy and comfortable way to press the strip against the structure during the entire curing process. The gradient is approached by a stepwise bonding with decreasing prestressing force. The result is a prestressed CFRP strip without any external anchorage systems. In the near future, experiments on concrete beams reinforced with prestressed CFRP strips will show the performance capability of this system.

## References

[1] Martin Deuring (1993), "Verstärken von Stahlbeton mit gespannten Faserverbund-werkstoffen", EMPA Dübendorf Bericht Nr. 224

[2] Peter Holzenkämpfer (1997), "Ingenieurmodelle des Verbunds geklebter Bewehrung für Betonbauteile", Beuth Verlag GmbH Berlin

# FRPs in seismic conditions

# Advanced Wrapping System with CF-anchor - Seismic strengthening of RC columns with Wing Walls

K. MASUO and S. MORITA, General Building Research Corporation, Osaka, Japan
Y. JINNO, Shimizu Corporation, Tokyo, Japan
H. WATANABE, Taisei Corporation, Tokyo, Japan

## INTRODUCTION

The failures of columns with wing walls caused severe damages of exiting RC buildings in the 1995 Hanshin-Awaji Earthquake (1). One reason for the failures of these columns was that the increased rigidity resulting from the connection with wing walls resulted in the concentration of earthquake forces on these columns in comparison with isolated rectangular columns. The other reason was the decreased ductility of such columns under horizontal loading. Therefore the strengthening of these columns becomes an important task for the seismic retrofitting of exiting RC buildings.

Masuo studied some strengthening methods using CFRP sheet jacketing (1). He clarified that the wrapping of CFRP sheets around columns was effective in improving their ductility. In this method, both wing walls were cut off from the column, and then CFRP sheets were wrapped around the column. However, this type of construction is difficult to accomplish in exiting building.

In the present wrapping system with CF-anchors, after CFRP sheets are horizontally set on the column faces with impregnating epoxy resign, CF-anchors are jointed to CFRP sheets by passing the anchor strands through the penetrating holes of the wing walls next to the column face, as shown in Fig. 1. In order to clarify the strengthening effects of this method, column specimens with wing walls were tested under in-plane and out-of-plane horizontal load, respectively. This paper shows the results of this experiment and presents a method for estimating the improvements of this strengthening method.

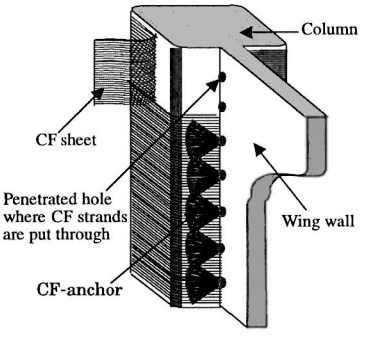



Fig. 1 Idea of CF-anchor

## IN-PLANE LOADING

### Test program

In this series, thirteen specimens were tested, as shown in Table 1. The test parameters were (1) type of reinforcement, (2) position of wing wall, (3) axial force level, (4) length of wing wall, (5) thickness of wing wall, (6) type of anchor system, and (7) number of layers of CFRP sheet. Specimen WI3 was the fundamental specimen, and specimen WI5 was completely wrapped with CFRP sheets around the column. These were compared with the other specimens using CF-anchors. Notations are defined as follows.

N : Axial force,
b, D : Width and depth of column,
$t_w$ : Thickness of wing walls
$\sigma_B$ : Compressive strength of concrete
$\beta$ D : Length of wing wall

Fig. 2 shows the configuration of test specimens and Fig.3 shows the arrangement of CFRP sheets and CF-anchors. Specimen scale was about 1/2 of actual building scale. Dimensions and reinforcement arrangements of all columns coincide with each other.

The width of each CFRP sheet for all of the specimens was 120 mm or 160 mm, and coincided with the spacing of wall horizontal reinforcements. A CF-anchor was produced with a CFRP strand which was composed of the same carbon fiber strings used in a CFRP sheet. Also, a vertical CFRP sheet was set on the end of the horizontal CFRP sheet to enhance the bond strength of CF anchors. The mechanical properties of materials used are shown in Table 2.

Table 1 Outline of in-plane loading test

| Specimen | Test Parameters | | | | | | |
|---|---|---|---|---|---|---|---|
| | (1) | (2) | $N/\sigma_B bD$ | $\beta$ | $t_w/b$ | (6) | (7) |
| WI1 | [D] | [C] | 0.2 | 1 | 1/4 | CF | 0 |
| WI2 | | | | | | | CF1 |
| WI3 | | | | | | | CF2 |
| WI4 | | | | | | | CF3 |
| WI5 | | | | | | Com | CF2 |
| WI6 | | | | | 1/3 | CF | CF2 |
| WI7 | | | | 0.5 | 1/4 | | 0 |
| WI8 | | | | | | | CF2 |
| WI9 | | | | | 1/3 | | CF2 |
| WI10 | | | 0.4 | 1 | 1/4 | | CF2 |
| WI11 | | [E] | 0.2 | 1 | 1/4 | | 0 |
| WI12 | | | | | | | CF2 |
| WI13 | [R] | [C] | 0.2 | 1 | 1/4 | | CF2 |

【Parameters】
(1) Type of reinforcement for main bar of column
[D] : Deformed bar, [R] : Round bar
(2) Position of wing wall
[C] : Centrally, [E] : Eccentrically
(6) Type of anchor system
CF : CF-Anchor, Com : Complete wrapping
(7) Number of layers of CFRP sheet
0 : Unstrengthening
CF1 : one layer of 150 g/m$^2$ sheet
CF2 : one layer of 300 g/m$^2$ sheet
CF3 : two layers of 300 g/m$^2$ and 150 g/m$^2$ sheets

### Loading method

In this test, the specimens were subjected to repeating horizontal force under constant axial force. The test equipment provides that both end stubs of the specimen remain parallel with each other in the horizontal direction (1).

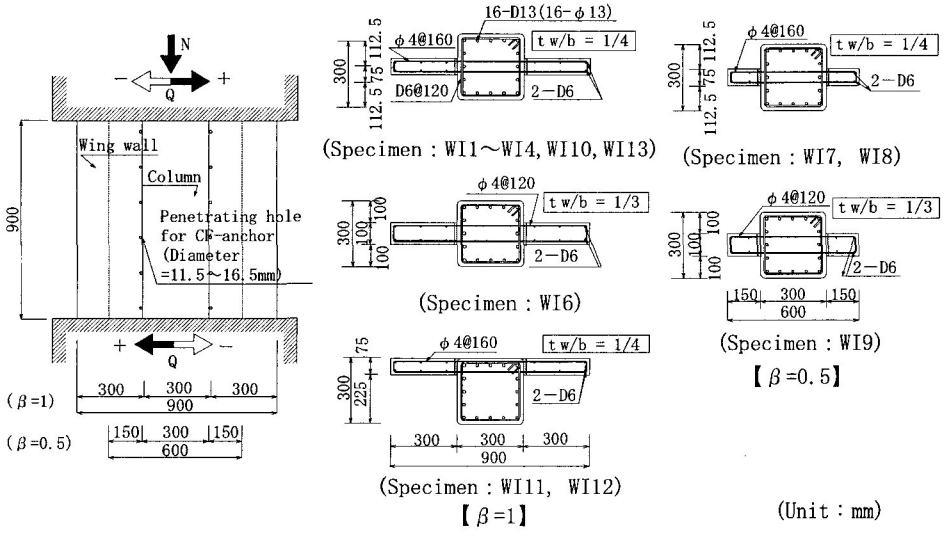



Fig. 2 Configuration of test specimens under in-plane loading

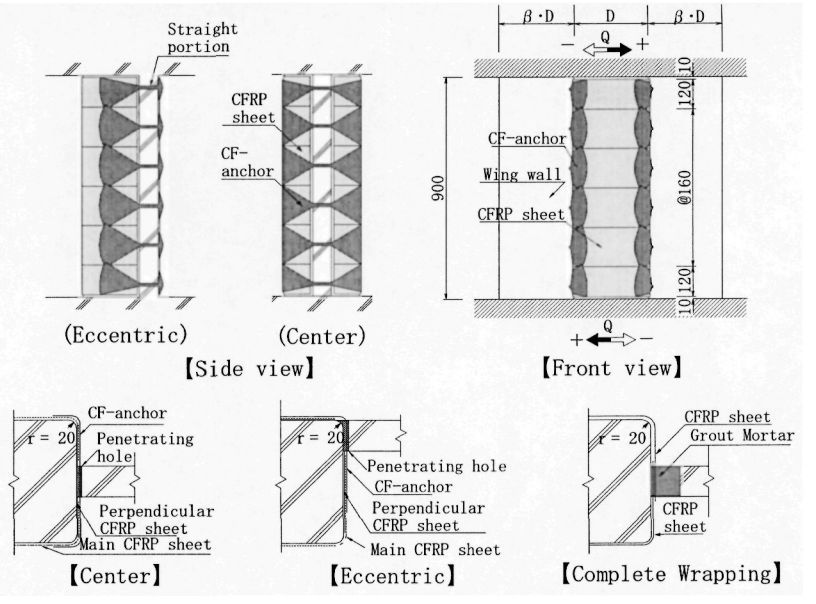



Fig. 3 Arrangement of CFRP sheets and CF-anchors

**Effects of strengthening**

The failure modes and the relation between shear force and drift angle of the typical specimens are shown in Photo. 1 and Fig. 4. Unstrengthened specimen WI1 failed in shear with diagonal shear cracks at 0.6/100 radian of drift angle.

Table 2 Mechanical properties of materials

(a) Concrete and grout mortar

| | | $\sigma_B$ (MPa) | $\varepsilon_{co}$ (%) | $E_c$ (GP) |
|---|---|---|---|---|
| In-plane loading | Concrete | 32.2 | 0.21 | 29.1 |
| | Grout Mortar | 52.9 | 0.56 | 23.3 |
| Out-of-plane loading | Concrete | 34.0-38.0 | 0.21-0.22 | 28.7-29.7 |
| | Grout Mortar | 57.9 | 0.52 | 23.6 |

$\sigma_B$ : Compressive Strength, $\varepsilon_{co}$ : Strain at $\sigma_B$, $E_c$ : Young Modulus

(b) Reinforcement

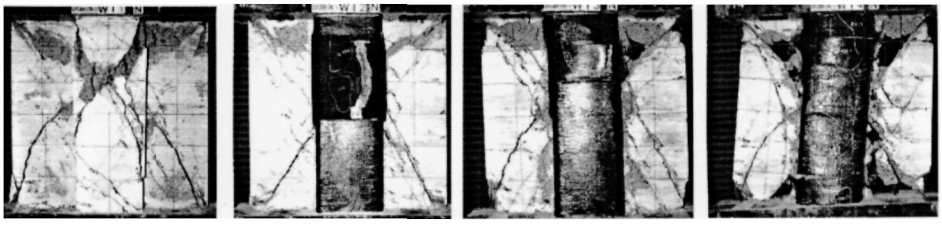
| | | $\sigma_y$ (MPa) | $\sigma_u$ (MPa) | Elong. (%) |
|---|---|---|---|---|
| Shear R. | D6 | 408 | 531 | 27 |
| Main R. | D13 | 328 | 466 | 28 |
| | $\phi$ 13 | 337 | 473 | 40 |
| Wall R. | D6 | 450 | 503 | 36 |

$\sigma_y$ : Yield Strength, $\sigma_u$ : Tensile Strength

(c) CFRP sheet

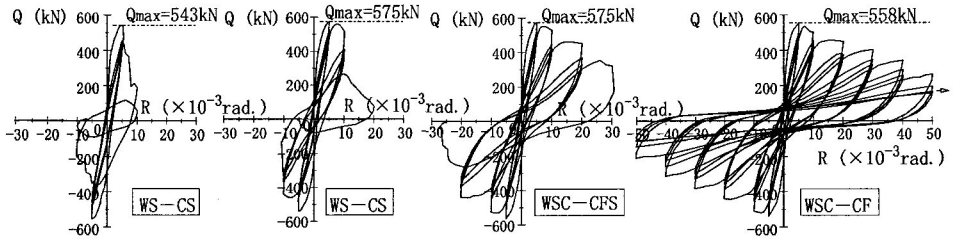
| | | $\sigma_{fu}$ (MPa) |
|---|---|---|
| In-plane loading | CF1 | 3283 |
| | CF2 | 3612 |
| | CF3 | 3133 |
| Out-of-plane loading | CF2 | 3893 |

$\sigma_{fu}$ : Tensile strength



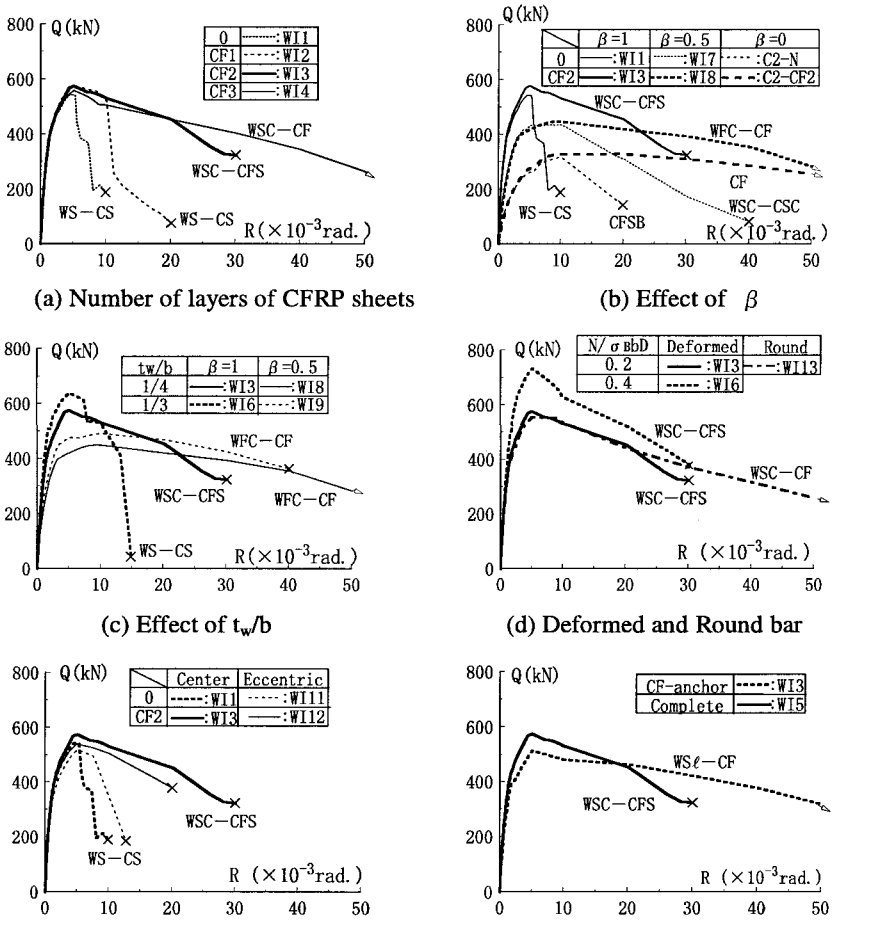
(a) WI1 (0) (b) WI2 (CF1) (c) WI3 (CF2) (d) WI4 (CF3)

Photo. 1 Failure modes of typical specimens ( $\beta$ =1, $t_w$/b=1/4) under in-plane loading




(a) WI1 (0) (b) WI2 (CF1) (c) WI3 (CF2) (d) WI4 (CF3)

Fig. 4 Relation between shear force (Q) and drift angle (R) of typical specimens ( $\beta$ =1, $t_w$/b=1/4) under in-plane loading




(a) Number of layers of CFRP sheets

(b) Effect of $\beta$

(c) Effect of $t_w/b$

(d) Deformed and Round bar

(e) Center and Eccentric

(f) CF-anchor versus Complete wrapping

Fig. 5 Curves of load-deformation relationships for in-plane loading

The ductility of strengthened specimens WI2, WI3 and WI4 gradually increased with the number of layers of CFRP sheets. In specimens WI2, CFRP sheets ruptured at the center of the column in the loading plane. Therefore, such CFRP sheets resisted as shear reinforcements of columns. In specimens WI3, after the main reinforcements of the column flexurally yielded at the ends of the column, the straight portion of CF-anchors ruptured in the perpendicular direction to the loading plane. This rupture was caused by the confining action of CFRP sheet jacketing to the reinforced concrete column section.

In specimens WI4, though wing walls spalled near both ends by flexural compression, the CF-anchors and CFRP sheets did not rupture until 5/100 radian of drift angle. This system provided sufficient confinement and was able to remarkably improve the ductility of these columns.

The ultimate strength and the ductility of these columns were influenced by the length and the thickness of the wing walls, as shown in Fig. 5. In each case, this strengthening system was able to improve the ductility of these columns. However its effectiveness with eccentrically arranged wing walls tended to decrease in comparison with that of centrally arranged wing walls.

The axial force enhanced the ultimate shear capacity, and decreased the ductility of the columns. The difference between deformed bars and round bars for the main reinforcements of columns did not significantly influence the behavior of these columns. Also, though the ultimate strength of specimen WI3 strengthened by this system was larger than that of specimen WI5 strengthened by the complete wrapping system, the ductility of specimen WI3 decreased in comparison with that of specimen WI5.

**Estimation of ultimate strength**

The ultimate flexural strength ($Q_{fu}$) was calculated according to the accumulative law. Namely, the interactive relation between axial force (N) and bending moment (M) of these columns at the ultimate state was calculated by summing up such interactive relation of the rectangular column and the vectors ($M_{wu}$, $N_{wu}$) of the ultimate strength of wing walls, as shown in Fog. 6. $Q_{fu} = M_{wu} / h_o$, where $h_o$ is the clear height of column.

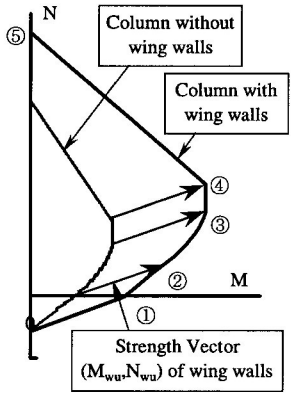
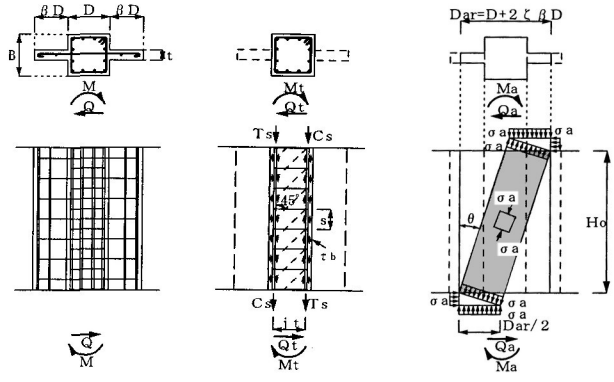



Fig. 6 Interactive relation of columns with wing walls




(a) Prototype (b) Truss mech. (c) Arch mech.

Fig. 7 Analytical model for estimation of ultimate shear

The ultimate shear strength ($Q_{su}$) was calculated by using the truss-arch model (1) shown in Fig. 7. In this model, the truss mechanism is effective for only the column, but the arch mechanism is effective over the total area of the column and wing walls.The strengthening effect was estimated by using the replaced reinforcement intensity ($p_f \sigma_{fd}$) of CFRP sheets. $p_f = 2\, t_f / b$, where $t_f$ is design thickness of CFRP sheet, $\sigma_{fd}$ is the design tensile strength of CFRP sheet. It is assumed that $\sigma_{fd}$ equals about two-thirds of the material tensile strength, namely, $\sigma_{fd} = 1960$ MPa.

The calculated values of the ultimate strength coincide closely with the tested values, as shown in Fig. 8. Also, the failure modes could be predicted by comparing these calculated values.

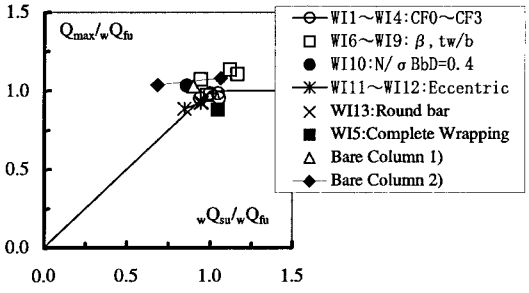



Fig. 8 $Q_{max}/Q_{fu} - Q_{su}/Q_{fu}$ relation

**Estimation of ductility**

The typical load-deformation relation of the columns with wing walls can be idealized, as shown in Fig. 9. The ultimate strength ($_wQ_u$, $_cQ_u$) of columns with and without wing walls is expressed by using the following equations.

$$_wQ_u = \min(_wQ_{su}, {}_wQ_{fu}), \quad {}_cQ_u = \min(_cQ_{su}, {}_cQ_{fu}) \tag{1}$$

Where, $_wQ_{su}$, $_wQ_{fu}$: Ultimate shear and flexural strength of columns with wing walls

$_cQ_{su}$, $_cQ_{fu}$: Ultimate shear and flexural strength of columns without wing walls

Fig. 10 shows the relation between $(R_u)_{test}$ and $_wQ_{su}/_wQ_{fu}$. $(R_u)_{test}$ is defined as the ultimate drift angle at 0.8 $Q_{max}$ after the ultimate strength and $Q_{max}$ is the tested value of the load carrying capacity. Then, the design ductility ratio $\mu_{wc}$ is defined as the ductility ratio at 0.9 $_wQ_u$, as follows (see Fig. 9).

$$\mu_{wc} = \mu_w + 0.1(\mu_c - \mu_w) \cdot {}_wQ_u / ({}_wQ_u - {}_cQ_u) \tag{2}$$

The ductility ratio $\mu_w$ and $\mu_c$ can be calculated by the following equation. The coefficient $_wq_{so}$ and $_cq_{so}$ in these equations can be estimated from the tested results.

$$\mu_w = R_u / R_y = 10 \cdot ({}_wQ_{su}/{}_wQ_{fu} - {}_wq_{so}) \tag{3}$$

$$\mu_c = 10 \cdot (0.3 / n) \cdot ({}_cQ_{su} / {}_cQ_{fu} - {}_cq_{so}) \tag{4}$$

Where, $R_y$ : Yield drift angle (It is assumed that $R_y$ equals 1/150 radian.)

$n = N / (\sigma_B bD)$ : Axial force level

For unstrengthened columns, $_wq_{so} = 1$

For strengthened columns, $_wq_{so} = 0.9$ (Deformed bar), $_wq_{so} = 0.8$ (Round bar.)

$$cqso = \gamma_B \cdot \gamma_t \cdot \gamma_e \cdot \gamma_r \leqq 1 \tag{5}$$

$\gamma_B$, $\gamma_t$, $\gamma_e$, $\gamma_r$ : Coefficient shown in Table 3

The ultimate drift angle calculated by Eq. (2) was estimated conservatively in comparison with the tested values, as shown in Fig. 11.

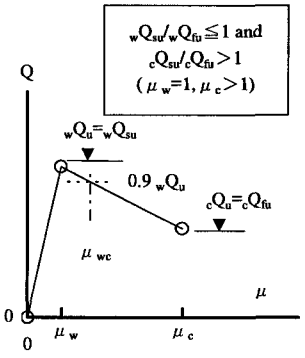



Fig. 9 Typical load-deformation relation of columns with wing walls under in-plane loading

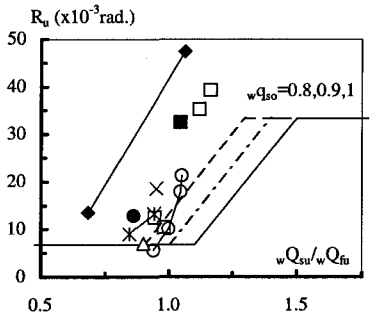
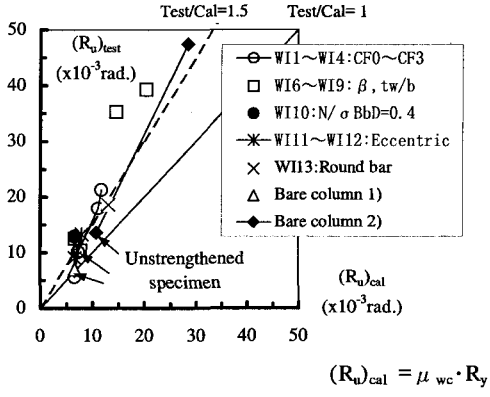



Fig. 10 $(R_u)_{test} - {}_wQ_{su}/{}_wQ_{fu}$ relation

Table 3 Coefficient $\gamma_B$, $\gamma_t$, $\gamma_e$, $\gamma_r$

| $\gamma_B = 1 + 0.2\beta$ | | $\gamma_t = 0.2 + 2.4t_w/b \geqq 1$ | |
|---|---|---|---|
| | $\gamma_e$ | | $\gamma_r$ |
| Center | 1.0 | Deformed bar | 1.0 |
| Eccentric | 1.1 | Round bar | 0.6 |

$\gamma_B, \gamma_t, \gamma_e, \gamma_r$ : Coefficient decided from $\beta$, $t_w/b$, position of wing walls and kind of reinforcement,




$(R_u)_{cal} = \mu_{wc} \cdot R_y$

Fig. 11 $(R_u)_{test} - (R_u)_{cal}$ relation

## OUT-OF-PLANE LOADING

### Test Program

In this series, eight specimens with five parameters were tested, as shown in Table 4. Specimen WO2 was the fundamental specimen, and specimen WO3 was completely wrapped with CFRP sheets around the column. The configuration of specimens and the arrangement of CFRP sheets and CF-anchors coincided with that of in-plane loading test, as shown in Fig. 12. The mechanical properties of materials used are shown in Table 2. Also, this test was carried out with the same equipment that was used under in-plane loading.

#### Effects of strengthening

The failure modes and the curves of load-deformation relationships are shown in Photo. 2 and Fig. 13. The load-deformation behavior of strengthened specimen WO2 almost equals to that of square column specimen C2-CF2 (2), as shown in Fig.13. In both specimens, CF-anchors and CFRP sheets did not rupture until 5/100 radian of drift angle. Also, the difference between CF-anchors and complete wrapping (WO2 and WO3) had very little influence on the behavior of these columns.

Table 4 Outline of out-of-plane loading test

| Specimen | Test Parameters | | | | |
|---|---|---|---|---|---|
| | (1) | (2) | N/ $\sigma_B$bD | (6) | (7) |
| WO1 | [D] | [C] | 0.2 | — | 0 |
| WO2 | | | | CF | CF2 |
| WO3 | | | | Com. | |
| WO4 | | | 0.4 | CF | |
| WO5 | | | 0.6 | | |
| WO6 | | [E] | 0.2 | | |
| WO7 | | | 0.4 | | |
| WO8 | [R] | [C] | 0.2 | | |

1) Definission of test parameters and notaions are shown in Tabale 1.

2) $t_w$/b of all specimens equals 1/4.

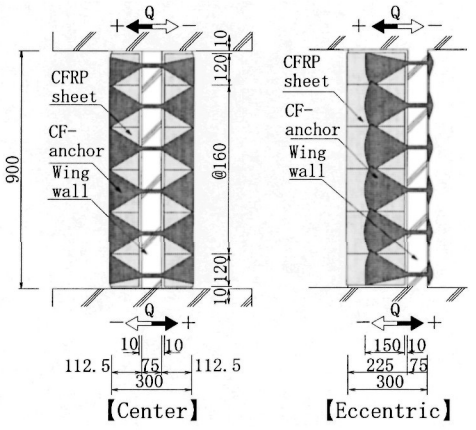
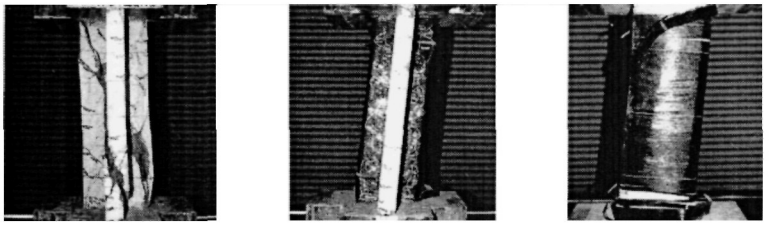



Fig. 12 Configuration of test specimens under out-of-plane loading

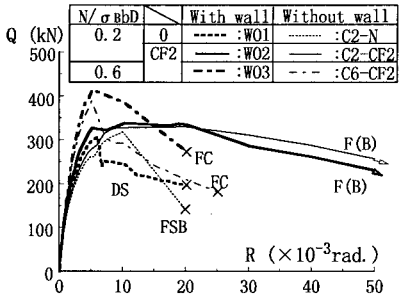
The ultimate strength of specimen WO5 subjected to large axial force level (N/ $\sigma_B$bD =0.6) was not only higher than that of square column specimen C6-CF2 (2), but also the ductility of both specimens was almost equal. In the column with wing walls, since the wing walls resisted to the axial force, the ultimate shear strength increased and the ductility did not decrease.

Though the ultimate strength of the strengthened specimens WO6 and WO7 with eccentrically arranged wing walls was larger than that of the strengthened specimens WO2 and WO4 with centrally arranged wing walls, the ductility of WO6 and WO7 decreased. These behaviors were influenced by the resistance of the eccentrically arranged wing walls for flexural compressive stress. Also, the difference between deformed bars and round bars for the main reinforcements of the columns had little influence on the behavior of the columns.

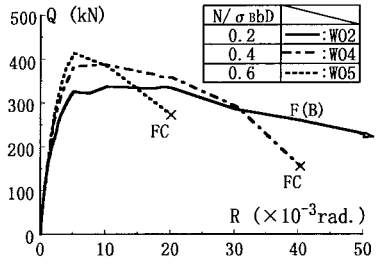


(a) WO1 (Unstrengthened) (b) WO2 (With wing wall) (c) C2-CF2 (Without wing wall)

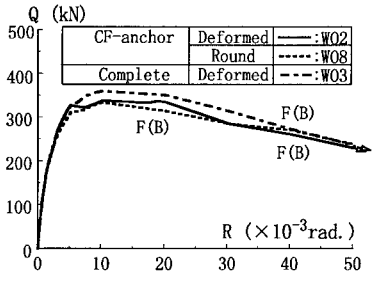
Photo. 2 Failure modes of typical specimens under out-of-plane loading



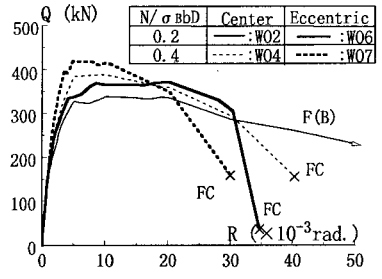

(a) With and Without wing wall




(b) Effect of N/ $\sigma_B$bD




(c) Deformed and Round bar
(CF-anchor and Complete wrapping)




(d) Center and Eccentric

Fig. 13 Curves of load-deformation relationships for out-of-plane loading

## CONCLUSIONS

1) From the in-plane loading test, it was verified that this system was effective for the improvement of ductility.
2) These strengthening effects could be estimated by consideration of several parameters, including the number of layers of CF sheets and the dimensions of wing walls, etc.
3) From the out-of-plane loading test, it was shown that the load-deformation behavior of the columns strengthened by this proposed wrapping system almost coincided with that of the completely wrapped columns. The design ductility of the strengthened columns was not determined by the rupture of CF-anchors.

## REFERENCES

1) Masuo, K. : Seimic Retrofitting of Reinforced Concrete Columns with Wing Walls Using Carbon Fiber Reinforced Plastic Sheets, SP188-18, pp.193-204, Oct. 1999.
2) Masuo, K. :et al. : Experimental Study on Strengthening Effects of CFRP Sheet and Steel Plate Jacketing for Reinforced Concrete Columns, GBRC, No.88, pp.22-44, Oct. 1997, No.92, pp.13-24, Oct. 1998. (In Japanese)

# Seismic Rehabilitation of Reinforced Concrete Building Corner Joints

C. P. PANTELIDES, C. CLYDE, C. P. LAU, and L. D. REAVELEY
Dept. of Civil and Environmental Engineering, University of Utah, Salt Lake City, Utah, USA

## ABSTRACT
Three half-scale reinforced concrete building corner joints were rehabilitated externally with carbon FRP composites and tested under quasi-static, cyclic loads. The rehabilitation goal was to improve joint shear capacity and displacement ductility. The three joints had steel reinforcement details typical of non-ductile concrete buildings. Two of the specimens were reinforced with hoop steel in the joint, while one specimen did not have any hoop steel reinforcement. Two of the specimens, one with and one without hoop steel were tested with an axial column load of $0.1f'_cA_g$. The third specimen, with hoop steel, was tested with a column load of $0.25f'_cA_g$. The performance of the rehabilitated specimens is compared to that of six baseline specimens, four with hoop steel in the joint and two without hoop steel. The comparisons include hysteretic behavior, joint shear stress, and joint shear strength coefficient as defined by ACI-352. Two different failure modes were observed for the CFRP composite rehabilitated joints. The shear capacity of the rehabilitated joints with hoop steel was slightly improved in comparison to the baseline. The rehabilitated joint without hoop steel showed even more improvement in shear capacity and in addition the displacement ductility was increased significantly.

## INTRODUCTION
Reinforced concrete buildings that were built in the 1960's do not meet current design criteria and behave in a non-ductile manner. Reinforced concrete frames can achieve ductile behavior provided that brittle failure of structural elements and instability can be prevented in severe earthquakes. The design and detailing of beam-column joints is important in achieving satisfactory performance of R/C building frames. The design should be able to: (a) prevent brittle shear failure of the joint, (b) maintain integrity of the joint so that the ultimate strength of the connecting beams and columns can be developed, and (c) reduce joint stiffness degradation by minimizing cracking of the joint concrete and by preventing the loss of bond between the concrete and longitudinal beam and column reinforcement. Joints in existing structures built prior to the development of current design guidelines such as ACI 352R-91 (1991) do not conform to the current seismic requirements (ACI SP-123, 1991). The proposed method of strengthening the beam-column joint with FRP composite jackets is relatively new; existing techniques include R/C jackets, glued steel plates, and X-shaped prestressed collars.

## TEST SPECIMENS
### Reinforced Concrete Corner Joints
A typical exterior beam-column joint in a reinforced concrete frame building built in 1964 was chosen as a model for this project. The dimensions of the original joint were reduced by

*FRPRCS-5*, Thomas Telford, London, 2001.

half, and reinforcing details were reduced based on shear stress calculations. The longitudinal beam reinforcement was increased to prevent early degradation of the beam, forcing a shear mode of failure in the joint. However, the beam longitudinal bars were not adequately anchored in the connection as in the original building joint. There was no transverse reinforcement within the joint core in one of the test specimens (Test #3) and light joint core reinforcement was used in two of the test specimens (Test #5 and Test #6). In addition, the lap splice length and column confining reinforcement details were inadequate according to current seismic criteria (ACI 352, 1991).

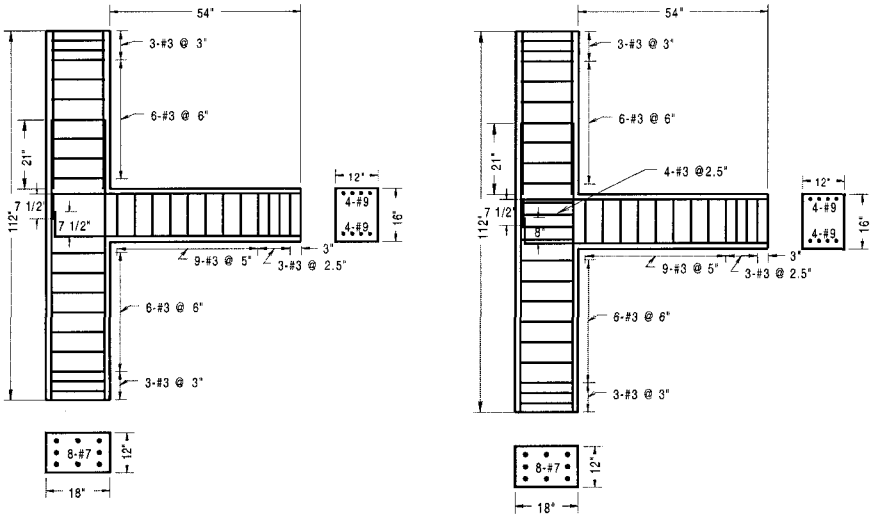
The original design of the specimens called for a concrete strength of 4,000 psi (28 MPa). However, due to resource restrictions higher strengths were achieved. The average concrete compressive strength for the three specimens was 6,000 psi (41 MPa). Three sizes of steel rebar were used as reinforcement in the beam-column joint. The longitudinal beam reinforcement was #9 (29 mm) bars with yield strength of 65.9 ksi (454 MPa), and the column longitudinal reinforcement was #7 (22 mm) bars with a yield strength of 68.1 ksi (470 MPa). The shear reinforcement in both the beam and column was #3 (10 mm) stirrups with yield strength of 62.0 ksi (428 MPa).

The three beam-column joint specimens had exactly the same dimensions and detailing except at the joint region. The specimen dimensions and reinforcement details for the two types of corner joints, with and without joint reinforcing, are shown in Fig. 1. The beam is 12 in. (305 mm) wide and 16 in. (406 mm) deep; it is symmetrically reinforced with 4-#9 (4x29 mm) bars for both the positive and negative reinforcement; the steel ratio is 2.47% at both top and bottom. Each longitudinal bar has a 7.5 in. (193 mm) hook bent at 90°. The bottom beam reinforcement is bent up into a hook at the joint, and the top reinforcement is bent down into a hook at the joint. The hooks overlap approximately 2 in. (51 mm) and are tied together, as shown in Fig. 1. The transverse reinforcement is a #3 (10 mm) closed stirrup with a 140° bend and a 2.5 in. (64 mm) extension on both ends. The stirrups are spaced at 5 in. (127 mm) along the beam, except at the beam end, where the spacing is reduced to 2.5 in. (64 mm) to give adequate strength at the location where the force is applied during the test. It should be noted that the original half-scale calculations required a reinforcement ratio $\rho$=0.76% at the top of the beam and $\rho$=0.48% at the bottom. The decision to increase the beam longitudinal reinforcement was based on the stated objective of studying joint shear failure at high drift levels. The 2.47% ratio of longitudinal steel meant that the joint core shear forces developed would be high.

The column is 12 in. (305 mm) wide and 18 in. (457 mm) deep. It is reinforced with 8-#7 (8x22 mm) bars evenly distributed around the perimeter of the column, thus having a steel ratio of 2.54%. The longitudinal reinforcement in the bottom column extends continuously up through the joint and 21 in. (533 mm) into the top column, as shown in Fig. 1. The top column longitudinal reinforcement is spliced over the 21 in. (533 mm) length and extends to the upper end of the column, or a distance $24d_b$, which is insufficient by current standards. The transverse reinforcement in the column consists of #3 (10 mm) closed stirrups with 140° bends and 2.5 in. (64 mm) extensions at both ends. The stirrups are spaced at 6 in. (152 mm) along the height of the column. The spacing is decreased to 3 in. (76 mm) at the upper and lower ends of the column, where the column was supported during the test. For the two test specimens with steel reinforcement in the joint region, 4-#3 (4x10 mm) hoops were placed at 2.5 in. (64 mm) in the joint.

**CFRP Composite Wrapping**

The design of the FRP composite for the joint region was determined by a procedure, which was similar to the guidelines developed for bridge beam column joints (Gergely et al. 2000):




(a) Test #3 specimen (b) Test #5 and Test #6 specimens

Figure 1. Reinforcement details for corner joint specimens

(a) the horizontal and vertical shear forces and consequently shear stresses in the center of the joint were calculated at the peak load; (b) the principal stresses in the joint were determined; (c) the principal angle was calculated to be 39° and therefore the optimum orientation of the fibers was found to be 51°; (d) the width and thickness of the FRP composite fabric was then designed to increase the diagonal tension capacity of the joint by 25 percent. From this procedure it was determined that four layers of carbon fiber composite should be placed in both the ± 51° directions. The composite strips were wrapped around the joint on all four sides except where the beam framed into the column and where the floor slab would be if the joint were part of an actual building. The CFRP composite was attached for only 3 in. (76 mm) on each beam side, resulting in an open beam face as shown in Fig. 2. A 1-in. (25.4 mm) gap was left at the interface between beam and column so the two elements could move independently (see Fig. 2). The following properties of the FRP composite were used to design the layup: (1) the material was 48,000 fibers per tow unidirectional carbon fiber; (2) the fiber sheets were 6 in. (152.4 mm) and 18 in. (457.2 mm) wide; (3) the CFRP composite tensile strength was 91.1 ksi (628 MPa) (ASTM, 1996); (4) the ultimate strain was 0.01; (5) the modulus of elasticity of the composite was 9,388 ksi (64,730 MPa).

## TEST SETUP

**Instrumentation**

Strain gages were attached to the longitudinal and transverse reinforcement at selected locations within the concrete beam-column joints. Strain gages were attached to the CFRP composite at the beam, columns, and in the joint. Linear variable differential transducers (LVDT) were mounted at the face of the joint and in the lap splice to calculate shear strains.

Displacement transducers were attached to measure curvature in the beam, rotation in the joint, deflection at the end of the beam, and rigid body movement of the specimen.

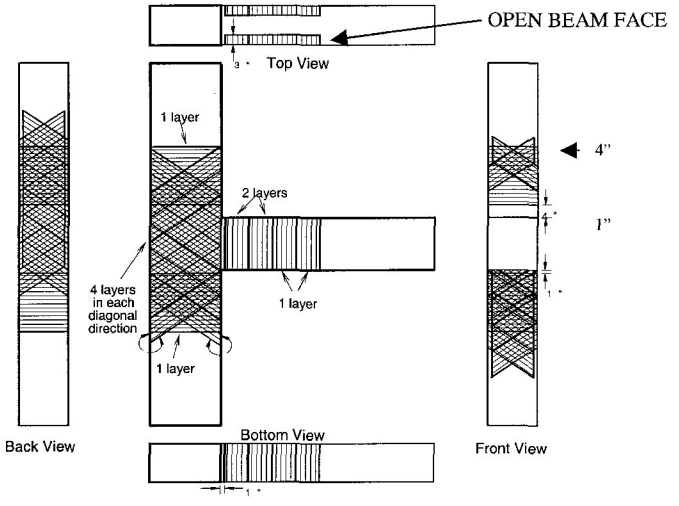



Figure 2. CFRP composite layout

**Loading Apparatus**

A schematic of the loading apparatus is shown in Fig. 3. The column was mounted horizontally with pinned supports at both ends. The axial load was applied using a small hydraulic cylinder and transferred to the column through four threaded rods, which were instrumented with strain gages for measuring the axial column load. The lateral load was applied at the end of the beam through a loading collar, as shown. A load cell, between the actuator and the loading collar, measured the quasi-static cyclic load applied to the beam.

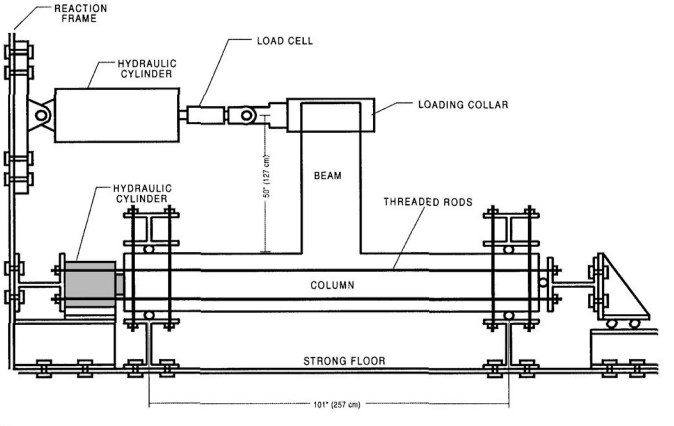



Figure 3. Loading apparatus

**Test Procedure**

First, the axial load was applied to the column portion of the specimen. An axial compressive load equal to $0.1f'_cA_g$ was applied to two of the specimens, Test #3 and Test #6. The other specimen, Test #5, received an axial compressive load equal to $0.25f'_cA_g$. The axial load was set to the calculated initial value and then left to change at will, as the beam was subjected to lateral load reversals. The lateral load was applied cyclically through the loading collar, in a quasi-static fashion at the end of the beam. The first portion of the test was load-controlled wherein the lateral load was increased in 5 kip (22.2 kN) increments. At every load step, three cycles were performed, and each cycle contained a push and pull segment. After the first yielding of the longitudinal reinforcement, the testing was carried out using displacement-control. Three cycles were performed at each displacement step, and the displacement was increased as a fraction of the initial yield displacement. The test continued until the lateral load either dropped below 50% of the peak value or until failure occurred.

## EXPERIMENTAL RESULTS

### Test #3 – Axial load of $0.1\,f'_c A_g$ without joint hoop steel

The load versus drift curve for the rehabilitated specimen without hoop joint reinforcement is shown in Fig. 4. The full loops are indicative of the ductile behavior of the joint. The first yielding in the steel reinforcement occurred at a lateral load of 42.2 kips (187.7 kN). Small cracks began to occur at the interface between the beam and the column at this load; these cracks widened as the test progressed, leading to ultimate failure of the joint specimen, as shown in Fig. 5. The CFRP wrap showed minimal evidence of damage; delamination of the CFRP from the concrete occurred in small patches along the column and at the beam. A minor fiber tensile failure occurred in the CFRP hoops at the top column, just above the beam. No CFRP damage occurred at the joint region other than the adhesive failure of the concrete, which opened up the CFRP composite jacket in the joint.

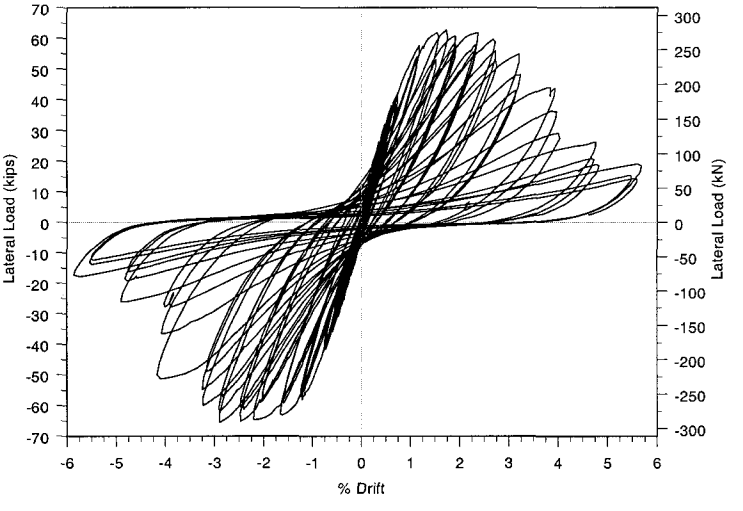



Figure 4. Hysteresis behavior of Test #3 at an axial load of $0.1f'_cA_g$

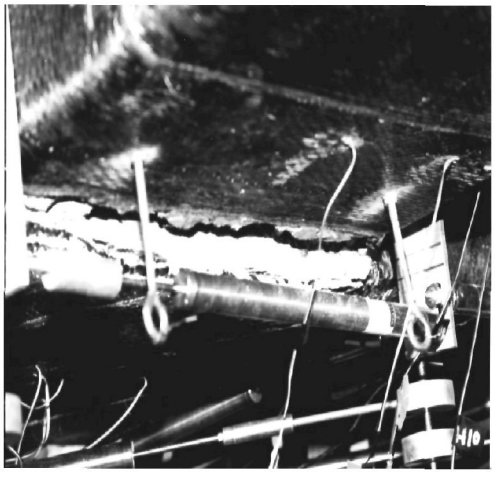


Figure 5. Failure at beam-column interface in Test #3

Figure 6 illustrates the joint shear behavior of the rehabilitated corner joint of Test #3. The maximum joint shear stress reached was 1,048 psi (7.2 MPa) which normalized by $\sqrt{f'_c}$ is $\gamma$=13.0 (psi) [1.08 (MPa)]. As seen in the diagram, this stress level exceeds that prescribed by the *Guidelines* of FEMA 273 (BSSC, 1997) and that of ACI 352 (1991).

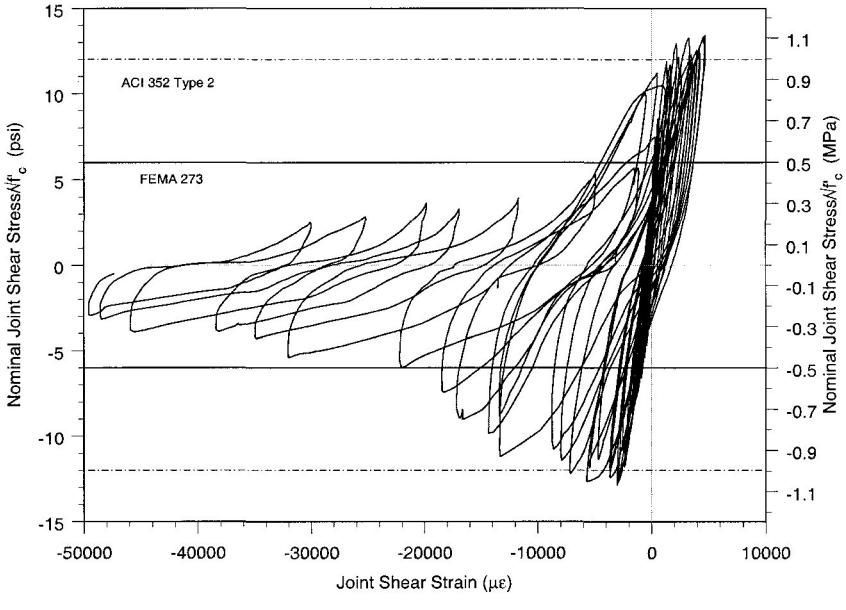



Figure 6. Joint shear stress-strain behavior for Test #3 at an axial load of $0.1f'_cA_g$

The strain in the CFRP composite jacket at the joint region is shown in Fig. 7. As the lateral load increased so did the strain in the CFRP composite at a fairly proportional rate. The strain was higher toward the edge of the column due to stress concentration at the corner where the carbon fiber material was bent.

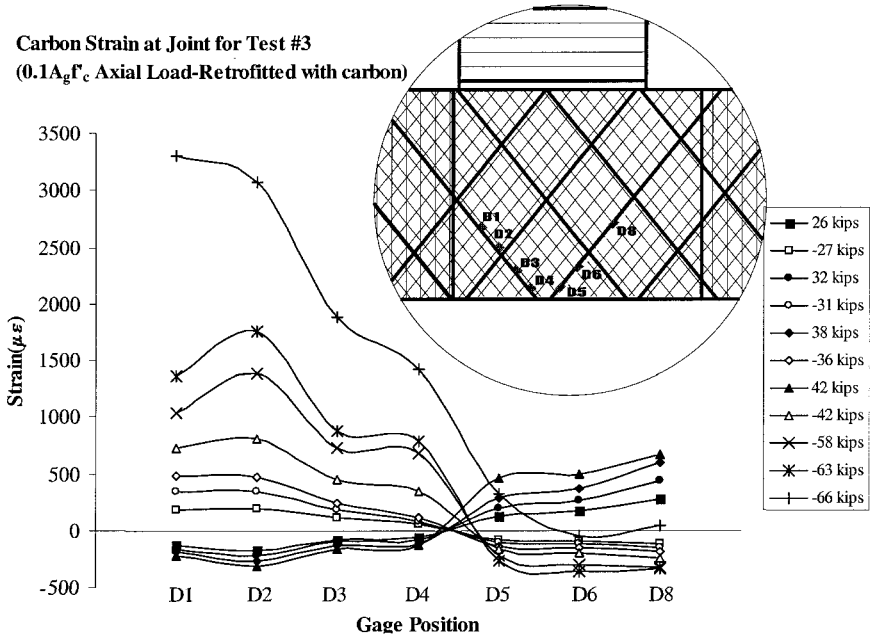



Figure 7. Carbon fiber composite strains in the joint region for Test #3

**Test #6 and Test #5 – with joint hoop steel**

In Test #6 with an axial load of 0.1f 'cAg axial load, the first steel yielding occurred in a top longitudinal beam bar at a lateral load of 51.1 kips (227.5 kN). As shown in Fig. 8, the specimen developed an unsymmetrical load-drift curve. The push segment shows improved behavior, however the pull segment (negative drifts and loads) shows very little ductility. This is due to debonding of the CFRP composite, which occurred at the open face of the beam, shown in Fig. 2, during the test. Failure of the beam occurred at a lateral load of 67 kips (298 kN) and is attributed to a type of symmetrical debonding of the concrete from the beam reinforcement by the CFRP composite. Cracks at the ends of the CFRP composite at the open face of the beam, and hairline cracks at the joint interface developed at the early stages of the test. Subsequently, a beam crack occurred all along the length of the beam on the open face which eventually led to total failure. The concrete essentially broke out through the gap in the CFRP wrap along this crack at the top the beam. The presence of the steel hoop reinforcement in the joint region as well as the CFRP wrap sufficiently provided confinement and shear strength for the joint. The beam-column specimen in Test #5 showed very similar behavior to that of Test #6 as shown in Fig. 9. Yielding first occurred in a longitudinal bottom beam bar at a lateral load of 64.64 kips (287.5 kN). Cracks then formed similar to those in Test #6 and ultimately the beam failed in a concrete debonding failure mode.

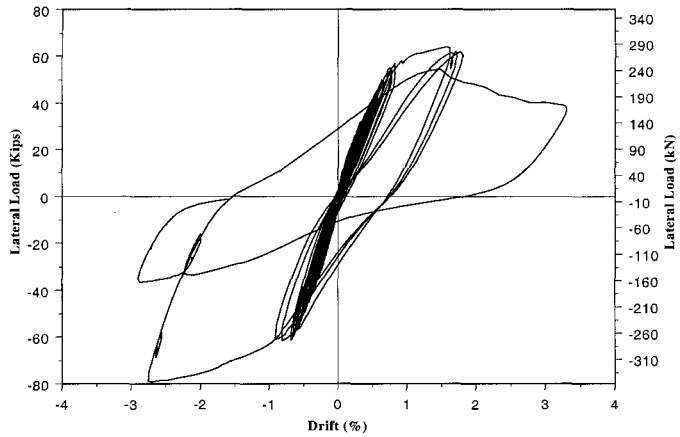



Figure 8. Hysteresis behavior of Test #6 at an axial load of $0.1f'_cA_g$

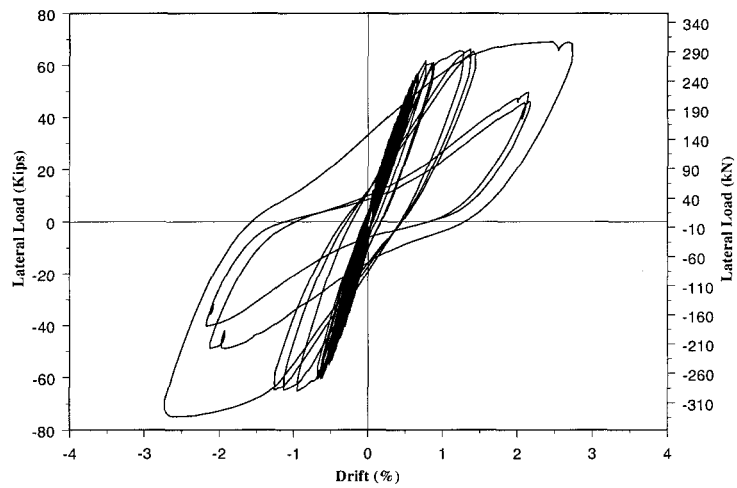



Figure 9. Hysteresis behavior of Test #5 at an axial load of $0.25f'_cA_g$

Figure 10 illustrates the joint shear behavior of the two rehabilitated corner joints with joint hoop steel. The maximum joint shear stresses reached in Test #5 and Test #6 were 1,139 psi (7.85 MPa) and 1,055 psi (7.27 MPa), respectively, which normalized by $\sqrt{f'_c}$ correspond to joint strength coefficients of $\gamma$=13.9 (psi) [$\gamma$=1.16 (MPa)] for Test #5 and $\gamma$=12.7 (psi) [$\gamma$=1.03

(MPa)] for Test #6. Figure 10 shows that these values exceed those prescribed in the *Guidelines* of FEMA 273 (BSSC, 1997) of $\gamma$=8 (psi) [$\gamma$=0.67 (MPa)], and ACI 352 (1991) of $\gamma$=12 (psi) [$\gamma$=1 (MPa)] for this type of joint.

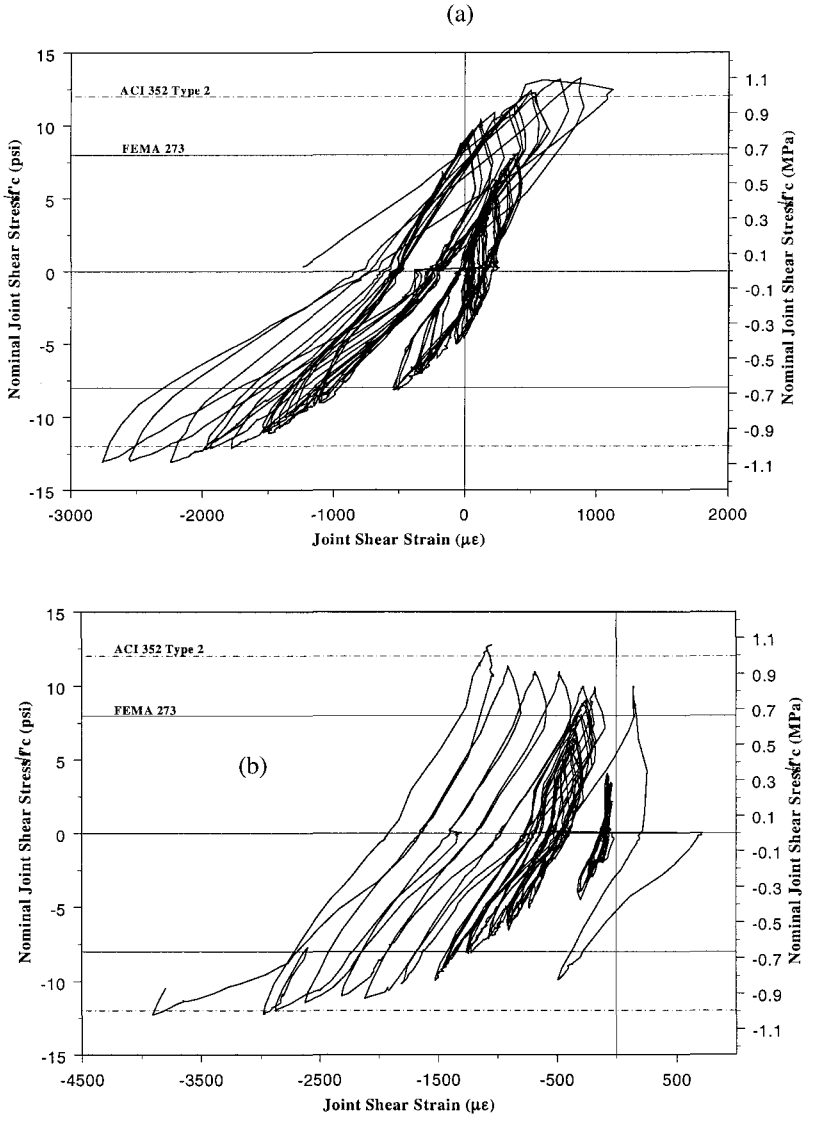



Figure 10. Joint shear stress-strain behavior: (a) Test #5 - 0.25f ′cAg axial load, (b) Test #6 – 0.1f ′cAg axial load

## COMPARISON AND CONCLUSION

A comparison of the three rehabilitated corner joints with six baseline specimens is presented in Table 1. Test #3, the specimen without steel joint reinforcement, showed increased strength and ductility. The CFRP composite wrap provided a joint shear strength increase of 5% from the as-is specimens. More importantly, a 44% increase in displacement ductility was reached, as well as an increase of 78% in drift capacity. The joint shear type failure seen in the baseline of the beam-column joint specimens was successfully prevented. Failure was moved to the beam, a less critical part of the sub assemblage, with significant gains in performance. No CFRP damage occurred at the joint region other than the adhesive failure of the concrete, which opened up the CFRP composite jacket in the joint.

The specimens in Test #5 and Test #6, on the other hand, showed little improvement in performance from the baseline specimens. Minimal increases in strength and a decrease in drift capacity of the rehabilitated joints were observed. The failure mode changed from joint shear failure in the as-is joints to brittle beam failure in the joints rehabilitated with CFRP composites. The objective of preventing joint shear failure was achieved but little was gained in performance. These two tests showed the importance of clamping the beam CFRP composite reinforcement to avoid concrete debonding failure from the open beam face. This could be achieved by either mechanical anchorage along the beam sides or by anchors through the beam width.

Table 1. Performance comparison between rehabilitated and baseline specimens

| | Baseline Specimens | | | CFRP Specimens | | |
|---|---|---|---|---|---|---|
| Axial Load Level | γ, psi (MPa) | % Drift | Displacement Ductility | γ, psi (MPa) | % Drift | Displacement Ductility |
| WITHOUT JOINT HOOP STEEL | | | | | | |
| $0.1f'_cA_g$ | 12.1 (1.00) | 2.95 | 2.8 | 13.0 (1.08) | 5.77 | 3.9 |
| $0.1f'_cA_g$ | 12.7 (1.05) | 3.57 | 2.6 | | | |
| WITH JOINT HOOP STEEL | | | | | | |
| $0.1f'_cA_g$ | 13.1 (1.09) | 3.79 | 2.3 | 12.7 (1.05) | 2.85 | 3.9 |
| $0.1f'_cA_g$ | 12.4 (1.03) | 4.93 | 4.6 | | | |
| $0.25f'_cA_g$ | 13.3 (1.10) | 4.87 | 2.9 | 13.9 (1.15) | 2.36 | 2.3 |
| $0.25f'_cA_g$ | 12.6 (1.05) | 2.97 | 2.1 | | | |

## ACKNOWLEDGMENTS

The work was financially supported in part by the Center for Composites in Construction at the University of Utah, and the Pacific Earthquake Engineering Research Center. Support was also received through in-kind contribution from Eagle Precast Co., Salt Lake City, Utah.

## REFERENCES

ACI Committee 352, 1991, Recommendations for design of beam-column joints in monolithic reinforced concrete structures, *American Conc. Inst.*, Farmington Hills, MI.

ACI SP-123, 1991, Design of Beam-Column Joints for Seismic Resistance, *American Conc. Inst.*, Report SP-123, Farmington Hills, MI.

ASTM, ASTM D 3039, 1996, Standard Test Method for Tensile Proerties of Polymer Matrix Composite Materials, *Amer. Soc. for Testing Materials.* D3039/D 3039 M-95a.

BSSC, 1997, NEHRP Guidelines for the Seismic Rehabilitation of Buildings, *FEMA 273 and FEMA 274*, Washington, D.C.

Gergely, J., Pantelides, C.P., and Reaveley, L.D., 2000, Shear strengthening of R/C T-Joints using CFRP composites, *ASCE, J. of Composites for Construction,* 4(2), 56-64.

# Seismic performance of hybrid RC columns with aramid fiber reinforced polymer square tube and steel reinforcement

P. ZHONG, University of the Ryukyus, Okinawa, Japan
T. YAMAKAWA, University of the Ryukyus, Okinawa, Japan
H. SATOH, Yokohama Rubber Co., Tokyo, Japan
K. KOMESU, University of the Ryukyus, Okinawa, Japan

## INTRODUCTION

Since 1990, continuous fiber sheet has been applied to seismic retrofit in Japan. Especially after the 1995 Hyogoken-Nanbu Earthquake, the seismic diagnosis and retrofit technology are taken seriously. The related research results have been applied positively to retrofit construction, and the construction experiences have been piled up. In September 1999, a design guideline for seismic repair using continuous fiber materials was published in Japan[1].

Carbon shell system was proposed by Seible at University of California, Los Angles, United States of America in 1997[2]. It was a new concept that can be used for bridge. Instead of steel tube, the carbon fiber tube was filled with concrete, and composed a truss element. It should be noted that longitudinal and transverse reinforcement were not arranged, therefore, the method should be seen as concrete-filled-tube.

The authors devised a study independent to Seible's approach. Continuous fiber tube is utilized to confine concrete transversely and improve its ductility and strength. Impregnating the continuous fiber sheets by epoxy resin in square shape, the square tube performs the dual functions of stay-in-place formwork and transverse reinforcement. The tube can not play a role of structural member alone, but it can hybridize concrete and reinforcement to form a hybrid element, which is probable behave well in seismic strength and ductility. A pilot loading test was carried out on columns with carbon fiber square tube, and the experimental results showed that the hybrid columns had almost equivalent improved strength and ductility as columns reinforced by steel tube[3]. To investigate the possibility of applying circular aramid fiber tube, four circular columns were loaded[4].

In this paper, the square aramid fiber tube is utilized in hybrid columns as stay-in-place formwork and transverse reinforcement. The purpose of this study is to validate the effectiveness and the perspective of the suggestion, as well as the seismic performance of the hybrid columns subjected to constant axial load and lateral cyclic forces simultaneously.

## TEST PLAN

Twelve columns are provided with 250 mm square, 750 mm height and shear span to depth ratio of 1.5. Details of the columns are listed in Table 1. According to the amount of longitudinal reinforcement, the specimens are divided into two series. In series D19, the columns were reinforced vertically with eight deformed steel bars, of which nominal diameter was 19 mm. In series D13, longitudinal reinforcement was 12 deformed steel bars, of which nominal diameter was 13 mm. The nominal diameter of steel hoops was 6 mm.

The mechanical properties of the materials are shown in Table 2. The aramid fiber square tube was made of aramid fiber sheet, which had a width of 300 mm and fiber content of 280 g/m$^2$. The fiber sheet was wrapped transversely with an overlap of 200 mm, and impregnated by epoxy resin. After hardening, the thickness of tube plate was about 1.3 mm for 1-ply-tube, 3.6 mm for 4-ply-tube and 5.2 mm for 6-ply-tube. In order to avoid the stress concentration

Table 1. Details of columns

| specimen | rebar | $p_g$ (%) | steel hoop | $p_w$ (%) | ply of sheet | $p_{wf}$ (%) | $\sigma_B$ (MPa) | N/(bD$\sigma_B$) |
|---|---|---|---|---|---|---|---|---|
| H98M-A0 | 8-D19 | 3.67 | 2-D6-@40 | 0.64 | -- | -- | 37.3 | 0.35 |
| H98M-A44 | | | -- | -- | 4 | 0.62 | | |
| H98M-A44h | | | 2-D6-@40 | 0.64 | | | | |
| H99M-A44t | | | 3-D6-@30 | 1.28 | | | 26.8 | |
| H00M-A66t | | | | | 6 | 0.93 | 37.9 | |
| H98M-S33h | | | 2-D6-@40 | 0.64 | (steel tube) | 2.56 | 37.3 | |
| H00M-S33t | | | 3-D6-@40 | 0.96 | | | 37.9 | |
| H99M-A0 | 12-D13 | 2.44 | 4-D6-@40 | 1.28 | -- | -- | 36.8 | 0.35 |
| H00M-A11h | | | | | 1 | 0.15 | 37.9 | |
| H99M-A44 | | | -- | -- | 4 | 0.62 | 36.8 | |
| H99M-A44h | | | 4-D6-@40 | 1.28 | | | | |
| H99M-A66h | | | | | 6 | 0.93 | | 0.70 |

* $N$ = axial force, $b$ = section width, $D$ = section depth, $\sigma_B$ = compressive strength of concrete cylinder, $p_g$ = longitudinal reinforcement ratio, $p_w$ = transverse reinforcement ratio of hoop, $p_{wf}$ = transverse reinforcement ratio of AFRP or steel tube.

Table 2. Properties of reinforcing materials

| reinforcing material | t (mm) | $\sigma_y$ (MPa) | $E_s$ (GPa) | $\varepsilon_y$ (%) |
|---|---|---|---|---|
| steel tube | 3.2 | 286 | 181 | 0.16 |
| rebar, D19 (SD345) | -- | 380 | 189 | 0.20 |
| rebar, D13 (SD295) | -- | 359 | 202 | 0.18 |
| hoop for specimen with H98M, D6 | -- | 388 | 184 | 0.21 |
| hoop for specimen with H99M and H00M, D6 | -- | 466 | 223 | 0.21 |
| AFRP sheet (1 ply) | 0.193 | 2059 | 118 | 1.80 |

* $t$ = thickness, $\sigma_y$ = tensile yield strength of steel, or standard tensile strength of AFRP sheet, $E$ = modulus of elasticity, $\varepsilon_y$ = strain corresponding to $\sigma_y$.

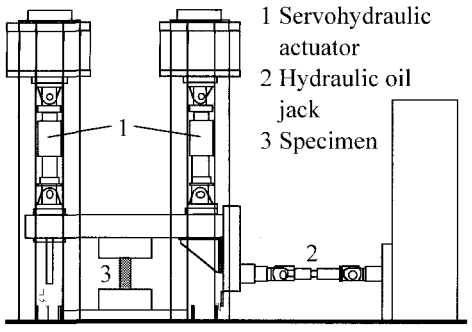



Figure 1. Schematic test setup

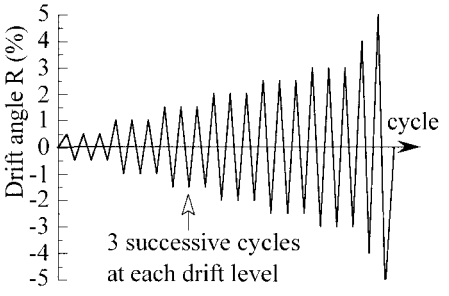



Figure 2. Loading program

of fiber sheet in column corner, curvature radius was adopted as 25 mm. Between tube and stubs, gaps of about 10 mm were provided in order to avoid influence of the axial load.

All the columns were tested under cyclic lateral forces while simultaneously subjected to constant axial load. Loading test setup is shown in Figure 1, and loading program is depicted in Figure 2. Story drift angle was controlled at 0.5% and at each stage three cycles were repeated. As indicated in "Design Guidelines for Earthquake Resistant Reinforced Concrete Buildings Based on Inelastic Displacement Concept" by Architectural Institute of Japan [5], the drift angle $R$=1.5% shall be ensured for columns in design limit state. In this loading test, the drift angle $R$ =5% was adopted as final deformation. The drift angle $R$ is story drift angle given by dividing story drift by height of column.

## EXPERIMENTAL RESULTS

Experimental results and failure modes obtained from loading test are summarized in Table 3. The AFRP tube columns H98M-A44, H98M-A44h and H99M-A44t were of bond failure, because of the large amount of longitudinal reinforcement. With much transverse confinement, the columns of Series D13 generated flexural yield except for the specimen H99M-A44.

After loading test, the AFRP or steel tubes were tore off and the failure conditions of concrete were observed. In Series D19, bond slip cracks occurred along the longitudinal steel and shear cracks were found at the upper and lower ends of columns, and the bond slip was of side splitting failure mode. The column H98M-S33h, H00M-S33t and H00M-A66t showed flexural cracks at the both ends.

In Series D13, smaller amount of longitudinal reinforcement was arranged, in addition to the same shear span ratio as in Series D19. Much shear and flexural cracks occurred, and seldom bond split cracks were found except for the AFRP tubed column H99M-A44.

Lateral shear force $V$ versus drift angle $R$ hysteresis loops are depicted in Figure 3, in which the dotted line represents calculated flexural yield strength $V_f$ including $P$-$\delta$ effect by the simplified equation[6]. This equation for flexural yield strength is widely used in Japan and is introduced in the design guidelines by Architectural Institute of Japan.

Table 3. Summary of experimental results

| specimen | $V_{exp}$ (kN) | $R_{Vexp}$ (%) | $R_f$ (%) | $R_y$ (%) | $\mu = R_f/R_y$ | failure mode | mark |
|---|---|---|---|---|---|---|---|
| H98M-A0 | 271.0 | 0.41 | 1.00 | 1.08 | 0.92 | S | ▲ |
| H98M-A44 | 277.2 | 0.52 | 2.60 | 1.08 | 2.40 | B | ▲ |
| H98M-A44h | 299.5 | 1.00 | 2.49 | 1.08 | 2.30 | B | ▲ |
| H99M-A44t | 274.2 | 1.46 | > 5.00 | 1.10 | 4.55 | B | ▲ |
| H00M-A66t | 376.8 | 2.43 | > 5.00 | 1.08 | 4.61 | F | △ |
| H98M-S33h | 358.7 | 1.41 | 2.61 | 1.08 | 2.41 | FB | ◆ |
| H00M-S33t | 399.3 | 1.97 | > 5.00 | 1.08 | 4.61 | F | ◇ |
| H99M-A0 | 277.2 | 0.95 | 2.83 | 0.84 | 3.35 | FB | ● |
| H00M-A11h | 326.5 | 1.42 | > 5.00 | 0.85 | 5.89 | F | ○ |
| H99M-A44 | 255.5 | 0.48 | 2.13 | 0.84 | 2.52 | B | ● |
| H99M-A44h | 304.1 | 1.91 | > 5.00 | 0.84 | > 5.92 | F | ○ |
| H99M-A66h | 354.2 | 1.96 | > 3.00 | 0.69 | > 4.38 | F | □ |

* $V_{exp}$ = experimental peak shear force in push loading direction, $R_{exp}$ = the drift angle corresponding to $V_{exp}$, $R_f$ = the drift angle corresponding to the shear force being 80% of $V_{exp}$, $\mu$ = ductility factor, $R_y$ = the drift angle corresponding to the first yield of longitudinal steel.
** S = shear failure, B = bond failure, FB= bond failure after flexural yielding, F = flexural failure.

In the ordinary column H98M-A0, at peak of drift angle $R$=0.5%, lateral shear force descended immediately when shear cracks occurred. For the longitudinal steel bars of large diameter and amount, the axial load was sustained by the confined concrete and longitudinal steel, therefore, brittle failure did not occur although shear failure occurred. Under cyclic loading, small shear cracks connected each other and bond splitting cracks formed. After the bond cracks became dominant, as a response, bond slip appeared in the $V$-$R$ hysteresis loops. The longitudinal steel did not yield at all during loading.

Confined by 4-ply-sheet AFRP tube, the specimen H98M-A44 showed bond slip at drift angle $R$=0.5%. When the drift angle got 2.5%, the measure instrumentation could not work. Hence, loading test was stopped at drift angle $R$=2.5%.

Doubly confined by AFRP tube and hoops, the specimen H98M-A44h showed stable performance at drift angle $R$=0.5%. At drift angle $R$=1.0%, lateral force degraded with bond slip. After loading test, bond splitting cracks were observed along longitudinal steel, and the bond failure occurred.

Adding cross ties and reducing the spacing of transverse steel, the specimen H99M-A44t depicted a rather stable response during loading, but did not get its flexural yield. It is considered that the lower concrete strength caused a poor bond capacity between concrete and embedded longitudinal steel bars.

With 6-ply-sheet AFRP tube and the same amount of transverse steel, increasing the concrete strength into 37.9 MPa, the column H00M-A66t represented flexural failure and adequate ductile capacity. The effectiveness of double confinement of AFRP tube and transverse steel is significantly proved experimentally.

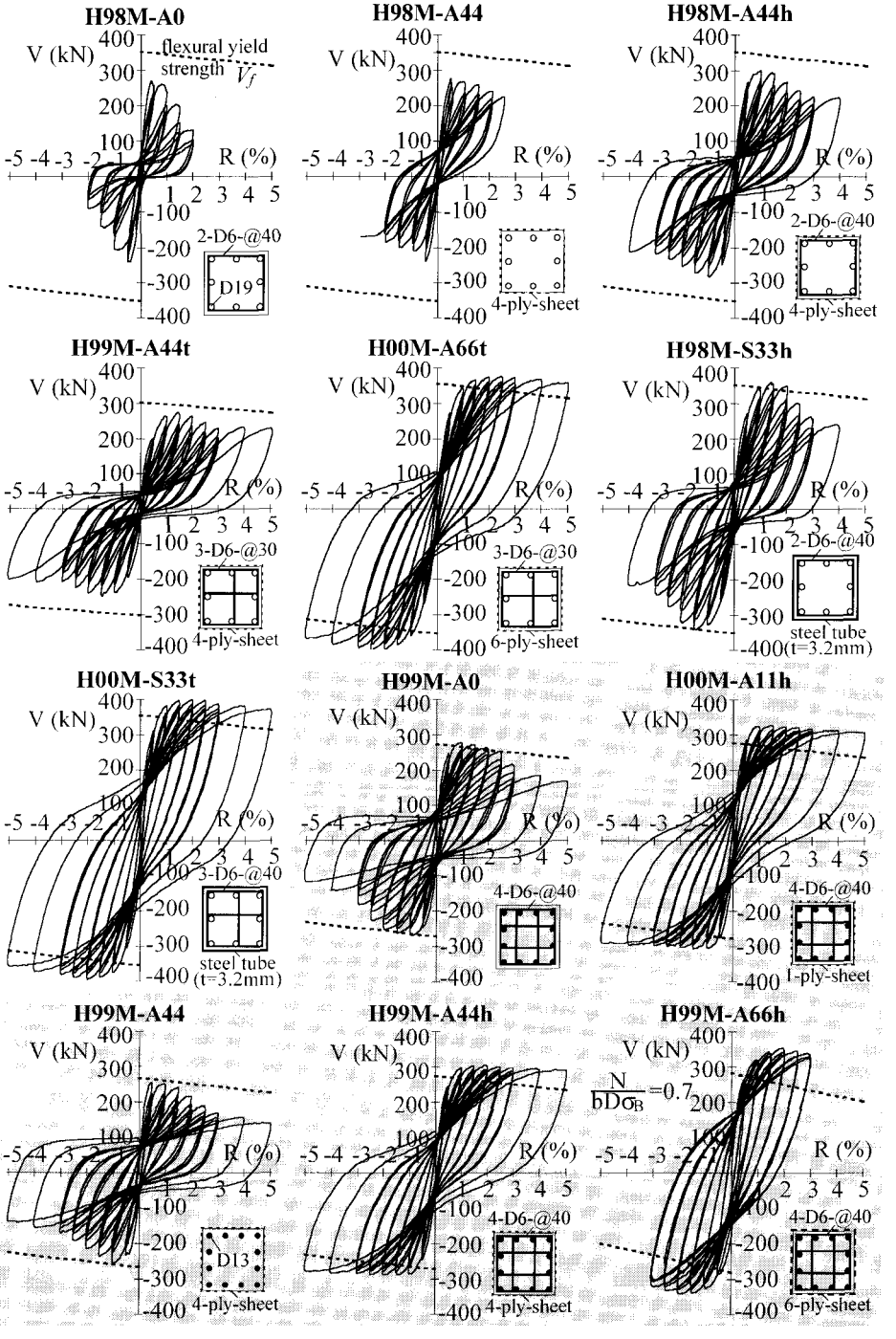



Figure 3. Measured shear force $V$ versus drift angle $R$ relationships

When confined by steel tube and hoops, longitudinal steel of the specimen H98M-S33h yielded at drift angle $R$=1.0%. From drift angle $R$=1.5%, bond slip appeared on $V$-$R$ curves, and the bond deterioration became severe. After flexural yield, the bond failure occurred in the end of column.

By adding cross ties, the column H00M-S33t drew a ductile resistant response after flexural yield of longitudinal steel. It is apparent that supplementary ties have a noticeable effect on increasing bond strength.

On the other hand, arranged with much transverse steel and less amount of longitudinal steel, different seismic performance was observed in the specimens of Series D13.

The ordinary specimen H99M-A0 showed flexural cracks in the end of the column at drift angle $R$=0.5%. At drift angle $R$=1.0%, the longitudinal steel got its tensile yield and the peak shear force was obtained. After drift angle $R$=2.0%, the deterioration of lateral force indicated that bond failure occurred due to the falling of the cover concrete in the end region of column.

Just only confined by 1-ply-sheet ARFP tube additionally, the column H00M-A11h did not perform any deterioration in lateral force, and the stable response remained until the final drift angle $R$=5%.

Confined by 4-ply-sheet AFRP tube, column H99M-A44 got its peak shear force at drift angle $R$=0.5%, then showed degradation until the end of loading. After test, it was observed that all the longitudinal bars buckled, and the cover concrete among bond splitting cracks along the inside longitudinal bars spalled off. The confinement condition of the inside bars was weaker than that of the corner bars, therefore the inside bars buckled prior to the corner bars. For the poor transverse confinement, this column is of bond failure accompanying with buckling of the longitudinal bars.

The column specimen H99M-A44h doubly confined by 4-ply-sheet AFRP tube and hoops depicted stable flexural behavior in hysteresis loops. Although some bond splitting cracks were observed, flexural failure governed the seismic behavior of the column.

With 6-ply-sheet AFRP tube and the same amount of hoops, subjected to high axial load level $N/(bD\sigma_B)$=0.7, the column specimen H99M-A66h presented flexural capacity. The loading could not be applied by the loading setup when the drift angle was greater than 3.0%. Hence, the loading test was conducted until drift angle $R$=3.0%. Since some compression cracks and bond splitting cracks were observed, the flexural failure was the main mode in the column.

Typical skeleton curves of shear force - drift angle hysteresis loops are compared in Figure 4, and accumulated energy absorption capacity curves are compared in Figure 5. It is apparent that the seismic behavior was improved by the double confinement of AFRP tube and steel hoop. In Series D13, lateral force response and accumulated energy absorption capacity of the specimen H00M-A11h are greater than that of the specimen H99M-A44h. It is considered that during casting concrete, the 1-ply-sheet tube expanded transversely under the lateral pressure of fresh concrete. When working as confining material, the AFRP tube behaved a confining effect much than that of square tube but less than that of circular tube. Hence, the experimental lateral response of the column H00M-A11h exceeds expected capacity.

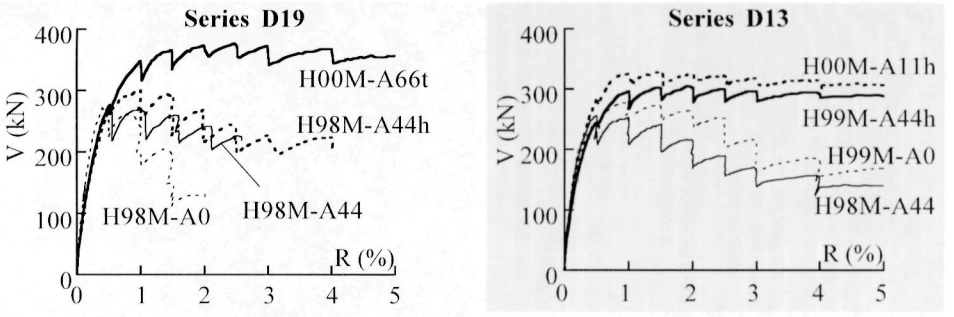



Figure 4. Comparison of shear force - drift angle skeleton curves

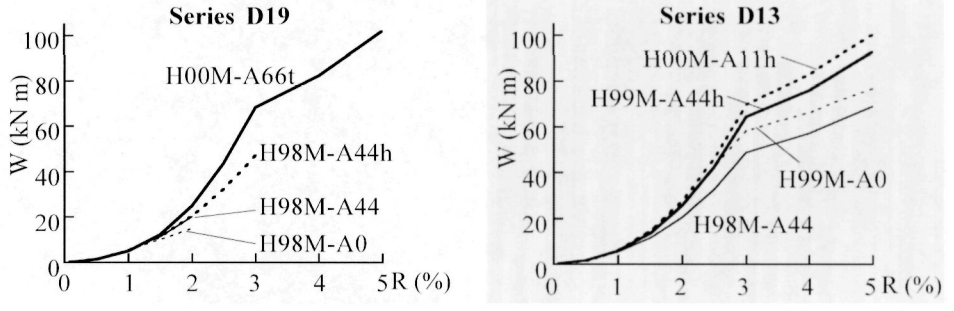



Figure 5. Comparison of accumulated energy absorption capacity results

## THEORETICAL INVESTIGATION

Shear strength of column was calculated by AIJ Design Guidelines' equation[5]. The drift angle $R_y$ when plastic hinge occurred was calculated by Sugano's equation, and shear strength degraded according to rotation of the plastic hinge. For the columns confined by the AFRP tube, the transverse reinforcing stress provided by the AFRP tube were determined corresponding to a lateral dilation strain of 0.7%, according to "Guidelines for Seismic Retrofit Design and Construction of Existing Reinforced Concrete and Steel Reinforced Concrete Buildings Utilizing Continuous Fiber Reinforcing Material" by the Building Disaster Prevention Association of Japan[1].

After examining bond stress and bond strength of longitudinal steel in columns, the shear strength due to bond slip was estimated by AIJ Design Guidelines' equation[5]. The influence of the AFRP tube was superposed into the transverse hoop ratio as $(p_{wf} \cdot E_f / E_s)$.

For flexural capacity, calculated results by simplified equation were adopted. Under low axial load level, flexural capacity by simplified equations could predict test results to a certain degree, however under high axial load level it could not.

For each specimen, the calculated and experimental results are compared in Figure 6. The test results of specimen H98M-A0 is close to the calculated shear strength. The *V-R* skeleton curve of the column H98M-A44 does not reach the flexural and shear capacity, however it exceeds the bond strength. The column H98M-A44h shows the same bond failure behavior in

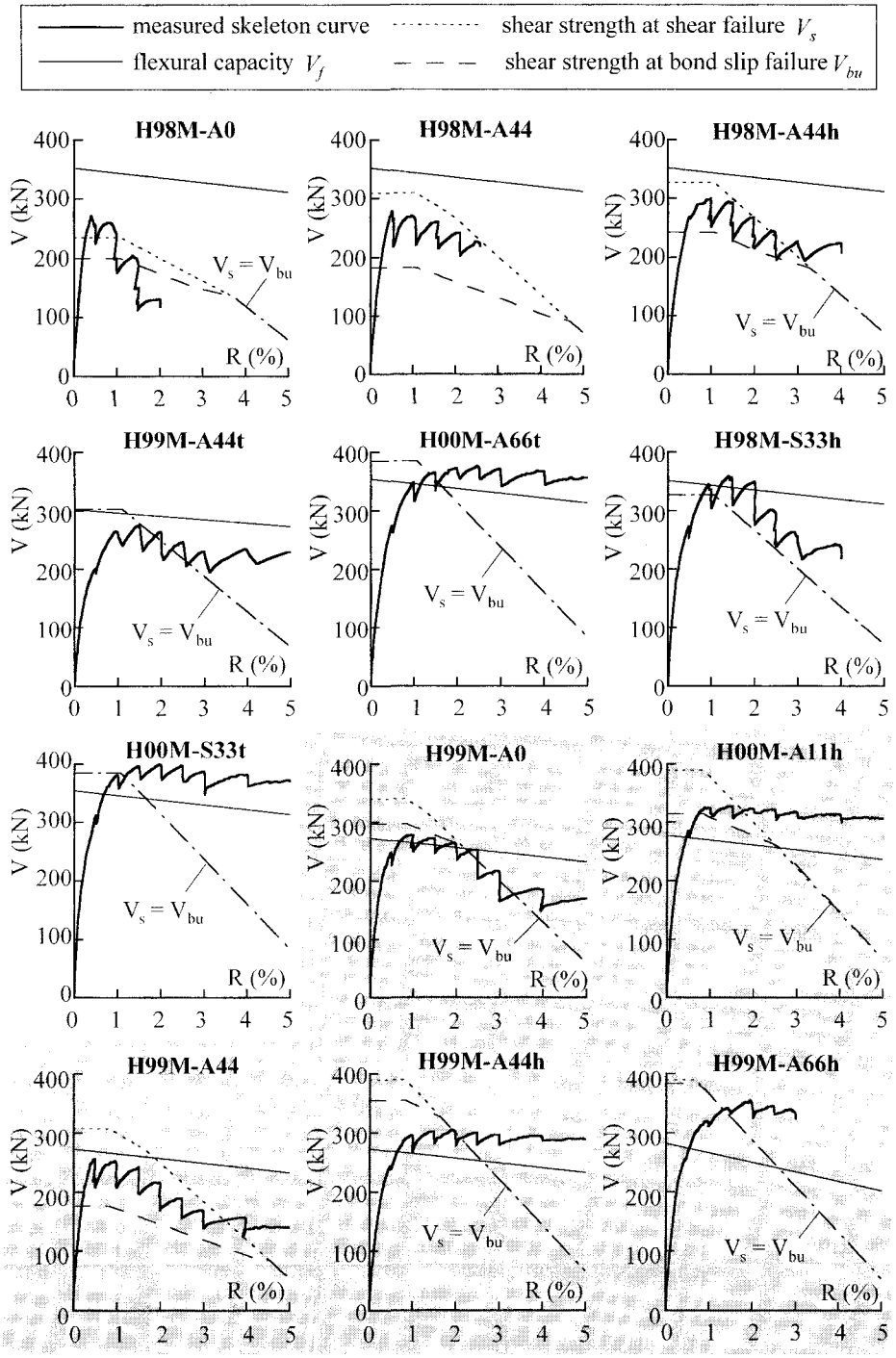



Figure 6. Comparison of experimental and analytical results

a higher level for the enhanced bond capacity. The column H98M-S33h obtained peak shear force close to calculated flexural result, however could not keep it until the end of loading.

In the specimen H99M-A0, the flexural yield was ensured, but when the plastic hinge rotating, the cover concrete fell off and the bond strength descended more fast than the flexural and shear capacity, hence bond the failure occurred finally. The measured skeleton curves the specimen H99M-A44 is lower than the flexural and shear forces, because the bond slip occurred. Specimen H99M-A44h and H99M-A66h depict *V-R* skeleton curves higher than calculated flexural results, however the bond and shear capacity does not seem sufficient as drift angle increases.

Above-mentioned calculated results are compared with the experimental results in Figure 7. In which, the $V_{exp}$ shows experimental peak shear force, the $V_s$ represents calculated shear strength before plastic hinge occurred, the $V_f$ means calculated flexural capacity by simplified equation, the $V_{bu}$ is calculated shear strength due to bond slip. Especially, the degradation of bond strength is dominant in comparison with shear strength in the specimens being of bond failure, such as the specimen H98M-A44, H98M-A44h, H99M-A44t and H99M-A44. When the shear strength and the bond strength exceed the flexural capacity, the flexural yield shall occur. This also can be applied to design.

In Figure 8, the ductility factors $\mu=R_f/R_y$ of specimens are compared with the analytical

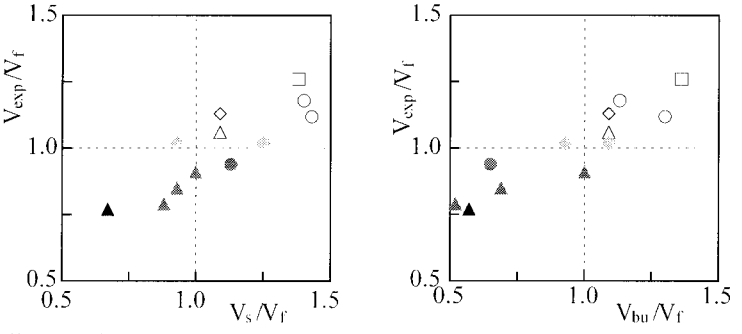



Figure 7. Failure modes

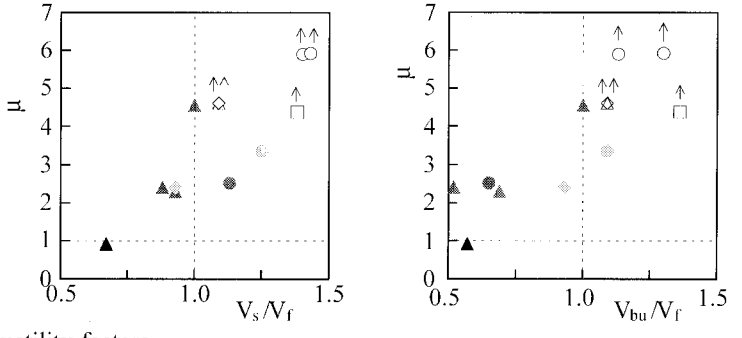



Figure 8. Ductility factors

strength, where the $R_f$ is experimental drift angle when shear force descends for 80% of peak shear force, the $R_y$ is drift angle when column yields and calculated by Sugano's approach. The arrows depicted in figures indicate that the column should have more ductility because the drift angle $R_f$ corresponding to the ultimate state deformation could not be obtained in loading test. Namely, the shear force did not descend for 80% of the peak shear force until final drift $R$=5%. As shown in Figure 8, the greater the value of $V_s/V_f$ and $V_{bu}/V_f$ becomes, the larger the ductility factor $\mu$ is. However, for the ordinary column H99M-A0, it is difficult to prevent the cover concrete from spalling off, hence the ductility can not be expected. Even if arranged by too many hoops, there is a limit of ductility to the ordinary hooped columns without AFRP tube, just as specimen H99M-A0.

## CONCLUSIONS

1) To investigate the effectiveness of the AFRP tube confinement, twelve columns were loaded under cyclic lateral force while simultaneously subjected to constant axial load. By impregnating aramid fiber sheet by epoxy resin, the premanufactured AFRP tube in hybrid column played the roles of transverse reinforcing material and stay-in-place.

2) Experimental results showed that bond failure was not prevented when columns were confined by the AFRP tube or hoop only. However, double confinement of the AFRP tube and hoop was effective to cause ductile flexural failure in the hybrid columns. The effectiveness of double confinement of the AFRP tube and transverse steel was proved experimentally.

3) For the hybrid columns confined by the AFRP tube and hoop, when the shear strength and the bond strength exceeded flexural capacity simultaneously, flexural failure with high ductility and high strength could be obtained.

## REFERENCES:

1) The Building Disaster Prevention Association of Japan. 1999. Guidelines for Seismic Retrofit Design and Construction of Existing Reinforced Concrete and Steel Reinforced Concrete Buildings Utilizing Continuous Fiber Reinforcing Material: 43-45. (In Japanese)

2) Seible, F., Hegemier. G., Karbhari, V., Burgueno.R. & Davol, A. 1997. The carbon shell system for modular short and medium span bridges. International Composites EXPO'97: Session 3-D/1-66.

3) Yamakawa T. & Zhong P. 1999. Seismic performance of RC columns laterally confined by carbon fiber reinforcing plastic tube. Specialist Techniques and Materials for Concrete Construction, Thomas Telford: 455-463.

4) Yamakawa T., Satoh H., & Zhong P. 1999. Seismic performance of Hybrid Reinforced concrete circular columns confined in aramid fiber reinforced polymer tube. Fourth International Symposium on Fiber Reinforced Polymer Reinforcement for Reinforced Concrete Structures, American Concrete Institute: 1089-1102.

5) Architectural Institute of Japan. 1999. Design guidelines for earthquake resistant reinforced concrete buildings based on inelastic displacement concept: 142-162, 175-192. (In Japanese)

6) Architectural Institute of Japan. 1999. AIJ Standard for Structural Calculation of Reinforced Concrete Structures-Based on Allowable Stress Concept-revised 1999: 154-155, 52-57. (In Japanese)

# Experimental investigation of FRP-strengthened RC beam-column joints

C. P. ANTONOPOULOS, T. C. TRIANTAFILLOU and C. G. PAPANICOLAOU
Department of Civil Engineering., University. of Patras, Greece.

## ABSTRACT
The results of a comprehensive experimental program, aiming at providing a fundamental understanding of the behavior of shear-critical exterior RC joints strengthened with fiber reinforced polymers (FRP) under simulated seismic load are presented in this study. The role of various parameters on the effectiveness of FRP is examined through 2/3-scale testing of eighteen exterior RC joints and conclusions are drawn on the basis of certain load versus imposed displacement response characteristics, comprising the strength (maximum lateral load), the stiffness and the cumulative energy dissipation capacity.

## INTRODUCTION AND BACKGROUND
Recent earthquakes worldwide have illustrated the vulnerability of existing reinforced concrete (RC) beam-column joints to seismic loading. Poorly detailed joints, especially exterior ones, have been identified as critical structural elements, which appear to fail prematurely, thus performing as "weak links" in RC frames. A typical failure mode in poorly designed joints is concrete shear, in the form of diagonal tension. Bond failure of rebars has been observed too, especially in interior joints where rebars are not properly anchored with standard hooks.

The authors started a research program about four years ago, aiming at expanding the range of applicability of the FRP strengthening technique to poorly detailed shear-critical RC joints. The simplest way to strengthen such joints is to attach (through epoxy bonding) FRP sheets or strips to the joint region, with the fibers in two orthogonal directions, those of the beams and columns meeting at the joint. This concept combines ease of application with effectiveness, as the two-dimensional fiber system in the joint will act as shear reinforcement. Studies in the area of FRP-strengthened joints have been conducted by other researchers too (e.g. Pantelides et al. 1999, Gergely et al. 2000). In the present study, the authors present the results of a comprehensive experimental program, which aimed at providing a fundamental understanding of the behavior of shear-critical exterior RC joints strengthened with composite materials under simulated seismic load, through the investigation of several design parameters. Details are provided next.

## EXPERIMENTAL PROGRAM
A total of eighteen, 2/3-scale, RC joints were constructed and tested, as shown in Fig. 1. All specimens had identical dimensions, and were reinforced such that they would represent a poorly detailed exterior T joint of a RC frame (Fig. 2). Reinforcement consisted of four 14 mm diameter rebars in the column, three 14 mm diameter rebars in each side (top, bottom) of the beam, 8 mm stirrups at a spacing of 10 mm in the column and 8 mm stirrups at a spacing

*FRPRCS-5*, Thomas Telford, London, 2001.

of 15 mm in the beam. Longitudinal steel was of type S500 and stirrups were of type S220, with measured average yield stress equal to 585 MPa and 260 MPa, respectively. Sixteen of the specimens had no stirrups in the joint and the remaining two specimens (specimens S-C and S-F22) had only one column stirrup in the joint. Three of the sixteen specimens (without stirrup in the joint) were not planar, but they were constructed with a transverse beam in one side, in order to account for the effect of confinement provided by transverse elements (specimens T-C, T-F33, T-F22S2). Reinforcement in the transverse beams consisted of four 14 mm diameter longitudinal rebars.

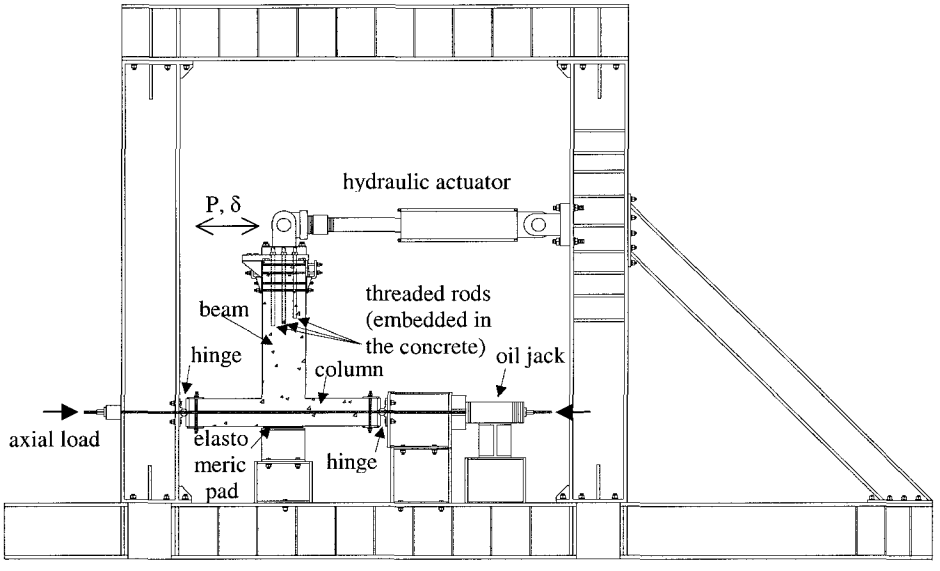



Figure 1. Schematic view of test setup and geometry of specimens.

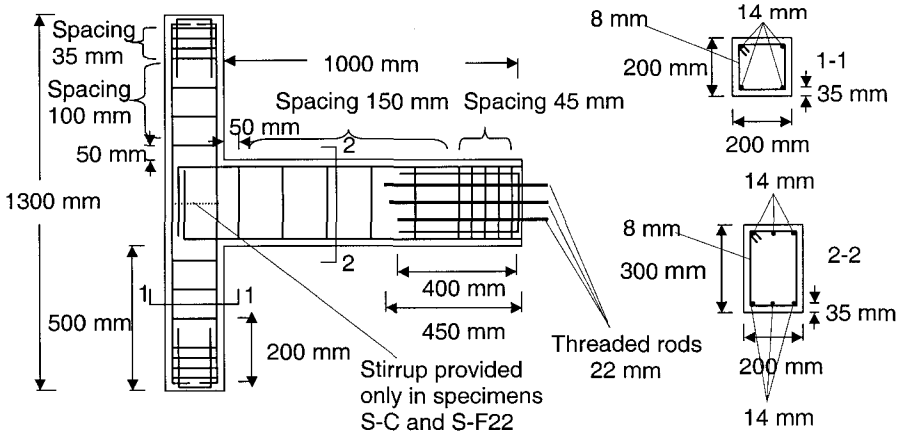



Figure 2. Details of reinforcement.

All specimens were designed such that failure would be due to shear in the joint. This was an important requirement, as one of the main objectives in this study was to evaluate the contribution of FRP to the shear capacity of RC joints. Moreover, the specimens were designed such that the effect of a series of factors on the shear capacity of joints could be investigated; these factors include the following: *effectiveness of strips versus sheets*, *number of strips* or *number of sheet layers*, *mechanical anchorages*, type of *fibers* (carbon versus glass), level of *axial load* in the column (equal to 46 kN in all specimens and 115 kN in F22A), *damage* in the joint prior to strengthening (F22in suffered initial damage by imposing a displacement of 10 mm which was removed prior to application of the FRP), effect of *transverse beam*. The designs of all the joints tested and details of the alternative strengthening configurations examined are given in Fig. 3.

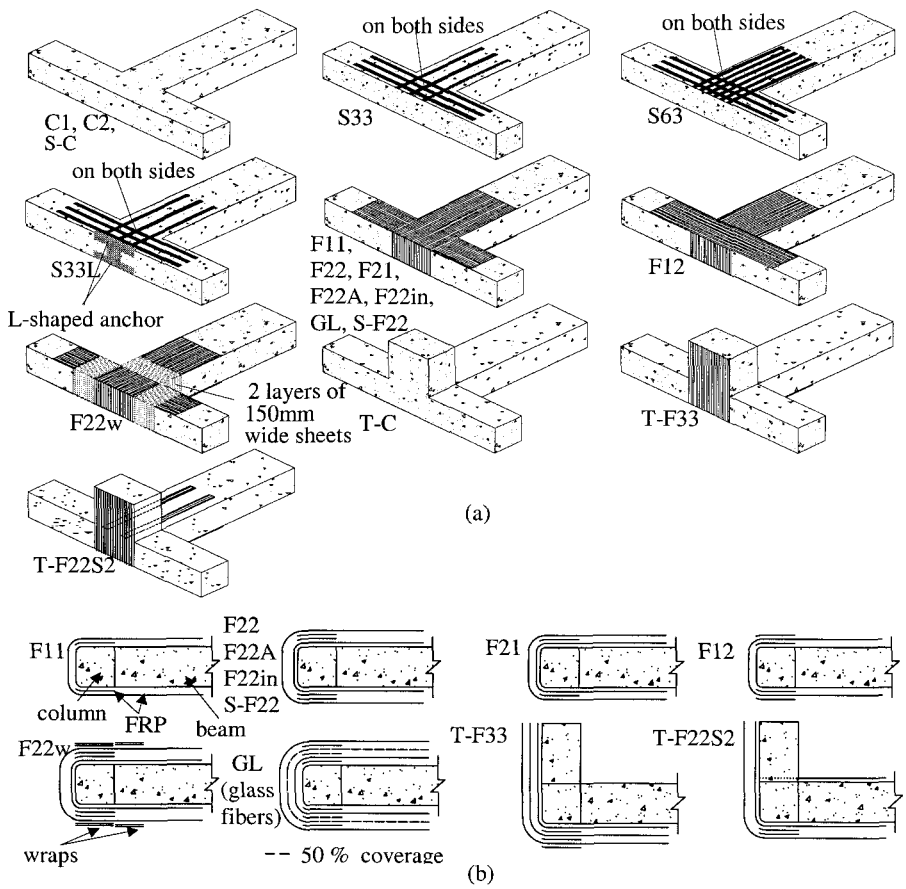



Figure 3. (a) Description of joints and strengthening alternatives; (b) layout of FRP layers.

The FRP strips used to strengthen specimens S33, S63 and S33L were 25 mm wide and 1.05 mm thick, and those for specimen T-F22S2 were 37.5 mm wide and 1.05 mm thick. The nominal thickness of sheets was 0.13 mm and 0.17 mm for carbon and glass, respectively.

The resulting area fractions of FRP reinforcement (defined as the cross sectional area of FRP divided by the member's cross sectional area) in the beam and the column, $\rho_{fb}$ and $\rho_{fc}$, respectively, are given in Table 1 (which gives also the 28 day average compressive strength of concrete). Finally, in all cases the FRP covered the joint region and extended 450 mm and 300 mm in the beam and the column, respectively.

The following properties (average values) were provided by the manufactures for the composite materials: elastic modulus and failure strain of carbon strips = 150 GPa and 0.016, respectively; elastic modulus and failure strain of carbon sheets = 230 GPa and 0.015, respectively; elastic modulus and failure strain of glass sheets = 70 GPa and 0.031, respectively.

Table 1. Specimen data and results.

| Specimen | 28 day concrete strength (MPa) | FRP area fraction | | Maximum load (kN) | | % difference with control | | Energy dissipated (kNmm) | |
|---|---|---|---|---|---|---|---|---|---|
| | | Beam $\rho_{fb}$ (%) | Column $\rho_{fc}$ (%) | Push | Pull | Push | Pull | 40 mm | % diff. |
| C1 | 19.5 | 0 | 0 | 31.32 | 27.13 | | | | |
| C2 | 23.7 | 0 | 0 | 30.82 | 31.08 | | | | |
| Aver. C1,C2 | 21.6 | 0 | 0 | **31.07** | **29.10** | **0** | **0** | 4995 | **0** |
| S33 | 26.0 | 0.26 | 0.39 | 34.66 | 35.28 | 11.6 | 21.2 | * | * |
| S63 | 24.2 | 0.52 | 0.39 | 39.36 | 40.24 | 26.7 | 38.3 | 5763 | **15.4** |
| S33L | 26.3 | 0.26 | 0.39 | 44.63 | 40.40 | 43.6 | 38.8 | 6015 | **20.4** |
| F11 | 22.8 | 0.13 | 0.13 | 42.76 | 42.44 | 37.6 | 45.8 | 6395 | **28.0** |
| F22 | 27.2 | 0.26 | 0.26 | 50.04 | 49.14 | 61.0 | 68.1 | 7477 | **49.7** |
| F21 | 27.0 | 0.26 | 0.13 | 51.08 | 50.29 | 64.4 | 72.8 | 7050 | **41.1** |
| F12 | 29.5 | 0.13 | 0.26 | 44.45 | 44.40 | 43.1 | 52.6 | 6085 | **21.8** |
| F22A | 27.8 | 0.26 | 0.26 | 57.38 | 52.56 | 84.7 | 80.6 | 8417 | **68.6** |
| F22W | 29.2 | 0.26 | 0.26 | 55.84 | 54.89 | 79.7 | 88.6 | 8532 | **70.8** |
| F22in | 21.0 | 0.26 | 0.26 | 41.93 | 41.59 | 35.0 | 42.9 | 5641 | **12.9** |
| GL | 19.5 | 0.42 | 0.42 | 44.13 | 43.04 | 42.0 | 47.9 | 6912 | **38.4** |
| S-C | 19.3 | 0 | 0 | **33.27** | **32.22** | **0** | **0** | 5494 | **0** |
| S-F22 | 19.0 | 0.26 | 0.26 | 44.09 | 43.23 | 32.5 | 34.2 | 6472 | **17.8** |
| T-C | 24.6 | 0 | 0 | **36.02** | **33.86** | **0** | **0** | 5873 | **0** |
| T-F33 | 26.0 | 0.19 | 0.19 | 44.26 | 44.45 | 22.9 | 31.3 | 7695 | **31.0** |
| T-F22S2 | 22.0 | 0.26 | 0.13 | 40.07 | 39.75 | 11.2 | 17.4 | 6207 | **5.7** |

* part of the hysteresis loops for this specimen is not correct and the energy results are not reliable; hence they are omitted.

Bonding of the composite materials took place at a concrete age of about 30-35 days. In order to ensure a high quality bond between the concrete and the FRP reinforcement, the specimens were thoroughly wire brushed (surfaces which received strips were roughened using a small hammer), until any loose material was removed, and vacuumed. In those specimens where the external reinforcement had to turn around sharp edges (column edges), grinding of the concrete was provided to a radius of about 25-30 mm.

In order to take advantage of the ability provided by the sheets to turn around the column (thus ensuring a good anchorage of the FRP reinforcement in the vicinity of the two column

edges), in most specimens the last FRP layer was always applied on the beam. Details about the application sequence of the various layers are given in Fig. 3b.

Specimen GL (strengthened with glass sheets) deserves special mention. The number of layers for this specimen was determined such that the FRP jacket would have the same axial rigidity as that for specimen F11 (with one layer in the column and one in the beam). The ratio of the products (thickness of sheet)x(elastic modulus) for carbon and glass sheets was calculated approximately equal to 2.5, meaning that the equivalent of one layer of carbon sheet would be "two and a half" layers of glass sheet. The "half" layer was achieved by cutting the sheet in narrow strips and using them to construct the second layer of the jacket (in both the beam and the column) with partial (50%) coverage of the beam and column sides. Three 33 mm wide strips were used for the column at a 63 mm spacing, and three 50 mm wide strips were used for the beam, at a 95 mm spacing.

An interesting feature was introduced in specimen T-F22S2. In addition to the sheets, this joint received two strips in the interior side of the beam. The strips were inserted into about 45 mm maximum diameter elliptical holes, which were first drilled and then wire brushed and thoroughly cleaned. Following placement of the strips, the holes were filled with epoxy mortar through injection. An interesting feature of the strips used for this joint was the preparation of their ends, in order to maximize their anchoring capacity inside the holes. These ends were first covered by an epoxy adhesive layer of varying thickness and then sand-coated (before hardening of the adhesive), in order to increase interlock with the surrounding epoxy mortar.

The full axial load was applied first (and held constant during testing) through high strength rods and a pair of oil jacks. Earthquake lateral loads were simulated by applying an alternating force to the end of the beam through an idealized pin. This force was applied in a quasistatic cyclic pattern using a horizontally positioned 500 kN MTS actuator. Data from the load cell and the actuator's displacement transducer were recorded using a computer controlled data acquisition system. The displacement-controlled loading sequence for each specimen consisted of three cycles at a series of progressively increasing (by 5 mm) displacement amplitudes in each direction (push and pull).

## EXPERIMENTAL RESULTS

Selective load-displacement curves are given in Fig. 4. The hysteresis loops obtained are characterized by substantial pinching, which is typical of joint shear failure. This failure mechanism developed in the form of diagonal cracking in the joint and was observed in all tests (for other than the control specimens where the concrete surface was not visible, the FRP had to be removed in order to allow for visual inspections). Hence, the key objective of strengthening the joints while maintaining the shear failure mode was achieved. A typical diagonal cracking pattern corresponding to shear failure is illustrated in Fig. 5a. Details about the failure modes and their sequence for each joint tested are given by Antonopoulos and Triantafillou (2000). In general, the strips and multi-layer sheets debonded prematurely (e.g. Fig. 5b,c), whereas single layer or well-anchored sheets fractured prior to debonding (see Fig. 5d).

In order to evaluate the effectiveness of the various FRP reinforcement configurations, the strength, the stiffness and the energy dissipation capacity for every load cycle were recorded. The strength (maximum load) in both the push and the pull direction is given in Table 1. Typical stiffness versus displacement curves are shown in Fig. 6. Finally, energy dissipation

due to inelastic action within and near the joint panel was computed by summing the area enclosed within the load versus displacement curves. The cumulative energy corresponding to 40 mm displacement level is given in Table 1, and in graphical form for some of the specimens tested in Fig. 7.

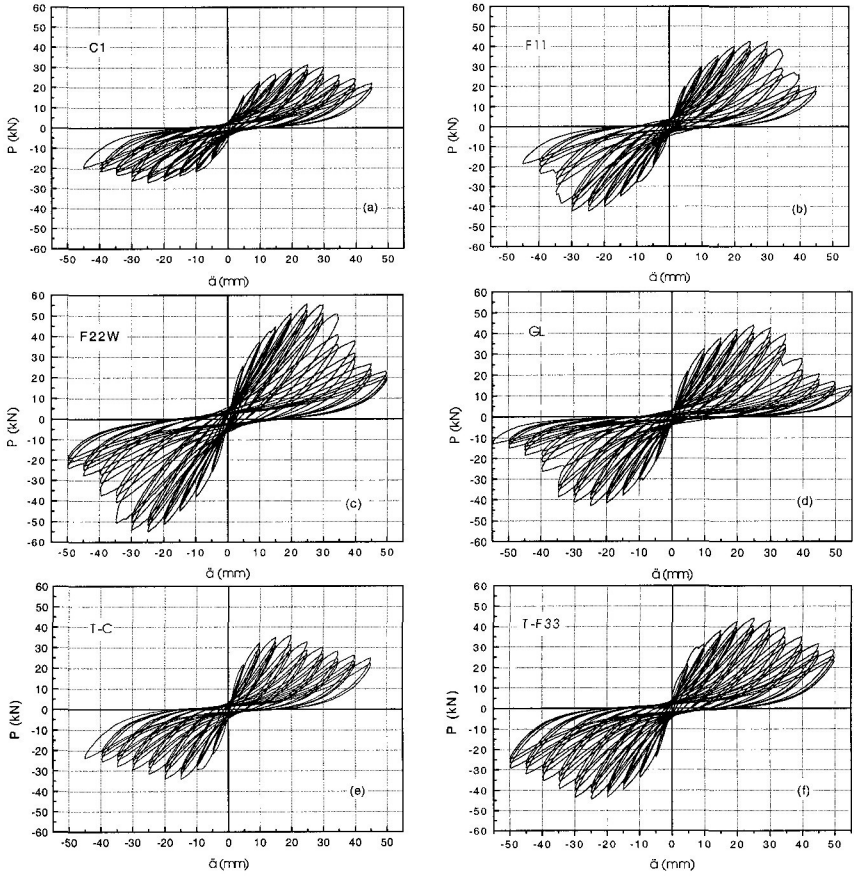
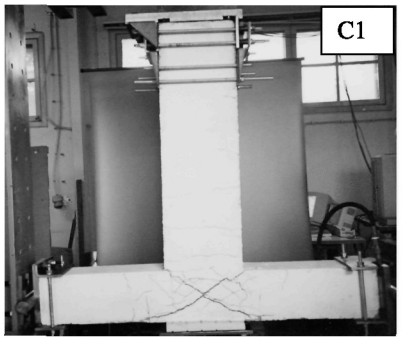
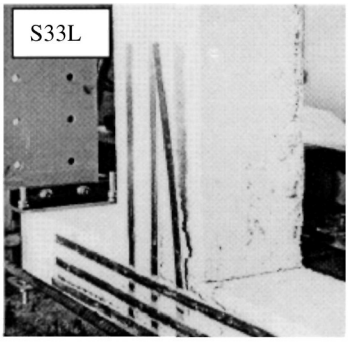


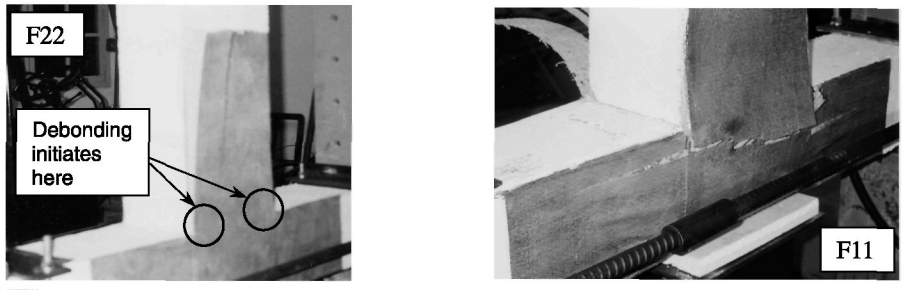

Figure 4. Typical load versus displacement curves.




(a)




(b)




(c) (d)

Figure 5. Typical photographs of specimens tested.

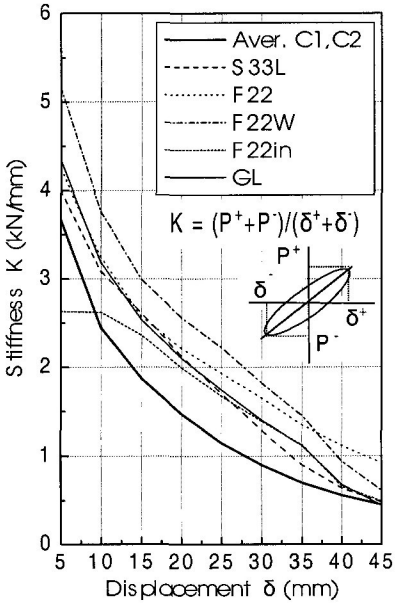



Figure 6. Typical curves of stiffness versus displacement.

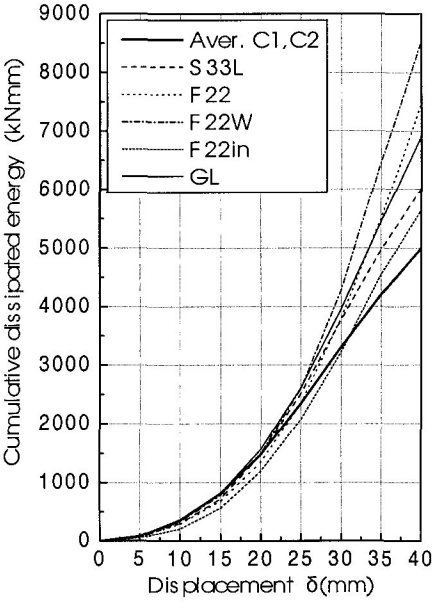



Figure 7. Typical curves of energy dissipation versus displacement.

## ANALYSIS OF RESULTS

All the joints tested failed as designed, that is in shear, which developed in the form of diagonal cracks in the concrete. In terms of the various factors examined in this investigation, careful examination of the test results in terms of strength (average increase in the push and pull direction) and energy dissipation (at the end of the 40 mm cycles) revealed the following information:

- *Increased area fraction in both the beam and the column* (average of C1-C2 versus F11 and F22): Both the strength and the dissipated energy increase considerably with – but not proportionally to - the number of FRP layers. The strength increase is about 40% and

65% for $\rho_{fb} = \rho_{fc} = 0.0013$ and 0.0026, respectively; and the associated values for energy dissipation are about 30% and 50%.

- *Increased area fraction in the beam only* (average of C1-C2 versus S33 and S63, and versus F11, F21): In terms of strength, increasing the FRP area fraction in the beam is nearly as effective as it is for equal increase in both the beam and the column, implying that the effectiveness of column FRP is rather limited. The strength increase in joints with strips is about 15% and 30% for $\rho_{fb} = 0.0026$ and 0.0052 (with $\rho_{fc} = 0.0039$ in both cases), respectively; the associated energy values are about 15% and 20%. In joints with sheets, the strength increase is about 40% and 70% for $\rho_{fb} = 0.0013$ and 0.0026 (with $\rho_{fc} = 0.0013$ in both cases), respectively; and the associated energy values are about 30% and 40%.
- *Effectiveness of beam versus column FRP reinforcement* (average of C1-C2 versus F21, F12): Beam reinforcement is much more effective than column reinforcement. This may be seen by comparison of results for specimens with $\rho_{fb} = 2\rho_{fc} = 0.0026$ and $\rho_{fc} = 2\rho_{fb} = 0.0026$, which indicate a strength increase in the order of 70% and 50%, respectively. The corresponding values for energy dissipation are approximately 40% and 20%.
- *Effect of mechanical anchorage* (F22 versus F22W, S33 versus S33L): The mechanical anchorages employed in this study increased the effectiveness of FRP sheets in terms of strength and energy by about 30% (from 65% increase to 85%) and 40% (from 50% increase to 70%), respectively. For strips, the effectiveness of anchorage was much higher, in the order of 150%: strength increases of about 15% (S33) jumped up to about 40% (S33L).
- *Effect of axial load on strengthened joints* (F22 versus F22A): The favorable effect of high axial load on the shear capacity of FRP-strengthened joints was confirmed. A 2.5 times higher load pushed the strength increase from 65% to about 85% and the energy increase from 50% to 70%.
- *Effect of initial damage* (F22 versus F22in): The initial damage affected adversely the response of the strengthened joint. Strength and energy increases for the undamaged joint were about 65% and 50%, respectively. For the pre-cracked joint these values dropped to about 40% and 15%, indicating that if the strengthened joint is damaged (but not repaired), FRP materials are less effective in terms of energy dissipation as opposed to strength increase.
- *Carbon versus glass FRP* (F11 versus GL): Glass fibers proved only slightly more effective than carbon fibers in terms of strength, but more effective in terms of energy dissipation (about 30% energy increase in F11 versus 40% in GL).
- *Sheets versus strips* (S33L versus F22): Joints S33L and F22 had the same FRP area fraction in the beam and different in the column. Despite the higher FRP area fraction in the column (0.0039 versus 0.0026), the specimen with strips performed worse than that with sheets. The increase in strength and energy was 40% and 20%, respectively, in S33L, whereas the corresponding values for F22 reached 65% and 50%. This result is not surprising, as the achievement of proper anchorages for strips is a much more difficult task than for sheets; yet, the sheets provide a more even transfer of forces over the joint region.
- *Effectiveness of FRP versus steel reinforcement* (stirrups) in the joint (average of C1-C2 versus F22 and S-C versus S-F22): As the transverse steel reinforcement in the joint increased, the FRP became less effective. Area fractions $\rho_{fb} = \rho_{fc} = 0.0026$ in the joint without the extra stirrup provided a 65% and 50% increase in the strength and the energy, respectively, whereas the associated values for the joint with one extra stirrup were about 35% and 20%.
- *Effectiveness of FRP on joints with transverse beam* (T-C versus T-F33 and average of C1-C2 versus average of F11-F22; T-C versus T-F22S2 and average of C1-C2 versus F21): For the case of FRP sheets making a 90° turn, the presence of a transverse beam

decreased the effectiveness of the FRP by about 50% and 20% in terms of strength and energy, respectively. The associated reduction in the case of sheets combined with straight strips was even higher, in the order of 80% (strength) and 85% (energy).

When a comparison of the test results is made in terms of stiffness, most strengthening configurations resulted in higher stiffness values compared with the control joints. These values ranged from about 5% to 40% in the early cycles ($\delta$ = 5 mm), from 20% to 90% at $\delta$ = 25 mm, and from nearly 0% to 100% at the end of the displacement history ($\delta$ = 45 mm). The highest increases were obtained when FRP sheets were anchored using transverse wrapping (joint F22W). The results for the pre-damaged joint (F22in) demonstrated that after a certain displacement level (about 10 mm in this study) even low FRP area fractions ($\rho_{fb}$ = $\rho_{fc}$ = 0.0026 here) result in considerable stiffness increase, which was up to about 50% in this study. Finally, when the comparison is made in terms of the rate of stiffness degradation, the conclusion is that this quantity is not affected much by the configuration of the FRP strengthening system.

## CONCLUSIONS

The tests performed in this study demonstrated that externally bonded FRP reinforcement is a viable solution towards enhancing the strength, energy dissipation and stiffness characteristics of poorly detailed (in shear) RC joints subjected to simulated seismic loads. Relatively low FRP area fractions increased both the strength (peak lateral load capacity) and the cumulative dissipated energy up to about 70-80%. The increase in stiffness varied with the imposed displacement level and reached values in the order of 100%.

The design of specimens allowed for an investigation of several variables. The main conclusions, in terms of strength and energy dissipation, may be summarized in a rather simplified and qualitative manner as follows:

- Debonding dominates the behavior of external reinforcement unless very low area fractions are employed or proper mechanical anchorages are provided.
- Both the strength and the dissipated energy increase considerably with – but not proportionally (due to premature debonding) to - the number of FRP layers.
- Increasing the FRP area fraction in the beam is nearly as effective as it is for equal increase in both the beam and the column, implying that the effectiveness of column FRP is rather limited.
- Mechanical anchorages increase the effectiveness of both strips and sheets. Wrapping of longitudinal FRP sheets with transverse layers proved to be a highly effective anchorage system.
- The effect of high axial load on the shear capacity of FRP-strengthened joints is quite positive.
- If the strengthened joint is damaged (but not repaired), FRP materials are less effective in terms of energy dissipation as opposed to strength increase (both quantities increase, though).
- On the basis of the same axial rigidity, glass fiber sheets proved marginally more effective than carbon fiber sheets.
- The effectiveness of FRP increases as the transverse steel reinforcement in the joint decreases.
- Compared with planar specimens, the effectiveness of FRP sheets in joints with a transverse beam is reduced (not so much for the energy as for the strength).

**ACKNOWLEDGEMENTS**

Partial support to this research has been provided by the Research Committee of the University of Patras ("K. Karatheodoris" Program). The authors wish to thank Assistant Professor S. Bousias and Mrs. D. Grammenou for their invaluable assistance in the experimental program; and SIKA Hellas for providing the composite materials used in this investigation.

**REFERENCES**

Antonopoulos, T. C. and Triantafillou, T. C. (2000). "Experimental investigation of FRP-strengthened RC beam-column joints". *J. Comp. Constr.*, ASCE, submitted.

Gergely, J., Pantelides, C. P. and Reaveley, L. D. (2000). "Shear strengthening of RC T-Joints using CFRP composites". *J. Comp. Constr.*, ASCE, 4(2), 56-64.

Pantelides, C. P., Gergely, J., Reaveley, L. D. and Volnyy, V. (1999). "Retrofit of RC bridge pier with CFRP advanced composites". *J. Struct. Engrg., ASCE*, 125(10), 1094-1099.

# Seismic Upgrade of Beam-Column Joints with FRP Reinforcement

ANDREA PROTA and ANTONIO NANNI, University of Missouri-Rolla, USA
GAETANO MANFREDI and EDOARDO COSENZA, University of Naples Federico II, Italy

## SUMMARY
Many opportunities are becoming available for using composite materials to strengthen/upgrade existing reinforced concrete (RC) structures. This paper focuses on a new technique for the seismic upgrade of RC beam-column connections in gravity load-designed frames by the application of FRP rods and/or laminates. The near surface mounted FRP rods provide flexural strengthening, whereas the lay-up laminates provide confinement and shear strengthening. Along with the modeling of such upgraded connections to assess the increase in strength and/or ductility exhibited by the composite reinforced connection, an experimental program was planned and it is being undertaken. A preview is given in this paper together with an explanation of its philosophy; furthermore, interesting preliminary results are presented and discussed. If confirmed, the proposed upgrade method will have a significant impact on the engineering practice in the near future.

## INTRODUCTION
RC frames, designed without seismic provisions, are often characterized by an unsatisfactory structural behavior due to low ductility and lack of a strength hierarchy of global failure mechanisms. A critical region in an RC frame is the beam-column connection, where different construction details can originate local failures, such as the shear collapse of the panel due to the lack of transverse reinforcement. In general, the lack of a design based on the strength hierarchy influences the global behavior of GLD frames and is responsible for the low dissipative capacity [Cosenza and Manfredi 1997, White and Mosalam 1997].

The present paper focuses on the problems associated with the seismic upgrade of GLD frames and, in particular, of beam-column joints that can be knee, interior, exterior, or corner joints depending on their vertical and horizontal position in the structure. On interior and exterior GLD connections (a large part of the joints in a building), an experimental study was performed by Beres et al. [1996]. They underlined seven critical details that could be potential causes of failure in a GLD structure subject to an earthquake. Four of the seven were related to the columns, they are:

- Longitudinal reinforcement less than 2% of the concrete cross section
- Lapped splices of the longitudinal reinforcement above the construction joint
- Insufficient confinement provided by the ties, and
- Construction joints above and below the beam-column connection

*FRPRCS-5*, Thomas Telford, London, 2001.

The remaining three are related to:

- Discontinuous positive reinforcement in the beam
- Lack of transverse reinforcement in the panel, and
- Weak column-strong beam condition.

Composite materials, known as fiber reinforced polymers (FRP), have shown a great potential for the strengthening of RC structures [Dolan et al. 1999] in the forms of:

- Lay-up laminates externally bonded to a concrete member to increase flexural and shear capacity as well as to provide concrete confinement [Alkhrdaji et al. 1999], and
- Near surface mounted (NSM) reinforcement to increase flexural and shear strength [De Lorenzis et al. 2000].

At present, studies on the possible application of composite materials for the seismic upgrade of RC beam-column connections are at an early stage [Pantelides et al. 2000]. The present research focuses on this topic with the objective of evaluating the opportunities offered by using FRP sheets and NSM rods in strengthening GLD joints. In order to assess the validity of this strengthening methodology, a detailed experimental program is proposed.

The program analyzes the effects of FRP reinforcement detailing and the other parameters on the global behavior of the beam-column connection and its failure mechanisms. The test results and their analysis will be used to compile design and construction guidelines on the seismic retrofitting and upgrade of RC beam-column joints with FRP sheets and NSM rods. This paper provides a first insight on the research program previously described. The outcomes of the first five tests are presented and the encouraging results are discussed.

## RESEARCH OBJECTIVES

The goal of this research is to investigate the effects of FRP reinforcement detailing on the behavior of the beam-column connection, its failure mechanisms, and its ductility. In particular, the planned experimental program is expected to demonstrate that, by means of targeted strengthening, it is possible to establish a strength hierarchy in the member. This hierarchy starts from the lowest level (i.e., column failure) given by the virgin joint. The first level of FRP upgrade moves the failure to the panel, and then, further strengthening moves it to the beam. The influence of the axial load applied to the column is also investigated. The experimented results will be used to develop design guidelines that, for different situations, would allow the choice of the upgrade level for the joint depending on the desired strength and/or ductility. Ultimately, the engineer could have the tools to modify the performance of an existing structure with an economical and sound technology.

## TEST SPECIMENS

In choosing the dimensions of the specimen, typical frame and geometrical ratios were taken into account even though some scaling was adopted to maintain the specimen size and weight to a manageable level. The specimen's cross section and the steel reinforcement used are shown in Figure 1. The specimen design was carried out following the recommendations of a building code [ACI 318-63] pre-dating the current one, as it is representative of a large number of existing buildings. These code provisions were used to determine the spacing of steel stirrups and ties. The amount of longitudinal steel reinforcement for the column was fixed equal to about 2% of its concrete gross cross-sectional area (ACI 318-63 allows a

minimum of 1%). The concrete cover was equal to 38 mm. Regarding materials, concrete had a compressive strength, $f'_c$, equal to 31.7 MPa and steel was characterized by a yield strength, $f_y$, equal to 420 MPa.

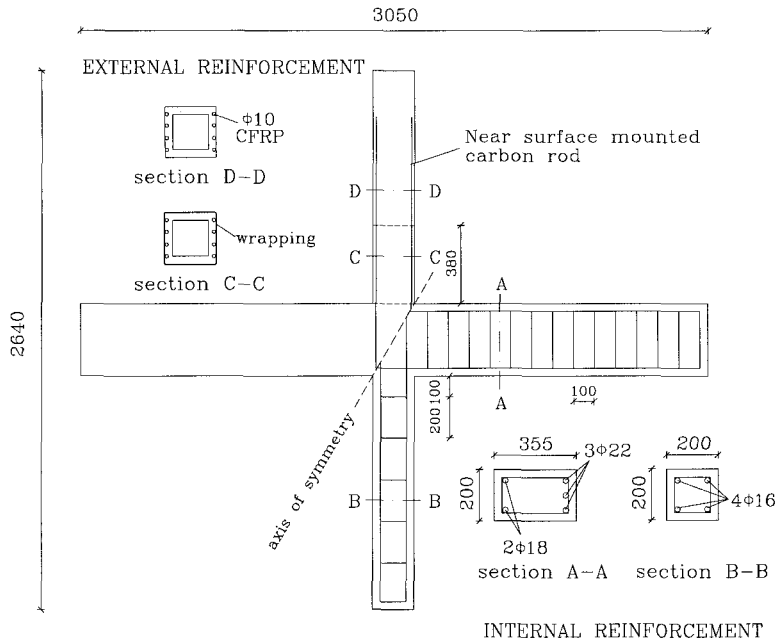



Figure 1. Specimen geometry (all the dimensions are in mm)

The confinement by lay-up jacketing was accomplished with two plies of CFRP. Each ply had a fiber-only thickness of 0.165 mm and was characterized by a modulus of elasticity, $E_{fs}$, equal to 229,600 MPa and the ultimate tensile strength, $f^*_{su}$, equal to 3,465 MPa. As shown in section C-C of Figure 1, the FRP wrapping was extended for 380 mm over the length of the column with an overlap of 100 mm for each ply.

For the specimen where the column is to be strengthened with NSM rods, eight ϕ10 CFRP rods were used. These rods, 2,200 mm long, were installed through the panel using near surface mounted technology and provided a continuous flexural reinforcement fully effective in the critical column sections close to the nodal zone. See section D-D in Figure 1. The CFRP rods had the modulus of elasticity, $E_f$, equal to 106,400 MPa and an ultimate tensile strength, $f^*_{ru}$, equal to 1,900 MPa. To facilitate installation of the NSM rods, eight wooden strips were nailed to the forms so that grooving the column and drilling through the panel for the subsequent installation of the rods could be performed with less difficulty and greater precision. However, it has been demonstrated in other projects that the grooving and drilling is possible in the field with conventional tools.

The set-up of each specimen on the laboratory floor is shown in Figure 2. At one of the column ends a constant axial load, P, is applied by means of an hydraulic jack independently operated. At the other end of the column, a load cell is placed to record the applied load P.

The restraints at the extremes of the columns simulate hinges that allow rotation by means of a pair of steel bars on both sides of the element. Two additional shear loads are applied on the extremes of each beam with independently operated jacks. A load cell on each cylinder contacting the beam records the applied force. During the test the cylinders can be switched so that load can be applied on the opposite face of the beams (see Figure 2). A greased plywood sheet between the specimen and the floor limits the friction and allows for the free movement of the beams and column.

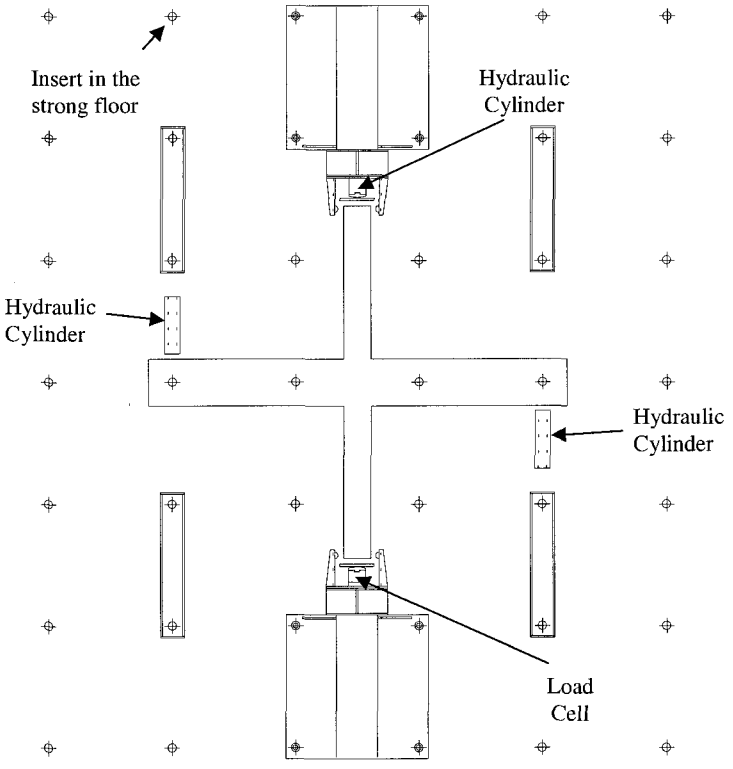



Figure 2. Test set-up

## EXPERIMENTAL PROGRAM

The first phase of the experimental program consists of 12 tests (see Table 1). In particular, two series of tests are planned. Each series is characterized by the same axial load applied to the column. The difference among the six specimens relates to the level of upgrading, designed to verify expected levels of the strength hierarchy. The first specimen is the "virgin" joint (1.a or 2.a), like those designed and built without seismic provisions. The other five are upgraded with FRP reinforcement in the following ways: two of them show respectively wrapping (1.b or 2.b) and wrapping combined with NSM rods in the column (1.c or 2.c). In the following two, both column and panel are strengthened, the latter with sheets (1.d or 2.d) and sheets and rods (1.e and 2.e), respectively. In the last one, the wrapping of the beams is added to the strengthening of columns and panel (1.f or 2.f).

In Table 1 P is the axial load acting on the column, B the dimension of each side of the column and of minimum side of the beam, H the maximum dimension of the beam, $A_{col}$ the total longitudinal steel reinforcement of the column, $A_s$ and $A_s$' respectively top and bottom longitudinal steel reinforcement of the beam.

Table 1. Experimental program

| Specimen | COLUMN | | | | | PANEL | BEAM | | | | |
|---|---|---|---|---|---|---|---|---|---|---|---|
| | P | B | $A_{col}$ steel | FRP sheet | FRP NSM | upgraded by | B | H | $A_s$ steel | $A_s$' steel | FRP sheet |
| | kN | mm | rods | plies | rods | | mm | mm | rods | rods | plies |
| 1.a | 250 | 200 | 4φ16 | 0 | 0 | ------- | 200 | 355 | 3φ22 | 2φ18 | 0 |
| 1.b | 250 | 200 | 4φ16 | 2 | 0 | ------- | 200 | 355 | 3φ22 | 2φ18 | 0 |
| 1.c | 250 | 200 | 4φ16 | 2 | 8φ10 | ------- | 200 | 355 | 3φ22 | 2φ18 | 0 |
| 1.d | 250 | 200 | 4φ16 | 2 | 8φ10 | sheets | 200 | 355 | 3φ22 | 2φ18 | 0 |
| 1.e | 250 | 200 | 4φ16 | 2 | 8φ10 | sh.+rods | 200 | 355 | 3φ22 | 2φ18 | 0 |
| 1.f | 250 | 200 | 4φ16 | 2 | 8φ10 | sh.+rods | 200 | 355 | 3φ22 | 2φ18 | 2 |
| 2.a | 125 | 200 | 4φ16 | 0 | 0 | ------- | 200 | 355 | 3φ22 | 2φ18 | 0 |
| 2.b | 125 | 200 | 4φ16 | 2 | 0 | ------- | 200 | 355 | 3φ22 | 2φ18 | 0 |
| 2.c | 125 | 200 | 4φ16 | 2 | 8φ10 | ------- | 200 | 355 | 3φ22 | 2φ18 | 0 |
| 2.d | 125 | 200 | 4φ16 | 2 | 8φ10 | sheets | 200 | 355 | 3φ22 | 2φ18 | 0 |
| 2.e | 125 | 200 | 4φ16 | 2 | 8φ10 | sh.+rods | 200 | 355 | 3φ22 | 2φ18 | 0 |
| 2.f | 125 | 200 | 4φ16 | 2 | 8φ10 | sh.+rods | 200 | 355 | 3φ22 | 2φ18 | 2 |

The influence of the compressive stress applied to the column on the resistant mechanism of the connection will be assessed by comparing specimens belonging to the two series. Axial loads reported in Table 1 induce in the columns an average compressive stress equal to 6 MPa for series 1 and 3 MPa for series 2. The former takes into account the increase of axial load due to a seismic event, while the latter refers to a serviceability condition.

## LOADING ARRANGEMENT

Once the specimen is in place, the loading process includes the following steps:

- *Axial column load application*: this is the preliminary step, during which the prefixed load P is gradually applied to the column. During the application of the axial load, the beam ends are free in order to allow the small displacements in their transverse direction.

- *Gravity beam loads application*: after the axial load has reached the fixed value and is kept constant, the beam load setup is arranged. Two equal shear forces are then applied to the beam ends in order to simulate the effect of gravity loads. The amount of the total load was calculated to reproduce on the beams the service condition. In particular, the adopted value of shear force, $V_V$, equal to 40 kN generates a maximum flexural moment equal to half of the design moment obtained according to ACI provisions. The jack configuration during this phase is shown in the Figure 3.

- *Reversed load cycles*: with this step the earthquake simulation starts. As soon as the beam shear is unequal at each side of the connection, a flexural moment and shear force are generated in the column to maintain equilibrium. An increment/decrement in shear force, $\Delta V$, equal to 4.45 kN was established so that at least six reversed load cycles were needed before reaching the design moment strength in the column calculated according to ACI provisions. The algebric sum of beam shear forces and compressive column axial force is kept constant during the test. In the beginning the shear force application is performed by

maintaining the jacks from the same side of the beams and increasing/decreasing their forces. For every shear force increment/decrement, three repetitions are carried out. Once zero shear force is reached at one of the beam ends (i.e., nine load cycles), the cylinders are switched at the beam ends.

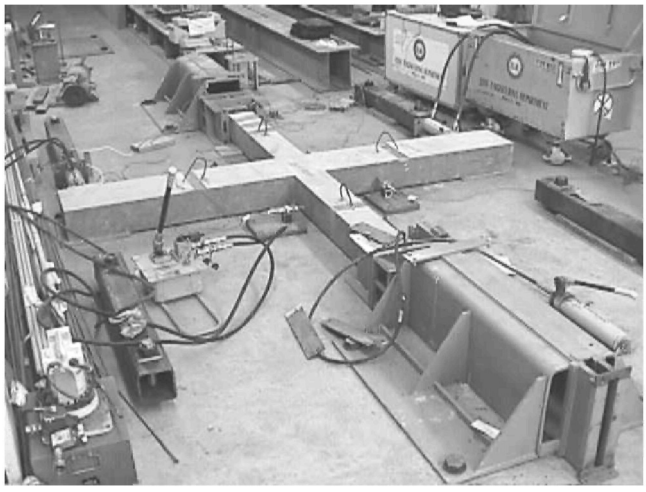


Figure 3. Gravity beam loads application

The three load phases described above are shown in Figure 4, which represents the load history recorded during a test. $V_V$ is the gravity shear force on both the beams; $V_1$ and $V_2$ are the shear forces on the beams during the reverse load application.

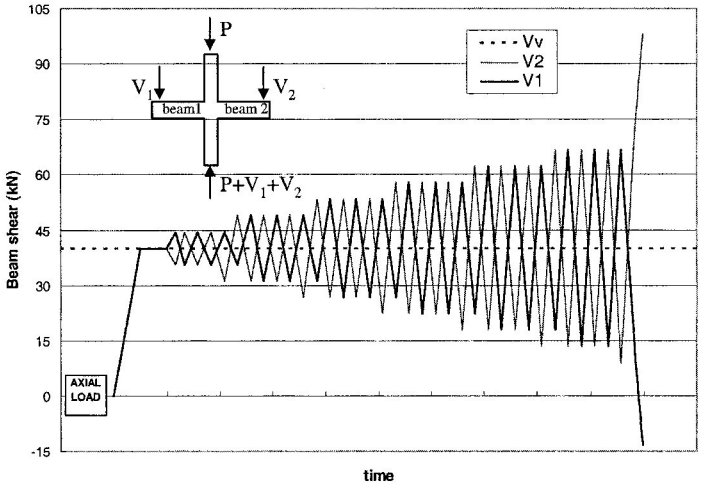



Figure 4. Load history

## PRELIMINARY EXPERIMENTAL RESULTS

After the first five tests (1.a, 1.b, 1.c, 2.a and 2.c in Table 1), some significant results were obtained. First, a comparison between virgin and strengthened joints belonging to the same

series underlines a significant increase of the column strength; a change also in the column stiffness can be observed. This is depicted in Figure 5, where a comparison between joints 1.a, 1.b and 1.c is provided in terms of the envelopes of shear column versus average displacement. This displacement was calculated by averaging the values recorded by the LVDTs placed 280 mm from the beam-column interface on opposing sides of the column.

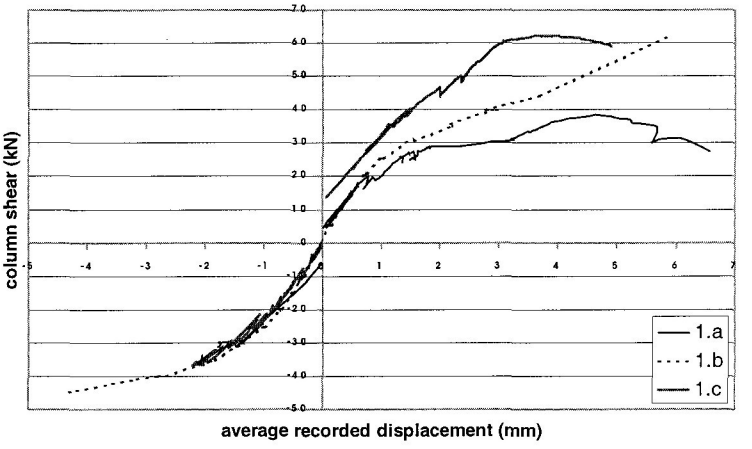



Figure 5. Column shear-displacement: 1.a (control joint), 1.b and 1.c (upgraded joints)

For both the series, while the control joint (1.a and 2.a) collapsed by compressive failure at the critical cross sections in the column, in the upgraded connections (1.b, 1.c and 2.c) the crisis migrated to the panel (Figure 6).

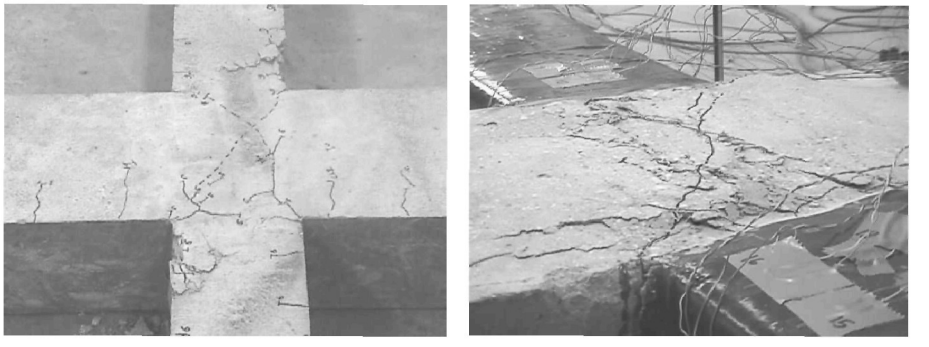


Figure 6. Failure mode of the control 1.a (left) and of the upgraded joint 2.c (right)

In the strengthened specimens, panel failure occurred without using the total column capacity; however, in spite of this, the maximum column shear was much higher than that of the virgin column. A comparison between the control joints of the two series (1.a and 2.a) allows to underline the higher ultimate strength of the column subjected to the lower axial load P. However, the column shear at failure for connection 1.c is higher than that of 2.c. Table 2

summarizes these results, reporting the recorded shear in the columns at failure, $V_{col}$, and the joint failure mode.

Table 2. Column shear at failure and failure modes

| Specimen | $V_{col}$ (kN) | Failure mode |
|---|---|---|
| 1.a | 38.4 | concrete crushing in the column |
| 1.b | 61.5 | shear failure of the panel |
| 1.c | 62.3 | shear failure of the panel |
| 2.a | 40.3 | concrete crushing in the column |
| 2.c | 57.8 | shear failure of the panel |

Additional information was provided by the strain gauges applied to the CFRP laminate (1.b, 1.c and 2.c) in the direction of the fibers (i.e., hoop direction) on two lines parallel to the axis of the beam and placed at 50 mm and 100 mm from the end of the column. For example, in joint 1.b, strain gages #20, #15 and #17 are along the first line (50 mm) and gages #19, #16 and #18 along the second (100 mm) (see Figure 7). Whereas the strains recorded by gages #15 and #16 are almost constant during the cyclic load application, the values recorded by gages #20 and #17, #19 and #18 (faces in the flexural plane) change substantially depending on the acting moment (tensile or compressive). For tensile stress, they are low and similar to those recorded on the perpendicular face. However, for compressive stress, they increase due to the high demand of confinement. The relatively high strains in the FRP wrapping (about 0.0023 mm/mm), recorded for the three specimens at failure of the panel, underline the effectiveness of its confinement function. Finally, a comparison between the two data points representative of ultimate strains recorded on the two lines (#20 and #17 versus #19 and #18 respectively in Figure 7) allows to point out how rapidly the demand in confinement decreases when the distance from the nodal zone increases.

## PRELIMINARY ANALYSIS

Confirmation of the validity of the test set up and loading procedure was provided by a preliminary analysis of the results obtained for the control joints. For 1.a for example, the moment-curvature relationship shows that the ultimate moment of the column, 42.3 kNm, is practically identical to the experimental moment, 42.5 kNm, calculated by equilibrium of the applied loads. As experimentally observed, the analysis confirms that the failure was due to concrete crushing, while at that instant the steel reinforcement on the tension side was yielded. For the strengthened specimens, a similar analysis is being carried out, adding the contribution of the FRP rods and the effect of the FRP jacketing on flexural strength.

## CONCLUSIONS

Preliminary results of an experimental program confirmed that the combined action by FRP jacketing and near surface mounted FRP rods can be a promising and flexible retrofit technique for beam-column connections in GLD frames. In fact, it could make it possible to modify strength and/or ductility of the joints by varying the combination of FRP wrapping and NSM rods. In this way, the design of the retrofitting could result in a choice of collapse mode of the upgraded frame.

In order to accurately assess the influence of different key parameters (e.g., axial force, amount and type of FRP reinforcement), it is necessary to complete the experimental program

described herein. The goal of the research is to define design criteria so that, known the initial conditions and loads, it becomes possible to design the structural retrofit changing the failure mode and varying the improvement in terms of strength and/or ductility.

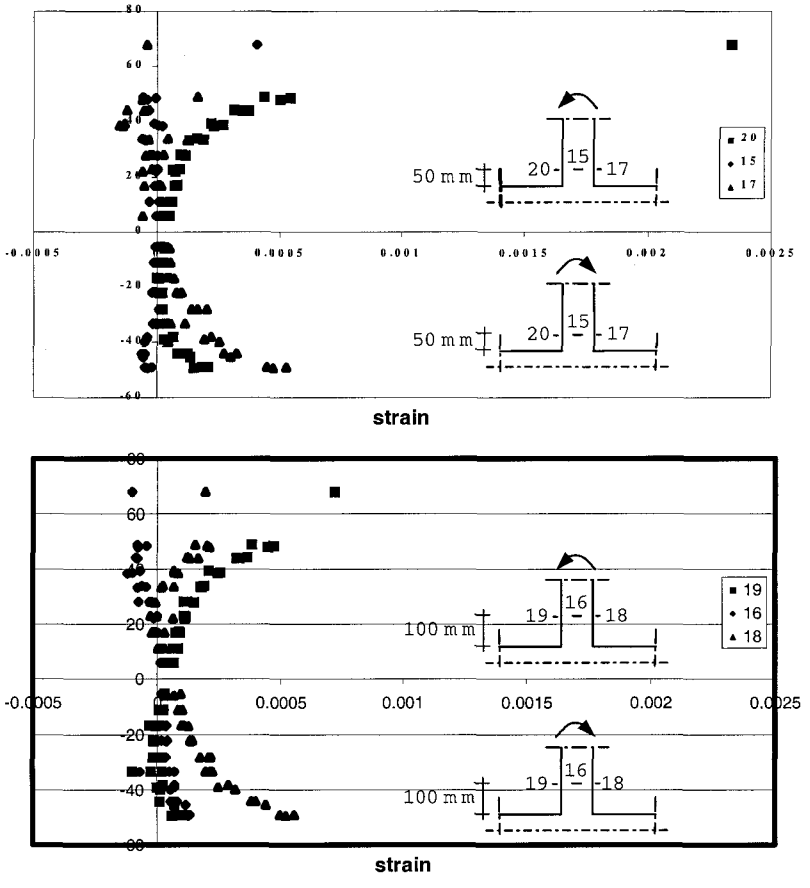



Figure 7. Column moment versus FRP strain at different locations (1.b)

## ACKNOWLEDGEMENTS

This project is the result of a collaborative effort between The University of Missouri – Rolla (UMR) and the University of Naples Federico II. The authors acknowledge the support of the NSF Industry/University Cooperative Research Center on Repair of Buildings and Bridges with Composites based at UMR and MAC SpA, Treviso, Italy.

## REFERENCES

American Concrete Institute Committee, (1963) *"Building Code Requirements for Reinforced Concrete"* ACI 318-63, Detroit USA.

Alkhrdaji, T., Nanni., A., Chen, G., and Barker, M., (1999) *"Upgrading The Transportation Infrastructure: Solid RC Decks Strengthened with FRP,"* Concrete International: Design and Construction, Vol. 21, No. 10, Oct. 1999, pp. 37-41.

Alkhrdaji, T and A. Nanni, (2000) *"Flexural Strengthening of Bridge Piers Using FRP Composites,"* ASCE Structures Congress 2000, Philadelphia, PA M. Elgaaly, Ed., May 8-10, CD version, #40492-046-008, 8 pp.

Beres, A., Pessiki, S.P., White, R. N. and Gergely, P., (1996), *"Implications of Experiments on the seismic behavior of Gravity Load Designed RC Beam-to-Column Connections"*, Earthquake Spectra, Vol. 12, No. 2, May, pp. 185-198.

Cosenza, E. and Manfredi G., (1997), *"Some Remarks on the Evaluation and Strengthening of Underdesigned R.C. Frame Buildings"*, Technical Report, NCEER-97-0003 - State University of New York at Buffalo, pp.157-175.

De Lorenzis, L., A. Nanni, and A. La Tegola, (2000) *"Strengthening of Reinforced Concrete Structures with Near Surface Mounted FRP Rods,"* International Meeting on Composite Materials, PLAST 2000, Proceedings, Advancing with Composites 2000, Ed. I. Crivelli-Visconti, Milan, Italy, May 9-11, 2000, pp. 419-426.

Dolan, C.W., S. Rizkalla and A. Nanni, Editors, (1999), *Fiber Reinforced-Polymer Reinforcement for Concrete Structures – Fourth International Symposium (FRPRCS4)*, ACI Special Publication No. 188, American Concrete Institute, Farmington Hills, MI, 1999, 1182 pp.

Pantelides, C., Clyde, C. and Reaveley, L., (2000), *"Rehabilitation of R/C Building Joints with FRP Composites"*, 12th World Conference on Earthquake Engineering, Auckland, New Zealand.

White R.N. and Mosalam, K., (1997), *"Seismic Evaluation and Rehabilitation of Concrete Buildings"*, Technical Report, NCEER-97-0003 - State University of New York at Buffalo, pp.177-196.

# Assessment of Seismic Rehabilitation and Repair of RC Bridges with CFRP Composites

C. P. PANTELIDES and L. D. REAVELEY
Dept. of Civil and Environmental Engineering, University of Utah, Salt Lake City, Utah, USA

## ABSTRACT
An assessment of the effectiveness of the seismic rehabilitation of a bridge sub-assembly, and the repair of another with Carbon Fiber Reinforced Polymer (CFRP) composites is presented. The assessment is based on the results of in-situ tests carried out on two three-column bridge bents and the deck slab between them. The performance of the two bents is compared to that of an as-built bent; the as-built bent was tested first; the bent was then repaired using epoxy injection, shotcrete, and CFRP composites. A damage assessment and a performance assessment is made for the as-built, the rehabilitated, and the repaired bents in terms of the *Caltrans Seismic Design Criteria* for new bridges, and the *Seismic Retrofitting Manual* of existing bridges. Parameters include column shear strength, plastic hinge length, anchorage and splices of longitudinal reinforcement, and cap beam-column joint shear capacity. The demand was determined from seismic design spectra of the site for a 10% probability of exceedance in 50 years, 100 years, and 250 years earthquakes. Comparisons of demand versus capacity are made for the as-built and rehabilitated bent for the three earthquakes.

## INTRODUCTION
Recent earthquakes have repeatedly demonstrated the vulnerabilities of older RC bridges to seismic deformation demands. In the 1994 Northridge earthquake, the primary cause of all collapse and major damage was insufficient ductility in the structural frames (Zelinski 1999). All bridge structures in the region of strong ground motion shaking during the 1994 Northridge earthquake, that were retrofitted since the 1989 Loma Prieta earthquake performed adequately without damage requiring repairs, thus demonstrating the validity of the adopted Caltrans retrofit procedures (Seible and Priestley 1999). The retrofitted structures as a whole resisted the earthquake motions much better than the unretrofitted structures.

Prefabricated fiber reinforced polymer jackets have been used for repair of damaged columns with inadequate lap splices in the longitudinal reinforcement, with satisfactory performance (Xiao and Ma 1997). Various circular and rectangular columns with carbon CFRP composite retrofits were tested in the laboratory (Seible at al. 1997), which exhibited stable hysteretic load-displacement behavior up to a large displacement ductility, while maintaining a constant load capacity level without significant cyclic capacity degradation. In-situ tests of RC circular columns were performed in St. Louis (Gamble and Hawkins 1996); several columns were tested in the as-built condition, after being retrofitted with tensioned steel bands, or glass CFRP composite jackets. All of the retrofits functioned adequately, and prevented the lap splices from failure at significant force and deformation levels. Three joints of the Highland Drive Bridge, in Salt Lake City, Utah, were wrapped with carbon CFRP composites in 1996, while the bridge was in service. The details of the field application, analytical techniques for the retrofit design, and comparison with full-scale experiments of similar joints have been

*FRPRCS-5*, Thomas Telford, London, 2001.

presented (Pantelides et al. 1997, Gergely et al. 1998). Detailed procedures for improving the shear capacity of RC T-joints using CFRP composites were recently established based on laboratory tests (Gergely et al. 2000).

The South Temple Bridge, on Interstate 15 in Salt Lake City, Utah, was designed and built in 1962, and was missing the reinforcement details necessary to provide adequate lateral load capacity and ductility. Three in-situ tests were performed: (a) test of a bent in the as-built condition (Bent #5), (b) test of a bent rehabilitated with CFRP composites (Bent #6), and (c) test of the repaired Bent #5 rehabilitated with CFRP composites (Bent #5R). The paper describes the results for in-situ tests (a), (b) and (c) of the as-built, rehabilitated, and repaired bents. The purpose of the tests was to demonstrate the ability of CFRP composites to improve the performance of the bents under simulated seismic loading. Specifically, the CFRP composite retrofit of Bent #6 was designed to double the displacement ductility of Bent #5 in the as-built condition. Bent #5R simulates a bridge bent that might have been damaged in a previous earthquake, and was subsequently repaired with epoxy resin grout injection, shotcrete, and CFRP composites.

## SOUTH TEMPLE BRIDGE DETAILS

Two 19.51m bents and the 21.87m deck between them were left standing after demolition of the South Temple Bridge. The elevation of Bent #5 is shown in Fig. 1. The design concrete compressive strength was $f_c'$=20 MPa, and the yield stress of the reinforcement was $f_y$=276 MPa; the measured in-situ properties were $1.9f_c'$ for concrete and $1.2\,f_y$ for the reinforcement. The bent sections consisted of a 0.914 x 1.219m beam cap and three 0.914 x 0.914m columns, which were supported on three pile caps. Each of the exterior columns was supported on a 2.134m square pile cap with four 0.305m diameter concrete-filled steel pipe piles. A 2.75 m square pile cap with five piles supported the center column. The piles had an average length of 19.81 m, and were embedded in the 0.914m thick pile cap a distance of 0.305 m. As part of the rehabilitation, the piles were epoxy grouted using a 2.438m Dywidag bar per pile; the bars were 32 mm in diameter (1030 MPa ultimate stress) and were used to prevent pullout failure of the piles; this detail was implemented for the four corner piles of the three pile caps of each bent. In addition, horizontal Dywidag bars were provided to complete the load path. The deck supports were modified to "roller" for Bent #6 and "fixed" for Bent #5 in order to perform the tests in a safe manner and still be able to include the dead load of the deck (Pantelides et al. 2000). A horizontal quasi-static cyclic load was applied at the beam cap level, as shown in Fig. 1. The load was applied in three-cycle load steps; initially, the load was applied in a force-controlled mode until yielding of the reinforcement, after which the test was performed in a displacement-controlled mode.

## CFRP COMPOSITE DESIGN FOR SEISMIC REHABILITATION

The bridge bents had several deficiencies in the reinforcement details required for good performance under seismic excitations, including the lack of confinement of column reinforcement in the plastic hinge regions, the insufficient anchorage length of the column reinforcement into the beam cap and the pile cap, minimum embedment of the reinforcement from the piles to the pile cap, the size and reinforcement of the grade beam connecting the pile caps, insufficient column splice length, and inadequate shear reinforcement in the beam cap-column and pile cap-column joints. The beam cap stirrups had substantial corrosion, but there was no obvious sign of corrosion in the columns. The goal of the rehabilitation was to improve the displacement ductility of Bent #6 by a factor of two, with the associated strength improvement. The capacity of the columns and the beam cap-column joints had to be improved to allow this ductility increase. The material properties of the CFRP composite

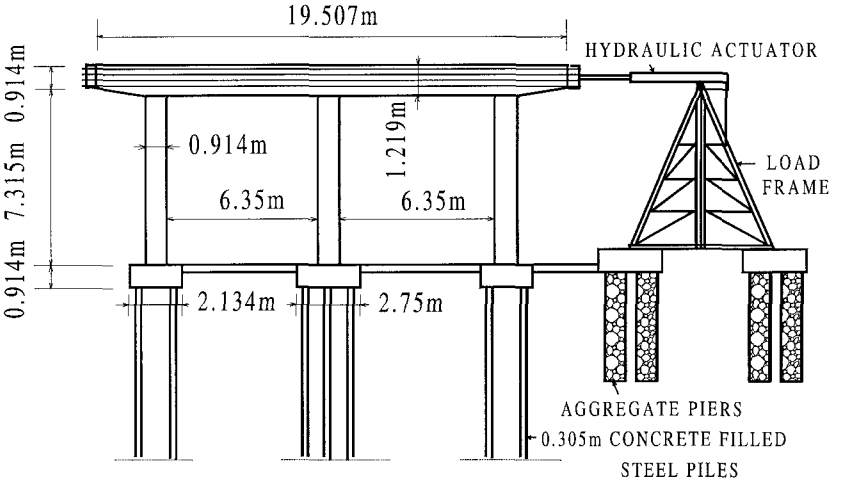



Figure 1. Test configuration

were determined using tensile coupons prepared according to ASTM D-3039 specifications (ASTM 1996). The material used in this application was 48,000 fibers per tow unidirectional woven carbon fibers at six picks per 25.4 mm, and weighed 9.14 N/m$^2$. The width of the carbon fiber sheets used was 457 mm. The thickness of one CFRP composite layer was 1.32 mm, the tensile strength of the composite was 630 MPa, and the modulus of elasticity of the composite was 64.7 GPa. The application of the CFRP composite included: (a) removal of loose concrete and cover from the entire beam cap; (b) shotcreting and surface preparation of the beam cap using high pressure water jet; (c) application of bonding agent to the columns and beam cap; and (d) application of CFRP sheets using hand lay-up and impregnation with epoxy resin at ambient temperature curing.

The design included flexural plastic hinge confinement and shear strengthening of the columns, as well as lap splice clamping of the bottom column bars. The composite layout for the retrofitted bent is shown in Fig. 2. The total number of CFRP composite layers at any location is denoted as L (number of layers). In Fig. 2 there are ten layers at the column base for lap splice clamping, flexural plastic hinge confinement, and shear strengthening. Next, two layers were placed for flexural plastic hinge confinement and shear strengthening, and finally one layer for flexural plastic hinge confinement. The jacket for the top of the column is similar to the jacket for the column base, except that there is no requirement in this case for lap splice clamping. A 51-mm gap was left between the column and pile cap, and the column and beam cap, as shown in Fig. 2, to avoid any strength and stiffness increase from the retrofit. In addition, the corners of the beam cap and columns were rounded to 51 mm to provide better anchorage and confinement. Two new design elements were also used: the "Ankle-wrap" concept for strengthening beam column joints, and the "U-strap" concept for improving column bar anchorage into the beam column joint.

**New "Ankle-Wrap" Concept for Shear Strengthening of Beam Cap-Column Joint**

The difference between the joint principal tensile stress of the rehabilitated Bent #6 and the as-built Bent #5, was used as the design tensile stress to be provided by the CFRP composite. The number of CFRP composite layers, inclined at the principal angle, was determined by dividing the principal tensile stress difference between Bent #5 and Bent #6 by the tensile

stress developed in one CFRP composite layer; this stress is limited by the strain, at which debonding of the CFRP composite from the concrete occurs, times the modulus of elasticity of the CFRP composite. This strain was determined experimentally in laboratory tests of T-joints to be 20% of the ultimate strain of the CFRP composite (Gergely et al. 2000); at a higher strain, the CFRP composite debonds from the concrete and is ineffective in resisting diagonal tension. The analysis showed that 3.65 layers were needed; to construct a symmetric jacket, four layers of CFRP composite were applied, which were provided in both directions (±45°) to resist the cyclic nature of the simulated seismic loads as shown in Fig. 2.

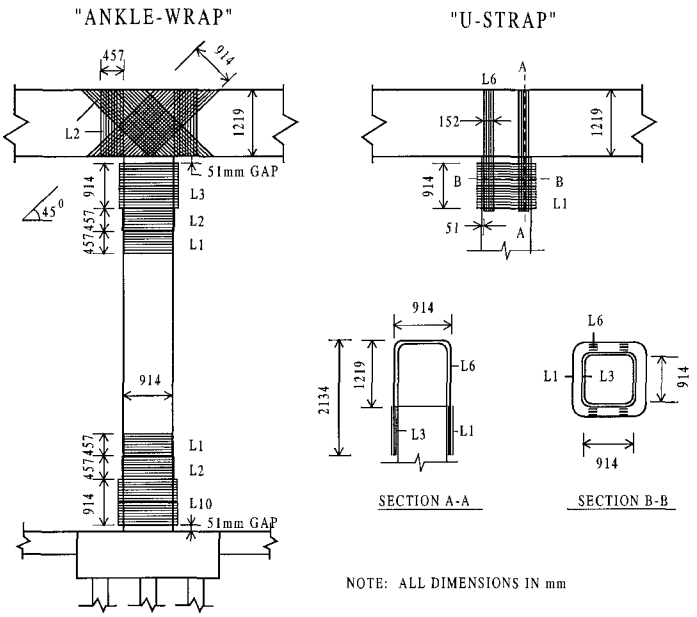



Figure 2. CFRP Composite Design

**New "U-strap" Concept for improving column bar anchorage into the joint**

Six layers of 152 mm-wide CFRP composite U-straps, shown in Fig. 2, were provided in order to improve the anchorage of the longitudinal steel reinforcement at the top of the column extending into the joint; this steel reinforcement had insufficient development length in the joint. The U-straps were designed by providing the CFRP composite area for resisting the tensile forces at the column joint interface. Complete details of the CFRP composite design are given in Pantelides et al. (1999a, 1999b, 2000), and Gergely et al. (2000).

## DAMAGE ASSESSMENT

### As-built Bent #5

From a bilinear approximation of the load-displacement behavior, the displacement ductility of the bent was found as $\mu = 2.8$ (Fig. 3). Plastic hinges formed at the top and base of the three columns, which is satisfactory by current seismic guidelines. Flexural cracks developed at the top of the columns, and shear cracks formed in the beam cap-column joints, the largest being 2 mm at the interface of the column and the beam cap. The cracks went all around the column perimeter in the plastic hinge region. Radial and circumferential spalling of the concrete at the top of the pile cap around the column perimeter was observed.

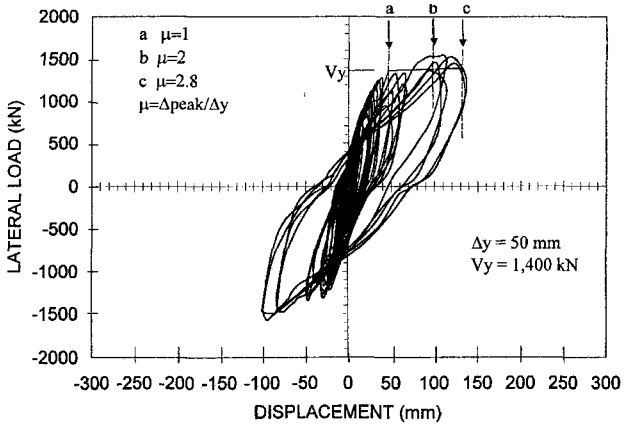



Figure 3. Hysteresis of as-built Bent #5

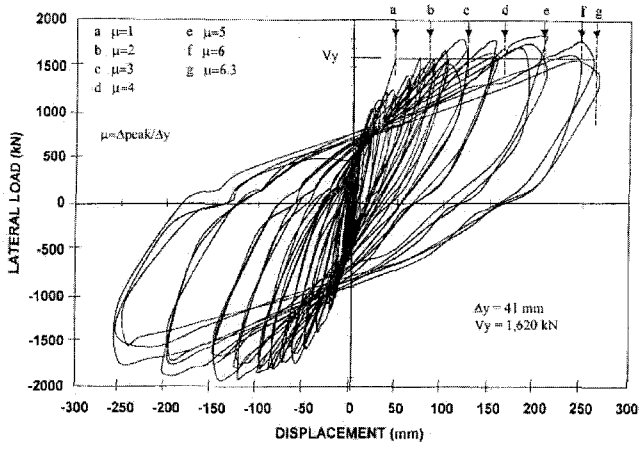



Figure 4. Hysteresis of Rehabilitated Bent #6

**Rehabilitated Bent #6**

The peak load capacity was 2203 kN, which dropped by 16 percent by the end of the test. The applied displacement reached a maximum of 265 mm. From a bilinear approximation of the load-displacement behavior, the displacement ductility of the bent at the end of the test was $\mu$=6.3, as shown in Fig. 4. The goal of doubling the displacement ductility of the as-built Bent #5 was achieved. The ductility achieved during the test is higher than the target design displacement ductility of $\mu$=5 used by Caltrans for multicolumn bents (Caltrans 1999). Large cracks in the concrete were visible at the interface between the column and the beam cap, which were 6 mm wide. The interface cracks propagated from the concrete into the CFRP composite as tensile cracks. In addition, at both column ends, spalling cracks in the 51-mm gaps were formed at the ankle-wrap. The CFRP composite layers delaminated in the beam cap-column joint region and at the top and bottom of the columns. This failure mechanism was also observed in the laboratory (Gergely et al. 2000). A second failure mechanism was the debonding/tensile failure of the 152 mm CFRP composite U-straps (Fig. 5). After completion of the test, the CFRP composite was removed from the faces of the column (Fig. 6). The concrete had several small cracks but the condition of the plastic hinge region was intact, indicating that the CFRP composite confined the column and maintained its integrity.

**Repaired Bent #5R**

The composite layout for the repaired Bent #5R was identical to that for Bent #6 as shown in Fig. 2. The cracks resulting from the initial test of Bent #5 were filled to a great extend using a resin grout injection. The application of the composite included: (a) removal of loose concrete both originally present and that resulting from extensive cracking after the first test for Bent #5, especially in the plastic hinge area at the top of the columns; (b) crack injection using the Sho-Bond Bics system, which makes use of the contraction pressure of a rubber tube to inject a special epoxy resin grout deep into cracks; (c) shotcreting of the four faces of the beam cap to bring it to its original shape; (d) application of a bonding agent; and (e) application of the carbon fiber sheets using hand lay-up. The peak load during the test was 2033 kN and the maximum displacement was 280 mm. From a bilinear approximation of the

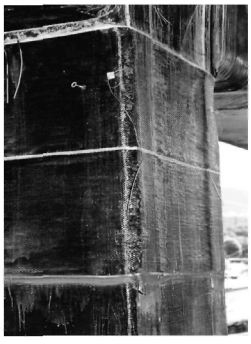


Figure 5. Debonding/tensile failure of U-straps



Figure 6. Bent #6 column top after removing CFRP

load-displacement behavior, the displacement ductility of the bent was $\mu = 4.0$, as shown in Fig. 7. This compares well with the performance of Bent #6 which had a ductility of $\mu = 6.3$; it can be observed that the ductility of the repaired bent is 63 percent of the ductility of Bent #6 with undisturbed concrete rehabilitated with CFRP composites. Compared to Bent #5, tested in the as-is condition that had a displacement ductility of $\mu = 2.8$, the repaired Bent #5R has a higher ductility by a factor of 1.43. This implies that even damaged bridges, such as from a previous earthquake, can benefit from application of CFRP composites as a seismic retrofit measure.

The initial stiffness of Bent #5R was reduced by 40 percent compared to Bent #5 as can be seen from Figs. 3 and 7, due to buckling of the longitudinal bars observed in the plastic hinge zone at the top and base of the columns, and concrete cracking. However, the peak load in the push and pull direction was approximately equal for Bent #5R and Bent #6. Large cracks in the concrete were visible at the interface between the column and the beam cap, which reached 8 mm in width, and propagated into the CFRP composite as tension cracks. The CFRP composite layers delaminated in the column-beam cap joint region, and some of the 152mm-wide CFRP composite U-straps failed in debonding/tension, in a similar manner as in Bent #6. Removal of the CFRP composite revealed 2mm-wide diagonal shear cracks in the plastic hinge region of the top of the columns, extending more than 2/3 of the column width; in addition, on the west-facing side of the top of the middle column, the longitudinal column bars had buckled as shown in Fig. 8. The bars buckled between the column ties, and a large portion of the concrete between the ties was pulverized and had fallen out, as the CFRP

composite sheet was being removed. This is in contrast to the condition observed for Bent #6, and is due to the fact that Bent #5R had already been damaged in the first test of Bent #5.

## PERFORMANCE ASSESSMENT

### Column Shear Strength

The largest applied shear in the plastic hinge region of the middle column during the test of the as-built Bent #5 was 68% of the capacity, whereas for the rehabilitated Bent #6 the shear during the test was 90% of the capacity, calculated according to the Caltrans *Seismic Design Criteria* (Caltrans 1999).

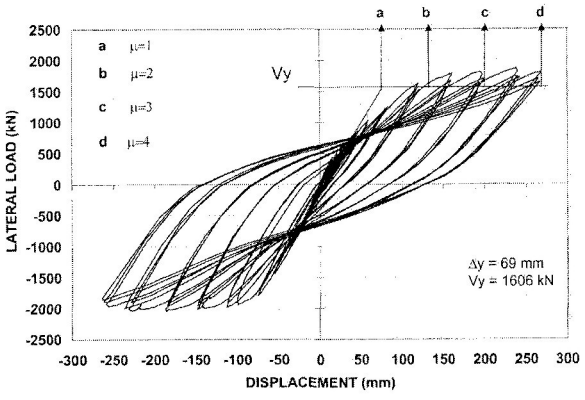



Figure 7. Hysteresis of repaired Bent #5R



Figure 8. Buckled bars at top of middle column of Bent #5R

### Plastic Hinge Length

The analytical plastic hinge length in the middle column of Bent #5 was calculated as 528 mm or 57% of the column width according to the *Seismic Retrofitting Manual* (FHWA 1995); from the in-situ test of Bent #5, it was observed that the plastic hinge at the top of the middle column, was 508 mm below the beam cap, or 55% of the column width. Plastic hinges formed at the top and base of the three columns as evidenced by strain gage measurements of Bent #6 (Pantelides et al. 2000); the CFRP composite confined the column and maintained its integrity, as shown in Fig. 6. This observation supports laboratory experimental evidence of the effectiveness of CFRP composites to increase the ductility of concrete columns with relatively little concrete degradation (Priestley et al. 1996).

### Anchorage of Longitudinal Reinforcement

The longitudinal column bars extended 864 mm into the beam cap. According to the *Seismic Retrofitting Manual* (FHWA 1995), the required effective anchorage length is 968 mm. The length provided into the beam cap was only 89% of the required length and anchorage failure was actually evidenced by bar slippage from the concrete in the joint region of the beam cap for Bent #5, but not for Bent #6. Due to the presence of the CFRP composite U-straps, some of which failed in debonding/tension, the anchorage of the reinforcement for Bent #6 was maintained until the last cycles of the test.

### Splices in Longitudinal Reinforcement

The key to preventing a splice failure is the presence of sufficient, closely spaced transverse reinforcement that will prevent initiation of splitting. The minimum area of transverse reinforcement in the columns, required to prevent a splice failure was calculated according to the *Seismic Retrofitting Manual* (FHWA 1995) as 394 $mm^2$; the original area provided was

129 $mm^2$, which is 33% of that required; the clear spacing between spliced bars should not be more than 129 mm; in the actual bent the clear spacing between bars was 137 mm, which violates the requirement. In addition, the splice length should not be less than 795 mm; here, the splice length at the pile cap-column interface was only 635 mm, which again violates the requirements. Splitting failure was observed in the bottom of the columns of Bent #5.

**Cap Beam-column Joint Shear Strain**

The shear strain at the cap beam-column joint of the middle column reached a maximum strain of 0.3 percent for Bent #5. Strain gages measured the peak value of the strain in the CFRP composite of Bent #6 at the beam cap-column joints as 0.22 percent, which was about a fifth of the ultimate strain value of 1 percent. This low strain level in the composite verifies the limiting maximum strain value used in the design of the CFRP composite for shear strengthening of the beam cap-column joints. The maximum shear strain in the joint of Bent #6 was 1.3 percent, which is four times the strain observed for Bent #5.

**Cap Beam-column Principal Tensile and Compressive Stress**

The principal tensile stress for the middle column joint was $\sigma_t$ =1.99 MPa or 0.44 $(f'_c)^{0.5}$ MPa; at this stress, diagonal tension cracks and joint degradation was observed; this stress is slightly higher than 0.42 $(f'_c)^{0.5}$ MPa which is predicted to cause joint degradation (Priestley et al. 1996). The principal compression stress was $\sigma_c$ = 0.12 $f'_c$, which is less than the recommended stress for design of 0.3 $f'_c$ (Priestley et al. 1996). For Bent #6, the principal tensile stress was 2.73 MPa or 0.60 $(f'_c)^{0.5}$ MPa, which is 37 percent higher than Bent #5; it is also 44 percent higher than the stress predicted to cause joint degradation. The principal compressive stress was $\sigma_c$ = 0.16 $f'_c$, which is 33 percent higher than Bent #5; it is less than the recommended stress for design of 0.3 $f'_c$.

**Overall performance**

The lateral load capacity of the rehabilitated Bent #6 was the highest, followed closely by that of the repaired bent as shown in Table 1. The ratio of the maximum lateral load to that of the as-built Bent #5 was 1.16 for Bent #6, and 1.15 for Bent #5R. The displacement ductility calculated using a bilinear model for the rehabilitated Bent #6 was 2.25 times the ductility of Bent #5, and the displacement ductility of the repaired Bent #5R was 1.43 times that of the as-built Bent #5. The rehabilitated Bent #6 and repaired Bent #5R showed exceptional energy dissipation due to the confinement provided by the CFRP composite. The ratios for energy of Bent #6 and Bent #5R as compared to Bent #5 were 2.44 and 2.50, respectively. Even though Bent #5R was originally damaged, repair with CFRP composites had restored the lateral load capacity and ductility and increased them by a considerable amount compared to Bent #5 without CFRP composites.

Table 1. Performance comparisons between as-built, rehabilitated, and repaired bents

| Quantity | As-built Bent #5 | Rehabilitated Bent #6 | Repaired Bent #5R | Ratio of Bent #6 over Bent#5 | Ratio of Bent #5R over Bent #5 |
|---|---|---|---|---|---|
| Displacement ductility | 2.8 | 6.3 | 4.0 | 2.25 | 1.43 |
| Lateral load capacity | 1401 kN | 1619 kN | 1606 kN | 1.16 | 1.15 |
| Energy dissipation | 2034 kJ | 4350 kJ | 5084 kJ | 2.14 | 2.50 |

**Capacity Vs Demand**

The design spectra were obtained from design criteria for the new Interstate 15 bridges. The peak spectral acceleration for the 10% in 50 years earthquake was 0.6g, the one for the 10% in 100 years was 1.0g, and the one for the 10% in 250 years was 1.6g. The performance of Bent #5 and Bent #6 was evaluated using an elastoplastic model of the bent (Pantelides et al. 2000) and the results are shown in Table 2. From the hysteresis curve for Bent #5, the peak lateral force capacity is 1500 kN and the peak lateral displacement is 150 mm. Therefore, the as-built Bent #5 will survive the 10% in 50 years earthquake, it will sustain damage in the 10% in 100 years earthquake, and would be very close to collapse in the 10% in 250 years earthquake. The peak lateral force capacity from the hysteresis curve for Bent #6 is 1943 kN and the peak lateral displacement is 267 mm. It is expected that Bent #6 will survive the 10% in 50 years earthquake, and the 10% in 100 years earthquake; for the 10% in 250 years earthquake some damage due to large displacements is expected, but the bridge should be functional and carry the gravity loads, as was demonstrated by the in-situ tests.

Table 2. Lateral force and displacement demands

| | As-Built Bent #5 | | Rehabilitated Bent #6 | |
|---|---|---|---|---|
| Design Spectrum | Force, kN | Displacement, mm | Force, kN | Displacement, mm |
| 10% in 50 Years | 1170 | 60 | 565 | 93 |
| 10% in 100 Years | 2073 | 107 | 1001 | 165 |
| 10% in 250 Years | 3456 | 179 | 1672 | 276 |

## CONCLUSIONS

The lateral load and displacement capacity of the as-built Bent #5 was higher than expected due to redundancy, pinning of the piles, and overstrength. The dominant modes of failure of the CFRP composite for the rehabilitated Bent #6, were delamination from the concrete surface and debonding/tensile failure of the CFRP composite U-straps. The CFRP composite was designed to increase the displacement ductility of Bent #5 by a factor of 2; a displacement ductility 2.25 times that of Bent #5 was reached in the tests. The lateral load capacity was increased by a factor of 1.16. The energy absorbed by Bent #6 was 2.14 times that of Bent #5. The rehabilitated Bent #6 would survive the 10% in 250 years earthquake with minor damage and the bridge would remain functional, largely due to the increased ductility provided by the CFRP composite; on the other hand, the as-built Bent #5 would be very near collapse in the 10% in 250 years earthquake, and sustain considerable damage in the 10% in 100 years earthquake. Overall, it must be concluded that the FRP composite seismic rehabilitation of Bent #6 was successful.

The repaired Bent #5R showed an increase of the displacement ductility by a factor of 1.43 compared to the as-built Bent #5. The lateral load capacity was increased by a factor of 1.15. The energy absorbed by the repaired Bent #5R was 2.50 times that of Bent #5. The repair of the damaged bent using CFRP composites actually improved the seismic performance to a level beyond the original capacity Bent #5 in the as-built condition. This is significant because even after suffering substantial damage, repair of the bridge bent using CFRP composites was effective.

## ACKNOWLEDGMENTS

The authors would like to acknowledge the financial support provided by the National Science Foundation under Grant No. CMS 9712761. Financial support from the Federal Highway Administration, the Utah Department of Transportation, the Idaho National

Engineering and Environmental Laboratory, and the Center for Composites in Construction, a State of Utah Center of Excellence, is also acknowledged.

## REFERENCES

ASTM, ASTM D 3039, 1996, Standard Test Method for Tensile Properties of Polymer Matrix Composite Materials, *Amer. Soc. For Test. Mater.* D3039/D 3039 M-95a.

California Department of Transportation, 1999, Caltrans Seismic Design Criteria-Version 1.1, *California Department of Transportation*, Engrg. Service Center, Sacramento, CA.

Federal Highway Administration, 1995, Seismic Retrofitting Manual for Highway Bridges, *U.S. Dept. of Transportation, Publication No. FHWA-RD-94-052,* McLean, VA.

Gamble, W.L., and Hawkins, N.M., 1996, Seismic retrofitting of bridge pier columns, *Proc. Struct. Congress XIV, ASCE*, Vol. 1, 16-23, Chicago, IL.

Gergely, I., Pantelides, C.P., Nuismer, R.J., and Reaveley, L.D., 1998, Bridge pier retrofit using fiber-reinforced plastic composites, *ASCE, J. of Compos. for Constr.,* 2(4), 165- 174.

Gergely, I., Pantelides, and Reaveley, L.D., 2000, Shear strengthening of R/C T-joints using CFRP composites, *ASCE, J. of Compos. for Constr.,* 4(2), 56-64.

Pantelides, C. P., Gergely, I., Reaveley, L. D., and Nuismer, R. J., 1997, Rehabilitation of cap beam-column joints with carbon fiber jackets, *Proc. of the Third Intern. Symp. On Non-Metallic (CFRP) Reinforcement for Concrete Structures*, Sapporo, V. 1, 587-595.

Pantelides, C. P., Gergely, I., and Reaveley, L. D., 1999a, Advanced composite retrofit design for R/C bridges, *Proc. of the Transportation Research Board 78th Annual Meeting*, Washington, D.C.

Pantelides, C.P., Gergely, J., Reaveley, L.D., and Volnyy, V.A., 1999b, Retrofit of R/C bridge pier with CFRP advanced composites, *ASCE, J. Struct. Engrg.*, 125(10), 1094-1099.

Pantelides, C. P., Gergely, J., Marriott, N., and Reaveley, L.D., 2000, Seismic rehabilitation of concrete bridges: Verification using in-situ tests at South Temple Bridge on Interstate 15, *Research Report UUCVEEN 00/1*, Dept. of Civil and Envir. Engrg., Univ.of Utah, Salt Lake City, Utah.

Priestley, M.J.N., Seible, F., and Calvi, G.M., 1996, *Seismic Design and Retrofit of Bridges,* John Wiley & Sons, Inc., New York.

Seible, F., Priestley, M.J.N., Hegemier, G., and Innamorato, D., 1997, Seismic retrofitting of RC columns with continuous carbon fiber jackets, *ASCE, J. of Compos. for Constr.,* 1(2), 52-62.

Seible, F., and Priestley, M.J.N., 1999, Lessons learned from bridge performance during the Northridge earthquake, *ACI International SP-187, Seismic Response of Concrete Bridges*, ed. Krishnan, K., Farmington Hills, MI, SP 187-3, 29-55.

Xiao, Y., and Ma, R., 1997, Seismic retrofit of RC circular columns using prefabricated composite jacketing, *ASCE, J. Struct. Engrg.*, 123(10), 1357-1364.

Zelinski, R., 1999, Northridge earthquake influence on bridge design code, *ACI International SP-187, Seismic Response of Concrete Bridges*, ed. Krishnan, K., Farmington Hills, MI, SP 187-2, 17-28.

# Bond

# Prediction of debonding failure load due to flexural cracks of concrete for FRP-strengthened structures

HEDONG NIU and ZHISHEN WU
Dept. of Urban & Civil Eng., Ibaraki University, Hitachi, Japan

## ABSTRACT

The use of fiber reinforced polymers (FRP) as externally bonded reinforcement has gained widespread acceptance as an innovative method for the maintenance, rehabilitation and upgrading of existing concrete structures. Significant increases in stiffness, strength and seismic response of the structures can be achieved by this technique, but yet little is known about the debonding failure along the FRP-concrete interface initiated from the end of a flexural crack of concrete. This study mainly focuses on developing a methodology for predicting the debonding failure load due to flexural cracks in FRP-strengthened R/C beams based on the fracture energy criterion. A closed-form analytical solution for predicting interfacial shear stresses induced by flexural cracks is presented by adopting a bilinear bond stress-slip model with softening behavior and validated by comparing with both finite element and experimental results. On the basis of our previous work, a quantitative criterion governing the debonding failure for FRP-strengthened R/C beams is established by combining RC beam theory with the solution from the simple shear test. Through application of the proposed method to existing experimental results, the interfacial fracture energy consumed for the debonding failure is identified. It is realized that the present study can provide a rational design methodology, which can be easily included in the design guideline, for design and performance evaluation of FRP-strengthened concrete structures.

**Key Words:** fiber reinforced polymers (FRP), flexural crack, debonding failure, interfacial fracture energy, design methodology

## 1. INTRODUCTION

The need to rehabilitate or retrofit the deteriorated civil infrastructure is becoming a major and urgent problem facing the world. The use of fiber reinforced polymers (FRP) as externally bonded reinforcement has gained widespread acceptance as an innovative method for the maintenance, rehabilitation and upgrading of existing concrete structures due to their much more beneficial characteristics such as high strength- and stiffness-to-weight ratio, high corrosion resistance, electromagnetic neutrality, inherent tailorability and ease of application in field. Many studies [1-7] have shown that significant increases in stiffness, strength and seismic response can be achieved by this technique; however, a wide variety of failure modes is also observed in the retrofitted concrete beams: crushing of concrete, shear failure, rupture of FRP, debonding or peeling-off of FRP along the adhesive-concrete interface. Among these failure modes, the first three modes of failure can be avoided in the structural design and their corresponding ultimate strength of the structural member can be predicted by using

conventional or modified RC flexural theory. The debonding or peeling-off of FRP is a new failure mode, which invalidates the composite action between concrete and FRP and often significantly lowers the expected load-carrying capacity of the retrofit system. Thus there poses an urgent need for rational evaluating or predicting the structural capacity due to this type of failure mode.

Many researchers have done much work on the premature failure at the cut-off point of steel/FRP plates in steel/FRP-strengthened beams and developed the corresponding failure criteria for predicting the premature failure load [8-11]. However, very limited literatures concerning with debonding due to flexural cracks in the maximum moment region can be found, which is considered to be more dominant than the delamination induced by the stress concentrations at curtailment zone for the strengthened beam with FRP sheets. Täljsten [12] used fracture mechanics approach to derive closed-form formula for the case of linear elastic shear-slip relationship. Kamiharako et al. [13] and Yoshizawa et al. [14] found that the interfacial local shear stress distribution can be well described by using the linearly ascending and descending branch of interfacial stress-slip relationship in the pure shear tests of FRP. Yuan et al. [15] theoretically investigated the nonlinear interfacial shear stress transfer problems for pure shear test of FRP. Till now, nonlinear closed-form formula have not yet been derived for FRP-strengthened flexural structures.

In this paper, we mainly focus on developing a sound methodology for predicting the debonding failure load due to flexural cracks in the FRP-strengthened R/C beam based on our previous work [16-18]. First, a closed-form analytical solution is presented to give a clear insight into interfacial shear stress distribution induced by a flexural crack by adopting a bilinear bond stress-slip model with softening behavior and its validity is confirmed by comparing with both FEM and experimental results. Second, an iterative analytical method is developed to predict the response of the strengthened beams based on the strain compatibility. Third, an energy-based procedure is established to evaluate or predict the debonding failure load for the retrofitted beams. Finally, the interfacial fracture energy consumed for debonding failure is identified through applying the proposed method to the existing available experiments.

## 2. SHEAR TRANSFER ALONG FRP-CONCRETE INTERFACE

### 2.1 Shear transfer influenced by a flexural crack in FRP-strengthened beams

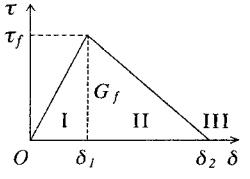



Fig. 1 Bilinear bond stress-slip model

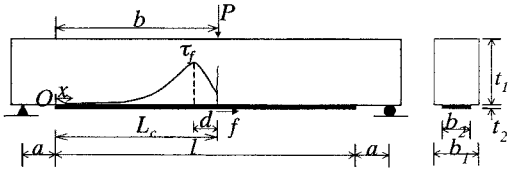



Fig. 2 Three-point bending with a flexural crack

In the present analysis, the following assumptions are made for simplicity in the derivation of shear stress:

(a) All the materials (R/C and FRP) are regarded to be homogeneous and linear elastic;

(b) The adhesive is assumed to only play a role in transferring the stresses from the above concrete to FRP and its thickness can be negligible;
(c) The bending stiffness of FRP is far less than that of the beam to be strengthened so that the bending moment in FRP can be neglected;

Here we only give a study of a three-point bending beam with a flexural crack as shown in Fig. 2, where interfacial shear stresses conform to the bilinear relationship in Fig. 1. According to [18], the theoretical equations are given in what follows.

*2.1.1Fundamental equations*

(1)Linearly ascending branch
The interfacial shear stresses can be written as:

$$\tau^{I}(x) = C_1 \cosh(\alpha_1 x) + C_2 \sinh(\alpha_1 x) + \frac{\tau_f}{\alpha_1^2 \delta_1 E_1 W_1} V_1(x) \tag{1}$$

where $\alpha_1^2 = \frac{\tau_f b_2}{\delta_1}\left[\frac{1}{E_2 A_2} + \frac{1}{E_1 A_1} + \frac{e}{E_1 W_1}\right]$, $\tau_f$ and $\delta_1$ are defined in Fig.1, $E_2, A_2, b_2$ are elastic modulus, section area and width of FRP, respectively, $E_1, A_1, W_1$ are elastic modulus, section area and section modulus of R/C beam to be strengthened, respectively, $e$ is the distance from the neutral axis to the bottom of R/C beam; $V_1(x)$ is shear force at section x due to externally applied loads since the shear force in FRP is neglected; $C_1$ and $C_2$ are integration constants to be determined by the boundary conditions.

The axial force of FRP can be expressed as:

$$N_2^{I}(x) = \frac{b_2}{\alpha_1^2}\left[\frac{d\tau^{I}(x)}{dx} + \frac{\tau_f}{\delta_1}\frac{M(x)}{E_1 W_1}\right] \tag{2}$$

where $M(x)$ is the bending moment at section $x$.

(2)Linearly descending branch
The interfacial shear stresses can be written as:

$$\tau^{II}(x) = C_3 \sin[\alpha_2(x - L_c + d)] + C_4 \cos[\alpha_2(x - L_c + d)] + \frac{\tau_f V_1(x)}{\alpha_2^2(\delta_2 - \delta_1)E_1 W_1} \tag{3}$$

where $\alpha_2^2 = \frac{\tau_f b_2}{\delta_2 - \delta_1}\left[\frac{1}{E_2 A_2} + \frac{1}{E_1 A_1} + \frac{e}{E_1 W_1}\right]$, $\delta_2$ is defined in Fig.1; $L_c$ and $d$ are defined in Fig.2; $C_3$ and $C_4$ are integration constants to be determined by the boundary conditions.

The axial force of FRP in the soft branch can be expressed as:

$$N_2^{II}(x) = \frac{b_2}{\alpha_2^2}\left[-\frac{d\tau(x)}{dx} + \frac{\tau_f}{(\delta_2 - \delta_1)}\frac{M(x)}{E_1 W_1} + \frac{\tau_f}{(\delta_2 - \delta_1)}\frac{N_2^{I}(L_c - d)e}{E_1 W_1}\right] \tag{4}$$

*2.1.2Determination of integration constants*
(1)The shear stresses only locate in linearly ascending branch
The integration constants are obtained as:

$$C_1 = \frac{\dfrac{\tau_f}{\delta_1\alpha_1 E_1 W_1}\left\{a\left[\cosh(\alpha_1 L_c)-1\right]-L_c\right\}V_1(x)+\dfrac{\alpha_1 f}{b_2}}{\sinh(\alpha L_c)}, C_2 = -\frac{\tau_f V_1(x) a}{\delta_1\alpha_1 E_1 W_1} \tag{5}$$

(2)The shear stresses enter the softening branch
The integration constants are obtained as:

$$\begin{aligned}
C_1 &= \frac{\tau_f + \dfrac{\tau_f V_1(x)}{\alpha_1^2\delta_1 E_1 W_1}\left\{\alpha_1 a \sinh\left[\alpha_1(L_c-d)\right]-1\right\}}{\cosh\left[\alpha_1(L_c-d)\right]}, C_2 = -\frac{\tau_f V_1(x) a}{\alpha_1\delta_1 E_1 W_1}, C_4 = \tau_f - \frac{\tau_f V_1(x)}{\alpha_2^2(\delta_2-\delta_1)E_1 W_1},\\
C_3 &= -\frac{\alpha_2}{\alpha_1}\left\{\left[\tau_f - \frac{\tau_f V_1(x)}{\alpha_1^2\delta_1 E_1 W_1}\right]\tanh\left[\alpha_1(L_c-d)\right]-\frac{1}{\cosh\left[\alpha_1(L_c-d)\right]}\frac{\tau_f V_1(x) a}{\alpha_1\delta_1 E_1 W_1}\right\}\\
&\quad + \left[\frac{\tau_f}{\alpha_2(\delta_2-\delta_1)} - \frac{\alpha_2\tau_f}{\alpha_1^2\delta_1}\right]\frac{V_1(x)(L_c-d+a)}{E_1 W_1}
\end{aligned} \tag{6}$$

$$b_2\left\{\frac{1}{\alpha_2}\left[C_4\sin(\alpha_2 d)-C_3\cos(\alpha_2 d)\right]+\frac{\tau_f}{\alpha_2^2(\delta_2-\delta_1)}\frac{V_1(x)(L_c+a)}{E_1 W_1}\right\} = f \tag{7}$$

The length of descending branch, $d$, can be calculated by equation (7) and then integration constants can be obtained according to equation (6).

According to [14], $\delta_1 = 0.05$mm, $\delta_2 = 0.3$mm and $\tau_f = 8$MPa are adopted in what follows to verify the correctness of the aforementioned equations by comparing to both FEM and experimental results.

A FRP-strengthened beam shown in Fig.2 is analyzed with the "ABAQUS" finite element program (ABAQUS, Version 5.8, 1998) and the derived equations. The dimension of the beam is: $b$=35cm, $l$=70cm, $a$=2.5cm, $t_1$ =15cm, $b_1$=10cm and $b_2$=9cm, the material properties are listed in Table 1. The detailed information can be referred to [18].

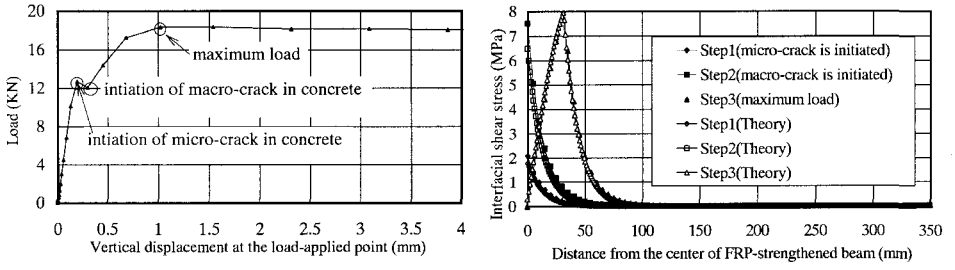
Table 1 Material properties for the studied specimen

| | | |
|---|---|---|
| Concrete | Young's modulus [GPa] | 30 |
| | Compressive strength [MPa] | 39.2 |
| | Poisson's ratio | 0.16 |
| CFRP sheets | Young's modulus [GPa] | 235 |
| | Tensile strength [GPa] | 3.2 |
| | Thickness [mm] | 0.11 |
| | Poisson's ratio | 0.3 |

Fig.3(a) shows the response of the FRP-strengthened beam for initiation and propagation of a unique flexural crack at the mid-span. As seen from Fig.3(b), three stages marked as micro-cracking initiation, macro-cracking initiation and maximum load are used to compare FEM simulation to the predicted results by theoretical equations. It is found that once a complete debonding (the shear slip at the flexural crack attains the ultimate tolerant value and the shear

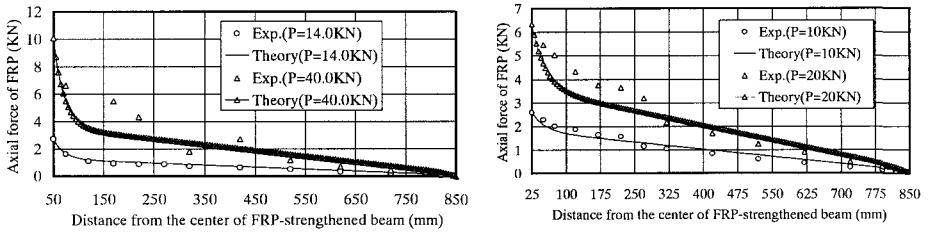
stress becomes zero) is formed the load-carrying capacity keeps nearly constant. The theoretical prediction is in a good agreement with that by FEM.

By assuming that only one flexural crack occurs in the composite beam, the predicted axial forces of FRP are compared with the experimental ones [6] as shown in Fig.4. The predicted values show much deviation from the experimental ones with increase of the external load, which may be attributed to occurrence of multiple flexural cracks in the tested beam.




(a) Structural response simulated by FEM (b) Shear stress distribution for different stages

Fig. 3 Simulation of FRP-strengthened beam with one flexural crack at the mid-span




(a) Case for 1mm CFRP plate (b) Case for 2mm CFRP plate

Fig. 4 Comparison of the predicted results with the experimental ones [6]

## 2.2 Application of theory on simple shear test to FRP-strengthened R/C beams

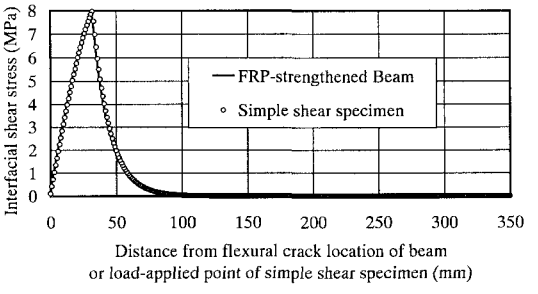



Fig. 5 Interfacial shear stress distribution in FRP-strengthened beam predicted by the present formula and the equations derived by Yuan et al [15] for simple shear specimen at the axial force of FRP=22.4KN

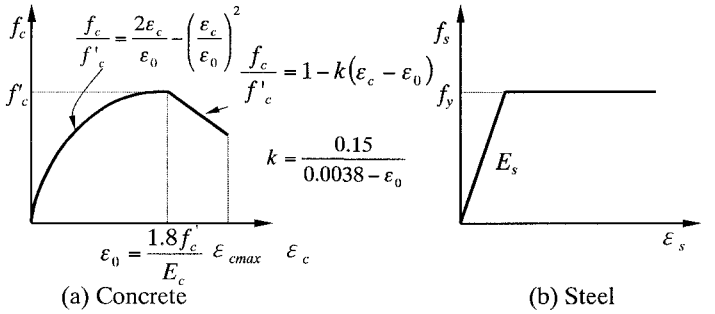
Fig.5 shows that interfacial shear stresses in FRP-strengthened beam predicted by the derived equations agree well with the ones derived by Yuan et al [15] for simple shear specimen. By adopting linear elastic bond stress-slip relationship Wu and Niu [17] investigated the shear stress distributions near flexural cracks in FRP-strengthened beam for several load cases and found that the shear transfer is similar to that in a simple shear test. Therefore, the formula on simple shear test can be applied to FRP-strengthened R/C beams.

Provided that the bonding length is larger than the effective bond length that provides effective force transfer between FRP and concrete, the equations for determining the maximum load in both linear and bilinear stress-slip relationship can be expressed in the same form [15]:

$$P_{\max} = b_2\sqrt{2G_f E_2 t_2} \tag{8}$$

where $E_2$, $t_2$ and $b_2$ are elastic modulus, thickness and width of FRP, respectively; $G_f$ is the area of the complete $\tau - \delta$ curve for the bilinear relationship illustrated in Fig. 1.

## 3. ANALTYTICAL METHOD TO PREDICT THE RESPONSE OF COMPOSITE BEAMS




(a) Concrete (b) Steel

Fig. 6 Constitutive relationship for materials

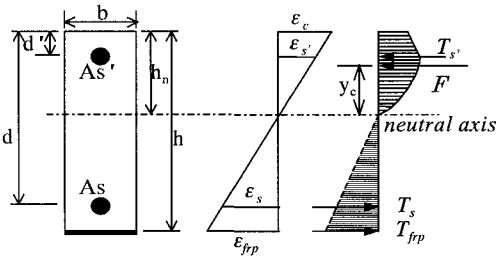



Fig. 7 Analytical model based on strain compatibility

To simulating the real response of the FRP-strengthened R/C beam accurately, nonlinear constitutive relationships for concrete and steel reinforcement in the composite beam are used in the analysis as shown in Fig.6. FRP composites are assumed to behave linearly elastic up to failure. In the analysis, it is assumed that failure is reached when either the concrete strain reaches 0.0035 or FRP composites reach their ultimate strains [1][16][17].

In the analysis presented in this section, the following assumptions are made [1][16][17]:

(a) Linear strain distribution throughout the full depth of the section;
(b) No slip between the longitudinal reinforcing steel and the surrounding concrete;
(c) No slip between the external FRP reinforcement and the concrete base;
(d) No premature FRP separation or shear failure is accounted for, composite action is maintained up to failure;
(e) The tensile strength of the adhesive is ignored.

Based on the above assumptions and the analytical model illustrated in Fig.7, an iterative procedure can be easily implemented in the computer program to determine the applied load with the known measuring position and tension strain of FRP or the axial force of FRP at a specific position when the applied load is known [16][17]. The validity of the strain compatibility is confirmed by comparing to the experimental results illustrated in Fig.8.

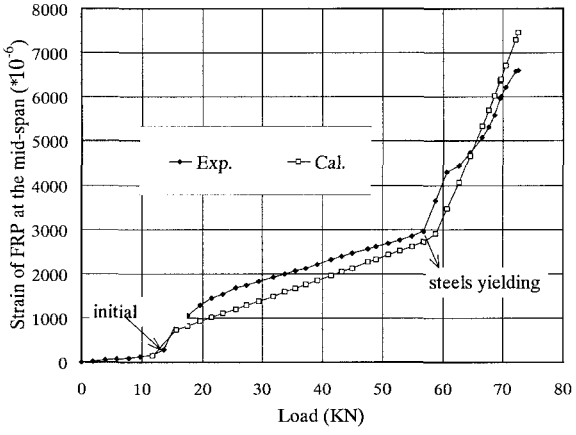
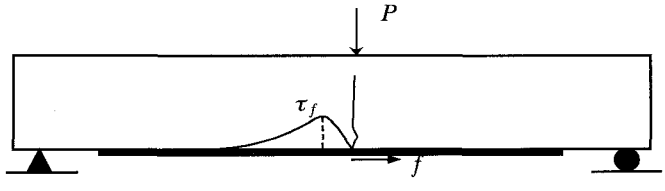



Fig. 8 Experimental result versus the predicted one for RCS_1 [17]

## 4. PROPOSED METHOD FOR PREDICTING DEBONDING FAILURE LOAD

### 4.1 An energy-based procedure for predicting debonding failure load




① $f = b_2\sqrt{2G_f E_2 t_2}$

② $f \Rightarrow P$

Fig. 9 Procedure for predicting the debonding failure load in the case of one centralized flexural crack appearing in FRP-strengthened beams

Generally, there are two typical crack patterns for debonding failure observed in the experiments conducted by Wu et al. [3][4][5][6]: 1) one or two centralized flexural cracks

appearing in the maximum moment region; 2) many distributed flexural cracks. For the case of centralized crack, once a complete interfacial crack at the end of flexural crack is initiated the final debonding failure occurs. But this does not hold true for the case of distributed cracks, where the debonding mechanism becomes more complicated with the occurrence of multiple cracks [18]. Based on the above statement, we propose an energy-based methodology for predicting the debonding failure load in what follows.

Fig.9 shows a procedure for predicting the debonding failure load in FRP-strengthened beams where only one centralized flexural crack appears. The axial force of FRP at the flexural crack located in the maximum moment region can be easily obtained by equation (8) if the interfacial fracture energy is known from a simple shear test. And then the debonding failure load can be predicted according to the strain compatibility presented in section 3.

As for the case of distributed flexural cracks, it can be assumed that flexural cracks are smeared in the strengthened beam. Considering that the interfacial shear stresses are mainly produced by the difference of axial forces in FRP, we predict debonding failure load for FRP-strengthened RC beams by assuming that a complete debonding is exactly formed between two flexural cracks with a spacing of an effective transfer length. The predicting procedure is briefly illustrated in Fig.10.

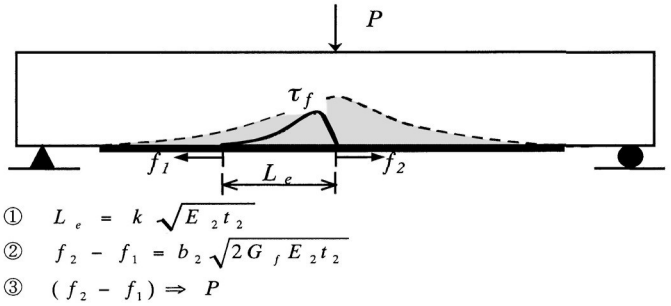



Fig. 10 Procedure for predicting the debonding failure load in the case of distributed flexural cracks appearing in FRP-strengthened RC beams

According to equation (8), the effective transfer length can be expressed as:

$$L_e \approx \frac{2P_{\max}}{\tau_f b_2} = \frac{2\sqrt{2G_f E_2 t_2}}{\tau_f} \propto \sqrt{E_2 t_2} \Rightarrow L_e(mm) = k\sqrt{E_2 t_2 (MPa \cdot mm)} \tag{9}$$

where $k$ is a coefficient determined by experiment.

Bizindavyi and Neale [19] observed that the effective transfer length increases with debonding propagation and are in the range of 15 to 20cm for concrete joints bonded with 1- and 2-ply GFRP ($E_2 t_2$ = 29.2 GPa·mm per ply) and CFRP ($E_2 t_2$ = 25.0 GPa·mm per ply). Based on this kind of studies, here we suggest that $k$ be approximately taken as 0.94 in equation (9).

### 4.2 Identification of the interfacial fracture energy from the available experiments

Based on the aforementioned methods, it is very simple to identify the interfacial fracture energy for debonding failure in the case of one centralized flexural crack appearing in FRP-

strengthened beams through a simple shear test [14][16]. Herein we give an application example to use the proposed method to identify the interfacial fracture energy for the case of distributed flexural cracks appearing in FRP-strengthened RC beams as shown in Table 2, according to the proposed method and the available experimental results.

Table 2 Identification of the interfacial fracture energy consumed for debonding failure

| Ref. | Specimen types | Properties of FRP | | | | Failure load (KN) | Identified fracture energy (N/mm) | Failure mode |
|---|---|---|---|---|---|---|---|---|
| | | Layer number | Width (cm) | $E_{FRP}$ (GPa) | Thickness per layer (mm) | | | |
| [7] | No.2 | 1 | 14 | 230 | 0.167 | 67.7 | 0.40 | Deb. |
| | No.3 | 1 | 14 | 230 | 0.167 | 76.7 | 0.49 | Deb. |
| | No.4 | 1 | 14 | 230 | 0.167 | 87.0 | 0.62 | Deb. |
| | No.8 | 1 | 14 | 230 | 0.167 | 74.9 | 0.48 | Deb. |

## 5. CONCLUSIONS

(1) A closed-form solution for predicting interfacial shear stress distribution due to a flexural crack in FRP-strengthened beams is presented by adopting bilinear bond stress-slip relationship with softening behavior.

(2) An iterative analytical method is developed to predict the response of the composite beams based on the strain compatibility, which is verified by comparison of the analytical calculation with the experiment.

(3) An energy-based criterion for predicting debonding failure load of the FRP-strengthened beams is proposed based on our previous work.

(4) By applying the proposed method to the available experiments, the interfacial fracture energy consumed for debonding failure is identified.

## REFRERNCES

1) An, W., Saadatmanesh, H. and Ehsani, M. R., *RC beams strengthened with FRP plates II: Analysis and parametric study*, Journal of Structural Engineering, ASCE, Vol. 117, No. 11, pp.3434-3455, November, 1991

2) Wu, Z. S., *Research trends onretrofitting and strengthening concrete structures by FRP sheets and plates*, pp.9-17, October, 1997, Guangzhou, China

3) Wu, Z. S., Matsuzaki, T. and Tanabe, K., *Experimental study on fracture mechanism of FRP-reinforced concrete beams*, Symposium on Non-Metallic (FRP) Reinforcement for Concrete Structures, Japan Concrete Institute, pp.119-126, May, 1998 (In Japanese)

4) Ichikawa, M. and Wu, Z. S., *Experimental study on flexural and shear behavior of RC beams strengthened with FRP sheets*, Proceedings of the Japan Concrete Institute, Vol. 20, No. 1, pp.449-454, 1998 (In Japanese)

5) Wu, Z. S., Matsuzaki, T., Fukuzawa, K. and Kanda, T., *Strengthening effects on RC beams with externally prestressed carbon fiber sheets*, Journal of Materials, Concrete Structures and Pavements, JSCE, pp.153-165, 2000 (In Japanese)

6) Kurokawa, T., Wu, Z. S. and Youshizawa, H., *Experimental investigation on crack characteristics of RC beams strengthened with CFRP plate*, Proceedings of the 54th annual conference of the JSCE, Part 5, pp.702-703, 1999 (In Japanese)

7) Takeo, K., Matsushita, H., Sagawa, Y. and Ushigome, T., *Experiment of RC beam reinforced with CFRP adhesive method having variety of shear-span ratio*, Proceedings of the Japan Concrete Institute, Vol. 21, No. 2, pp.205-210, 1999 (In Japanese)

8) Roberts, T. M., *Approximate analysis of shear and normal stress concentrations in the adhesive layer of plated RC beams*, The Structural Engineer, Vol. 67, No. 12, pp.229-233, 20 June, 1989
9) Ziraba, Y. N., Baluch, M. H., Basunbul, I. A., Sharif, A. M., Azad, A. K., and Al-Sulaimani, G. J., *Guidelines toward the design of reinforced concrete beams with external plates*, ACI Structural Journal, Vol. 91, No. 6, pp.639-646, November-December, 1994
10) Täljsten, B., *Strengthening of beams by plate bonding,* Journal of Materials in Civil Engineering, ASCE, Vol. 9, No. 4, pp.206-212, November, 1997
11) Malek, A. M., Saadatmanesh, H., and Ehsani, M. R., *Prediction of failure load of R/C beams strengthened with FRP plate due to stress concentration at the plate end*, ACI Structural Journal, Vol. 95, No. 1, pp.142-152, January-February, 1998
12) Täljsten, B., *Strengthening of concrete prisms using the plate-bonding technique*, International Journal of Fracture, Vol. 82, pp.253-266, 1996
13) Kamiharako, A., Shimomura, T., Maruyama, K. and Nishida, H., *Stress transfer and peeling-off behavior of continuous fiber reinforced sheet-concrete system*, The Seventh East Asia-Pacific Conference on Structural Engineering & Construction, pp.1283-1288, August 27-29, 1999, Kochi, Japan
14) Yoshizawa, H., Wu, Z. S., Yuan, H. and Kanakubo, T., *Study on FRP-concrete interface bond performance,* Journal of Materials, Concrete Structures and Pavements, JSCE, Vol. 49, No. 662, pp.105-119, November, 2000 (In Japanese)
15) Yuan, H., Wu, Z. S. and Yoshizawa, H., *Theoretical solutions on interfacial stress transfer of externally bonded steel/composite laminates,* Journal of Structural Mechanics and Earthquake Engineering, JSCE, April, 2001 (In press)
16) Wu, Z. S. and Niu, H. D., *Study on debonding failure load of RC beams strengthened with FRP sheets,* Journal of Structural Engineering, JSCE, Vol. 46A, pp.1431-1441, March, 2000
17) Wu, Z. S. and Niu, H. D., *Shear transfer along FRP-concrete interface in flexural members,* Journal of Materials, Concrete Structures and Pavements, JSCE, Vol. 49, No. 662, pp.231-245, November, 2000
18) Niu, H. D. and Wu, Z. S., *Interfacial debonding mechanism influenced by flexural cracks in FRP-strengthened beams,* Journal of Structural Engineering, JSCE, March, 2001 (In press)
19) Bizindavyi, L. and Neale, K. W., *Transfer lengths and bond strengths for composites bonded to concrete*, Journal of Composites for Construction, ASCE, Vol. 3, No. 4, pp.153-160, November, 1999

# Study on the bond between concrete and externally bonded CFRP sheet

BIMAL BABU ADHIKARY and HIROSHI MUTSUYOSHI
Department of Civil & Env. Engineering, Saitama University, Urawa, Japan

## ABSTRACT
Strengthening of concrete structures with CFRP sheet has emerged as one of the effective techniques. However, the effectiveness of such strengthening system depends largely on the performance of the interface between concrete and CFRP sheet in epoxy joint. For strengthening design with epoxy bonded CFRP sheets; the bond between concrete and CFRP is a major factor to be kept in mind. The bond strength of such joints depends on concrete strength, type and thickness of CFRP and bonded length. In this paper, experimental results are reported on the bond strength of CFRP sheet externally bonded to concrete with epoxy adhesive. The failure types of the system and average as well as the maximum bond strengths are reported. The effects of concrete strength, bond length and the thickness of CFRP sheet on average bond strength are described. Finally a simple expression to estimate the average bond strength of joint for flexible CFRP sheet used in this study is suggested on the basis of experimental results.

## INTRODUCTION
A number of civil infrastructures are in state of serious deterioration all over the world due to variety of reasons. Moreover, infrastructures constructed many years ago can no longer serve added needs of today's society. Besides, there are numerous structures in field that have faulty design and improper construction. As far as reinforced concrete structures (RC) are concerned, deterioration can be severe due to carbonation, chloride attack, freeze and thaw, reinforcement corrosion, etc. Several RC Bridge structures have been found seriously deteriorated in many parts of the world due to such environmental effects. However, the most important reason for strengthening of RC structures in bridges is due to continuous upgrading of design codes with time and increased live load requirements due to heavier vehicles. This increased load requirement has put the safety and integrity of several existing bridge structures in question by causing bridges deficient in their load carrying capacities. Such deficient structures have to be either replaced completely or somehow upgraded or strengthened if they require providing uninterrupted service without serious risk to human lives and properties. Strengthening and retrofitting is obvious choice if speedy, economic, reliable, and simple strengthening techniques are available.

With the advent of epoxy adhesives and availability of several composite materials such as fiber reinforcement polymers (FRP), it has been possible to use epoxy bonding of FRP to strengthen the existing concrete structures and repair the damaged ones. These materials come into variety of forms such as flexible sheets, laminates and plates. From the past studies, it has been known that the externally bonded Carbon Fiber Reinforced Polymer (CFRP) can be used effectively to enhance the shear as well as flexural capacities of RC

*FRPRCS-5*, Thomas Telford, London, 2001.

structures such as beams, columns and slabs. Due to flexible nature and ease of handling and application, combined with high tensile strength and stiffness, the flexible Carbon Fiber Sheets (hereafter CFRP sheet) are found to be highly effective for strengthening and retrofitting of RC structures. These sheets can be bonded to external surfaces of structures in different configurations, since they can follow the contour of the structures easily. Further, the application of sheet is quite simple and speedy that does not require heavy machinery for lifting and placement. Due to these advantages, CFRP sheet has emerged as one of the best-suited materials for strengthening concrete structures. The performance of the strengthened systems largely depends on the behavior of bond between concrete and CFRP sheet in epoxy joint. The failure of the system sometimes occurs from the bond line failure. Since epoxy is a brittle material once it hardens; the failure due to debonding of sheet from concrete is very sudden, which occurs without any warning. To understand the behavior of such CFRP strengthened systems; study on the bond characteristic of such joints is of great importance. There have been a number of studies in this aspect around the world, Bronsens & Van Germert (1997), Chajes et al. (1996), Horiguchi & Saeki (1997), Izumo et al. (1997). The bond between the sheet and concrete depends on a number of parameters such as concrete strength, bond length of sheet and types of sheet. Thus the experimental database for such studies is always inadequate. The objective of this paper is to enhance the understanding of bond behavior of CFRP-epoxy-concrete interface as affected by various parameters. In this study, seven reinforced concrete prisms bonded with CFRP sheets were tested. Concrete strength, type of CFRP, number of CFRP layers and bond length were taken as variables. Ultimate shearing force, average bond strength of the joint, maximum bond stress at failure, strain distribution in CFRP sheet and failure modes of specimens were investigated.

## EXPERIMENTAL DETAILS

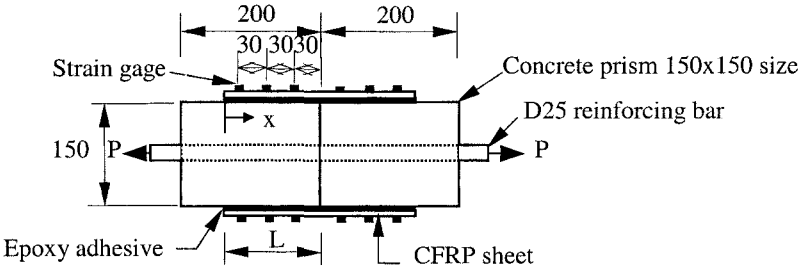



Figure 1. Layout of experiment

The CFRP sheets used in this research were high strength unidirectional sheets (FTS-C1-30 and FTS-C1-20) manufactured by Tonen Corporation, Japan. The sheets were provided in 50 meters length having 500-mm width with paper backing. Paper backing was removed after cutting the sheets into required sizes just before bonding. Primer for concrete surface and epoxy adhesive used were also supplied by Tonen, which have been developed specifically for these types of CFRP sheets. Two 100 mm wide sheets were bonded on the opposite sides of two reinforced concrete prisms 150 mm x 150 mm x 200 mm in size as shown in Figure 1. The concrete prisms were adequately reinforced both with longitudinal bars as well as stirrups. Before bonding, the bonding faces of concrete prisms were roughened by

mechanical grinding machine and cleaned thoroughly with acetone. Primer was applied on bonding surfaces uniformly and kept overnight. After the lapse of 24 hours, a two-part epoxy adhesive was applied in thin layer over the primer and pre-cut CFS were placed over it. The sheets were pressed firmly and rolled uniformly by plastic rollers to squeeze out excess epoxy. Then a slightly hot iron roller was rolled over the impregnated sheets to make a smooth surface and squeeze out all air bubbles. In case of second layer, epoxy was poured over the first layer and the procedure was repeated. Bonding was done in stages for each side of prism. In case of dry CFRP sheet as used in this study, epoxy resin serves both as adhesive and the matrix. Table 1 shows the material properties of two types of sheets and Table 2 shows the properties of epoxy adhesives used in the tests.

Table 1. Properties of CFRP sheets

| Property | Type 1 (FTS-C1-30) | Type 2 (FTS-C1-20) |
|---|---|---|
| Fiber amount ($g/m^2$) | 300 | 200 |
| Thickness of sheet (mm) | 0.167 | 0.111 |
| Tensile strength (MPa) | 3400 | 3400 |
| Tensile stiffness (N/mm) | 38400 | 25500 |
| Modulus of elasticity (GPa) | 230 | 230 |
| Maximum elongation at failure (%) | 1.5 | 1.5 |

Table 2. Properties of epoxy adhesive

| Property | Value |
|---|---|
| Pot life (minutes) | 35 |
| Compressive strength (MPa) | 34 |
| Tensile shear strength (MPa) | 9.8 |
| Adherence strength to concrete (MPa) | 1.9-2.0 |

Table 3 shows the experimental variables used in the test. Concrete prisms were tested in direct tension in a universal testing machine so that the CFRP-epoxy-concrete joint is subjected to pure shear. Strains at different locations of CFRP sheets in the direction of applied force were recorded during the test.

Table 3. Experimental variables

| Specimen number | Concrete compressive strength (MPa) | CFRP type / layer | Bond length (L) (mm) |
|---|---|---|---|
| CF-1 | 24.0 | 1 / 1 | 100 |
| CF-2 | 24.8 | 1 / 1 | 100 |
| CF-3 | 33.1 | 1 / 1 | 150 |
| CF-4 | 33.1 | 1 / 2 | 100 |
| CF-5 | 32.7 | 2 / 2 | 100 |
| CF-6 | 36.5 | 2 / 1 | 150 |
| CF-7 | 29.7 | 2 / 2 | 100 |

* Sheet width (b): 100 mm

## RESULTS AND DISCUSSION

Experimental results are shown in Table 4. Specimens CF-3 and CF-7 failed by pure debonding of CFRP sheet from concrete, whereas CFRP rupture was accompanied in the

specimens CF-6 along with debonding. Rest specimens showed concrete splitting with either CFRP debonding or CFRP rupture. Figure 2 shows the debonding failure of CFRP sheet in specimen CF-6. In all specimens, the debonded CFRP retained some chunks of concrete on their bonded surface. This suggests that the actual failure is somewhat shearing-off of concrete just below the CFRP sheets. Thus the concrete surface tensile strength is one of the most important factors in CFRP strengthened structures. The surface tensile strength of concrete can be related to the concrete compressive strength for the ease of study. The average bond stress at failure was found in between 1.1 to 2.8 MPa whereas the maximum bond stress varied from 3.6 to 6.3 MPa. The average bond stress of the joint is calculated from eq. 1, whereas maximum bond stress is calculated using eq. 2.

$$\tau_{avg.} = \frac{P}{2bL} \tag{1}$$

$$\tau_{\max.} = E_{CFRP} t_{CFRP} \frac{\Delta\varepsilon}{\Delta x} \tag{2}$$

where, $P$ : total load at failure (N)
$b$ : width of CFRP sheet (mm)
$L$ : bond length (mm)
$E_{CFRP}$ : Elastic modulus of CFRP sheet (MPa)
$t_{CFRP}$ : thickness of CFRP sheet (mm)
$\frac{\Delta\varepsilon}{\Delta x}$ : strain gradient between two consecutive strain gages in CFRP sheet

Table 4. Experimental results

| Specimen number | Ultimate failure load P (kN) | Average bond stress (MPa) | Maximum bond stress (MPa) |
|---|---|---|---|
| CF-1 | 44.0 | 2.2 | 5.0 |
| CF-2 | 40.2 | 2.0 | 4.9 |
| CF-3 | 40.9 | 1.4 | 4.3 |
| CF-4 | 51.8 | 2.6 | 3.6 |
| CF-5 | 56.5 | 2.8 | 6.3 |
| CF-6 | 33.5 | 1.1 | 3.6 |
| CF-7 | 49.2 | 2.5 | 5.6 |

Effects of concrete strength and bond length on average bond strength of CFRP-epoxy-concrete interface are shown in Figure 3 and Figure 4 respectively. Relationship between ultimate shearing force and bond length is shown in Figure 5. It is seen that the average bond strength of interface increases with concrete strength. It is found that the ultimate shearing force remained somewhat constant for both bond lengths 100 mm and 150 mm, whereas the average bond stress decreases. This implies that for specimens with longer bond length, some portion of bond takes only nominal part in force transfer before the failure of highly stressed end. Once the first debonding occurs, stress at that point decreases and the location of maximum stress shifts towards the other end. This way a progressive debonding occurs. This observation suggests that the effective bond length of CFRP sheet falls somewhere around 100 mm. Chajes et al. (1996) have reported effective bond length of 90 mm for FRP sheets.

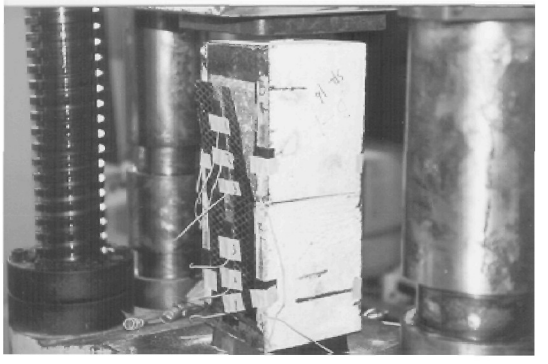


Figure 2. Photograph of CFRP debonding in specimen CF-6

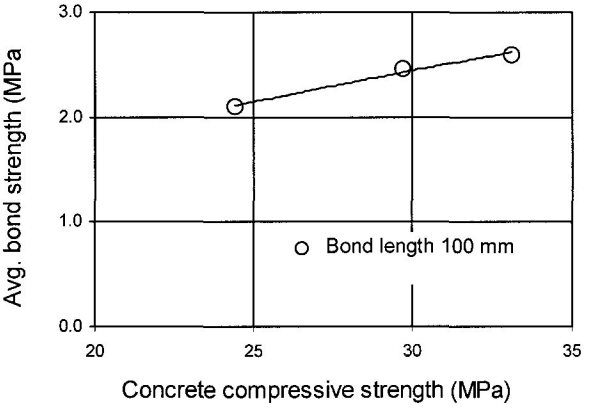



Figure 3. Average bond strength versus concrete strength relationship

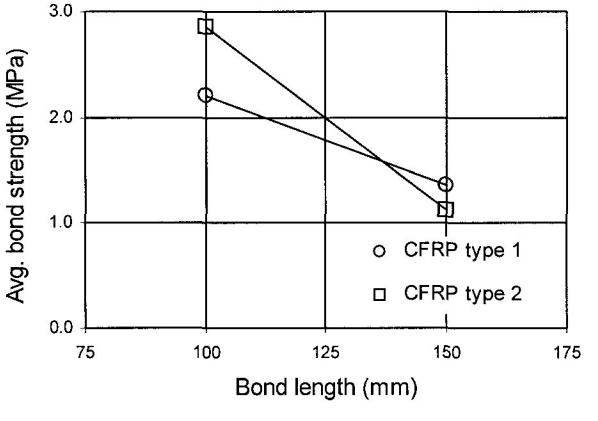



Figure 4. Average bond strength versus bond length relationship

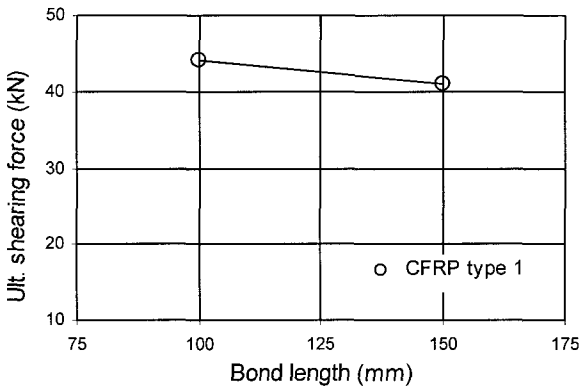



Figure 5. Ultimate shearing force versus bond length relationship

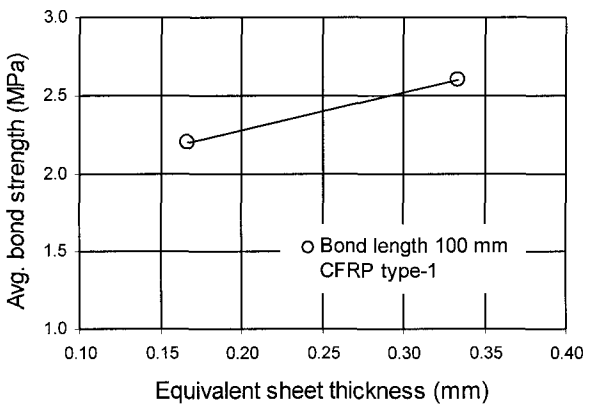



Figure 6. Average bond strength versus equivalent sheet thickness relationship

The effect of number of sheet layers in terms of equivalent sheet thickness on the average bond strength of interface is shown in Figure 6 for CFRP type 1. It is seen from this figure that the bond strength increases little by increasing the number of sheet layers. The high concentration of bond stress near the loaded end of CFRP sheet can be confirmed by the sheet strain distribution for typical specimen CF-5 shown in Figure 7.

## EXPRESSION FOR BOND STRENGTH

Since for specific type of CFRP sheet specific epoxy is generally used in practice and for CFRP sheets used in this study, the effective bond length was found about 100 mm; the estimation of the average bond strength of the joint can be related to concrete strength. The validity of this assumption has been observed from the debonding failure of sheet that occurs in thin layer of concrete just below the sheet. Effect of the thickness of CFRP sheet is ignored for the sake of simplicity. From the experimental results, the average bond strength of CFRP sheet to concrete in epoxy joint can be estimated from eq. 3.

$$\tau_u = 0.25\left(f_c'\right)^{\frac{2}{3}} \tag{3}$$

where, $\tau_u$ is average bond strength and $f_c'$ is concrete compressive strength respectively.

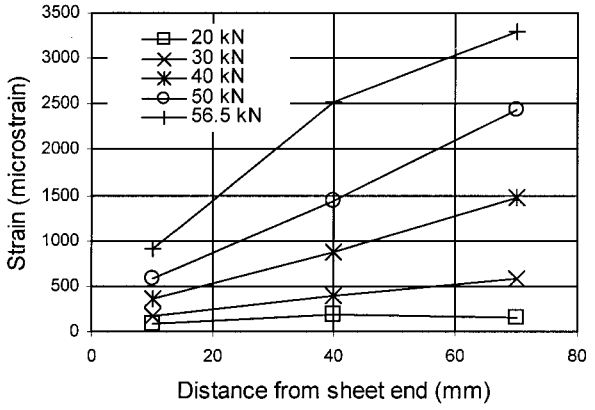



Figure 7. Strain distribution in CFRP sheet for specimen CF-5

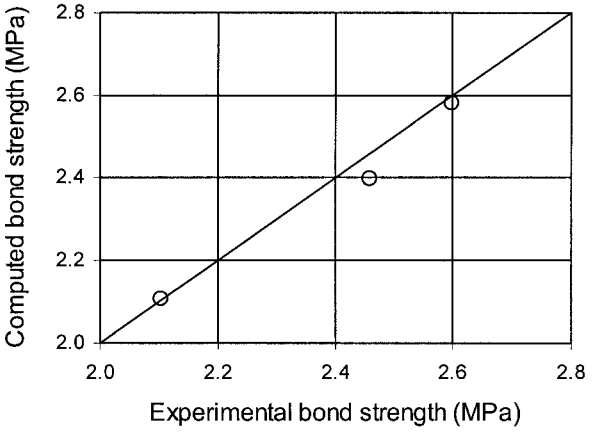



Figure 8. Correlation graph for average bond strength

Figure 8 shows the correlation graph of bond strength predicted from eq. 3 and experiment. It is seen that the present expression predicts the bond strength quite well to test results.

## CONCLUSIONS

The average bond strength and maximum bond stress at failure are found in the range of 1.1-2.8 MPa and 3.6-6.3 MPa for the CFRP-epoxy- concrete interface. However, the strain distribution is not uniform along the bonded length. The highest bond stress occurs at the end of sheet near the applied force where the first debonding starts and progresses towards the

other end. This causes the average bond strength to decrease, as the bond length becomes longer. However, the ultimate shearing force remains somewhat constant. Thus it is suggested that the effective bond length is somewhere around 100 mm for CFRP sheets used in this study. The average bond stress at failure increases with concrete strength. CFRP sheet bonded specimens exhibited shearing-off of concrete just below the sheet with CFRP rupture in some cases. Thus the concrete strength is the major factor in determining bond strength of concrete to CFRP sheet in such joints. The simple expression suggested for bond strength can be used satisfactorily to predict the bond strength of this type of CFRP sheet to concrete for practical applications.

## ACKNOWLEDGMENTS

The authors would like to express their sincere thanks to Tonen Corporation, Japan for providing the CFRP sheets and epoxy adhesive used in this study.

## REFERENCES

Brosens, K. and Van Gemert, D. (1997), "Anchoring Stress Between Concrete and Carbon Fiber Reinforced Laminates," Non-Metallic (FRP) Reinforcement for Concrete Structures, Proceedings of the Third International Symposium, Sapporo, Vol. 1, pp. 271-278.

Chajes, M. J., Finch Jr, W. W., Januska, T. F., and Thomson Jr., T. A. (1996), "Bond and Force Transfer of Composite Material Plate Bonded to Concrete," ACI Structural Journal, Vol. 93, No. 2, pp. 208-217.

Horiguchi, T. and Saeki, N. (1997), "Effects of Test Methods and Quality of Concrete on Bond Strength of CFRP sheet," Non-Metallic (FRP) Reinforcement for Concrete Structures, Proceedings of the Third International Symposium, Sapporo, Vol. 1, pp. 265-270.

Izumo, K., Saeki, N., Asamizu, T. and Shimura, K. (1997), "Strengthening Reinforced Concrete Beams by Using Prestressed Fiber Sheets," Non-Metallic (FRP) Reinforcement for Concrete Structures, Proceedings of the Third International Symposium, Sapporo, Vol. 1, pp. 379-386.

Lee, Y. J., Boothby, T. E., Bakis, C. E. and Nanni, A. (1999), "Slip Modulus of FRP Sheets Bonded to Concrete," Journal of Composites in Construction, ASCE, Vol. 3, No. 4, pp. 161-167.

Rostasy, Ferdinand S. and Neubauer, Uwe (1997), "Bond Behavior of CFRP-Laminates for the Strengthening of Concrete Members," Composite Construction - Conventional and Innovative, Proceedings of the International Conference, Innsbruck, Austria, pp. 717-722.

Swamy, R. N., Jones, R. and Charif, A. (1986), "Shear Adhesion Properties of Epoxy Resin Adhesives," Adhesion between Polymers and Concrete, Edited by H. R. Sasse (RILEM), pp. 741-755.

# Advanced wrapping system with CF-anchor —Stress transfer mechanism of CF-anchor—

K. KOBAYASHI, Fukui University, Fukui, Japan,
S. FUJII, Kyoto University, Kyoto, Japan,
Y. YABE, Shimizu Corporation, Tokyo, Japan,
H. TSUKAGOSHI, Shimizu Corporation, Tokyo, Japan, and
T. SUGIYAMA, Nippon Steel Composite Co., Ltd., Tokyo, Japan

## IDEA OF CF-ANCHOR

CF sheet wrapping technology for bare columns has been documented [1]-[3]. However, the number of bare columns in buildings is relatively small and there is considerable variety in them such as columns with wing walls, columns with spandrel/suspended walls, columns with shear walls, etc. When columns have walls, CF sheet wrapping is split between both side of the wall. Several ideas to achieve a semi-closed wrapping through the walls have been proposed. It is, however, difficult to obtain sufficient strengthening effect without partially removing the walls and achieving a closed wrapping. This would reduce the strength and rigidity of the wall. CF-Anchor is an idea to connect the CF sheet wrapping split by walls, keeping them in the original condition as shown in Fig.1. Penetrating holes are drilled through the wall close to the column surface. A bundle of CF strands is put through the hole, and then they form a fan outside of the hole. The distributed strand in a shape of fan is spliced with CF sheet on the column. The advantage is that the CF-anchor hardly affects the strength and rigidity of the walls. A column strengthened by this system would not fail in a shear mode, even after the failure of the walls. The walls would work as energy absorption elements. In early stages, the rigidity and strength as columns with walls could be expected, and after the failure of the walls, a performance of bare columns with high ductility could be expected.
CF-Anchor is applicable to beams with slabs, in-filled shear walls in the frame, etc. as well as columns with walls.

## STRESS TRANSFER MECHANISM

Figure 2 shows a basic unit of CF-anchor. A tensile force on the CF sheet changes its direction in the fan shaped portion of CF-anchor and again changes its direction at the key portion of CF-anchor, and travels to a straight line portion. The force (F2) for changing the direction of tensile force at the key portion of CF-anchor can be fully expected on the inside of the penetrating hole drilled in the wall. In order to change the direction of tensile force in the fan shaped portion of CF-anchor, the force (F3) in the orthogonal direction to CF sheet is needed, such as an adhesive strength of CF sheet on the concrete of column surface. If the force of F3 is small, the tensile strength of the CF sheet is not fully demonstrated.
CF sheet would demonstrate full strength in the central part, since it is not necessary to change the direction of

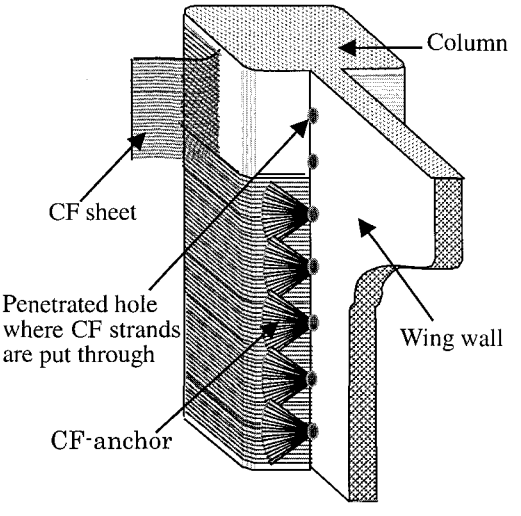



Fig.1 Idea of CF-anchor

tensile force. Then, if it is assumed that CF sheet demonstrates $\alpha$ times the full tensile strength depending on the distance from the center as described in Eq.1, 50% of the tensile capacity of CF sheet would transmit to the CF-anchor.

$$\alpha = 1 - \theta / \theta_0 \quad \text{(Eq.1)}$$

($\theta$ and $\theta_0$ are defined in Fig.2.)

If Eq.2 is assumed, 100% of the tensile capacity of CF sheet would transmit to the CF-anchor.

$$\alpha \equiv 1 \quad \text{(Eq.2)}$$

A detail to assure the force of F3 should be developed and $\alpha$ should come close to the distribution of Eq.2.

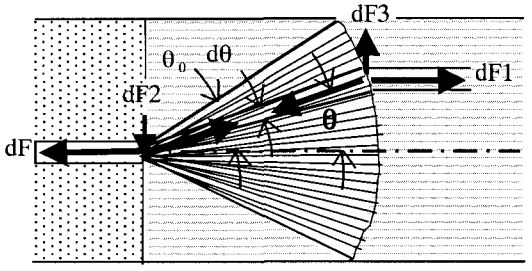



Fig.2 Stress transfer mechanism of a basic unit of CF-anchor

Therefore, the problems to be resolved in the CF-anchor system are as follows:

(1) Adhesive strength of CF-anchor and CF sheet
(2) A detail to assure the force (F3) to change the direction of tensile force of the CF sheet in the fan shaped portion of the CF-anchor
(3) A capacity of the key portion of the CF-anchor, since uniform stress is not applied to CF strands in the key portion of the CF-anchor
(4) A suitable amount of CF strand of the CF-anchor to the amount of CF sheets

## EXPERIMENTAL VERIFICATION OF STRESS TRANSFER MECHANISM

### Outline of Experiment

A fundamental test was conducted for the verification of the above mentioned stress transfer mechanism. Two types of specimens are shown in Fig.3. The parameters are listed in Table 1. S-type is a unit specimen with a CF-anchor in the center. The experimental variable is CF-anchor length (L). When the width of a unit CF-anchor is constant, the opening angle of a fan becomes larger as the CF-anchor length (L) decreases. D-type is a unit specimen that simulates the region between two adjoining CF-anchors. The experimental variable is the non-overlapped length (W) of the fans that are located side by side. The opening angle of a fan becomes larger as the non-overlapped length (W) decreases. Three kinds of specimen models were produced for both S- and D-types. The BA-model details the most disadvantageous situation where CF sheet does not bond with concrete. In the LA-model, a steel plate with 3.2mm in thickness was laminated on the opposite side of CF sheet in the spliced portion with CF-anchor. This was thought to model the condition where CF sheet has bonded with concrete and the force (F3) of Fig. 2 can be assured. The SW-model is similar to the LA-model. A steel plate with 3.2mm in thickness was inserted between the CF sheet and CF-anchor. This was thought to model the condition of good bond of CF-anchor with CF sheet in addition to the condition of LA-model.
CF sheet used is 20cm in width and one layer of 300g/m$^2$ in density. The area of cross-section is

20cmx0.0167cm=0.334cm$^2$. The specified tensile strength is 3430N/mm$^2$. The tensile capacity of CF sheet used is 3.430kN/mm$^2$x33.4mm$^2$=114.6kN. CF strand for CF-anchor is the same as that used for the production of CF sheet. The amount of sizing agent is 2%. The amount of fiber in CF sheet and CF-anchor is the same. For the introduction of uniform stress distribution into the CF sheet, the CF sheet at the loading end was sandwiched between a pair of steel plates with 4.5mm in thickness. The tensile force was applied through a pin joint. The steel pipe was attached in the straight portion of the CF-anchor. In case of D-Type specimens, the tensile force was applied fixing the distance between two attached steel pipes.

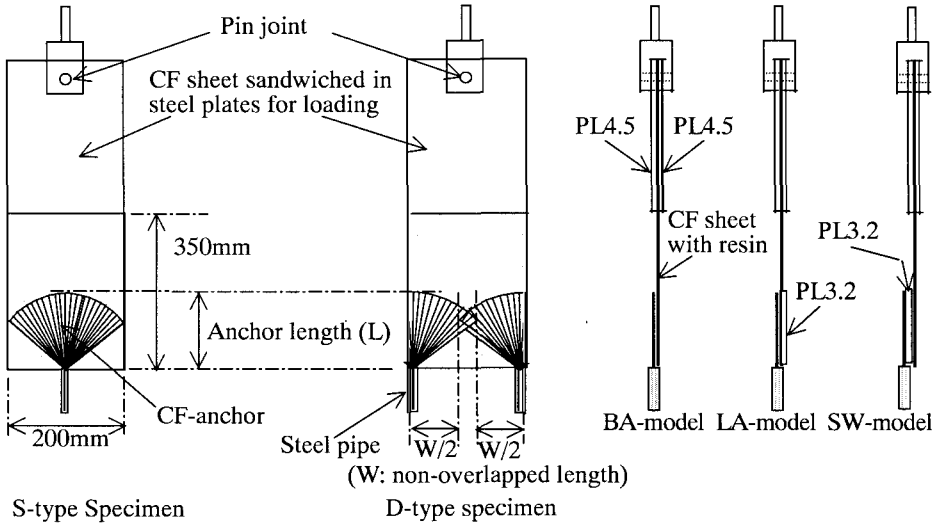



Fig.3 Illustration of two types of specimens

**Test Result**

The experiment results are shown in the right hand column of Table 1. The relation between the maximum load and CF-anchor length (L) is shown in Fig.4 for S-type specimens and in Fig.5 for D-type specimens.

The maximum load becomes larger according to the increase of CF-anchor length. If CF-anchor length is the same, the maximum load is largest and smallest for the LA-model, BA- and SW-model, respectively. The maximum load was determined by the rupture of CF sheet for BA-model and the rupture of the key portion of CF-anchor for LA-model. In the SW-model, the CF-anchor was peeled off the sandwiched steel plate, because of the eccentric tensioning of the CF-anchor and CF sheet. As a result the maximum load became small.

An example of strain distribution on CF sheet is shown in Fig.6. In the BA-model of the S-type, it approached the distribution predicted by Eq.1, and the strain decreased in proportion to the distance from the center of CF sheet. The maximum load was about 48kN when CF anchor length was 20cm. This means that about 40% of the tensile capacity of CF sheet are transmitted to the CF-anchor. In case of the LA- and SW-models of S-type, it approached the distribution expected by Eq.2. But the magnitude of strain was much smaller than the ultimate strain of the CF sheet. Eventually the key portion of CF-anchor ruptured in case of the LA-model of S-type, and the fan shaped portion of CF-anchor was peeled off the steel plate in case of SW-model of S-type. As a result, the maximum load of both LA- and SW-model was around 40% of tensile capacity of the CF sheet when the CF-anchor length was 20cm.

From this experimental result, it was demonstrated that a larger part of the tensile capacity of CF sheet could be transmitted to the CF-anchor if the capacity of the key portion of the CF-anchor could be improved. The force of F3 for changing the direction of tensile force on the CF sheet, explained in Fig.1, is absolutely required even after the CF sheet loses the bond with concrete. It is necessary to assure the force of F3 by a certain method.

Table 1 List of specimens

| Specimen's name | CF-anchor length L(cm) | Non-overlapped length W(cm) | Opening angle of fan-shape (degree) | Maximum load (kN) |
|---|---|---|---|---|
| S12-BA-1, 2, 3 | 11.5 | 20 | 120 | 35.8 |
| S12-LA-1 | | | | 37.4 |
| S12-SW-1 | | | | 26.6 |
| S15-BA-1, 2, 3 | 15.0 | | 84 | 43.1 |
| S15-LA-1 | | | | 51.2 |
| S15-SW-1 | | | | 29.7 |
| S20-BA-1, 2, 3 | 20.0 | | 60 | 47.5 |
| S20-LA-1 | | | | 53.6 |
| S20-SW-1 | | | | 43.0 |
| S25-BA-1, 2, 3 | 25.0 | | 47 | 51.2 |
| S25-LA-1 | | | | 57.4 |
| S25-SW-1 | | | | 47.6 |
| D05-BA-2, 3 | 20 | 5.0 | 120 | 45.1 |
| D05-LA-1 | | | | (29.4)* |
| D05-SW-1 | | | | (30.1)* |
| D10-BA-1, 2, 3 | | 10.0 | 100 | 51.3 |
| D10-LA-1 | | | | (29.0)* |
| D10-SW-1 | | | | 36.5 |
| D15-BA-1, 3 | | 15.0 | 80 | 51.2 |
| D15-LA-1 | | | | 43.7 |
| D15-SW-1 | | | | 34.4 |

Note: ( )* was excluded from the discussion, because the distance between two CF-anchors was not satisfactorily restrained.
The maximum load of BA-model is the average value of two or three specimens.

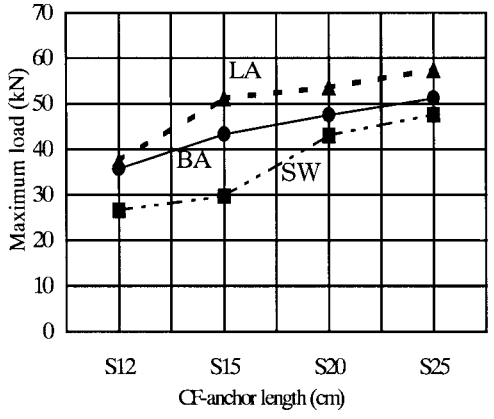



Fig.4 Relation between the maximum load and CF-anchor length for S-type

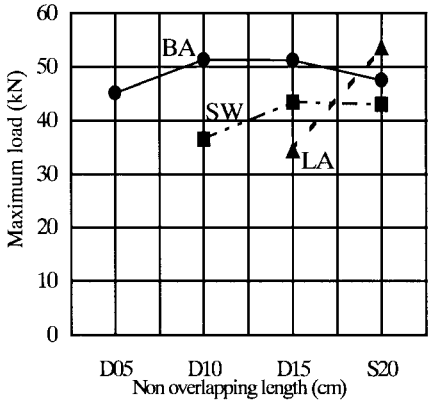



Fig.5 Relation between the maximum load and CF-anchor length for D-type

In D-type specimens, the strain concentration at the center of the CF sheet was considerably eased by a slight overlapping of the fan shaped portion of the CF-anchors, even in the BA-model, and the rupture of the key portion of the CF-anchor preceded the rupture of CF sheet. Adjoining CF-anchors mutually share the force of F3 in Fig.2. It could be expected that stress transfer is performed efficiently when multiple CF-anchors are installed. The maximum load of D-type specimens was constantly about 50kN regardless the overlapping length of the fan shaped portion of CF-anchor. SW-models of D-type fundamentally showed a similar behavior

to that of LA-models. However, peeling-off of CF-anchor is promoted by the eccentric tensioning of CF-anchor and CF sheet, and the maximum load becomes small. Since a level gap of CF sheet and CF-anchor causes peeling off, a specification for reducing the eccentricity is required.

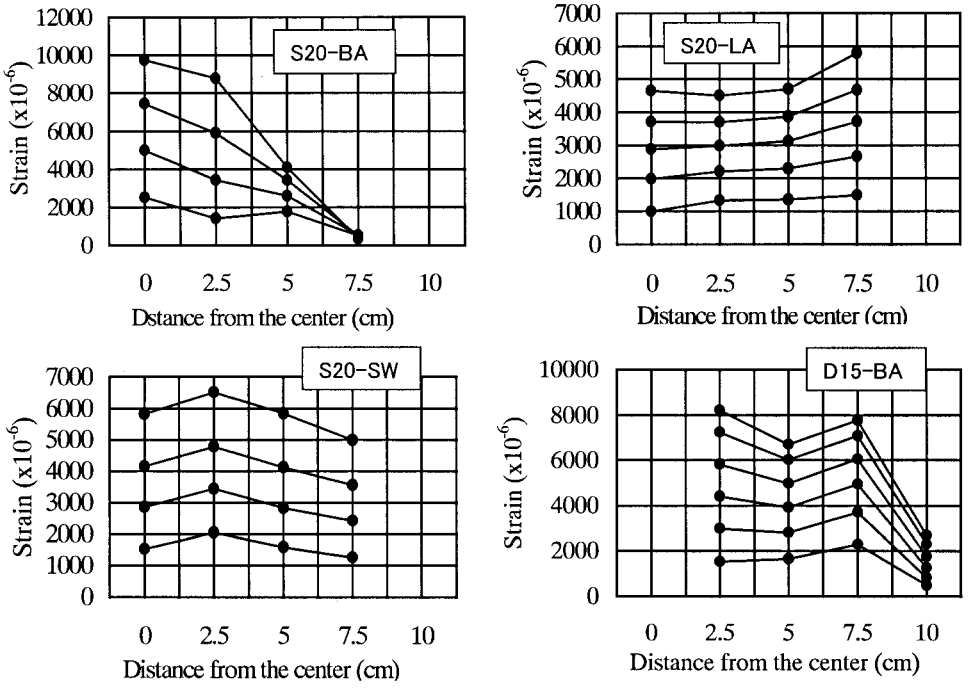



Fig. 6 Typical strain distribution on CF sheet

## SPECIFICATION OF CF-ANCHOR

A standard detail of the CF-anchor system is shown in Fig.7. CF-anchor with larger length (L) has larger maximum load. A larger CF-anchor length also means a small opening angle of the fan, and it should be limited to less than 90 degrees. By overlapping of the fan shaped portions of adjoining CF-anchors, the force of F3 in Fig.2 can be expected. So the fan shaped portions of

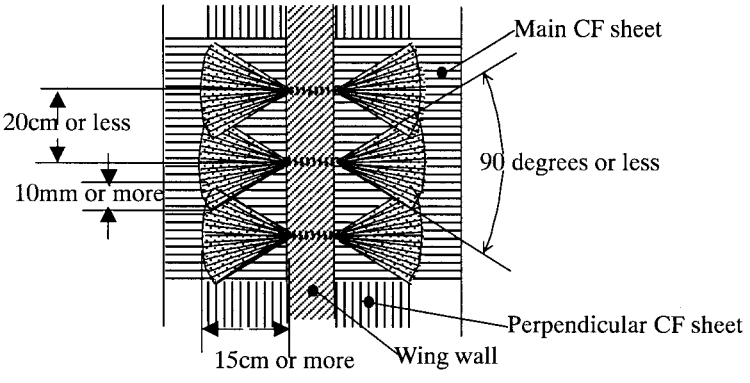



Fig. 7 A standard detail of CF-anchor system

adjoining CF-anchors should be arranged so that they overlap. If the CF-anchor length (L) is 15cm, then the interval of CF-anchor is inevitably set to less than 20cm.
The perpendicular CF sheet is required under the fan shaped portion of CF-anchor. Its amount would be more than a half of main CF sheet.
As for the amount of fibers contained in the CF-anchor, it should at least be more than that in main CF sheet, so that the capacity of the key portion of CF-anchor would be assured.
CF strand with sizing agents of 0.2% must be used for CF-anchor. From an experiment conducted separately, it was shown that permeability of the resin into the key portion of CF-anchor is much improved, and the capacity of the key portion of CF-anchor increases, if the amount of sizing agents in the CF strand is lowered to about 0.2%.

## EXPERIMENTAL EVALUATION OF CAPACITY OF CF-ANCHOR

### Modeling of Specimens

Three models of specimen were designed supposing the cracking pattern shown in Fig.8.
Illustrative detail of three models is shown in Fig. 9. The upper block and the lower block are produced separately. A-model simulates the cracking pattern where a shear crack extends along the interface between column and wing wall. The total applied tensile force acts at the key portion of the CF-anchor.
B-model simulates the cracking pattern where another shear crack is crossing the fan shaped portion of CF-anchor in addition to the condition of A-model. The total applied tensile force acts at the key portion of CF-anchor and on CF sheet at the position of an introduced crack.

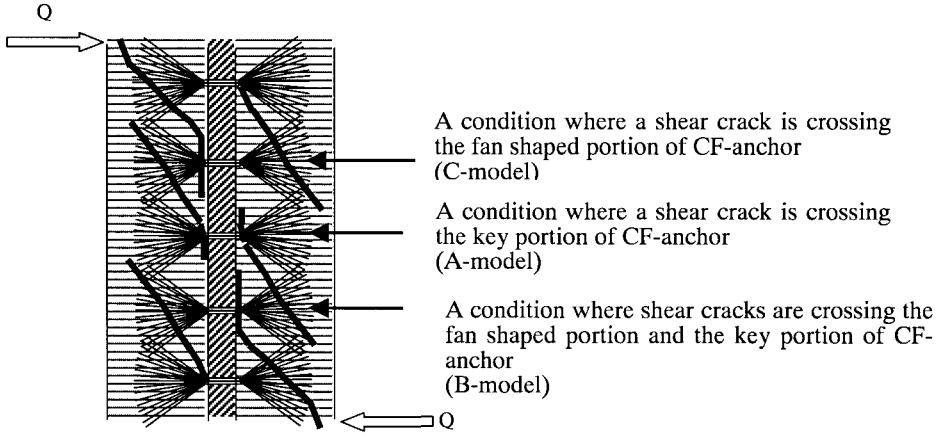



Fig. 8 Modeling of specimens

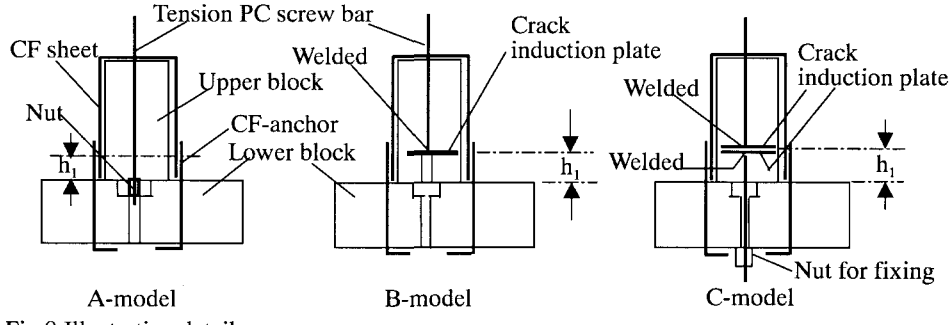



Fig.9 Illustrative detail

C-model simulates the cracking pattern where a shear crack is crossing just the fan shaped portion of the CF- anchor. The bottom part of the upper block is fixed to the lower block by a PC screw bar. The total applied tensile force acts on the CF sheet at the position of an introduced crack.

**Outline of Experiment**

The dimension of the lower block is 400x200x600mm. The penetrating holes with a diameter of 16mm, where the straight portion of CF-anchor was put through, were pre-installed. The dimension of the upper block is 240x200x500mm. In order to install the perpendicular CF sheet, the corners of the upper block were rounded with a radius of 20mm. The specimens are listed in Table 2. The concrete strength for the first 20 specimens of Table 2 was 33.7N/mm$^2$, and 26.1N/mm$^2$ for another 20 specimens. The amount of sizing agents of the used CF strand was 0.2%.

In a part of the A-model specimens, the bond between the perpendicular CF sheet and concrete was removed in the region of $h_1$(mm) measured from the bottom of the upper block. In S15-2A150N-12 and D15-2A150N-12, the bond between the main CF sheet and concrete was removed under the fan shaped portion of the CF-anchor.

Loading setup is shown in Photo.1. The lower block was fixed in the reaction frame and a tensile force was applied by tensioning PC screw bar D25 through an oil jack with center-hole. Applied load was measured by load cell that was installed at the tip of the oil jack. Moreover, strain gages were attached on the main CF sheet, perpendicular CF sheet and the fan shaped portion of CF-anchor.

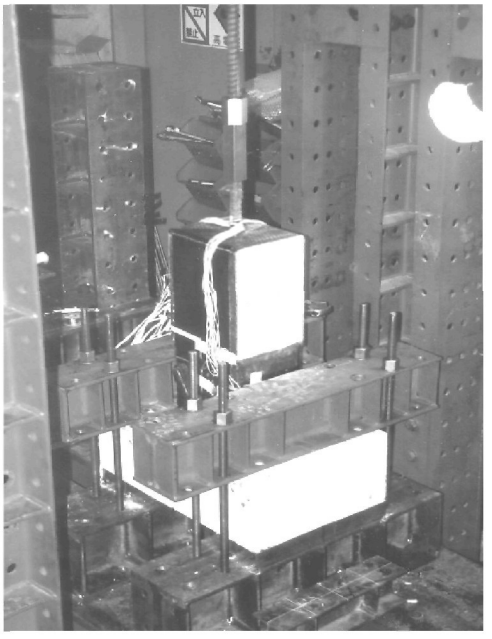


Photo.1 Loading setup

**Test Results**

The maximum load and the failure mode are shown in the right hand column of Table 2. There is considerable fiber in the region where the fan shaped portion of CF-anchor is spliced with CF sheet. So a failure in this portion hardly occurs. In S20-2C150H-12, this failure mode appeared, but it was only secondary and partial. Since CF strand with sizing agents of 0.2% was used and the strength of the key portion of CF-anchor was much improved, the CF-anchor was dislocated in plane from the main CF sheet in many specimens.

When there was no perpendicular CF sheet, the maximum load was low. After de-bonding of CF sheet from concrete, CF-anchor of S-type was distorted by tensioning and showed a similar behavior to that of S-type in Fig. 3. In D-type, the center of a main CF sheet was torn. The necessity for a perpendicular CF sheet was recognized. In D-type specimens, some strain gages on a perpendicular CF sheet with fiber density of 300g/m$^2$ showed a large strain of 0.6-1%. Some strain gages on a perpendicular CF sheet with fiber density of 150g/m$^2$ showed a larger strain of 1.3-1.4% just before the maximum load and the rupture of a perpendicular CF sheet partially appeared. Although it is not certain whether the rupture of a perpendicular CF sheet triggered the rupture of the CF-anchor system, a perpendicular CF sheet would undoubtedly play an important role.

Figure 10 shows the comparison of the maximum load of S-type specimens and D-type specimens. There is a tendency for the maximum load of D-type to be larger than that of S-type. When two or more CF-anchors are actually constructed, they would work cooperatively. Therefore this experiment is conducted under more severe conditions.

Table 2 List of Specimens

| Specimen's Name | | $h_1$ mm | Per. CF sheet g/m$^2$ | Main CF sheet g/m$^2$ | CF-anchor | | | Test Result | |
|---|---|---|---|---|---|---|---|---|---|
| | | | | | L mm | No. of strand | γ | $P_{max}$ (kN) | Failure mode |
| S15-2A000Y-12 | A | 0 | 300 | 300 | 150 | 92×1 | 1.2 | 97.4 | P |
| S15-2A075Y-12 | A | 75 | 300 | 300 | 150 | 92×1 | 1.2 | 97.7 | N |
| S15-2A150Y-12 | A | 150 | 300 | 300 | 150 | 92×1 | 1.2 | 123.3 | N S1 |
| S15-2A150N-12 | A | 0 | None | 300 | 150 | 92×1 | 1.2 | 69.8 | P |
| S15-2B075Y-12 | B | 75 | 300 | 300 | 150 | 92×1 | 1.2 | 84.7 | N |
| S15-2B150Y-12 | B | 150 | 300 | 300 | 150 | 92×1 | 1.2 | 114.9 | P |
| S15-2B150N-12 | B | 150 | None | 300 | 150 | 92×1 | 1.2 | 77.6 | P |
| S15-2C075Y-12 | C | 75 | 300 | 300 | 150 | 92×1 | 1.2 | 94.6 | N |
| S15-2C150Y-12 | C | 150 | 300 | 300 | 150 | 92×1 | 1.2 | 132.9 | N |
| S15-2C150N-12 | C | 150 | None | 300 | 150 | 92×1 | 1.2 | 96.8 | P |
| D15-2A000Y-12 | A | 0 | 300 | 300 | 150 | 46×2 | 1.2 | 95.1 | P |
| D15-2A075Y-12 | A | 75 | 300 | 300 | 150 | 46×2 | 1.2 | 89.6 | P |
| D15-2A150Y-12 | A | 150 | 300 | 300 | 150 | 46×2 | 1.2 | 135.9 | P N |
| D15-2A150N-12 | A | 0 | None | 300 | 150 | 46×2 | 1.2 | 58.1 | P |
| D15-2B075Y-12 | B | 75 | 300 | 300 | 150 | 46×2 | 1.2 | 113.1 | P N |
| D15-2B150Y-12 | B | 150 | 300 | 300 | 150 | 46×2 | 1.2 | 138.5 | P |
| D15-2B150N-12 | B | 150 | None | 300 | 150 | 46×2 | 1.2 | 82.2 | P S1 |
| D15-2C075Y-12 | C | 75 | 300 | 300 | 150 | 46×2 | 1.2 | 140.4 | N S1 |
| D15-2C150Y-12 | C | 150 | 300 | 300 | 150 | 46×2 | 1.2 | 128.3 | P |
| D15-2C150N-12 | C | 150 | None | 300 | 150 | 46×2 | 1.2 | 89.6 | P |
| S15-2A150H-10 | A | 150 | 150 | 300 | 150 | 76×1 | 1.0 | 93.4 | S1 P |
| S15-2B150H-10 | B | 150 | 150 | 300 | 150 | 76×1 | 1.0 | 114.2 | N P |
| S15-2C150H-10 | C | 150 | 150 | 300 | 150 | 76×1 | 1.0 | 115.4 | S2 N P |
| S20-2B150H-10 | B | 150 | 150 | 300 | 200 | 76×1 | 1.0 | 128.3 | S3 P |
| S20-2B150H-12 | B | 150 | 150 | 300 | 200 | 92×1 | 1.2 | 108.3 | N S3 P |
| S20-2C150H-12 | C | 150 | 150 | 300 | 200 | 92×1 | 1.2 | 107.6 | S2 N |
| S20-2B150H-15 | B | 150 | 150 | 300 | 200 | 114×1 | 1.5 | 117.2 | P |
| D15-2A150H-10 | A | 150 | 150 | 300 | 150 | 38×2 | 1.0 | 98.3 | P |
| D15-2B150H-10 | B | 150 | 150 | 300 | 150 | 38×2 | 1.0 | 109.7 | P |
| D15-2C150H-10 | C | 150 | 150 | 300 | 150 | 38×2 | 1.0 | 123.8 | S1 P S2 |
| D15-1A150H-12 | A | 150 | 150 | 150 | 150 | 23×2 | 1.2 | 74.1 | P |
| D15-3A150H-12 | A | 150 | 150 | 150+300 | 150 | 69×2 | 1.2 | 109.1 | P |
| D15-1B150H-12 | B | 150 | 150 | 150 | 150 | 23×2 | 1.2 | 84.8 | N |
| D15-3B150H-12 | B | 150 | 150 | 150+300 | 150 | 69×2 | 1.2 | 180.5 | P |
| D15-3B150Y-12 | B | 150 | 300 | 150+300 | 150 | 69×2 | 1.2 | 138.0 | P |
| D20-2B150H-12 | B | 150 | 150 | 300 | 200 | 46×2 | 1.2 | 165.0 | N P |
| D20-2C150H-12 | C | 150 | 150 | 300 | 200 | 46×2 | 1.2 | 139.5 | S1 P S2 |

Specimen's name represents (type, anchor length) -(main CF sheets, model, $h_1$, perpendicular CF sheets) - (γ)

$h_1$: Position of introduced crack for B-model and C-model, no bond length for A-model

$P_{max}$: Maximum load

γ: Ratio of the amount of fibers in CF-anchor to that in main CF sheet

Failure mode P: In-plane dislocation of CF-anchor from main CF sheet

N: Rupture of the key portion of CF-anchor

S1: Rupture of a perpendicular CF sheet

S2: Rupture of a main CF sheet

S3: Rupture of the fan shaped portion of CF-anchor

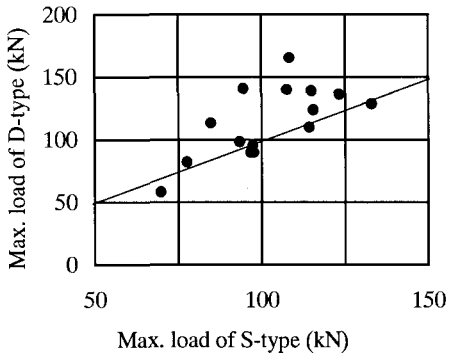



Fig.10 Comparison of the maximum load of S-type and D-type

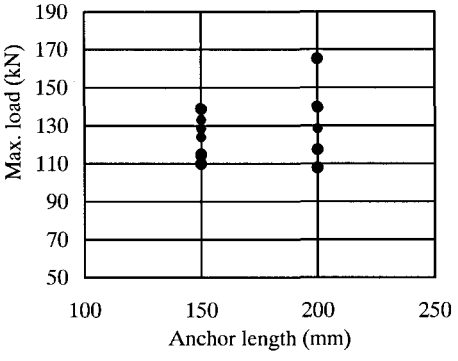



Fig.11 Effect of the CF-anchor length

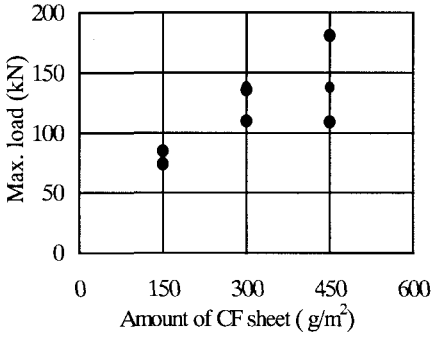



Fig.12 Effect of the amount of main CF sheet

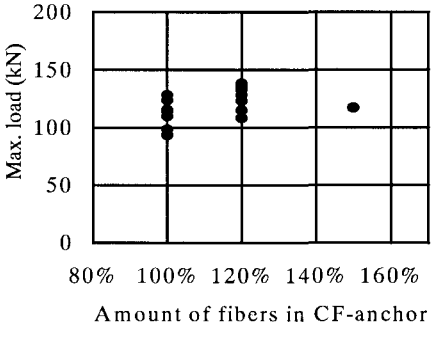



Fig.13 Effect of the amount of fibers in CF-anchor

Figure 11 shows an effect of the CF-anchor length on the maximum load. There is a tendency that specimens with 20cm of CF-anchor length show a larger maximum load. However, there is no difference of minimum value between the specimens with 15cm and those with 20cm. Once in-plane dislocation of CF-anchor from CF sheet starts from the fan tip, it will lead to the whole destruction and will determine the maximum load.
Figure 12 shows an effect of the amount of main CF sheet on the maximum load. The maximum load is approximately proportional to the amount of main CF sheet, even if it becomes the in-plane dislocation mode.
Figure 13 shows the effect on maximum load of the ratio of the amount of fibers in the CF-anchor to that in the main CF sheet. If the amount of fibers in CF-anchor increases, the maximum load has a tendency to increase regardless the failure mode.

## POSSIBLE APPLICATION TO VARIOUS MEMBERS

The CF-anchor system is a mechanism that collects the distributed tensile force on CF sheet into one place. This would be applicable to any case where the end of the CF sheet must be anchored. CF-anchor could be designed considering the capacity and the expected stress level on CF-sheet. Beams with slab are also possible targets.
Also there is a demand to strengthen shear walls. In this case, CF sheet on the shear wall must be anchored in the frame to demonstrate its strength. CF-anchor would be easily installed and the straight portion of CF-anchor should be anchored in beams and columns. Experimental verification of this anchoring performance is underway.

## CONCLUSIONS

(1) The capacity of the key portion of CF-anchor is increased if the ratio of the amount of fibers in the CF-anchor to those in main CF sheet increases. In this study, CF strand with sizing agents of 0.2% was used for CF-anchor, and a significant improvement was recognized.
(2) For the in-plane dislocation mode, the increase in the capacity of CF-anchor is not always expected even if the CF-anchor length is increased. In this case, another detail would be needed.
(3) In order to collect the tensile force on the main CF sheet at the key portion of CF-anchor, a perpendicular CF sheet is absolutely required and works very effectively. In this study, when one half the amount of main CF sheet was placed in the perpendicular direction, the rupture of a perpendicular CF sheet did not determine the capacity of the CF-anchor system.
(4) A capacity of at least 50kN per one CF-anchor could be expected under the following standard specification of CF-anchor system.
    CF-anchor length is more than 15cm.
    The interval of CF-anchors is less than 20cm.
    The amount of fibers in CF-anchor is more than that in main CF sheet.
    More than one half the amount of main CF sheet is constructed in perpendicular direction under the fan shaped portion of CF-anchor.
    The capacity would increase in proportion to the amount of main CF sheets

To determine the stress transfer capability of the CF-anchor system, the following three failure modes are considered:
(a) Rupture of main CF Sheet by stress concentration to the center
(b) Rupture of the key portion of CF-Anchor
(c) In-plane dislocation of the fan shaped portion of CF-anchor from a main CF sheet due to bond resistance limit.

Although the stress transfer capability of CF-anchor is influenced by a cracking pattern, the problem of (a) and (b) would be resolved by construction of perpendicular CF sheet, an improvement of CF strand used for CF-anchor, a specification for the suitable amount of fibers in CF-anchor, etc. It would be possible to increase the capacity of CF-anchor system.
It is difficult to resolve the problem of (c). If this problem is caused by the bond resistance limit, we would need to increase the bonding area. When more than two layers of CF sheet are constructed, one idea would be to insert the fan shaped portion of CF-anchor into the CF sheet layers. Another idea would be to extend the CF-anchor length so that it could catch the corner of the column.

## REFERENCES

[1] Katsumata, K., Kobayashi, K., Morita, S. and Matsuzaki, Y. (1999), "Japanese State of the art on seismic retrofit by fiber wrapping for building structures: Technologies and research and development activities", *Proceedings of the fourth International Symposium on Fiber Reinforced Polymer Reinforcement for Reinforced Concrete Structures,* ACI, SP-188, pp.865-878
[2] Matsuzaki, Y., Nakano, K., Fujii, S. and Fukuyama, H. (1999), "Japanese State of the art on seismic retrofit by fiber wrapping for building structures: Research", *Proceedings of the fourth International Symposium on Fiber Reinforced Polymer Reinforcement for Reinforced Concrete Structures,* ACI, SP-188, pp.879-893
[3] Fujii, S., Matsuzaki, Y., Nakano, K. and Fukuyama, H. (1999), "Japanese State of the art on seismic retrofit by fiber wrapping for building structures: Evaluations", *Proceedings of the fourth International Symposium on Fiber Reinforced Polymer Reinforcement for Reinforced Concrete Structures,* ACI, SP-188, pp.895-906

# Rapid Flexural Strengthening of RC beams using Powder Actuated Fasteners and FRP strips

ANTHONY J.LAMANNA, University of Wisconsin, Madison, WI, USA
LAWRENCE C. BANK, University of Wisconsin, Madison, WI, USA
DAVID W. SCOTT, Georgia Tech Regional Engineering Program, Savannah, GA, USA

## ABSTRACT
The current method of bonding FRP strengthening strips to concrete structures requires extensive time and skilled labor. An alternative method is to use a commercial off-the-shelf powder actuated fastening system to attach composite strips to concrete. Such tools are readily available, do not require sophisticated training to operate, and are inexpensive. Such a technique could meet requirements for rapid strengthening in situations where time is critical. This paper presents an overview of this novel procedure for rapidly strengthening reinforced concrete beams. Selected results from small scale and large scale tests are presented to demonstrate the potential of the proposed method.

## INTRODUCTION
A technology to rapidly strengthen and repair bridges for both military and civilian uses is needed. In a military environment this technology is needed to rapidly strengthen concrete bridges that are damaged or become unserviceable due to low load ratings, and consequently adversely impact the military's operational mission. In the civilian sector there exists an equal need to rapidly strengthen and repair highway bridges, as it is undesirable to close down a bridge for any length of time.

A method of repairing reinforced concrete beams by attaching FRP strengthening strips to the bottom surface using powder actuated fasteners has been developed. This method has the potential to be a rapid procedure that utilizes simple hand tools, light-weight materials, and unskilled labor. Unlike the conventional method of adhesively bonding FRP strips to the concrete surface, this method does not require significant surface preparation, and allows for immediate use of the strengthened structure.

A popular current method used to strengthen reinforced concrete beams is to adhesively bond strips of thin composite laminates, also known as fiber reinforced polymer (FRP) strengthening strips, to the surfaces of these beams to increase their capacity. Typically these strips are attached to the soffits to increase the flexural capacity of the reinforced concrete element. This method is time-consuming since it can take days per application to sand blast, clean, and smooth the concrete to make it suitable for bonding the strip. Following the application of the adhesive, the FRP strengthening strip "must not be disturbed for a minimum of 24 hours" according to one supplier of strengthening strips (SIKA 1999).

*FRPRCS-5*, Thomas Telford, London, 2001.

A number of authors have recommended that to prevent a catastrophic brittle failure of the strengthened beam by strip detachment, mechanical anchorage should be provided at the strip ends (Spadea et al. 1988, Garden and Hollaway 1998). Plate end anchorages have a greater effect in beams that are shorter, with a high ratio of shear force to bending moment, than in longer beams. Anchorage is usually provided by anchor bolts or cover plates. Similar anchorages have been recommended for use with epoxy-bonded steel plates (Hussain et al. 1995). In addition to being rapid and easy to use the proposed method provides the necessary anchoring mechanism as part of the procedure. The use of multiple small fasteners as opposed to large diameter bolts distributes the load more evenly over the strip and reduces stress concentrations at the holes in the strip which can lead to premature failure.

## BACKGROUND

A powder actuated fastening system drives a fastener into a concrete substrate. As the fastener penetrates the concrete is compressed as material is displaced. When the fastener is driven into the concrete, the surface of the fastener becomes deformed and generates friction with the surrounding material. The heat generated in this process causes sintering and creates a bond between the concrete and fastener (CEB 1994). These two factors give the fastener its holding capacity.

To determine the load capacity per fastened-connection, tests were performed at the University of Wisconsin – Madison. In these tests, a piece of FRP composite material strengthening strip was attached to a concrete block with a powder actuated fastener. Testing was carried out on a variety of different types of fasteners and strips, and on fasteners driven into pre-drilled holes and on fasteners driven into concrete without predrilled holes. The capacity of the connection is a function of the depth of fastener embedment in the concrete, the bearing strength and edge distances of the strengthening strip, and the strength and aggregate properties of the concrete. Figure 1 shows the load capacity per fastened-connection test set-up.

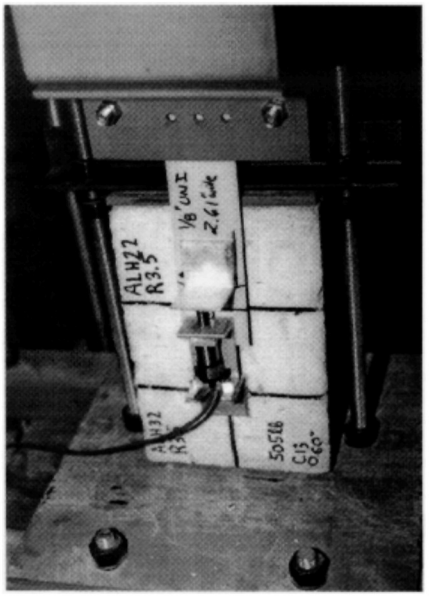



Figure 1: Load capacity per fastened-connection test set-up.

For the types of concrete, strengthening strips, and fasteners used in this study, the lower bound design capacity per fastened-connection was recommended as 2224 N (500 lb) for connections without a pre-drilled hole. A large amount of scatter was observed in these tests stemming from several failures in the concrete substrate at very low load. For connections with a pre-drilled hole, the lower bound design capacity was recommended as 4448 N (1000 lb). The pre-drilling greatly reduces the cratering that occurs in the surface of the concrete when the fastener first enters, and increases the capacity by eliminating the failures in the substrate at very low loads (Forrestal and Longcope 1982).

A preliminary investigation into the feasibility of this method of strengthening strip attachment was first conducted on 35 small scale reinforced concrete beams. The beams

measured 152 x 152 x 1219 mm (6 x 6 x 48 in.) and were tested on a span of 1067 mm (42 in.) with a moment span of 203 mm (8 in.). A variety of fasteners and fastener layouts were considered with a number of different strengthening strips, including steel. The strengthened small scale beams showed increases in yield and ultimate moments up to 36% and 30%, respectively, over the unstrengthened control beams (Lamanna et al. 2000).

The effect of increasing the scale of the proposed method was then investigated. The size of most components, the FRP strip, the concrete cross section, and the reinforcing steel, can all be increased; however, the fasteners are a fixed diameter and penetrate the same depth into the concrete regardless of the beam size. 15 large scale reinforced concrete beams were tested. The purpose of this testing was to examine the effect of different types of FRP strengthening strips, fasteners, and fastener layouts on large scale beams. Two beams strengthened by fastening and one by bonding strips are discussed here and compared to two control beams. Complete results will be discussed elsewhere.

## MATERIALS

The FRP composite material strengthening strips used were custom designed as part of this research and were pultruded by Strongwell (Chatfield Division). These "UW FRP" composite material strengthening strips contained carbon and glass fibers in a vinylester resin and are of a proprietary design. The target design modulus was 55.2 GPa (8,000 ksi). The strengthening strips were tested according to ASTM D3039, and the modulus and tensile strength were determined to be 59.4 ± 2.8 GPa (8,610 ± 400 ksi) and 862 ± 28 MPa (125 ± 4.0 ksi) based on ten tests. The strengthening strips had a cross section of 102 mm wide by 3.175 mm thick (4 in. by 0.125 in.) and were 3048 mm (120 in) long.

The large scale reinforced concrete beams were 3658 mm (144 in.) long and had a cross section of 305 mm by 305 mm (12 in. by 12 in.). They were cast at the US Army Engineering Research and Development Center in Vicksburg, Mississippi with concrete supplied by a local vendor. A pea gravel mix was used to facilitate casting. The measured concrete strength at 28 days was 32.7 MPa (4740 psi).

The beams were designed in accordance with ACI 318-99. Primary tension steel was provided by two #8 Grade 60 deformed bars. Two #3 Grade 60 deformed top bars were used in order to provide stability to the rebar cage during casting. Shear reinforcement was provided in the form of closed stirrups of #4 grade 60 deformed bars. These stirrups were placed at 102 mm (4 in.) on center throughout the shear span of the beam and into one-third of the moment span. Stirrup spacing was increased to 127 mm (5 in.) and then 152 mm (6 in.) in the center of the moment span. This stirrup spacing ensured that a shear failure in the strengthened beams would be avoided. Figure 2 shows the large scale beam dimensions and the location of the internal steel. The beam was tested on a 3353 mm (132 in.) total span, with each shear span and the moment span being 1118 mm (44 in.), so that the strengthening strip terminated 152 mm (6 in.) from the supports.

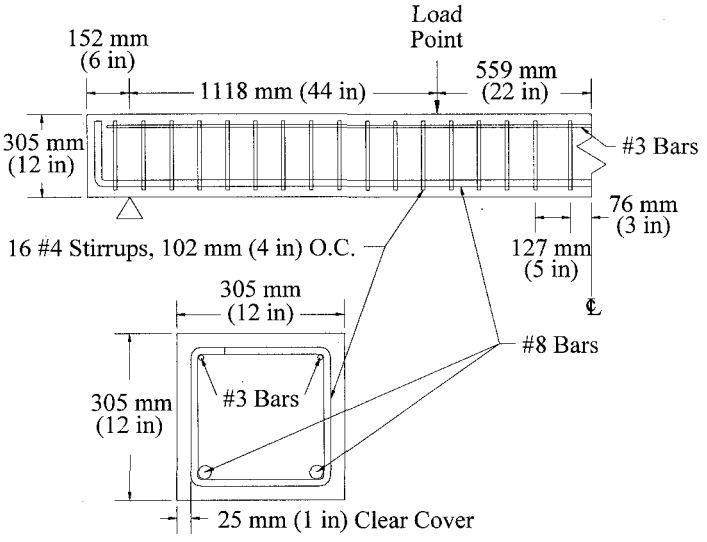



Figure 2: Large scale beam dimensions and internal reinforcement layout.

The fastening system used was a Hilti DX A41 Powder Actuated Fastening system. The DX A41 uses a 6.8 mm (0.27 in.) caliber short gunpowder booster. Purple boosters, signifying extra heavy charge, were used in conjunction with X-AL-H fasteners for attaching the strip. The X-AL-H fasteners are made of specially heat-treated high-strength steel that is zinc plated to resist corrosion. The fasteners used were the X-AL-H47, which were 47 mm (1.875 in.) long with a shank diameter of 4.5 mm (0.177 in.). Pre-drilling was done with a DX-Kwik bit, which had a diameter of 4.76 mm (0.188 in) and a drill bit length of 15.88 mm (0.625 in.). A standard hammer drill was used with this special bit.

Beams 1 and 2 were tested without strengthening as control beams. Beam 3 was prepared by sand blasting the bottom surface, then flushing it with water. The UW FRP strengthening strip was sanded with 400 grit sandpaper, then cleaned with acetone. After the beam was allowed to dry out, Sikadur Hex 300 two part epoxy resin was thickened with fumed silica and applied to the sand blasted surface and to the UW strip. The strip was then aligned and placed on the beam, and 7.3 N/cm (50 lb/ft) of weights were applied to the strip. The beam was covered in black plastic and left to cure in the sun for five days before testing. The UW strip was attached to beam 4 using two rows of fasteners that were 51 mm (2 in.) apart, and a spacing of 51 mm (2 in.) along the length of the beam. Attachment for beam 5 used two rows of fasteners 51 mm (2 in.) apart with a spacing of 76 mm (3 in.) along the length of the beam.

## ATTACHMENT PROCEDURE

The reinforced concrete beam was turned over, so that the tensile steel was facing upwards. The fastener locations were marked on the strengthening strip. The UW FRP strengthening strip was centered with the concrete beam from side-to-side and end-to-end and held in place at each end. At the center of the beam, two shallow pilot holes were drilled in a line perpendicular to the length of the beam. These holes were drilled through the 3.175 mm

(0.125 in.) thick strengthening strip so that they extended approximately 12.7 mm (0.5 in.) into the concrete. The two holes were drilled in approximately ten seconds.

Then the fasteners were inserted into the Hilti DX A41 tool, lined up with the holes, and driven into the concrete. The fasteners were drilled and driven by twos continuing to one end of the beam, and from the center to the other end of the beam. Very little spalling was observed, and the complete attachment of the UW FRP strengthening strip took about approximately 30 minutes. The beam was then turned back over, so that the tensile steel was on the bottom, taking care not to damage the attached strip or fasteners, and placed on the supports.

## TESTING

A lightweight aluminum frame was attached to the beam at half of the depth at the supports. Small plexiglass blocks were attached to the sides of the beam at half of the depth at the midspan with a two part epoxy. Two LVDTs were attached to the aluminum frame to read the deflection of the beam on both sides. The frame and LVDTs are shown in Figure 3. Micro Measurements strain gages CAE-06-250UW-350 were attached to the composite strip at midspan and one fastener spacing on either side of the midspan, and a gage WK-06-20CBW-350 was mounted on the top of the beam at midpan. An MTS Testar system was used to control the 490 kN (110 kip) hydraulic actuator. An Optim Megadac was used for data collection.

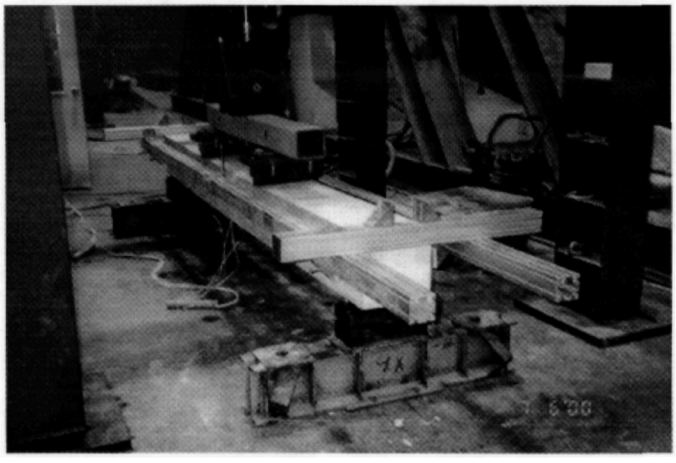


Figure 3: LVDT support frame shown in place on a large scale beam.

The beams were placed directly on the supports, and thin wood strips, similar to those used in split tensile tests, were placed under the load points. The beams were loaded at the rate of 1.3 mm/min (0.05 in./min) to an actuator displacement of 25 mm (1 in.), and then at a rate of 2.5 mm/min (0.1 in./min) to failure.

## DISCUSSION

Beams 4 and 5 showed an increased stiffness in the elastic range over the control beams 1 and 2 but less than that of beam 3. In beams 4 and 5 the concrete reached compression failure in the moment span while the FRP strengthening strip was still attached, resulting in the same

amount of strengthening as the bonded beam 3, at a much greater ductility. At concrete compression failure, the strip remained attached and was difficult to remove with a crowbar after the test.

Control beams 1 and 2 had yield moments of 122.3 kN-m (1082 k-in) and ultimate moments of 136.4 kN-m (1207 k-in). Beam 1 failed at a midspan deflection of about 53 mm (2.1 in.) while beam 2 failed at a deflection of 64 mm (2.5 in.), making the average failure deflection 58 mm (2.3 in.).

Beam 3 yielded at 148.0 kN-m (1310 k-in), a 21% increase over the yield moment of the control beams. This beam showed an increased stiffness in the elastic range, and a secondary stiffness post yield before it failed without warning in a sudden manner, by failure of the adhesive layer. This failure mechanism is described in detail by Buyukozturk and Hearing (1998). Failure occurred at an ultimate moment of 163.1 kN-m (1444 k-in), a 20% increase over the control beams. It is important to note that the beam failed at a midspan deflection of 36 mm (1.4 in.), showing much less ductility, or deflection capacity, than the control beams.

Beams 4 and 5 both yielded at 139.1 kN-m (1231 k-in), a 14% increase over the control beams. These beams showed an increased stiffness in the elastic range, but not as much as beam 3. The strip remained attached in both tests through concrete failure at ultimate strength. The ultimate moments of beams 4 and 5 were 163.8 kN-m (1450 k-in) and 159.4 kN-m (1411 k-in), increases of 20% and 17% over the control beams. These beams failed at a midspan deflection of 58 mm (2.3 in.), the average failure deflection of the two control beams. Figure 4 is a close up of the failure in the mechanical connection between the FRP strengthening strip and the concrete surface that occurs when the test is taken well beyond the ultimate moment.

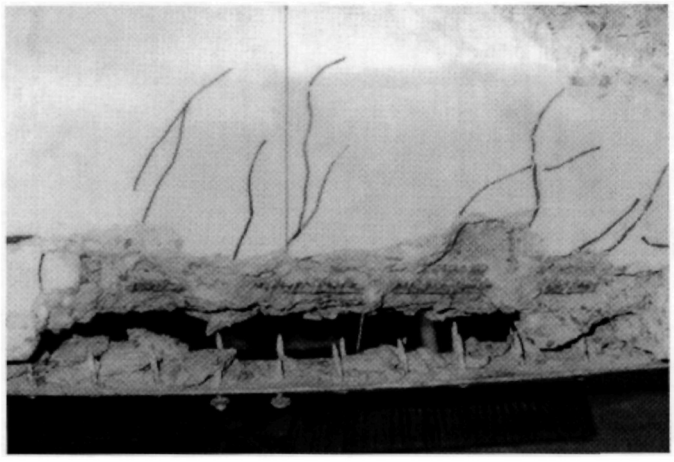


Figure 4: Close up of failure in mechanical fastenings in beam 4 well beyond ultimate moment.

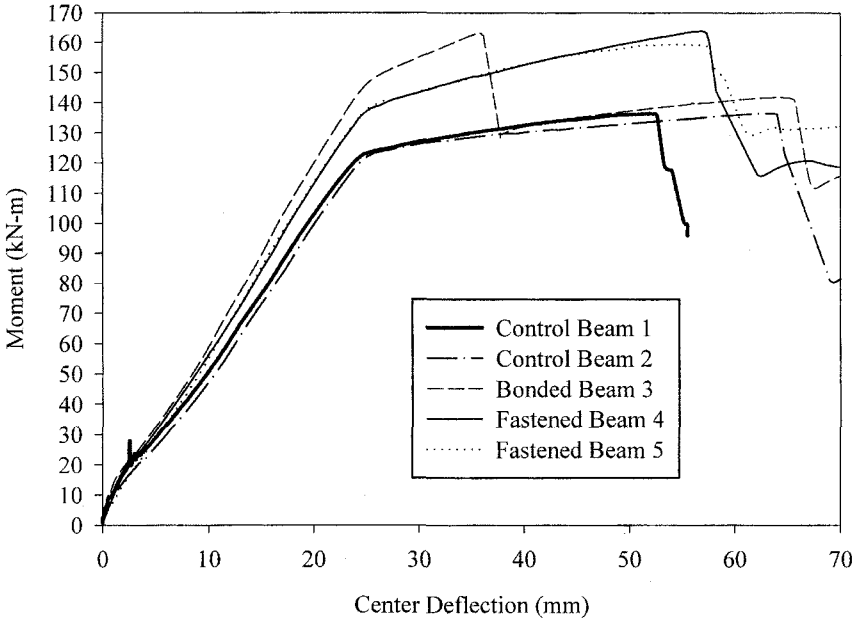



Figure 5: Moment-deflection curves for control beams 1 and 2, beam 3 strengthened using the conventional adhesively bonded method, and beams 4 and 5 strengthened using the powder actuated fastening method.

Figure 5 shows the moment-deflection curves of beams 1, 2, 3, 4, and 5. The moment-deflection behavior of beams 4 and 5 were identical up until within 3% of failure. Beams 4 and 5 have a post yield stiffness greater than the control beams, but much less than beam 3. This is likely due to slip between the strip and the concrete surface, caused by a combination of micro cracking in the concrete substrate and initiation of bearing failure in the FRP strengthening strip around the fasteners.

The midspan FRP strengthening strip strain was measured on beams 4 and 5 using three strain gages and taking the average value. The stress in the strip was then calculated using the strip modulus and measured strain. The load in the strip was calculated using the strip area. This is the load carried in the FRP strengthening strip in the center of the span, which is constant throughout the moment span.

Table 1 shows the midspan strain, stress, and load in the FRP strengthening strips for beams 4 and 5 at failure. The number of fasteners and number of fasteners per shear span are also given in table 1. Given the close spacing of the fasteners, it is appropriate to make the assumption that the load is equally distributed over all fasteners in the shear span. Thus the load per fastener can be calculated by dividing the load by the number of fasteners in the

shear span. The load per fastener for beam 4, with a 2 inch spacing was 3703 N (834 lbs) and the load per fastener for beam 5, with a 3 inch fastener spacing, was 4830 (1097 lbs). The fasteners in beam 5 were at a load level above the 4448 N (1000 lb) maximum design capacity determined previously by small testing of fastened-connections. This could explain the loss of strengthening at very high load levels close to failure.

Table 1: Beam 4 and 5 strip stress states and fastener information at failure.

| Beam | Midspan Strip Strain | Midspan Strip Stress | Strip Load in Midspan | No. of Fasteners | No. of Fasteners Per Shear Span | Load Per Fastener |
|---|---|---|---|---|---|---|
| | με | MPa (ksi) | kN (kips) | | | N (lb) |
| 4 | 7,740 | 459.8 (66.7) | 459.8 (25.4) | 124 | 40 | 3,707 (834) |
| 5 | 7,129 | 423.4 (61.4) | 423.4 (30.7) | 84 | 28 | 4,830 (1097) |

## CONCLUSION

A series of tests on large scale reinforced concrete beams strengthened with powder actuated fasteners and FRP strengthening strips has shown that with the correct fastener layout and strip properties, strengthening capacity equal to that of beams strengthened by bonding the strip to the beam can be achieved. The strengthening capacity of the two fastener layouts described in this paper is the same as the strengthening capacity of the traditional bonded method; however, the proposed method provides an added benefit of added ductility. Since micro cracking in the concrete begins and bearing failure is initiated in the strip around the fasteners, the system fails progressively in a pseudo ductile matter.

It appears that attaching FRP strengthening strips to reinforced concrete beams with powder actuated fasteners is as effective as the traditional method of bonding the strips to the beams and takes much less time, which makes it a viable option for instances where speed of installation is a major factor.

An analytical model is being developed to accurately predict the strengthening effect of FRP strips attached with mechanical fasteners. Slip between the strip and the concrete is being considered, which will allow the model to predict the reduction in strengthening as the individual connections reach their maximum capacity. Fatigue testing will be conducted to determine the effect of cyclic loading on reinforced concrete beams strengthened using this method.

## ACKNOWLEDGEMENTS

Support for this research was provided by the US Army Engineering Research and Development Center under grant #DACA42-00-P-0044. The authors would like to express their thanks to Gerardo Velazquez, James Ray, Dan Wilson, Cliff Gill, and Mike Hedrick at ERDC. The authors would also like to thank Dennis McMonigal at Strongwell (Chatfield Division) and Nicholas Holterman at the University of Wisconsin – Madison.

**REFERENCES**

Buyukozturk, O., and Hearing, B., "Failure Behavior of Precracked Concrete Beams Retrofitted with FRP," ASCE Journal of Composites for Construction, Vol. 2, No. 3, pp. 138-144, 1998.

Comite Euro-International du Beton (CEB), *Fastenings to Concrete and Masonry Structures*, Thomas Telford Services Ltd., London, England, 1994.

Forrestal M. J., and Longcope, D. B., "Closed-Form Solutions for Forces on Conical-Nosed Penetrators into Geological Targets with Constant Shear Strength," *Mechanics of Materials*, Vol. 1, No. 4, pp. 285-295, 1982.

Garden H. N., and Hollaway, L. C., "An Experimental Study of the Influence of Plate End Anchorage of Carbon Fibre Composite Plates Used to Strengthen Reinforced Concrete Beams," *Composite Structures*, Vol. 42, pp. 175-188, 1998.

Hussain, M., Sharif, A., Basunbul, I. A., Baluch, M. H., and Al-Sulaimani, G. J., "Flexural Behavior of Precracked Concrete Beams Strengthened Externally by Steel Plates," ACI Structural Journal, Vol. 92, No. 1, pp. 14-22, 1995.

Lamanna, A. J., Bank, L. C., and Scott, D. W., "Flexural Strengthening of RC Beams Using Fasteners and FRP Strips," submitted to *ACI Structures Journal* in June 2000.

SIKA Corporation, *Sika Carbodur Structural Strengthening System – Engineering Guidelines for Design and Application*, Sika Corporation, 1999.

Spadea, G., Bencardino, F., and Swamy, R. N., "Structural Behavior of Composite RC Beams with Externally Bonded CFRP," ASCE Journal of Composites for Construction, Vol. 2, No. 3, pp. 59-68, 1998.

# Bond Analysis of Curved Structural Concrete Elements Strengthened using FRP Materials

M.A. AIELLO, N. GALATI and A. LA TEGOLA
Department of Innovation Engineering, University of Lecce, Italy

## ABSTRACT

Repair and strengthening of reinforced concrete structures is becoming a very important topic in the field of the Civil Engineering because of the occurrence of concrete elements deterioration strictly linked to the durability of materials or the increase of the required performances for many structures.

On the other hand the success of FRP (Fibre Reinforced Plastic) in structural applications makes such materials very promising candidates for retrofitting concrete elements utilizing new techniques. In fact, composite materials are characterised from many advantageous properties with respect to traditional materials as steel, in particular the low weight, the good mechanical performances, the absence of corrosion that improves the durability of concrete structures reducing the maintenance costs.

As known the effectiveness of the repair technique depends, in more extend, on the bond between composites and concrete that influence the static behaviour of structural elements both under service and/or ultimate conditions. With reference to curved structural elements, as arches, in the paper an analysis of the bond performance between composite FRP sheets and concrete is carried out. The presence of curvature makes necessary the evaluation of bond-slip laws that take into account the presence of normal stresses besides that of shear stresses. Therefore the influence of the curvature both in terms of bond-slip laws and mechanisms of crisis is investigated.

## INTRODUCTION

The use of Fibre Reinforced Plastic (FRP) for repair and/or retrofitting concrete and masonry structures is becoming a successfully technique. In fact, composite materials are widely utilized as flexural and shear strengthening of concrete beams, to increase ductility and strength of masonry and concrete columns by FRP wrapping, mostly in seismic areas, for shear retrofitting of masonry panels, to strengthen curved structural elements, as vaults or arches. The increasing applications of such new materials world-wide are due to their well-known advantages with respect to more traditional techniques: the high strength and stiffness to weight ratio, the design flexibility on the basis of specific requirements, the easy application and the absence of electrochemical corrosion. In all cases the effectiveness of the repairing technique is strictly depending on the bond between the FRP reinforcement and the substrate.

*FRPRCS-5*, Thomas Telford, London, 2001.

As known the bond performance affects all aspects of the structural behaviour and in particular the serviceability conditions as well as the ultimate conditions. In fact, cracking and deformations are influenced from bond laws; in addition structural elements may undergo a premature collapse because of the crisis at the interface reinforcement-substrate. For these reasons many studies, theoretical and experimental, have been carried out to analyse the bond behaviour between reinforcement and substrate (1), (2), (3), (4), (5), (6), (7), (8). With reference to plates or sheets, mainly utilized in the field of repair and upgrade, interesting results have been found and some theoretical models have been proposed in order to provide useful design guidelines.

On the other hand few studies have been performed referring to the bond behaviour when curved structural elements are strengthened with FRP plates or sheets; however the need of repairing and upgrading curved elements is at present increasing because of arches are structural elements typically encountered in bridges and historical and/or artistic buildings. The bond behavior in this case can be more critical; in fact, the presence of the curvature causes radial stresses that combined with shear stresses at the interface may cause, in same cases, a reduction of the bond strength increasing the probability of a premature collapse of local type at the interface.

In the present paper the interface performance of curved structures strengthened with FRP sheets is analysed. Some considerations have been made on this topic with reference to masonry arches or vaults (9); however further theoretical and experimental researches are requested in order to assess theoretical models able to take into account the influence of the bond mechanism at the interface on the static behaviour of curved elements.

At this aim an experimental investigation, still in progress, has been planned in order to analyse the transfer mechanism of stresses at the interface and the bond strength between reinforcement and concrete. Obtained results are reported and discussed; specimens without curvature have been also tested for comparison.

Finally a theoretical analysis is performed to analyse the effectiveness of models, utilized in the case of straight elements, for curved structures and to evaluate the ultimate condition, corresponding to the reinforcement debonding, taking into account the influence of the curvature.

## EXPERIMENTAL INVESTIGATION

In order to analyse the bond behaviour between curved concrete elements and FRP sheets, glued at the intrados and/or at the extrados for repairing and/or upgrading structural arches, an experimental investigation has been carried out on three groups of beams characterized from different curvature values. Geometrical details of tested specimens are reported in Tab. 1 and Fig. 1. Carbon Fiber Sheets (CFS) have been utilized as reinforcement, bonded for 200 mm length and 50 mm width. Tensile strength and elastic modulus values of the reinforcement are 3400 MPa and 275 GPa respectively. The sheets have been glued at the intrados of the specimens corresponding to the curved piece of the beam. In addition CFS have been wrapped in correspondence of the straight part of the specimens in order to avoid the crisis in that zone.

Standard compression test have been made to determine the compression strength of the concrete, the corresponding mean value is 30.22 MPa. The bond test performed is a modified

RILEM bond-test; beams have been precracked in correspondence of the hinge, the scheme of the test apparatus is reported in Fig. 2.

Table 1. Tested Specimens

| Specimen | Width (mm) | Height (mm) | Curvature radius (mm) |
|---|---|---|---|
| A1–50, A2-50, A3-50 | 200 | 250 | 500 |
| A1 – 100, A2-100, A3-100 | 200 | 250 | 1000 |
| A1– 00, A2-00 | 200 | 300 | ∞ |

Strain gages have been glued on the reinforcement to measure the strain values and the strain path along the sheets. The uniformity of the strain distribution in the transverse direction has also been checked by strain gages glued along the width of the reinforcement at fixed positions. Details of strain gages positions are reported in Fig. 3.

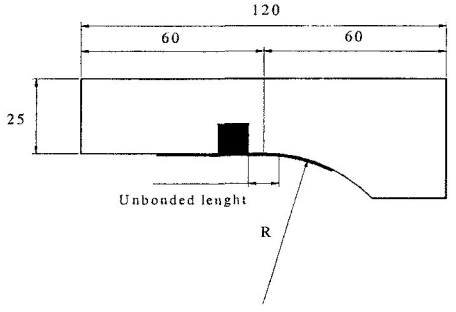



Figure 1.Geometrical details of specimens

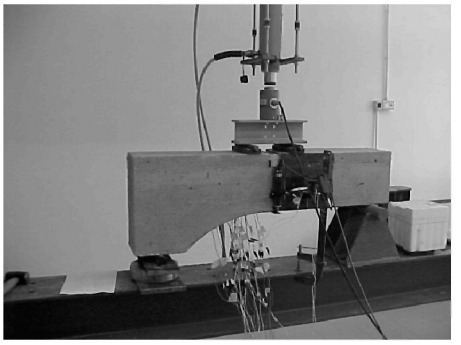
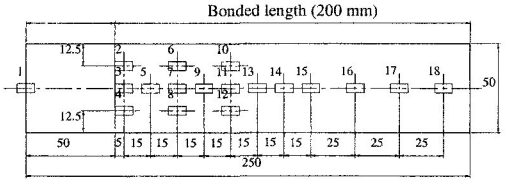
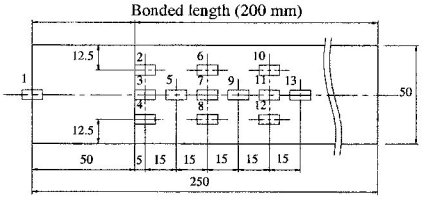


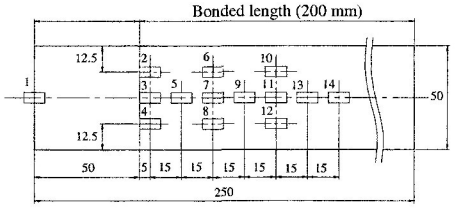
Fig.2. Test apparatus



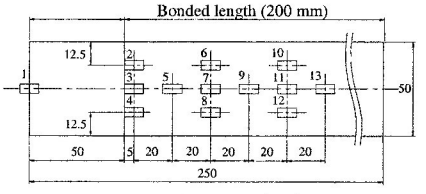

A1-100, A1-50




A2-50, A3-100, A3-50




A2-100




A1-00, A2-00

Fig. 3. Strain gages position

In the Figs. 4a÷4e the strains distributions along the sheets for some of the tested specimens are drawn. An interesting result can be observed analysing the figures; in fact the strains distribution referred to straight specimens is very different from that of the curved specimens. In particular, for straight beams the path of strains is almost exponential at low load level

while when load increases the peak of the strain shifts along the reinforcement till an almost uniform trend is recorded at high load level. Such an occurrence point out as the stresses transfer at low load level takes place within a very short length of the sheet while the reinforcement length involved increases with the load. On the other hand, for curved beams, the transfer mechanism of stresses is localised near the loaded end of the reinforcement up to the crisis of the interface; as one can see, from reported curves, the exponential trend is evidenced almost at any load level. Therefore the presence of radial stresses reduces the ultimate load, attained before the transfer mechanism could shift along the FRP sheet.

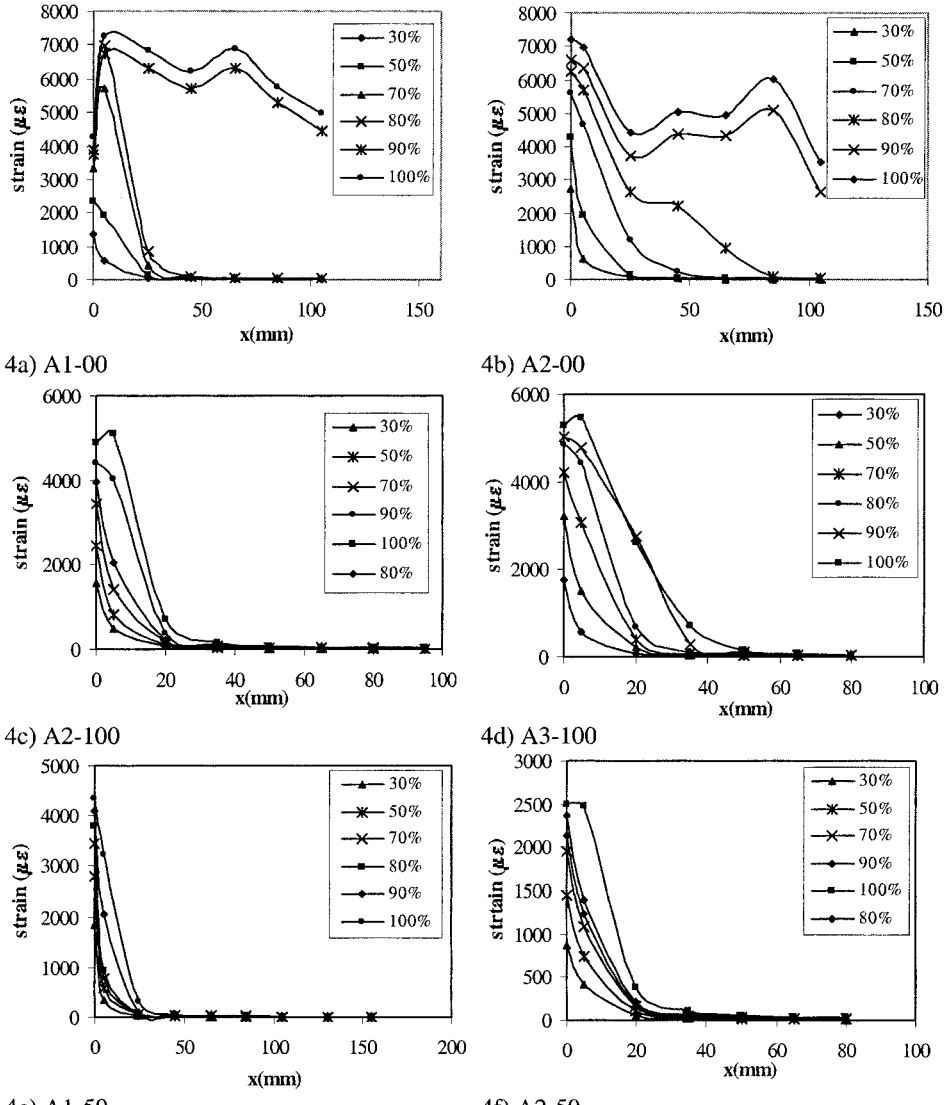
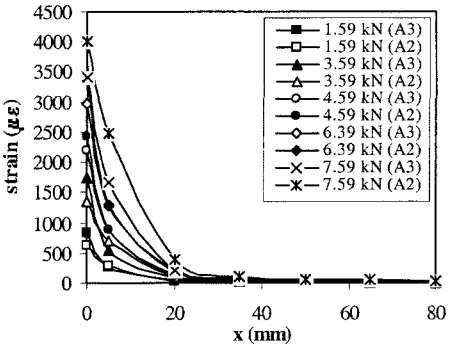


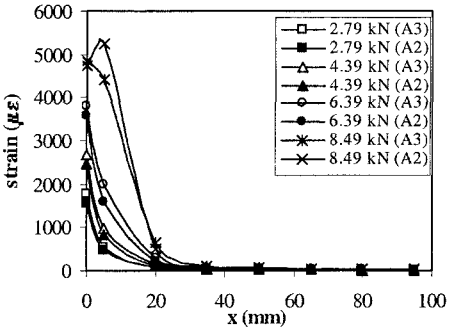

Fig. 4. Distribution of strains along the reinforcement at different load level: (30%, 50%, 70%, 80%, 90%, 100%) $F_u$

In the Figs. 5a÷5b comparisons between the strain distributions of similar tested specimens are reported; it can be evidenced as results for specimens with the same radius of curvature present very small scatter; only for high load level, approaching the ultimate load, some differences arise due to the beginning of the debonding phenomenon.

In the Figs. 6a÷6b load values are reported as function of the strain distribution in the transverse direction of the sheet. Results refer to specimens A2-00 and A2-100 even if similar trend have been recorded for the others. As one can see the strain distribution is almost uniform within the width of the sheet. Some differences between measured strains arise when the load increases and mostly at the transverse positions were the sheets debonding starts.




5a) A2-50, A3-50




5b) A2-100, A3-100

Fig 5. Comparisons between strain distribution of similar specimens

On the basis of measured strains and imposing equilibrium conditions the shear stresses and the radial stresses have been evaluated along the FRP sheets as follows:

$$\tau = \frac{E_r(\varepsilon_i - \varepsilon_{i+1})\cdot t_r}{x_i - x_{i+1}}; \quad \sigma_{ri} = \frac{\sigma_{li}}{R} t_r \tag{1}$$

where:

$E_r$ =elastic modulus of the reinforcement (MPa);

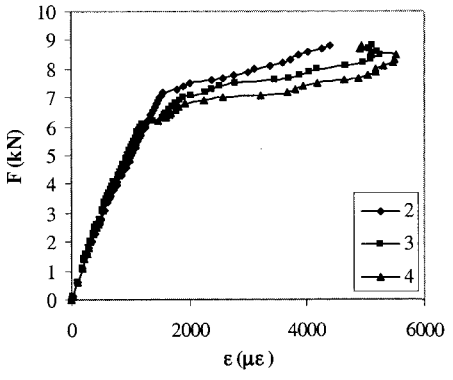
$t_r$ = thickness of the reinforcement(mm);

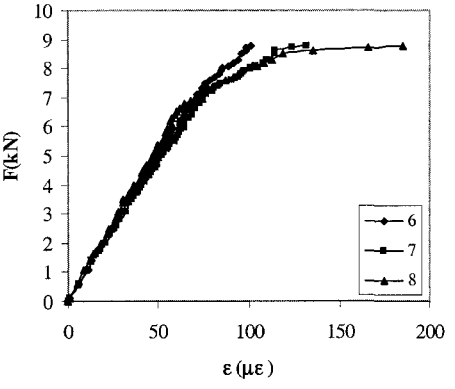
$x_i$, $x_{i+1}$= position along the sheet where the strain $\varepsilon_i$ and $\varepsilon_{i+1}$ are recorded (mm);

R=curvature radius (mm);

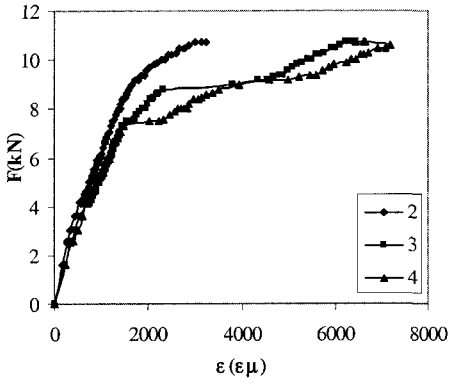
$\sigma_{li}$=normal stress at the position $x_i$ (MPa)

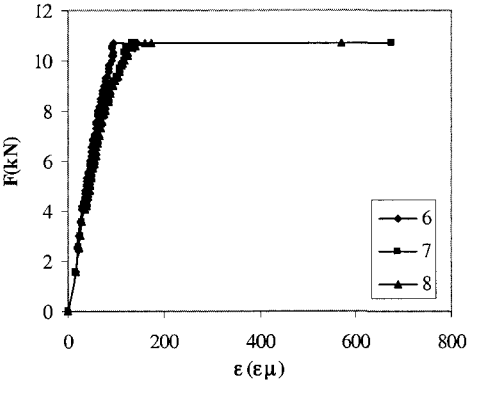
In the Figs. 7a÷7b the shear stresses distribution within the reinforcement is drawn for specimens A3-100 and A2-50. The curves confirm as an increase of curvature causes a reduction of the maximum shear stress and an almost exponential trend up to the debonding of the sheet. Such result is further evidenced in the Fig. 8, where curves $\tau_{max}$-s are reported, being *s* the slip determined integrating the measured strains along the sheet and $\tau_{max}$ the shear stress value at the loaded end of the specimens.



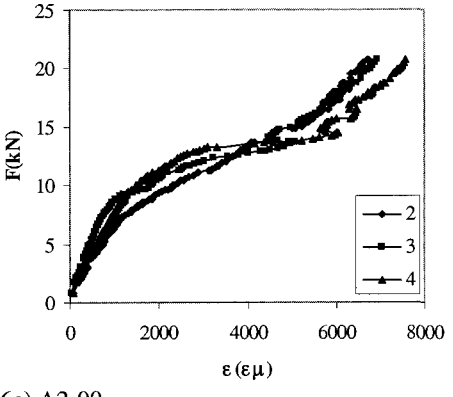



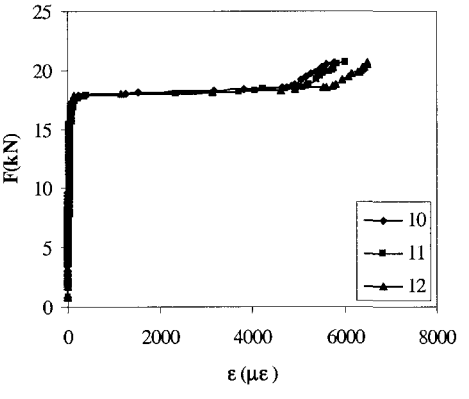

6a) A2-100



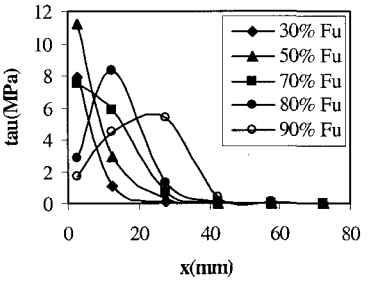

6b) A3-50

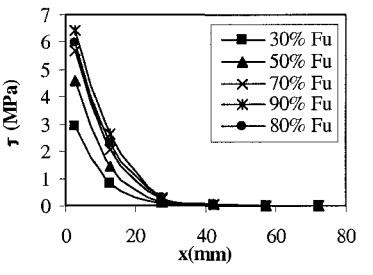



6c) A2-00

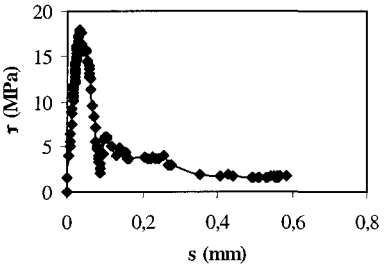
Fig. 6. Transverse strain distribution

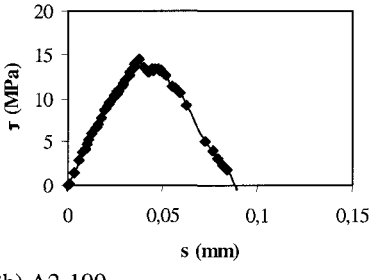


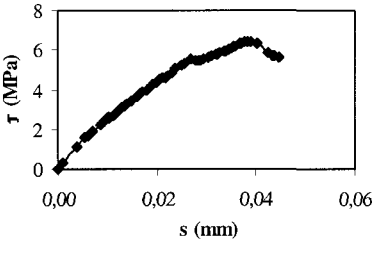

7a) A3-100 7b) A2-50

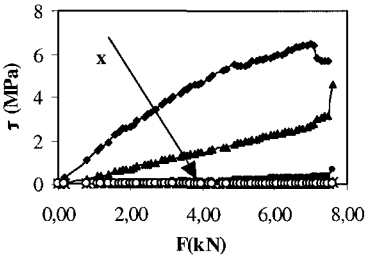
Fig.7. Shear stress distribution along the sheet




8a) A2-00 8b) A2-100




8c) A2-50 8d) A2-50

Fig.8a)÷8c). τ-s curves. Fig 8d). F-τ curves increasing x

Figs. 8a÷8c evidence as increasing the curvature the maximum shear stress decreases. In addition for straight specimens the curve τ-s is characterized from an ascending and a descending branch up to the debonding of the sheet corresponding to high slip values, while when curvature increases the debonding of the sheet takes place at low slip value, being almost absent the descending branch of the τ-s law when curvature increases. Finally in the Fig. 8d) one can observe as the transfer mechanism of the shear stress is limited to a very short length of the sheet, in fact the shear stress is very small for x>30÷40 mm.

## THEORETICAL ANALYSIS

Considering following hypotheses:

- Linear elastic behaviour of materials
- Flexural stiffness of sheets negligible

the theoretical distributions of strains, normal stresses and shear stresses can be evaluated by simple theoretical models referring to service conditions. Imposing the translational equilibrium of the sheet one obtain:

$\frac{dT}{dx} = -\tau \cdot b$, while the relationship between slip and shear stress is: $\tau = G_a \gamma$,

being :

T= axial force acting at the sheet (N)

b=sheet width (mm)

$G_a$=shear modulus of the adhesive (MPa)

γ=shear strain of the adhesive

Imposing the compatibility condition between the sheet, the concrete and the adhesive the following expression can be obtained:

$$\tau = \frac{G_a}{t_a}(u_c - u_r) \tag{2}$$

where $u_c$ and $u_r$ are the reinforcement and concrete displacements (mm) respectively.

Therefore utilizing the relation between the axial force and the normal strain:

$$\varepsilon_r = -\frac{N}{(EA)_r} \tag{3}$$

the solution can be found by solving the differential equation:

$$\frac{d^2\tau}{dx^2} + \lambda^2 \tau = 0 \tag{4}$$

where:

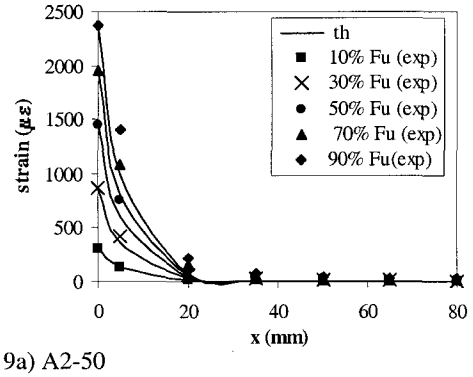
$$\lambda = \sqrt{\frac{G_a}{t_a}\frac{b}{(EA)_r}} \tag{5}$$

Finally the shear stress and the strain distributions are given by:

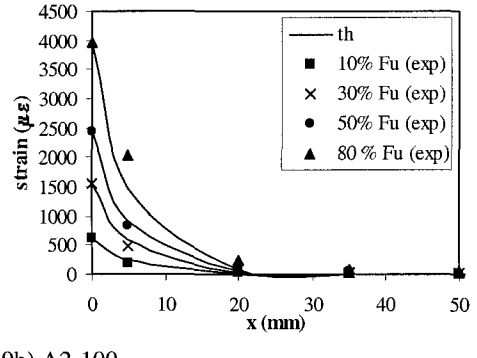
$$\tau(x) = \lambda L \tau_m e^{-\lambda x} \tag{6}$$

$$\varepsilon(x) = \frac{t_a}{G_a}\frac{d\tau(x)}{dx} = \varepsilon_0 e^{-\lambda x} \tag{7}$$

In the Figs. 9a÷9b a comparison between theoretical and experimental strains distribution is reported for two tested specimens. Comparing theoretical curves and experimental points it can be observed as the scatters are very small for low load level, corresponding to service condition, while some differences arise when the load increases, because of the considered hypotheses become not correct when the load approaches the ultimate value.




9a) A2-50




9b) A2-100

Fig. 9. Comparison between experimental and theoretical strains

At the ultimate condition the maximum load, corresponding to the debonding of the CFS, is greatly influenced from the presence of the curvature as it is evidenced in the Fig. 10, where the ultimate value corresponding to the force, T, acting at the CFS is reported versus the curvature values of the specimens. The ultimate load in the Fig. 10 is obtained averaging the ultimate load of tested specimens, while $T=F_u/(2\ l_1\ h^*)$, being $l_1$ the distance between the support and the position of the applied load and h* the distance between the centroid of the compression stresses and that of the tensile stresses.

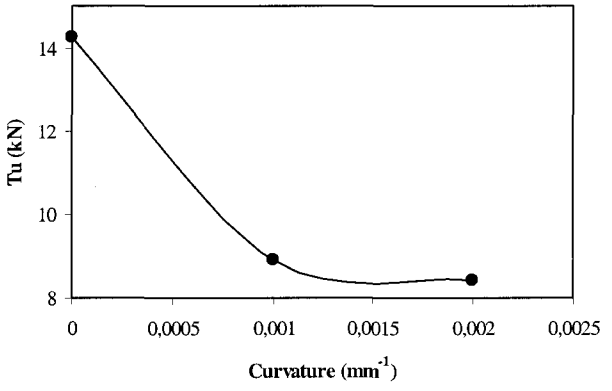



Fig.10. Ultimate tensile load versus curvature value

On the basis of the obtained results, it is suggested to define an interaction law between radial stresses and shear stresses at the ultimate condition. The proposed relationship could be expressed as:

$$\left(\frac{\sigma_r}{f_r}\right)^{k_1}+\left(\frac{\tau}{\tau_r}\right)^{k_2}\le 1 \qquad (8)$$

where:
$f_r$=pull-off strength (MPa)
$\tau_r$= bond strength (MPa)
$\sigma_r$, $\tau$ = radial stress and shear stress at the collapse (MPa).
$k_1$ , $k_2$ = parameters to be experimentally calibrated
Once the pull-off strength and the bond strength are known, the proposed law would allow to evaluate the combination of radial and shear stress causing the crisis of the interface.

## CONCLUSIONS

In the paper results of an on going experimental analysis on bond between curved concrete elements and FRP sheets are reported and discussed. In particular the following remarks can be drawn:

- The presence of the curvature involves a reduction of the ultimate load value corresponding to the debonding of the sheet from the substrate.

- The occurrence of radial stresses at the interface of curved elements influences the mechanism transfer of stresses. In fact increasing the curvature the bonded length of the sheet, involved in the transfer mechanism reduces, because of the crisis occurs before a shift of the transfer mechanism takes place.

- Theoretical models, available in the literature, are effective to predict the strain distributions along the reinforcement at the service stage.

- A theoretical relationship between shear stress and radial stresses at the ultimate conditions is proposed. However further experimental and theoretical investigations are needed to calibrate parameters involved aiming to carry out reliable theoretical models.

## REFERENCES

1. Bizindavy, L., and Neale, K. W. (1999), "Transfer Length and Bond strength for Composites bonded to Concrete". Journal of Composites for Construction, Vol. 3, No. 4, 153-160.
2. Brosens, K., and Van Gemert, D. (1997), " Anchoring stresses between concrete and carbon fibre reinforced laminates". *Proc., Third Int. Symposium on Non Metallic (FRP) Reinforcement for concrete structures*, JCI , Vol.1, 271-278.
3. Brosens, K., and Van Gemert, D. (1999), " Anchorage Design for externally Bonded carbon Fiber Reinforced Polymer Laminates". *Proc., Fourth Int. Symposium on FRP Reinforcement for concrete structures*, Baltimore, 635-645.
4. Maeda, T., Asano, Y., Sato, Y., Ueda, T., and Kakuta, Y. (1997), " A study on bond mechanism of carbon fiber sheet". *Proc., Third Int. Symposium on Non Metallic (FRP) Reinforcement for concrete structures*, Vol.1, 279-286.
5. Nanni, A., Bakis, C., Boothby, T., (1997), " Externally bonded FRP composites for repair of RC structures". *Proc., Third Int. Symposium on Non Metallic (FRP) Reinforcement for concrete structures*, Vol.1, 303-310.
6. Saadatmanesh, H., M. Malek, A, .(1997), " Prediction of shear and peeling stresses at the plate ends of beams strengthened with FRP plates". *Proc., Third Int. Symposium on Non Metallic (FRP) Reinforcement for concrete structures*, Vol.1, 311-318.
7. Täljsten, B. (1994), "Plate Bonding. Strengthening of existing concrete structures with epoxy bonded plates of steel or fibre reinforced plastics". Doctoral Thesis, Luleå University of technology, Sweden.
8. Bisby, L. A., Green, M. F., Beaudoin, Y., Laboissière, P., (2000)," FRP Plates and Sheets Bonded to Reinforced Concrete Beams", *Proc., Advanced composite materials in Bridges and Structures*, J. Humar, A. Ghani Razaqpur, ed., Canadian Society for Civil Engineering, Montreal, Quebec, 209-216.
9. Faccio, P., Foraboschi, P., Siviero, E., (2000), "Collapse of Masonry Arch Bridges Strengthened Using FRP Laminates", ", *Proc., Advanced composite materials in Bridges and Structures*, J. Humar, A. Ghani Razaqpur, ed., Canadian Society for Civil Engineering, Montreal, Quebec, 505-512.

# Anchoring Method of Carbon Fiber Sheet for Strengthening of Reinforced Concrete Beams

YASUTAKA SAGAWA, HIROMICHI MATSUSHITA and HIROAKI TSURUTA
Kyushu University, Fukuoka, Japan

## INTRODUCTION

The use of carbon fiber sheet (CFS) to strengthen and rehabilitate existing concrete structures has recently increased because of its corrosion resistance, high strength, light weight and low maintenance cost. CFS shows totally elastic behavior until failure, and the bond mechanism of CFS is different from that of reinforcing bar. Applying CFS as a reinforcing material is effective in enhancing both strength and stiffness, but it has been observed that CFS bonded to the tension face of reinforced concrete (RC) beam for flexural strengthening can debond prematurely before the CFS reaches its ultimate strain.

Many anchoring methods of CFS for flexural strengthening of RC members have been investigated. Mechanical anchoring, using steel angles, steel plates, or anchor bolts is one of the popular methods. However, there is quite a possibility that holes bored in order to insert anchor bolts into the concrete can cause stress concentration and tearing of the CFS, and damage to the concrete which is to be strengthened.

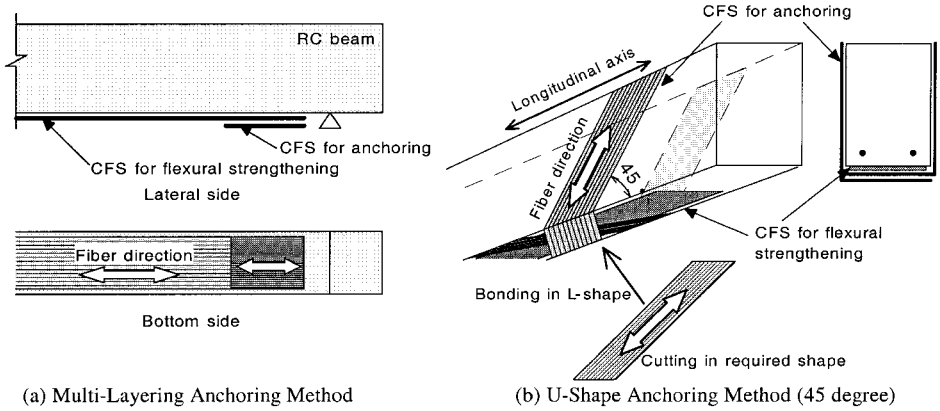
In this study, two anchoring methods were examined; one was the "Multi-Layering Anchoring Method" in which extra CFS for anchoring was bonded at the end of the CFS for flexural strengthening, while the other was the "U-Shape Anchoring Method", in which CFS for anchoring wrapped the RC beams in a U-shape.

## ANCHORING METHOD

Figure 1(a) shows the "Multi-Layering Anchoring Method". After CFS for flexural strengthening has been bonded to the tension face of the beam, CFS for anchoring is bonded on top of the end of CFS bonded previously. The fiber direction of the CFS for anchoring is oriented perpendicular to the longitudinal axis of the beam as well as to the CFS for flexural strengthening. This method reduces concentration of bonding stress, and delays the subsequent debonding of the CFS for flexural strengthening.

Orienting the fiber direction of CFS for anchoring perpendicular to the longitudinal axis of the beam has been examined [1,2]. However, the CFS used widely is typically an orthotropic material and it can hardly tolerate external force transverse to the fiber direction. Therefore, inclining the CFS for anchoring seems to be an advantageous method. In this study an anchoring method was proposed in which the fiber direction of the

*FRPRCS-5*, Thomas Telford, London, 2001.




(a) Multi-Layering Anchoring Method (b) U-Shape Anchoring Method (45 degree)

Figure 1. Procedure of anchoring of Carbon Fiber Sheet

anchoring CFS was inclined 45 degrees to the longitudinal axis of the beam, and the effect of this method was compared with the fiber direction oriented perpendicular to the beam axis.

Figure 1(b) shows the procedure of bonding CFS for anchoring. CFS cut out in a parallelogram was bonded to one of the lateral sides and the bottom of the beam in an L-shape. A U-shaped anchor consisted of two L-shaped pieces of CFS that were bonded together on the bottom. The corner of the beam had a 10 mm radius to prevent the CFS breaking at the corner due to stress concentration. Because two L-shaped pieces of CFS for anchoring were bonded to the CFS for flexural strengthening, a reduction of bond stress concentration was expected as in the "Multi-Layering Anchoring Method", and a reduction of the transverse deformation of the flexural strengthening CFS was expected.

## TEST SPECIMENS AND MATERIALS

The mechanical properties of reinforcing steel bar and CFS used for specimens are shown in Table 1 and Table 2, respectively. CFS was high strength grade with weight/unit area

Table 1. Properties of steel bars

| | D13 (Reinforcing bars) | D6 (Stirrups) |
|---|---|---|
| Modulus of elasticity | 179kN/mm$^2$ | 160kN/mm$^2$ |
| Yield point | 341N/mm$^2$ | 310N/mm$^2$ |
| Tensile strength | 503N/mm$^2$ | 514N/mm$^2$ |
| Elongation at ultimate | 23% | 18% |

Table 2. Properties of CFS

| | |
|---|---|
| Modulus of elasticity | 230kN/mm$^2$ |
| Tensile strength | 3480N/mm$^2$ |
| Design thickness | 0.165mm |
| Areal weight | 300g/m$^2$ |
| Elongation at ultimate | 15,000• 40$^{-6}$ (1.5%) |

Table 3. Mix proportion of concrete

| W/C | s/a | Unit content (kg/m$^3$) | | | | |
|---|---|---|---|---|---|---|
| | | C | W | S | G | Admixture* |
| 49% | 43.0% | 163 | 333 | 755 | 1087 | 0.832 |

* Air-entraining and water-reducing admixture

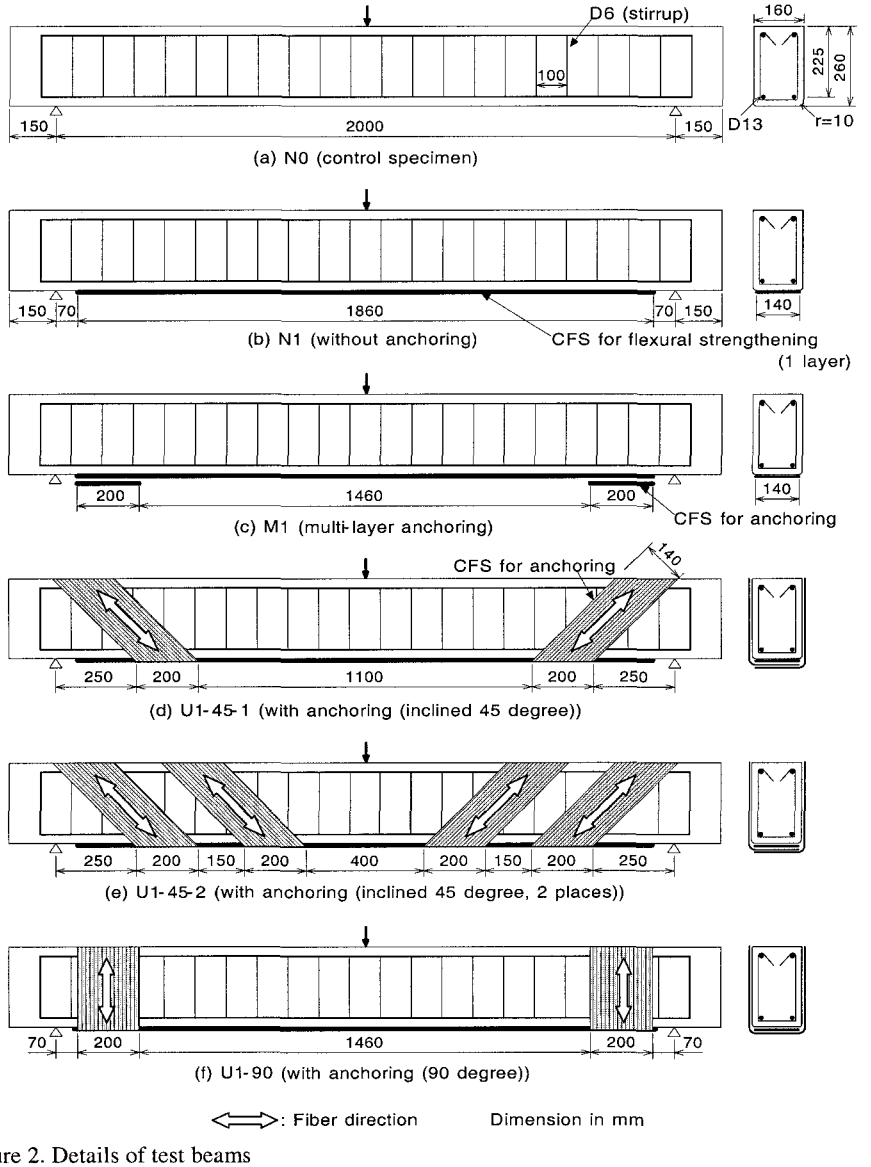



Figure 2. Details of test beams

of 300 g/m$^2$ (FTS-C1-30) manufactured by Nippon Steel Composite Co. Ltd. Table 3 shows mix proportions of concrete. At the age of 21 days, the surface of concrete was prepared by a disk sander, and was coated with an epoxy-based primer, which penetrated the concrete pores and provided better bond strength. The first layer of epoxy-based impregnant resin was then applied to bonding area, and the CFS was impregnated with resin by using a plastic roller. This was repeated for the second layer of coated CFS. Bending tests were carried out at the age of about 28 days.

Details and dimensions of specimens are shown Figure 2. Stirrups were arranged at intervals of 10 cm so as to prevent shear failure. Seven beams were tested. They consisted of three groups; three beams that have no anchoring (N series), one beam to which "Multi-Layering Anchoring Method" was applied (M series) and three beams to which "U-Shape Anchoring Method" was applied (U series). Beam N0 was the control specimen. CFS for flexural strengthening was bonded to the tension face of beam N1, M1, U1-45-1, U1-45-2 and U1-90 in 140 mm width and one layer. In beam M1, CFS for anchoring was bonded over a 200mm length at the end of the flexural strengthening CFS. In beam U1-45-1, the end of the flexural strengthening CFS was strengthened by CFS inclined at 45 degree to the axis. In beam U1-45-2, CFS inclined at 45 degree was bonded at two places. There was a distance of 150 mm between the two CFS anchoring areas. In beam U1-90, the CFS for anchoring was oriented perpendicular to the axis.

## TEST PROCEDURE

To measure strain, wire strain gauges of 2 mm and 30 mm were bonded to the reinforcing bar and CFS respectively, at a distance of 100 mm apart. Two displacement meters were located at mid-span on each side of the beams. The load was applied stepwise by hydraulic jack and measured with load cell. Cracks were sketched at each step.

## RESULTS OF TESTS

Experimental results are presented in Table 4, which summarizes loads and deflections at yielding of the tension steel bar and the ultimate stage as well as compressive strength of the concrete determined by a cylinder test ($\phi$ 10 cm×20 cm). The ultimate load was defined as when the beam could not sustain additional load because of rupture or debonding of the CFS. In Table 3, the figures enclosed in brackets are given to the ratio to N1.

Table 4. Experimental results

| Specimen | Compressive strength of concrete (N/mm$^2$) | At yielding | | At ultimate | | Mode of failure |
|---|---|---|---|---|---|---|
| | | Load (kN) | Deflection (mm) | Load (kN) | Deflection (mm) | |
| N0 | 31.3 | 40.8 | 4.8 | 45.3 | 37.0 | Crushing of concrete |
| N1 | 31.3 | 52.0 | 4.8 | 62.1 (1.00) | 16.5 (1.00) | Debonding of CFS |
| M1 | 39.0 | 49.2 | 4.5 | 74.9 (1.21) | 28.3 (1.72) | Debonding of CFS |
| U1-45-1 | 27.3 | 50.2 | 5.0 | 86.2 (1.39) | 40.7 (2.47) | Rupture of CFS |
| U1-45-2 | 27.3 | 50.1 | 4.6 | 83.3 (1.34) | 19.8 (1.20) | Rupture of CFS |
| U1-90 | 27.3 | 50.2 | 5.3 | 53.6 (0.86) | 47.7 (2.89) | Rupture of CFS |

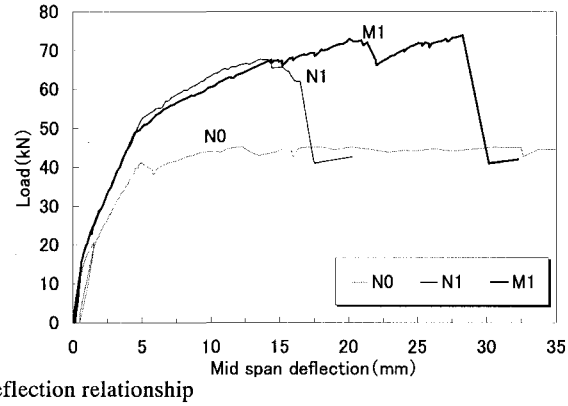
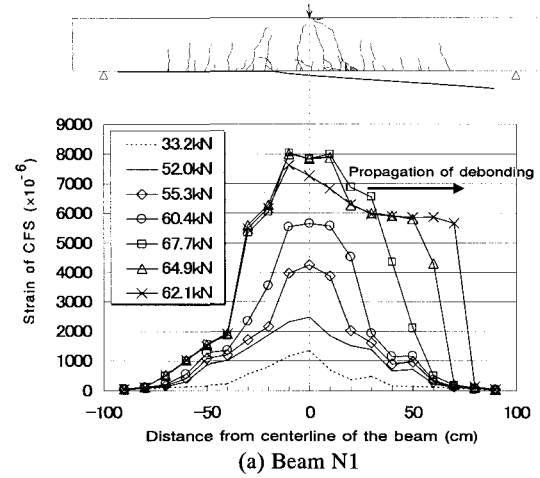
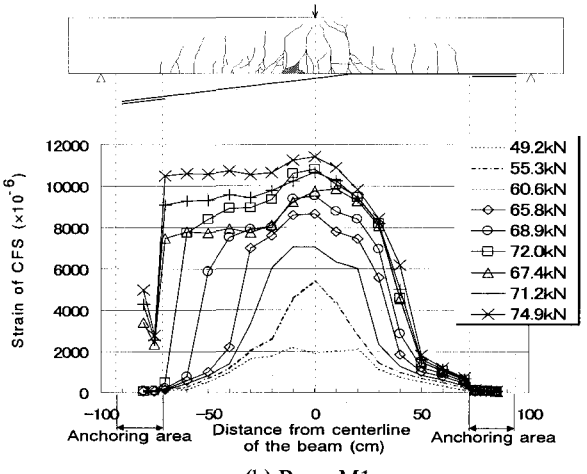



Figure 3. Load-deflection relationship




(a) Beam N1




(b) Beam M1

Figure 4. Strain distribution of CFS and crack pattern

## EFFECTIVENESS OF MULTI-LAYERING

Load-deflection curves of beam N0, N1 and M1 are shown in Figure 3. Beam N0 behaved like a typical underreinforced concrete beam. In N1, the debonding area of the CFS propagated from the center of span to the end of bonding area, and the load capacity fell rapidly. As a consequence, the flexural strengthening effect of the CFS was lost. In M1, debonding of CFS propagated as in N1, but propagation of debonding stopped at the anchoring area where extra CFS was bonded and the deflection then increased significantly. The deflection of M1 at ultimate was 73% bigger than that of N1.

The strain distribution of the CFS and the crack pattern at the ultimate stage for N1 are shown in Figure 4(a). After 60.4 kN load, the debonding area expanded from the center of span to the right support.

The strain distribution of CFS and the crack pattern at ultimate for M1 are shown in Figure 4(b). Debonding of CFS propagated to the left support after 65.8 kN. At the same time as debonding reached the anchoring area, the strain of the CFS at the anchoring area increased suddenly. After that, the strain of debonding area increased in a similar way. The maximum strain was about $11{,}000\times10^{-6}$, while that of N1 was about $8{,}000\times10^{-6}$. The effect of the CFS was lost immediately after 74.9 kN.

## EFFECTIVENESS OF WRAPPING IN A U-SHAPE

In U1-45-1, after the debonding area had reached the anchoring CFS, the effect of the anchoring CFS became apparent, and the load increased linearly. At the ultimate stage, the entire length of CFS for flexural strengthening broke into fragments. In U1-45-2, the flexural strengthening CFS broke at the center of span, and the debonding area of the CFS only extended to the inside of the anchoring CFS. In U1-90, at the same time as the debonding area of the flexural strengthening CFS reached the anchoring CFS, the bottom of the anchoring CFS slipped from the required position (Figure 5). Subsequently, the

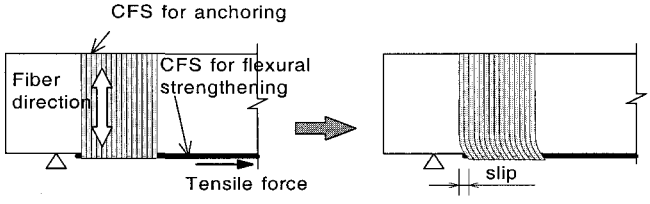



Figure 5. Slip of anchoring sheet

deflection increased at virtually constant load. The flexural strengthening CFS ruptured at the anchoring area.

Load-deflection curves of the U-series are shown in Figure 6. The load-deflection curves of U1-45-1 and U1-45-2 were linear after yielding. Although the load in U1-90 reduced temporarily due to the slip of the anchoring CFS, the deflection increased while sustaining a bigger load bigger than N0.

The load capacities of U1-45-1 and U1-45-2 were almost equal because they were determined by rupture of the strengthening CFS. However, the inclination of load-deflection curve after yielding of U1-45-2 was bigger than that of U1-45-1. This is

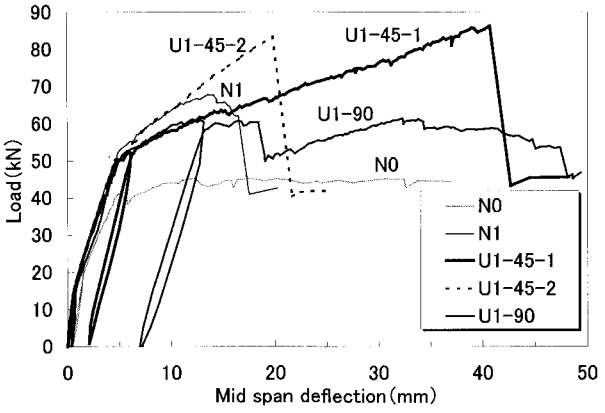


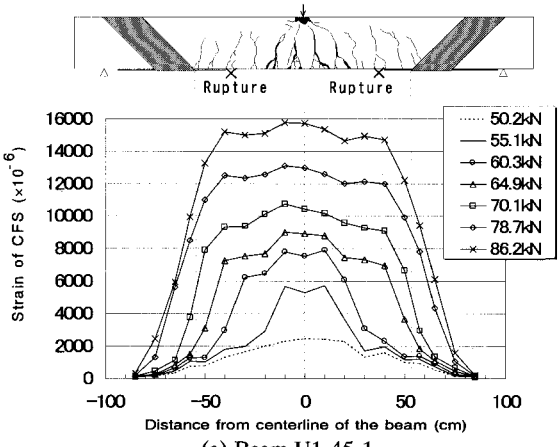

Figure 6. Load-deflection relationship

because the area that it is possible to debond is limited due to the inside anchoring CFS, and the stiffness of the beam itself become higher. This shows that the deformation characteristics depend on the position of anchoring CFS. After the CFS ruptured or debonded, theload-deflection relationships of the beam strengthened with CFS were similar to that of beam N0.

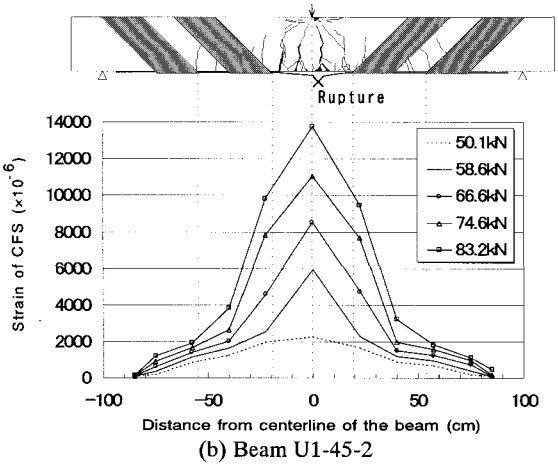
Figure 7 shows the strain distribution of the flexural strengthening CFS and the crack patterns at ultimate for U1-45-1, U1-45-2 and U1-90. In U1-45-1, the area in which strain was uniform in the direction of the beam axis appeared in the vicinity of the center of span at 55.1 kN, and then debonding propagated toward the end of the bonding area of CFS. After 70.1 kN, exlargement of the debonding area stopped and the strain of the CFS increased uniformly. After the strain attained the nominal breaking strain ($15{,}000\times10^{-6}$), the CFS fractured at 86.2 kN.

Because the anchoring CFS in U1-45-2 was bonded to two areas and propagation of debonding was prevented, only the strain near the center of the span increased significantly. Although distribution of the strain took the form of a triangle in Figure 7(b), it was presumed from the result of U1-45-1 that there was an area in which the strain was uniform in the direction of the beam axis.

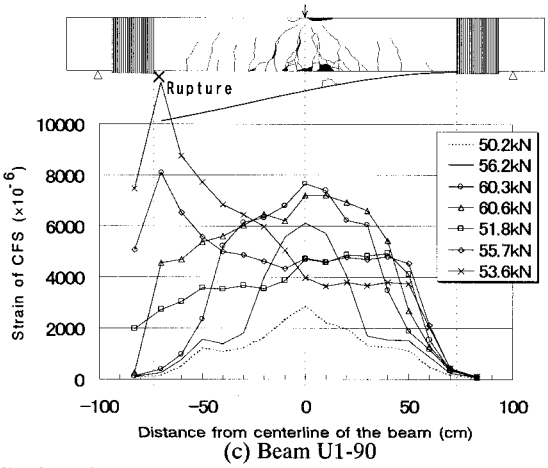
Figure 7(c) shows that after the debonding area reached the left anchoring CFS at 60.6 kN, the load fell rapidly, and then only the strain of the left end of the CFS increased. The greatest value of strain at the center of span was about $7{,}700\times10^{-6}$ which was under half the ultimate strain.




(a) Beam U1-45-1




(b) Beam U1-45-2




(c) Beam U1-90

Figure 7. Strain distribution of CFS and crack pattern

## CONCLUSION

In this study, the effectiveness of two anchoring methods of CFS were investigated. In these methods, only high quality CFS was used. Results obtained in this study are as follows:

- The "Multi-Layering Anchoring Method" could limit propagation of debonding of the CFS. Deflection of the beam with the "Multi-Layering Anchorage Method" was about 70 % larger than that of the beam without anchoring.
- "U-Shape Anchoring Method" also could limit propagation of debonding of the CFS. However, the effectiveness of anchoring depended upon the fiber direction and the bonding area of the anchoring CFS.
- In the case where the fiber direction of the CFS was perpendicular to the beam axis, the bottom of the anchoring CFS slipped from the required position at the same time as debonding of the flexural strengthening CFS reached the anchoring area. Subsequently, only deflection increased, while the load hardly increased.
- Where the fiber direction of the CFS was inclined at 45 degree to the beam axis, load and deflection increased linearly without debonding of the anchoring CFS. The strain of the CFS for flexural strengthening reached breaking strain ($15{,}000 \times 10^{-6}$) and the CFS ruptured at the ultimate load.
- In the specimen where the anchoring CFS was inclined at 45 degree and bonded at two places, the gradient of the load-deflection after yielding was bigger than when the anchoring CFS was bonded only at one place. However, the load capacities of both beams were the same.

## REFERENCES

[1] Sato, Y., et al. "Bond Behavior Between CFRP Sheet and Concrete (Part 2) -Improvement of bond strength by out-of-plane confinement-", Journal of Structural and Construction Engineering (Transaction of AIJ), AIJ, No. 509, Jul. 1998, pp. 127-134.

[2] Takahashi, Y., et al. "Experimental Study of Flexural Behavior of Aramid FRP Rods Reinforced Concrete Beam with Externally Bonded Carbon Fiber Sheet", Proceedings of the Japan Concrete Institute, JCI, Vol. 20, No. 1, 1998, pp. 509-514.

# Strength Models for Plate End Debonding in FRP-Strengthened RC Beams

S.T. SMITH and J.G. TENG,
Dept of Civil and Struct. Eng, The Hong Kong Polytechnic University, Hong Kong, China.

## ABSTRACT
Substantial experimental investigations over the last decade have been conducted into reinforced concrete (RC) beams strengthened in flexure by the bonding of a fibre reinforced polymer (FRP) soffit plate. Many of these studies have reported premature brittle failures by debonding of the soffit plate with or without the concrete cover attached. Among the various modes of premature failures, debonding at the plate end, by either separation of the concrete cover or interfacial debonding of the FRP plate from the concrete, has been most commonly reported. This paper is concerned with strength models for such debonding failures. The paper first presents a review of existing debonding strength models and then assesses them with experimental data collected from the literature. The relative strengths and weaknesses of each model are revealed and finally a new simple model is proposed.

## KEYWORDS
RC beams, strengthening, FRP, debonding, strength models

## INTRODUCTION
Reinforced concrete (RC) beams can be strengthened by bonding fibre reinforced polymer (FRP) plates to their soffit. Extensive testing of such strengthened beams has been carried out over the last ten years (e.g. Arduini and Nanni 1997, Garden *et al.* 1998) and their strengths have been found to be limited often by the plate being suddenly separated from the RC beam rather than by the ultimate flexural capacity of the section. Such failures are commonly referred to as debonding failures.




(a) Concrete cover separation (b) Plate end interfacial debonding

Figure 1. Plate end debonding failure modes of FRP strengthened RC beams

The observed modes of debonding can be broadly classified into two types (Teng *et al.* 2000): (a) those that initiate at or near a plate end and then propagate from the plate end; and (b) those that initiate at an intermediate flexural or flexural-shear crack and then propagate from such a crack towards a plate end. The first type of debonding is referred to as *plate end debonding* here and occurs in one of the two possible modes: (i) separation of the concrete cover with the FRP plate still attached which is referred to as *concrete cover separation* (Fig. 1a), and (ii) separation of the FRP plate, generally with a thin layer of concrete, which is

referred to as *plate end interfacial debonding* (Fig. 1b). Of these two failure modes, concrete cover separation is by far the more commonly reported failure mode. Debonding failures of the second type generally occur in the concrete but adjacent to the adhesive-to-concrete interface, and is referred to as *intermediate crack induced interfacial debonding*. Although less commonly reported, they are likely to control the strength of a significant portion of FRP strengthened beams. This paper is only concerned with strength models for FRP strengthened RC beams which fail by plate end debonding.

## REVIEW OF DEBONDING STRENGTH MODELS

Several strength models for plate end debonding have been developed for FRP plated RC beams in the last decade (Varastehpour and Hamelin 1997, Saadatmanesh and Malek 1998, Wang and Ling 1998, Ahmed and van Gemert 1999, Tumialan *et al.* 1999, Raoof and Hassanen 2000). In addition, a number of strength models have also been developed for plate end debonding in steel plated beams (Oehlers 1992, Ziraba *et al.* 1994, Jansze 1997, Raoof and Zhang 1997). As plate end debonding occurs by either concrete cover separation or adjacent to the adhesive-to-concrete interface in the concrete, models developed for steel plated beams may well be applicable to FRP plated beams, with modifications if necessary. Therefore, all the above-mentioned models are reviewed and assessed herein.

In terms of approaches, existing debonding strength models can be divided into three categories, namely (a) shear capacity based models, (b) concrete tooth models, and (c) interfacial stress based models. All existing models are classified into one of these approaches and briefly reviewed below, while a more detailed review is given in Smith and Teng (2001). It is worth noting that all the models developed specifically for FRP strengthened RC beams (Varastehpour and Hamelin 1997, Saadatmanesh and Malek 1998, Tumialan *et al.* 1999) follow the interfacial stress based approach. On the other hand, three of the five models specifically developed for steel plated beams follow either the shear capacity approach (Oehlers 1992, Jansze 1997) or a combined shear capacity and interfacial stress approach (model II of Ziraba *et al.* 1994).

Of these available models, model I of Ziraba *et al.* (1994) and Varastehpour and Hamelin's (1997) model are for plate end interfacial debonding only. All the concrete tooth models are for cover separation only, while the remainder of interfacial stress based models and all the shear capacity based models appear to be suitable for both cover separation and plate end interfacial debonding, although their applicability to plate end interfacial debonding has not been found to be clearly stated in the descriptions of these models.

### Shear Capacity Based Models

Oehlers and Moran (1990) and Oehlers (1992) investigated simply supported steel plated beams subjected to four and three point bending respectively and developed a strength model by first considering two extreme positions of soffit plate termination. For a plate terminated in the constant moment region, an expression for the flexural peeling moment $M_{peel}$ at the end of the plate was proposed and calibrated with steel plated beam tests. It was suggested that in design, this moment needs only to be compared to the additional moment applied to the beam at the plate end after the plate is bonded. For a plate terminated near the support, it was proposed that debonding (shear peeling) occurs when the shear force at the plate end $V_{peel}$ reaches the shear capacity of the concrete in the RC beam alone, without the contribution from the steel shear reinforcement, based on experimental observations. For general cases where both the shear force and the moment at the plate end are important, an interaction equation was suggested based on test results (Oehlers 1992).

Jansze (1997) also proposed a debonding strength model for steel plated beams but the background information to the model (Jansze 1997) could not be obtained. Only the final form of the model with general comments given in Ahmed and van Gemert (1999) is available to the present authors. It appears that Jansze's (1997) model is also based on the initiation of shear cracking in an RC beam without the contribution of shear reinforcement. Ahmed and van Gemert (1999) later modified Jansze's (1997) model and calibrated the modified model with test results of FRP plated RC beams reported to have failed by concrete cover separation. Ahmed and van Gemert (1999) did not explain in detail the basis of their modification, but inspection of their debonding strength equation reveals that the increase in shear strength offered by shear reinforcement is included.

**Concrete Tooth Models**

Raoof and Zhang (1997) presented a strength model to predict concrete cover separation failures in steel plated beams modified from an earlier version (Zhang *et al.* 1995). The model makes use of the concept of a concrete "tooth" between two adjacent cracks deforming like a cantilever beam under the action of horizontal shear stresses at the beam-plate interface (Fig. 2). Debonding is deemed to occur when these shear stresses lead to tensile stresses at the root of the "tooth" that exceeds the tensile strength of the concrete. The stress in the soffit plate at debonding can then be easily determined as it is directly related to the size of the concrete tooth and the shear stress at the beam-plate interface. Once the stress in the plate is known, the moment to cause separation of the plate can be calculated using a conventional section analysis with the assumption of plane section bending as explained in Zhang *et al.* (1995). An upper and a lower bound bending moment are determined as a consequence of the assumed minimum ($l^p_{min}$) and maximum stabilised crack spacings differing by a factor of two.

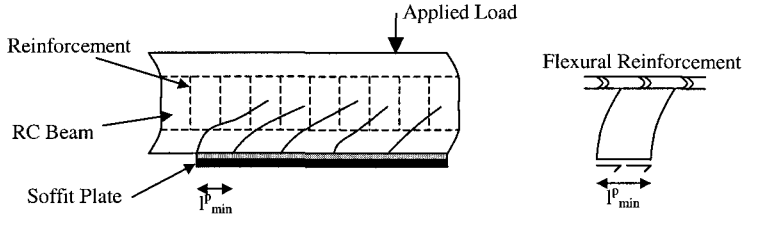



Figure 2. Concrete tooth model (Raoof and Zhang 1997)

Raoof and Hassanen (2000) recently modified Raoof and Zhang's (1997) model for application to FRP plated beams in which two expressions were presented for the effective length of the FRP plate for end anchorage, with two corresponding values for the bond strength between the FRP and the RC beam. These expressions were calibrated in the same manner as that described in Raoof and Zhang (1997) but with FRP-plated RC beam test results. Earlier, Wang and Ling (1998) proposed a modification to the 1995 version of the "tooth" model (Zhang *et al.* 1995) by slightly redefining the minimum crack spacing formula for application to FRP plated RC beams.

**Interfacial Stress Based Models**

A logical assumption is that concrete cover separation or plate end interfacial debonding is due to high interfacial stresses at the end of the soffit plate. Figure 3 shows the stresses acting on an element of concrete adjacent to the end of the adhesive layer where $\tau$ and $\sigma_y$ denote the

shear and transverse normal (peeling) stresses respectively while $\sigma_x$ is the longitudinal stress. Interfacial stress based debonding strength models are generally based on interfacial stresses from an existing closed-form solution (e.g. Roberts 1989) and a concrete failure criterion. Models of this type include model I of Ziraba *et al.* (1994), and those of Varastehpour and Hamelin (1997), Saadatmanesh and Malek (1998) and Tumialan *et al.* (1999).

An alternative use of the interfacial stresses was made in model II of Ziraba *et al.* (1994). The ACI concrete code (ACI-318 1999) prediction of the shear capacity of an RC beam was modified by adjusting the contribution of the shear stirrups to the shear capacity of the plated RC beam. The stirrup efficiency factor was related to the peak interfacial normal stress at the end of the soffit plate and calibrated with experimental data. This model therefore combines the shear capacity approach discussed above with interfacial stresses.

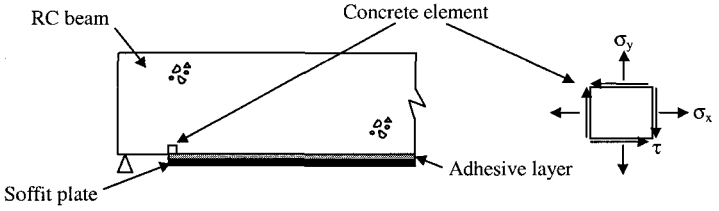



Figure 3. Stresses in the concrete near the plate end

## EXPERIMENTAL DATA

Smith and Teng (2001) compiled an experimental database of seventy-two data points collected from sixteen studies for unstressed and unanchored FRP plated RC beams that were reported to have failed prematurely by plate end debonding. All collected test results are for simply supported beams without any loading before plating, rectangular in cross-section, conventionally reinforced, loaded in three or four point bending, and strengthened with a glass or carbon FRP soffit plate. Tests that were not sufficiently well documented were excluded from the database. This database is much larger than that used in developing any of the existing debonding strength models for FRP strengthened RC beams, and provides a solid basis for assessing the performance of all the debonding strength models reviewed above.

For beams with pultruded plates, the adhesive layer thickness was sometimes not reported. In such cases, the thickness of the adhesive layer was assumed to be 2 mm, a value similar to the average of those reported for the remaining beams with pultruded plates. This is believed to be the most rational approach one can take without having to exclude some test data from the database, and to have minimised errors due to assumed adhesive layer thicknesses. This assumption may be further justified by noting that any model which is overly sensitive to adhesive layer thicknesses is unlikely to be suitable as design models as adhesive layer thicknesses are difficult to control on site and have been found to have a limited effect on test debonding loads (Swamy *et al.* 1987, Quantrill *et al.* 1996, Oehlers and Ali 1998).

For beams strengthened with FRP plates constructed in a wet lay-up process, more uncertainty exists. For many of the tests reported on such beams, the thickness of the FRP plate versus the thickness of the adhesive, was generally not available. Although in a small number of cases, both the fibre sheet thickness alone $t_{sheet}$ and the gross thickness of the fibre sheet plus the applied adhesive $t_{frp,g}$ were given, only the sheet thickness $t_{sheet}$ was given in most cases. For the former cases, the adhesive layer thickness and FRP plate thickness were worked out using the following formulas for a single layer of FRP (Smith and Teng 2001):

$$t_a = (t_{frp,g} - t_{sheet})/2 \quad (1)$$

$$t_{frp} = t_a + t_{sheet} \quad (2)$$

based on the assumptions that the sheet sits in the middle of the adhesive, and the sheet and the outside adhesive form the plate. For the latter cases, $t_a$ was assumed to be 0.42 mm based on measurements of plate samples formed from carbon fibre sheets by wet lay-up (Smith and Teng 2001), and the FRP plate thickness, $t_{frp}$, was worked out from Eq. 2 for a single layer of FRP. For cases where the FRP plate was formed from a number of layers, the total plate thickness was found by multiplying the single layer thickness by the number of layers by assuming that the adhesive thickness between two sheets is $t_a$. The above rational process is believed to have minimised the effect of uncertainty in the existing test data. Furthermore, any debonding strength model that is overly sensitive to this uncertainty is unlikely to be suitable for design use for a wet lay-up process as adhesive and plate thicknesses are difficult to control on site or to define for calculations. For these reasons, test data of beams strengthened with wet lay-up plates are included here for comparisons, but are separated from those beams with pultruded plates to explore differences between the two types of beams.

In addition, the elastic modulus of the adhesive was not reported in many studies. For these cases, the elastic modulus was assumed to be 8500 MPa, a value close to the average of the values reported for the other cases of the database. Again, this is a rational approach, and is not expected to compromise the usefulness of the database.

Table 1. Test-to-predicted debonding strength ratios: pultruded and wet lay-up plates

| Category | Model | Average | Standard Deviation | Coeff. of Variation | Percentage of exceedence | No. of tests |
|---|---|---|---|---|---|---|
| Shear capacity Based models | Oehlers | 2.33 | 0.48 | 20% | 0.3% | 49 |
| | Jansze | 1.46 | 0.43 | 29% | 14% | 44 |
| | Ahmed and van Gemert | 1.11 | 0.25 | 22% | 33% | 44 |
| | New Model ($V_{db}$=1.2$V_{wc}$) | 1.93 | 0.40 | 21% | 1.0% | 49 |
| | New Model ($V_{db}$=1.5$V_{wc}$) | 1.55 | 0.32 | 21% | 4.4% | 49 |
| Concrete Tooth Models | Raoof and Zhang: Lower | 1.37 | 0.36 | 26% | 15% | 49 |
| | Raoof and Zhang: Upper | 1.03 | 0.26 | 25% | 46% | 49 |
| | Wang and Ling: Lower | 1.23 | 0.38 | 31% | 27% | 48 |
| | Wang and Ling: Upper | 0.88 | 0.15 | 17% | 77% | 48 |
| | Raoof and Hassanen I: Lower | 1.43 | 0.38 | 27% | 13% | 49 |
| | Raoof and Hassanen I: Upper | 1.17 | 0.42 | 36% | 35% | 49 |
| | Raoof and Hassanen II: Lower | 1.43 | 0.42 | 29% | 15% | 49 |
| | Raoof and Hassanen II: Upper | 1.14 | 0.38 | 34% | 36% | 49 |
| Interfacial Stress Based Models | Ziraba *et al.* II | 1.61 | 0.51 | 32% | 12% | 49 |
| | Saadatmanesh and Malek | 3.26 | 2.96 | 91% | 22% | 44 |
| | Tumialan *et al.* | 1.79 | 1.25 | 70% | 26% | 44 |

## ASSESSMENT OF DEBONDING STRENGTH MODELS

A through assessment of existing debonding strength models using the test database described above is given in Smith and Teng (2001). The models are assessed there with and without differentiating between cover separation and plate end interfacial debonding. The test data for cover separation are the more reliable in that the failure mode is generally clearly described in the literature, while there is some uncertainty in this aspect for the test data for plate end interfacial debonding. For the above reason and due to space limitation, only a brief assessment of those models suitable for concrete cover separation is presented here. The general conclusions with regard to the merits of various models reached here remain more or less the same when the test data for plate end interfacial debonding are also included in the assessment (Teng and Smith 2001).

Tables 1-3 present the statistical characteristics of the test-to-predicted debonding strength ratios as assessed using only the collected test data for concrete cover separation in FRP plated RC beams. The three tables are for all test results combined, results for beams with pultruded plates only and results for beams with wet lay-up plates only, respectively. It should be noted that the models of Jansze (1997), Ahmed and van Gemert (1999), Saadatmanesh and Malek (1998) and Tumialan *et al.* (1999) cannot be used for plates terminated at the support, while Wang and Ling's (1998) model cannot be used for plates terminated in the constant moment region. These limitations account for the smaller number of test data used to asses these models (Tables 1-3).

Table 2. Test-to-predicted debonding strength ratios: pultruded plates only

| Category | Model | Average | Standard Deviation | Coeff. of Variation | Percentage of exceedence | No. of tests |
|---|---|---|---|---|---|---|
| Shear capacity Based models | Oehlers | 2.12 | 0.28 | 13% | 0% | 29 |
| | Jansze | 1.20 | 0.32 | 26% | 26% | 27 |
| | Ahmed and van Gemert | 1.02 | 0.23 | 23% | 46% | 27 |
| | New Model ($V_{db}$=1.2$V_{uc}$) | 1.75 | 0.23 | 13% | 0% | 29 |
| | New Model ($V_{db}$=1.5$V_{uc}$) | 1.40 | 0.18 | 13% | 1.3% | 29 |
| Concrete Tooth Models | Raoof and Zhang: Lower | 1.30 | 0.28 | 22% | 14% | 29 |
| | Raoof and Zhang: Upper | 0.99 | 0.26 | 26% | 52% | 29 |
| | Wang and Ling: Lower | 1.21 | 0.39 | 32% | 30% | 29 |
| | Wang and Ling: Upper | 0.83 | 0.15 | 18% | 87% | 29 |
| | Raoof and Hassanen I: Lower | 1.34 | 0.33 | 25% | 15% | 29 |
| | Raoof and Hassanen I: Upper | 1.06 | 0.31 | 29% | 43% | 29 |
| | Raoof and Hassanen II: Lower | 1.34 | 0.33 | 25% | 16% | 29 |
| | Raoof and Hassanen II: Upper | 1.06 | 0.32 | 31% | 43% | 29 |
| Interfacial Stress Based Models | Ziraba *et al.* II | 1.55 | 0.39 | 25% | 8.1% | 29 |
| | Saadatmanesh and Malek | 2.74 | 3.09 | 113% | 29% | 27 |
| | Tumialan *et al.* | 1.54 | 1.43 | 93% | 35% | 27 |

Based on the statistical performance of each model (Tables 1-3), the models of Raoof and Zhang (1997) (upper bound predictions), Saadaatmanesh and Malek (1998), Wang and Ling (1998) (both lower and upper bound predictions), Ahmed and van Gemert (1999), Tumialan *et al.* (1999) and Raoof and Hassanen's (2000) (upper bound predictions) are identified to be the worse performing models in terms of giving close and safe predictions. Ahmed and van Gemert's (1999) model, which was modified from Jansze's (1997) model, is rather un-conservative for the combined data of pultruded and wet lay-up plates (Table 1) and for pultruded plates alone (Table 2) as evidenced by the high percentages of exceedence, but is satisfactory for wet lay-up plates alone (Table 3). Raoof and Zhang's (1997) and Raoof and Hassanen's (2000) upper bound predictions are understandably un-conservative. Wang and Ling's (1998) model performs poorly in both the lower and upper bound predictions compared to Raoof and Zhang's (1997) model. Overall, the interfacial stress based models of Saadatmanesh and Malek (1998) and Tumialan *et al.* (1999) show unsatisfactory performance (Tables 1-3), although their performance is much better if only wet lay-up plates are considered (Table 3). The main shortcoming of these models is the large scatter in their predictions (Tables 1-3). An obvious disadvantage of these models is that interfacial stresses are sensitive to the adhesive layer thickness which is often hard to define in practice and has been found to have limited effect on test debonding loads (Swamy *et al.* 1987, Quantrill *et al.* 1996, Oehlers and Ali 1998).

Table 3. Test-to-predicted debonding strength ratios: wet lay-up plates only

| Category | Model | Average | Standard Deviation | Coeff. of Variation | Percentageof exceedence | No. of tests |
|---|---|---|---|---|---|---|
| Shear capacity Based models | Oehlers | 2.64 | 0.54 | 21% | 0.1% | 20 |
| | Jansze | 1.88 | 0.19 | 10% | 0% | 17 |
| | Ahmed and van Gemert | 1.24 | 0.21 | 17% | 12% | 17 |
| | New Model ($V_{db}$=1.2$V_{uc}$) | 2.20 | 0.45 | 21% | 0% | 20 |
| | New Model ($V_{db}$=1.5$V_{uc}$) | 1.76 | 0.36 | 21% | 1.8% | 20 |
| Concrete Tooth Models | Raoof and Zhang: Lower | 1.47 | 0.44 | 30% | 15% | 20 |
| | Raoof and Zhang: Upper | 1.09 | 0.26 | 24% | 37% | 20 |
| | Wang and Ling: Lower | 1.27 | 0.38 | 29% | 23% | 19 |
| | Wang and Ling: Upper | 0.96 | 0.13 | 13% | 62% | 19 |
| | Raoof and Hassanen I: Lower | 1.55 | 0.43 | 28% | 9.9% | 20 |
| | Raoof and Hassanen I: Upper | 1.32 | 0.52 | 39% | 27% | 20 |
| | Raoof and Hassanen II: Lower | 1.56 | 0.49 | 32% | 13% | 20 |
| | Raoof and Hassanen II: Upper | 1.26 | 0.44 | 35% | 28% | 20 |
| Interfacial Stress Based Models | Ziraba *et al.* II | 1.71 | 0.65 | 38% | 14% | 20 |
| | Saadatmanesh and Malek | 4.09 | 2.64 | 65% | 12% | 17 |
| | Tumialan *et al.* | 2.18 | 0.78 | 36% | 6.4% | 17 |

The better performing debonding strength models are the models of Oehlers (1992), Ziraba *et al.* (1994) (model II), Jansze (1997), Raoof and Zhang (1997) (lower bound predictions) and Raoof and Hassanen (lower bound predictions of both of their models). Raoof and Hassanen's (2000) lower bound predictions, using either of the two expressions for the effective length of the FRP plate for end anchorage, are similar to but slightly less satisfactory than the lower bound predictions of Raoof and Zhang (1997), as the former predictions are higher on average and show a greater scatter. For both the combined data and for pultruded plates alone, Oehlers's (1992) model and Raoof and Zhang's (1997) model (lower bound predictions) show a smaller scatter in predictions than model II of Ziraba *et al.* (1994) and Jansze's (1997) model based on the coefficients of variation. Jansze's (1997) model has the lowest coefficient of variation over the other five models when wet lay-up plates alone are examined (Table 3) but this model is rather un-conservative for pultruded plates. Oehlers' (1992) model gives safe predictions but can be considered overly conservative, and its scatter does not vary significantly with types of plates. Raoof and Zhang's (1997) model shows similar performance for both types of plates, while Ziraba *et al.*'s (1994) model II performs better for pultruded plates than for wet lay-up plates. The application of Ziraba *et al.*'s (1994) model II is however more laborious than the other four models, as interfacial stresses have to be calculated.

A more illustrative comparison of the test data with Oehlers' (1992) model is given in Fig. 4, where the test data are differentiated based both plate types. In these figures, $M_u$ is the theoretical ultimate moment capacity of the beam section without the influence of debonding, $M_{exp}$ is the maximum experimental moment in the beam at debonding, and $M_{db}$ is the corresponding debonding moment predicted by the strength models. It is worth noting that Oehlers' (1992) model is more conservative for wet lay-up plates than for pultruded plates.

Of the six better performing models, Oehlers' (1992) model is the only one which gives safe but slightly conservative predictions for design use. It also has the smallest scatter for the combined data (Table 1). Oehlers' (1992) model does have a drawback for direct application to FRP strengthened beams as discussed in the next section. A new model is therefore proposed in the next section by modifying Oehlers' (1992) model. It is also worth noting that of the six better performing models, three of them (Oehlers 1992, Ziraba *et al.*'s 1994 model II, Jansze 1997) relate the debonding strength to the shear strength of concrete in an RC beam, while the other three are concrete tooth models from the same group with only small

differences from each other. The shear capacity based approach independently proposed by three different groups appears to be a promising approach, which is another reason for building a new model on the basis of Oehlers' model (1992).

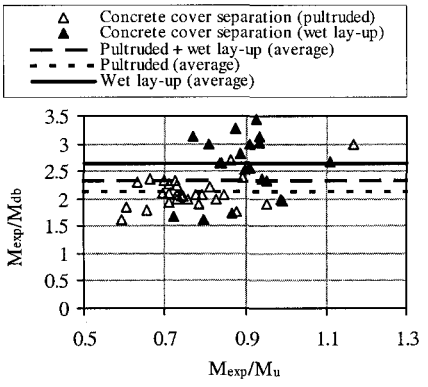



Figure 4. Performance of Oehlers' (1992) model

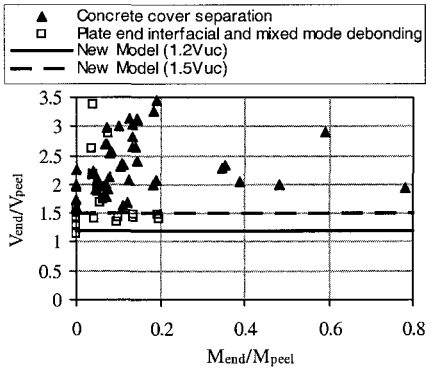



Figure 5. Comparison of new proposed model and test data

## A SIMPLE NEW MODEL

Oehlers' (1992) model is given by

$$\frac{M_{end}}{M_{peel}} + \frac{V_{end}}{V_{peel}} \leq 1.17 \tag{3}$$

where $M_{end} \leq M_{peel}$, $V_{end} \leq V_{peel}$ and $M_{end}$ and $V_{end}$ are the bending moment and the shear force at the plate end. The bending moment is based on the load applied after plating while the shear force includes the part from loading before plating. Oehlers (1992) equated $V_{peel}$ to the shear capacity of the concrete in the RC beam $V_{uc}$ and used the following expression for $V_{uc}$ which is taken from the Australian concrete code (AS 3600 1988):

$$V_{uc} = [1.4 - (d/2000)]bd\left[\frac{A_{st} f_c'}{bd}\right]^{\frac{1}{3}} \tag{4}$$

where it is required that $1.4 - (d/2000) \geq 1.1$, $f'_c$ is the concrete cylinder strength, $A_{st}$ the area of flexural tensile steel reinforcement, $b$ the section width and $d$ the effective depth of the section. In Figure 5, the plate end debonding test data of FRP-plated beams are plotted to determine the interaction between plate end shear force and moment. Both the test data for cover separation as used in the assessment of models presented above and the other test data for plate end interfacial debonding or a mixed mode of these two as described in detail in Teng and Smith (2001) are shown. It is interesting to note that no interaction appears to exist between the moment and the shear force, with the shear force at failure being always greater than $V_{peel}$ of Eq. 4, so the following simple debonding strength model can be proposed:

$$V_{db} = \alpha V_{uc} \tag{5}$$

This equation with $\alpha = 1.2$ and with $V_{uc}$ given by Eq. 4 provides a 94.9 percentile lower bound prediction to all the data shown in Fig. 5 and is shown as the solid line in Fig. 5 (Table 1). If only cover separation is considered, the value of $\alpha$ can be raised to 1.5 which provides a 95.6 percentile lower bound prediction to the cover separation test data and is shown as the dashed line in Fig. 5 (Table 1). The good statistical performance of the new model with $\alpha$ =1.2 or 1.5 is shown in Tables 1-3 for cover separation failures.

In practical design, since it is difficult to ascertain whether cover separation will be the failure mode, Eq. 5 with $\alpha$ = 1.2 is recommended for use to design against all forms of plate end debonding failures. An obvious advantage of this model is that $V_{uc}$ may be evaluated according to any national or international design code, and this facilitates the inclusion of the model in any national code on FRP strengthening. At this stage, it is necessary to limit the range of applicability of the model to that of the collected data in terms of the magnitude of the moment at the plate end. It is suggested that the above proposed model can only be used when $M_{end}/M_u \leq$ 0.72 as this approximates the upper limit of the test data (Smith and Teng 2001). The choice of this ratio as a parameter means that little extra work is required as $M_u$ is expected to be calculated in any flexural strengthening design. The use of the alternative ratio of $M_{end}/M_{peel}$ may be considered with its value limited to 0.78 (Fig. 5), but this would require the extra work of evaluating $M_{peel}$. The use of $M_{end}/M_u$ thus appears to be preferable unless evidence to the contrary emerges.

This new model has a number of advantages over the six better models identified in the previous section. These include: (a) the new model is calibrated with a large test database of FRP strengthened beams and provides a suitable lower bound for design use; (b) the new model is simpler to apply as the shear capacity of the concrete in the RC beam is either known or has to be evaluated in flexural strengthening design so little extra work is required for checking plate end debonding; and (c) the new model gives designers a better intuitive feel of the possibility of plate end debonding as it is directly related to the shear capacity of the concrete in the beam, particularly when steel shear reinforcement is not present as often is the case for slabs.

## CONCLUSIONS

An assessment of existing strength models for plate end debonding in FRP strengthened RC beams using available test data has identified the models of Oehlers (1992), Ziraba *et al.* (1994) (model II), Jansze (1997), Raoof and Zhang (1997) and Raoof and Hassanen (2000) to be the more accurate ones. Surprisingly, all but those of Raoof and Hassanen (2000) were developed for steel plated beams, while those specifically developed for FRP plated beams give poorer predictions. A simple new model was also proposed by modifying Oehlers' (1992) model. This new model is suitable for direct application in design, and can be included easily in any national codes.

## ACKNOWLEDGEMENTS

Both authors wish to thank The Hong Kong Polytechnic University for the provision of a postdoctoral fellowship to the first author.

## REFERENCES

ACI 318-95 (1999) *Building Code Requirements for Structural Concrete (318-95) and Commentary (318R-95)*, American Concrete Institute, Fifth Printing, Detroit, U.S.A.

Ahmed, O. and van Gemert, D. (1999) "Effect of longitudinal carbon fibre reinforced plastic laminates on shear capacity of reinforced concrete beams", *Proceedings, Fourth International Symposium on Fibre Reinforced Polymer Reinforcement for Reinforced Concrete Structures*, Maryland, U.S.A., 933-943.

Arduini, M. and Nanni, A. (1997) "Behaviour of pecracked RC beams strengthened with carbon FRP sheets", *Journal of Composites for Construction, ASCE,* 1(2), 63-70.

AS 3600 (1988) *Concrete Structures, AS 3600*, Standards Australia, Sydney, Australia.

Garden, H.N., Quantrill, R.J., Hollaway, L.C., Thorne, A.M. and Parke, G.A.R. (1998) "An experimental study of the anchorage length of carbon fibre composite plates used to

strengthen reinforced concrete beams", *Construction and Building Materials*, 12, 203-219.

Jansze, W. (1997) *Strengthening of R.C. Members in Bending by Externally Bonded Steel Plates*, PhD Thesis, Delft University of Technology, Delft.

Oehlers, D.J. (1992) "Reinforced concrete beams with plates glued to their soffits", *Journal of Structural Engineering, ASCE*, 118(8), 2023-2038.

Oehlers, D.J. and Moran, J.P. (1990) "Premature failure of externally plated reinforced concrete beams", *Journal of Structural Engineering, ASCE*, 116(4), 978-995.

Oehlers, D.J. and Ali, M. (1998) "Discussion on 'Predictions of the maximum plate end stresses of FRP strengthened beams: Part II – by Quantrill, R.J., Hollaway, L.C. and Thorne, A.M.' ", *Magazine of Concrete Research*, 50(1), 91-92.

Quantrill, R.J., Hollaway, L.C. and Thorne, A.M. (1996) "Predictions of the maximum plate end stresses of FRP strengthened beams: Part II", *Magazine of Concrete Research*, 48(177), 343-351.

Raoof, M. and Zhang, S. (1997) "An insight into the structural behaviour of reinforced concrete beams with externally bonded plates", *Proceedings of the Institution of Civil Engineers: Structures and Buildings*, 122, 477-492.

Raoof, M. and Hassanen, M.A.H. (2000) "Peeling failure of reinforced concrete beams with fibre-reinforced plastic or steel plates glued to their soffits", *Proceedings of the Institution of Civil Engineers, Structures and Buildings*, 140, 291-305.

Roberts, T.M. (1989) "Approximate analysis of shear and normal stress concentrations in the adhesive layer of plated RC beams", *The Structural Engineer*, 67(12), 229-233.

Saadatmanesh, H. and Malek, A.M. (1998) "Design guidelines for flexural strengthening of RC beams with FRP plates", *Journal of Composites for Construction, ASCE*, 2(4), 158-164.

Smith, S.T. and Teng, J.G. (2001) "FRP strengthened RC beams-I: review of debonding strength models, and II: assessment of debonding strength models", to be published.

Swamy, R.N., Jones, R. and Bloxham, J.W. (1987) "Structural behaviour of reinforced concrete beams strengthened by epoxy-bonded steel plates", *The Structural Engineer*, 65A(2), 59-68.

Teng, J.G., Chen, J.F., Smith, S.T. and Lam, L. (2000) *RC Structures Strengthened with FRP Composites*, Research Centre for Advanced Technology in Structural Engineering, Department of Civil and Structural Engineering, The Hong Kong Polytechnic University, Hong Kong, China, December.

Tumialan, G., Belarbi, A. and Nanni, A. (1999) *Reinforced Concrete Beams Strengthened with CFRP Composites: Failure Due to Concrete Cover Delamination*, Report No. CIES-99/01, Department of Civil Engineering, Centre for Infrastructure Engineering Studies, University of Missouri-Rolla, U.S.A.

Varastehpour, H. and Hamelin, P. (1997) "Strengthening of concrete beams using fibre-reinforced plastics", *Materials and Structures*, 30, 160-166.

Wang, C.Y. and Ling, F.S. (1998) "Prediction model for the debonding failure of cracked RC beams with externally bonded FRP sheets", *Proceedings, Second International Conference on Composites in Infrastructure (ICCI 98)*, Arizona, U.S.A., 548-562.

Zhang, S., Raoof, M. and Wood, L.A. (1995) "Prediction of peeling failure of reinforced concrete beams with externally bonded steel plates", *Proceedings of the Institution of Civil Engineers: Structures and Buildings*, 110, 257-268.

Ziraba, Y.N., Baluch, M.H., Basunbul, I.A., Sharif, A.M., Azad, A.K. and Al-Sulaimani, G.J. (1994) "Guidelines towards the design of reinforced concrete beams with external plates", *ACI Structural Journal*, 91(6), 639-646.

# Effect of Test Methods on Plate-to-Concrete Bond Strength

J.F. CHEN, School of the Built Environment, Nottingham University, UK
Z.J. YANG, School of Eng. and the Built Environment, Wolverhampton University, UK
X.M. PAN, Wenzhou Public Utilities Development Co., Wenzhou, Zhejiang, China, and
G.D. HOLT, School of Eng. and the Built Environment, Wolverhampton University, UK

## ABSTRACT
The strengthening of reinforced concrete structures using externally bonded steel or advanced fibre reinforced plastic (FRP) composites is becoming increasingly common in civil engineering applications. A key factor affecting the behaviour and reliability of such strengthened structures is the bond strength between the steel or FRP plate and the concrete substrate. Several different experimental set-ups have previously been used to determine bond strength. Within this paper, a finite element analysis on the stress distributions in these test set-ups is presented. Results show that stress distribution can be significantly different among different set-ups, for similar materials and geometry.

**KEYWORDS**: Shear test, concrete, FRP, steel plate, strengthening, bond, test method

## INTRODUCTION
Strengthening of reinforced concrete (RC) structures using externally bonded steel or advanced fibre reinforced plastic (FRP) composites, has been increasingly used in civil engineering applications. One of the major factors affecting the behaviour of such strengthened structures is the bond strength between the reinforcement plate and the concrete substrate. Recent studies have shown that understanding of bond behaviour is essential, for example, in predicting various de-bonding failure modes such as intermediate crack induced debonding in flexurally strengthened beams and slabs (Teng *et al.* 2000; Smith *et al.*, 2001) and debonding of side plates in shear strengthened beams (Chen and Teng 2001a). The accurate determination of bond strength is thus essential, for safe design of strengthening schemes for RC structures using externally bonded plates.

There is presently a lack of standards concerning the test method for determining bond strength. Several different experimental set-ups, including various shear tests and modified beam tests have been used. Although substantial research has been carried out on understanding bond strength (see Chen and Teng 2001b), Horiguchi and Saeki (1997) appear to the first to have experimentally investigated the effect of different test methods on test results. They concluded that different test set-ups have significant effect on the tested bond strength. This paper first presents a review of different test methods. A finite element (FE) study on the stress distributions in these set-ups is then carried out. A comparison is made to investigate the difference between the different test methods.

Based on an extensive literature review, Chen and Teng (2001b) indicated that most bond strength test specimens failed a few millimetres in the concrete underneath the concrete/ adhesive interface. In this failure mode, a good bond strength model should be applicable to

both FRP and steel plate bonded to concrete. No distinction is therefore made between FRP and steel plates in this paper.

## BOND STRENGTH TEST METHODS

### Classification

Bond strength between FRP or steel plates and concrete blocks has commonly been tested using a shear test or modified beam test. According to the differences invoked by mechanical behaviour, the test set-ups can be classified as: a) double shear pulling (DoublePull) test; b) double shear pushing (DoublePush) test; c) single shear pulling (SinglePull) test; d) single shear pushing (SinglePush) test; and e) bending or beam test (BeamTest).

It may be noted that numerous studies have been performed on flexurally strengthened beams. Some of these were concerned with the anchorage length of the bonded plates (e.g. Garden *et al.* 1998; Jones *et al.* 1980). These are "true beam bending" test and the results cannot be easily related to the bond strength. They are thus beyond the remit of this paper.

### Double Shear Pulling (DoublePull) Test

The DoublePull test has been the most popular test method to date (e.g. van Gemert 1980; Kobatake *et al.* 1993; Brosens and van Gemert 1997; Maeda *et al.* 1997; Hiroyuki and Wu 1997; Fukuzawa *et al.* 1997). There are slight differences regarding the test set-up details, but the loading mechanism is similar (Fig. 1). Two test plates are bonded on the opposite sides of a concrete block and equal tensile forces $P_p$ are applied in the plates. These forces are balanced by a pulling force applied in the concrete $P_c$ which may be applied either through a steel bar embedded at centre of the concrete block, or through steel plates bonded on the sides of the concrete block.

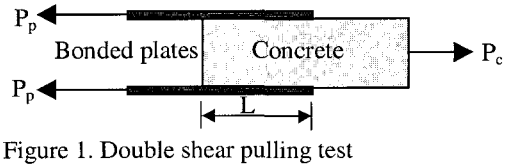



Figure 1. Double shear pulling test

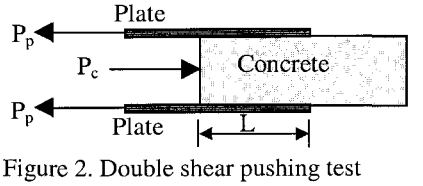



Figure 2. Double shear pushing test

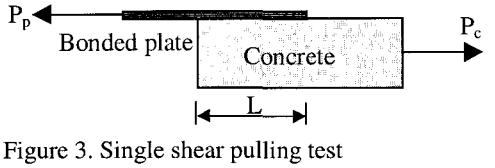



Figure 3. Single shear pulling test

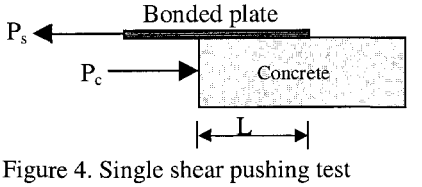



Figure 4. Single shear pushing test

### Double Shear Pushing (DoublePush) Test

The pushing force acting on the concrete block in a DoublePush test (Fig. 2) was usually applied through a supporting wedge (e.g. Swamy *et al.* 1986; Neubauer and Rostásy 1997). Neubauer and Rostásy (1997) believed that this can well simulate the stress state in the anchorage zone of a flexurally strengthened beam. Obviously, the stresses in the loading direction are compressive in the concrete block in this set-up; whilst that in a DoublePull test such stresses are tensile. This difference may lead to discrepancies among test results.

**Single Shear Pulling (SinglePull) Test**
Although no studies have appeared to use such a test set-up in the literature, theoretically a SinglePull test could be used (Fig. 3). Only one plate is bonded on one side of the concrete in a SinglePull test. This leads to a loss of the symmetry (as in a DoublePull test).

**Single Shear Pushing (SinglePush) Test**
The SinglePush test (Fig. 4) has possibly been the second most popular set-up after the DoublePull test (e.g. Chajes *et al.* 1996, 1996; Täljsten 1997; Bizindavyi and Neale 1999). This can obviously offer savings in both materials and labour because only one plate coupon is bonded to the concrete.

**Bending or Beam Test (BeamTest)**
BeamTest can well simulate the effects of moment variation and shear force in the concrete block. Similar test set-ups were adopted by van Gemert (1980) to investigate steel-concrete anchorage behaviour (Fig 5) and Ziraba *et al.* (1995) to investigate the effect of concrete compressive strength on steel-concrete bond strength (Fig. 6). Ziraba *et al.* (1995) found no dependence of the failure of the joint to the concrete strength and concluded that the concrete-glue-plate interface behaviour was rather a surface phenomenon. However, this contradicts other experimental observations (e.g. Chajes et al 1996); that concrete strength does have significant effect on bond strength.

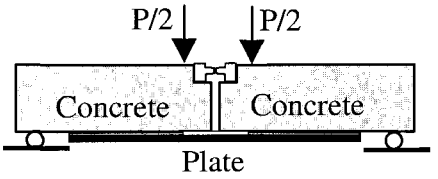


Figure 5. Beam test (van Gemert 1980)

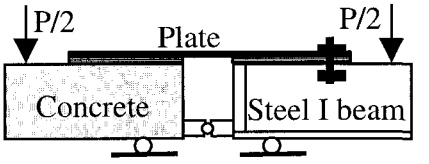


Figure 6. Modified beam test (Ziraba *et al.* 1995)

## FINITE ELEMENT MODELLING

### General

Linear elastic FE analyses were carried out in this study to compare the stress states in different test schemes. The concrete block was taken to have a size of 500mm in length and 150mm in thickness so that various bond lengths (of the plate to the block) could be analysed without changing the block's dimensions. A plate thickness of 3mm and adhesive thickness of 1mm were assumed in all of the analyses. Young's modulus was assumed to be 200, 1 and 30 GPa for the plate, adhesive and concrete respectively. The corresponding Poisson's ratio was 0.3, 0.25 and 0.17 respectively. The geometry, the loading and boundary conditions, as assumed for all five test schemes, are as shown in Fig. 7. For symmetrical configurations, only half of the structure was modelled. The pulling force in the plate was applied by a uniformly distributed tension force q with an intensity of 55.55MPa at the loading end for shear tests. The point load P applied in the modified beam test was obtained based on static equilibrium by assuming the same uniform stress in the plate.

The analyses were conducted using an FE analysis package which is being specially developed for analysing the behaviour of RC structures strengthened with externally bonded plates using fracture mechanics approach. All materials were modelled using 8-node quadrilateral isoparametric plane stress elements. A perfect bond between the adhesive and the plate and between the adhesive and the concrete was assumed.

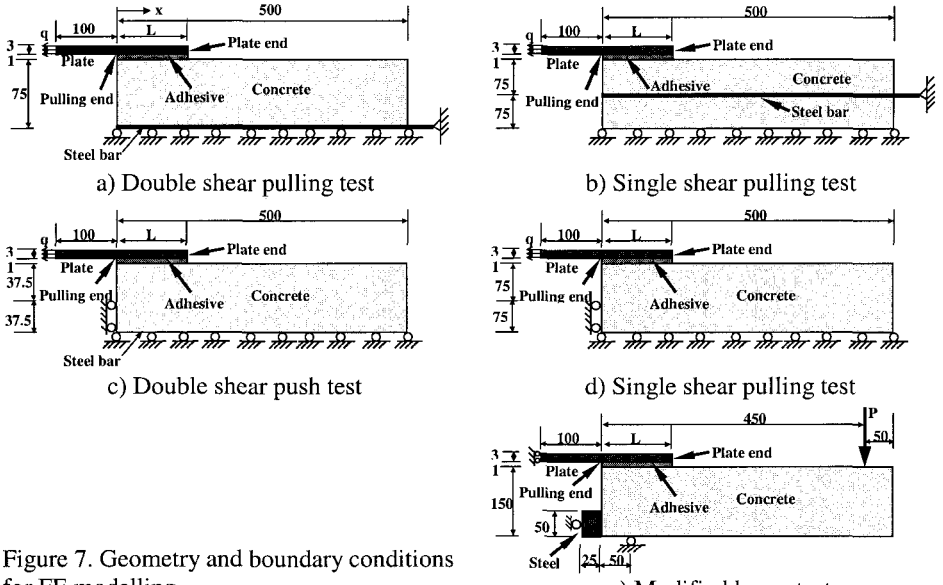


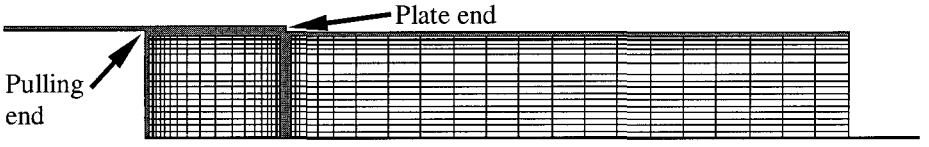

Figure 7. Geometry and boundary conditions for FE modelling

**Mesh Convergence Test**

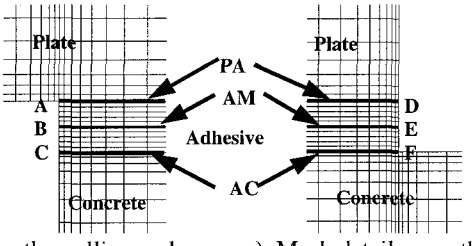
A mesh convergence test was conducted for the double shear pulling test (bond length L=100mm). Results from four typical meshes are compared here. All meshes have 8 layers of elements for the plate and 30 layers of elements for the concrete block in the vertical direction. Meshes were finest near the pulling end and the plate end where possible stress singularities exist (Fig. 8a). They gradually became coarser towards other parts of the structure. The number of element layers used for the adhesive layer for these four meshes were 2, 4, 10 and 20 respectively. Corresponding smallest element sizes for them were 0.5, 0.25, 0.1, and 0.05mm respectively. Figure 8a shows the mesh with the smallest element size of 0.1mm. Mesh details around the pulling and the plate end are shown in Figs 8b and 8c respectively. For brevity, the plate-adhesive interface, adhesive-concrete interface and the mid-section of the adhesive (Fig. 8) are respectively referred to as PA, AC and AM hereafter.

Figures 9a and 9b show distributions of the normal interfacial stress $\sigma_y$ (or peeling stress) at PA near the pulling and plate ends respectively. Maximum stresses near the ends increase as the mesh becomes finer. This is due to stress singularities at two-material wedges (Hein and Erdogan 1971). There are four stress singular points in this problem (Points A, C, D and F in Figs 8b and c). The normal stress is compressive at PA but tensile at AC near the plate end, which is similar to the stress distribution near the plate end in a RC beam bonded with a soffit plate as investigated by Teng *et al.* (2001). The normal stresses near the pulling end have similar distribution and amplitude, to those near the plate end (the sign is, however, reversed). A similar trend is seen for the shear stress distributions (Figs 9c and d). They also show that the two coarse meshes failed to capture the descending part of the curves.

Although the stress will never converge because of stress singularities, differences between predictions using meshes with 0.1 and 0.05mm smallest elements are only within 0.2mm from the ends. Comparable meshes to that with 0.1mm smallest elements were thus used for all other calculations hereafter.

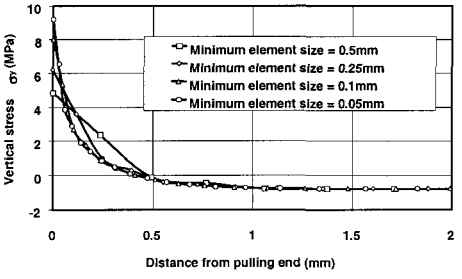



a) Mesh for the whole double shear pulling test model

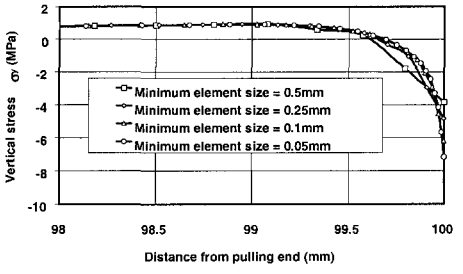



b) Mesh details near the pulling end c) Mesh details near the plate end

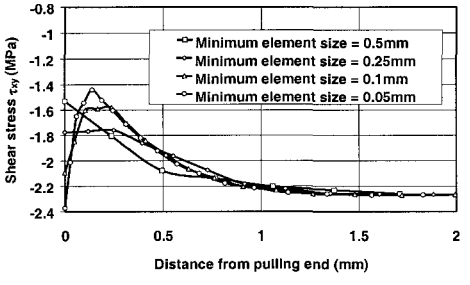
Figure 8. A typical FE mesh



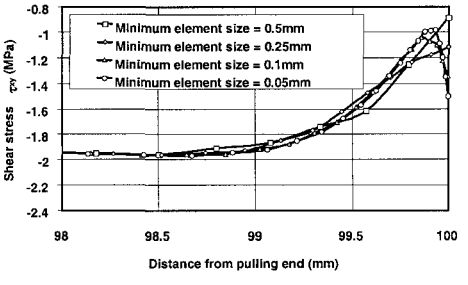

a) Normal stress $\sigma_y$ near pulling end




b) Normal stress $\sigma_y$ near plate end



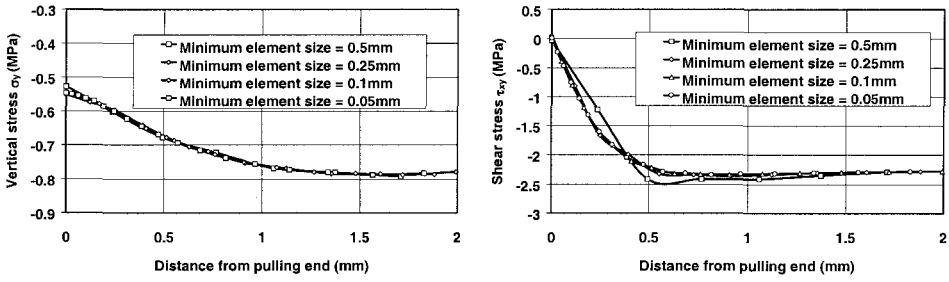

c) Shear stress $\tau_{xy}$ near pulling end




d) Shear stress $\tau_{xy}$ near plate end

Figure 9. Stresses on PA interface

All four meshes predicted similar normal stress distributions at AM near the pulling end (Fig. 10a). Except for the coarsest mesh, all other meshes predicted the same shear stress at AM (Fig. 10b). All predictions converged to zero shear stress at the free surface. Because most shear tests failed in concrete near the AC interface, it would be ideal to compare stresses in the concrete near this interface. However, this is impractical because stress singularities at C and F (Fig. 8) mean the stresses in the concrete at the AC interface near the pulling and plate ends can not be accurately predicted. For this reason, the stresses at AM, which are much less sensitive to the mesh and are not singular, are used for comparison in the rest of this paper.




a) Normal stress $\sigma_y$ b) Shear stress $\tau_{xy}$

Figure 10. Stresses in the adhesive on AM section near the pulling end

**Stresses in the Plate**

Figure 11 shows the distribution of the longitudinal stress on the upper and lower surfaces of the plate in a DoublePull test with a bond length L=100mm. Two boundary conditions were explored for the plate at the loading point: free or fixed vertically. When the loading point is free, the free part of the plate is subjected to pure tension. Within the bonded part of the plate, there are significant bending stresses near the pulling end, with the stress on the upper surface about 30% larger than that on the lower surface at about 10mm from the pulling end. The bending effect decreases gradually as distance from the pulling end x (Fig. 7a) increases and becomes insignificant at about x=40mm. Near the plate end, the bending effect becomes significant again though the average stress approaches zero. The stress is larger on the lower surface than that on the upper surface here.

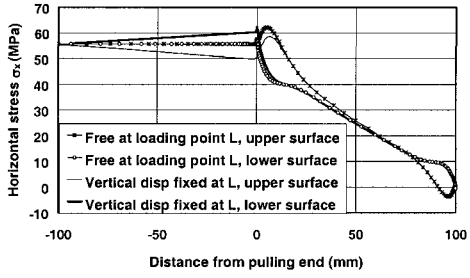



Figure 11. Horizontal stress $\sigma_x$ in the plate for double shear pulling test

When the loading point is fixed vertically, the reaction force there results in linearly increasing bending stresses in the plate within the free part of the plate. The distributions of bending stresses within the bonded part of the plate are almost identical to those with a free loading point, except they are slightly smaller within x<20mm. The interfacial shear stress at PA is usually found from the difference of adjacent two strains, measured on the upper surface along the bonded part of the plate in experimental studies (e.g. Swamy *et al.* 1986). This method is accurate only when the plate is subjected to pure tension within the bonded part. The existence of significant bending stresses within the plate means that the method can lead to significant errors, especially near the pulling end.

These results show that the two boundary conditions at the loading point result in similar stress distributions within the bonded part of the plate excepting small differences within x<20mm. Results show that this statement also stands for stresses at AP, AC and AM. In all following analyses, the loading point was fixed (which may be closer to practical conditions).

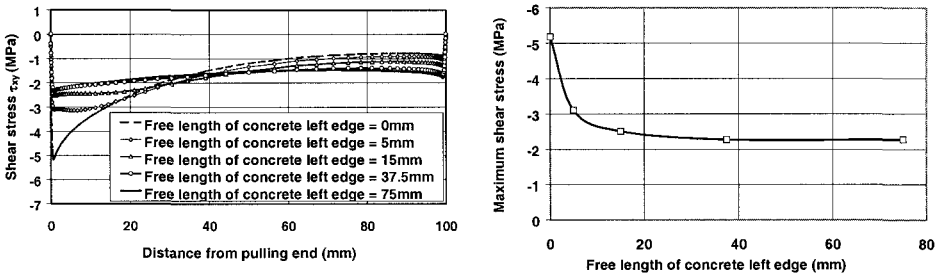
**Boundary Conditions for Double Shear Pushing Test**

In double or single shear pushing tests (Figs. 2 and 4), the pushing force on the concrete block is usually the reaction force at the supporting wedge or plate. The plate is usually very thick so it was modelled as a stiff support here. The effect of the plate size, which naturally varies in practical tests, is the chief objective of this study. Only the DoublePush test was modelled here, but the results shall also apply to the single shear-pushing test.

Five boundary conditions at the left edge of the concrete block were used. They are identified with the length of the free edge near the pulling end (the rest of the left edge was constrained horizontally). These lengths were 0, 5, 15, 37.5 and 75mm respectively for the five cases, corresponding to that the whole edge, 14/15, 4/5, 1/2 and only the mid-height point of the left edge were horizontally constrained respectively. Figure 12a shows the shear stress distribution on AM. When the free edge is greater than 37.5mm, the size of the support has little effect. When it is reduced to 15mm, the shear stress is up to 25% larger near the pulling end and up to 25% smaller near the plate end compared with only one mid-height point support. When the whole concrete edge is constrained, the shear stress is up to 100% larger than that with only one point constraint.

Figure 12b shows that the maximum shear stress near the pulling end decreases very fast when the length of free concrete edge increases if this length is small (<15mm). Shear stress in the adhesive is believed to play a key role in the failure of such joints. Although it is difficult to quantitatively relate the linear elastic predictions here to the bond strength (failure load), it can be expected that a large support plate can result in smaller bond strength. If the support plate has the similar size of the concrete cross-section, a few millimetres difference of the plate size may lead to significant difference of the test result.

Because results are insensitive to the length of concrete free edge when it is greater than 37.5mm, one half of the left concrete edge was constrained for DoublePush (Fig. 7c) and SinglePush (Fig. 7d) tests in the following analyses. However, it should be kept in mind that such predicted maximum shear stresses are the lower bound for these tests.



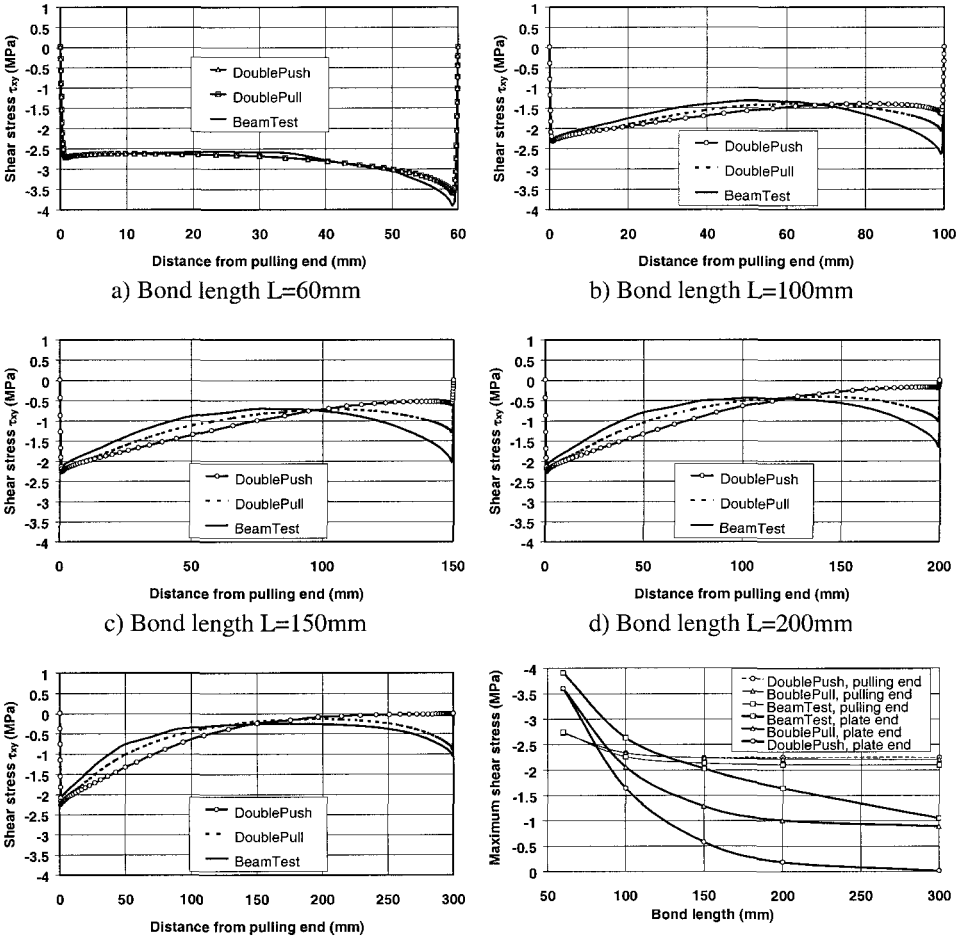

a) Shear stress b) Maximum shear stress near pulling end

Figure 12. Effect of support at the left edge of the concrete on shear stress on AM

## EFFECT OF TEST METHODS

An extensive parametric study was carried out to compare the stress distributions in the five test set-ups. Comparison showed that stress distribution has little difference between the double and single shear pushing tests and between the double and single shear pulling tests.

Therefore, only DoublePull, DoublePush and BeamTest are compared in the following discussion. Due to the limits on discussion length, only the shear stress at AM is compared. There is little difference between the shear stress distributions for DoublePush and DoublePull tests when the bond length L=60mm (Fig. 13a). Shear stresses vary little within x<30mm for all the three methods and they gradually increase thereafter to reach peaks near the plate end. Compared with shear tests, shear stress in BeamTest is slightly smaller in mid-parts of the adhesive length but larger near the plate end.




a) Bond length L=60mm

b) Bond length L=100mm

c) Bond length L=150mm

d) Bond length L=200mm

e) Bond length L=300mm

f) Maximum shear stress

Figure 13. Shear stresses at AM

When L is increased to 100mm (Fig. 13b), both DoublePush and DoublePull tests again predicted almost the same shear stress near the pulling end. The shear stress decreases continuously from the pulling end but starts to increase again at between x=70-90mm and peaks near the plate end in both shear test methods. The peak near the plate end is significantly larger in the pulling (than pushing) test, but it is smaller than that near the pulling end in both tests. The shear stress in DoublePull is now smaller in the mid-parts of the

adhesive length and larger near the plate end than that in DoublePush. In BeamTest, the shear stress decreases more quickly when x<40mm and increases more quickly when x>60mm than that in the shear tests. The peak near the plate end has a much higher value than in shear tests and it is still higher than that near the pulling end. A similar trend exists when L increases to 150mm (Fig. 13c) and 200mm (Fig. 13d), except that the peak near the plate end vanishes in DoublePush and its value is now smaller than that near the pulling end in other two tests. When L increases to 300mm, the shear stress reduces to zero at about x=230mm and keeps at zero thereafter in DoublePush test (Fig. 13e).

Figure 13f shows variation of the peak shear stresses near the pulling and the plate ends with L. The peak stress near the pulling end reduces slightly as L increases from 60 to 150mm for all three tests. They remain almost unchanged when L further increases. The value in BeamTest is slightly smaller than that in shear tests. This value is the same in both shear tests, but it should be noted that the value in the pushing test is the lower bound due to the effect of the support plate size as discussed earlier. It may thus be expected that the bond strength would be lowest if obtained from shear pushing tests when the specimen fails from the pulling end.

The peak shear stress near the plate end is higher than that near the pulling end when L is small in all the three test methods. It reduces quickly as L increases and becomes smaller than that near the pulling end. It decreases fastest in DoublePush test and reaches zero when L is sufficiently large. This peak stress decreases slower in DoublePull test and remains almost unchanged as L further increases from 200mm to 300mm. It decreases slowest in BeamTest. Based on this analysis, it may be expected that the failure of a specimen may start from the plate end if L is small but may start from the pulling end if L is large. The value of L for the transition of these two failure modes would be dependent on the adopted test method, with that in BeamTest being the largest and that in DoublePush test the smallest.

## CONCLUSIONS

This paper has presented a review of experimental methods used for the FRP or steel plate to concrete bond strength test. An FE study has analysed the stress distributions in these different methods. Based on interpretation of numerical results, it is concluded that the size of support plate in shear pushing tests can have very significant effect on the tested bond strength if its size is close to the cross-sectional area of the concrete block. Numerical results also indicate that two failure modes are possible: one starting from the plate end when the bond length is small and another starting from the pulling end if the bond length is larger. The transition bond length between these two failure modes would be dependent on the adopted test method, with that in the bending test being largest and in the shear pushing tests being smallest. The bond strength can be significantly dependent on the adopted test method. In general, the bond strength obtained using the bending test can be highest and that obtained using the shear pushing tests can be the lowest. Little difference can be expected between the double and single shear pushing tests, and between the double and single shear pulling tests.

## REFERENCES

Bizindavyi, L. and Neale, K.W. (1999) "Transfer lengths and bond strengths for composites bonded to concrete", *ASCE Jnl of Composites for Constructions*, 3(4), 153-160.

Brosens, K. and Van Gemert, D. (1997) "Anchoring stresses between concrete and carbon fibre reinforced laminates", *Non-Metallic (FRP) Reinforced Concrete Structures, Proc., 3rd Int. Symp.*, 1, Oct., 271-278.

Chajes, M.J., Finch, W.W., Jr., Januszka, T.F. and Thonson, T.A., Jr. (1996) "Bond and force transfer of composite material plates bonded to concrete", *ACI structural Jnl*, 93(2), 295-303.

Chen, J.F. and Teng, J.G. (2001a) "Shear capacity of FRP strengthened RC beams: FRP debonding", To be published.

Chen, J.F. and Teng, J.G. (2001b) "Anchorage strength models for FRP and steel plates bonded to Concrete", accepted by *ASCE Journal of Structural Engineering*.

Fukuzawa, K., Numao, T, Wu, Z., Yoshizawa, H. and Mitsui, M. (1997) "Critical strain energy release rate of interface debonding between carbon fibre sheet and mortar", *Non-Metallic (FRP) Reinforcement for Concrete Structures, Proc., 3rd Int. Symp.*, 1, 295-302.

Garden H. N. and Hollaway L. C. (1998) "An experimental study of the anchorage length of carbon fibre composite plates used to strengthen reinforced concrete beams", *Construction and Building Materials*, 12(4), 203-219.

Hein, V.L. and Erdogan, F. (1971) "Stress singularities in a two-material wedge", *International Journal of Fracture Mechanics*, 7(3), 317-330.

Hiroyuki, Y. and Wu, Z. (1997) "Analysis of debonding fracture properties of CFS strengthened member subject to tension", *Non-Metallic (FRP) Reinforcement for Concrete Structures, Proc., 3rd Int. Symp.*, 1, Oct., 287-294.

Horiguchi, T. and Saeki, N. (1997) "Effect of test methods and quality of concrete on bond strength of CFRP sheet", *Non-metallic (FRP) Reinforcement for Concrete Structures, Proc., 3rd Int. Symp.*, 1, 265-270.

Jones, R., Swamy, R.N., Bloxham, J. and Bouderbalah, A. (1980) "Composite behaviour of concrete beams with epoxy bonded external reinforcement', *Int. Jnl Cement Composites*, 2, 91-107.

Kobatake, Y., Kimura, K. and Ktsumata, H. (1993) "A retrofitting method for reinforced concrete structures using carbon fibre", *Fibre-reinforced-plastic (FRP) reinforcement for concrete structures: properties and applications,* Elsevier Science Publishers, 435-450.

Maeda, T., Asano, Y., Sato, Y., Ueda, T. and Kakuta, Y. (1997) "A study on bond mechanism of carbon fiber sheet", *Non-Metallic (FRP) Reinforcement for Concrete Structures, Proc. 3rd Int. Symp.*, 1, 279-285.

Neubauer, U. and Rostásy, F.S. (1997) "Design aspects of concrete structures strengthened with externally bonded CFRP plates", *Proc., 7th Int. Conf. on Structural Faults and Repairs*, ECS Publications, Edinburgh, 2, 109-118.

Smith, S.T., Teng, J.G. and Chen, J.F. (2001) "Debonding in FRP plated RC beams induced by intermediate cracking", Proceedings, *ACUN-3 International Composites Conference: Technology Convergence in Composites Applications*, 6-9 February, Sydney, Australia.

Swamy, R.N., Jones, R. and Charif, A. (1986) "Shear adhesion properties of epoxy resin adhesives", *Proc., Int. Symp. on Adhesion between Polymers and Concrete*, 741-755.

Täljsten, B. (1997) "Defining anchor lengths of steel and CFRP plates bonded to concrete", *Int. Jnl Adhesion and Adhesives*, 17(4), 319-327.

Teng, J.G., Chen, J.F., Smith, S.T. and Lam, L. (2000) "*Structural Retrofitting using FRP Composites*", The Hong Kong Polytechnic University, Hong Kong, China, 134pp.

Teng, J.G., Zhang, J.W. and Smith, S.T. (2001) "Interfacial stresses in RC beams bonded with a soffit plate: a finite element study", to be published.

Van Gemert, D. (1980) "Force transfer in Epoxy-bonded steel-concrete joints", *Int. Jnl of Adhesion and Adhesives,* No. 1, 67-72.

Ziraba, Y.N., Baluch, M.H., Basunbul, A.M., Azad, A.K., Al-Sulaimani, G.J. and Sharif, I.A. (1995), "Combined experimental – numerical approach to characterisation of steel-glue-concrete interface", *Materials and Structures*, 28, 518-525.

# Codes

# JSCE Design Recommendations for Upgrading of RC Members by FRP Sheet

K. MARUYAMA, Nagaoka University of Technology, Nagaoka, Japan,
T. UEDA, Hokkaido University, Hokkaido, Japan

## INTRODUCTION

Continuous fiber reinforced polymers (FRP's) have become attractive for design engineers as retrofit or strengthening materials for the existing RC structures after the disaster caused by the Great Hanshin Earthquake in 1995. High strength, lightweight and easy handling of FRP sheets become strongly beneficial for retrofit or strengthening of RC structures. Authorities in Japan, such as Railway Technical Research Institute, Japan Highway Public Corporation as well as the Ministries of Construction and Transportation, have been studying the effectiveness of FRP sheets for retrofit or strengthening of existing RC structures. With a lot of experimental works they have made their own design guidelines for their specific applications with specified type of fiber [1-5].

Considering the situation of FRP sheets applications in Japan, the Japan Society of Civil Engineers (JSCE) decided to establish the unified and more widely applicable design recommendations of FRP sheets for retrofit or strengthening of the existing concrete structures as well as repair and enhancement of durability of concrete structures. Since 1998 the authors have been working as a chairman and co-chairman in the JSCE research committee to establish the design recommendations of FRP sheet for upgrading of RC structures. The recommendations are now published both in Japanese and in English.

Different from the other recommendations, the recommendations are formatted and described based on the performance of RC structures with FRP sheets [6-8]. It means that the descriptions in the design part are made as how to evaluate the contribution of FRP sheets in terms of flexure, shear and ductility of RC members as well as enhancement of durability.

The recommendations involve other features, such as the construction part, the proposed test methods for FRP sheets and field applications. This paper describes the essence of the recommendations.

## CONTRIBUTION OF FRP SHEET TO THE FLEXURAL CAPACITY

The contribution of FRP sheet to the flexural capacity of concrete members can be evaluated by the traditional flexural theory such that plane sections remain planes, only when the peeling of sheet is not expected. The happening of peeling can be estimated by examination of tensile stress of the sheet at the location of flexural cracking. When the tensile stress of sheet can satisfies the eq.(1), then peeling can be neglected.

In the equation, the interfacial fracture energy Gf is introduced. The value can be obtained by the proposed test method for the bond properties of FRP sheet. When there is no test

*FRPRCS-5*, Thomas Telford, London, 2001.

date, then 0.5 N/mm is recommended.

$$f_f \le \sqrt{2G_f E_f / n_f \cdot t_f} \tag{1}$$

where, $f_f$: tensile stress of sheet calculated at flexural cracking, $G_f$: fracture energy of peeling of sheet, $E_f$: elastic modulus of sheet, $n_f$: number of layers of attached sheet, $t_f$: thickness of sheet

## CONTRIBUTION TO SHEAR CAPACITY

The contribution of FRP sheet to the shear capacity of RC member can be evaluated by the traditional truss model as shown below. However, the ultimate stress of sheet in the truss model should be estimated properly because the FRP sheet is quite elastic up to failure and has no stress redistribution (Fig.1).

$$Vu = Vc + Vs + Vf \tag{2}$$

$$Vf = K \cdot Af \cdot f_f \cdot z \cdot (\sin\alpha + \cos\alpha)/s_f \tag{3}$$

Where, $Vu$: ultimate shear capacity of RC members with FRP sheet, $Vc$: concrete contribution, $Vs$: contribution of shear reinforcing bars, $Vf$: contribution of FRP sheet, $K$: coefficient of effectiveness of CFRP sheet, $Af$: cross sectional area of FRP sheet, $f_f$: tensile strength of FRP sheet, $z$: lever arm length, $\alpha$: angle of fiber to longitudinal direction, $s_f$: =1 or spacing of FRP strip.

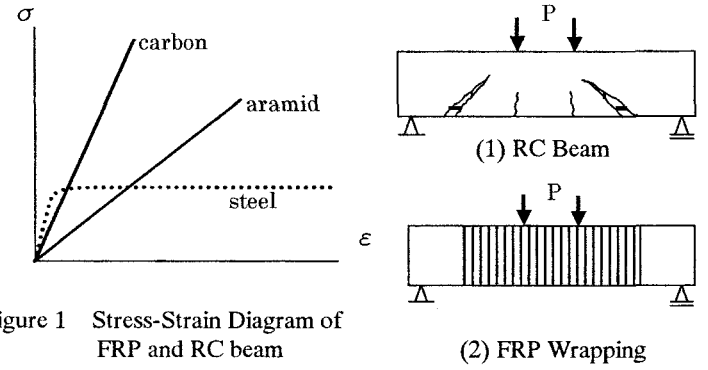



Figure 1 Stress-Strain Diagram of FRP and RC beam

Comparing with steel reinforcement, FRP's (both carbon fiber and aramid fiber) are quite elastic up to failure with less ultimate strain as shown in Fig.1. This property prevents strain redistribution which is typical phenomenon with steel reinforcement because steel has yielding property. In other words all steel stirrups within the length equivalent to the effective depth in a shear span, can carry the yield stress at the ultimate. On the other hand, FRP sheet can not transfer stresses uniformly within a shear span and has the stress concentration. Therefore, the equation derived from the truss model should account for the non strain redistribution of FRP using K factor. Otherwise, the contribution of FRP sheet to the shear capacity can not be evaluated properly.

The committee surveyed previous test results widely and reevaluated the contribution of the sheet using the tensile strength, the modulus of elasticity, the cross sectional area of FRP sheet as well as the concrete strength. With a lot of parametric studies, the K factor is proposed in the following form.

$$0.4 \le K = 1.68 - 0.67R \le 0.8 \tag{4}$$

$$R = (\rho_f \cdot E_f)^{1/4} \left(\frac{f_{fud}}{E_f}\right)^{2/3} \left(\frac{1}{f'_{cd}}\right)^{1/3} \qquad 0.5 \le R \le 2.0 \tag{5}$$

Where, $\rho_f = A_f/(b_w \cdot s_f)$ , $E_f$: modulus of elasticity of FRP sheet, $f_{fud}$: design strength of FRP sheet, $f'_{cd}$: concrete strength.

The effectiveness of the equation is shown in Fig.3 . The equation is still empirical and has a limit for application because the collected data are limited within the ranges of d=200-540 mm, a/d=1.1-3.6, f'c=21-45MPa, $f_f$=2480-4300MPa, $E_f$=87-252GPa.

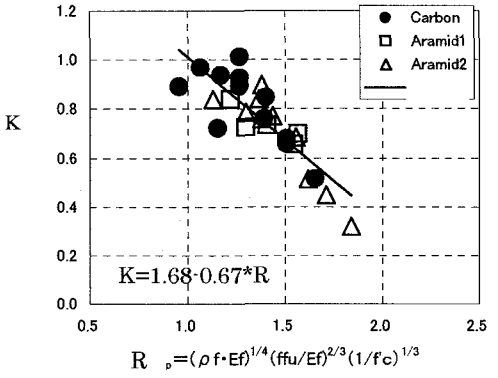



Fig.2 Correlation of K with R by test results

## CONTRIBUTION TO DUCTILITY

Mechanism on how FRP sheet contributes to the ductility of RC members is much more complicate than that on how the sheet contributes to the shear capacity. Even for ordinary RC members, the ductility is still difficult to determine analytically. It is, however, observed in the experimental works that RC members with relatively higher shear capacity to flexural capacity exhibit large ductility. This fact is taken in the JSCE seismic design code for concrete structures expressing that the ductility ratio is a linear function of the ratio of shear capacity to flexural capacity.

The contribution of FRP sheet to ductility can not be attributed only to the increase of shear capacity by sheet, but also to the confinement of cracked concrete by sheet wrapping (Fig.3). Conducting the parametric study of existing experimental data, the following equation is proposed.

$$\mu = 1.16 \cdot \frac{(0.5V_c + V_s)}{V_{mu}} \cdot \left(1 + \alpha_o \cdot \frac{\varepsilon_f \cdot p_f}{V_{mu}/(B \cdot z)}\right) + 3.58 \tag{6}$$

where, $\mu$: ductility ratio (ratio of yield deformation to ultimate deformation), Vmu: shear force at the ultimate flexural capacity, B: width, $\alpha o$: coefficient (same value of Young's modulus of steel can be taken) .

The equation is verified as shown in Fig.3. The equation has also a limit for application since the collected data are within the ranges of d=300-800 mm, a/d=4.0-5.7, f'c=18-24MPa, ff=2050-3430MPa, Ef=78-252Gpa, axial stress=3.2-5.9MPa. Different from the contribution to shear capacity, the contribution of sheet to ductility depends upon the existing structural performance. As mentioned before, FRP sheet wrapping increases both the shear capacity and the confinement effect of cracked concrete. These effects should provide the member a large deformation capacity.

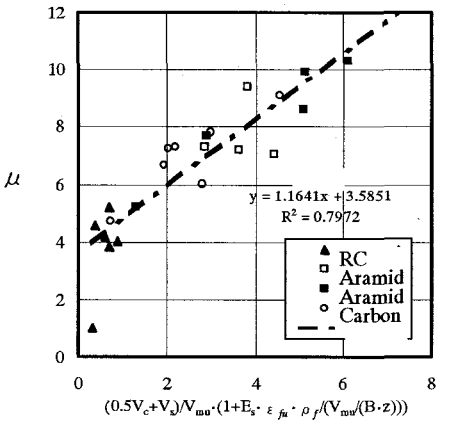



Fig. 3 Correlation of $\mu$

## CONSTRUCTION PRACTICE

The proposed evaluation equations in the recommendations are based on the proper construction practice. In particular, the bond between FRP sheet and concrete is most of importance. A lot of attention has to be paid on how to treat adhesive materials, on how to treat the surface of concrete, on how to attach sheets and to cure them. The chapter of construction practice represents a summary of extended experiences from the actual execution of upgrading works on site. Inspection at each stage of construction is necessary for completing the good works. Finally, there are still many things left to the workmanship for conducting the upgrading works by use of FRP sheet. It may be necessary to establish a system to examine the workmanship for ensuring the proper construction practice of FRP sheets.

## TEST METHODS

The committee proposed 9 test methods to determine the mechanical and durable properties of FRP sheet. Those are to determine (1) tensile strength of sheet, (2) anchorage strength between sheets, (3) bond strength between sheet and concrete, (4) bond strength between sheet and steel plate, (5) adhesive strength between sheet and concrete, (6) tensile fatigue strength of sheet, (7) accelerated exposure test, (8) freezing and thawing test, and (9) resistance against water, acid and alkali. Most of test methods are concerned with the property of sheet itself, but the bond test represents the interface strength among sheet, adhesive material and the surface condition of concrete. Since the tensile strength of sheet and the bond strength between sheet and concrete are important to the contribution of sheet to the flexural and shear capacity of RC members, some aspect of the test method is discussed.

**Tensile Strength Test Specimens**

The shape and size of specimen are shown in Fig.4 and table 1. The previous studies show that the specimen gives good results for both carbon fiber sheet and aramid fiber sheet.

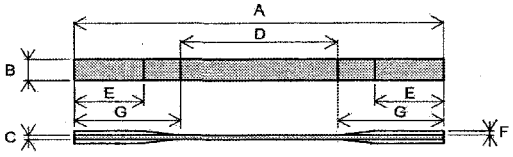



Fig. 4 Tensile test specimen

Table 1: Dimension of specimen (unit: mm)

| A | B | C | D | E | F | G |
|---|---|---|---|---|---|---|
| ≧200 | 12.5±0.5 | ≦2.5 | ≧100 | ≧35 | 1 - 2 | ≧50 |

**Bond Strength Test**

Test specimen is shown in Fig. 5. Two concrete blocks (100 x 100 x 300 mm) are aligned to match the center of cross section. Each has a steel bar mounted at the center of cross section. After alignment of two blocks, two FRP sheets (more than 50 mm width x 400mm length) are attached on the opposite sides. In order to obtain consistent data, sheets in one side should be anchored sufficiently. The left parts of sheets are measured. The load is applied by pulling a steel bar at the both ends. Strain gages should be attached on the both surfaces of sheet. Based on the strain distribution of sheet as shown in Fig. 6, the bond strength is determined.

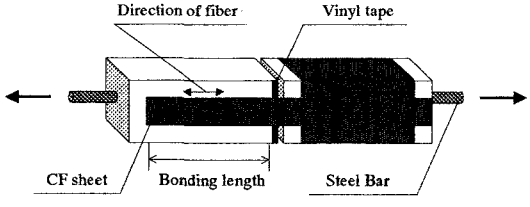



Fig. 5 Test Specimen for Bond

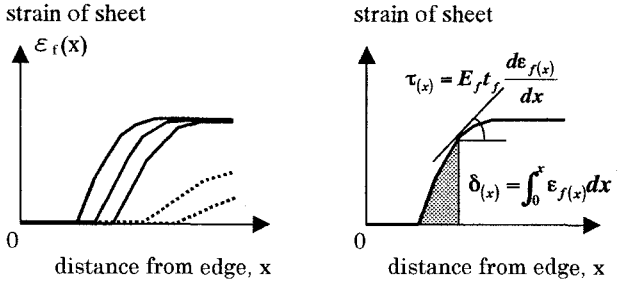



Fig. 6 Strain Distribution of Sheet

## CONCLUDING REMARKS

FRP sheets have advantageous material properties, such as high strength, lightweight, high resistance to corrosion. Making the application of FRP sheets to upgrading structures more effective, the contribution of the sheet should be evaluated sufficiently in the performance of structures as a whole. JSCE has surveyed the current technical state of the art and published the recommendations for the retrofit and strengthening of RC structures by FRP sheets. The recommendations are, of course, not perfect. With further understandings on the mechanism and with computational invention, the evaluation could be improved by numerical analyses.

## REFERENCES

1. Experimental Research Institute, The Japan Highway Public Corporation, 'Design/Construction Guidelines on the Retrofitting of Reinforced Concrete Bridge Piers using Carbon Fiber (proposal)',(1995) (in Japanese).
2. Railway Technical Research Institute (RTRI), 'Design/Construction Guidelines on the Seismic Retrofitting of Railway Viaduct Columns using Carbon Fiber Sheet', (1996) (in Japanese).
3. Railway Technical Research Institute (RTRI), 'Design/Construction Guidelines on the Seismic Retrofitting of Railway Viaduct Columns using Aramid Fiber Sheet', (1996) (in Japanese).
4. Railway Technical Research Institute (RTRI), 'Design/Construction Guidelines on the Seismic Retrofitting of Subway RC Columns using Carbon Fiber Sheet', (1997) (in Japanese).
5. The Hanshin Highway Public Corporation, 'Design/Construction Guidelines on the Seismic Retrofitting of RC Bridge Piers using Carbon Fiber Sheet', (1997) (in Japanese).
6. The Building Research Institute of Japan, 'US-Japan Research Collaboration on the Hybrid Structures – The Retrofitting Design Guidelines on the Application of Continuous Fiber Sheets', (1998).
7. ACI Committee 440, 'Guidelines for the Selection, Design, and Installation of Fiber Reinforced Polymer (FRP) Systems for Externally Strengthening Concrete Structures', (1999).
8. JSCE Concrete Committee, 'Recommendations for Upgrading of Concrete Structures with Use of CFRP Sheet', (2000)

# Outline of the Japanese Guidelines for Seismic Retrofitting of RC Buildings using FRP Materials

HIROSHI FUKUYAMA, Building Research Institute, Japan,
GUSTAVO TUMIALAN, University of Missouri-Rolla, USA,
YASUHIRO MATSUZAKI, Science University of Tokyo, Japan

## INTRODUCTION

In 1995, the Hyogoken-Nanbu Earthquake caused to the city of Kobe the greatest disaster of the postwar era in Japan. As a result of the inflicted damage and to reduce the impact of potential seismic events in other parts of the country, the Ministry of Construction of Japan promoted a program for the development of effective strategies for seismic retrofitting of buildings. One of the areas targeted by this program was the use of Fiber Reinforced Polymer (FRP) materials.

In September 1999, the Japan Building Disaster Prevention Association (JBDPA) published the "Seismic Retrofitting Design and Construction Guidelines for Existing Reinforced Concrete (RC) Buildings with FRP Materials". These guidelines were developed based on the results of investigations conducted in Japan, mainly after 1995, and reflect the combined efforts of the Japanese academy, industry, and governmental agencies.

## SEISMIC CAPACITY EVALUATION

The "Seismic Capacity Evaluation Standards" [1] and "Guidelines for Seismic Rehabilitation of RC Buildings" [2] are used in conjunction with the guidelines for seismic retrofitting of RC buildings. These guidelines have been used since 1977 as an instrument to evaluate the seismic capacity of existing RC buildings. Since these provisions represent the first step in the retrofitting process, their basic concepts are briefly described in this section. The seismic capacity of a building is quantified by the seismic index $I_s$, which should be estimated for every story and frame direction. It is defined as follows:

$$I_s = E_o \, S_D \, T \tag{1}$$

Where $E_o$ expresses the basic seismic index, $S_D$ is the structural design index, which accounts for plan or story-height irregularities, gravitational and stiffness centroid eccentricities. T represents the time index to account for the degree of deterioration of the building, manifested by cracks and permanent deformations.

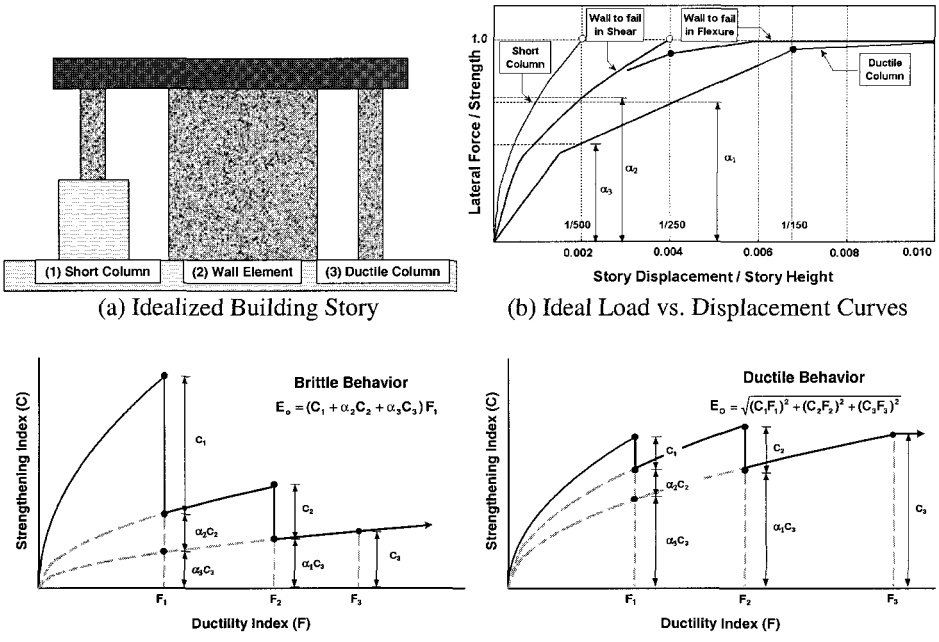
The basic seismic index is a function of the strength index C, and the ductility index F. The basic seismic index $E_o$ is expressed as:

$$E_o = \frac{n+1}{n+i} \, f(C, F) \tag{2}$$

where 'n' is the number of stories and 'i' is the story being analyzed. The seismic index intends to represent the capability of the building story being analyzed to absorb energy. Thus, if a story is assumed to consist of a series of vertical members, such as those illustrated in Figure 1a, the load deflection curves for this story subject to a monotonic load can be

*FRPRCS-5*, Thomas Telford, London, 2001.

represented by the curve shown in Figures 1b. The variable $\alpha$ represents the ratio between the lateral force acting in the element and the capacity of the element. For the computation of $E_o$, predetermined values for $\alpha$ and F are provided by the "Seismic Capacity Standards". The largest value obtained by using the equations illustrated in Figure 1c and 1d is used for the computation of $I_s$.




(a) Idealized Building Story (b) Ideal Load vs. Displacement Curves

(c) Brittle Behavior (d) Ductile Behavior

Figure 1. Seismic Capacity Evaluation

Three procedures are recommended to estimate $I_s$, which are dependable on the characteristics of the story to be analyzed. These procedures can be described as:

- The first procedure is the simplest, which is used for stories with a large density of walls. The ultimate strength is estimated based on the concrete shear strength and cross section area of columns and walls.
- The second procedure requires the calculation of the ultimate capacity and ductility of columns and walls. The beams are usually assumed to be rigid. This procedure is used for "weak column-strong beam" frames.
- The third procedure implies to calculate the ultimate capacity and ductility of the vertical members as well as beams. All the possible mechanisms of failure are taken into account.

Once the seismic index $I_s$ is estimated, this value is compared to a limit index $I_{so}$. If the $I_s$ index is larger than the limit index, the building is expected to have a good performance during a seismic event. Otherwise, the structures must be retrofitted to comply with the requirements of current building standards. Evaluations conducted on damaged buildings due to earthquakes indicated that whenever the $I_s$ indices were less than 0.3 severe damage was observed. Also, when the values of the $I_s$ indices were larger than 0.6, the damage observed in the buildings was moderate. This was evident from the evaluations performed to the building structures after the Hyogoken-Nanbu Earthquake in 1995, where a value of 0.6

indicated the border limit between severe and moderate damage. Thereby, the "Standards for Seismic Capacity Evaluation of RC Buildings" specify a value equal to 0.6 as limit index $I_{so}$ to prevent collapse or severe damage.
When the structures is found to be structurally deficient, new values for C and/or F have to be estimated to meet the structural demand.

## SCOPE OF THE JBDPA GUIDELINES FOR STRENGTHENING WITH FRP

The Japanese guidelines for seismic retrofitting of RC building structures [3] provide specifications on the characteristics of the FRP materials commonly used in Japan, their proper handling and installation. Also, pertaining design and detailing recommendations are provided, which mainly target the shear strengthening of either columns or beams. Some of the main provisions are described in the subsequent sections. The guidelines are part of the "Guidelines for Seismic Rehabilitation of RC Buildings", a comprehensive publication that documents different retrofitting methods utilized in Japan.

## MATERIALS

The JBDPA guidelines describe the properties of PAN-class high-strength carbon fiber sheets, and aramid fiber sheets. In its turn, aramid is sub-classified as aramid 1 (homopolymer) and aramid 2 (copolymer). Carbon fiber sheets are labeled based on the tensile strength of the fiber; whereas, the denomination of the aramid fiber sheets is based on the tensile strength in a width of one meter. The values of tensile strength and modulus of elasticity have been estimated from laminates made of carbon or aramid fibers bound in a resin matrix. Table 1 presents the properties of fibers bound by epoxy or methacrylate resin.

Table 1. Properties of FRP Sheets

| Characteristic | Carbon Fiber | | Aramid Fiber | |
|---|---|---|---|---|
| | 3400 MPa Class | 2900 MPa Class | Aramid 1 | Aramid 2 |
| Type of Fiber | PAN-class High-Strength | | Homopolymer | Copolymer |
| Tensile Strength | $\geq$3400 MPa | $\geq$2900 MPa | $\geq$2060 MPa | $\geq$2350 MPa |
| Young's Modulus | $230^{+45}_{-15}$ GPa | | 118 $\pm$ 20GPa | 78 $\pm$ 15GPa |
| Fiber Density | 1.80 $\pm$ 0.05 | | 1.45 $\pm$ 0.05 | 1.39 $\pm$ 0.05 |

The viscosity of the adhesive resins influences the efficiency of the strengthening work. Thus, if sagging is likely to occur, a resin of higher viscosity is recommended. Also, if smooth impregnation in the fiber is required, a resin with lower viscosity should be used. In the case of primers, epoxy and methacrylate resin are commonly used. Due to potential alterations of the hardening process, it is not allowed to use an epoxy-based primer in combination with a methacrylate-based adhesive or vice versa. In similar way, if the putty material is not compatible with the adhesive and primer resins, imperfect adhesion may occur.

## DESIGN APPROACHES FOR STRENGTHENING OF COLUMNS AND BEAMS

In order to determine the required amount of FRP strengthening, the Japanese guidelines provide expressions to calculate the flexural and shear strengths, and ductility index of RC members. The equations are based on those presented by the "Standards for Seismic Capacity Evaluation" and the "Guidelines for Seismic Rehabilitation of RC Buildings". These equations were developed by Arakawa and Hirosawa, and have been widely used for the design of new construction. Initially, Arakawa developed expressions to calculate the structural capacities of RC beams. Hirosawa modified those equations to make them suitable

to be applied in the analysis of axially loaded members. The definitions of the variables used hereafter are presented at the end of this section.

**Strengthening of Columns**

***Ultimate Flexural Capacity***

The ultimate flexural capacity of a RC column is calculated from the following expressions, which are originally included in the "Structural Regulations of Buildings" (Building Center of Japan, 1997), a guide for structural design of new buildings, which must comply with the "Japanese Building Standard Law".

For $N_{max} \geq N > N_b$:

$$M_u = \left[0.5a_g\sigma_y g_1 D + 0.024(1+g_1)(3.6-g_1)bD^2F_c\right]\left(\frac{N_{max}-N}{N_{max}-N_b}\right) \quad \text{(N-mm)} \tag{3a}$$

For $N_b \geq N \geq 0$:

$$M_u = 0.5a_g\sigma_y g_1 D + 0.5ND\left(1-\frac{N}{bDF_c}\right) \quad \text{(N-mm)} \tag{3b}$$

For $0 > N \geq N_{min}$:

$$M_u = 0.5a_g\sigma_y g_1 D + 0.5Ng_1 D \text{ (N-mm)} \tag{3c}$$

$N_b$, $N_{max}$ and $N_{min}$ can be computed from:

Balanced Axial Force: $N_b = 0.22(1+g_1)bDF_c$ (N) (4a)

Ultimate Axial Force in Compression: $N_{max} = bDF_c + a_g\sigma_y$ (N) (4b)

Ultimate Axial Force in Tension: $N_{min} = -a_g\sigma_y$ (N) (4c)

The shear force associated to the flexural capacity $M_u$ can be computed as:

$$Q_{mu} = \frac{\alpha M_u}{h_o} \quad \text{(N)} \tag{5}$$

A $\alpha$ value equal to two may be used to estimate the shear arm. Figure 2 shows the agreement between the experimental and predicted values when using the previous equations.

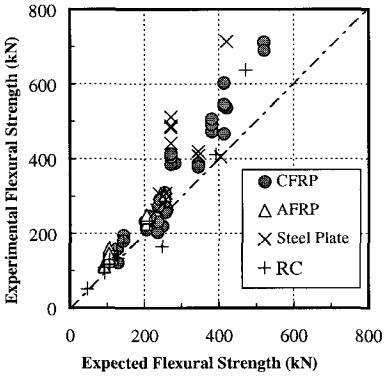



Figure 2. Validation of the Equation for Flexural Strength of Columns

***Ultimate Shear Capacity***

The equation used to quantify the shear capacity of an RC member strengthened with FRP composite systems is also similar to that provided by the "Structural Regulations of Building"

(Building Center of Japan, 1997). The only modification is the addition of the product $p_{wf}\sigma_{fd}$ to the summation $\Sigma p_w\sigma_{wy}$, which intends to take into account the contribution of the FRP reinforcement. Thus:

$$Q_{su} = \left[\frac{0.053p_t^{0.23}(17.6+F_c)}{M/Qd+0.12} + 0.845\sqrt{\sum p_w\sigma_{wy}} + 0.1\sigma_o\right]bj \qquad (N) \qquad (6a)$$

where:

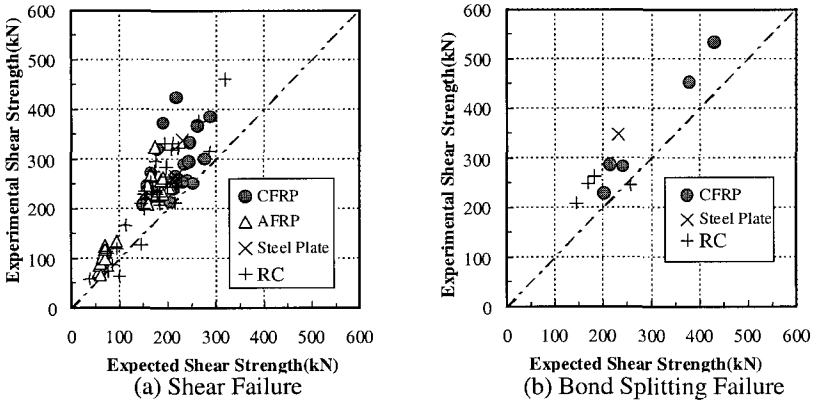
$$\sum p_w\sigma_{wy} = p_{ws}\sigma_{wys} + p_{wf}\sigma_{fd} \le 10MPa \qquad (6b)$$

An upper limit of 10 MPa is imposed to $\Sigma p_w\sigma_{wy}$ based on the fact that a larger amount of strengthening would not significantly increase the shear capacity of the strengthened member. Equation 6a can also be applied to predict the ultimate capacity of columns failing by bond splitting, and columns having longitudinal round reinforcing bars.

Another consideration to mention is that the value of the shear span-to-depth ratio expressed as M/Qd must not be less than one nor larger than three. The tensile strength of FRP for shear design is estimated as: $\sigma_{fd} = \min\{E_{fd}\varepsilon_{fd}, 2/3\sigma_f\}$

The value of $\varepsilon_{fd}$ equal to 0.7% is adopted based on previous investigations, which have shown that the measured strain in the FRP laminate at the final stage, was between 0.5% and 1.5%. These investigations have also shown that specimens strengthened with a large amount of external reinforcement ($p_{wf}E_{fd}$) possessed smaller strains at failure. Along with the first consideration, to avoid the rupture of the FRP laminate, a value of two-thirds of the tensile strength of the FRP laminate was adopted as a margin of safety, when designing for shear.

Figure 2 illustrates a good agreement between experimental and predicted values for shear strength of RC members strengthened with FRP material when shear failure (rupture of the laminate or compression failure of the concrete strut) and bond splitting are observed.




(a) Shear Failure (b) Bond Splitting Failure

Figure 2. Validation of the Equation for Shear Strength of Columns

***Ductility Factors and Ductility Index***

The ductility index F is a function of the ductility factor $\mu$, and can be expressed by the following relationships obtained from a degrading tri-linear hysteresis model.

$$F = \phi\sqrt{2\mu - 1} \qquad (7a)$$

where:

$$\phi = \frac{1}{0.75(1+0.05\mu)} \qquad (7b)$$

The ultimate ductility factor $\mu$ of columns strengthened with FRP materials is expressed as the margin ratio of the shear strength to the shear force associated to the flexural strength. This factor can be calculated as follows:

$$\mu = 10\left(\frac{Q_{su}}{Q_{mu}} - 0.9\right), \text{ where } 1 \le \mu \le 5 \tag{8}$$

It is known that the ultimate shear strength increases when the axial force in the column is increased. Also, the ultimate flexural strength decreases when the axial force is larger than the balanced axial force. This will cause that the associated shear force $Q_{mu}$ decreases, leading to a larger value of ultimate ductility factor $\mu$. Thereby, to avoid the use of larger ductility values, the code specifies to calculate $Q_{mu}$ based on the balanced moment, whenever the axial force exceeds the balanced axial force.

## Strengthening of Beams

### *Ultimate Flexural Capacity*

The ultimate flexural capacity of RC beams is computed by using the following equation:

$$M_u = 0.9a_t\sigma_y d \qquad \text{(N-mm)} \tag{9}$$

The flexural capacity may also be calculated with equation 3b considering a value of axial force equal to zero. The equations provided for the guidelines are for strengthening rectangular RC beams; the influence of the reinforcement of slabs is not considered. The shear force associated to the flexural capacity $M_u$ is calculated as:

$$Q_{mu} = \frac{\alpha M_u}{L_o} \quad \text{(N)} \tag{10}$$

### *Ultimate Shear Capacity*

To estimate the ultimate shear capacity of RC beams strengthened, the term representing the influence of the axial force in equation 6a is dropped, thus:

$$Q_{su} = \left[\frac{0.053p_t^{0.23}(17.6 + F_c)}{M/Qd + 0.12} + 0.845\sqrt{\sum p_w\sigma_{wy}}\right]bj \qquad \text{(N)} \tag{12}$$

Similarly to the case of columns, the value of the shear span-to-depth ratio expressed as M/Qd must not be less than one nor larger than three. In addition the term $\Sigma p_w\sigma_{wy}$ must satisfy the relationship given by equation 6b.

Figure 4 compares the experimental and predicted values for the maximum strength of RC beams strengthened in shear with FRP materials. It is observed that the calculated values by using equation 10 are on the safe side.

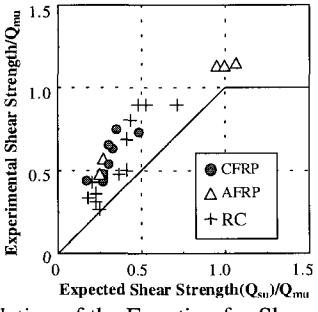



Figure 4. Validation of the Equation for Shear Strength of Beams

***Notation***

$a_g$ : Overall area of the longitudinal reinforcement of the column ($mm^2$)
$a_t$ : Area of the reinforcement in tension of a column or beam ($mm^2$)
$a_v$ : Area of shear reinforcement within a distance equal to the spacing "s" ($mm^2$)
B, D : Dimensions of the columns ($D \geq b$) (mm)
D : Effective depth (mm)
$E_{fd}$ : Modulus of elasticity of the FRP (MPa)
F : Ductility Index
$F_c$ : Compressive strength of concrete (MPa)
$g_1$ : Ratio of distance between the centers of longitudinal reinforcement in tension and compression to the column width.
$h_o$ : Clear height of column
j : Distance between the tensile and compressive force resultants.
(In columns: j = 0.80D. In beams: j = $^7/_8$ d)
$M_u$ : Ultimate Flexural Capacity (N-mm)
M/Q : Shear span (mm). A value equal to half of the column height can be used
N : Axial Force in the Column (N)
$p_t$ : Ratio of tensile reinforcement = $a_t/bd$ (%)
$p_{ws}$ : Ratio of existing shear steel reinforcement to area of contact surface = $a_v/bd$ (%)
$p_{wf}$ : Ratio of FRP reinforcement to area of contact surface = Area FRP/bD (%)
$Q_{mu}$ : Shear force associated to the ultimate flexural capacity (N)
$Q_{su}$ : Ultimate Shear Capacity (N)
$\varepsilon_{fd}$ : Effective Strain of the FRP, taken as 0.7%
$\mu$ : Ultimate ductility factor
$\sigma_y$ : Specified yielding strength of the longitudinal reinforcement (MPa)
For round steel bars: $f_y$ = 295 MPa
For deformed steel bars: $f_y$ = specified strength + 49 (MPa)
$\sigma_{wys}$ : Specified yield strength of the existing transversal reinforcement (MPa)
$\sigma_{fd}$ : Tensile strength of FRP for shear design (MPa)
$\sigma_f$ : Tensile Strength of FRP (MPa)
$\sigma_o$ : Axial stress (MPa), no larger than 7.84 MPa

## SPECIAL PROVISIONS

### Strengthening Without Removal of Mortar Finishing

An advantage of using FRP materials for strengthening RC elements is that the disruption to the building occupants or other individuals in the nearby area is minimum. One source of disruption is that caused by noise, dust and vibration when removing the finishing mortar. Surfaces finished with mortar were very common in Japan up to the mid-1970s, when the need for mortar finishing was basically eliminated with the improvement in formworks. As a principle, the Japanese guidelines require the removal of finishing mortar for strengthening of columns. However, the guidelines present special specifications for the strengthening of RC rectangular columns without removing the finishing mortar, which can be carried out when appropriate control during the execution of the strengthening work is provided. These specifications are based on previous experimental programs, which demonstrated that the shear capacity and ductility are not reduced when columns are wrapped around with FRP materials with the presence of finishing mortar. In addition, based on those researches, to be the strengthening effective, any existing cracks on the finishing mortar have to be repaired prior to installing the FRP system.

It is also specified that surfaces of mortar finishing painted with layers of thick painting materials may remain. The bond strength of these materials must be at least 1 MPa; in addition, they must not have any adverse chemical reaction with the epoxy adhesives. It is not recommended to attach FRP materials to surfaces constituted of plastering, finishing tiles, wallpaper, etc.

The survey of the conditions of the finishing mortar should be based on the number of years of service of the structure, the surface conditions, history of previous repair works and characteristics of finishing mortar. The strength of the mortar is estimated by means of any suitable tool such as Schmidt rebound hammers. Defining $t_m$ as the thickness of finishing mortar and D as the largest cross sectional dimension of the column the following recommendations are provided for the design of the strengthening:

- If $t_m \leq D/15$ and the results of the survey indicate that the mortar finishing can remain, the design is conducted as the mortar finishing had been removed.
- If $t_m > D/15$, the mortar finishing needs to be removed unless a special study is conducted.

In any case, with or without removal of mortar finishing, the lap length is specified to be larger than 200 mm. The radius corner must be larger than 10 mm when AFRP is used, and larger than 20 mm for the case of CFRP wrapping. Due to concrete cover consideration, the radii should not exceed 30 mm for any case.

**Anchoring Systems**

FRP systems that do not completely wrap the entire section will likely peel off from the concrete surface. To develop larger tensile stresses in the laminate, mechanical anchorages can be used at the termination points. Previous investigations demonstrated the use of Schemes C, D, E and F in Figure 5, increased the shear capacity. However, these schemes may not be effective in beams having short span or when the amount of reinforcement increases. It has been observed that the beam can split from the slab along the corners, as illustrated in Scheme C. To account for this, it is advisable to check the level of shear stresses at those corners to foresee the splitting. If the splitting is likely to occur, the guidelines recommend the use of anchorage schemes as those labeled as Schemes A and B.

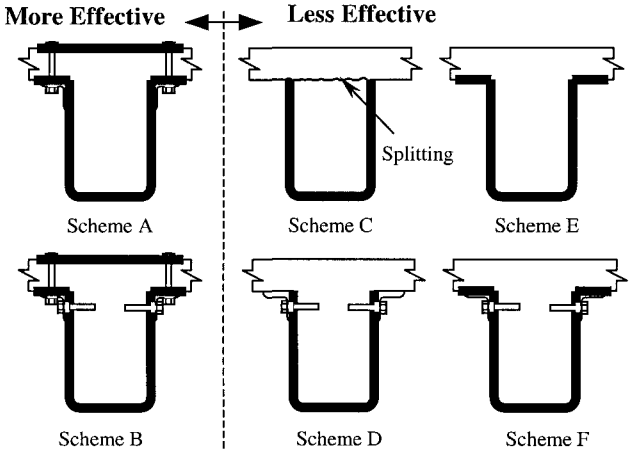



Figure 5. Anchorage Schemes

Specifications should be provided to fully guarantee the effectiveness of angles and bolts, which will ensure the increase of shear strength. The specifications should include the number and strength of bolts. Also, the "L" shapes must be designed to avoid rotation or plastic deformation caused by the tensile stresses in the laminate. Since the corners are not necessarily at 90° degrees, the designer should also provide specifications on the corner preparation and anchorage installation procedures.

## CONSTRUCTION PRACTICE

### Execution of the Strengthening Work

The work activities related to the strengthening of RC building structures should comply with the Contractors Law of the Ministry of Construction of Japan. The JBDPA guidelines provide adequate guidance for strengthening RC members with different combinations of continuous fibers and impregnating resins. These combinations include CFRP/epoxy resin, CFRP/methacrylate, and AFRP/epoxy resin. In its turn, the resins can be one-part or two-parts. Since there are no test results available on AFRP/methacrylate, specifications about this particular combination are not provided. Depending on the fiber-resin combination to be used, the required weight by square meter and the time interval for each step of the FRP installation are specified. As an example, Table 2 presents some specifications when FRP sheets are attached by using epoxy resins or a methacrylate resins.

The strengthening work requires to be inspected after the installation of the FRP systems. This is done to ensure the absence of defects such as blisters, partial peeling and residual resin. If blisters are observed, a resin compatible with the primary resin can be injected. When partial peeling is observed, it is recommended to remove the attached area without damaging the FRP lower layers, and replace it with a new sheet. The new sheet should overlap the existing sheet at least 200 mm. If residual resin is detected, it should be removed using sandpaper without damaging the FRP sheet.

Table 2. Specification for Installation of FRP with one-part resins

| Process | FRP/Epoxy Resin | | FRP/Methacrylate Resin | |
|---|---|---|---|---|
| | Weight of Material ($kg/m^2$) | Time Interval | Weight of Material ($kg/m^2$) | Time Interval |
| Primer | 0.2-0.3 | ≥4 hrs., within 3 days | 0.075-0.1 | ≥60 min. |
| First layer of resin | 0.4-0.5 | Immediately | 0.4-0.5 | ≥5 min. |
| FRP sheet installation | 1.15 $m^2/m^2$ | ≥ 2 min. (for fabric type); ≥ 20 min. (for pre-preg type), within 90 min. | 1.5 $m^2/m^2$ | Within10 min. |
| Second layer of resin | 0.3-0.4 | Immediately | 0.4-0.5 | Within10 min. |
| Air voids elimination | ----- | ≥4 hrs., within 3 days | ----- | ≥60 min. |

### Contractor Qualifications

The engineers and technicians, carrying out the strengthening work, must have been properly trained on the handling of the raw materials and installation of FRP systems. Manufacturers

and public agencies involved with the use FRP materials provide appropriate professional training and certification.

## FINAL REMARKS

Some of the most important provisions of the Japanese guidelines for the retrofitting of RC building structures with FRP materials are presented. The JBDPA guidelines condense the research on seismic retrofitting of RC building structures using FRP materials, which has been conducted in Japan mainly after the Kobe Earthquake. These provisions deal with the proper handling, design and installation of FRP systems used in Japan. Special considerations such as the detailing of anchorage and strengthening of columns in the presence of finishing mortar are also described.

## REFERENCES

[1] Japan Building Disaster Prevention Association (JBDPA). "Standards for Seismic Capacity Evaluation of RC Buildings", April 1977, revised in December 1990 (in Japanese).

[2] Japan Building Disaster Prevention Association (JBDPA). "Guidelines for Seismic Rehabilitation of RC Buildings", April 1977, revised in December 1990 (in Japanese).

[3] Japan Building Disaster Prevention Association (JBDPA). "Seismic Retrofitting Design and Construction Guidelines for Existing Reinforced Concrete (RC) Buildings with FRP Materials", September 1999 (in Japanese).

# Japanese and North American Guidelines for Strengthening Concrete Structures with FRP: A Comparative Review of Shear Provisions

GUSTAVO TUMIALAN, University of Missouri-Rolla, USA
KATSUHIKO NAKANO, Science University of Tokyo, Japan,
HIROSHI FUKUYAMA, Building Research Institute, Japan,
ANTONIO NANNI, Professor, University of Missouri-Rolla, USA

## INTRODUCTION

The increasing uses of FRP materials for the strengthening and upgrade of buildings and infrastructure has motivated the international engineering community to produce guidelines for the proper design, handling and installation of the externally bonded FRP systems. Thus, independent efforts coordinated by different organizations such as the Japan Building Disaster Prevention Association (JBDPA) and the American Concrete Institute (ACI) have led to implementing appropriate provisions. For the case of JBDPA, these provisions were published in 1999, whereas for ACI, they are in the final stages of the approval process, and changes are still possible.

The JBDPA guidelines mainly focus on seismic retrofitting of structural elements, which implies the strengthening for shear of deficient structural elements. This paper describes and comments on some of the design approaches provided in the guidelines of the two aforementioned organizations, particularly, those addressing the shear strengthening of columns. This was one of the main targets of the Japanese experience on infrastructure strengthening, which became an imperative task after the post-earthquake observations of the damage caused by the Kobe earthquake in 1995. Solved examples are developed to better illustrate the guidelines presented in the two documents, and to objectively compare the design procedures.

## DESIGN CONSIDERATIONS

### Shear Provisions in the JBDPA Code [1]

When designing the shear strengthening for columns, the protocol of the JBDPA Code requires the assignment of a ductility index to provide adequate ductility to the member to be retrofitted. This index depends on the ultimate flexural and shear capacities, and is estimated by seismic capacity evaluation standards.

#### *Ultimate Flexural Capacity*

The ultimate flexural capacity of a RC column can be computed as follows:
For $N_{max} \geq N > N_b$:

$$M_u = \left[0.5a_g\sigma_y g_1 D + 0.024(1+g_1)(3.6-g_1)bD^2F_c\right]\left(\frac{N_{max}-N}{N_{max}-N_b}\right) \quad \text{(N-mm)} \quad (1a)$$

For $N_b \geq N \geq 0$:

$$M_u = 0.5a_g\sigma_y g_1 D + 0.5ND\left(1-\frac{N}{bDF_c}\right) \quad \text{(N-mm)} \quad (1b)$$

For $0 > N \geq N_{min}$:

$$M_u = 0.5a_g\sigma_y g_1 D + 0.5Ng_1 D \quad \text{(N-mm)} \quad (1c)$$

The values for $N_b$, $N_{max}$ and $N_{min}$ are estimated as follows:

Balanced Axial Force: $N_b = 0.22(1+g_1)bDF_c$ (N) (2a)

Axial Force in Compression: $N_{max} = bDF_c + a_g\sigma_y$ (N) (2b)

Axial Force in Tension: $N_{min} = -a_g\sigma_y$ (N) (2c)

The remaining variables are defined as:

- N : Axial Force in the Column (N)
- $a_g$ : Overall area of the longitudinal reinforcement of the column ($mm^2$)
- b, D : Dimensions of the columns ($D \geq b$) (mm)
- $g_1$ : Ratio of distance between the centers of longitudinal reinforcement in tension and compression to the column width.
- $\sigma_y$ : Specified yielding strength of the longitudinal reinforcement (MPa)
  - For smooth steel bars: $f_y = 295$ MPa
  - For deformed steel bars: $f_y$ = specified strength + 49 MPa
- $F_c$ : Compressive strength of concrete (MPa)

For the case of RC beams, the ultimate flexural capacity can be estimated as follows:

$$M_u = 0.9a_t\sigma_y d \quad \text{(N-mm)} \quad (3)$$

Another approach to estimate the beam flexural capacity is by considering the axial force equal to zero in equation 1b.

The shear force associated to the flexural capacity estimated by equation is calculated as follows:

$$Q_{mu} = \frac{\alpha M_u}{h_o} \quad \text{(N)} \quad (4)$$

The coefficient $\alpha$ should be accurately calculated; however a value equal to two may be used to estimate the shear arm. The variable $h_o$, represents the clear height of the RC column. The clear span $L_o$ replaces $h_o$ when a RC beam is being analyzed.

***Ultimate Shear Capacity***

The ultimate shear capacity of a RC column strengthened with FRP materials can be calculated by using the following equation:

$$Q_{su} = \left[\frac{0.053p_t^{0.23}(17.6+F_c)}{\frac{M}{Qd}+0.12} + 0.845\sqrt{\sum p_w\sigma_{wy}} + 0.1\sigma_o\right]bj \quad \text{(N)} \quad (5a)$$

where:

$$\sum p_w \sigma_{wy} = p_{ws}\sigma_{wys} + p_{wf}\sigma_{fd} \leq 10 \text{ MPa} \quad (5b)$$

For the analysis of a RC beam the term $0.1\sigma_o$ is disregarded; the rest of the equation remains the same. An upper limit of 10 MPa is imposed to $\Sigma p_w \sigma_{wy}$ based on research, which demonstrated that a larger amount of strengthening would not significantly increase the shear capacity. The value of the shear span-to-depth ratio expressed as M/Qd must not be less than one nor larger than three. If M/Qd is not within this range, the limit values should be taken.

The variables used are defined as follows:

- $p_t$ : Ratio of tension reinforcement
- $p_{ws}$ : Ratio of existing shear steel reinforcement to area of contact surface
- $p_{wf}$ : Ratio of FRP reinforcement to area of contact surface
- $\sigma_{wys}$ : Specified yield strength of the transversal reinforcement in a column
- $\sigma_{fd}$ : Tensile strength of FRP for shear design

$$\sigma_{fd} = \min\left\{E_{fd}\varepsilon_{fd}, \frac{2}{3}\sigma_f\right\}$$

  $E_{fd}$: Modulus of elasticity of the FRP
  $\varepsilon_{fd}$: Effective Strain of the FRP, taken as 0.7%
  $\sigma_f$: Tensile Strength of FRP

- $\sigma_o$ : Axial stress (MPa), no larger than 7.84 MPa
- M/Q : Shear span (mm). A value equal to half of the column height can be used
- d : Effective depth
- j : Distance between the tensile and compressive force resultants. For the case of columns, this value can be estimated as 0.80D, whereas for beams as $^7/_8$d

The value of $\varepsilon_{fd}$ equal to 0.7% is adopted based on investigations, which have shown that the measured strain in the FRP laminate at the final stage was between 0.5% and 1.5%. These investigations have also shown that specimens strengthened with a large amount of external reinforcement ($p_{wf}E_{fd}$) possessed smaller strains at failure. Along with the first consideration and with the purpose to avoid the rupture of the FRP laminate, a value of two-thirds the tensile strength of for design was adopted as a margin of safety, when designing for shear.

***Ductility Factors and Ductility Index***

The ductility index F is a function of the ductility factor $\mu$, which is used when designing the strengthening of columns. It is expressed by the following relationships obtained from a tri-linear degrading hysteresis model:

$$F = \phi\sqrt{2\mu - 1} \quad (6a)$$

where:

$$\phi = \frac{1}{0.75(1 + 0.05\mu)} \quad (6b)$$

The ultimate ductility factor $\mu$ of columns strengthened with FRP materials is calculated as:

$$\mu = 10\left(\frac{Q_{su}}{Q_{mu}} - 0.9\right), \text{ where } 1 \leq \mu \leq 5 \quad (7)$$

To avoid large values of $\mu$, whenever the axial force exceeds the balanced axial force, $Q_{mu}$ should be the shear force associated to the balanced moment.

**Shear Provisions in the ACI Code [2]**

The ultimate shear strength of a RC member strengthened with FRP materials must be larger than the shear demand. Thus:

$$\phi V_n \geq V_u$$

The shear demand is calculated according to the governing load combination specified by the ACI 318 [3]. In similar way the strength reduction factor $\phi$ is equal to 0.85, similar to that adopted by the ACI 318 when designing for shear. The nominal shear capacity of an RC member strengthened with FRP is computed by adding $V_f$, shear contribution of the FRP reinforcement, to the shear contributions of concrete and steel. In this way, the well-known equation provided by the ACI 318 can be modified as follows:

$$\phi V_n = \phi(V_c + V_s + \psi_f V_f) \tag{8}$$

An additional reduction factor, $\psi_f$, is considered to account for the wrapping scheme to be used. Thus, the ACI 440 recommends the use of the $\psi_f$ factors shown in Table 1, for normal-weight concrete applications.

Table 1. Reduction Factor $\psi_f$

| $\psi_f$ | Wrapping Scheme |
|---|---|
| 0.95 | Completely wrapped elements |
| 0.85 | 3-sided "U-wraps" or bonded face plies |

The shear contribution of concrete and the existing internal reinforcement can be calculated by using equations 11-4 and 11-15 in the ACI 318 code. The shear contribution of the FRP is estimated using the following equation:

$$V_f = \frac{A_{fv} f_{fe} (\sin\alpha + \cos\alpha) d_f}{s_f} \tag{9a}$$

where the effective stress $f_{fe}$ in the FRP is the product of the effective strain $\varepsilon_{fe}$ and the modulus of elasticity $E_f$. The area of FRP shear reinforcement with spacing '$s_f$' is computed by:

$$A_{fv} = 2nt_f w_f \tag{9b}$$

The remaining variables are defined as follows:

- $\alpha$ : Angle of inclination of the FRP reinforcement.
- $d_f$ : Depth of the FRP shear reinforcement (in. or mm)
- $s_f$ : Stirrup spacing or pitch of continuous spirals (in or mm)
- $n$ : Number of plies of FRP reinforcement
- $t_f$ : Thickness of one ply of the FRP reinforcement (in. or mm)
- $w_f$ : Width of the plies of FRP (in. or mm)
- $\varepsilon_{fe}$ : Effective strain of the FRP reinforcement at failure (in./in. or mm/mm)
- $E_f$ : Tensile modulus of elasticity of FRP (psi or MPa)

The effective strain $\varepsilon_{fe}$ developed by the FRP system depends on the controlling mode of failure. The ACI code provides recommendations for the determination of this value, which depend on the wrapping scheme to be used. The suggested maximum strain is 0.4%, which is based on experimental results [4]. This limit strain, associated to narrow cracks, assures that aggregate interlock forces can still be transmitted through the shear plane. For completely wrapped elements (all four sides), the following relationship must be satisfied:

$$\varepsilon_{fe} = 0.004 \leq 0.75\varepsilon_{fu} \tag{10}$$

When the strengthening scheme includes the use of U-wraps or laminates bonded to the two shear resisting sides, a debonding failure will likely control the behavior of the strengthened member. Thereby, a reduction of the bond stresses needs to be considered, which is achieved by introducing the bond reduction $\kappa_v$, thus:

$$\varepsilon_{fe} = \kappa_v \varepsilon_{fu} \leq 0.004 \tag{11}$$

The bond reduction factor is a function of concrete strength, strengthening scheme, and laminate stiffness. Khalifa [4] provided a methodology for the computation of the aforementioned factor when U-wraps or two-sides bonded schemes are to be used. Following the philosophy of the ACI 318 code for crack control the total shear reinforcement needs to be limited, thus:

$$V_s + V_f \leq 0.66\sqrt{f'_c}bd \qquad \text{(SI units)} \tag{12}$$

**Environmental Considerations**

The ACI guidelines take account of the durability of the FRP materials when exposed to different environments. The code takes into account the long-term exposure to the environment by multiplying the design ultimate tensile strength $f_{fu}$ and the design rupture stress $\varepsilon_{fu}$, by the so-called environmental reduction factor $C_E$.

$$f_{fu} = C_E f^*_{fu} \tag{7a}$$

$$\varepsilon_{fu} = C_E \varepsilon^*_{fu} \tag{7b}$$

Where, $f^*_{fu}$ and $\varepsilon^*_{fu}$ are the ultimate tensile strength of the ultimate rupture strain of the FRP as reported by the manufacturer. Environmental reduction factors under various exposure conditions for different FRP systems are shown in Table 2. It is understood that these values are conservative and based on the relative durability of each fiber type.

Table 2. Environmental Reduction Factors $C_E$

| Exposure Condition | CFRP | AFRP | GFRP |
|---|---|---|---|
| Interior | 0.95 | 0.85 | 0.75 |
| Exterior | 0.85 | 0.75 | 0.65 |
| Aggressive Environment | 0.85 | 0.70 | 0.50 |

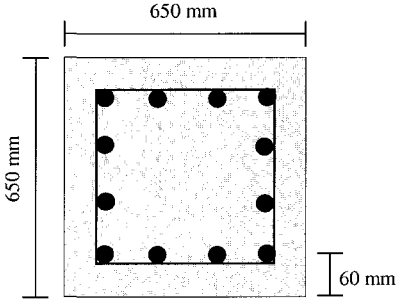
The JBDPA guidelines do not require the reduction of the tensile strength and modulus of elasticity of the FRP materials. The Japanese code requires from the manufacturer to perform heat, alkali and weather resistance tests. It has been demonstrated that the value of the reduced tensile strength due to environment effects is larger that the design tensile strength.

**Anchorage Considerations**

Mechanical anchorages at the end points of the laminates are used as a mean to increase the tensile forces in the in the laminates. When the strengthening strategy requires the anchoring of the reinforcement, the ACI guidelines recommend verifying their effectiveness by a representative testing. The JBDPA guidelines provide different schemes to be considered by the designer. In short-span beams, it has been observed that the beam can split from the slab along the corners; as a result, some of the conventional anchoring schemes may not be effective. Thereby, the level of shear stresses at those corners should be checked to prevent the splitting. If splitting will occur, the JBDPA guidelines provide special anchoring schemes.

**Example of Strengthening Design of a RC Column**

The shear capacity of an interior square column of 650 x 650 mm dimensions requires upgrade. A complete wrapping scheme (Carbon/Epoxy system) has been selected to upgrade the shear capacity of the column in the amount of 245 kN. The ductility index F is estimated as 2.5.




**Material Properties**
Compressive Concrete Strength = 21 MPa
Yielding Strength (longitudinal reinf.) = 345 MPa
Yielding Strength (transversal reinf.) = 295 MPa
Area Longitudinal Bars: 387mm$^2$
Area Transversal Bars: 64 mm$^2$ (spacing=200 mm)
**FRP Properties (according to the manufacturer)**
Guaranteed Ultimate Tensile Strength = 3400 MPa
Guaranteed Rupture Strain = 0.015 mm/mm
Modulus of Elasticity = 230 GPa
Thickness per ply = 0.167 mm

***Preliminary Considerations***

- The depth of the reinforcement 'd' is defined as the distance from the compressive face to the centroid of the tensile steel reinforcement. According to the Japanese practice in the cross section shown above, 'd' is calculated having in consideration the six lower bars; whereas, in the American practice, 'd' would be computed based on the four lower bars.
- In the American practice, the design loads (factored loads) are calculated using different load combinations for the dead, live and seismic loads in order to find the most critical condition. On the other hand, in the Japanese practice the computation of the loads acting on a particular element to be retrofitted consists on just adding those loads.

For the examples the "unfactored" axial forces to be considered are:
Dead Load = 1500 kN
Live Load = 450 kN
Seismic Load = +/- 15

***Design Protocol according to the JBDPA Guidelines***

- Estimate a value for Ductility Index F. The "Japanese Standard for Seismic Capacity Evaluation" provides three screening methods to evaluate the seismic capacity of structural members. The so-called Method 1 has been traditionally known as too conservative. Methods 2 and 3 provide more realistic values for F.
- Calculate the flexural strength of the column by using the appropriate expression of the sets of equations 1 and 2.
- Compute the shear force $Q_{mu}$ associated to the flexural strength by using equation 4.
- Calculate the Ductility Factor $\mu$, which can be computed by using equations 6a and 6b.
- Calculate the required shear strength $Q_{su}$ to satisfy the predetermined ductility index F, by means of equation 7.
- Estimate the required additional reinforcement, which can be achieved by solving equations 5a and 5b for $p_{wf}$.

Strengthening Design:
Calculate $M_u$:
The axial force is calculated as:

N=1500 kN + 450 kN +15 kN =1965 kN
It was previously determined that adding the seismic load rather than subtracting, will cause the most critical condition.

Estimate the balanced axial force $N_b$ from equation 2a:

$$g_1 = \frac{(374\text{mm})}{(650\text{mm})} = 0.575$$

$$N_b = 0.22(1+0.575)(650\text{mm})(650\text{mm})(21\text{MPa}) = 3074\text{kN}$$

Since $N<N_b$ use equation 1b to calculate the flexural capacity:

$$M_u = 0.5(4644\text{mm}^2)(0.394\text{GPa})(0.575)(650\text{mm}) + 0.5(1935\text{kN})(650\text{mm})\left(1-\frac{(1965\text{kN})}{(650\text{mm})(650\text{mm})(0.021\text{GPa})}\right) = 839.1\,\text{kN}-\text{m}$$

Thus, in equation 4: $Q_{mu} = \frac{2(832.4\text{kN}-\text{m})}{(2.4\text{m})} = 699.3\,\text{kN}$

Calculate $Q_{su}$:

$$F = \frac{\sqrt{2\mu-1}}{0.75(1+.05\mu)} = 2.5 \quad \therefore \mu = 2.73$$

Replacing this value in equation 7: $2.73 = 10\left(\frac{Q_{su}}{699.3\text{kN}} - 0.9\right) \quad \therefore Q_{su} = 820.3\,\text{kN}$

Calculate the amount of additional reinforcement:

The ratio of tension reinforcement: $p_t = \frac{As}{bd} = \frac{(6\text{bars})(387\text{mm}^2)}{(650\text{mm})(512\text{mm})} = 0.007$

The shear span-to-depth ratio: $\frac{M}{Qd} = \frac{(1200\text{mm})}{(512\text{mm})} = 2.34$

The axial stress due to N: $\sigma_o = \frac{(1965\,\text{kN})}{(650\text{mm})(650\text{mm})} = 4.65\ \text{MPa}$

In equation 5a:

$$(820.3\text{kN})(1000) = \left[\frac{0.053\left((0.007)(100)\right)^{0.23}\left(17.6+(21\text{MPa})\right)}{(2.34)+0.12} + 0.845\sqrt{\sum p_w \sigma_{wy}} + 0.1(4.65\text{MPa})\right](650\text{mm})\left((0.8)(650\text{mm})\right)$$

$$\therefore \sqrt{\sum p_w \sigma_{wy}} = 1.415$$

Then, the amount of steel reinforcement: $p_{ws} = \frac{A_v}{bs} = \frac{2(64\text{mm}^2)}{(650\text{mm})(200\text{mm})} = 0.0010$

The tensile strength of FRP is calculated as:

$$\sigma_{fd} = \min\left\{(230\text{x}10^3\,\text{MPa})(0.007), \frac{2}{3}(3400\text{x}10^3\,\text{MPa})\right\} \quad \therefore \sigma_{fd} = 1610\text{MPa}$$

From equation 5b: $1.402^2 = (0.0010)(295\text{MPa}) + p_{wf}(1610\text{MPa}) \quad \therefore p_{wf} = 0.0011$

Finally, the number of sheets is:

$$p_{wf} = \frac{2t_{wf}}{b}, \text{ then: } t_{wf} = \frac{(0.0010)(650\text{mm})}{2} = 0.357\text{mm}$$

$$N_f = \frac{t_{wf}}{t_f} = \frac{(0.357\text{mm})}{(0.167\text{mm})} = 2.14 \quad \therefore \text{Use 3 plies of CFRP}$$

***Design Protocol according to the ACI Guidelines***

- Calculate the additional shear force to be resisted by the RC element, which is achieved by subtracting the shear demand $V_u$ from the initial shear capacity due to concrete and steel contributions. The shear demand can be estimated by any suitable structural analysis method.
- Modify the ultimate stress and strain to take into account the service environment conditions by using equations 7a and 7b, and Table 2.
- The shear force to be carried by the FRP material, $V_f$ is estimated by a $\phi$ factor equal to 0.85 and a suitable $\psi$ factor from Table 1.
- Determine the value of the effective strain $\varepsilon_{fe}$ according to the strengthening scheme to be utilized, by using equations (10) or (11).
- The amount of FRP material is computed by means of equations 8a and 8b.
- Verify that the relationship given by equation 12 is satisfied.

Strengthening Design:
Estimate the factored load according the ACI 318 provisions. It was found that the critical condition corresponds to:
$Nu = 0.9N_D + 1.43N_E = 0.9(1500\text{ kN}) + 1.43(15\text{ kN}) = 1371.5\text{ kN}$

The shear contributions of concrete and steel reinforcement are calculated using the equations 11-4 and 11-5 provided by the ACI 318:

$$V_c = \left(1 + \frac{N_u}{14A_g}\right)\left(\frac{\sqrt{f'_c}}{6}\right) bd \text{ (in SI)}$$

$$= \left(1 + \frac{(1371.5\text{kN})(1000)}{14(650\text{mm})(650\text{mm})}\right)\left(\frac{\sqrt{(21\text{MPa})}}{6}\right)(650\text{mm})(590\text{mm}) = 361000\text{N} = 361\text{kN}$$

$$V_s = \frac{A_v f_y d}{s} = \frac{\left(2(64\text{mm}^2)\right)(295\text{MPa})(590\text{mm})}{(200\text{mm})} = 101200\text{N} = 101.2\text{kN}$$

Estimate the design ultimate tensile stress and rupture strain:

Adopting a $C_E$ value of 0.85

$f^*_{fu} = (0.85)(3400\text{MPa}) = 2890\text{MPa}$

$\varepsilon^*_{fu} = (0.85)(0.015) = 0.013$

$\varepsilon_{fe} = 0.004 < 0.75(0.013) = 0.010$

Estimate the shear force to be carried by the FRP material:

$$V_f = \frac{\Delta V_u}{(\phi)(\psi)} = \frac{(245\text{kN})}{(0.85)(0.95)} = 303.4\text{kN}$$

The amount of FRP is calculated by rearranging equation 9a:

$$A_{fv} = \frac{(303.4\text{kN})s_f}{(0.004)(230\text{GPa})(650\text{mm})} = 0.507s_f\,\text{mm}^2$$

Number of plies:

$$n = \frac{0.507s_f}{2(0.167)w_f} = 1.5 \quad \therefore \text{Use 2 plies of CFRP}$$

Then, the shear contribution of the FRP needs to be recalculated by using equation 9b:

$A_{fv} = 2(2\text{plies})(0.167\text{mm})w_f = 0.668w_f\text{mm}^2$

Since the column will be wrapped in its entire height, $w_f = s_f$:

$$V_f = \frac{(0.668w_f\text{mm}^2)(0.004)(230\text{GPa})(650\text{mm})}{s_f} = 400\text{kN}$$

Verify the relationship given by equation 12:

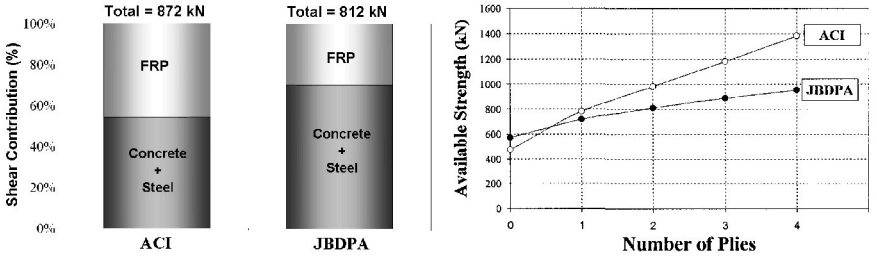
$$V_s + V_f = (101.2\text{kN}) + (400\text{kN}) = 501.2\text{kN} \le 0.66\sqrt{(21\text{MPa})}(650\text{mm})(590\text{mm}) = 1160\text{l}$$

$\therefore$ The condition is satisfied

## SHEAR STRENGTH EVALUATION

The recommendations provided by ACI allow for a larger contribution of the FRP reinforcement. This is evident from Figure 1a which illustrates the percentage of FRP shear contribution to the overall shear strength calculated based on the JBDPA and ACI approaches for a column strengthened with two plies of CFRP. For a column similar to that shown in the example and strengthened with two plies of CFRP, it is observed that according to the ACI guidelines the FRP reinforcement is assumed to carry 45% of capacity. For the case of the JBDPA the FRP contribution represents 30 % of the expected shear capacity.

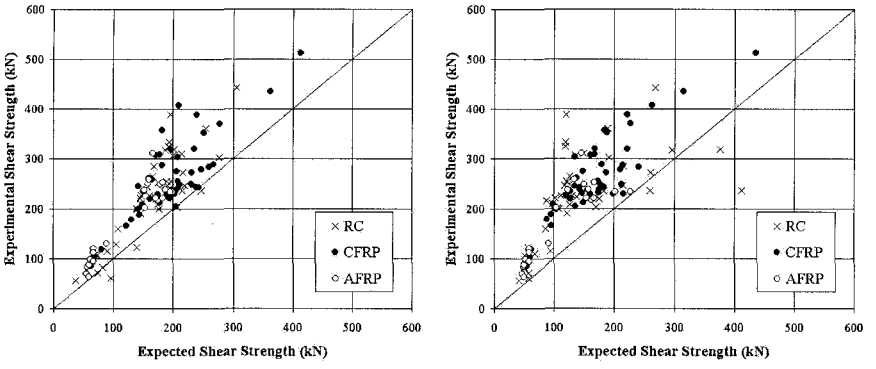
Figure 1b depicts shear strength as a function of the number of plies. The JBDPA guidelines express the contribution of the shear reinforcement as the square root of the summation of the steel and FRP contributions. Compared to the ACI guidelines, this approach increases the difference in the expected values of FRP shear contribution when the number of plies is increased.




(a) Shear Contribution (b) Available Strength

Figure 1. Shear Strength Evaluation

In Figure 2, the data utilized to correlate the experimental and expected values according to the two codes were obtained from over one hundred columns tested in Japan [5]. Most of these specimens were strengthened with one or two plies of FRP laminates, mainly, carbon and aramid. It is observed that the JBDPA approach provides less dispersion of data. It should also be noted that the ACI Code may provide less conservative values only for columns without FRP confinement.




(a) JBDPA Code (b) ACI Code

Figure 2. Shear Strength Comparison

## CONCLUDING REMARKS

The shear provisions provided by the Japan Building Disaster Prevention Association (JBDPA) and the American Concrete Institute (ACI) for the retrofitting of RC members with FRP materials are presented. Comparisons of the design approaches, environmental and anchoring considerations were presented.

## ACKNOWLEDGEMENTS

Special thanks to the Japan International Science and Technology Exchange Center (JISTEC) and the U.S. National Science Foundation (NSF) for providing the funding that made the exchange opportunity with Japan possible; and to the Building Research Institute of the Ministry of Construction of Japan for hosting an exchange researcher. The support of the National Science Foundation Industry/University Cooperative Research Center at the University of Missouri – Rolla is also acknowledged.

## REFERENCES

[1] Japan Building Disaster Prevention Association (JBDPA). "Seismic Retrofitting Design and Construction Guidelines for Existing Reinforced Concrete (RC) Buildings with FRP Materials", September 1999 (in Japanese).

[2] American Concrete Institute (ACI), Committee 440. "Guide for the Design and Construction of Externally Bonded FRP Systems for Strengthening Concrete Structures," September 2000 (document under review).

[3] American Concrete Institute (ACI), Committee 318, "Building Code Requirements for Reinforced Concrete and Commentary," American Concrete Institute, Detroit Michigan, 1999.

[4] Khalifa, A. "Shear Performance of Reinforced Concrete Beams Strengthened with Composites," Doctoral Thesis, Structural Engineering Department, Alexandria University, Egypt, 1999.

[5] Fujii, S., Matsuzaki, Y., Nakano, K., and Fukuyama, H. "Japanese State of the Art on Seismic Retrofitting by Fiber Wrapping for Building Structures: Evaluations," Fourth International Symposium on Fiber Reinforced Polymer (FRP) for Reinforced Concrete Structures, pp. 895-906, Baltimore, Maryland, November 1999.

# Durability of fibre reinforced plastics

# Durability of GFRP composites reinforcing rods in concrete environment

BENMOKRANE, B., WANG, P., TON-THAT, M.T., and LAOUBI, K.
ISIS Canada, Department of Civil Engineering, University of Sherbrooke, Sherbrooke Québec, Canada

## ABSTRACT
Extensive studies have been conducted on the durability of FRP composites for construction at the University of Sherbrooke. Some results from the study on fundamental material properties of GFRP rebars with respect to durability are presented in this paper. More than 400 accelerated ageing tests have been conducted on GFRP bars manufactured by FRP industrial partners. GFRP rebars are grouped into more than 20 types of specimens with different combination of resin matrix, glass fibres, manufacturing parameters, sizing chemistry, sizes and shapes, and surface coatings. The FRP bars have been subjected to different tensile sustained load (22-68% of ultimate strength) using three different loading systems, in various alkaline environments, such as NaOH, simulated alkaline pore water solution, and embedded in moist concrete samples. Time to rupture or residual strength, as applicable, has been determined. Additionally, various micro-structural analysis techniques and absorption measurements have been carried out to understand stress corrosion mechanism of the bars. The results showed clearly that alkaline ions and moisture could penetrate or diffuse through the resin (or through cracks and voids) to the inter-phases and the fibres and damage the FRP reinforcements through many mechanisms which change depending on the type of resin matrix, sizing, stress level, pH of the alkaline environment, and manufacturing process. Furthermore, most of the studied GFRP reinforcing rods in this research project are quite durable in alkaline environments under stress levels corresponding to 25% of the tensile ultimate stress.

## INTRODUCTION
Fibre-reinforced polymer (FRP) composites are increasingly being used in civil infrastructure in applications ranging from reinforcing rods and tendons, wraps for seismic retrofit of columns and externally bonded reinforcement for strengthening of walls, beams, and slabs, composite bridge decks, and composite structural systems. Their use in these applications is predicated on performance attributes linked to their lightweight, high stiffness-to-weight and strength-weight ratios, ease of installation in the field, potential lower systems level cost, and potential high overall durability. Since FRP composites are still relatively unknown to the practising civil engineer and infrastructure systems planner, there are heightened concerns related to the overall durability of these materials, especially as related to their capacity for sustained performance under harsh and changing environmental conditions under load.

Acknowledging that if FRP composites are to be widely accepted in the near future by practicing civil engineers, architects, and planners as construction materials at the same level as conventional materials such as timber, steel and concrete. It is essential to have a reliable database of material properties and a compressive understanding of fracture and failure

*FRPRCS-5*, Thomas Telford, London, 2001.

mechanism of FRP composites with exposed to complex civil engineering infrastructure environments. The international conference [Benmokrane and Rahman, 1998] has clearly demonstrated that durability of FRP composites is still a controversial issue among the engineering community. Recent survey by the ACI subcommittee 440D also indicate that durability is top priority for future research needs with respect to the application of FRP composites in civil engineering infrastructure [Porter 1999]. A gap analysis has been undertaken recently under the agencies of the Civil Engineering Research Foundation (CERF) and the Market Development Alliance (MDA) of the FRP Composites Industry to identify critical gaps in existed durability data for such application. Experts in this field formed seven sub panels to focus on specific information. These sub panels include: moisture/solution, alkali effects, thermal effects, fatigue, creep/relaxation, UV, and fire. Each of the panels complied information against the high priority applications defined by the user panel, which included bridge decks, concrete reinforcement and repair, and structural elements. The preliminary results indicate that there are significant gaps in durability data that need to be addressed [Vistasp et al 2000].

In view of this technical obstacle, a long-term research program has been carried out regarding the durability of FRP rebars for civil infrastructure application at the University of Sherbrooke. The main objectives of this research program aim to improve the durability of FRP rebars for concrete structures, to develop test methodology for the evaluation of alkaline effects on durability of FRP rebars, to establish long term durability database of FRP composites, and to develop service prediction model. This will assist industrial companies to improve the characteristics of their FRP products (types of resins and fibres, manufacturing processes, surface coating, etc) and to enhance their properties regarding long-term durability, and to help engineers and users to utilize this innovative technology with enhanced confidence. Accelerated ageing conditions such as alkaline, saline and acid solution, ultraviolet radiation, wet/dry and freeze-thaw cycles, as well as loading (monotonic, cycles and sustained) are being considered. A major part of this program deals with the fundamental material properties of FRP bars with respect to durability by means of accelerated ageing tests and micro-structural analysis. Some results from the accelerated ageing tests on GFRP rebars under various alkaline environments will be presented in this paper.

## MATERIALS

GFRP rebars (HB, C and IS) produced by three FRP manufacturers, were used in this research program. They were grouped into more than 20 types of specimens with different combinations of matrix types (i.e. vinyl ester, polyester), glass fibre types (i.e. E-glass 366, Advantex 366, and Advantex 712, alkaline resistance glass fibre (AR)); manufacturing parameters; sizes and shapes; and sizing chemistry. Additionally, HB rebar was external helically wrapped bar [Figure 1a]. The C rebar surface had lugs or protrusions [ribbed bar] [Figure 1b]. The IS rebar surface had sand coating (sand coated bar) [Figure 1c]. The tensile strengths of these rebars varied from 530 MPa to 960 MPa and the modulus of elasticity varied from 40 GPa to 50 GPa. The properties of tested rebars are given in Table1.




Figure 1. Some GFRP bars used in this project (a) typical helically wrapped rebar [type HB], (b) typical ribbed rebar [type C], and (c) typical sand coated rebar [type IS]

Table 1. Properties of some tested GFRP specimens

| Rebar types | Fibre type | Matrix type | Fibre content | Diameter (mm) | Manufacturing parameter |
|---|---|---|---|---|---|
| (8*) HB | E-glass 366, AR glass, | P, 5P2V, 1P1V, V | 73-78% | 9.3, 12.4 | MP1 |
| (7*) C | E-glass E/A2, E/A1 | V-PET, V, IS, VE2 | 63-73% | 12 | P1, P2, P3 |
| (7*) IS | E-glass | P, V1, V2 | 71-76% | 9.5, 12.4 | IP1, IP2 |

*Note: P: polyester resin, V, V1, V2: vinyl ester resin, vinyl ester resin 1, vinyl ester resin 2*
*E/A1: Advantex 366, E/A2: Advantex 712*
*AR: alkaline resistance glass fibre*
** : number of GFRP bars types*

## EXPERIMENTAL PROGRAM

GFRP rebar specimens were subjected to a sustained load of 25-68% of the tensile strength in various alkaline environments at different stress levels for a specific period of time. The time to rupture of specimens was recorded and if no rupture occurred during the tests, the residual tensile strength of the aged rebar was evaluated. Figure 2 shows typical GFRP rebar embedded in concrete for durability evaluation, and Figure 3 shows typical test set-up for durability test. Micro-structural analyses were also conducted to study the most significant mechanisms of the stress corrosion, such as matrix cracking, matrix degradation, matrix diffusion, fibre damage, fibre-matrix interface damage, which cause degradation of the rebars were identified. These results yield valuable information on the means to improve rebar durability.



Figure 2. GFRP rebar embedded in concrete for durability evaluation (using loading System 3)

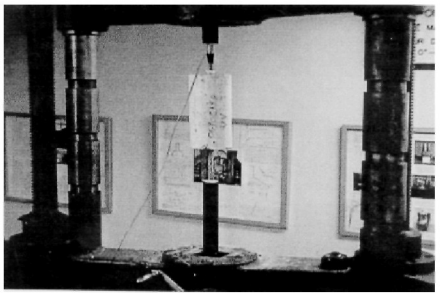
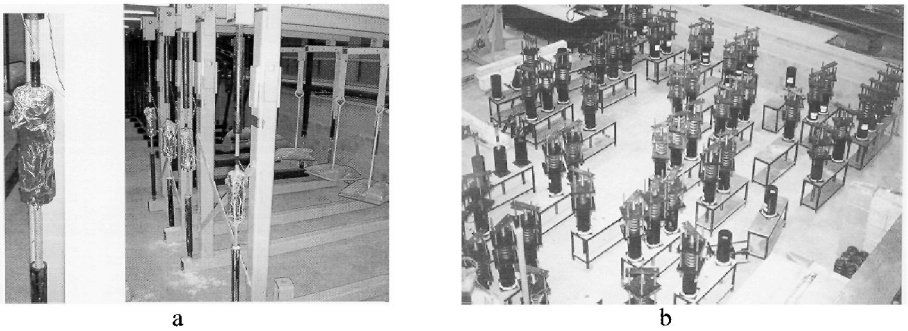


Figure 3. Typical test set-up (Evaluation of residual tensile strength)

### Development of loading systems

Up to now, there was no standard method for evaluating the durability of FRP reinforcing rods used for concrete structures. Therefore, several test methods involving gripping and loading techniques for subjecting GFRP rebar specimens to a constant load as well as in alkaline environments have been investigated [Benmokrane et al 1998]. Because of the relaxation characteristics of the FRP composites, it is very difficult to maintain a specimen under a constant load for a long period of time. In order to choose the most suitable loading techniques for durability tests, several loading Systems have been considered. To overcome disadvantages of the present existing system, new loading Systems were developed, namely loading Systems 1, 2, 3, and 4 [Benmokrane 2000]. Systems 1, 2, and 3 were developed to study the durability of GFRP bars System 4 was developed to evaluate the durability of concrete elements (such as beams) reinforced with FRP bars under different environmental conditions (e.g. freeze-thaw cycles, thermal cycles, moisture, alkalinity and salinity combined

with different loading conditions). Figure 4 shows overview of loading System 2 and loading System 3.



a b

Figure 4. Overview of loading Systems (a) loading System 2, and (b) loading System 3

**Simulated alkaline environments**

The next important issue for the tests was to simulate the alkaline environment of concrete. Currently there are no standard test methodologies for the evaluation of alkaline effects on FRP composites for concrete structures. At first, NaOH solution was used. Even NaOH, one of the strongest alkalis, is not the real alkaline composition of the pore water solution; it was used to accelerate a degradation of the specimens in order to choose the most alkaline resistant bars for the later tests. A more realistic solution simulated from the main alkaline components of pore water solution, such as Ca(OH)2, NaOH and KOH, which has been used to study the durability of GFRP bars.

Degradation of FRP reinforcements in concrete is a complicated process, involving various chemical reactions. For short term, degradation of the GFRP composite bars can be mainly due to reactions with alkali, but for long term, reactions with other components of the pore water solution should also be taken into account. An example of this reaction is oxidation accelerated by heavy metal ions of pore water solution. For a realistic evaluation of the durability of GFRP bars in concrete, it was necessary to do the tests with specimens embedded in concrete.

**Microstructural analysis**

Fundamental material properties of aged and unaged GFRP rebars have been studied using micro-structural analyses techniques to evaluate degradation mechanism (i.e. fibre dominated mechanism, matrix dominated mechanism, inter-phase dominated mechanism or combined mechanism), and penetration of chemical solution into the GFRP bars. Matrix degradation was studied by Infrared Spectrosscopy (IR), Thermal Gravimetry Analysis (TGA), and Differential Scanning Calorimetry (DSC), Matrix cracking was investigated by Energy Dispersive X-ray (EDX), X-ray Elemental Mapping (XEM), light microscopy (LM) and SEM analysis. Fibre damage and inter-phase damage were observed by LM and SEM techniques. Chemical penetrations were determined by EDX, XEM and TGA analysis. Each of these techniques is critical to the complete characterization of GFRP composites as function of environmental exposure and mechanical loading. Diffusibility of polymer matrix is critical to durability of FRP reinforcements. Higher the diffusibility of the matrix, easier the transportation of the moisture, alkaline molecules, and degraded products through the material, resulting in faster degradation process. Since absorption is related to the diffusion behaviour, absorption tests on GFRP bars were conducted to evaluate diffusibility of GFRP bars by means of weight changes and micro-structural analysis.

## SELECTED RESULTS AND DISCUSSIONS

Some selected results from the on-going research project are presented as follows to describe some important factors, which influence the durability of GFRP rebars in alkaline environments.

### Effect of resin matrix

Effect of resin type on the stress-corrosion characteristics of the rebars was investigated. From Table 2 it can be seen that tensile strength of all rebars slightly decreased after aging in simulated pore-water solution under a stress level of 30% for 90 days. The results clearly show that durability of GFRP rebars was influenced by the matrix used. The rebar HB4 made of 100% vinyl ester resin exhibited the highest resistant to stress corrosion in alkali. It is well known that vinyl ester resin has better chemical resistance, even in alkaline environment. A fundamental reason is that in vinyl ester resin the weakest ester linkage is partly replaced by the stronger ether linkage that is highly resistant to alkali. Furthermore, vinylester resin is tougher than polyester because of a longer distance between crosslinks. Thus, if flaws/microcracks pre-exist in a specimen, their growth under stress would be at lower rate in vinyl ester than in polyester.

Table 2. Effect of resin type

| Rebar type | Number of specimens | Stress levels (% of tensile strength) | Number of days under tension | Average retention in tensile strength (%) |
|---|---|---|---|---|
| HB2 | 3 | 30 | 90 | 84.8 ± 5.1 |
| HB3 | 3 | 30 | 90 | 85.6 ± 3.5 |
| HB4 | 3 | 30 | 90 | 96.0 ± 1.1 |

Fujii et al (1993) confirmed that GFRP composites with a tougher vinyl ester matrix performs better than one with a less tough polyester matrix in 5% $HNO_3$ in terms of resisting crack generation. However, crack resistance of tougher vinyl ester matrix only appears to a certain extent. Current studies indicate that vinyl ester resin can provide protection at relatively lower stress level, which was found to be 25% of ultimate tensile strength in NaOH solution (pH=13.6). This value was believed to be critical stress level which was required to initiate micro-cracking for vinyl ester resin matrix in NaOH solution (pH=13.6).

### Effect of fibre types

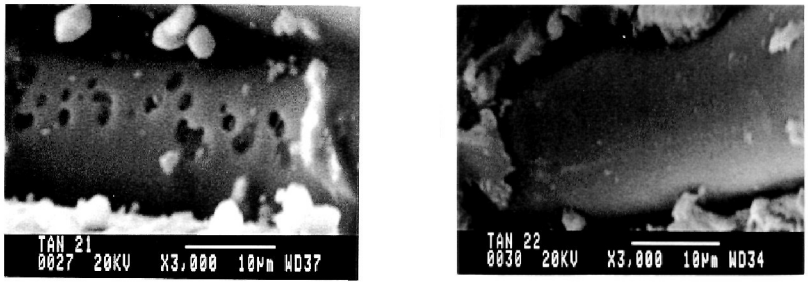
Rebar specimens were immersed in simulated pore water solution and kept at the same constant stress level of 30% for 90 days and 140 days. SEM analysis was conducted on two specimens C6 and C7, which were produced with same resin matrix but different glass fibre types. More fibre pullout and less fibre damage were observed in the C7 than in the C6 [Figure 5]. The difference in failure morphologies between the two is due to the glass fibre used. C7 is based on E-glass 366 Advantex, and C6 is based on normal E-glass fibre. This indicates that E-glass 366 Advantex, is more alkaline resistance than the normal E-glass.

Accelerated aging tests were conducted on three types of alkaline resistance glass fibre (AR) reinforced GFRP rebars with different resin matrix, namely, HB5 (AR/polyester), HB6(AR/vinyl ester), HB7(AR/polyester and vinyl ester), and one E-glass reinforced GFRP rebars (E glass/vinyl ester), namely HB8. Table 3 shows residual tensile strengths of GFRP rebar specimens after immersed in simulated pore solution and embedded in concrete under 30% stress level for 140 days. For specimens immersed in simulated pore water solution, no significant decrease in their tensile strength was observed for HB5, HB6, and HB7. However, 17% loss was observed for the result on HB8. For specimens embedded in concrete, HB5,

HB6, and HB7 did not show any loss in their residual strength. On the other hand, HB8 showed 16% loss in their residual tensile strength under the same conditions and the same time period. These results indicate that GFRP rebar reinforced with AR glass fibre show better alkaline resistance than the GFRP rebars reinforced with E-glass.

Table 3. Typical residual strengths of GFRP rebar

| GFRP type | Alkaline environments | Stress level (%) | Number of days | Load at rupture | Residual tensile strength (MPa) | Strength variation (%) |
|---|---|---|---|---|---|---|
| HB5 | | 30 | 140 | 44±2.5 | 618.3±35.3 | -5 |
| HB6 | In simulated | 30 | 140 | 44±0 | 624.5±0 | +1 |
| HB7 | pore water | 30 | 140 | 38.3±1.6 | 537±22.5 | +1 |
| HB8 | | 30 | 140 | 56.8±1.1 | 797.9±15.5 | -17 |
| HB5 | | 30 | 140 | 47±1.7 | 659.9±23.6 | +2 |
| HB6 | Embedded in | 30 | 140 | 44.3±0.4 | 621±5.4 | -1 |
| HB7 | concrete | 30 | 140 | 37.4±0.6 | 525.6±9 | -1 |
| HB8 | | 30 | 140 | 57.3±1.6 | 804.3±22.1 | -16 |




a b

Figure 5. Typical SEM photos for fibre surface of aged specimen in pore water
(a) C6 specimen, (b) C7 specimen

**Effect of manufacture parameters**

Effect of manufacturing parameters on durability was illustrated by a study of the C rebars. Rebar C2 was manufactured with condition described as P1 while rebar C3 by P2. Two rebars were subjected to a NaOH solution (pH=13.1) under stress level of 30% for duration of 60 days. No significant difference in their residual tensile strength could be observed. However, when rebars were subjected to the high stress level of 65% in air, the results indicated a difference [Table 4]. The P1 impaired a weakness in the rebar C2 at the location of mould joints. Rupture of rebar specimens C2-1 and C2-2 began at this position and then developed further. This was possible reason for a faster rupture of these specimens as seen in Table 4. For specimens C2-3 and C2-4 that did not have this part within their lengths, the time to rupture is significantly longer as seen from the Table 4. It appears that P2 could rectify the problem of P1 as rupture of specimens C3-1 and C3-2 took longer.

Table 4. Typical results for effects of manufacturing parameters in stress-rupture tests

| Rebar type | Manufacture Parameter | Stress level (% of tensile strength) | Loading system | Number of days at rupture | Note |
|---|---|---|---|---|---|
| C2-1 | P1 | 64 | 2 | 90 | |
| C2-2 | P1 | 65 | 2 | 83 | |
| C2-3 | P1 | 65 | 2 | 176 | Out of weakest part |
| C2-4 | P1 | 65 | 2 | 198 | Out of weakest part |
| C3-1 | P2 | 65 | 2 | 193 | |
| C3-2 | P2 | 65 | 2 | 248 | |

**Effect of curing degree**

Effect of curing degree on durability was described on a study of IS rebar. The difference between V4 (E-glass/vinylester1) and V6 (E-glass/vinylester2) was resin matrix. V7 had the same composition asV6, but the surface of V6 is smooth than that of V7. Table 5 shows the DSC results for V4, V6, and V7. DSC analysis indicates that core and coating of specimen V4 have a lower curing degree after processing, compared to V6 and V7 ones. V6 has higher cross-linking at core and lower cross-linking at the coating

Table 5. DSC results for GFRP bars

| GFRP type | Coating | | Core | |
|---|---|---|---|---|
| | Heat* (J/g) | Tg (°C) | Heat* (J/g) | Tg (°C) |
| V4 | -10.71 | 67.1 | -4.09 | 107.1 |
| V6 | -4.25 | 76.8 | -2.16 | 113.8 |
| V7 | -6.17 | 78.3 | -2.61 | 116.4 |

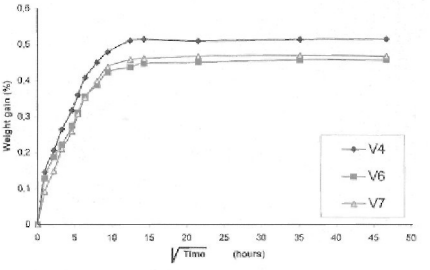
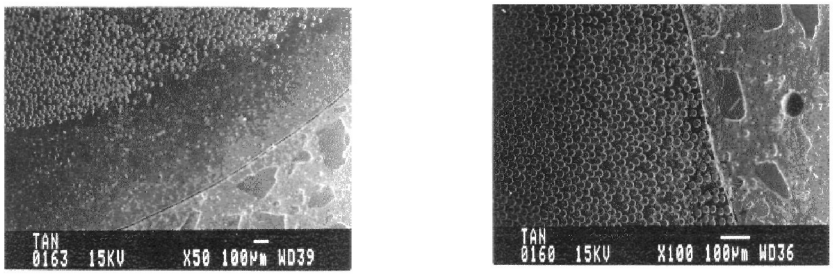



Figure 6. Water absorption test results

Figure 6 shows V4 has the highest water absorption at the early and later steps, while V6 absorbed water faster at the early stage and then slower at the later stage. It is believed that at the early stage of absorption, the contribution of the coating is much more dominantly but at the later step, the core determined the rate of water absorption. Compared to V7. The higher water absorption of V4 is due to poorer curing degree. Clearly, GFRP bars with lower curing degree resin present an increase in moisture and ions penetration compared to fully cured products.

**Effect of resin rich zone**

Figure 7a and Figure 7b show SEM images of GFRP specimens embedded in concrete and subjected to a stress level of 30% of the ultimate strength for 30 days. A larger gap was observed at resin rich zone of the interface between GFRP rebar and concrete. Since the resin rich zone has higher Possion's ratio, transverse shrinkage due to tension in this zone is higher, resulting a larger gap at the interface. At the fibre rich zone, only a narrow gap was observed. This result provides useful information to optimize bonding behaviour of GFRP rebars. With reduced resin rich zone thickness or increased fibre rich zone thickness in the areas near the surface of GFRP rebars, the bond behaviour of GFRP rebar can be improved.




a b

Figure 7. SEM images of interface between GFRP and concrete (a) at resin rich zone, and (b) at fibre rich zone

**Effect of alkaline environments**

Typical tests results for GFRP bars exposed to different alkaline environments and different stress levels are given in Table 6 to Table 8. The time to rupture of specimens was recorded and if no rupture occurred during the tests, the residual strength of the aged rebar was evaluated. The retention in tensile strength decreased with the increased in applied level and time. It is believed that the increase of applied stress increases the growth of flaws or microcracks on the resin matrix, allowing the alkali to diffuse deeper into the material and hence, damaging the GFRP specimen faster. NaOH solution is more aggressive environment, therefore, it is not surprising that the retention in tensile strength of specimens aged in this solution is much lower than that of specimens aged in simulated pore water solution. Samples embedded in concrete have the highest retention, some specimens embedded in concrete under sustained tensile load up to 1295 days, did not show any rupture. These differences mainly dues to different degradation mechanism caused by such alkaline environments. Fibre, matrix, and interface damage can be obviously observed in specimens aged in NaOH solution [Figure 8a and Figure 8b] while only matrix and interface damage are clearly seen in specimens aged in pore water solution [Figure 8c] and just few matrix microcracking and interface damage can be found in specimens embedded in concrete [Figure 8d]. From the obtained results, it is clear that most of the studied GFRP rebars are quite durable in alkaline environments under tensile stress levels corresponding to 25% of the ultimate tensile strength.

Table 6. Typical results of the tests in NaOH solution

| Rebar type | Number of specimens | Stress level (%) | Rupture or not | Days at rupture | Days under tension | Retention in tensile strength (%) |
|---|---|---|---|---|---|---|
| C1 | 5 | 13-22 | No | - | 121, 120 | 41,57,67,88,90 |
| C1 | 6 | 29-50 | Yes | 31-81 | - | - |

Table 7. Typical results of the tests in simulated pore water solution

| Rebar type | Number of specimens | Stress level (%) | Rupture or not | Duration of tests | Average retention (%) |
|---|---|---|---|---|---|
| C5 | 6 | 0 | No | 99, 140 | 88, 96 |
| C5. | 6 | 30 | No | 93, 120 | 73, 91 |
| C6. | 6 | 0 | No | 99, 140 | 88, 96 |
| C6. | 6 | 30 | No | 90, 93 | 90, 92 |

Table 8. Typical results of GFRP bars embedded in concrete and subjected to sustained load

| GFRP Bar type | Number of specimens | Stress level (%) | Duration* (days) | Number of days at rupture |
|---|---|---|---|---|
| IS0 | 8 | 21-44 | 1145-1295 | On going |
| IS0 | 1 | 54 | | 664 |
| IS4 | 4 | 25-39 | 863-800 | On-going |
| IS4 | 5 | 48-65 | | 1-27 |
| HB2 | 4 | 24-47 | 936 | On-going |
| HB2 | 4 | 46-66 | | 1-135 |
| HB3 | 4 | 19-37 | 1082 | On-going |
| HB3 | 3 | 54-68 | | 3-34 |

*Note. *The duration is up-to-date measurement for the on-going durability tests on GFRP rebars which is not ruptured and still under sustained load*
*Stress level is the % of the ultimate tensile strength*

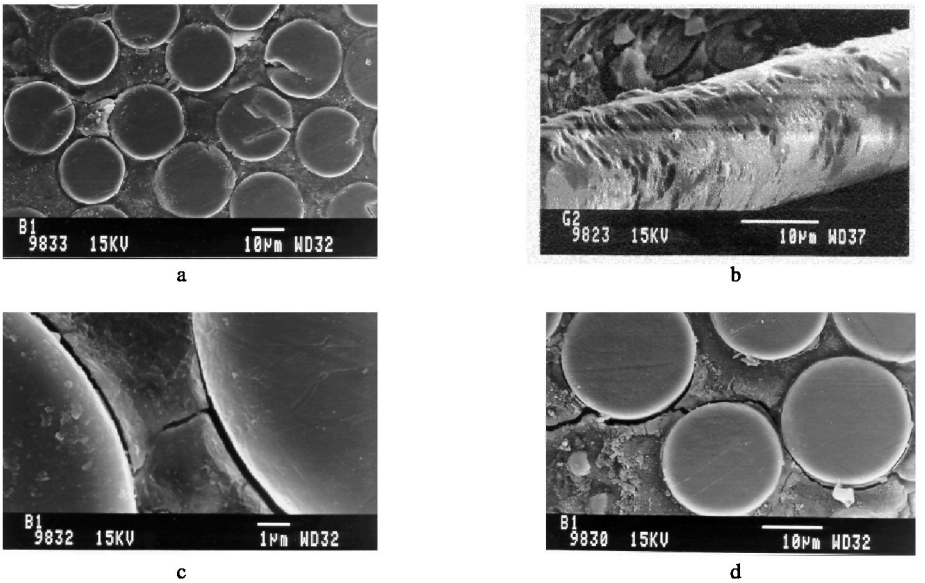



Figure 7. SEM photos of cross section of specimens aged in (a) and (b) NaOH solution (c) simulated pore water solution, and (d) embedded in concrete

## CONCLUSIONS

Results from the on-going research project on effects of alkaline environment on durability of GFRP bars were presented, from which the following conclusions and recommendations can be drawn:

(1) The test methodology to evaluate the alkaline effects on durability of GFRP reinforcing rods should include FRP reinforcing rods embedded in, or directly in contact with concrete. The concrete should be moist/wet. FRP bars should be under certain amount of stress close or over to the stress level experienced in service. Loading system 2 may be used for FRP bars durability evaluation, and loading system 4 may be used for evaluating durability of concrete elements reinforced with FRP bars. Elevated temperatures can be used to accelerate the ageing in the laboratory. However, these temperatures should not exceed the glass transition temperature of the matrix and temperature at which different mechanisms of degradation may creep in, the temperature of 60°C has been suggested.

(2) Alkaline ions and moisture could penetrate or diffuse through the resin (or through cracks and voids) to the inter-phase and fibres and damage the FRP rebars through many mechanisms which change depending on the type of resin matrix, sizing, stress level, pH of the alkaline environment, and manufacturing process

(3) Micro-structural techniques are very useful in evaluating the short and long-term performance and changes taking place in FRP reinforcements under stress and environmental effects (evaluation of the resin matrix, fibre, inter-phase, Tg, voids and cracks, fibre volume fraction, etc.). Such analyses, as those described in this paper, should be considered as standards in the Quality Control/Assurance tests by the FRP industrial manufacturers, engineers and users (Codes and Specifications). These techniques definitely help the

industrial manufacturers to produce high quality FRP reinforcing rods and to maintain thereby high standard of their products.

(4) The results obtained have also shown that type of glass fibres, manufacturing process, additional factors determining the long-term durability of the GFRP reinforcing rods. In particular, it has been shown that E-glass 366 Advantex and AR glass fibres have a better resistance to alkaline environments than the normal E-glass. The resin and FRP reinforcing bars should be fully cured prior to their use in concrete structures. Tests have shown that GFRP bars with under-cured resins present an increase in moisture and ions penetration compared to fully cured products. Voids, holes or other imperfections on the FRP rebar surface should be eliminated. All tested GFRP bars having these imperfections have shown lesser durability compared to GFRP bars not presenting these imperfections

(5) The resin plays also an important role in protecting the fibre and slowing diffusion process. Vinyl ester resin (or epoxy) shows low diffusibility, high resistance to alkaline attack and quite tough to resist micro-crack development. Therefore it has the highest potential to protect the glass fibre in the reinforcing rod from the alkaline attack and should be used in manufacturing GFRP bars. The polyester resin is not recommended.

Finally, from the obtained results, it is clear that GFRP reinforcing rods can be used in structural concrete considering the two following conditions: 1) Stress level in the GFRP rods should be limited under sustained factored loads at less than 25% of guaranteed design strength (guaranteed design strength may be taken as average ultimate tensile strength minus three times the standard deviation); 2) It is assumed that properly specified and proven materials and manufacturing process for FRP reinforcing rods have been used by the manufacturers.

## ACKNOWLEDGEMENTS

This research was supported by the National Science and Engineering Research Council of Canada (NSERC), the Canadian Network of Centres of Excellence on Intelligent Sensing for Innovative Structures (ISIS Canada), Hughes Brothers Inc., Pultrall Inc., Marshall Industries Composites Inc., Reichhold Chemicals Inc., and Owens Corning.

## REFERENCES

Benmokrane. B. 2000 "Improvement of the durability performance of GFRP reinforcements for concrete structures," Research report, Department of Civil Engineering, University of Sherbrooke, Sherbrooke, Québec, Canada pp 50.

Benmokrane. B., H. Rahman, M.-T. Ton-That and J.-F. Robert 1998 "Improvement of the durability performance of FRP reinforcement for concrete structures," Proceedings of the First International Conference, Sherbrooke, Québec, Canada, pp 571-578.

Porter. L. M 1999 "Durability issues for FRP reinforcement to concrete structures," SAMPE Vol. 44 pp 2246-2254.

Vistasp. M.K., Chin, J. W., and Reynaud. D. 2000 "Critical gaps in durability data for FRP composites in civil infrastructure," 45th International SAMPE Symposium pp 549 – 563.

Fujii, Y., et al 1993 "Evaluation of initial damage and stress corrosion of GFRP," Proceedings of the 5th International Conference on Composite Materials (ICCM93), Madrid, Spain, July 12-16.pp562-568.

# Alkali Resistance of Fibers, FRP Rods and Epoxy Resins

HIROSHI MUTSUYOSHI, Saitama University, Urawa, Japan
ATSUSHI SUMIDA, Dupont-Toray Co. Ltd., Tokyo, Japan
TAKETO UOMOTO, Collaborative Research Center, The University of Tokyo, Japan

## ABSTRACT

FRP rods made of carbon, aramid and glass fibers are increasingly being used as alternative reinforcements in concrete structures due to their non-corrosive characteristics. However, alkali resistance characteristics of FRP rods made of above mentioned fibers as well as the resins, which are used to harden the fibers have hardly been clarified. Furthermore, an appropriate test method to study the alkali resistance of FRP rods has never been established. The objectives of this paper are to establish a suitable test method to study the alkali resistance of FRP rods and to investigate eleven kinds of FRP rods, ten kinds of different fibers and four kinds of resins in terms of their alkali resistance. A series of tests have been done during the past three years to establish an appropriate test method proposed in this paper. This paper also describes some mechanical properties such as tensile strength, Young's modulus and load carrying capacities of the FRP rods, fibers and resins after they have been immersed in alkali solution for two years.

## INTRODUCTION

Deterioration of concrete structures is a worldwide problem nowadays. Corrosion of reinforcing bars is one of the major factors for concrete deterioration. Recently, there have been a lot of researches in the use of rods made of fiber reinforced polymers (FRP) as an alternative reinforcement in concrete structures. Many kinds of FRP rods have been recently developed to use them as reinforcements in concrete; these rods are generally made of carbon fiber, aramid fiber, glass fiber and vinylon fibers. Since these rods are corrosion proof and lightweight, they are increasingly being used for new concrete structures utilizing their advantages. Though there have been some researches in the short term mechanical properties of concrete members reinforced with FRP rods, long term durability of FRP rods placed inside concrete has hardly been clarified. In order to build durable structures, long term performance of these new types of FRP rods should be studied. The purpose of this paper is to throw some lights on the durability aspect of some types of FRP rods with regard to their alkali resistance. In order to investigate the long-term durability of FRP rods in concrete, the alkali resistance test for FRP rods was proposed newly and the tests were carried out on eleven kinds of FRP rods, four kinds of resins and ten kinds of fibers. The tests were done in such a way that the alkali solutions used in the tests could simulate the composition that is found in the pore solution in concrete. The rods, resins and fibers were immersed in alkali solutions for specified time periods ranging from 4 weeks to two years. Results of the tests on their performance in regard to tensile strength, modulus and load carrying capacities of fibers after immersing them in an alkali solution for specified time period are presented.

*FRPRCS-5*, Thomas Telford, London, 2001.

## TEST PROGRAM

### Alkali Resistance of FRP Rods

The test method used herein for alkali resistance of FRP rods, see appendix, is newly proposed and endorsed by JSCE. In order to investigate the alkali resistance of FRP rods, eleven kinds of FRP rods such as carbon FRP (CFRP), aramid FRP (AFRP), glass FRP (GFRP) and vinylon FRP (VFRP) were immersed in an alkali solution, which had the same composition as that found in the pore solution in concrete. The alkali solution was composed of NaOH (10g/l), KOH (14g/l) and $Ca(OH)_2$ (2g/l). The pH value of the solution was between 13.2 to13.4. The lengths of FRP rods were 400 mm and the diameter of each specimen varied between 3 to 11 mm. Both ends of FRP rods with the length of 200-300 mm were fixed in the anchorage. Figure 1 shows the photograph of typical specimens of FRP rods used in the tests. In order to prevent the infiltration of solution through the ends of test pieces during immersion, both ends of the test pieces were covered with epoxy resin. The temperature during the immersion was kept constant at 60 degree Celsius and 80 degree Celsius to accelerate the chemical reaction. The periods of immersion were 4 weeks, 13 weeks, one year and two years. Table 1 shows the detail experimental variables. The original mechanical properties of FRP rods before immersing into the alkaline solution are presented in Table 2. Five FRP rods were tested for each experimental parameter. After each period of immersion, change in the mass of FRP rods was measured and tensile tests of FRP rods were carried out.

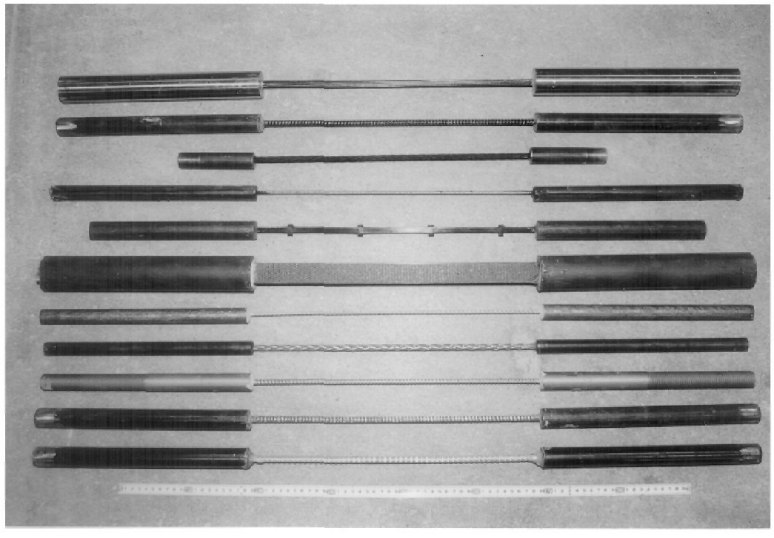


Figure 1. Photograph of typical FRP rods used in the tests

### Alkali Resistance of Resins

Four kinds of resins that are used for binding and hardening in the above-mentioned FRP rods were also immersed in alkali solution under the same condition as FRP rods. The resins were molded into special shapes and allowed to harden fully before immersion. The typical specimen of resin used in the test is shown in Figure 2. The thickness of the each specimen was 12 mm. After each period of immersion, tensile tests were conducted on the resin specimens. Three specimens were used for each experimental parameter.

Table 1. Experimental variables used in the tests

| Spe. no. | Configuration of rods | Material* | Resin no. | Fiber no. | 4 weeks 60°C + | 13 weeks 60°C + | 1 year 60°C + | 2 year 60°C + | 4 weeks 80°C + |
|---|---|---|---|---|---|---|---|---|---|
| A | Strand | CF | Ar | Af | O | - | - | - | - |
| B | Rod | CF | Br | Bf | O | O | O | O | - |
| C | Strand | CF | Cr | Cf | O | - | - | - | - |
| D | Strand | CF | Dr | - | O | - | - | - | - |
| E | Lattice | CF | Er | Ef | O | - | - | - | - |
| F | Rectangular | CF | Fr | Ff | O | - | - | - | - |
| G | Rod | AF | GJr | Gf | O | - | - | - | - |
| H | Braided | AF | Hr | Hf | O | - | - | - | - |
| I | Rod | AF | Ir | If | O | O | O | O | O |
| J | Rod | GF | GJr | Jf | O | O | O | O | O |
| K | Rod | VF | Kr | Kf | O | O | O | O | O |

* CF: Carbon fiber, AF: Aramid fiber, GF: Glass fiber**, VF: Vinylon fiber
+ Alkali solution: Ca $(OH)_2$ 2g/l + NaOH 10 g/l + KOH 14 g/l
** Glass fibers and GFRP rods are made of E-Glass

Table 2. Mechanical properties of FRP rods

| Spe. no. | Nominal diameter (mm) | Load carrying capacity (kN) | Tensile strength ($kN/mm^2$) | Young's modulus ($kN/mm^2$) | Ultimate elongation (%) |
|---|---|---|---|---|---|
| A | 9.6 | 90.9 | 1.64 | 109.0 | 1.5 |
| B | 8.0 | 101.8 | 2.02 | 127.2 | 1.0 |
| C | 7.5 | 52.7 | 1.73 | 130.8 | 1.3 |
| D | 5.0 | 41.6 | 2.12 | 145.4 | 1.4 |
| E | 4.7 | 19.1 | 1.09 | 90.9 | 1.2 |
| F | 11.0 | 172.6 | 1.82 | 113.6 | 1.6 |
| G | 3.0 | 4.9 | 0.69 | 63.6 | 2.0 |
| H | 7.3 | 58.2 | 1.38 | 63.6 | 2.0 |
| I | 6.0 | 46.3 | 1.64 | 49.1 | 3.7 |
| J | 8.0 | 68.1 | 1.35 | 38.2 | 2.7 |
| K | 8.0 | 27.3 | 0.55 | 20.0 | 3.0 |

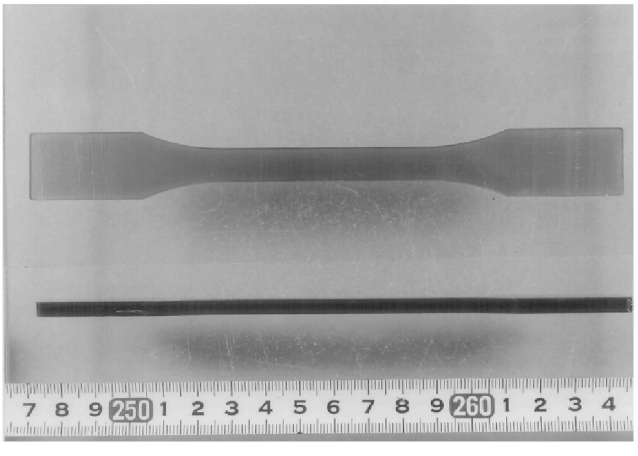



Figure 2. Photograph of typical resin specimen used in the tests (scale shown in cm)

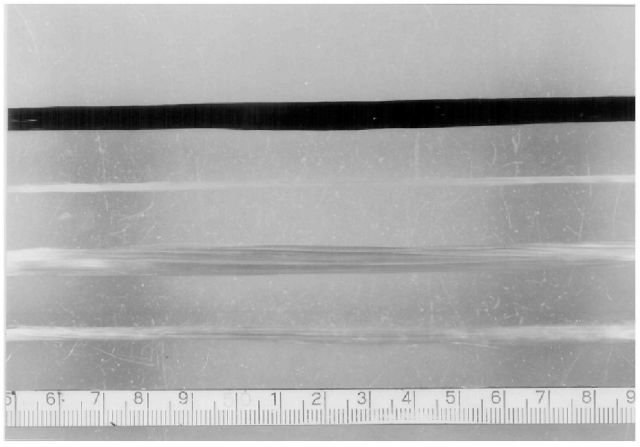



Figure 3. Photograph of typical fiber filaments used in the tests (scale shown in cm)

**Alkali Resistance of Fibers**

Ten kinds of fibers that are used for the above-mentioned FRP rods were also immersed in alkali solution containing the same composition to investigate the fiber properties. The typical fibers that were used in the tests are as shown in Figure 3. After the immersion for a period ranging from several hours to 2 years, tensile tests were conducted. The original mechanical properties of fibers (not-impregnated in resin) before immersing into the alkaline solution are presented in Table 3.

Table 3. Mechanical properties of fibers

| Specimen no. | Fiber tensile strength ($kN/mm^2$) | Fiber modulus ($kN/mm^2$) | Fiber specific gravity | Elongation (%) |
|---|---|---|---|---|
| A | 4.41 | 218.1 | 1.80 | 1.90 |
| B | 3.43 | 218.1 | 1.77 | 1.45 |
| C | 3.63 | 218.1 | 1.77 | 1.50 |
| D | 4.95 | 213.5 | 1.80 | 2.10 |
| E | 4.95 | 213.5 | 1.80 | 2.10 |
| F | 4.90 | 213.5 | 1.80 | 2.10 |
| G | 2.94 | 100.9 | 1.45 | 2.40 |
| H | 2.94 | 100.9 | 1.45 | 2.40 |
| I | 3.43 | 67.2 | 1.39 | 4.60 |
| J | 2.45 | 67.2 | 2.54 | 4.50 |
| K | 2.01 | 41.4 | 1.30 | 5.00 |

## TEST RESULTS

The results in terms of change in tensile strength, modulus and the load carrying capacities were studied for each FRP rods, resins and the fibers. Figure 4 shows the relationship between the tensile strength after immersion and the immersion period for CFRP rod, AFRP rod, GFRP rod and VFRP rod. It is seen that the tensile strength remains somewhat constant in the case of CFRP, AFRP rods, but there is a remarkable decrease in the strength for GFRP rods. VFRP rod shows a little change in its tensile strength.

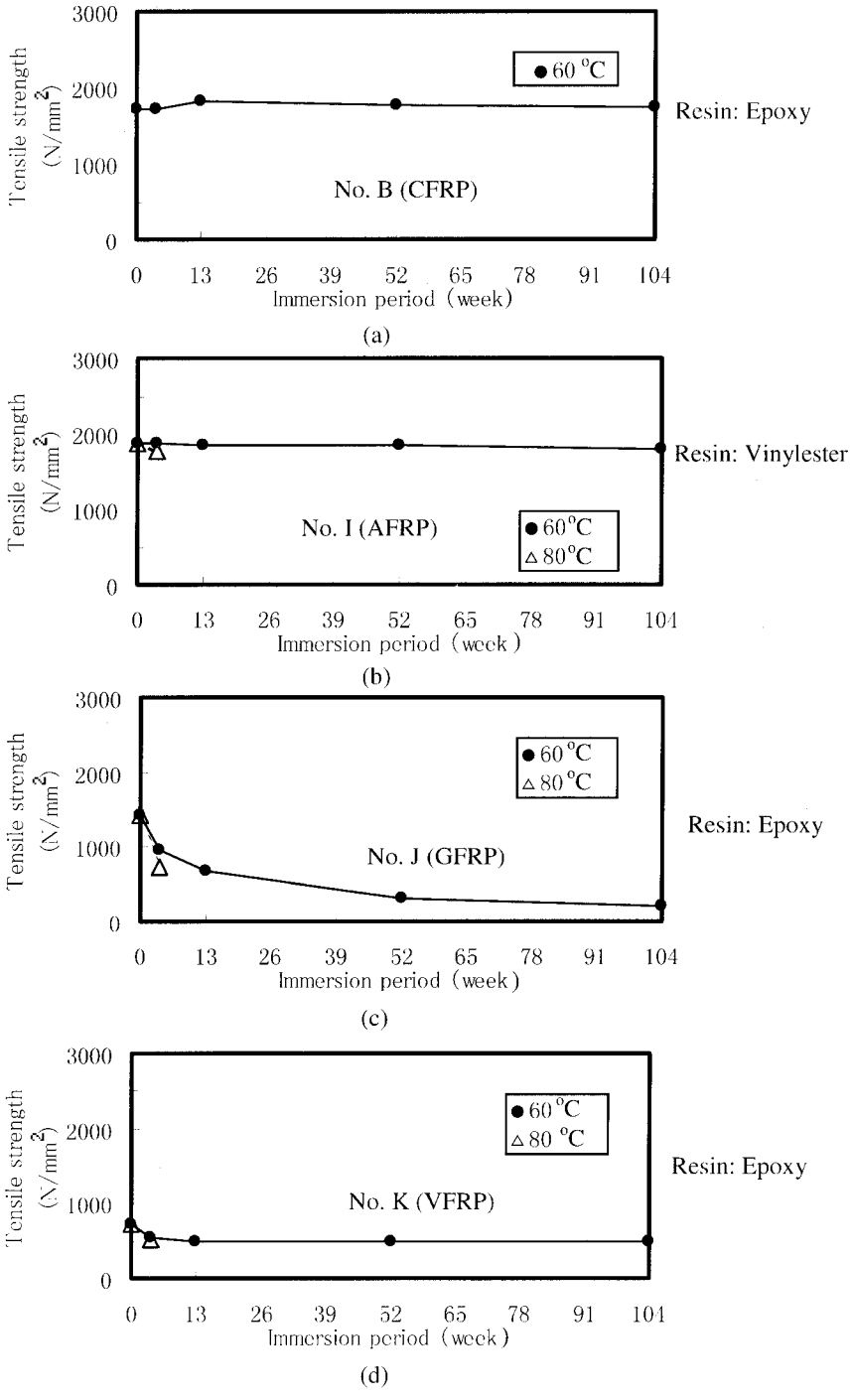



Figure. 4 Relationship between tensile strength and immersion period for FRP rods

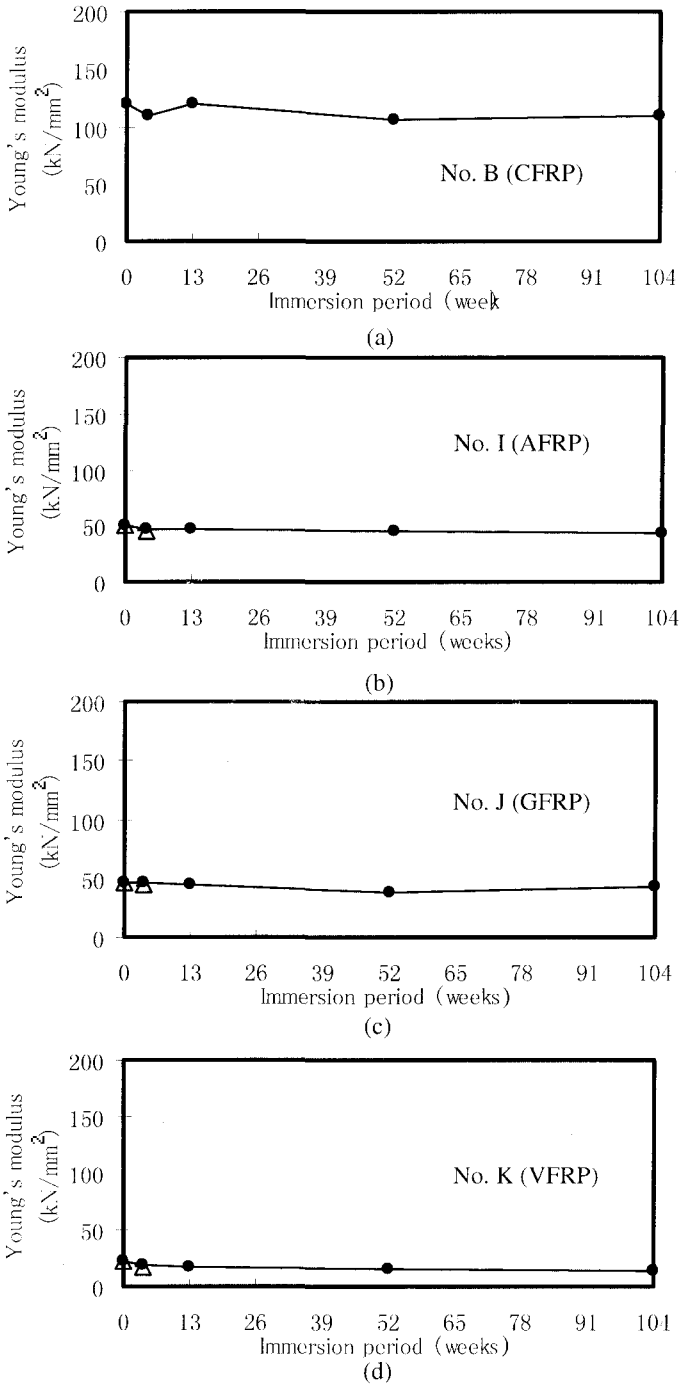
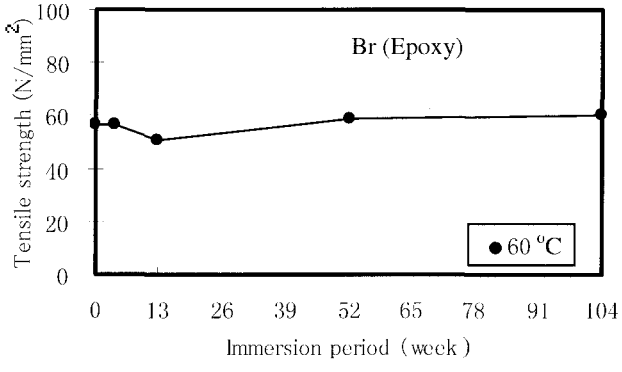


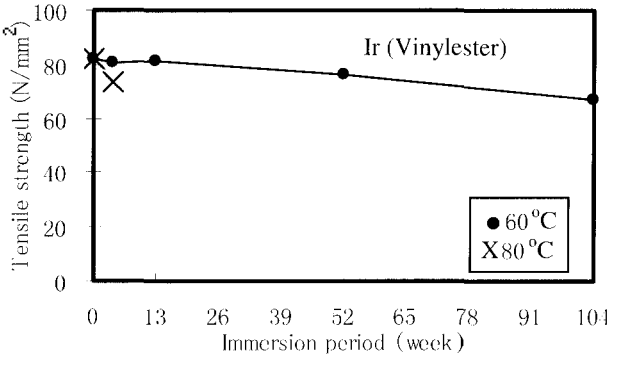

Figure. 5 Relationship between Young's modulus and immersion period for FRP rods

Figure 5 shows the relationship between the Young's modulus of FRP rods and immersion period. It is seen that the modulus remains almost the same even up to 2 years of immersion for all kinds of FRP rods. The ultimate strains sustained by different rods were also investigated. It was found that for CFRP, AFRP and VFRP, the ultimate strains after 2 years of immersion were almost the same as the original ones. However, the GFRP rod shows decrease in ultimate strain. At the end of two years the drop was approximately 75%. These results show that the durability of GFRP rod is very poor, whereas the other FRP rods are satisfactory in their durability performance.

Figure 6 shows the relationship between tensile strength and immersion period for the epoxy resin and vinylester resin. It is seen that the epoxy resin has almost constant strength whereas vinylester resin shows a decreasing trend in strength with time. Figure 7 shows the load carrying capacities of each Aramid fiber, Glass fiber and Vinylon fiber after immersion into alkali solution. It is seen that the capacity decreases for all fibers, but there is a sharp decrease in load carrying capacity for Glass fiber even after 24 hours of immersion. For Vinylon fiber, there is no capacity left after 90 weeks of immersion.

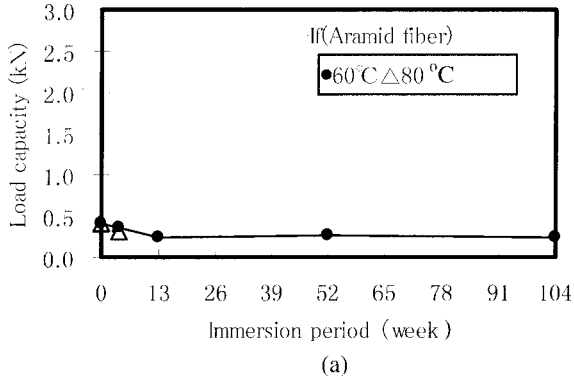



(a)

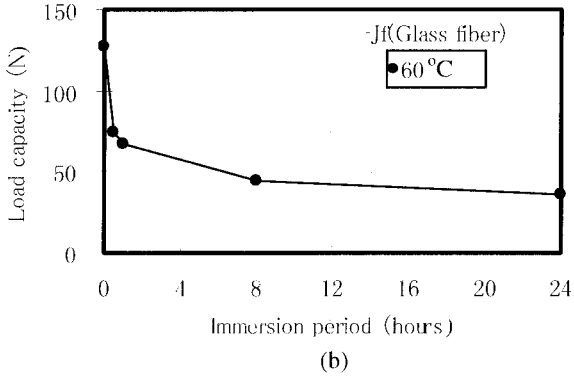



(b)

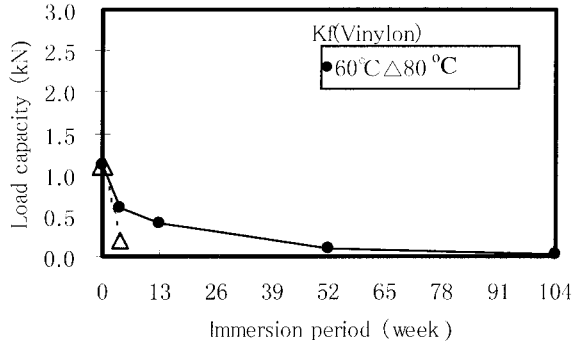
Figure. 6 Relationship between tensile strength and immersion period for resins




(a)




(b)




(c)

Figure. 7 Relationship between load carrying capacity and immersion period for fibers

## CONCLUSIONS

To investigate the durability of FRP rods under alkaline condition, the alkali resistance tests were carried out using four different types of FRP rods namely CFRP, AFRP, GFRP and VFRP based on the new test method proposed by JSCE. From the test results, the following conclusions can be drawn.

1. Alkali resistance of CFRP rod is superior to those of other FRP rods.

2. Though the alkali resistance of aramid fiber itself is not good compared to carbon fiber, AFRP rods impregnated with epoxy resin have good resistance against alkali.
3. It is cleared that the alkali resistance of glass fiber is very poor. Even GFRP rods impregnated with epoxy resin showed poor alkali resistance.
4. The test method for alkali resistance of FRP rods proposed herein and endorsed by JSCE is generally appropriate to judge durability of FRP rods under alkali conditions.

## ACKNOWLEDGEMENT

This study was carried out by the committee on durability of FRP supported by MITI, Japan. The authors would like to express their gratitude to all the committee members.

## APPENDIX: TEST METHOD FOR ALKALI RESISTANCE OF CONTINUOUS FIBER REINFORCING MATERIALS

### SCOPE

This specification specifies mainly the test method for evaluating alkali resistance of CFRM used in place of steel reinforcement or prestressing tendon in concrete by immersion in an aqueous alkaline solution.

### TEST PIECES

#### Preparation of Test Pieces

Test pieces shall as a rule not be subjected to any processing. For mesh-type CFRM, linear test pieces may be prepared by cutting away extraneous parts in such a way as not to affect the performance of the part to be tested.

#### Handling of Test Pieces

During sampling and preparation of test pieces, all deformation, heating, outdoor exposure to ultraviolet light, etc. causing to the material properties of the test section of the test piece must be avoided.

#### Length of Test Pieces

The length of the test section shall not be less than 100mm, and not less than 40 times the nominal diameter of the CFRM. For CFRM in strand form, as an additional condition, the length shall not be less than 2 times the standard pitch.

#### Number of Test Pieces

The number of test pieces for pre- and post-immersion tensile testing shall not be less than five. If the test piece is found clearly to have failed at the anchoring section, or to have slipped out of the anchoring section, an additional test shall be performed on a separate test piece taken from the same lot.

### IMMERSION IN ALKALINE SOLUTION

#### Preparation of Alkaline Solution

The alkaline solution used for immersion shall have the same composition as the pore solution found in concrete.

#### Prevention of Infiltration of Solution into Test Piece

In order to prevent infiltration of solution via the ends of the test pieces during immersion, both ends of the test pieces shall be covered with epoxy resin.

#### Immersion Temperature

The specification temperature for immersion shall be 60 degree Celsius.

**Mounting of Test Piece**
The test piece shall be mounted on the immersion apparatus. If necessary a tensioning load just to stretch it shall be applied to the test piece. The alkaline solution must be prevented from absorbing $CO_2$ from air and from the evaporation of water during immersion.

**Period of Immersion and Post-Immersion Treatment**
The specification immersion period shall be one month. The test piece shall be washed in water after immersion.

## EXTERNAL APPEARANCE AND MASS CHANGE

**Inspection of Alkaline Solution**
The pH value of the alkaline solution shall be measured before and after alkali resistance test.

**External Appearance**
The external appearance of the test piece shall be examined before and after the alkali resistance test, for comparison of color, surface condition, and change of shape. If necessary the test piece may be sectioned and polished and the condition of the cross-section examined using a microscope, etc.

**Measurement of Mass Change**
After immersion, the hardened epoxy resin shall be removed from the ends of the test piece, which shall then be dried and the mass measured until the mass is constant. The rate of mass change shall be calculated according to eq.1.

$$\text{Rate of mass change } (\%) = \{(W_0/L_0 - W_1/L_1)/(W_0/L_0)\} \times 100 \quad (1)$$

where, $W_0$ = mass before immersion (g) $L_0$ = length before immersion (mm)
$W_1$ = mass after immersion (g) $L_1$ = length after immersion (mm)

## TENSILE TEST

**Testing Machine and Devices**
Testing machine and devices shall be in accordance with the "Test Method for Tensile Properties of Continuous Fiber Reinforcing Materials" suggested by JSCE.

**Test Temperature and Test Method**
Test temperature and test method shall be in accordance with the "Test Method for Tensile Properties of Continuous Fiber Reinforcing Materials" suggested by JSCE.

## CALUCULATION AND EXPRESSION OF TEST RESULTS

**Handling of Data**
The material properties of CFRM shall be assessed on the basis only of test pieces undergoing failure in the test section. In cases where tensile failure or slippage has clearly taken place at the anchoring section, the date shall be disregarded and additional tests shall be preformed until the number of test pieces failing in the test section is not less than five.

**Tensile Capacity Retention Rate**
The tensile capacity retention rate (%) shall be calculated according to eq.2 and rounded off to two significant places.

$$\text{Ret} = (F_{u1}/F_{u0}) \times 100 \quad (2)$$

where, $F_{u1}$ = tensile capacity after immersion (N)
$F_{u0}$ = tensile capacity before immersion (N)

# Durability of FRP sheet used for concrete in sulphuric acid environment

A. HATTORI, Kyoto University, Japan
Y. OHNISHI, Nishimatsu Construction Co., Ltd., Japan
T. MIYAGAWA, Kyoto University, Japan

## INTRODUCTION

Degradation of repair and strengthening by the FRP sheet may be caused by deterioration of concrete, FRP sheet and/or interfacial property between them. In order to evaluate the degradation of concrete structures strengthened with the FRP sheet, it is important to confirm applicability of various inspection methods.

In this study, several types of the FRP sheet using some combinations of fibre sheet and resin were applied for mortar specimens. A surface with the FRP sheet of mortar specimens was immersed into sulphuric acid solution, which was an accelerating environment simulating such as the sewerage facilities, for 1 month. After the degradation acceleration, the mortar specimens were investigated by surface and cross section observation using scanning electron microscope (SEM) with the element distribution analysis, and by measuring ultrasonic pulse propagation velocity and acoustic emission (AE). Flexural loading test was also carried out. Obtained results were summarized to make clear the applicability of the evaluation methods for the FRP sheet using different fibre sheet and resin materials. Degradation process of the FRP sheet–strengthened concrete structures under the accelerated degradation environment was also discussed.

## EXPERIMENT OUTLINE

On a side surface of the $40 \times 40 \times 160$mm standard mortar specimens, one layer of FRP sheet was axially applied. Properties of materials used for FRP sheet composites are shown in Table 1. Mix proportion of the mortar is shown in Table 2. In order to accelerate degradation, some of the mortar specimens were immersed in 20°C/10% sulphuric acid solution for one month. Those immersed were applied thick epoxy coating on the surfaces other than that immersed with the FRP sheet. Following investigations were conducted for the mortar specimens.

### SEM observation and element distribution analysis

In addition to visual observation, surface and cross section of the FRP sheet were observed by SEM (Figure 1, acceleration voltage: 20kV, working distance: 28mm). During the SEM observation, element distribution analysis of the cross section (line profile) was also carried out on elemental sulphur (S). Neutralization depth of cross section was also measured by using the phenolphthalein solution.

Table 1. Properties of fibre sheets and resins for FRP sheet

| Fibre sheet | Carbon fibre (High strength type) | Carbon fibre (High modulus type) |
|---|---|---|
| Designation | HS | HM |
| Tensile strength (kN/mm$^2$) | 4900 | 4200 |
| Elastic modulus (kN/mm$^2$) | 230 | 436 |
| Elongation (%) | 2.1 | 1.0 |
| Weave Density (g/m$^2$) | 300 | 300 |

| Resin | Epoxy (Normal type) | Epoxy (Acid proof type) | Epoxy (Flexible type) |
|---|---|---|---|
| Designation | N | A | F |
| Tensile strength (kN/mm$^2$) | 42.7 | 25.0 | 20.6 |
| Elastic modulus (kN/mm$^2$) | 2.2 | 0.98 | 0.88 |
| Elongation (%) | 3.0 | 8.0 | 20 |

* Specimens were named with combinations of fibre sheet and resin used for a FRP sheet composite; ex. "HS–N", and specimens without FRP sheet were named "0–0".

Table 2. Mix proportion of mortar

| Flow | Unit mass (g/*l*) | | |
|---|---|---|---|
| (mm) | W | C | S |
| 162 | 225 | 450 | 1350 |

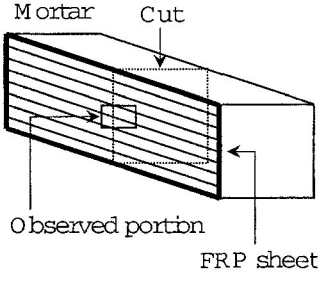



Figure 1. SEM observation (cross section)

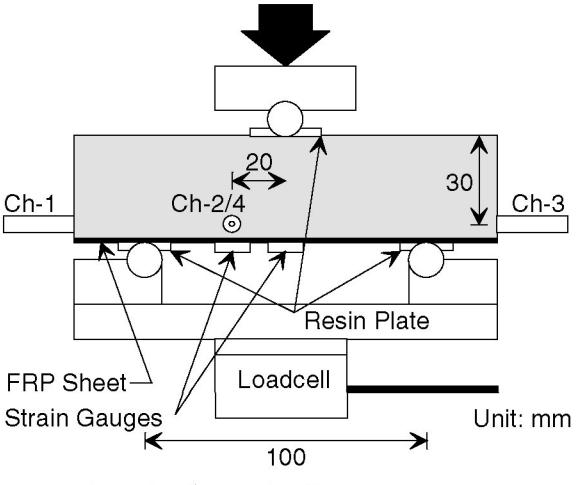



Figure 2. Flexural loading test

**Ultrasonic pulse propagation velocity**

By the symmetric method (radiator and pickup: 50mm in diameter, 50kHz), ultrasonic pulse propagation velocity was axially measured between both end surfaces (distance: 160mm).

**Flexural loading with AE measurement**

Loading test setup is shown in Figure 2. Unidirectional monotonic load or unidirectional cyclic load were applied statically. In the cyclic loading, load was applied up to $0.5P_{cr}$, $1P_{cr}$, $2P_{cr}$, ... (where $P_{cr}$: flexural cracking load of each specimen) and then unloaded down to small load in every cycle. Load and surface strain of FRP sheet at two points including the span centre (gauge length: 5mm) were measured.

In addition, AE events were counted by the ring down method (sensor: 150kHz resonant type, gain: 40dB by both pre– and main–amplifier, discriminate level: 1V). Using the AE count, Fericity ratio[1] (= $P_{AE}/P_{1st}$, $P_{1st}$: maximum load experienced in a loading history, $P_{AE}$: load when AE count increases remarkably in later loading process), which shows stability of the Kaiser effect (if Fericity ratio = 1, Kaiser effect is perfect), was obtained. The unidimensional position rating of the AE source was also carried out.

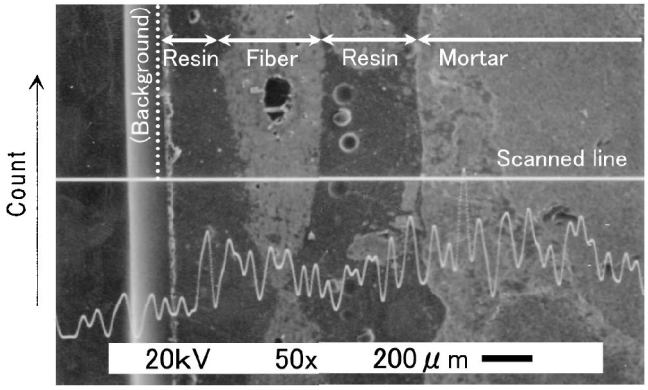
## RESULTS AND DISCUSSIONS

Neutralization depth of mortar cross section was 0mm for all of the specimens with FRP sheet. All kinds of FRP sheet protected mortar against the sulphuric acid in the immersion period (1 month).

**SEM observation and element distribution analysis**

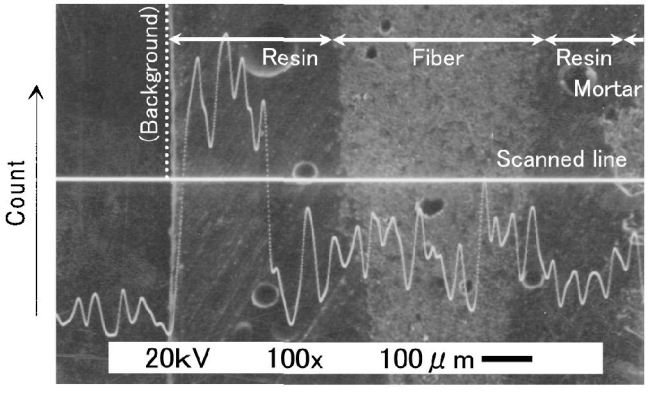
Any change such as crack generation was not recognized by the visual and SEM observation in/on the FRP sheet. However, infiltration depth of sulphur (S) measured by the element distribution analysis increased clearly from those without immersion, as shown in Figure 3 (not immersed) and Figure 4 (immersed). Therefore, the infiltration depth can be adopted as an index of influence of sulphuric acid on the FRP sheet.

While the infiltration depth was small in the acid proof resin (A), it advanced close to the edge of the fibre bundle in the FRP sheet in the flexible resin (F) (Figure 4). This means that barrier performance increases as the cross–link density of resin is larger. The infiltration depth is correspondent to reduction of tensile strength and weight increase tendency[2] after immersion in the same resins respectively.

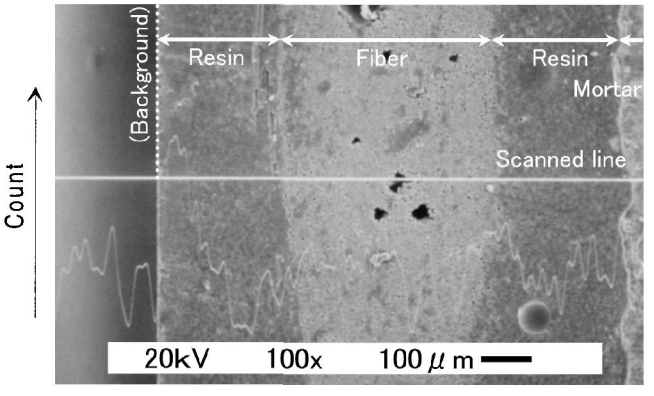



HS–N

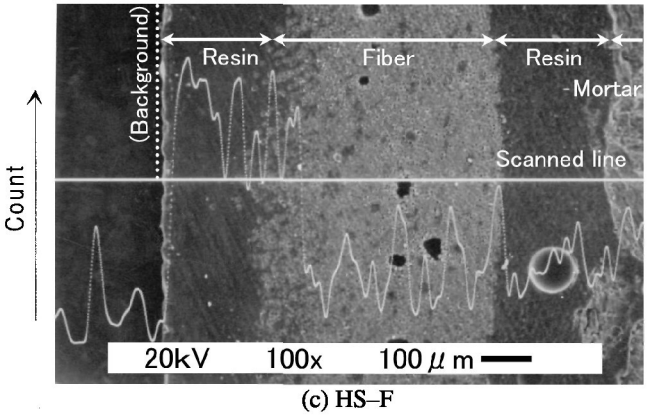
Figure 3. Sulphur distribution (Not immersed)




(a) HS–N




(b) HS–A




(c) HS–F

Figure 4. Sulphur distribution (Immersed)

**Ultrasonic pulse propagation velocity**

*Effect of materials*

Significant difference was observed among the material combinations of the FRP sheet composites, as shown in Figure 5. Influence of fibre sheet was more remarkable than that of resin. The velocity was also affected by the position of the radiator and pickup; that is, the velocity increased as they were placed closer to the FRP sheet in the both end surfaces. The fibre sheet itself can have high velocity owing to its high elastic modulus. Besides, the fibre sheet stiffened the mortar and the resin fulfilled pores near the surface of the mortar.

*Effect of immersion*

The velocity decreased a little after the immersion. Reduction in elastic modulus of the resin surface may cause the velocity reduction.

**Flexural loading**

*Failure mode*

After a flexural crack was generated near the span centre, cracks due to diagonal tension stress were observed in both sides of the flexural crack. The diagonal cracks developed to the FRP sheet, and then caused sudden debonding of the FRP sheet, when maximum load was obtained.

*Flexural cracking and maximum load*

With the tensile rigidity of the fibre sheet being the x–axis, ratio of the flexural cracking load to that of the specimen without strengthening is shown in Figure 6, and ratio of the maximum load is shown in Figure 7. Although the flexural cracking load was the highest in the high modulus carbon sheet (HM), the maximum load was not. Since stress at an equal strain is larger due to the high elastic modulus, the HM sheet could restrain cracks. On the contrary, the HM sheet required large

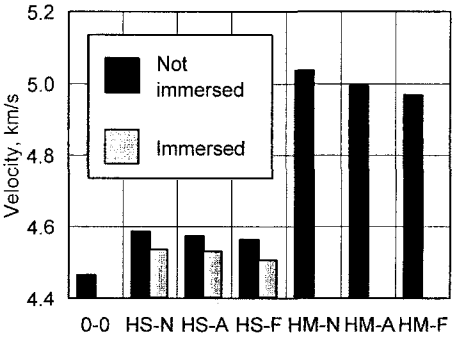



Figure 5. Ultrasonic pulse propagation velocity

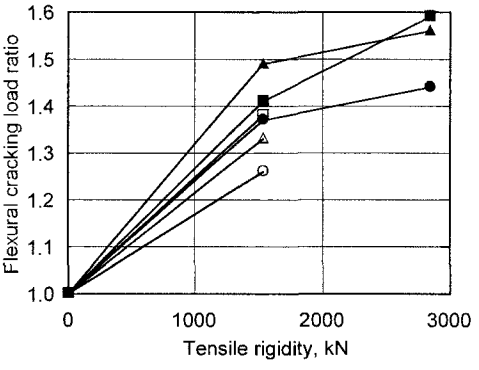



Figure 6. Flexural cracking load ratio

■, ●, ▲: Not immersed, Resin=N, A, F

□, ○, △: Immersed, Resin=N, A, F

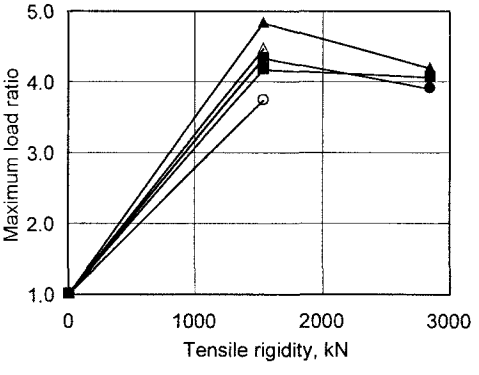



Figure 7. Maximum load ratio

■, ●, ▲: Not immersed, Resin=N, A, F

□, ○, △: Immersed, Resin=N, A, F

bond strength so that the debonding could easily occur.

*FRP sheet surface strain*

The FRP sheet surface strain of the HM sheet was one half of that of high strength carbon sheet (HS). The strain was small when the flexible resin (F) was used. In the case of the F resin, slip deformation might occur in wide area.

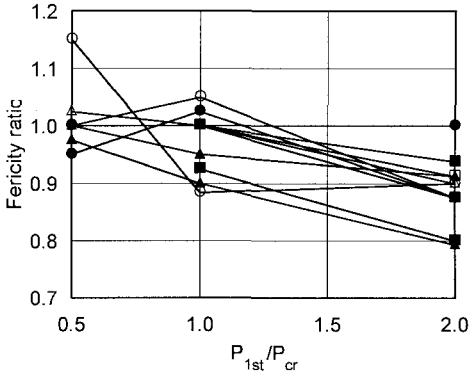
*Effect of immersion*

After the immersion, the flexural cracking load decreased 15% at most when the F resin was used, which is due to significant degradation of F resin. However, the maximum load reduction and the surface strain reduction at a certain load were not significant.

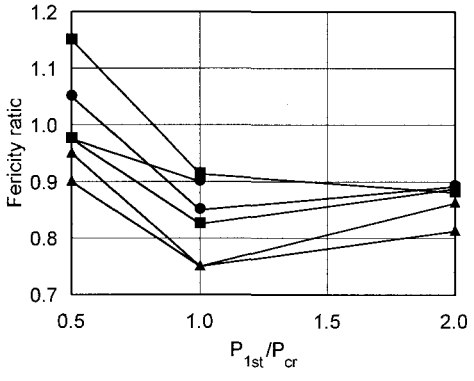
**AE measurement in flexural loading**

*Effect of immersion*

With increase in $P_{1st}$, the Fericity ratio decreased, as shown in Figure 8 (a), which indicates that the specimens fell into unstable conditions. After the immersion, the Fericity ratio decreased significantly at $P_{1st}/P_{cr}=1$ as shown in Figure 8 (b). Therefore, the Fericity ratio is effective for degradation estimation. On the contrary, the Fericity ratio did not decrease in the immersed specimens at $P_{1st}/P_{cr}=2$. This means that degradation which made the Fericity ratio decrease greatly occurred at $P=P_{cr}$ by the immersion.




(a) Not immersed




(b) Immersed

Figure 8. Fericity ratio
■, ●, ▲: HS, Resin=N, A, F
□, ○, △: HM, Resin=N, A, F

*Unidimensional position rating*

In the unidimensional position rating, remarkable AE counts were obtained near the span centre when the flexural crack was generated, as shown in Figure 9. Afterwards, AE count frequency got small in some load increase. Subsequently AE generation area extended with load increase, which was corresponding to the generation and development of the diagonal and debonding cracks. In this way, unidimensional position rating could follow the cracks observed in the specimens. However, difference of materials and immersion effect were not clear.

## CONCLUSIONS

In this study, applicability of some evaluation methods for FRP sheet using different fibre sheet and resin materials combination was discussed. Basic findings with regard to degradation process of the FRP sheet–strengthened concrete structures under accelerated

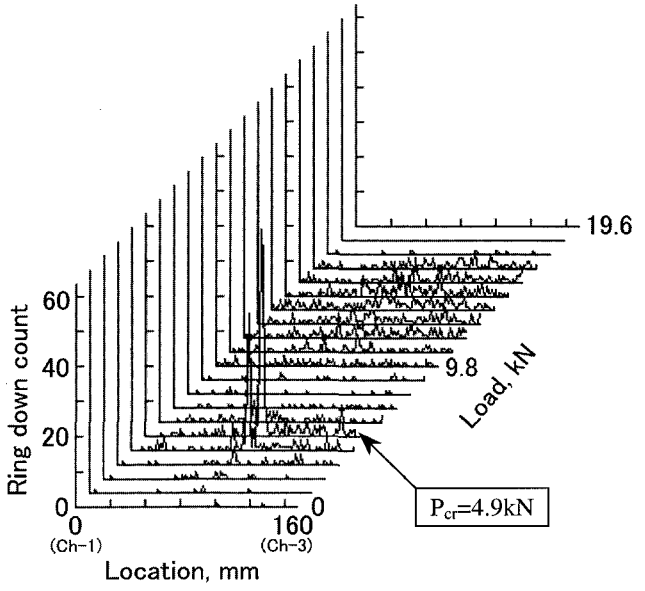



Figure 9. Unidimensional position rating (HS–N, Immersed)

sulphuric acid environment simulating sewerage facilities were also obtained. The main results obtained in this study are summarized as follows:

1. In sulphuric acid solution environment, degradation of the FRP sheets used in this study proceeds as a constituent in the solution infiltrates into them in a certain rate according to cross–link density of resin. The degradation can be evaluated by the element distribution analysis of sulphur (S).
2. The ultrasonic pulse propagation velocity of the mortar with a 40×40mm cross section by the symmetric method is significantly affected by attached FRP sheet. Especially the elastic modulus of fibre sheet used for the FRP sheet has great influence.
3. While flexural cracking load increases as tensile rigidity of the fibre sheet is larger, influence of the resin is not clear. However, by immersion of 10% sulphuric acid solution for one month, 15% reduction at most was observed in the case of the flexible resin. Severe degradation in resin can cause reduction in the flexural cracking load.
4. The degradation under sulphuric acid solution environment can be expressed in reduction degree in Fericity ratio due to flexural cracking.
5. AE source position rating can indicate the generation and propagation of diagonal cracks in a mortar specimen and debonding cracks of the FRP sheet, as well as the mortar flexural crack.

## REFERENCE

[1] Masayasu Ohtsu (1988), "Characteristics and Theory of Acoustic Emission", Morikita Shuppan Co., Ltd. (in Japanese)

[2] Atsushi Hattori, Takashi Yamamoto, Seiji Kashi and Toyoaki Miyagawa (1998), "Repair and Strengthening of Sewerage Concrete Structures Using Fibre Sheet", Journal of Construction Management and Engineering, No. 599/V–40, pp.59–69 (in Japanese).

# Durability of FRP Rebars After Four Years of Exposure

A. KATZ, Technion-Israel Institute of Technology, Haifa, Israel
L.C. BANK, University of Wisconsin-Madison, USA
M. PUTERMAN, Technion-Israel Institute of Technology, Haifa, Israel

## ABSTRACT

Six types of glass fiber reinforced polymer rods were embedded in concrete blocks in order to study the long-term properties of the rods and the rod-concrete interface. The specimens were submerged in water at 80°C for 14 and 84 days, at 20°C for 4.5 years and in air for 84 days and 4.5 years.

The results indicated a significant increase in the bond strength of smooth rods after 4.5 years in water but no significant change between 4.5 years in air or 84 days in hot water. Scanning Electron Microscopy (SEM) of the surface of the rod indicated significant deterioration of the polymer at the surface of the rods (mainly of those made from polyester) either after exposure to hot water for 84 days or to 20°C water for 4.5 years.

## INTRODUCTION

Durability of FRP bars proposed as replacement for conventional reinforcing steel in concrete structures is of a significant importance. The FRP rebars are proposed as a durable replacement for the conventional steel that suffers from a severe deterioration in an aggressive environment (marine structures, road pavements in cold regions, etc.). As such, the long-term properties of the FRP rebars must be well established in order to validate its superiority over conventional steel reinforcement in different environments (Tannous and Saadatmanesh 1999, Bank 1993, Uomoto and Ohga 1996). Special attention is given to the processes at the surface of the rods. The transfer of loads from the concrete to the load-carrying fibers at the core of the rod occurs through the resin, which also needsto provide an effective protection to the fibers that might be susceptible to the alkaline environment of the concrete (Ehsani et al., 1993, Nanni et al, 1998, Bentur and Mindess, 1990).

In this light a study was started in 1994 (Bank et al., 1998) in order to (i) establish an accelerated test method to determine the durability of FRP rebars in concrete and (ii) test the durability of FRP rebars encased in concrete blocks under accelerated conditions and normal conditions. Partial results from 4.5 years of exposure to wet and dry environments are reported here.

*FRPRCS-5*, Thomas Telford, London, 2001.

## TEST METHOD

Materials: six FRP bars, with properties as listed in Table 1, were tested. It should be noted that these bars were selected in 1994 and thus their properties might be different from bars produced today for concrete reinforcement. The concrete was a normal strength concrete having a 28-day compressive strength of 44 MPa.

Table 1: Properties of the FRP rods.

| Rod designation | Nominal diameter, in. | Fiber type | Resin type | Description |
|---|---|---|---|---|
| R1 | 1/2" | Glass | Polyester | Smooth |
| R2 | 1/2" | Glass | Vinylester | Smooth |
| R3 | 1/2" | Glass | Vinylester | Helical wraps |
| R4 | 1/2" | Glass | Polyester* | Helical wraps + sand coating |
| R5 | 1/4" | Glass | Polyester | Smooth |
| R6 | 1/4" | Glass | Vinylester | Smooth |

* assumed

The FRP rebars were embedded at the center of a concrete cylinder having the dimensions of 100 mm diameter and 250 mm length. The rod protruded from the concrete for 240 mm on one end of the cylinder and 10 mm on the other end. All specimens were cured for 7 days under water followed by additional 21 days in laboratory conditions (21°C, 60% R.H.) before beginning with additional aging according to the experimental program.

Aging program: five aging regimes were tested as follows:

Table 2: Aging regimes.

| Notation | Aging time | Environment | Conditions |
|---|---|---|---|
| E1 | 14 days | Water | 80°C |
| E2 | 84 days | Water | 80°C |
| E3 | 84 days | Air | 20°C, 60% R.H |
| E4 | 4.5 years | Air | 20°C, 60% R.H |
| E5 | 4.5 years | Water | 20°C |

An embedded rod test (ERT) was specifically designed for this test (Bank et al., 1998). This setup (shown in Figure 1) enables one to obtain a variety of information from a single test sample that has been subjected to environmental conditioning. Three test specimens are obtained from each sample after sectioning the concrete: one for pullout of the rod to determine the bond properties, one rod segment that is removed from the concrete cylinder after splitting of the concrete, and one that provides a slice of concrete with the rod embedded in it.

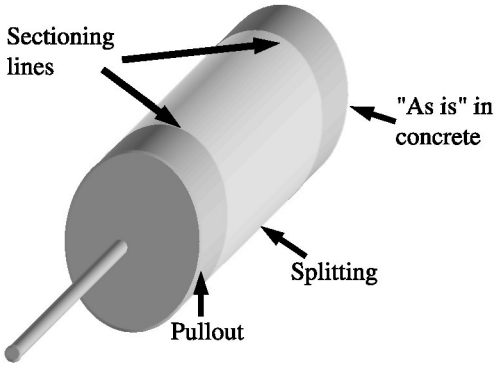



Figure 1: Embedded Rod Test (ERT) specimen.

The average bond strength, τ, was determined by dividing the maximum pullout load ($P_{max}$) with the embedded surface area of the rod in the concrete as shown in the following equation:

$$\tau = \frac{P_{\max}}{\pi d l}$$

where: *d*- rod diameter and *l*- embedded length (65 mm).

## RESULTS AND DISCUSSION

### Bond strength

Bond strength of the smooth bars was relatively very low. The bond strength of the deformed bars R3 and R4 was much larger but splitting of the concrete block before beginning of slippage prevented the calculation of the maximum bond strength. Therefore, these rods were excluded from this report. A different study (Katz, 1999), however, done by using a modified ERT configuration, yielded bond strength values of approximately 11 MPs and 4 MPa for rods R3 and R4, respectively. Figure 2 presents the results of bond strength for the various testing environments of rods R1, R2, R5 and R6.

Bond strength of the smooth rods was approximately 0.5-1.5 MPa for aging in environments E1 through E4. Significantly larger bond values were obtained for the specimens exposed to E5 conditions (submerged in water for 4.5 years). The bond mechanism of the smooth rods depends mainly on the friction between the rod and the surrounding concrete; therefore, densification of the interfacial layer during time in the presence of continuous moisture probably yielded an improved bond.

## PULLOUT BEHAVIOR

Figure 3 presents the pullout curves of the smooth rods R1 and R2 under the different aging conditions. Similar curves were obtained for rods R5 and R6 at lower load levels, expected form their smaller diameter.

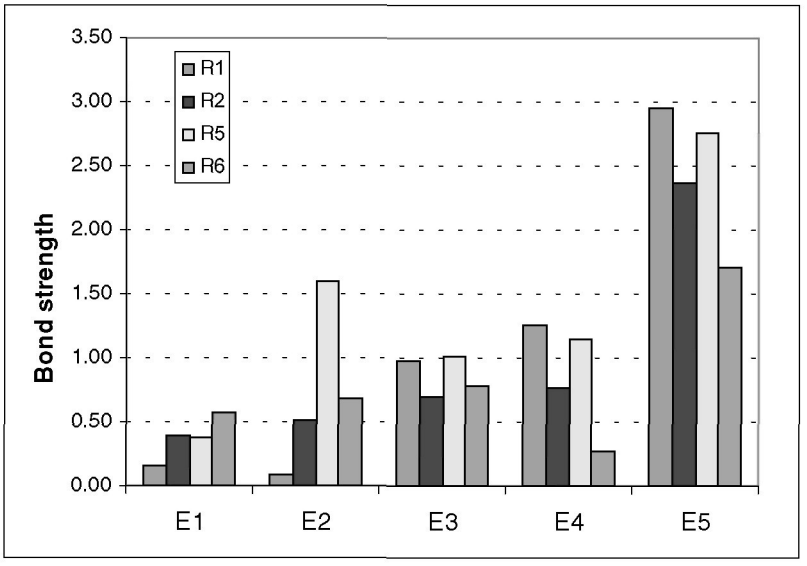



Figure 2: Results of bond strength (MPa) for the smooth rods in different environments.

The pullout behavior of the rods depends very much on the friction between the smooth surface of the rod and the surrounding concrete. In some cases, entrapment of a concrete crumb in the interface led to a local increase in the pullout load by a wedging effect until the crumb was crushed and stopped preventing the rod movement. Visual examination of the rod's surface clearly showed the locations of wedging on the surface after pullout. Without this effect a linear reduction of the load in the post-peak zone is expected. This phenomenon was more pronounced in rods R5 and R6 due to the lower pullout loads seen for these rods.

Aging in high temperature (E1 and E2) led to a significant low bond strength for the polyester (R1) rods compared with the aging in water in room temperature for the short or long period of time (E3 and E4, respectively). Pullout curves of the vinylester rod (R2) in all environments exhibited the same trends (see Figure 3) except for environment E5. The curves of both rod types look similar for environment E5.

It seems that the polyester rods were more susceptible to the high temperature of the aging in environments E1 and E2, leading to deterioration of the outer surface of the rod and to lower bond/friction between the rod and its surrounding concrete. Aging in room conditions did not change the properties of the surface, even after a long time. The vinylester that has a better resistance to the concrete environment did not suffer as much from deterioration in the high temperature as the polyester, exhibiting the same properties in environments E1 through E4. It seems that after a long period of time in which the specimens were submerged under water in 20°C (environment E5) the interface between the rods and their surrounding concrete became denser, leading to increased friction between the rod and the concrete, exhibiting better bond and more uniform slip behavior.

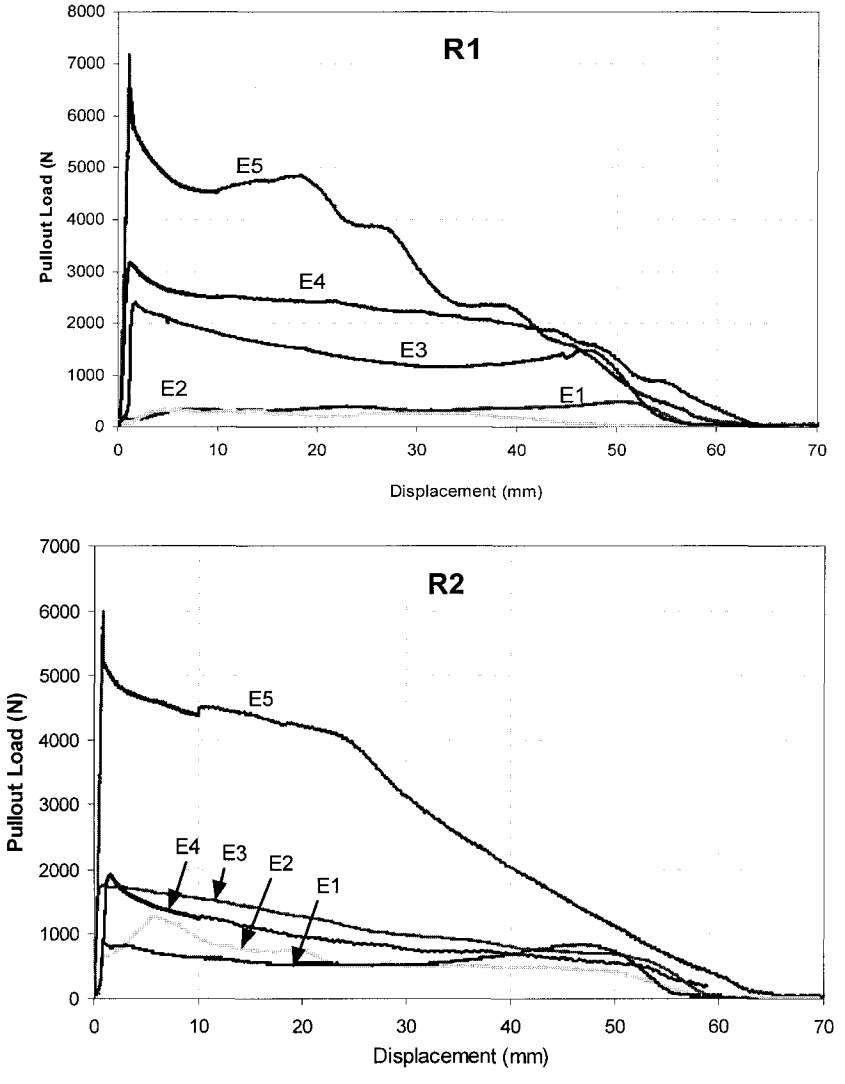



Figure 3: Typical curves of pullout load vs. displacement of rods R1 and R2.

## SURFACE MICROSCOPY

The surface of the rods was tested by a scanning electron microscope (SEM). Figure 4 shows the examination of rods R1 and R2 exposed to environments E4 and E5. Extensive deterioration of the surface accompanied with extensive cracking along the fibers is seen on the surface of rod R1 exposed to environment E5. Some cracking and signs of deterioration were also seen on the surface of rod R2 but to a lesser extent. The surface of the rod subjected to environment E4 showed no sign of visible deterioration as was seen in the other environment. Results from the early age testing of the rods (Bank et al, 1998) showed

deterioration of the surface of rod R1 under environments E1 and E2 but almost no damage when it was exposed to environment E3. Rod R2 showed less damage when it was exposed to environments E1 and E2. These findings correlate well with the other results from pullout tests, both for the bond strength and for the slip behavior discussed before.

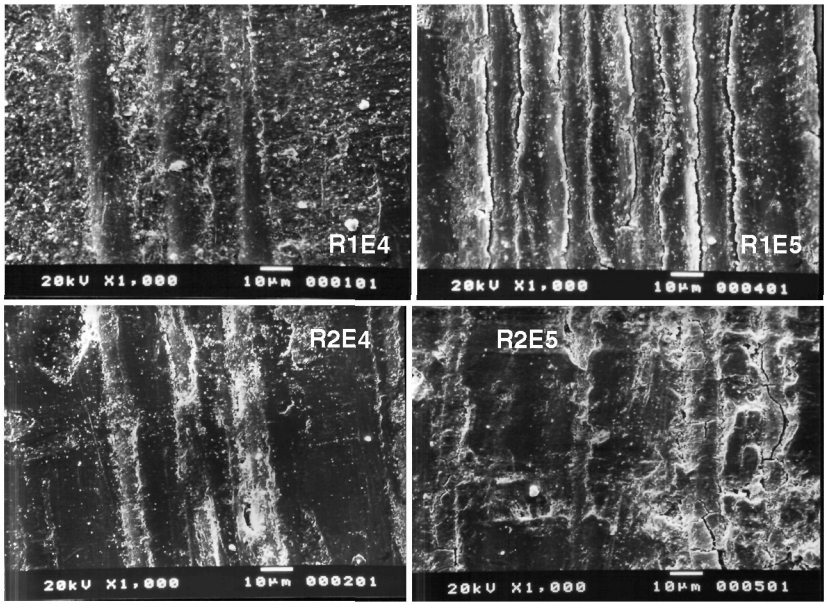



Figure 4: SEM micrographs of the surface of rod R1 in different environments.

## CONCLUSIONS

1. Aging in hot water accelerates the deterioration of the FRP rebars in concrete. However, it is not certain that a temperature of 80°C represents well the processes that develop in the actual material during time under natural conditions, due to the differences seen in slip behavior of the rods. Other than that, SEM micrographs showed a similar deterioration pattern.
2. Prolonged curing in water probably densens the zone around the rod due to:

   -Additional cementitious activity

   -Swelling of the polymer

   This phenomenon can increase the bond strength of the smooth rods in which the bond is based on pure friction between the rod and the surrounding concrete.
3. The extent of damage into the rod and to the structural fibers needs further study in order to determine the possibility of structural damage to the rods during time, and not only to their surface.

## ACKNOWLEDGMENTS

This research was partially supported by the Fund for the Promotion of Research at the Technion

**REFERENCES**

Bank L. C., 1993, "Properties of FRP reinforcement for concrete", in proceedings *Fiber Reinforced Plastic (FRP) for Concrete Structure: Properties and Applications*, Nanni A. Ed., Elsevier Science Publishers, pp. 59-86.

Bank L. C., Puterman M. and Katz A., 1998, "The effect of materials degradation on bond properties of fiber reinforced plastic reinforcing bars in concrete", *ACI Materials Journal*, Vol. 95, No. 3, pp. 232-243.

Bentur A. and Mindess S., 1990, "*Fiber Reinforced Cementitious Composites*", Elsevier Science Publishers.

Ehsani M. R., Saadatmanesh H. and Tao S., 1993, "Bond of GFRP rebars to ordinary strength concrete", in Proceedings of *Fiber Reinforced Plastic Reinforcement for Concrete Structures*, Nanni A. and Dolan C. W. Eds., American Concrete Institute (ACI) Special Publication SP-138, pp. 333-345.

Katz, A., 1999, "Bond Mechanism of FRP Rebars to Concrete", *Materials and Structures*, Vol. 32, pp. 761-768.

Nanni A., Bakis C. E. and Mathew J. A., 1998, "Acceleration of FRP bond degradation", in Proceedings of *Durability of Fiber Reinforced Polymer (FRP) Composites for Construction*, Benmokrane B. and Rahman H. Eds., University of Sherbrooke,Canada, pp. 45-56.

Tannous F. E. and Saadatmanesh H., 1999, "Durability of AR glass fiber reinforced plastic bars", *Journal of Composites for Construction*, Vol. 3 No. 1, pp. 12-19.

Uomoto, T. and Ohga H, 1996, "Performance of fiber reinforced plastics for construction reinforcement, in Proceedings *Advanced Composite Materials in Bridges and Structures*, El-Brady et al. Eds., Canadian Society for Civil Engineers, Montreal, Canada, pp. 125-132.

# Durability and service life prediction of GFRP for concrete reinforcement

VALTER DEJKE and RALEJS TEPFERS
Department of Building Materials, Chalmers University of Technology, Göteborg, Sweden

## INTRODUCTION

In recent years FRP (Fibre Reinforced Polymer) reinforcement has emerged as an alternative to conventional steel reinforcement in aggressive environments. The most important benefit is that it is not susceptible to carbonation- and chloride initiated corrosion like steel. Of the FRP types available, glass-FRP (GFRP) is the cheapest, and consequently has the highest potential of being cost effective.

However, GFRP reinforcement may deteriorate due to degradation mechanisms other than those for steel. Concrete is a highly alkaline environment having a pH value of approximately 13-14 (before carbonation or leakage have occurred). Under these circumstances steel is passivated and cannot corrode. For GFRP (and also for aramid-FRP) on the other hand, the high alkalinity of concrete may instead lead to a slow deterioration in mechanical properties due to base hydrolysis. Furthermore, GFRP are prone to fail due to stress-rupture (or stress-corrosion) when subjected to long-term sustained tensile stress. In the existing design guidelines the stress-rupture problem is handled by introducing upper stress limits, while the deterioration in mechanical properties due to environmental influence is compensated for by using strength reduction factors.

A great deal of research has been addressing durability of FRP for concrete reinforcement in recent years. The required service life of concrete reinforcement is usually in the order of 50 to 100 years, and as results is desirable within only one or a few years, accelerated ageing is generally used to speed up the degradation. However, so far the durability research conducted in this area have been predominantly qualitative, comparing different FRP types to determine which perform better. For this new material to be generally accepted by the building industry, a good durability must be proven also in quantitative terms. Hence, a big challenge for researchers within this field is to determine the deterioration rate, and thereby the service life of GFRP in concrete. This knowledge is needed for safe design of concrete structures using FRP reinforcement.

## PROJECT OBJECTIVE

At Chalmers University of Technology/Department of Building Materials, a research project on the durability of GFRP in concrete is now going on. The project objective is to make a quantitative assessment of the durability and service life of GFRP reinforcement in concrete. Hopefully the results obtained within this project can contribute to the determination of allowable design strength of GFRP used as concrete reinforcement.

*FRPRCS-5*, Thomas Telford, London, 2001.

## DEGRADATION MECHANISMS

### General consideration

FRP consists of fibres, a polymer matrix and the fibre/polymer interface region. Hence, degradation of FRP occurs as a consequence of degradation of one or several of its constituents. In GFRP, the fibres are generally considered to be the weakest link, as E-glass (the most commonly used glass fibre type) is known to degrade when in contact with an alkaline solution. Therefore an important role of the matrix is to protect the fibres from the OH-ions in the concrete pore solution. In general, degradation of the fibres mainly affects the tensile properties of the composite, while degradation in the matrix or fibre/matrix interface region essentially affects the inter laminar shear strength (ILSS), which in turn control the bond strength (between concrete and FRP reinforcement). Hence, a good resistance to degradation of all the constituents are important for FRP to meet the requirements for concrete reinforcement.

### Degradation of fibres

In the literature, several possible degradation mechanisms for glass in alkaline environment are described.

One important mechanism that results in dissolution of the silica oxygen network is shown in Equation 1 (Yilmaz and Glasser, 1991; Yilmaz, 1992; Veysel et al, 1991).

$$\text{-Si-O-Si-} + OH^- \rightarrow \text{-Si-OH (solid)} + \text{Si-}O^- \quad \text{(solution)} \qquad (1)$$

Furthermore, in alkaline solutions (especially if pH is more than 10) $HSiO_3^-$, $SiO_3^{2-}$ and $H_2SiO_3$ may be leached from the glass surface as a result of the reaction (Yilmaz and Glasser, 1991).

Another important degradation mechanism for E-glass has been claimed to be the attack by alkali on the $SiO_2$-CaO structure (Rostásy, 1997). Yet another suggested mechanism is given in Equation 2 (Adams, 1984):

$$2 \text{ x } NaOH + (SiO_2)_X \rightarrow \text{x } Na_2SiO_3 + \text{x } H_2O \qquad (2)$$

However, in a composite the fibres are embedded in the polymer matrix and hence, degradation of fibres must involve transport of the aggressive agent through the matrix. Therefore, a composite of good quality can exhibit a good resistance to alkali attack even though the fibres are prone to degradation when in direct contact with alkali solution.

### Degradation of the polymer matrix

The chemical durability of thermosetting resins is governed to a large extent by the chemical nature of the backbone of the polymer. A possible degradation mechanism is base hydrolysis of the ester linkages. All resin types contain ester bonds and these are generally the weakest part of a polymer. As concrete represents a highly alkaline environment base hydrolysis can be expected to take place to some extent. An ester linkage and the chemical reaction of base hydrolysis are shown in Figure 1.

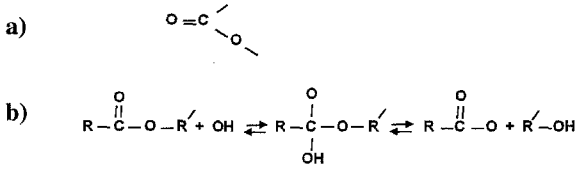


*Figure 1*
*a) An ester, b) base hydrolysis of ester (Jones, 1984).*

Polyesters are prone to undergo saponification in an alkaline environment. This occurs as a result of hydroxyl attack on the ester linkages and the great susceptibility is a consequence of the large number of ester linkages present in the backbone of this type of resin (Comyn, 1985). In contradiction to polyesters the ester linkages in vinyl esters are terminal and shielded by methyl groups and hence, are less susceptible to hydrolysis (Chin et al, 1997). In addition the epoxy backbone in vinyl esters is very resistant to chemical attack and due to the fact that the vinyl groups are very reactive complete cure of the backbone is easily accomplished (Theodore, 1988), which improves the environmental resistance.

### Degradation of the fibre/matrix interface

A coupling agent is generally used with the primary function to provide a good bond between the glass fibre and the polymer (Hull and Clyne, 1981). For E glass fibre reinforced polyester or vinyl ester the *silane coupling agent* is commonly used. However, the chemical bond between silane and glass have been reported to be susceptible to water and alkali and may therefore degrade in such environments.

## EXPERIMENTS

The durability experiments at Chalmers University of Technology were started in late spring 1999, and are still going on (at the time this paper was written).

### Material

Four types of GFRP bars from two manufacturers are examined. The bars differ regarding type of glass fibre and polymer matrix according to Table 1.

*Table 1 Fibre type and matrix material for the bars tested.*

| | Fibre type | Matrix material |
|---|---|---|
| **GFRP bar A** | E-glass | vinyl ester |
| **GFRP bar B** | AR-glass | vinyl ester |
| **GFRP bar C** | AR-glass | polyester |
| **GFRP bar D** | E-glass | vinyl ester |

### Exposure conditions

Specimens are subjected to accelerated as well as non-accelerated exposure under three environmental conditions (concrete, alkali solution and water) at 20, 40, 60 and 80°C, to study the influence on the GFRP material. The environmental conditions are as follows:

The ***concrete*** used is made of Swedish low alkali Portland cement and has a water/cement ratio of 0.5. The specimens are embedded in the concrete and stored at 100% RH (relative humidity) to simulate a real concrete structure under moist conditions. The concrete has been

cast in a way that makes it easy to extract the bars from it without causing any damage on them, before testing of aged samples.

***Alkaline solution*** was used to be able to compare the aggressiveness to that of concrete. The solution consists of sodium hydroxide (NaOH), potassium hydroxide (KOH), and calcium hydroxide ($Ca(OH)_2$), in a composition simulating the concrete described above, and giving a pH value of 13.7.

***Tap water*** was chosen as a reference environment to be able to determine how large part of the total deterioration that was caused by the alkali solution and water respectively.

**Test methods**

Aged GFRP bars are being tested regarding there mechanical as well as physical properties, to evaluate how the environmental exposure affects the material.

The mechanical properties tested after environmental exposure are tensile strength and ILSS (Inter Laminar Shear Strength). ILSS is a property dominated by the condition of the polymer matrix and the fibre/matrix interface and is considered to be intimately related to the bond strength between concrete and FRP reinforcement (Sheard et al, 1997). ILSS is determined by measuring the load capacity in three point bending of a short GFRP beam with fibres oriented parallel to the length of the beam. The failure takes place between the fibres resulting in a failure surface parallel to the length of the beam. ILSS is a useful test method as it is easier to carry out than pullout tests.

Samples have also been analysed using LA-ICPMS (Laser Ablation Inductive Coupled Plasma Mass Spectroscopy) to detect signs of degradation or alkali ingress taking place in the material.

**Results**

Deterioration in tensile strength and ILSS has been found for all GFRP types and for all exposure conditions used. However the magnitude of deterioration was found to vary considerably between the GFRP types tested. A summary of the tensile strength and ILSS results for bars A-D after being embedded in concrete at 60°C for approximately 1 year is shown in Figure 2.

A conclusion that can be drawn from the results is that different mechanical properties may deteriorate at different rate. As a consequence, to study only one mechanical property may not be enough to determine which one of two bar types is the more durable. For instance, testing only tensile strength would not reveal the poor ILSS performance of Bar C and consequently give the impression that Bar C is more durable than Bar D. However, testing also ILSS would lead to the conclusion that Bar D has the better overall durability.

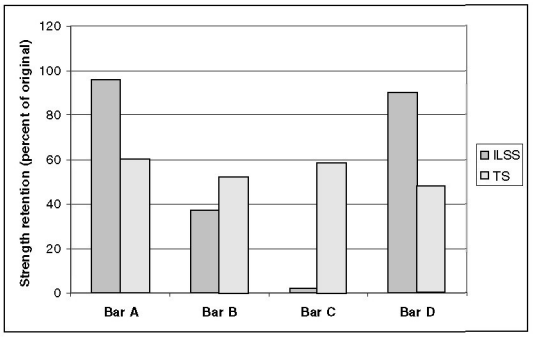



*Figure 2*
*Inter Laminar Shear Strength (ILSS) and tensile strength (TS) for GFRP bars after being embedded in concrete at 60°C for approximately 1 year (10 months for Bar D in tensile strength).*

It is evident from Figure 2 that the E-glass/vinyl ester systems (Bar A and Bar D) have considerably better environmental resistance regarding ILSS compared to the other systems investigated. Bar C almost completely lost it's ILSS after the exposure. The poor performance of glass/polyester composites after exposure in alkaline environments has been reported by several researchers (Comyn 1985) and was expected. For all bars, including those with AR-glass, significant losses in tensile strength were observed. It appears from Figure 2 that the E-glass/vinyl ester systems have the best overall durability.

Figure 3 gives an indication of the severity of different exposure environments and temperature levels. In the figure, the course of tensile strength, and ILSS deterioration for Bar A is shown. Considering tensile strength, alkali solution appears to be a slightly more aggressive environment than concrete at 100% RH. Note also that pure tap water can cause considerable weakening of the material. Regarding ILSS only small deteriorations were experienced and it's difficult to draw conclusions regarding the relative aggressiveness of the different exposure conditions.

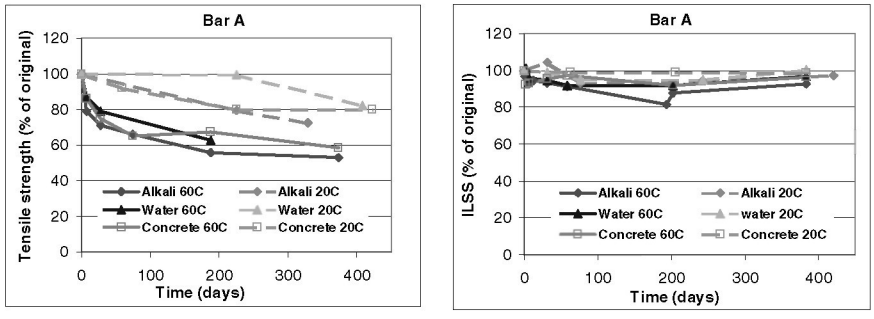



*Figure 3* *Tensile strength and ILSS retention for bar A exposed to alkali solution, concrete and water at 20°C and 60°C. Each data point in the diagram represents the average of one to six test results.*

To examine ingress of elements from the alkali solution LA-ICPMS analysis was conducted. With this equipment it is possible to detect elements heavier than sodium at very low concentrations. The specimens were examined along lines with a length of 2-4 mm starting in the core of the bar and ended at the surface in a direction perpendicular to the surface. To be

able to determine where the surface of the bar were, a "trace paint" (TipEx) was used. This paint contains Titanium at considerably higher concentration than that in the GFRP bars and thus, provides a clear indication on when the surface has been reached. The results were found to differ a lot between the bar types studied. This is believed to depend on the quality of the polymer surface layer. For bar A, having a surface layer of good quality no alkali ingress could be detected. For bar type D, the quality of this layer was poor and come loose after only a few days in alkaline solution at 60°C. For this bar detectable concentration levels of Na and K was found at a depth of approximately 0.5 mm from the surface for specimens exposed to alkali solution at 60°C for 7 months. LA-ICPMS results for this bar type are shown in Figure 4.

Thermosetting resins are known to be semi-permeable allowing water to penetrate while the transport of larger molecules or inorganic ions are restricted (Jones, 1998). It is therefore believed that the alkali transport in bar D took place in micro-cracks. This result shows the importance of a polymer surface layer of good quality.

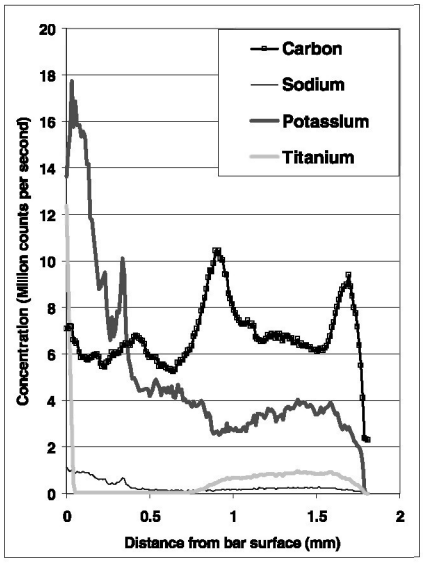



*Figure 4*
*Concentration of various elements in GFRP bar D. The bar had been immersed in alkali solution (pH 13.7 at 60°C) for 7 months prior to the measurement, which was conducted using LA-ICPMS.*

## ON SERVICE LIFE PREDICTION

### Methods suggested in the literature

Katsuki and Uomoto (1997) have used Fick's law to simulate the deterioration of GFRP rods quantitatively. GFRP bars were immersed in alkaline solution and the sodium (Na) penetration depth in the GFRP material could be determined after different exposure duration using an EPMA (Electron Probe Microscope Analyser). The diffusion coefficient of alkali in GFRP was calculated using the same equation. By assuming that the strength in the GFRP material was totally lost in parts reached by the Sodium front, the deterioration in tensile strength could be predicted by calculating the theoretical ingress depth after a chosen period of time. The same approach was used by Saadatmanesh and Tannous (1997) to predict the reduction in tensile strength of various FRP tendons. This approach presupposes that the

ingress of alkali ions in the GFRP material can be measured. However, it is doubtful if modern, high quality GFRP materials actually allow ingress of alkali ions in measurable quantities. Furthermore, a bar that loses all tensile strength in a layer penetrated by alkali ions probably also loses its bond strength. Hence, for the assumptions made in that method, deterioration in bond strength is likely to control the service life rather than the tensile strength.

Another approach that has been suggested (Porter and Barnes, 1998; Vijay and GangaRao, 1999) is to utilise the time-temperature relationship established for *glass fibre reinforced concrete, GRC* (Litherland et al, 1981). This relationship is used to transform time under accelerated exposure of GFRP bars (in alkali solution or embedded in concrete) to time at a real application. The benefit of using this approach is that reliable time-temperature relationships for GRC are available for relatively long exposure times (at least 10 years). However, it is not obvious that the time-temperature relationship that applies for the degradation of GRC is valid also for GFRP. For instance movements of various agents are more restricted in thermosetting plastics than in concrete and, furthermore, the time dependence of degradation mechanisms taking place in the fibre/polymer interface is not included in the "time-shift factor" that apply for GRC.

**Suggested approach**

In this project an aim is to quantify the time shift factor describing the relationship between accelerated and non-accelerated exposure, by using data exclusively from tests on GFRP. If the shape of the curve describing the change in some mechanical property with time is similar for different exposure temperatures then an Arrhenius type relationship can be expected (Litherland et al, 1981). In that case the "time shift factor" can be obtained from the distance between two such curves, established for different temperatures, in a diagram having logarithmic time scale.

Preliminary time shift factors have been established for Bar A. In Figure 5 the strength reductions after exposure in concrete and alkaline solution at 20°C and 60°C are shown. In the diagram (having a logarithmic time scale) the shape of the strength retention curves have been approximated by straight parallel lines. Comparing the displacement of the curves with respect to temperature gives a time shift factor of approximately 21. That is, one year exposure in moisture-saturated concrete at 60°C should give the same reduction in tensile strength as 21 years in moisture saturated concrete at 20°C. However this value of the time shift factor is only valid for tensile strength and under the above assumptions and environmental conditions. This approach can be used to determine the relative time-shift factor between any two exposure temperatures, under the assumption that Arrhenius time-temperature relationship is valid for the whole temperature range considered. For example, under the above assumption, 18 months in concrete at 60°C correspond to 100 years at outdoor conditions in the southwest of Sweden (where the mean annual temperature is 7°C). The calculation procedure is shown in Equation 3.

$$TSF = e^{\frac{B}{T_1+273.15} - \frac{B}{T_2+273.15}} \tag{3}$$

Where:

$TSF$ is the Time Shift Factor

$B$ is a constant determined using the time-shift shown in Figure 4

$T_1, T_2$ are the temperatures (in °C) between which the $TSF$ is calculated

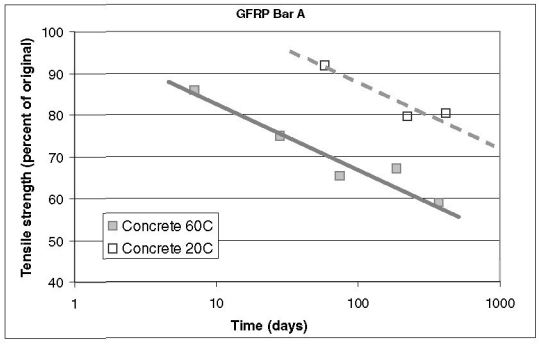



*Figure 5*
*Strength retention versus time for Bar A after being embedded in concrete at 20°C and 60°C. Straight lines have approximated the shapes of the strength retention curves.*

These kinds of predictions are important, as the maximum tensile strength utilizable in design with FRP is that of the material at the end of the service life. The experimental results discussed in this article mainly apply for tensile strength retention of GFRP bars exposed to moisture-saturated concrete and without any stress acting on them. In the majority of real applications the RH of the concrete is not 100% but considerably less (in Sweden the RH in outdoor concrete is generally around 80%). Hence, under outdoor conditions the degradation is likely to take place at a lower rate than that for moisture saturated concrete in the lab. However, in a real application reinforcement is usually subjected to tensile load to some degree, which probably will make any degradation to take place at a higher rate (for example by open up micro cracks that allow ingress of water and harmful agents into the composite). It is therefore important to determine the strength retentions and time shift factors for all the conditions (regarding environment and stress) faced by GFRP when used as concrete reinforcement. Nevertheless, a reasonable assumption should be that the time-temperature relationship suggested in this article applies fairly well with that for GFRP reinforced concrete in an outdoor application with moderate stress acting on the reinforcement.

The influence on degradation rate of different moisture contents of the concrete in which the GFRP reinforcement is embedded will be the subject for future research at Chalmers University of Technology.

## CONCLUSIONS

This article summarises a research project carried out at Chalmers University of Technology, Department of Building Materials, on the durability GFRP used for concrete reinforcement. Possible degradation mechanisms of GFRP material in alkaline environments have been discussed and experimental results obtained so far reported. Furthermore, an approach for prediction of strength retention of GFRP bars in concrete has been presented.

From the work conducted so far within the project the following conclusions can be drawn:

- ✓ Different properties may deteriorate at different rates during environmental exposure. Hence, it is not enough to test only one mechanical property (for instance tensile strength) in order to evaluate the durability.

- ✓ A polymer surface layer of good quality on GFRP bars appears to, to a large extent, prevent alkali ions to penetrate the composite, which probably results in a better environmental resistance.

- ✓ Of the GFRP systems tested, it appears as if the E-glass/vinyl ester composite have the best overall durability in alkaline environments. This is probably due to the good quality of the fibre/matrix interface in this system.

- ✓ Alkaline solution seams to represent a slightly more aggressive environment than that of moisture saturated concrete (both having the same pH value).

- ✓ Time-temperature relationships can be determined from strength retention curves obtained for GFRP exposed to concrete at different temperatures. According to preliminary results, 18 months in concrete at 60°C corresponds to 100 years under outdoor conditions (in the south-west of Sweden).

## ACKNOWLEDGEMENTS

The support of SBUF (The Development Fund of the Swedish Construction Industry), BFR (Swedish Council for Building Research), NCC (Nordic Construction Company), ConFibreCrete (Training and Mobility of Researchers, EU project) and my supervisors: Professor Ralejs Tepfers and Professor Lars-Olof Nilsson are gratefully acknowledged.

## REFERENCES

Adams P. B., "Glass corrosion -A record of the past? A predictor of the future", Journal of Non-Crystalline Solids 67, Amsterdam, North-Holland, 1984, pp. 193-205.

Chin J. W., Nguyen T., Aouadi K., "Effects of environmental exposure on fiber-reinforced plastic (FRP) materials used in construction", Journal of Composites Technology and Research, Vol 19, No 4, Oct 1997, pp. 205-213.

Comyn J., "Polymer permeability", Chapman and hull, Printed in Great Britain by Ipswich Book Co, Ipswich, Suffolk, 1985, (reprinted 1994).

Hull D. and Clyne T. W., "An introduction to composite materials", Cambridge University Press, First published 1981, Second edition 1996.

Jones F. R., "A review of deterioration mechanisms of sewer renovation materials", Department of Metallurgy & Materials Technology University of Surrey, guildford GU2 5XH, February 1984.

Jones F. R., "Designing composites for durability in aqueous and corrosive environments", Designing Cost Effective composites, Editor Banks W., 1998, pp. 65-81.

Katsuki F. and Uomoto T., "Evaluation of alkali resistance of GFRP Rods", Concrete Library of JSCE No. 29, June 1997.

Litherland K L, Oakley D R, Proctor B A, "The Use of Accelerated Ageing Procedures to Predict the Long Term Strength of GRC Composites", Cement and Concrete Research - *An International Journal*- Vol 11, No 3, New York, Pergamon Press, May, 1981, pp. 455-466.

Porter M. L. and Barnes B. A., "Accelerated aging degradation of glass fiber composites", Fiber Composites in Infrastructure, Proceedings of the Second International Conference on Fibre Composites in Infrastructure ICCI'98, Vol. 2, Tucson, 1998, pp. 446-459.

Rostásy F. S., "On durability of FRP in aggressive environments", Non-Metallic (FRP) Reinforcement for Concrete Structures: *Proceedings of the Third International Symposium*, Vol 2, Sapporo, Oct. 1997, pp. 107-114.

Saadatmanesh H, Tannous F, "Durability of FRP Rebars and Tendons", Non-Metallic (FRP) Reinforcement for Concrete Structures: *Proceedings of the Third International Symposium*, Vol 2, Sapporo, Oct. 1997, pp. 147-154.

Sheard P, Clarke J, Dill M, Hammersley G, Richardson D, "Eurocrete - Taking Account of Durability for Design of FRP Reinforced Concrete Structures", Non-Metallic (FRP) Reinforcement for Concrete Structures: *Proceedings of the Third International Symposium*, Vol 2, Sapporo, Oct. 1997, pp. 75-82.

Theodore J. R., "Engineered materials handbook, Vol. 2: Engineering Plastics, ASM International, Ohio 1988, pp. 272-275.

Veysel T., Yilmaz, Lachowski E. E., and Glasser F. P., "chemical and microstructural changes at alali-resistant glass fibre-cement interfaces", J. Am. Ceram. Soc. 74 (12), 1991, pp. 3054-60.

Vijay P. V., and GangaRao V. S., "Accelerated and Natural Weathering of Glass Fiber Reinforced Plastic Bars", Proceedings from Fourth international Symposium, Fiber Reinforced Polymer Reinforcement for Reinforced concrete Structures, ACI Ed. Dolan C. W., Rizkalla S. H. and Nanni A., Baltomore 1999, pp. 605-614.

Yilmaz V. T. and Glasser F P, "Reaction of alkali-resistant glass fibres with cement. Part 1. Review, assessment, and microscopy", Glass Technology, Vol. 32, No. 3, Sheffield, Society of glass technology, June 1991, pp. 91-98.

Yilmaz V. T., "Chemical attack on alkali-resistant fibres in a hydrating cement matrix: characterization of corrosion products", Journal of Non-Crystalline Solids 151, 1992, pp. 236-244.

# Creep and long-term behaviour

# Stress-rupture of FRP: state of the art

K. AUDENAERT, Magnel Laboratory for Concrete Research, Department of Structural Engineering, Ghent University, Belgium.
L. TAERWE, Magnel Laboratory for Concrete Research, Ghent University, Belgium.
D. GAZOULI, Department of Civil Engineering, University of Patras, Greece

## INTRODUCTION

The use of advanced composite materials, like non-metallic tendons based on high strength fibres in a polymeric matrix, introduces materials of which the characteristics and their long-term behaviour are not well known up to now. These composite materials based on glass, aramid or carbon fibres, have strength capacities in the range of prestressing steel. However several other material characteristics differ considerably from those of prestressing steel. This is especially important for those -less familiar- phenomena or characteristics that may become critical or decisive in the design process.The mechanical, physical and chemical properties in relation to long term use have to be investigated and evaluated.

Of particular importance is the stress-rupture behaviour of FRP. This is the process which leads to failure if the material is subjected to a sustained high load lower than the short-term failure load. In the first part of this paper, this process is described. The stress-rupture behaviour is strongly influenced by the sustained stress level, the type of FRP and the environmental conditions. These influencing factors are discussed in the second part. Most high strength fibres are perfectly resistant in environments where steel will corrode, but in the alkaline environment of the concrete matrix, where steel behaves perfectly, some types of FRP face problems. This inherently means that the long term interaction with concrete may become critical. To assess the reliability of applications on the longer term, the extrapolation of the residual strength based on the Arrhenius approach is discussed. The existing test methods are briefly described in the next part, followed by known models and test results of several researchers. In the last part, a summary of different recommended stress limits is given.

## STRESS-RUPTURE BEHAVIOUR

Stress-rupture is the process which leads to failure of the material if subjected to a sustained high load. For a specific type of FRP, the time to failure depends primarily on two factors. The first factor is the ratio of the applied load to the short-term tensile strength. If this ratio increases, the time to failure will decrease. The environment is the second factor. For example, permanent contact of an GFRP element with an alkaline solution – chemically similar to the concrete's pore water- will definitely damage the fibres, resulting in a decrease of the failure time.

Stress-rupture is usually preceded by creep and can be thought of as a creep-to-failure, which leads to the alternative name of creep-rupture. The behaviour of most fibrous materials is characterized by an initial elastic response, followed by a fairly rapid primary creep phase, a

long, relatively slow secondary creep phase and a rapid tertiary creep towards failure, as shown in fig. 1.

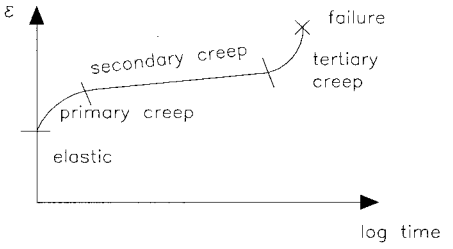



Fig. 1: Creep behaviour of FRP [1]

Stress-rupture does not represent a reduction in short-term strength with time. If fibres are subjected to a load which would cause failure by stress-rupture after some long time $t_f$ but are instead tested after a proportion of that time, they will usually have a strength, equalling the initial short-term strength. Only those elements tested just before $t_f$ will show a reduction in strength. This process is known as strength retention and is illustrated in fig 2.
The basic mechanism of this behaviour can be summarized as follows. The fibre can be regarded as a chain of elements in series, whose strengths vary because the fibre is not uniform at a molecular level along its length. When subject to a short-term load, the fibre will fail at its weakest element. When subjected to a long-term load, weaknesses will develop, either by crack propagation (for glass) or bond slippage (for aramid). But, until only a short time before the eventual failure, the particular place of final failure does not stand out as particularly weak by comparison with its neighbours. The element thus retains its full apparent strength. The difference between stress-rupture and strength retention is shown in fig. 2.

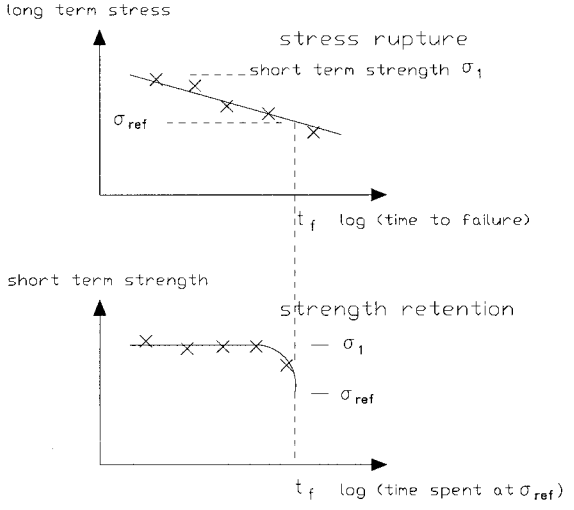



Fig. 2: Stress-rupture and strength retention behaviour [1]

## FACTORS INFLUENCING THE STRESS-RUPTURE BEHAVIOUR

### Stress level

Yamaguchi et al. [2] performed stress-rupture tests on AFRP, CFRP and GFRP rods, at different stress levels in air at 22±1°C. More than ten tests were carried out at each stress level. The results of these tests are shown in fig. 3, and indicate that a linear relationship exists between stress-rupture strength and the logarithm of time. The obtained relationships between the time until failure and the applied stress can be used for extrapolations to determine the admissible stress when the target service live of the structure is known.

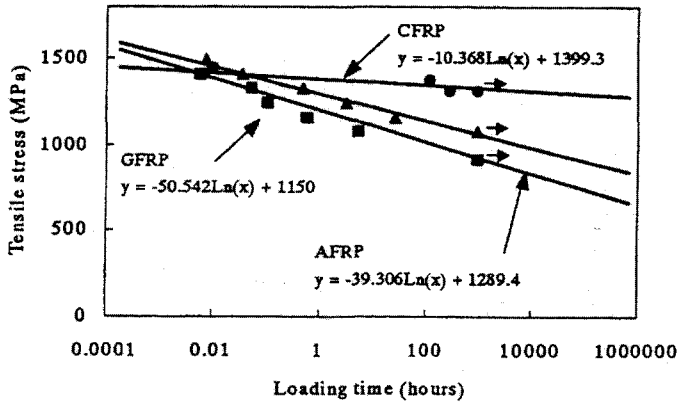



Fig. 3: Stress-rupture time of FRP rods [2]

### Type of FRP

Although all the analytical relationships between the stress and rupture time seem to be of the same type (fig. 3), creep strains and failure modes of each type of FRP are quite different. The appearance of each type of FRP after failure and the measured creep strains are described in [3]. In case of AFRP rods, the creep strain gradually increases during loading time. This creep strain behaviour can be divided into three periods from the beginning to the failure (see also fig. 1). In case of GFRP rods, creep strains of the rod increased step by step during the loading time. In case of CFRP rods, failure occurs without any creep strain throughout the loading time.

### Environment

The environment is of great influence on the creep-rupture behaviour of most FRP materials. The FRP suited for pre- and post-tensioning of concrete members will not be damaged by ions from usual acidic solutions. But more important is the influence of alkaline solutions with pH>12.5, e.g. fresh concrete or the pore solution of hardened concrete. Not all fibres are equally sensitive. Glass fibres are attacked by $OH^-$ - as well as by $Cl^-$ -ions. Aramid fibres are only slightly attacked by $OH^-$ -ions and are not vulnerable to chlorides. Carbon fibres are nearly inert to most environments. It is clear that the survival of these alternative reinforcements in an alkaline environment is an imperative requirement to practical application in direct contact with concrete. For some fibres, especially for aramid, even moisture is an environment to take into account. These are relatively slow processes of which the effects will only become apparent after a considerable time-span.

In order to avoid disappointing evidence after years, it is necessary to develop or define accelerated methods to simulate long-term behaviour. The investigation and evaluation of "accelerated " aging has shown that the Arrhenius aproach is very sensible. The Arrhenius approach accelerates the process by increasing the temperature in the range from 0°C to 100°C (increasing the movement of ions) and is applicable if no other disturbing processes occur. In this approach the temperature indications are plotted along the vertical axis on a linear scale for 1/T, where T is the temperature in Kelvin. At each temperature, the process develops at a certain velocity. By measuring the residual strength values of samples at regular intervals, the rate of decrease in strength can be determined at each temperature. It will appear that, if a range of measurements is carried out at several temperatures (minimum 3) lines can be drawn connecting the same residual strength levels (fig. 4). The lines found, ought to be straight to signify that no other chemical processes have interfered. Thus, if a significant part of these lines, which are principally parallel, can be established, an extrapolation of the rate of degradation to be expected, e.g. at room temperature in the given environment, can be obtained by measurements at higher temperatures. The lines will shift to the left if less resistant (e.g. glass) or less protected fibres (e.g. pure fibres) are chosen. The slopes can differ slightly dependent on the particular resin chosen.
In the case of FRP elements in concrete, the agressors are mainly the free $OH^-$ - and $Cl^-$ -ions. Most of the resins used are nearly not vulnerable to this attack but some fibres are. The fibres are attacked if the ions are able to reach them. In this respect, also long-term strain capacity of the resin is important. Cracks in the resin due to insufficient strain capacity can be harmful.

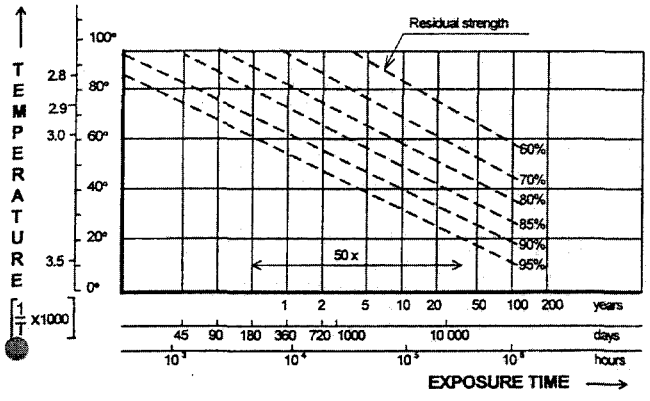



Fig. 4: Extrapolation of the residual strength according to Arrhenius for an aramid-epoxy tendon in saturated $CaOH_2$ [4]

Scheibe et al. [5,6] performed several test series on Arapree (AFRP) under constant long-term load. These series differed with respect to the environment during the test. The first test series was executed in air at 20°C, the second under the influence of an alkaline solution at the same temperature. The third series was performed in an alkaline solution at higher temperatures up to 60°C. As solution a saturated $Ca(OH)_2$ + 0.4nKOH solution was used, which is chemically comparable to the concrete pore solution. It was concluded that (see also fig. 5) an alkaline environment in combination with higher temperatures represents the greatest damage potential for AFRP bars. Another conclusion was that a comparison of test results at 20°C and 60°C for the same load level and environmental conditions shows that the influence of an increasing temperature is much more important than the influence of the

alkaline environment. One should take into account that, using a solution to simulate the effect of concrete, the movement of ions in a solution is much higher than in the concrete matrix.

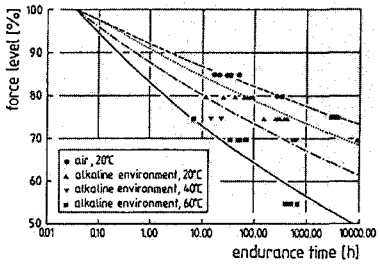



Fig. 5: Test results of stress-rupture testing on AFRP [5,6]

## TEST METHODS

The creep-rupture behaviour of FRP bars is important for defining the admissible prestress. For the prediction of endurance, extensive testing is necessary. The characteristic short-term tensile strength is used as a basis for creep-rupture tests. Unlike other construction materials, standard test methods have yet to be established for FRP materials to determine constitutive properties for these materials in civil engineering constructions. Consequently, the loading conditions and material characteristics for civil engineering applications must be determined in consultation with the manufacturer. Throughout the world, research has been conducted to determine FRP material properties, but test methods vary and are not fully documented or standardized in the literature.

Budelmann et al. [7] are proposing that creep-rupture behaviour should be investigated on at least three distinctly different force levels, e.g. 80%,70%,60% of the characteristic short-term tensile strength. The force should be maintained constant until failure occurs, the fracture times should be recorded. The range of endurance times should cover up to $10^4$ hours. Their experience shows that at least 10 to 15 results per force level are necessary.

The Japan Society of Civil Engineers (1997) has proposed a test method "Test method on tensile creep-rupture of fibre reinforced materials" [8,9]. According to the recommended test procedure, test temperature should be maintained at 20±1 °C throughout the test and at least five levels of initial loading should be executed. The number of test specimens for each load level shall not be less than three and in case of premature failure due to anchorage, additional tests should be performed on specimens from the same lot until the test results from at least three specimens have been acquired.

Some manufacturers give results for relaxation-rupture lifetimes rather than creep-rupture lifetimes. In relaxation-rupture tests, lifetimes appear longer for a given initial load since the force drops with time. So, they are more attractive to the fibre manufacturer than creep-rupture results. They would also be useful for designers, provided that a consistent global theory for creep, relaxation and rupture can be established.

## MODELLING

In a previous section, it was mentioned that a linear relationship exists between stress-rupture strength and the logarithm of time. This can be written as follows (with $\sigma_{sust}$ the sustained applied stress, $f_t$ the short term tensile strength, t the time in hours, A and B are constants) [10]:

$$\frac{\sigma_{sust}}{f_t} = A + B \log t$$

In some documents the following equation for design is proposed:

$$1.15\sigma_P(t) \leq (A + B \log t) f_{tk} \qquad \text{for} \qquad t \leq T_{life}$$

where (A+B logt) $f_{tk}$ represents the characteristic value of the stress-rupture line and $T_{life}$ is the design life time of the concrete element. An additional safety factor 1.15 is used. This condition only assures that no failure occurs under service conditions, the ultimate limit state must be checked as well and should be based on a residual strength basis.

In [11] a model for the calculation of the creep-rupture time is proposed based on failure statistics of both the resin and the fibres. First a static failure simulation model is developed considering the static failure probability of fibres, the stress in the broken fibres, the stress distribution mechanism and the change of strength of the intact fibres. This model is followed by a simulation model for the creep rupture behaviour of FRP rods, using the creep failure probability of the fibre and the relaxation of the matrix. The predictions of the models are compared with test results on GFRP, AFRP and CFRP. The predictions are giving reasonable results. However, the behaviour of the fibre-matrix interface needs further research in order to improve the accuracy of the model.

## TEST RESULTS

In [2] experimental results are given for AFRP, GFRP and CFRP rods in air at 22±1°C. For all types of FRP a linear relationship between the logarithm of the creep-rupture time and the loading level is found.
In [10] stress-rupture of Arapree is described and a survey of different test programs is given.
Stress-rupture tests on CFRP and AFRP are described in [12]. The influence of the diameter of the specimen is investigated by testing specimens with a diameter of 5 mm and 12.5 mm for the CFRP and with a diameter of 5 and 15 mm for the AFRP. Regardless of the diameter of the specimen, it is found that the load ratio and the logarithm of the creep-rupture time are proportional to each other. In [13] stress-rupture tests on GFRP rods are described. The tests were performed in air at 20 °C following the JSCE test method [8,9]. The creep failure capacity (this is the load ratio causing failure after 1 million hours, approximately 114 years) is 53.1% (which is 423N/mm²). The creep strains were measured and were found to be extremely small just after loading. However, the creep strains of many specimens increased after a while, but some increased suddenly before the creep-rupture. The obtained values for the stress-ratio-failure time model are given in table 1.

Table 1: Coefficients in stress-rupture model

| Ref. | FRP type | FRP product | Temperature [°C] | pH | A | B |
|---|---|---|---|---|---|---|
| 2 | AFRP | Rods | 22 | Air | 0.337 | -0.010 |
| | CFRP | | | | 0.426 | -0.004 |
| | GFRP | | | | 0.358 | -0.016 |
| 10 | Arapree | Strips | 20 | 13 | 0.843 | -0.030 |
| | | | 60 | 13 | 0.843 | -0.051 |
| | | Rods | 20 | Air | 0.960 | -0.073 |
| | | | 20 | 13 | 0.864 | -0.043 |
| | | | 60 | 13 | 0.847 | -0.095 |
| 12 | CFRP | Strands | Room temp. | Air | 0.964 | -0.031 |
| | AFRP | | | | 0.959 | -0.054 |
| 13 | GFRP | Rods | 20 | Air | 0.784 | -0.042 |

An extensive series of stress-rupture tests were performed at the Technical University of Delft. The specimens were made of strips of high modulus aramid. The major part of the test specimens was submerged in an alkaline solution (pH13) which was kept at a temperature of 20 °C (38 tests) or 60°C (39 tests). It can be concluded that the strength decay under constant load and alkaline conditions is 10 to 15 times faster at 60 °C than at 20 °C (fig. 6). In this figure the regression curves are shown with their respective 95 % confidence interval. It is also seen that at 50% of the characteristic load to failure the time to failure in an alkaline liquid amounts to more than 100 years (0.88 $10^6$ hours). The increase of temperature at testing shows accelerated aging effects, indicating that progressive (e.g. chemical) damage to the fibre structure is enhanced. The tests have been performed in a highly alkaline liquid, which presents much more aggressive environment than hardened concrete (slower movement of $OH^-$ -ions).

At the Technical University of Braunschweig tests were performed on AFRP bars. Three different ambient conditions were considered: air at 20 °C and an alkaline solution at 20 °C and 60 °C. It was found that the stress-rupture phenomenon is amplified by an alkaline environment and an increased temperature (see fig. 5).

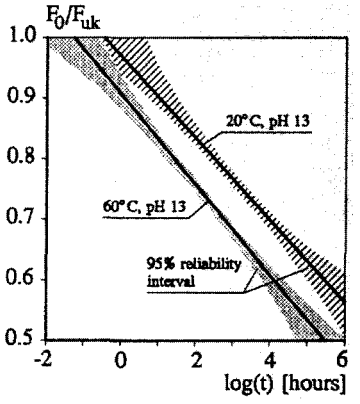



Fig. 6: Stress-rupture of Arapree in alkaline solution at different temperatures [14]

Since glass fibres are cheaper than carbon or aramid fibres, glass fibre reinforced plastics are most popular. But it is well known that the creep properties of GFRP are inferior to those of other FRP.

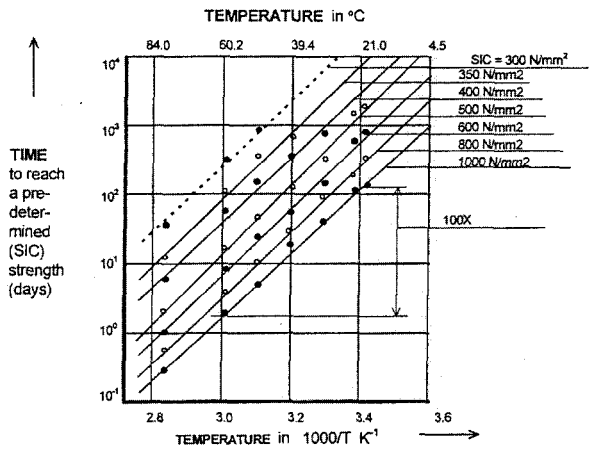



Fig. 7: Graphical representation of the Arrhenius approach for glass reinforced cement [15]

Litherland et al. [15] tested the Arrhenius approach with the evaluation of the durability of glass reinforced cement using AR-glass. They did their accelerated testing at a range of elevated temperatures and a range of time intervals with thin strips embedded in cement. It can be seen in fig. 7, that an acceleration factor of 100 is valid for a temperature increase from 20°C to 60°C. For slightly coated AR-glass under the same conditions, an acceleration factor of 200 was found. For other fibres (e.g. E-glass or S-glass), other resins and other solutions, different slopes and different distances between the lines are found. For each case, factors can be derived taking into account the kind of solution, type of fibres, coating of fibres, distance of fibres to the surface, etc. So for any case, the investigations with several temperatures on a range of time intervals has to be carried out before an acceleration factor can be established.

## RECOMMENDED STRESS LIMITS

The annex of the Canadian code limits the transfer stress in prestressing tendons as a result of the creep-rupture behaviour. Aramids are limited to 38% of the static strength and carbon to 60% of the static strength.

For AFRP, it has been proposed by Gerritse et al. [10] to limit the initial stress in the prestressing elements to 0.55 $f_{tk}$. At stressing, a value of 0.60 $f_{tk}$ is proposed.

In table 2, recommended stress limits for FRP reinforcement for different service lifes are given. These values are lower bounds from a statistical regression analysis based on tests conducted at 21±3 °C by Dolan et al. [16], Ando et al. [12], Yamaguchi et al. [2] and Seki et al. [13].

Table 2: Recommendations for stress limits

| | Service life (years) | |
|---|---|---|
| Fibre type | ≤ 50 | > 50 |
| GFRP | 0.30 | 0.25 |
| AFRP | 0.50 | 0.45 |
| CFRP | 0.80 | 0.75 |

## CONCLUSION

Stress-rupture is the process which leads to failure of the material if subjected to a sustained long term load and exists for almost all structural materials. For prestressing steel, it is of no practical relevance. However for FRP, the stress-rupture behaviour is very important and can become decisive. It is strongly influenced by the applied stress and the environment. If the applied stress is increasing, the time to failure will decrease. A linear relationship exists between the ratio of the applied stress to the short term tensile strength and the logarithm of time. The obtained relationships between the time to failure and the applied stress can be used for extrapolations to determine the admissible stress when the target service life of the structure is known. The environment is also of great influence, especially alkaline environments. Accelerated test methods using the Arrhenius approach in order to simulate long term behaviour are very sensitive. In this approach, the process is accelerated by increasing the temperature in the range of 0°C to 100°C. For a definite residual strength level, there is a linear relationship between the inverse of the temperature (in Kelvin) and the logarithm of time if no other disturbing processes occur. By extrapolating this relationship for a given environment to a temperature that will occur, the residual strength is known. Recommended stress limits are given and are varying between 40% and 55% of the short term tensile strength for AFRP. For CFRP and GFRP these ratio's are respectively 60% to 80% and 30%.

## REFERENCES

1. C. BURGOYNE, Long term behaviour of FRP composites, Discussion document for use at fib TG 9.3 meeting, Lisbon 1999
2. YAMAGUCHI, T. NISHIMURA, T. UOMOTO, Creep model of FRP rods based on fiber damaging rate, Proceedings of the first international conference (CDCC 1998), Durability of fibre reinforced polymer composites for construction, eds. B. Benmokrane, H. Rahman, 1998, p. 427-438
3. T. YAMAGUCHI, Y. KATO, T. NISHIMURA, T. UOMOTO, Creep-rupture of FRP rods made of aramid, carbon and glass fibers, Non-Metallic reinforcement for concrete structures, Proceedings of the third international symposium on non-metallic (FRP) reinforcement for concrete structures, Vol. 2, eds. S. Morita, H. Okamura, T. Uomoto, Oct. 1997, p. 179-186
4. A. GERRITSE, Assessment of long term performance of FRP bars in concrete structures, Proceedings of the first international conference (CDCC 1998), Durability of fibre reinforced polymer composites for construction, eds. B. Benmokrane, H. Rahman,1998, p. 285-298
5. M. SCHEIBE, F.S. ROSTASY, Engineering model of stress-rupture of AFRP in concrete, Proceedings of the second international symposium on non-metallic reinforcement for concrete structures, ed. L. Taerwe, 1995, p. 74-81
6. M. SCHEIBE, F.S. ROSTASY, Stress-rupture of AFRP subjected to alkaline solutions and elevated temperature – experiments, Proceedings of the second international

symposium on non-metallic reinforcement for concrete structures, ed. L. Taerwe, 1995, p. 67-73
7. H. BUDELMANN, F.S. ROSTASY, Creep-rupture behavior of FRP elements for prestressed concrete – phenomenon, results and forecast models, International Symposium on FRP Reinforcement for concrete structures, March 1993, p. 87-100
8. JSCE-E 533-1995, Test method for creep failure of continuous fiber reinforcing materials, Recommendation for design and construction of concrete structures using continuous fiber reinforcing materials, JSCE 1997, p.98-101
9. JSCE-E 533-1995, Commentary on the test method for creep failure of continuous fiber reinforcing materials, Recommendation for design and construction of concrete structures using continuous fiber reinforcing materials, JSCE 1997, p.136-139
10. A. GERRITSE, L. TAERWE, Recommended design aspects for concrete members pretensioned with aramid fiber reinforced polymers, Proceedings of the fourth international symposium on fiber reinforced polymer reinforcement for reinforced concrete structures, eds. C. W. Dolan, S. H. Rizkalla, A. Nanni, ACI SP-188, 1999, p. 829-841
11. T. YAMAGUCHI, T. NISHIMURA, T. UOMOTO, K. TAKEWAKA, Simulation for creep rupture of FRP rods based on statistical theory of fracture of fibres, Transactions of the Japan Concrete Institute, Vol. 21, 1999, p. 227-234
12. N. ANDO, H. MATSUKAWA, A. HATTORI, M. MASHIMA, Experimental studies of the long term tensile properties of FRP tendons, Proceedings of the third international symposium on non-metallic reinforcement for concrete structures, eds. S. Morita, H. Okamura, T. Uomoto, 1997, p. 203-210
13. H. SEKI, K. SEKIJIMA, T. KONNO, Test method on creep of continuous fiber reinforcing materials, Proceedings of the third international symposium on non-metallic reinforcement for concrete structures, eds. S. Morita, H. Okamura, T. Uomoto, 1997, p. 195-201
14. A. GERRITSE, J.A. DEN UIJL, Long-term behaviour of Arapree, Proceedings of the second International Symposium on Non-Metallic reinforcement for concrete structures, ed. L. Taerwe, 1995, p. 57-66
15. K. LITHERLAND, D. OAKLEY, B. PROCTOR, The use of accelerated ageing to predict long term strength of GRC composites, Cement and Concrete Research, vol. 11, 1981
16. C.W. DOLAN, B.L. LEU, A. HUNDLEY, Creep-rupture of fiber reinforced plastics in a concrete environment, Proceedings of the third international symposium on non-metallic reinforcement for concrete structures, eds. S. Morita, H. Okamura, T. Uomoto, 1997, p. 187-194

# Long-term creep of hybrid FRP bars

V. TAMUZS, R. MAKSIMOVS and J. MODNIKS
Institute of Polymer Mechanics, Riga, Latvia

## ABSTRACT
Five year long creep data for hybrid composites are reported. Glass-aramid-epoxy composites with different aramid and glass fiber ratios were investigated.

The theoretical prediction of creep is based on the knowledge of the creep properties of constituents. The long term creep of the matrix and fibers are predicted from the accelerated testing data using the time-temperature analogy. The theoretical and long term experimental results are compared and reveal a good coincidence.

It should be noted that, at some brittle-ductile fiber ratio and a certain load level, the fragmentation of brittle fibers can occur during the creep process. Such fragmentation leads to an unexpected creep acceleration. This phenomenon was observed and modeled using two year creep data for carbon-aramid composites.

## INTRODUCTION
At present, the most popular FRPs used for concrete reinforcement are based on carbon, glass, or aramid fibers. The first two fibers do not reveal creep deformations, whereas the aramid fibers exhibit pronounced creep under constant stresses. To be used as reinforcement in prestressed concrete the knowledge about expected the creep level of FRP rods in long periods of time is necessary. Such creep behavior can be predicted by short term tests using the WLF time-temperature superposition, but long-term control tests are necessary, too.

Hybrid FRPs with different ratios of carbon, glass, and aramid fibers can be produced to obtain the optimal relation between the stiffness, ductility and price of reinforced bars. Thermal deformation of some hybrid FRP (aramid-glass, aramid-carbon, and glass-carbon) has been studied in [1, 2]. Ductility of hybrid FRP at static loading were reported in [3]. Performance of concrete slabs with hybrid FRP reinforcement was studied [4]. If a hybrid FRP is used as reinforcement in prestressed concrete, then the creep properties of such material should be investigated.

In the present paper, the experimental long-term creep data for different glass-aramid and glass-carbon hybrids obtained in the Institute of Polymer Mechanics are reported and discussed.

## EXPERIMENTAL
The materials used were aramid SVM, glass fibers VMPS and epoxy resin EDT-10 (all produced in Russia). Hybrid glass-aramid composite plates of size 500x400x5 mm were

produced by winding technology on the basis of epoxy matrix. Six versions of samples were produced with different volume fractions of aramid, $\mu_a$,and glass, $\mu_g$,fibers, namely $\mu_a/\mu_g$ = 0.5/0, 0.40/0.10, 0.29/0.21, 0.18/0.32, 0.10/0.40, and 0/0.50. The total fiber volume content $\mu_a + \mu_g = \mu$ was 0.5 in all cases. Samples of size 5x15x180 mm were cut out in the fiber direction. The tensile creep tests were performed for a period of five years in a room adapted to long term creep tests at room temperature. The deformation level was measured by dial strain gages. Besides, the creep tests on pure aramid fibers and epoxy matrix were performed. As a part of a separate project, creep tests on a carbon-aramid hybrid were started two years ago, and the measurements are still going on. These data will be discussed later.

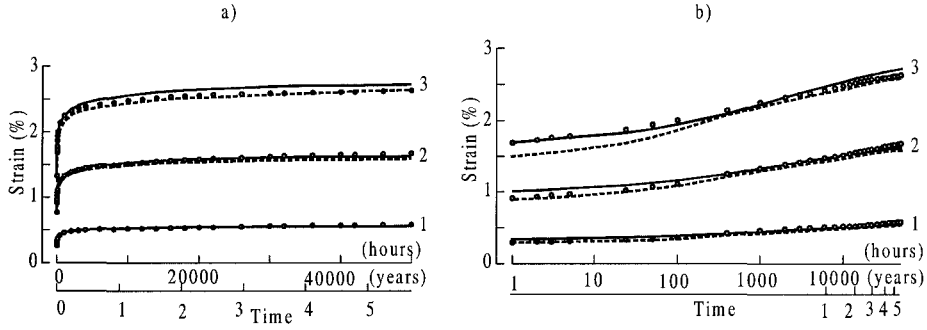



Fig. 1. Creep curves for aramid fibers at different stress levels: 330 (1), 1000 (2), and 1650 MPa (3). Dots are experimental data, solid lines are approximations according to Eq. (2), and dashed lines - prediction from short-term tests at elevated temperatures: a) linear time scale, b) logarithmic time scale.

On Fig. 1, the creep data for aramid fibers are presented in conventional and logarithmic time scales. The curves have a classical shape with an accelerated strain rate in the initial loading period, but it should be noted that the creep does not stabilize even in five years.

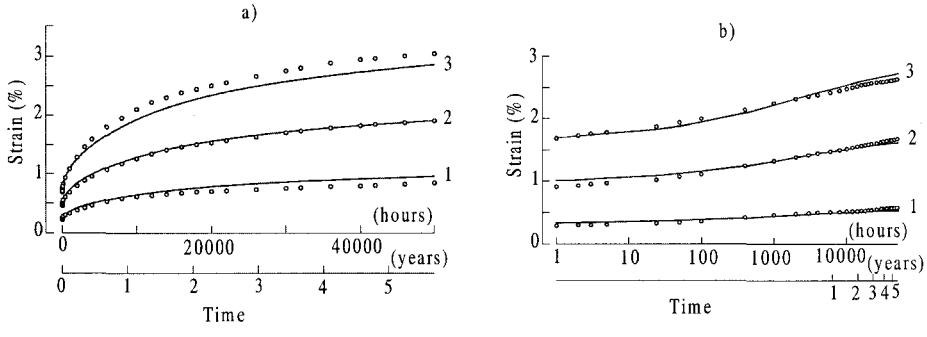



Fig. 2. Creep curves of epoxy resin at different stress levels: 6.8 (1), 13.6 (2), and 20.4 MPa (3). The dots are experimental data and the lines are approximations according to Eq. (2 ): a) linear time scale, b) logarithmic time scale.

The creep curves of epoxy resin at different stress levels are presented on Fig. 2. The creep curves for all hybrid glass-aramid composites at one stress level are given on Fig. 3.

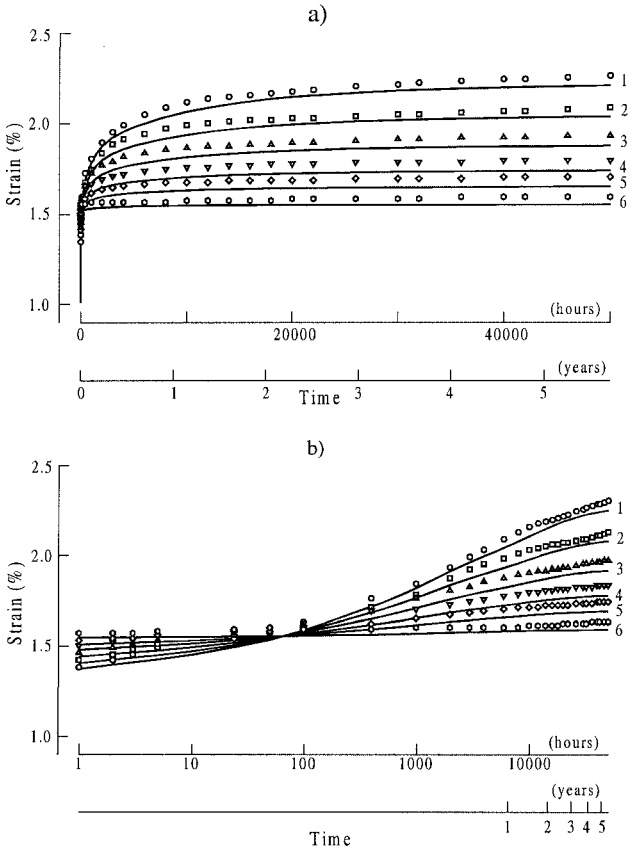



Fig. 3. Creep curves of unidirectional aramid - glass FRP with different volume contents of aramid ($\mu_a$) and glass ($\mu_g$) fibers, $\mu_a/\mu_g$: 0.50/0 (1), 0.40/0.10 (2), 0.29/0.21 (3), 0.18/0.32 (4), 0.10/0.40 (5), and 0/0.50 (6). The stress level, equal to 700MPa, was the same for all the specimens examined. The experimental values are given by dots and the predictions – by lines: a) linear time scale, b) logarithmic time scale.

## ANALYSIS AND DISCUSSION

The creep curves of aramid fibers (Fig. 1) can be described by the usual hereditary type viscoelasticity equation

$$\varepsilon(t) = \frac{1}{E_0}\left[\sigma(t) + \int_0^t k(t-s)\sigma(s)ds\right]. \qquad (1)$$

Expressing the kernel $k(t\text{-}s)$ as a sum of exponential functions, Eq. (1) for $\sigma = \text{const}$ gives

$$\varepsilon = \frac{\sigma}{E_0}\left(1 + \sum_{i=1}^{n} A_i\left(1 - \exp\left(-\frac{t}{\tau_i}\right)\right)\right) \quad \text{or} \quad \varepsilon = \frac{\sigma}{E_A(t)}, \qquad (2)$$

where

$$E(t) = \frac{E_0}{1 + \sum_{i=1}^{n} A_i \left(1 - \exp\left(-\frac{t}{\tau_i}\right)\right)}, \tag{3}$$

$\sigma$ is the applied stress, $E_0$ is the initial modulus of aramid fibers, $t$ is the time under load in hours, and $n$ is the number of terms used to approximate the creep diagram. The coefficients $A_i$ and $\tau_i$ are determined from the best fit to the measured curves.

It should be noted that, for a sufficiently precise approximation of creep curves over a long time interval, a rather large number of exponential functions is needed, which reflects the complex nature of deformational processes in polymers. The approximation curves in Figs. 1 and 2 are obtained at $n = 7$ and are shown by solid lines.

On Fig. 3, curve 6 describes the behavior of a unidirectional glass fiber composite. As is seen, both in the conventional and the logarithmic time scales, the creep deformation is negligible and therefore the glass fibers can be regarded as purely elastic with a modulus $E_g$,

$\sigma_g = \varepsilon \cdot E_g$.

To estimate the creep of the hybrid composites, the strains of all fibers in the hybrid composite were assumed to be equal. From this assumption follows the linear law of mixtures for the modulus of the hybrid composite:

$$\varepsilon(t) = \frac{\sigma_H}{E_H(t)}, \tag{4}$$

$$E_H(t) = E_a(t)\mu_a + E_g(t)\mu_g + E_m(t)(1 - \mu_a - \mu_g),$$

where $E_H(t)$ is the modulus of the glass-aramide composite, $\sigma_H$ is the average stress in the hybrid composite, and $E_a(t)$, $E_g$, $E_m(t)$, $\mu_a$, and $\mu_g$ are the corresponding moduli and volume fractions of aramid and carbon fibers and matrix. Since $E_m(t) << E_a(t), E_g$, the last term in Eq. (4) can be neglected.

Using Eqs. (2), (3), and (4), the creep of the hybrid composites was determined. On Fig. 3, the experimental creep data (dots 1-5) are compared with the predicted curves. The prediction accuracy is satisfactory. The stress in glass fibers increases during the creep process, which leads to a stress redistribution between the glass and aramid fibers. The corresponding equation is of the form

$$\sigma_g(t) = \frac{\sigma E_g}{\mu_g \{E_g - E_a(t)\} + \mu E_a(t)}, \tag{5}$$

where $\mu = \mu_a + \mu_g$ is the total fiber volume content.

In Fig.3b, it is seen that all creep curves with different aramid and glass fiber ratios cross in one point. Really, comparing the strain levels for two hybrid composites with different glass volume contents $\mu_{1g}$ and $\mu_{2g}$, keeping the total fiber volume $\mu$ unchanged, we find that the strains will be equal at

$$E_g\mu_{g1} + E_a(t)(\mu - \mu_{g1}) = E_g\mu_{g2} + E_a(t)(\mu - \mu_{g2}), \tag{6}$$

or

$E_a(t) = E_g$

i.e., when the stiffness of aramid, $E_a(t)$, becomes equal to the modulus of glass fibers.

## ACCELERATED PREDICTION OF CREEP

For direct calculation of hybrid composite creep deformation in the long period of time (Fig. 3) it is necessary to use the creep data for constituents on the same period of time (Fig. 1, Fig. 2) which significantly eliminates the advantages of calculation. Fortunately the creep of fibers and matrix as thermo relogically simple materials can be predicted by short tests at elevated temperature using the time-temperature analogy [1], [2].

To examine the possibility of predicting the long-term creep from the results of accelerated tests at elevated temperatures, the temperature dependence of the creep of aramid fibres has been investigated at four temperature levels in the range from 20 to 150°C. Fig. 4a presents the averaged experimental short-term (up to 5h) creep as function of log time for 20, 70, 100, and 150°C. The creep data are represented as creep compliance $D(t) = \varepsilon(t)/\sigma$.

On Fig. 4b the curves of short creep tests are shifted along $\log t$ axis to obtain the single master curve of compliance for the reference temperature 20°C. As it is seen the master curve covers the interval of time exceeding the duration of accelerated tests by several orders of magnitude.

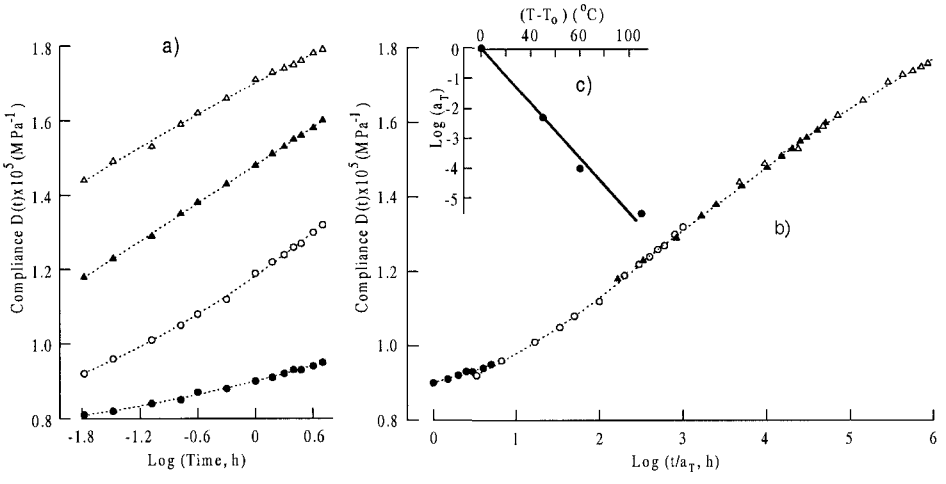



Fig. 4. Creep compliance curves for aramid fibres: a) initial short-time (up to 5h) creep at temperature of 20 (•), 70 (○), 100 (▲), and 150° (Δ); b) creep compliance master curve at the reference temperature 20°C; the symbols are the same as in Fig. 4a; c) the time-temperature shift factor $\log a_T$.

It is seen, that the procedure of time-temperature superposition to obtain a master curve can be performed without difficulty. This implies that the compliance curves in the investigated range of temperature differ only by the time scale, that is,

$D(\log t, T) = D(\log t - \log a_T) = D[\log(t/a_T)]$.

The shift factor $\log a_T$ is shown in Fig. 4c as a function of temperature.

The coefficients $A_i$ and $\tau_i$ in Eq. (2) were determined also from master curve for aramide fibres. For this purpose, a mean-square difference of all points of master curve from the curve computed according to Eq. (2) was minimized. Using the coefficients obtained, the long-term creep curves at different stress levels were calculated. The accuracy of prediction can be judged by Fig. 1, were creep curves predicted from the characteristics obtained from accelerated temperature tests are shown by dashed lines. The maximum deviation of these curves from experimental points is 13%, the relative mean-square error is 6% and does not exceed the confidence intervals of the experimental curves.

## THE INFLUENCE OF BRITTLE FIBER FRAGMENTATION ON THE CREEP PROCESS

The carbon-aramid hybrid composite was also tested in creep. The materials used were carbon fibers T400HB produced by "Toray" (Japan), aramid SVM (Russia), and polyester resin NORPOL440M850 (Norway).

Using Eqs. (2), (3), and (4), the creep strains of the hybrid composite was determined. The calculated curve for the carbon-aramid composite is shown in Fig. 5 in comparison with the test results.

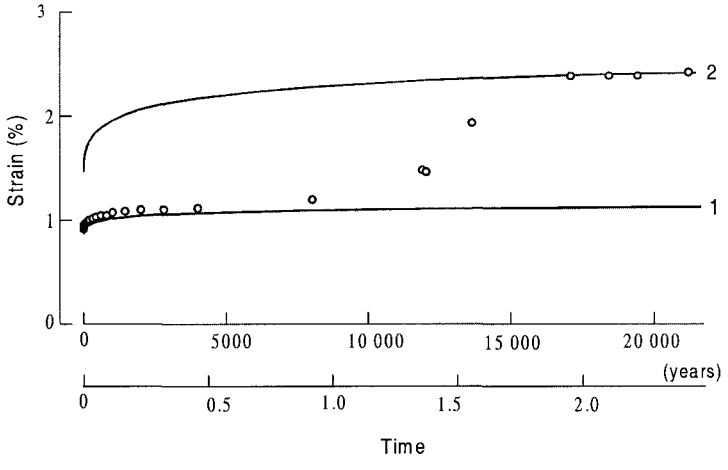



Fig. 5. Creep diagram of hybrid carbon-aramid UD composite (24% T400HB carbon + 76% aramid, with total fiber volume fraction equals 36%). Curve 1 - prediction of hybrid behavior, curve 2 - creep curve for pure aramid composite, dots - experimental results.

After 8000 hours, the creep strain of the carbon-aramid composite made up 38% of the elastic strain. Then, the creep strain increased nonlinearly, achieving about 180% of the elastic strain in 17000 hours (about two years). Such a creep acceleration can be explained only by damage processes (fragmentation of carbon fibers). A similar effect was observed in creep tests with a boron-aramid composite, where the boron fibers were overloaded due to large creep deformations of aramid fibers [5].

The creep curve 1 on Fig. 5 was calculated neglecting the fiber fragmentation, therefore it reflects only the linear creep behavior and does not predict the creep acceleration. The curve 2 on Fig. 5 was calculated by taking into account only the aramid fibers and neglecting the carbon fibers. The good coincidence with four last experimental dots confirms that carbon fibers have splitted in small delaminated fragments, which don't influence the creep of aramid significatly. The static tests with hybrid composites show that the carbon fails at 1.05 - 1.3 % strains ([3] (Fig. 6)). It means that the creep acceleration could be expected in 800 hours. After the fragmentation of carbon fibers, the stress in aramid fibers arises from 0.7 GPa to about 1.6 GPa, whereas the ultimate stress for aramid is 2.7 GPa, therefore the specimen will not fail but will deform with a higher rate. Using the formulas (2), (3), and (4) the creep curves of hybrid composites can be calculated for different stress levels and fiber ratio. Equating the creep strain to limit strain for carbon fibers in composite $\varepsilon = 1.1\%$ the time is determined at which the creep of hybrid will accelerate. On Fig. 7 the results of corresponding calculation are shown for carbon-aramid hybrid, used in the creep test desribed above.

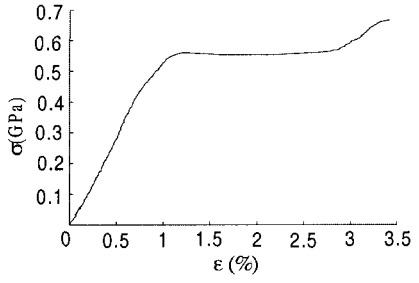



Fig. 6. σ-ε diagram of a carbon-aramid hybrid composite.

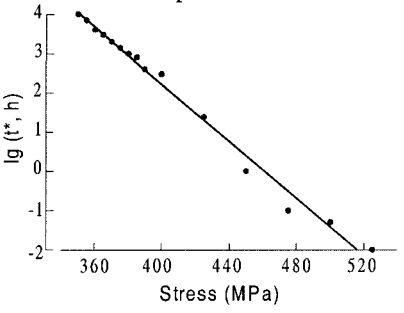



Fig. 7. Expected time of carbon fiber fragmentation in carbon-aramid hybrid composite as function of applied stress. Fiber volume fraction the same as in Fig. 5.

## CONCLUSIONS

The experimental results show that hybrid composites have a considerably higher creep resistance in comparison with pure aramid composites. For example, for a hybrid with the volume fraction of glass fibers $\mu_g = 0.21$ and aramid fibers $\mu_a = 0.29$, the initial modulus is lower only by 14%, but the creep strain is reduced 1.7 times in comparison with a pure aramid composite.

The behavior of hybrid composites can be predicted from the creep data of components with a satisfactory accuracy.

However, if brittle components such as carbon fibers are used in the hybrid composite, a certain risk of overloading this component exists due to the large creep of aramid fibers, as it can be seen from experimental results. After the breakage of carbon fibers the creep will accelerate and may lead to the failure of the whole composite if the load level for the remaining fibers is high.

## REFERENCES

1. Maksimov R. D, Kochetkov V.A. (1989) "Thermal deformation prediction of hybrid composites with viscoelastic components", Science and Engineering of Composite Materials, 1989, Vol. 1, No. 4, pp. 117-127
2. Kochetkov V.A., Maksimov R. D. (1994) "Prediction of deformative and thermal properties of hybrid fiber composites with polymer matrix.", Acta Polymerica, 1994, Vol. 45, No. 5, pp. 348-354.
3. Apinis R., Modniks J., Tamuzs V., Tepfers R. (1998). "Ductility of Hybrid Fiber Composite Reinforcement FRP for Concrete". Institute of Polymer Mechanics, Riga, Latvia. Chalmers University of Technology, Division of Building Technology, Work No 23. Riga, 1998. p. 16. Contribution to the ECCM8 Conference 1998-06-03/05, Naples. Volume 2. pp. 89-96.
4. Apinis R., Modniks J., Tamuzs V., Tepfers R. (1999). "Pull-out, flexural rotation capacity and creep tests using hybrid composite rods and CFCC rods for reinforcement in concrete". Chalmers University of Technology, Division of Building Technology, Work No 32. Publication 99:4. Göteborg, 1999. p. 49 + A1 to A5.
5. Kochetkov V.A. and Maksimov R. D. (1983) "Prediction of the creep of a unidirectional hybrid composite with allowance for the effect of fiber breakage", Mechanics of Composite Materials, 1983, No. 5, pp. 668-677.

# Analysis of Time-Dependent Behaviour of Concrete Beams Prestressed with FRP Tendons

X.W. ZOU, R.I. GILBERT and N. GOWRIPALAN
The University of New South Wales, Sydney, Australia

## ABSTRACT
In this paper, analyses are presented for determining the short-term and time-dependent behaviour of fully or partially prestressed concrete beams with Fibre Reinforced Polymer (FRP) tendons under sustained bending and axial force. The Age-adjusted Effective Modulus Method (AEMM) is used to model the creep behaviour in the concrete and the relaxation in the FRP prestressing tendons. The analytical values are compared to the test results of prestressed concrete beams containing carbon fibre rods (CFRP) or aramid fibre rods (AFRP) under service load condition. The comparisons include the change of the curvature and the deflection with time. A tension-stiffening model proposed by Gilbert (1988) was adopted for the cracked beams, and this model was then modified using the experimental results by introducing a material parameter $\beta_3$ to the model in order to use it for beams prestressed by FRP tendons.

## INTRODUCTION
If Fibre Reinforced Polymer (FRP) tendons are to be used as alternatives to steel tendons in prestressed concrete, it is important to understand the implications and effects on the time-dependent structural behaviour. The material properties of the tendons that most affect the service load performance of prestressed structures are the elastic modulus $E_p$ and the final percentage relaxation $R$ (or creep coefficient, $\phi_p$). Some FRP tendons may relax or creep more than prestressing steel tendons and the elastic modulus may be substantially lower than for steel. Higher creep in the tendons results in a greater loss of prestress (due to relaxation), whilst a smaller elastic modulus means that the time dependent deformations of the concrete (due to creep and shrinkage) cause smaller losses of prestress. This paper discusses the time-dependent behaviour of concrete beams prestressed with FRP tendons including experimental studies and theoretical analysis.

## SHORT-TERM ANALYSIS
### Uncracked Section
The short-term analysis of a cross-section can be carried out by transforming the bonded reinforcement into equivalent areas of concrete and performing a simple, elastic analysis on the equivalent concrete section. In the transformation, the ratios of the elastic modulus of the prestressing tendon and the concrete, $n_p$, is called the modulus ratio for the tendon and $n_p = E_p/E_c$. The corresponding modulus ratio for the conventional non-prestressed reinforcement is designated $n_s$ and $n_s = E_s/E_c$. The area $A$, the first and second moments $B$ and $\bar{I}$ of the transformed section are taken about the top fibre of the section. The initial strain and stress distributions on uncracked sections are assumed to be linear over the depth of the section. The

*FRPRCS-5*, Thomas Telford, London, 2001.

concrete strain at top fibre $\varepsilon_{oi}$ and the initial curvature $\kappa_i$ are given by (Gilbert and Mickleborough, 1990):

$$\varepsilon_{oi} = \frac{BM_i - \bar{I}N_i}{E_c\left(B^2 - A\bar{I}\right)} \tag{1}$$

and

$$\kappa_i = \frac{BN_i - AM_i}{E_c\left(B^2 - A\bar{I}\right)} \tag{2}$$

where

$N_i$ and $M_i$ are the stress resultants for the cross section (axial force and bending moment) with respect to the top fibre of the cross-sesction, while $E_c$ is the modulus of elasticity of concrete.

The initial concrete strain and stress at $y$ below the top fibre are

$$\varepsilon_i = \varepsilon_{oi} + y\kappa_i \tag{3}$$

$$\sigma_i = E_c\varepsilon_i = E_c(\varepsilon_{oi} + y\kappa_i) \tag{4}$$

The corresponding stresses in the tendons and the reinforcement can be determined using the linear material properties for FRP and steel.

**Cracked Section**

If the applied moment at any time $t$ is greater than the cracking moment, cracking will occur and at each crack the concrete below the neutral axis is ineffective. The short-term behaviour of the cracked cross-section may be calculated using a simple elastic analysis with the assumptions of: (i) plane sections remain plane and therefore the strain distribution is linear over the depth of the section; (ii) perfect bond exists between the concrete and both the prestressed and non-prestressed reinforcements; (iii) instantaneous material behaviour is linear-elastic for concrete, steel and FRP. For an applied sustained moment $M_s$ greater than the cracking moment, there are two unknowns associated with the strain diagram: the depth of the neutral axis $d_n$ and the instantaneous extreme fibre compressive strain $\varepsilon_{oi}$. When $\varepsilon_{oi}$ and $d_n$ are known, the strain diagram is defined and the concrete, tendon and reinforcement stresses are readily determined. To find these two unknowns, there are two equations of equilibrium available. By a trial and error procedure, the depth of neutral axis $d_n$ and the strain at top fibre $\varepsilon_{oi}$ can be found. Alternatively, the following equation may be solved for $d_n$ using a simple trial and error search (Gilbert, 1988).

$$\frac{\int_0^{d_n}(d_n - y)y\,dA + \sum_{k=1}^{m} nA_{sk}d_{sk}(d_n - d_{sk})}{\int_0^{d_n}(d_n - y)\,dA + \sum_{k=1}^{m} nA_{sk}(d_n - d_{sk})} = -\frac{M_i}{N_i} \tag{5}$$

Hence the curvature $\kappa_i$ can be determined:

$$\kappa_i = -\frac{\varepsilon_{oi}}{d_n} \tag{6}$$

After $d_n$ is determined, the properties of the fully cracked transformed section with respect to the top reference surface ($A$, $B$ and $\bar{I}$) may be calculated and the short-term strain at the top fibre, the curvature and hence the strain distribution may be determined.

## TIME-DEPENDENT ANALYSIS OF CROSS-SECTION

In prestressed concrete beams, the bonded tendons and the reinforcement provide restraint to the time-dependent shortening of concrete caused by creep and shrinkage. The tendon and reinforcement are gradually compressed. Equal and opposite tensile forces are applied to the concrete at each level of bonded tendon and conventional reinforcement, thereby reducing the compression caused by prestress. It is the tensile forces applied gradually at each level of bonded reinforcement that result in significant time-dependent changes in curvature and deflection (Gilbert and Mickleborough, 1990).

The sum of the time-dependent change of strain at any depth $y$ below the top fibre of the cross-section ($\Delta\varepsilon$) may be expressed in terms of the change in the top fibre strain ($\Delta\varepsilon_o$) and the change of curvature ($\Delta\kappa$):

$$\Delta\varepsilon = \Delta\varepsilon_o + y\Delta\kappa \tag{7}$$

The time analysis of the cross-section considered here uses the AEMM (Bazant, 1972) together with a relaxation approach (Bresler and Selna, 1964). The application was proposed by Gilbert (1988). In the relaxation procedure, the strain state is assumed to be held constant throughout a given time interval. If the total strain is held constant and the creep and shrinkage strains change, then the instantaneous component of strain must also change by an equal and opposite amount. As the instantaneous strain changes, so too does the concrete stress. The concrete stress on the cross-section is therefore allowed to vary due to relaxation. As a result, the internal actions change and equilibrium is not maintained. An axial force $\Delta N$ and a bending moment $\Delta M$ must, therefore, be applied to the cross-section to restore equilibrium. The actions required to restrain creep and shrinkage in the concrete and creep in the prestressing tendon are given by

$$\Delta N = \overline{E}_{ec}\left[\phi_{cr}\left(A_c\varepsilon_{oi} + B_c\kappa_i\right) + \varepsilon_{sh}A_c\right] + E_{ep}\phi_p\left(A_p\varepsilon_{oi} + A_p d_p\kappa_i\right) \tag{8}$$

$$\Delta M = \overline{E}_{ec}\left[\phi_{cr}\left(B_c\varepsilon_{oi} + \overline{I}_c\kappa_i\right) + \varepsilon_{sh}B_c\right] + E_{ep}\phi_p\left(A_p d_p\varepsilon_{oi} + A_p d_p{}^2\kappa_i\right) \tag{9}$$

where $\overline{E}_{ec}$ is the age-adjusted effective modulus for concrete and $E_{ep}$ is the effective modulus of the FRP prestressing tendon. The variables $A_c$, $B_c$ and $I_c$ are the area, first moment of area and second moment of area of the concrete part of the cross-section, with respect to the top surface. $\phi_{cr}$ and $\varepsilon_{sh}$ are the creep coefficient and shrinkage strain of the concrete and $\phi_p$ is the creep coefficient of the FRP tendon. The change of strain in the top fibre and the change of curvature with time are calculated using the equivalent properties $\overline{A}_e$, $\overline{B}_e$ and $\overline{I}_e$ of the age-adjusted transformed section using the equations below:

$$\Delta\varepsilon_o = \frac{\overline{B}_e\Delta M - \overline{I}_e\Delta N}{\overline{E}_{ec}\left(\overline{B}_e{}^2 - \overline{A}_e\overline{I}_e\right)} \tag{10}$$

$$\Delta\kappa = \frac{\overline{B}_e\Delta N - \overline{A}_e\Delta M}{\overline{E}_{ec}\left(\overline{B}_e{}^2 - \overline{A}_e\overline{I}_e\right)} \tag{11}$$

The modular ratios of the age-adjusted transformed section are given by $\overline{n} = E_{ep}/\overline{E}_{ec}$ and $\overline{n}_s = E_s/\overline{E}_{ec}$ and are used to determine the transformed area of the tendons and the non-prestressed reinforcements (if any).

The change in stress in the concrete at any depth $y$ is

$$\Delta\sigma = -\overline{E}_{ec}\left[\phi_{cr}(t,t_0)\left(\varepsilon_{oi} + y\kappa_i\right) + \varepsilon_{sh} - \left(\Delta\varepsilon_o + y\Delta\kappa\right)\right] \tag{12}$$

and the change in stress in the tendon is

$$\Delta\sigma_p = -E_{ep}\left[\phi_p\left(\varepsilon_{oi} + d_p\kappa_i\right) - \left(\Delta\varepsilon_o + d_p\Delta\kappa\right)\right] \tag{13}$$

After the time-dependent changes of strains, curvatures and stresses are determined, the final strains, curvatures and stresses at the cross-section are readily found by

$$\varepsilon(t) = \varepsilon_{oi} + \Delta\varepsilon(t) \tag{14}$$

$$\kappa(t) = \kappa_i + \Delta\kappa \tag{15}$$

$$\sigma(t) = \sigma_{oi} + \Delta\sigma \tag{16}$$

When a fully cracked cross-section is subjected to a period of sustained loading, creep causes a change of position of the neutral axis. In general, the depth to the neutral axis increases with time and so too does the area of concrete in compression. However, to include this in the calculations requires an iterative numerical solution that leads to increased complexity with little increase in accuracy. It is assumed here that the depth of the concrete in compression remains constant with time. This assumption is in fact necessary, if the short-term and time-dependent stress and strain increments are to be calculated separately and added together to obtain the final stresses and deformations. The assumption greatly simplies the analysis and usually results in relatively little error.

## DEFLECTION CALCULATION

In order to calculate the deflection of the beam, direct integration is used. By obtaining a variation of curvature at a number of sections, the deflection at midspan can be obtained by integrating the curvatures $\kappa(x)$ twice.

$$\Delta = \int_0^L \int_0^L \kappa(x)\, dx\, dx \tag{17}$$

This equation is a general equation and applicable for both elastic and inelastic material behaviour. It is also suitable for short-term and long-term deflection calculations.

### Tension stiffening

Noting that concrete has the ability to carry tensile stress between cracks in the tension zone due to the bond between the steel and concrete, a tension stiffening model should therefore be used in the cracked cross-sectional analysis of the beams. A model proposed by Gilbert (1988) is adopted in this study. It should be pointed out that the model was developed for concrete members with steel reinforcement or steel tendons. The approach for modelling tension stiffening is to assume that an area of concrete located at the tensile steel level is effective in providing stiffening. Figure 1 shows an average cross-section of a singly reinforced member. The properties of this average section are between those of fully-cracked cross-section and the uncracked cross-section between the primary cracks. The tensile concrete area $A_{ct}$, is assumed to contribute to the beam stiffness after cracking and depends on the magnitude of the maximum applied moment $M_s$, the area of tensile reinforcement $A_{st}$, the amount of concrete below the neutral axis, the tensile strength of the concrete (the cracking moment $M_{cr}$), and the duration of the sustained load. The tensile concrete area $A_{ct}$ may be calculated using Equation 18:

$$A_{ct} = \beta_1\beta_2\left(0.21b_w - nA_{st}\right)\left(\frac{M_{cr}}{M_s}\right)^2 \tag{18}$$

where

$\beta_1$ is 1.0 for deformed bars /tendons and 0.5 for round bars;

$\beta_2$ is 1.0 for initial loading and 0.5 for long-term load or cycles of load.

It should be pointed out that there are many other tension stiffening models and some of these are described below. The tension stiffening models specified in ACI 318 (1995) and CEB-FIP (1983) involve calculating effective second moment s of the cross-sectional area using Equations 19 and 20, respectively:

$$I_e = I_{cr} + (I_g - I_{cr})\left(\frac{M_{cr}}{M_s}\right)^3 \leq I_g \tag{19}$$

$$I_e = (1-\zeta)I_u + \zeta I_{av} \tag{20}$$

where

$$\zeta = 1 - \beta_1\beta_2\left(\frac{M_{cr}}{M_s}\right)^2 \tag{21}$$

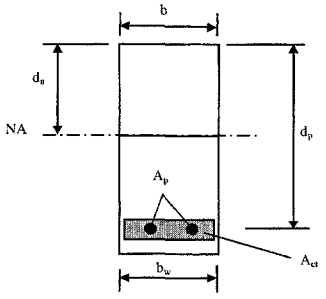



Figure 1 Tension stiffening model (Gilbert, 1988)

According to Gilbert and Mickleborough (1990), the CEB-FIP (1983) approach is recommended. It best accounts for the breakdown of tension stiffening under long-term or cyclic loading and allows for the reduction in tension stiffening when plain bars or bonded tendons only are present and the tendon-concrete bond is not perfect. For cracked beams, the deflection was calculated with and without accounting for tension stiffening. The tension stiffening models are discussed in a later section and the model proposed by Gilbert (1988) is used in this study.

### Long-Term Deflection

Long-term deflections due to concrete creep and shrinkage are affected by many variables, including load intensity, mix proportions, member size, age at first loading, curing conditions, total quantity of compressive and tensile reinforcement, level of prestress, relative humidity and temperature (Gilbert and Mickleborough, 1990). As for short-term deflection calculations, when the curvature at time *t* has been determined at each section, the long-term deflection at that time can be calculated by integrating the curvature twice.

## COMPARISONS OF THEORETICAL PREDICTIONS TO EXPERIMENTAL RESULTS

### Beams with Uncracked Sections

The predicted time-dependent behaviour of the beams prestressed with steel or FRP tendons is here compared with the experimental results obtained by Zou (1999). In the analysis, the actual measured concrete properties were used, to give close comparison to measured

experimental results. These include compressive strength, modulus of elasticity, creep coefficient and shrinkage. The relaxation of steel was modelled using the formula proposed in AS 3600 (1994), while the relaxation of CFRP was considered to be zero as obtained from the tests (Zou 1999). In the case of AFRP tendon, the empirical equation (Equation 22) was used to model the creep coefficient of the tendon.

$$\phi_{pt} = 0.0058\ln(t) + 0.0531, \quad (R^2 = 0.9185) \tag{22}$$

The effective modulus of the AFRP tendon is given by

$$E_{pe} = \frac{E_p}{1+\phi_{pt}} \tag{23}$$

The predicted long-term curvatures are compared to the experimental results in Figure 2 to Figure 3. In general, The predicted values are comparable to the experimental results The predicted midspan deflections are compared to the experimental results in Figure 4 to Figure 6. Full details of the experimental program are given by Zou (1999). A reasonable prediction of the deflection is achieved using the AEMM for the beams prestressed with both steel tendons and CFRP rods.

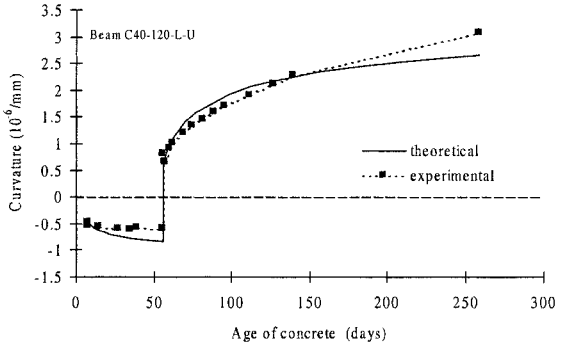



Figure 2 Theoretical predictions versus experimental results of curvature for the midspan section for a beam with CFRP (C40-120-L-U)

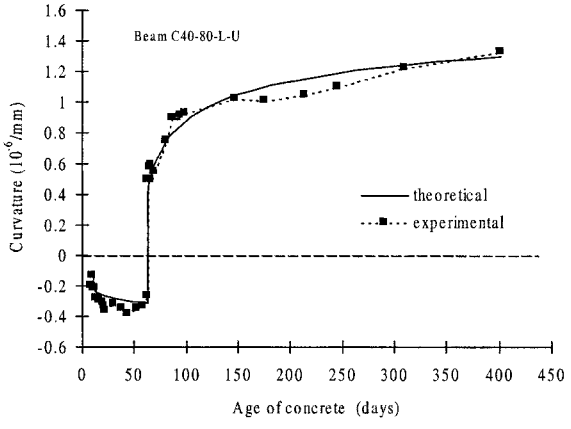



Figure 3 Theoretical predictions versus experimental results of curvature for the midspan section for a beam with CFRP (C40-80-L-U)

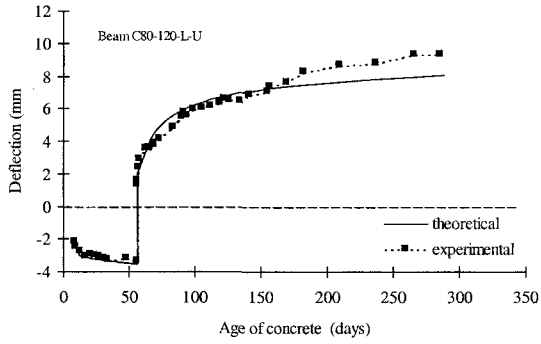



Figure 4 Theoretical predictions versus experimental results of midspan deflection for a beam with CFRP (C80-120-L-U) (6 fine cracks appeared after two weeks of loading)

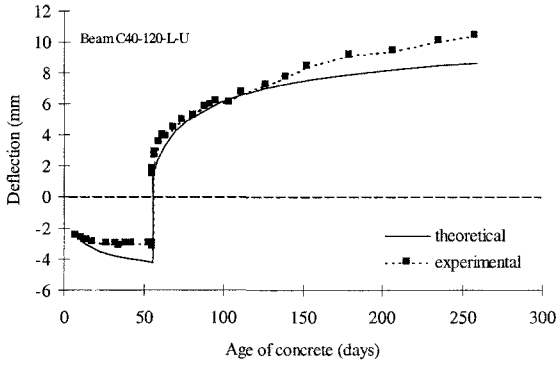



Figure 5 Theoretical predictions versus experimental results of the midspan deflection for a beam with CFRP (C40-120-L-U)

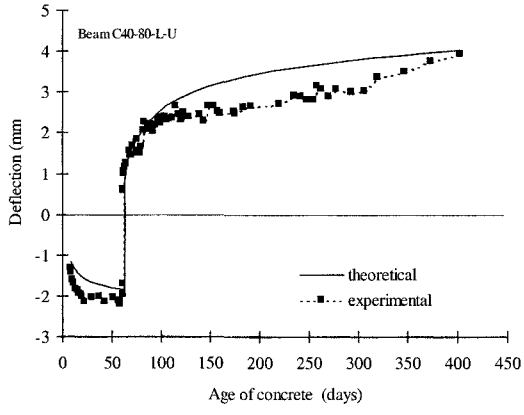



Figure 6 Theoretical predictions versus experimental results of the midspan deflection for Beam C40-80-L-U

**Beams with Cracked Sections**

This section compares the theoretical prediction to the experimental results of the beams subjected to a sustained load greater than their cracking load. The concrete strains at the top fibre and the deflections at the midspan are discussed. It should be pointed out that the depth of the neutral axis $d_n$, derived from the measurement of concrete strains cross the depth of the beam at midpsan section is used in the calculation. It should also be pointed out that a material parameter $\beta_3$ has been included in the determination of the tension stiffening effect and $\beta_3$ will be defined, discussed and calibrated in later section.

The computed midspan deflections (with and without tension stiffening) are compared to the experimental results in Figure 7, Figure 8 and Figure 9 for Beams S80-120-L-C, A80-120-L-C and C80-80-L-C respectively. The importance of including the effect of tension stiffening in deflection calculation is highlighted in these figures. It is clear that the calculation without the tension stiffening effect overestimates the deflection. However, if the tension stiffening is taken into account, then the calculated values are comparable to the experimental results. Moreover, best-fit curves were achieved by changing the value of $\beta_1$ to 0.75 for beam S80-120-L-C or by using $\beta_3$ =0.5 for beams A80-120-L-C and C80-80-L-C.

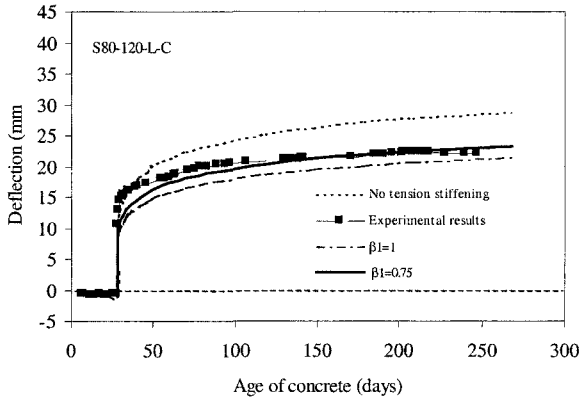



Figure 7 Comparison of theoretical values and experimental results of the midspan deflection for beam S80-120-L-C (6 cracks in the beam)

**Modified Tension Stiffening Model**

The model proposed by Gilbert (1988) for tension stiffening was originally developed for conventional reinforced concrete beams reinforced by steel round bars or deformed bars. There was no value specified for $\beta_1$ when using steel strand. For this reason, a suitable value of $\beta_1$ for 7-wire steel strand is required. It is also necessary to propose a material parameter $\beta_3$ in order to use this model for beams prestressed by FRP rods. Hence a modified tension stiffening model may be expressed as follows:

$$A_{ct} = \beta_1\beta_2\beta_3 \left[0.21 b_w d - nA_{st}\right]\left(\frac{M_{cr}}{M_s}\right)^2 \tag{24}$$

where

$\beta_1$ is the reinforcement surface condition parameter

$\beta_2$ is the load history parameter, and
$\beta_3$ is the material parameter.

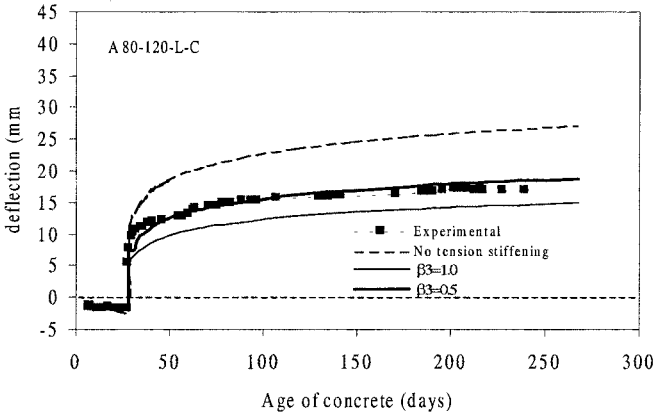



Figure 8 Comparison of theoretical values and experimental results of the midspan deflection of beam A80-120-L-C (4 cracks in the beam)

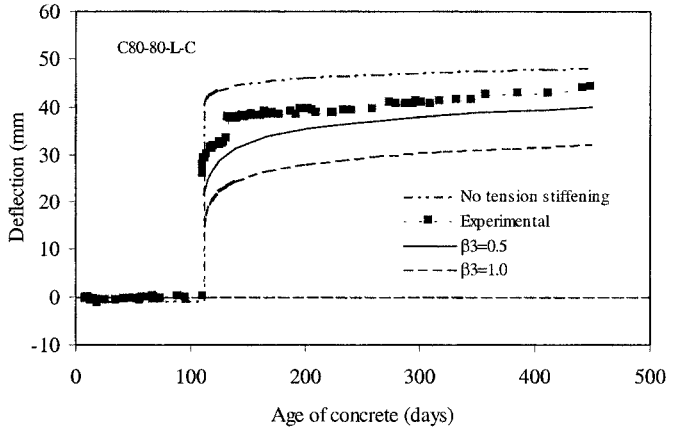



Figure 9 Comparison of theoretical values and experimental results of the midspan deflection for beam C80-80-L-C (7 cracks in the beam)

For beams prestressed by steel strands, it can be seen from the three theoretical curves of Figure 7 that the best fit is when $\beta_1$ is 0.75. $\beta_1$ may therefore be taken as 0.75 for 7-wire steel strand, while $\beta_2$ is 0.5 and$\beta_3$ is 1.0. Considering the surface of the AFRP is sand coated, $\beta_1$ was taken as 1.0 while $\beta_2$ was 0.5 for long-term loading. In the case of CFRP, due to its relatively smooth surface condition, $\beta_1$ was taken as 0.5 and $\beta_2$ as 0.5 for long-term loading. To determine the value of $\beta_3$, predictions with three different values of $\beta_3$ were made and they are compared to the experimental results. From the comparison of theoretical values to

experimental results, for time-dependent deflection calculations, the recommended values of these parameters are given in Table 1:

Table 1 Values of $\beta_1$, $\beta_2$ and $\beta_3$ for a modified tension stiffening model

| Parameters | Steel reinforcement | | Steel strand | AFRP rod | CFRP rod |
|---|---|---|---|---|---|
| | round | deformed | (7-wire) | (sand coated) | (indented) |
| $\beta_1$ *(surface)* | 0.5 | 1.0 | 0.75 | 1.0 | 0.5 |
| $\beta_2$ *(short-term)* | 1.0 | 1.0 | 1.0 | 1.0 | 1.0 |
| $\beta_2$ *(Long-term)* | 0.5 | 0.5 | 0.5 | 0.5 | 0.5 |
| $\beta_3$ *(material)* | 1.0 | 1.0 | 1.0 | 0.5 | 0.5 |

## CONCLUSIONS

1. For uncracked beams, good prediction of the curvature and deflection are achieved using the AEMM for the beams prestressed with either steel or CFRP tendons with different concrete strengths and different levels of prestress.
2. For cracked beams, tension stiffening is an important criteria in predicting the load-deflection response of beams after cracking. It is important to include tension stiffening in deflection calculation. Calculations without tension stiffening overestimate the deflection. If tension stiffening is taken into account, the calculated values are comparable to the experimental results.
3. A modified tension stiffening model which includes a material parameter $\beta_3$ in the equation has been proposed and is suitable for predicting the instantaneous and the time-dependent deflections of cracked concrete beams prestressed with AFRP rods or CFRP rods. The value of $\beta_3$ is dependent on the surface conditions and the modulus (stiffness) of the tendon.

## REFERENCES

Australian Standards AS3600 (1994), Concrete structures, Standards Association of Australia, pp75.

Branson, D. E. (1977), Deformation of concrete structures, McGraw-Hill.

CEB-FIP 1990, Model Code for concrete structures, Tomas Telford Editor, London.

Gilbert, R.I. (1988), Time effects on concrete structures, Elsvier, New York, 321pp.

Gilbert, R.I. and Mickleborough, N.C. (1990), Design of prestressed concrete, Unwin Hyman, London, 504pp.

Zou X.W. (1999), Short-term and time-dependent behaviour of concrete beams prestressed with fibre reinforeced polymers (FRP) tendons. PhD Dissertation, The Unveristy of New South Wales, Sydney Australia. 405pp.

# Thermal and external effects

# Fire Testing of Concrete Slabs Strengthened with Fibre Composite Laminates

H. BLONTROCK, L. TAERWE and P. VANDEVELDE
Magnel Laboratory, Ghent University, Belgium

## ABSTRACT:

Strenghtening of concrete elements by means of fibre composite laminates is an efficient technique for repairing or strenghtening of concrete elements. These fibre composite laminates are glued with epoxy resin to the concrete surface. In case of fire, the bond between the composite laminates and the concrete will be lost very quickly because of the low glass transition temperature of the epoxy. So there is a need for thermal protection of the external strengthening system of these elements. Fire tests on strengthened and protected slabs, loaded to service load level, are executed to evaluate fire resistance of these elements. Temperatures and deformations are measured during testing. The testing parameters of these elements include the use of different thermal protections (including different materials and geometric layouts of the protection) of the glued reinforcement.

## INTRODUCTION

Concrete elements can succesfully be repaired and/or rehabilitated by external strengthening with glued composite laminates. Under normal environmental conditions, the structural behaviour of these strengthened elements seems to be satisfactory. A lot of research has already been performed concerning the structural behaviour of these strengthened elements under ambient temperatures [1,2,3,4]. The behaviour under fire conditions of these strengthened elements may cause a problem. Indeed, the interaction between the glued composite laminate and the concrete will be lost very quickly in a fire, due to weakening of the adhesive layer, which has a low glass transition temperature (glass transition temperature of epoxies are usually in the range 50°C-100°C). Hence, in order to maintain the interaction between the composite laminate and the concrete during a certain time, a thermal protection of the external strengthening system will be necessary.

Concerning the fire resistance of these strengthened (protected) elements, only two test programmes have been reported up to now. At the EMPA Institute (Dübendorf, Switzerland), six concrete beams were tested in a fire test: one reference beam, one beam strengthened with a steel plate, and four beams strengthened with composite laminates [5]. For the FRP strenghtened beams, two beams were tested unprotected in the fire test (for one of the beams an adhesive with a higher thermal capacity was used), the two other beams were protected

*FRPRCS-5*, Thomas Telford, London, 2001.

with insulating plates of different thicknesses (Promatect L). The test results clearly show the need for a thermal protection of the external strengthening system. Interaction between the composite laminate and the concrete is lost very quickly for the unprotected elements, but only lost after about one hour for the protected elements.
As part of a testing programme dealing with the fire resistance of strengthened concrete elements at Ghent University, ten strenghtened beams were tested. The test results showed that a thermal protection (even only partially applied at the anchorage zones of the strengthening element) was able to maintain interaction between the composite and the concrete during a certain time [6].

In order to investigate the problem in more detail for strengthened concrete slabs, another test programme was performed at Ghent University, comprising a total of ten slabs. Three slabs (an unstrengthened reference slab and two strengthened reference slabs with different strengthening degrees) were statically loaded up to failure at room conditions. Two unprotected and unstrengthened slabs, loaded to the service load for an unstrenghtened slab and five protected and strengthened slabs, loaded to the service load for a strenghtened slab were submitted to a fire test. The protection for the externally strengthening system was applied in different ways with respect to thickness and shape.

## SURVEY OF THE EXPERIMENTAL PROGRAMME

### Test specimens

The dimensions of the tested slabs were: thickness of 150 mm, width of 400 mm and a length of 3150 mm. The lower reinforcement consists of 4 bars $\phi$ 8 mm. Transverse reinforcement $\phi$ 6 mm is provided with a spacing of 200 mm. The concrete cover on the steel reinforcement (Type S500) was 25 mm. The following concrete mix was used for the preparation of the slabs:

Table 1 : Concrete mix

| | |
|---|---|
| Gravel (Siliceous) 4/14 | 1350,0 kg |
| Coarse sand | 565,0 kg |
| Cement | 325,0 kg |
| Water | 162,5 kg |

The mechanical properties of the concrete, determined for each slab, are given in Table 2. The compressive strength is the average of four results on concrete cubes 158 mm. The bending tensile strength is determined on a concrete prism 150x150x600 mm. After the bending test, the splitting tensile strength is determined on the two pieces of the broken prism. The elastic modulus was determined on a concrete prism 150x150x600 mm

Table 2 : Concrete properties of tested slabs

| | Age at Testing [days] | Compressive Strength [N/mm²] | Bending Tensile Strength [N/mm²] | Splitting Tensile Strength [N/mm²] | Elastic Modulus [N/mm²] |
|---|---|---|---|---|---|
| **Slab 1** | 105 | 57,50 | 5,96 | 4,55 | 34600 |
| **Slab 2** | 107 | 55,55 | 5,63 | 4,19 | - |
| **Slab 3** | 106 | 57,23 | 6,16 | 4,19 | 33900 |
| **Slab 4** | 97 | 58,36 | 5,96 | 4,40 | 34400 |
| **Slab 5** | 97 | 57,15 | 5,76 | 4,19 | - |
| **Slab 6** | 84 | 55,03 | 5,50 | 4,51 | 34800 |
| **Slab 7** | 84 | 57,08 | 5,30 | 4,28 | - |
| **Slab 8** | 84 | 55,03 | 5,69 | 3,88 | 34800 |
| **Slab 9** | 84 | 56,43 | 5,41 | 4,40 | - |
| **Slab 10** | 91 | 56,40 | 6,08 | 4,14 | - |

The steel properties were determined on three test specimens and can be found in Table 3. The characteristics of the composite laminate S&P carbon sheet, supplied by the manufacturer, are summarized in Table 3. The glass transition temperature of the epoxy (Multipox), determined with a differential scanning calorimetric analysis according to prEN 12614, is 67°C.

The following procedure is followed for the application of the composite laminates to the strengthened slabs: the bottom face of the concrete slabs is roughened through sandblasting and is made dust-free afterwards. The epoxy resin (Multipox from Resiplast N.V.) is applied directly on the concrete. The composite sheet is pressed again the concrete surface and is fully impregnated with epoxy. For the application of two layers of carbon sheet, the same procedure is applied twice. The age of concrete at the time of strengthening was at least one month. The adhesive was cured for at least seven days at room conditions before testing. Slab 2 and slabs 6 to 9 are strenghtened with two layers of S&P carbon sheet, slab 3 and slab 10 are strenghtened with one layer of S&P carbon sheet. Slab 1 (unstrengthened reference slab) and slabs 2 and 3 (strengthened reference slabs) are statically loaded at room conditions. Slabs 4 and 5 (unstrenghtened unprotected slabs) and slabs 6 to 10 (strengthened and protected slabs) are submitted to a fire test.

Table 3 : Steel and Composite properties for tested slabs

| | Yield Strength [N/mm²] | Ultimate Strength [N/mm²] | Elastic Modulus [N/mm²] | Ultimate Strain [%] |
|---|---|---|---|---|
| **Steel (bar ϕ8)** | 576 | 699 | 210000 | 6,7 |
| **S&P C-Sheet** | - | 3900 | 240000 | 1,55 |

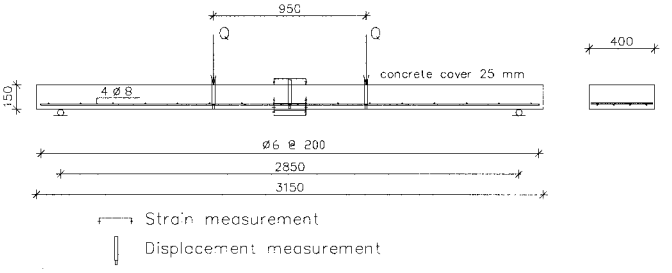



Figure 1 : Test set-up unstrengthened reference slab 1

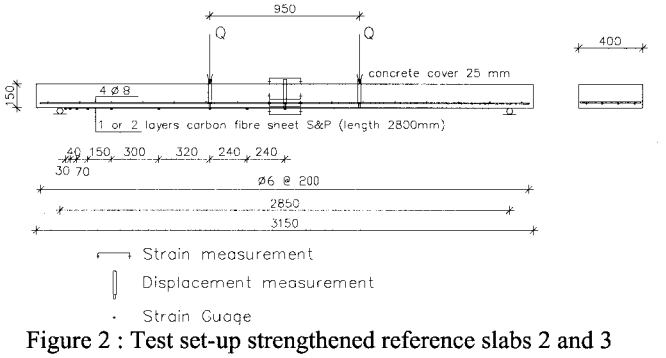



Figure 2 : Test set-up strengthened reference slabs 2 and 3

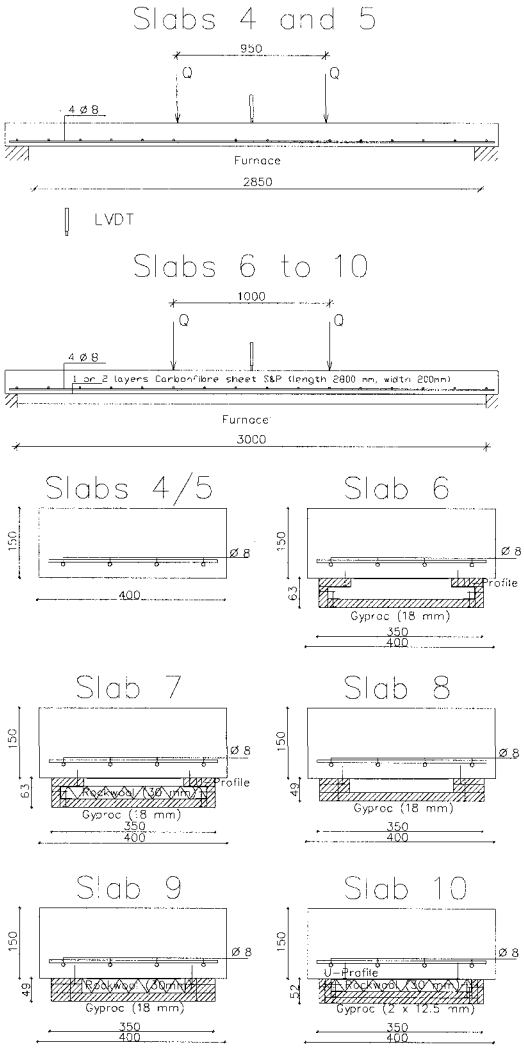



Figure 3 : Slabs 4-10 with lay-out of the protection system

The external strengthening of the slabs is protected with fire resistant plates (Gyproc Rf plates). The insulating Gyproc plates consist of two layers of cardboard with a gypsum core. For stability reasons in fire, some small glass fibres (about 0.2% in mass) are added to the gypsum core. The density of these insulating plates is 820 kg/m³. The thermal conductivity of the Gyproc Rf plates is 0.21 W/mK but there is an important absorption of heat during loss of the chemically bound water in the gypsum cristals.

Small U shaped steel profiles are mechanically fixed to the bottom of slabs 6 and 7 with insertion of a gyproc plate strip between the profile and the concrete. Gyproc plates (thickness 18 mm) are then screwed on the bottom and side faces of this profiles. The gap created in this way remains empty for slab 6, while for slab 7 the gap is filled with 30 mm Rockwool (an insulating mineral wool with thermal conductivity of 0.05 W/mK). The layout

of the protection for slabs 8 and 9 is similar to the one for slabs 6 and 7. The gap is created by means of Gyproc plate strips (width 75 mm, thickness 18 + 12 mm) fixed to the concrete beside the glued composite sheet. The gap is closed with a Gyproc plate (thickness 18 mm, width 350 mm). For plate 8 the gap remains empty and for plate 9 the gap is filled with 30 mm Rockwool. For slab 10 the U shaped profiles are fixed directly to the concrete surface and two layers of Gyproc plates (thickness 12.5 mm) are screwed onto the bottom and sidefaces profiles. The gap is filled with Rockwool (thickness 30 mm). Figure 3 shows the lay-out of the protection systems and the test set-up for slabs 4 to 10.

**Test procedure for static loading of reference elements**

A calculation of the maximum service load was made in accordance to Eurocode 2. The following assumptions are made for the calculation of the load corresponding with the ultimate limit state design for slab 1: the concrete quality is C35/45 (mean compressive strength on cubes 158 mm : 56.6 N/mm²) with a parabolic-rectangle stress-strain diagram, steel quality is S500 (mean yield strength : 577 N/mm²) with an elastic-perfectly plastic stress-strain relationship (E-modulus 210000 N/mm²). It is assumed that half of the loading is a permanent action and half of the loading is a variable action. With the design ultimate load, the two following conditions were checked for the serviceability limit state of slab 1: concrete stress at the most compressed fibre < 0.50 $f_{ck}$ (17.5 N/mm²) and steel stress < 0.80 $f_{yk}$ (400 N/mm²) for the infrequent load combination. The service loads for the strengthened slabs 2 and 3 are calculated as the loads for which the steel stresses equal the steel stress in the serviceability limit state for the unstrengthened slab 1. A perfectly elastic stress-strain relationship is assumed for the composite sheets (E-modulus 240000 N/mm²). The service loads with the corresponding stresses in concrete and steel and the strain in the laminate can be found in table 4.

Table 4 : Service loads and corresponding stresses/strains for Slabs 1 to 3

| | **Slab 1** (Unstrengthened) | **Slab 2** (2 layers C-sheet) | **Slab 3** (1 layer C-sheet) |
|---|---|---|---|
| **Load Q** | 2 x 5,86 kN | 2 x 9,07 kN | 2 x 7,46 kN |
| **Concrete stress $\sigma_c$** | 12,4 N/mm² | 14,4 N/mm² | 13,4 N/mm² |
| **Steel stress $\sigma_s$** | 300 N/mm² | 300 N/mm² | 300 N/mm² |
| **Laminate strain $\varepsilon_l$** | - | 2,0‰ | 2,0‰ |

Two reference slabs (slab 1 (unstrengthened) and slabs 2 and 3 (strengthened)) are loaded up to failure under room conditions. The slabs are first loaded in eight steps to the service load, are then unloaded and finally reloaded up to failure. During testing, the force applied by the jacks, the deflections at mid-span and at the third-points are measured. At mid-span, the strains for the most-compressed fibre and the most tensioned fibres, for the fibre at mid-height of the slab and for the fibre at the level of the internal steel reinforcement are measured with strain stirrups. Between successive steps the formation and the widths of the cracks are measured. For the strengthened slabs, the strains in the composite are measured at different locations with strain gauges. The test set-up for the reference slabs 1 to 3 can be found in figures 1 and 2.

**Test procedure for fire tests**

The horizontal furnace of the fire testing laboratory is 3m wide by 6m long. A reaction frame by which the tested elements are supported, is placed above the furnace. For the first test-series, the slabs are in the logitudinal direction of the furnace, the clear span of the slabs

being 2.85m. In the middle a water cooled steel profile is placed to support the elements. In the first series the two unprotected, unstrengthened reference slabs 4 and 5 are tested. For the second test-series, the slabs are all placed in the transverse direction of the furnace, the clear span of the slabs being 3.00 m. The five protected and strengthened slabs are tested in this second series. Before the start of the fire test, the slabs are loaded to the full service load level of an unstrengthened slab for slabs 4 and 5 and to the full service load level of a strengthened slab for slabs 6 to 10 (values shown in Table 4). This load is kept constant during the fire test. The slabs are loaded in pairs (two jacks connected to one hydraulic unit). They are unloaded when the span/deflection ratio of one of the two adjacent slabs reaches about l/35.

The fire test is executed according to ISO 834 (Fire Resistance : Test-Elements of Building Construction). This standard prescribes the heating by combustion gases in function of the time and is given by :

$$T_g = T_o + 345\log_{10}(8t+1)$$

where $T_g$ : temperature of the combustion gases [°C]
$T_o$ : initial temperature [°C]
t : time in minutes

The following values are measured during testing : the load on the slabs and the deflection of the slabs at mid-span during testing. Each slab is equipped with 20 thermocouples. Temperatures are measured in two concrete sections. In each section ten thermocouples are placed. Three thermocouples are fixed on the bottom face of the concrete slab to measure the temperature increase of the glue layer, two thermocouples are placed on the lower steel reinforcement and the remaining thermocouples are placed in the concrete section.

## TEST RESULTS

### Results of Static Loading Tests

The load-deflection curves for slabs 1 to 3 are given in figure 4. Comparison of the test results for the unstrengthened and strengthened slabs shows that the failure load increases from 2 x 16.7 kN to 2 x 25.2 kN for slab 2 (increase by 51%) and to 2 x 19.9 kN for slab 3 (increase by 20%). The cracking moment and the stiffness increase as well, but there is a decrease in ductility. Indeed, the deflection at mid-span at failure is reduced from more than 100 mm for the unstrengthened slab (the deformation at mid-span was larger than the stroke of the displacement transducer) to 47.1 mm for strengthened slab 2 and to 40.0 mm for strengthened slab 3.

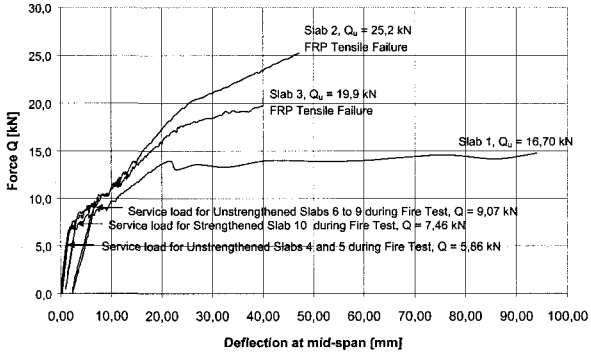



Figure 4 : Force-deflection diagram for slabs 1 to 3

The failure mode for the strengthened slabs is characterized by yielding of the internal steel reinforcement followed by tensile failure of the externally glued composite sheet.

**Results of Fire Tests**

*Test results of slabs 4 and 5*

Test results for slabs 4 and 5 can be found in figure 5. A time-deflection curve and a time-temperature curve for the internal steel reinforcement are shown. Slabs 4 and 5 are unloaded when the increase in deflection was about 87 mm, the temperature increase of the internal steel reinforcement was about 440 °C at that moment.

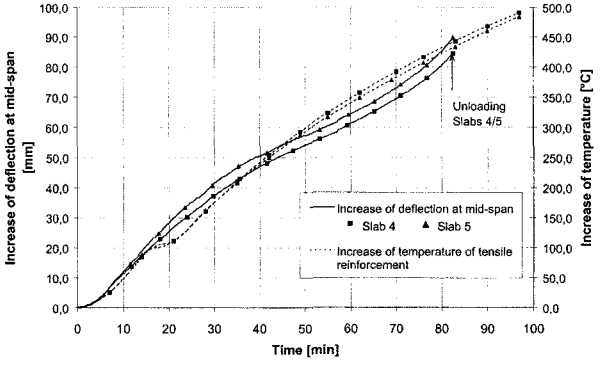



Figure 5 : Time-Deflection and Time-Temperature diagrams for Slabs 4 and 5

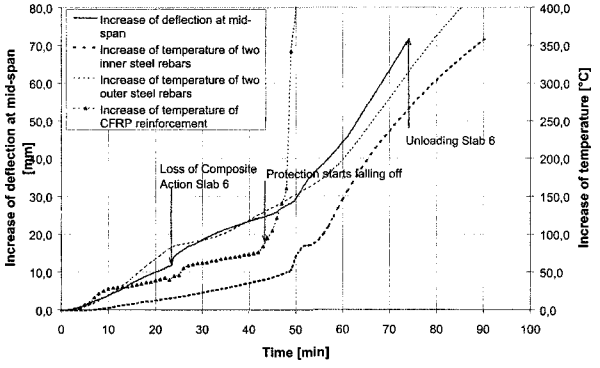



Figure 6 : Time-deflection and time-temperature diagrams for slab 6

*Test results of slabs 6 to 9*

Test results for slabs 6 to 9 can be found in figures 6 to 9. A time-deflection curve and three time-temperature curves are shown. Because of the partial protection of the bottom face of the slabs, temperature rise for the two inner steel rebars and for the two outer steel rebars is different. Hence, two time-temperature curves for the internal steel reinforcement are shown. The temperature increase of the glued composite sheet is measured in the middle of the sheet. The time-deflection curves all show a similar behaviour up to the point where a quite sudden increase in deflection occurs. At that time it may be assumed that the interaction between the composite laminate and the concrete is lost totally due to weakening of the glue layer. Filling of the air gap with a mineral insulating wool, results in an increase of the period during which interaction between composite and concrete is maintained (see test results slab 6 and 7).

However, for slabs 8 and 9 there is no significant difference for this time period due to the presence of the insulating mineral wool.

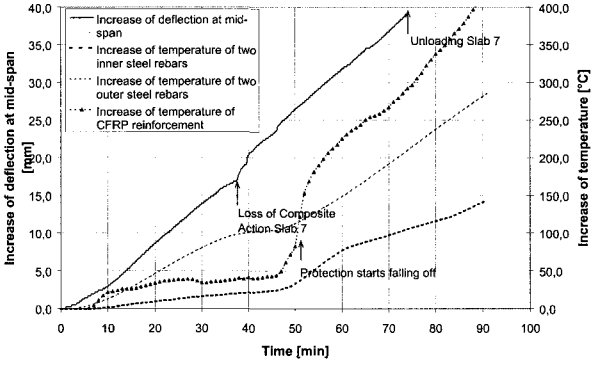



Figure 7 : Time-deflection and time-temperature diagrams for slab 7

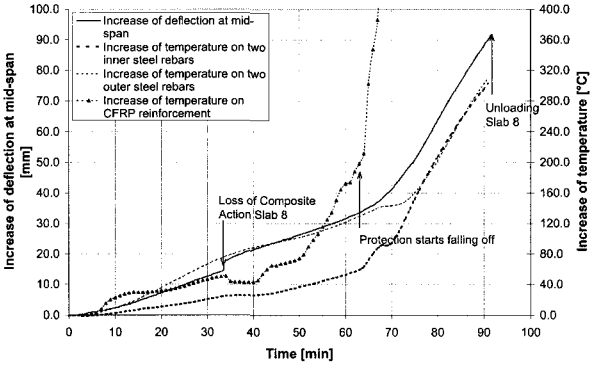



Figure 8 : Time-deflection and time-temperature diagrams for slab 8

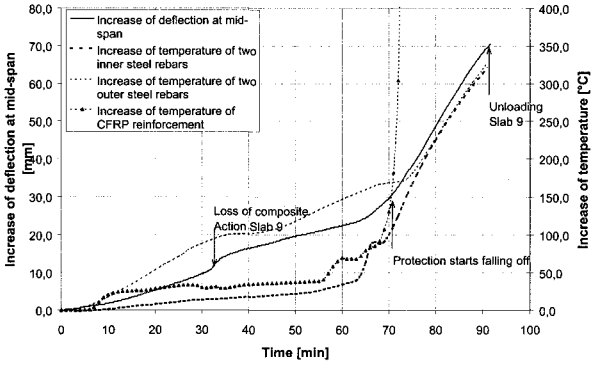



Figure 9 : Time-deflection and time-temperature diagrams for slab 9

*Test results of slab 10*

Test results for slab 10 can be found in figure 10. The time-deflection curve for slab 10 shows a sharp increase in deflection after 55 minutes due to the loss of interaction between the concrete and the laminate. Due to the lower strengthening degree compared with slabs 6

to 9, the increase in deflection at the moment of loss of interaction is smaller than compared with the increase in deflection for slabs 6 to 9. Application of the thermal protection in two layers seems to be favourable for the integrity of the protection system in fire. Indeed, the protection starts falling off after about 80 minutes. For slabs 6 to 9 where the protection is applied in one layer of 18 mm, the protection starts falling off between 40 and 70 minutes.

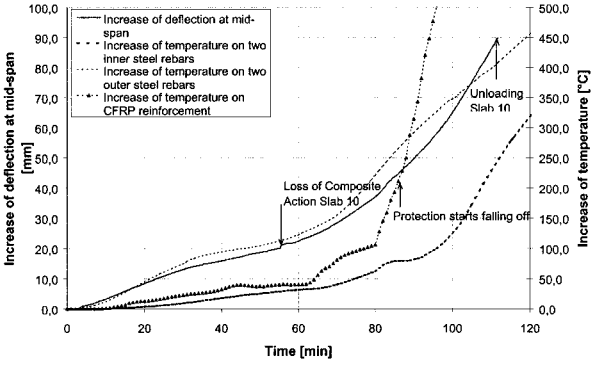



Figure 10 : Time-deflection and time-temperature diagrams for slab 10

*Summary of the test results*

A summary of test results for slab 4 to 10 can be found in table 5. The following values are given in the table:

- The time at which the interaction between the composite laminate and the concrete is lost (derived from the sudden increase in deflection)
- The temperature of the CFRP at that time
- The increase in deflection after 75 minutes of fire
- The temperature of the internal steel after 75 minutes (If two temperatures are given, the first is the temperature of the inner two steel rebars and the second is the temperature of the outer two steel rebars)

Table 5 : Summary of test results slabs 4-10

| | Loss of interaction FRP/Concrete [min] | $T_{CFRP}$ at time of loss of interaction FRP/Concrete [°C] | Increase in deflection at mid-span after 75 min [mm] | $T_{internal\ steel}$ after 75 min. [°C] |
|---|---|---|---|---|
| **Slab 4** | - | - | 74,3 | 412 |
| **Slab 5** | - | - | 78,3 | 403 |
| **Slab 6** | 24 | 63,0 | 71,8 | 273 / 323 |
| **Slab 7** | 38 | 58,3 | 39,4 | 107 / 215 |
| **Slab 8** | 34 | 68,9 | 50,7 | 152 / 161 |
| **Slab 9** | 34 | 47,0 | 38,4 | 168 / 182 |
| **Slab 10** | 55 | 58,3 | 32,6 | 50 / 185 |

## CONCLUSIONS

Based on the fire tests on the externally strengthened concrete slabs, the following conclusions can be drawn:

- A thermal protection for the externally strengthening system is needed to maintain interaction between the externally strengthening system and the concrete. Without

thermal protection, it is impossible to reach the same fire resistance as for the unprotected and unstrengthened slab.
- For the particular conditions of this testing programme, interaction between the externally glued sheet and the concrete was lost when the temperature of the adhesive reached a value in the range of 47°C to 69°C.
- The fire resistance of the strengthened and protected slabs is at least the same as for the unstrengthened and unprotected slabs.

**References**

[1] H. Kaiser (1989), "Bewehren von Stahlbeton mit kohlenstoffaserverstärkte Epoxidharzen", Dissertation ETH Nr. 8919, Zürich, Switzerland.
[2] B. Täljsten (1994), "Plate Bonding: Strengthening of Existing Concrete Structures with Epoxy Bonded Plates of Steel or Fibre Reinforced Plastics", Doctoral thesis 1994: 152 D, Lulea Technical University Sweden.
[3] L. Taerwe, Ed. (1995), Second International Symposium on Non-Metallic (FRP) Reinforcement for Concrete Structures (FRPRCS-2), Ghent, Belgium, RILEM Proceedings 29, E&FN Spon.
[4] Japan Concrete Institute (1997), Third International Symposium on Non-Metallic Reinforcement for Concrete Structures (FRPRCS-3), Sapporo, Japan.
[5] M. Deuring (1994), "Brandversuche an nachträglich verstärkten Trägern aus Beton", EMPA nr. 148'795, Dübendorf, Switzerland
[6] H. Blontrock (2000), "Fire Tests on Concrete Beams Strengthened with Fibre Composite Laminates", 3rd PhD-Symposium, Vienna, vol.2, pg. 151-161.

# Heat Resistance Of Continuous Fiber Reinforced Plastic Rods

ATSUSHI SUMIDA, Products & Application Technology, Dupont-Toray Co. Ltd., Japan
TADASHI FUJISAKI, Institute of Technology, Shimizu Corporation, Japan
KEN WATANABE, Institute of Technology, Tokyu Construction Co. Ltd., Japan
TAKEHIKO KATO, Marketing Division, Kumagai Gumi Co., Ltd., Japan

**ABSTRACT:** The thermal properties of FRP rods commercially available in Japan as well as those of each cured matrix resin specially prepared by rod manufacturer were examined in this paper. The bond strength in concrete under heat treatment was also examined referring to the thermal properties of rod and resin.
**KEYWORDS:** FRP rod, resin heat resistance, rod strength during heat treatment, rod strength after heat treatment, bonding strength during heat treatment

## INTRODUCTION

Continuous fiber reinforced plastic (FRP) rods have been widely applied to steel rebar replacement in Japan because of their light weight and non-corrosive properties, as well as being non-conductive and non-magnetic. Specifically, a considerable amount of FRP rods has been and will be used for electrically non-conductive and magnetic induction-free buildings such as computer rooms, NMR facilities and so on. Heat resistance of FRP rods in a fire is essential for steel rebar replacement in buildings. Therefore, the Association of Composite Materials Using Continuous Fiber for Concrete Reinforcement (CCC) has evaluated heat resistance of commercially available FRP rods in Japan. The thermal properties of each resin; the tensile strengths of FRP rods both during and after heat treatment, and bond strength in concrete during heat treatment were evaluated.

## ROD AND RESIN SAMPLES

The rods that are commercially available in Japan and the type of resin, as described in the manufacturers literature are summarized in Tables 1 and 2. The FRP rods and resin samples are shown in Photo 1 and 2.

Table 1 Description of Rods

| Sample | Description*1) | Fiber | | | | | Matrix Resin*2) |
|---|---|---|---|---|---|---|---|
| | | Type | Tensile Strength ($kN/mm^2$) | Modulus ($kN/mm^2$) | Density | Elong. (%) | |
| R－A | C S | CF | 4.41 | 218.1 | 1.80 | 1.9 | E P |
| R－B | C D | CF | 3.43 | 218.1 | 1.77 | 1.45 | E P |
| R－C | C S | CF | 3.63 | 218.1 | 1.77 | 1.5 | E P |
| R－D | C S | CF | 4.95 | 213.5 | 1.80 | 2.1 | E P |
| R－E | C L | CF | 4.95 | 213.5 | 1.80 | 2.1 | V E |
| R－F | C P | CF | 4.90 | 213.5 | 1.80 | 2.1 | E P |
| R－G | A D | AF | 2.94 | 100.9 | 1.45 | 2.4 | E P |
| R－H | A B | AF | 2.94 | 100.9 | 1.45 | 2.4 | E P |
| R－I | A D | AF | 3.43 | 67.2 | 1.39 | 4.6 | V E |
| R－J | G D | GF | 2.45 | 67.2 | 2.54 | 4.5 | E P |
| R－K | V D | VF | 2.01 | 41.4 | 1.30 | 5.0 | E P |

Table 2 Properties of Rods

| Sample | Description*1) | Properties of rods | | | | |
|---|---|---|---|---|---|---|
| | | Diameter (mm) | Strength (kN) | Tensile Strength ($kN/mm^2$) | Modulus ($kN/mm^2$) | Elongation (%) |
| R－A | C S | 9.6 | 90.9 | 1.64 | 109.0 | 1.5 |
| R－B | C D | 8 | 101.8 | 2.02 | 127.2 | 1.0 |
| R－C | C S | 7.5 | 52.7 | 1.73 | 130.8 | 1.3 |
| R－D | C S | 5 | 41.6 | 2.12 | 145.4 | 1.4 |
| R－E | C L | 4.7 | 19.1 | 1.09 | 90.9 | 1.2 |
| R－F | C P | 11 | 172.6 | 1.82 | 113.6 | 1.6 |
| R－G | A D | 3 | 4.9 | 0.69 | 63.6 | 2.0 |
| R－H | A B | 7.3 | 58.2 | 1.38 | 63.6 | 2.0 |
| R－I | A D | 6 | 46.3 | 1.64 | 49.1 | 3.7 |
| R－J | G D | 8 | 68.1 | 1.35 | 38.2 | 2.7 |
| R－K | V D | 8 | 27.3 | 0.55 | 20.0 | 3.0 |

*1) C: Carbon Fiber(CF), A: Aramid Fiber (AF), G: Glass Fiber(GF), V: Vinylon Fiber(VF) R: Rod, S: Strand, B: Braided, L: Lattice, P: Rectangular (Plate)

*2) EP: Epoxy, VE: Vinyl ester

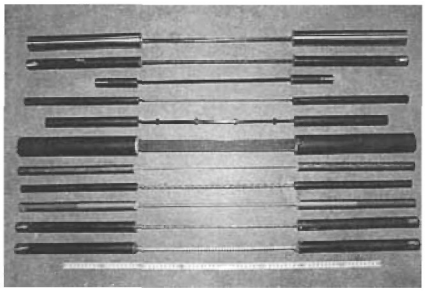


Photo 1 FRP Rods

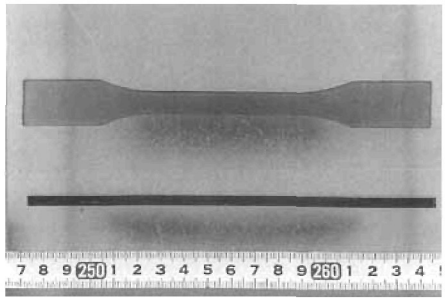


Photo 2 Resin Sample

## EXPERIMENTAL PROCEDURE

### Heat resistance of resins

(1) Weight Loss

The weight loss behavior of each resin was measured by thermogravimetry in both air and nitrogen.

A. Testing condition

Instrument : TG-40M by Shimazu Seisakusho

Atmosphere : Air and Nitrogen, 50ml/min.

Temperature Range : Room Temperature to 700℃

Heat Rate : 10℃/min.

Sample Weight : ca. 10mg

B. Results

Each resin sample started to decompose at about 300℃ and weight loss in nitrogen was less than that in air at the same temperature as shown in Table 3.

Table 3. Weight Loss of Resin

| | Resin | 1% weight loss ℃ | 5% weight loss ℃ | Peak of DTG ℃ | Residue at 700℃ % |
|---|---|---|---|---|---|
| A | Epoxy | 293 (313) | 334 (348) | 430 (429) | 0.3 (16.0) |
| B | Epoxy | 286 (304) | 368 (401) | 437 (454) | 0.0 ( 9.8) |
| C | Epoxy | 319 (-----) | 367 (-----) | 428 (-----) | 0.3 (-----) |
| D | Epoxy | 300 (313) | 347 (353) | 437 (442) | 0.1 (13.8) |
| E | Vinyl ester | 244 (-----) | 345 (-----) | 422 (-----) | 0.1 (-----) |
| F | Epoxy | 283 (300) | 360 (365) | 395 (402) | 0.4 (19.9) |
| H | Epoxy | 279 (297) | 350 (353) | 384 (399) | 0.2 (16.1) |
| I | Vinyl ester | 279 (273) | 355 (380) | 426 (435) | 0.1 ( 6.1) |
| J | Epoxy | 286 (-----) | 369 (-----) | 437 (-----) | 0.2 (-----) |
| K | Epoxy | 269 (296) | 366 (397) | 437 (446) | 0.2 ( 9.6) |

Bracketed figures (...) are in Nitrogen, other figures are in air.

**Glass Transition Temperature (Tg) and Modulus**

Both ends of the resin test piece were mounted in grips. One was connected to a transducer to measure displacement of the sample and the other was connected to a stress transducer. An actuator provided sinusoidal vibration to the sample during the raising of the temperature, while the displacement and stress were measured.

A. Testing Condition

| | |
|---|---|
| Instrument | : RHEOVIBRON DDV-Ⅱ-A by Orientec |
| Vibration | : 11Hz |
| Atmosphere | : Nitrogen |
| Temperature Range | : RT to 200℃ |
| Heat-up Ratio | : 2℃/min. |

B. Results

There were significant differences in the Tg of the resin samples that also resulted in differences in modulus values as shown in Table 4.

Table 4 Tg and Modulus of Resins

| | Resin | Tg(1) | Tg(2) | Modulus at Typical Temperature (GPa) | | | |
|---|---|---|---|---|---|---|---|
| | | ℃ | ℃ | RT | 100℃ | 150℃ | 200℃ |
| A | Epoxy | 126 | 122 | 1.7 | 1.30 | 0.018 | 0.016 |
| B | Epoxy | 99 | 90 | 1.8 | 0.45 | 0.043 | 0.027 |
| D | Epoxy | 140 | 135 | 1.9 | 1.20 | 0.11 | 0.019 |
| F | Epoxy | 177 | 169 | 2.1 | 1.50 | 0.83 | 0.037 |
| H | Epoxy | 176 | 167 | 2.3 | 1.60 | 1.30 | 0.046 |
| I | Vinyl ester | 126 | 120 | 2.0 | 1.60 | 0.017 | 0.014 |
| K | Epoxy | 93 | 85 | 2.0 | 0.32 | 0.045 | 0.033 |

Tg(1) : Peak temperature of main distribution, Tg(2) : SACMA method

**TENSILE STRENGTH OF RODS**

Samples R-D (carbon fiber) and R-I (aramid fiber) were selected for the tensile test because resins of these rods were a representative for each fiber.

**After Heat Treatment**

A. Preparation of Rods

Samples R-D and R-I (excluding the grips) were heated for ten minutes at 50, 100, 125, 150, 175, 200, 220, 240 and 260℃. After cooling, grips were attached to each rod by the rod manufacturer, as shown in Fig.1.

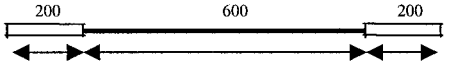



Fig.1 Shape Test Specimen

B. Testing Method

The test was performed in accordance with CONCRETE ENGINEERING SERIES 23 [1].

C. Test Results

Figs. 2 and 3 show the test results of the relationship between the heat treatment temperature and the retention of both breaking strength of rod and weight of resin.

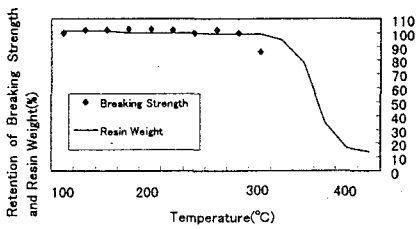



Fig.2 CFRP

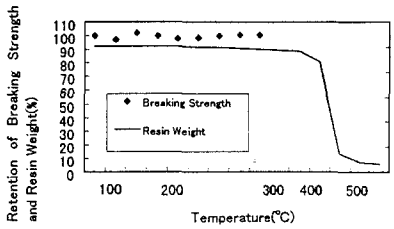



Fig.3 AFRP

**Tensile Strength at Elevated Temperatures**

A. Preparation of Rods and Testing Method

The grips were attached to each rod by the rod manufacturer and the testing method was as in Section A. A rod was mounted in the tensile tester with a furnace as shown in Fig.4.

The rod was heated to 50, 100, 125, 150, 175, 200, 220, 240 and 260℃ at 2℃/min. and after reaching the target temperature, a tensile test was performed.

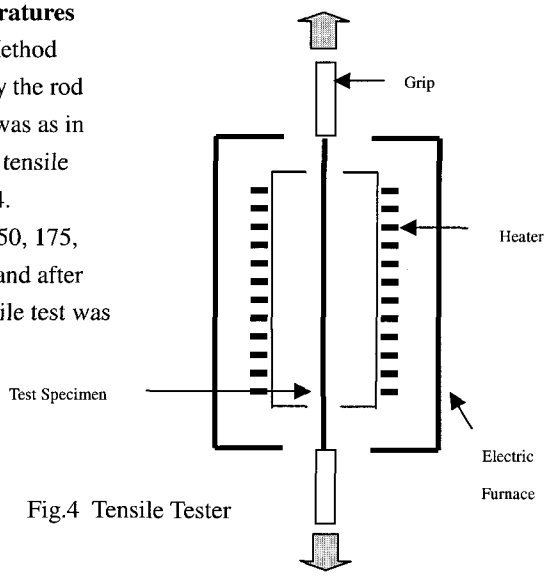



Fig.4 Tensile Tester

B. Test Results

The test results are plotted in Fig.5 and 6. The solid line shows the relationship between temperature and retention of modulus of resin while the dotted line gives the relationship between temperature and retention of fiber strength.

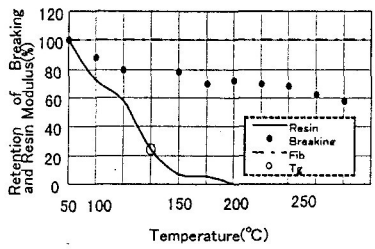



Fig.5 Carbon Fiber Rod

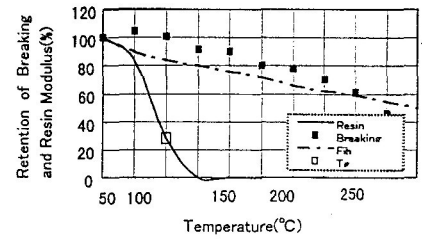



Fig.6 Aramid Fiber Rod

## BOND STRENGTH IN CONCRETE

### Preparation of Rod Samples

One end of each FRP rod that was limited to contact with concrete was embedded in concrete as shown in Photo 4, 5 and 6. The other end was embedded in steel pipe with epoxy resin.

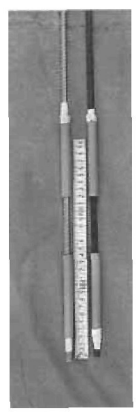


Photo 4 Rod Sample



Photo 5 Arrangement of Rod

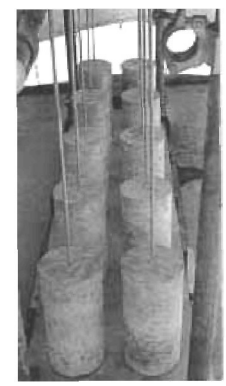


Photo 6 Test Specimen

**Testing Method**

The test specimen was mounted on the tensile tester with electric heater as shown in Fig.7. The slip length was measured with displacement gage.

**Test Results**

Figs.8 and 9 show the relationship between slip and average bond strength ( $\tau$ ). $\tau$ was calculated by:-

$\tau = P/(\pi \cdot D \cdot L)$

P : Load (N)

D : Diameter of FRP rod (mm)

L : Adhesive length (mm)

Figs.10 and 11 show the relationship between temperature vs. $\tau$ at each slip length and maximum $\tau$ .

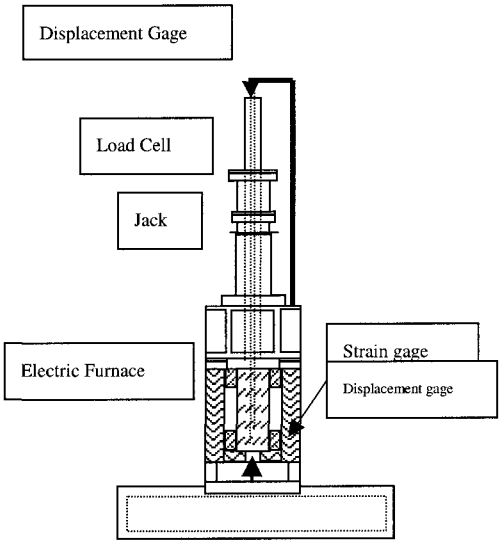



Fig.7 Tensile Tester

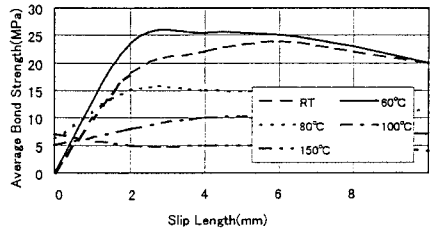



Fig.8 Carbon Fiber Rod

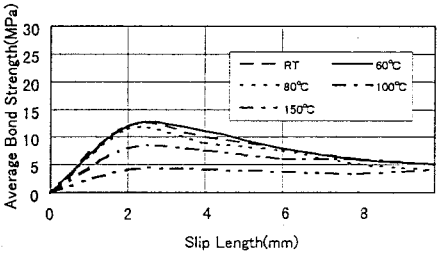



Fig.9 Aramid Fiber Rod

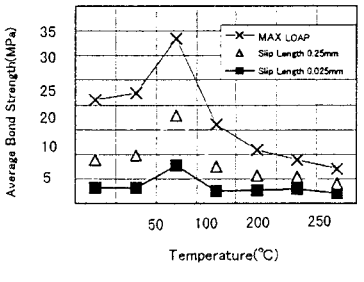



Fig.10 Carbon Fiber Rod

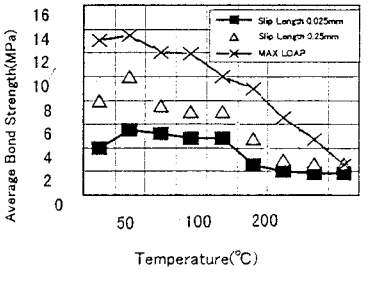



Fig.11 Aramid Fiber Rod

Figs.12 and 13 show the comparison between retention of $\tau$ at maximum load and retention of modulus of resin.

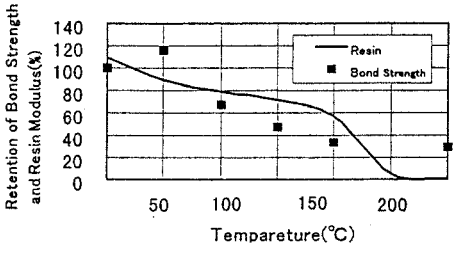



Fig.12 Carbon Fiber Rod

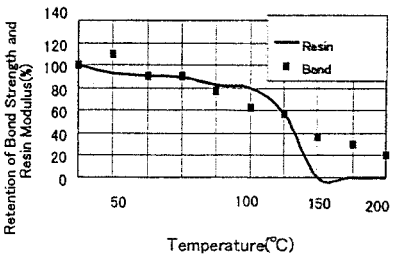



Fig.13 Aramid Fiber Rod

## RESULTS AND DISCUSSIONS

(1) Epoxy and vinyl ester are used as matrix resin in commercially available FRP rods.

The upper temperature limit for weight loss of all resins was essentially the same, about 300℃. However, the glass transition temperatures were lower and differed significantly. The retention of modulus of each resin was also significantly different.

(2) Tensile Strength of FRP after Heat Treatment

There was no observable loss in tensile strength of both carbon fiber rod and aramid fiber rod at temperatures below 250℃. It proposed that the retention of tensile strength of rods after heat treatment will depend on the weight retention of its resin in nitrogen, because the resin exposed to temperature in excess of 250℃ will lower the reinforcement ability of the fiber.

(3) Tensile Strength of FRP Rods during Heat Treatment

The retention of both carbon fiber rod and aramid fiber rod dropped significantly during exposure to temperatures in excess of 100℃. This is most likely to be a result of the significant drop in the resin modulus during heat treatment as shown in Fig.5 and 6, because the resin of low modulus will drop the reinforcement ability for fiber.

(4) Bond Strength in Concrete

The retention of bond strength in concrete was similar to the retention of tensile strength of the rod during heat treatment. It is likely that the bond strength is directly dependent on the resin modulus since the resin is directly in contact with concrete.

## CONCLUSIONS

1. In applications where FRP rods are used as replacement for steel rebar with low levels of permanent stress, the surface temperature of the rods should be kept below 250℃. Therefore, FRP rod can continue to be used after a fire provided this temperature was not exceeded.

2. In applications where FRP rods are used with levels of high permanent stress, the surface temperature of the rod should be kept below 100℃.

3. Improvement in heat resistance of FRP rods will require development of resin with better properties at higher temperatures.

## ACKNOWLEDGEMENTS

This work was supported by the Association of Composite Materials Using Continuous Fiber for Concrete Reinforcement (CCC) and by companies who supplied FRP rods and resin samples.

## REFERENCES

[1] JSCE, recommendation for design and construction of concrete structures using continuous fiber reinforcing materials, 1997, pp. 91 – 94

# Measurement of Electromagnetic Transmission through Structures Reinforced with High Strength Fibers

YUKIO KUROSAKI, Mitsui Construction Co., Ltd., Chiba, Japan
KOICHI ISHIBASHI, Mitsui Construction Co., Ltd., Chiba, Japan
YOSHIHIRO MURANO, Kandenko Co., Ltd., Tokyo, Japan

## BACKGROUND

The high strength fiber FRP as reinforcement for structures features not only excellent dynamic characteristics but also electric and magnetic neutrality. This new material, with unique characteristics not seen with conventional steel reinforcement, is expected to open up new possibilities in its application in the construction industry.

Computers, communication equipment and other electronics products, linear motor driven transportation, equipment for superconductivity, high-energy and other similar researches, etc., require proper electric and magnetic environments. In widening the range of applications of high strength fiber reinforcements, therefore, investigations into the effects of civil engineering and architectural structures using this material on the electric and magnetic environment will surely play a role of great importance.

In view of the absence of any established methods for measuring the electrical and magnetic characteristics of architectural structures at present, it is of urgent necessity that reliable methods be standardized.

Accordingly, we have aimed to establish and standardize the measuring methods of such electromagnetic characteristics as the electromagnetic wave characteristics of structures reinforced with high strength fibers.

This paper proposes specifications for the method of evaluating the electromagnetic wave transmission characteristics of structures using high strength fiber reinforcement capable of transmitting electromagnetic waves.

## SCOPE

The purpose of this paper is to determine the measuring method to be employed in evaluating the electromagnetic wave transmission characteristics of structures reinforced with high strength fibers. The method of measurement is to be applied to the measurement of electromagnetic waves of a specific range of frequencies, such as broadcast waves, that arrive at a structure (hereinafter referred to as incoming waves), that can be measured in a relatively steady state above background noise.

*FRPRCS-5*, Thomas Telford, London, 2001.

It is possible that the electromagnetic transmittance of a room or a structure is determined by the use of the shielding characteristic measurement. A measuring method is specified by MIL-STD-285 (Military Standard Specifications, but the results of measurement by this method may vary, depending on how the measuring equipment is handled, how the measuring positions are selected and who carries out the measurement. Also, methods for evaluating structural materials include the Advantest method, the KEC method, shield/sealed box method, etc. However, the evaluation results by these methods do not necessarily agree with each other, and do not necessarily prove valid when applied to those in structures. Hence, it is necessary to develop a testing method that can provide a reliable evaluation.

This paper, therefore, provides general guidelines for the measurement of the electromagnetic transmission characteristic of structures reinforced with high strength fibers.

## SELECTION of MEASURING METHOD

There is no established measuring method for measuring the electromagnetic transmittance of buildings. As discussed in the previous chapter, the electromagnetic transmittance of a room or a building can be determined by measuring its shielding characteristic. The technique of MIL-STD-285 is the most popular for measuring the shielding characteristic. However, this method is not suitable for determining the electromagnetic transmittance of building spaces for the following reasons. This paper selects the "incoming wave method". The rating by the incoming wave method is based on the difference between the level of wave arriving outside the subject space and that of wave transmitting to the subject space.

These are demerits of the MIL-STD-285 method.

(1) A single surface is subjected to measurement by this method. It is difficult to rate the electromagnetic performance of building space.

(2) It is intended for rating the shielding performance of thin components such as doors and windows, so it is not necessarily suitable for thick portions of buildings such as concrete walls.

(3) It requires both transmitting and receiving devices, whereas the incoming wave method can be conducted with a receiving device only.

(4) When a room of a building with many partition walls is subjected to the measurement, it is difficult to install the transmitting and receiving antennas.

## DEFINITIONS

The definitions of terms used in this paper shall be as specified below.

**High strength fiber reinforcement**

Bar-shaped fiber reinforced plastic (FRP) using high strength fibers, such as aramid fiber or carbon fiber, that can be used as reinforcement (reinforcing bars) for concrete structures.

For the purpose of this paper, the above reinforcement shall mean the aramid FRP (aramid reinforcement) which displays nonmagnetic characteristics.

**Electromagnetic wave transmission characteristics**
Transmittance of electromagnetic waves shown by the whole or part of a structure.

**Incoming wave method**
In the measurement of the electromagnetic wave transmission characteristics of structures reinforced with high strength fibers, the transmittance shall be determined by measuring the observation terminal voltage (hereinafter referred to as the receiving level) by the incoming wave method as specified below:

(1) Measure the receiving level (dBμV) of electromagnetic waves arriving outside the measuring space as the reference value: L.

(2) Measure the receiving level (dBμV) of electromagnetic waves that have transmitted through the measuring space: R.

(3) The difference between R and L shall be found to be the transmittance: T.
(R-L) = T (dB)
Note: 1μV = 0dBμV

## MEASURING EQUIPMENT

In deciding on the measuring equipment, reference was made to the "Electric Field Strength Measuring Method for Environmental Electromagnetic Noise (Draft)" in "Current Technology and Problems of Measurement of Electromagnetic Environment of Structures," a document used at the 2nd Symposium held by the Architectural Institute of Japan, the Environmental Engineering Committee and the Electromagnetic Environment Steering Committee.

**Antennas**
*(1) Antennas and frequencies to be measured*
Antennas to be used shall have known antenna factors and direction characteristic.

The types of antennas to be used shall be the loop antenna, the rod antenna, the biconical antenna, the log-periodic antenna, double rigid guide antenna (horn antenna), etc. The dipole antenna can also be used when measurement is limited to specific frequencies.

*(2) Polarization and feeding point*
Electromagnetic waves are waves consisting of electric and magnetic fields which are at right angles to each other. Electromagnetic waves whose electric field is parallel with the ground are called horizontally polarized waves, while those whose electric field is vertical to the ground are called vertically polarized waves. Polarized waves should be determined beforehand in a preliminary measurement. The position of an antenna normally means the position of the feeding point. Hence, the height of an antenna should be specified relative to this position. With the log-periodic antenna, however, the position of the antenna customarily means the center of the transmission line.

In installing an antenna, a tripod may often be used to fix its position. In such a case, however, it is desirable that a resin or wooden tripod be used instead of a metallic one which can reflect the electromagnetic waves or change the direction characteristic of the antenna.

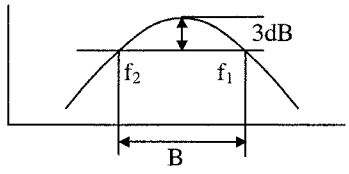
**Measuring devices**

Spectrum analyzers are generally used. Such standards as VDE and VCCI cover the internal noise of spectrum analyzers; otherwise, there seem to be no detailed provisions for the internal noise.

Detection methods can be classified into the average value detection, peak value detection, quasi-peak value detection and effective value detection types. CISPR uses the quasi-peak value detection. The measurement of environmental electromagnetic noise, such as incoming waves, which is often carried out to determine the maximum value at a specified position, generally employs the peak value detection. Also, the average value detection can be used for the measurement of broadcast waves.

The passing bandwidth is the difference between frequencies f1 and f2, which are the points 3dB below the maximum gain point of frequency characteristic (-3dB points) (See Fig. 1).

That is,
Bandwidth :
$B = f_1 - f_2$ (Hz)




$B = f_1 - f_2$
B: passing bandwidth

Fig. 1 Passing bandwidth

**Cables**

The cable to be used for the measurement of incoming waves is generally a double-shielded wire whose impedance is 50Ω. The cable types now in use in Japan include 3D-2W, 5D-2W, 8D-2W, RG-55A/U, RG-223/U, RG-5A/U, and RG-9B/U, which are all different in wire thickness. The impedance, wire diameter, capacity, conductor resistance, attenuation, etc., of these cables are specified in JIS C 3501 and other standards. The cable from the power amp to the antenna tends to be thick because a thicker wire allows the flow of greater current. As the attenuation of a coaxial cable is greater with longer distance and higher frequency, the cable type must be selected carefully for measurement at high frequencies.

It is important that these signal cables be connected securely to the measuring device. Improper connection can result in the entry of noise from the connection or unstable operation of the measuring device.

The connectors that connect the cable to the measuring device include the N type, SMA, BNC, APC-7, APC-3.5, 2.4mm, etc.

Spectrum analyzers often come with the N type or SMA connector as a standard feature. The combination of a 5D-2W cable and N type connector is widely used. The connection between connector and cable requires caution because the matching connectors vary with cable diameter.

## MEASURING METHOD

(1) Check the arrival bearing of electromagnetic waves, and adjust the directivity, orientation and polarization direction of antennas inside and outside the structure.

(2) The base of an antenna shall, as a rule, be 1.5 meters above the floor or the ground.

(3) Find the frequency of steady electromagnetic waves by a preliminary measurement in order to measure electromagnetic waves with minimal fluctuation. In this case, the electromagnetic waves of the steady frequency shall have a receiving level 10 dB or more above the background noise level.

(4) Carry out measurement with the measuring devices at a maximum value held for a certain period of time (max. hold: peak value detection), and record the data obtained. It shall be noted, however, that measurement by average value detection is also possible.

(5) Use, as the reference value, a measured value that has been least subject to the reflection and other environmental effects of the structure.

(6) As a rule, two sets or more of the measuring equipment shall be prepared.

The receiving levels of arriving waves inside and outside the measuring space shall be measured simultaneously. However, all the receiving equipment shall be subjected to an inspection before this testing to see whether they have any errors. If any of the equipment is found to have an error, compensation shall be made to the equipment or to the results of measurement.

When only one set of measuring instrument is available, the measurement shall be made twice or more in each position to determine whether or not there is an incoming wave which can be used as reference. The level of the reference incoming wave must be stable.

## CONCLUSION

We have proposed the incoming wave method to measure the electromagnetic transmission through structures reinforced with high strength fibers.

It can be said that this method is more effective for evaluating the structure space than the method of MIL-STD-285 that measures the shielding performance of some members such as walls.

In order to determine the electromagnetic wave quantitatively using the incoming wave method, it is necessary to study the properties of radio waves (frequency, intensity), setting of measurement positions and polarization direction, and how to grasp the variation with time of the radio wave environment.

In our future investigation, we will collect the measurement data of various purposes of structures, architectural styles and heights to establish a method of measuring electromagnetic transmittance resorting to the incoming wave method.

## REFERENCES

"Electric Field Strength Measuring Method for Environmental Electromagnetic Noise (Draft)" in "Current Technology and Problems of Measurement of Electromagnetic Environment of Structures," a document used at the 2nd Symposium held by the Architectural Institute of Japan, the Environmental Engineering Committee and the Electromagnetic Environment Steering Committee.

"Study on the Evaluation of Electromagnetic Wave Transmission Factor Using Incoming Wave."
"Part1 Evaluation and study on application to office buildings. "
Architectural Institute of Japan, Summaries of the lectures in the Symposium in 2000.
Koichi Ishibashi, Yukio Kurosaki, Keiichi Tashiro

"Architectural Design in Electromagnetic Environment"
Architectural Institute of Japan

## NOTICE

This paper was made as the working result of NEDO (New Energy and Industrial Technology Development Organization) in the 1997 fiscal year.

AIJ (Architectural Institute of Japan) supported the working group on making this paper.

# Behaviour and Design of Structural Concrete Reinforced with CFRP Rebars for Temperature Effects

MAMDOUH ELBADRY, University of Calgary, Calgary, Alberta, Canada
OMER ELZAROUG, Concordia University, Montréal, Québec, Canada

## ABSTRACT
The effects of thermal incompatibility of carbon fibre reinforced polymers (CFRP) and concrete on the behaviour reinforced concrete members is investigated. Concrete beams reinforced with CFRP rebars are tested under the effects of temperature gradients while the rotation at the beam ends are prevented. The bending moments and cracking developed by the temperature gradients are monitored. The results are compared with those obtained from tests on beams of the same dimensions but reinforced with steel bars. Reduction of the thermal moments due to progressive stiffness degradation with crack formation is studied analytically and compared with the moment values recorded in the tests. The test series includes beams with variable amounts of reinforcement to study their effects on thermal moments and on crack widths and spacing. Design charts are presented for determining the minimum amount of CFRP reinforcement necessary for control of cracking due to temperature.

## INTRODUCTION
Thermal characteristics of fibre reinforced polymers (FRP) vary from one product to another and depend on the type of fibre and resin matrix used, the fibre volume ratio and the modulus of elasticity. Carbon fibre reinforced polymers (CFRP), for example, have a coefficient of thermal expansion in the longitudinal direction, $\alpha_{fL}$, close to zero, while aramid fibre reinforced polymers (AFRP) have a negative coefficient varying from $-2\text{x}10^{-6}$ /°C to $-15\text{x}10^{-6}$ /°C. For glass fibre reinforced polymers (GFRP), while the longitudinal coefficient, $\alpha_{fL}$ is similar to that of hardened concrete, the transverse coefficient, $\alpha_{fT}$, is 5–8 times greater.

Under increasing temperature the small expansion of CFRP and the contraction of AFRP may lead to compressive stresses in the concrete and tensile stresses in the reinforcement. This can be beneficial in concrete members prestressed by CFRP or AFRP tendons. On the other hand, under temperature decrease, this may cause tensile stresses in the concrete and compressive stresses in the reinforcement and, hence, increase in the prestress losses in prestressed members. The difference in thermal expansion in the transverse direction may cause bursting stresses within the concrete around the reinforcing bars under high temperature or separation of the bars from the concrete under low temperature. This may adversely affect the bond of the reinforcement to the concrete and cause cracking of the concrete cover to the reinforcement.

This paper presents results of an experimental investigation into the behaviour of concrete members reinforced with CFRP rebars under the effects of thermal gradients. Concrete specimens (250x500x3350 mm) reinforced with variable amounts of CFRP reinforcement were tested to investigate the effects of thermal characteristics of FRP on the development of

*FRPRCS-5*, Thomas Telford, London, 2001.

thermal stresses and cracking and to examine the effectiveness of this type of reinforcement in controlling cracking due to temperature. Temperature gradients were produced by heating one side of the specimens using infrared lamps. End rotations were restrained to produce a constant moment along the specimen's tested length. The bending moment and the cracking developed by the thermal gradients were monitored and the strains, crack widths and spacing were recorded. The results were compared with those available from tests conducted on members of the same dimensions but reinforced with steel bars. The results are also used to calibrate a theoretical model developed to determine the effects of the progressive reduction in stiffness as cracks form on thermal stresses and internal forces in continuous structures reinforced with CFRP. Design charts are presented for determining the minimum amount of CFRP reinforcement required for control of cracking due to temperature.

## EXPERIMENTAL PROGRAM

Five concrete beams with 500 x 250 mm rectangular cross section and overall length of 3350 mm were reinforced with different amounts of CFRP bars and subjected to thermal gradients in the test frame shown in Fig. 1. CFRP Leadline rods of 8 and 10 mm nominal diameter were used as reinforcement. The five beams were provided with reinforcement ratios of 0.2, 0.4, 0.6, 0.8 and 1.0 %; accordingly, the beams are denoted here as L.2, L.4, L.6, L.8 and L1.0, respectively. The results were compared with those available from tests carried out on five concrete beams of the same dimensions but provided with steel bars of the same reinforcement ratios [1]. The beams are denoted S.2, S.4, S.6, S.8, and S1.0, respectively. Beams L.2, L.4 and S.2 to S1.0 were provided with 9.5 mm diameter steel stirrups placed at 400 mm spacing along the tested length. The reinforcement details for the test beams are given in Table 1.

In the tests, the beams were subjected to thermal gradient over the cross-section depth, $h$ = 250 mm. For convenience in instrumentation and measurement and to eliminate the effect of self-weight, the cross section is rotated 90°. The thermal gradient was produced by heating one vertical face of the beam, referred to here as the *hot face*, using ten infrared, 250 Watt heat bulbs mounted in an insulated wooden box over a length of 2000 mm of the beam. The opposite face of the beam, referred to as the *cool face*, was exposed to room temperature. The top and bottom faces were insulated. The temperature distributions over $h$ = 250 mm were monitored by five thermocouples at two sections within the heated length of each beam. Two external thermocouples were also installed on the hot and cool faces of the beams. The temperature difference between the two faces of the beam would produce end rotations, which were restrained by means of four relatively rigid steel arms (Fig. 1). Because of this restraint, a bending moment, causing tension on the cool face and compression on the hot face, developed along the tested length of the beam. Two load cells were used to measure the end moments developed ($M = PL$, where $P$ is the absolute value of the axial force measured by each load cell; and $L$ is the distance between the two axial forces).

### Material Properties

The Leadline rods are manufactured by pultrusion using linearly oriented coal tar pitch-based continuous fibre epoxy resin [2]. The longitudinal modulus of elasticity of Leadline, $E_{fL}$ = 147 GPa, and its ultimate strength, $F_{Fu}$ = 1970 MPa. The coefficient of thermal expansion, $\alpha_{fL}$ is $0.68 \times 10^{-6}$ /°C. The reinforcing steel used was of Grade 400 ($f_y$ = 435 MPa). The measured average compressive strength of the concrete used ranged from 30 MPa to 35 MPa at the time of testing. The secant modulus of elasticity at 0.5 $f_c'$ was $E_c$ = 24.7 GPa and the coefficient of thermal expansion was $\alpha_c = 10.6 \times 10^{-6}$ /°C.

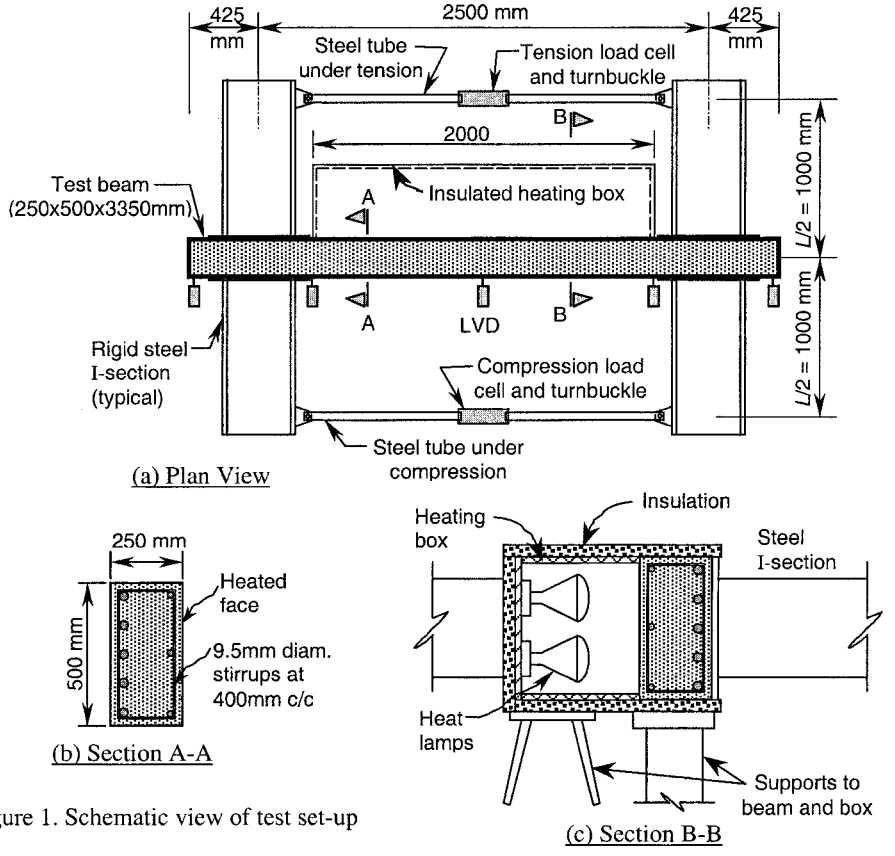



Figure 1. Schematic view of test set-up

Table 1 – CFRP and steel reinforcement in test beams

| Beam Designation | Reinforcing Material | On Tension Side | | | | On Compression Side | | |
|---|---|---|---|---|---|---|---|---|
| | | Number of Bars | Nominal Diameter (mm) | $A_r$ (mm$^2$) | $\rho_r$ (%) | Number of Bars | Nominal Diameter (mm) | $A'_r$ (mm$^2$) |
| **L.2** | Leadline | 4 | 8 | 200 | 0.2 | 2 | 8 | 100 |
| **L.4** | Leadline | 8 | 8 | 400 | 0.4 | 3 | 8 | 150 |
| **L.6** | Leadline | 8 | 10 | 600 | 0.6 | 3 | 8 | 150 |
| **L.8** | Leadline | 8 + 4 | 10 + 8 | 600 + 200 | 0.6 + 0.2 | 3 | 8 | 150 |
| **L1.0** | Leadline | 8 + 8 | 10 + 8 | 600 + 400 | 0.6 + 0.4 | 3 | 8 | 150 |
| **S.2** | Steel | 2 | 11.3 | 200 | 0.2 | 2 | 11.3 | 200 |
| **S.4** | Steel | 2 | 16 | 400 | 0.4 | 2 | 16 | 400 |
| **S.6** | Steel | 3 | 16 | 600 | 0.6 | 2 | 16 | 400 |
| **S.8** | Steel | 4 | 16 | 800 | 0.8 | 2 | 16 | 400 |
| **S1.0** | Steel | 5 | 16 | 1000 | 1.0 | 2 | 16 | 400 |

### Testing Procedure

Prior to heating, equal end moments were applied to the test beams using two turnbuckles provided with load cells (Fig. 1). These moments were acting in the same direction as those produced by the temperature gradient. The purpose of applying these initial moments was to cause the cracking to occur at lower temperature gradient and thus eliminate the need to heat the beams to very high temperatures. After application of these moments, the deflection at the center of the tested length relative to its ends was measured and kept constant during thermal loading.

The temperature increase was applied in 10 to 12 increments for each beam. Each increment required two to three hours to reach a stable temperature distribution. A variable autotransformer connected to the heating box was used to control temperature on the hot face. In each increment, due to gradual development of the temperature gradient, the increase in forces and strains were observed. In the last increment, the temperatures at the hot and the cool faces were 160 and 40 °C, respectively, causing a temperature difference of 120 degrees between the two faces. Testing of each beam required 24 to 26 hours for completion.

After stabilization of temperature readings in each increment, the turnbuckles attached to the load cells were adjusted to eliminate any change in central deflection and to make the forces in the two load cells always equal. This ensured that the beam tested length was subjected to pure bending moment equal to the initial moment plus the end moment produced by thermal loading.

## EXPERIMENTAL RESULTS

### Thermal Moment

Figures 2 to 4 show the variation of thermal moment with temperature difference, $\Delta T$, between the hot and cool faces for beams L.6, L.8 and L1.0 reinforced with Leadline of 0.6, 0.8 and 1.0% reinforcement ratios, respectively. The results for beams reinforced with steel of same reinforcement ratios are also plotted for comparison. The moment values plotted at $\Delta T$ = 0 degrees represent the initial applied moment. Smaller values of this moment were chosen for beams reinforced with Leadline because cracking of these beams was expected to take place at a lower moment than that for beams reinforced with steel [3]. The figures show that the thermal moment increases gradually with the increase in temperature difference for all beams until the total moment (initial plus thermal) reaches the cracking moment and the first crack occurs at the weakest section. Since the bending moment is constant along the tested length of the beam, the weakest section is located anywhere within the tested length. Cracking reduces the beam stiffness and, thus, a sudden drop in the thermal moment takes place after occurrence of the crack. The drop in the moment varies from one beam to another depending on the amount of reinforcement.

The increase in temperature gradient after the first crack results in further increase in the thermal moment until once again the cracking moment is reached and a second crack occurs at the next weakest section. The thermal moment at which the second crack takes place is higher than the moment at the first crack. This is attributed to the fact that the tensile strength of concrete is not equal at all sections and that the longitudinal coefficient of thermal expansion, $\alpha_{fL}$ of CFRP is close to zero. As explained above, when the temperature increases, the bond of the Leadline rods to the concrete restrains the large expansion of concrete relative to the reinforcement and creates compressive stresses that delays occurrence of the cracks due to thermal moment. The drop in thermal moment after the second crack is however smaller than that after the first crack. This is because of the further reduction in stiffness after occurrence of the second crack.

The three figures 2 to 4 show that for the same reinforcement ratio, the total moments of the beams reinforced with Leadline are higher than the moments in the beams reinforced with steel.

This is despite the fact that the initial moment applied to the Leadline reinforced beams was smaller than that applied to the steel reinforced beams. The beams reinforced with Leadline continued to show increase in the thermal moment up to the end of the test. On the other hand, the steel reinforced beams did not exhibit any significant increase in the thermal moment with the increase in temperature gradient as was noticed in the Leadline reinforced beams. A comparison between the five beams reinforced with Leadline is shown in Fig. 5, which indicates that increasing the reinforcement ratio from 0.2 to 1.0% improved the behaviour of the beams.

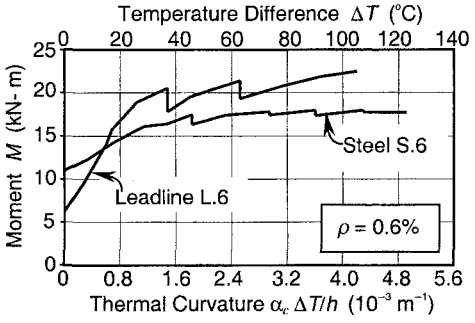



Figure 2. Bending moment versus $\Delta T$ in beams reinforced with 0.6% Leadline or steel

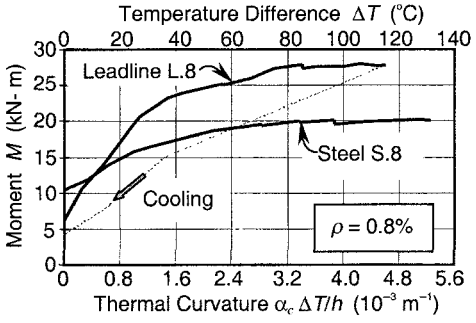



Figure 3. Bending moment versus $\Delta T$ in beams reinforced with 0.8% Leadline or steel

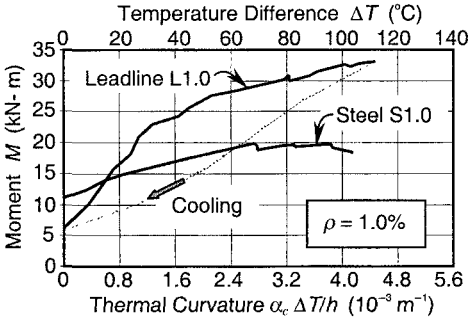



Figure 4. Bending moment versus $\Delta T$ in beams reinforced with 1.0% Leadline or steel

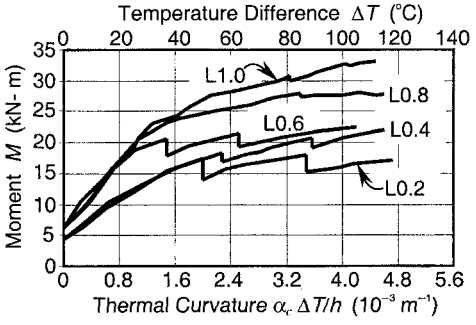



Figure 5. Bending moment versus $\Delta T$ in beams reinforced with Leadline

The thermal behaviour of beam L.8 and L1.0 reinforced with 0.8% and 1.0% Leadline was monitored during a cooling down process, which lasted for about two days. The thermal moment readings were recorded immediately after the heat flux was terminated and until all thermocouple readings reached the room temperature. The thermal moments during cooling of the two beams are plotted in Figs. 3 and 4 along with the moment during heating. As can be seen, the thermal moment decreased with the decrease in temperature until it reached the value of the initially applied moment. When the temperature difference became zero (i.e., room temperature at both sides of the beam), all the cracks that occurred during the thermal test closed.

**Crack Spacing and Maximum Crack Widths**

A typical view for the crack pattern is shown in Fig. 6 for beam L.8 reinforced with 0.8% Leadline. The average spacing between cracks varied from 270 to 460 mm in the Leadline reinforced beams. Figure 7 presents plots of the maximum crack width for beams L.6, L.8 and L1.0. A comparison with the crack widths in beams S.6, S.8 and S1.0 is shown in the same

figure. As can be seen, for reinforcement ratio smaller than 1.0%, the Leadline reinforced beams always exhibit larger cracks than the steel reinforced beams. Also, increasing the reinforcement ratio reduced the crack width from 0.33 to 0.1 mm in beams L.6 and L1.0, respectively. The crack width for beams L.8 and L1.0 increased at a very slow rate. This is attributed to the fact that Leadline has small coefficient of expansion relative to concrete, which produces compression in the concrete under temperature rise and, hence, reduced crack width. The maximum crack width measured in beams L.6 to L1.0 ranged from 0.1 to 0.33 mm which satisfied the requirements of CSA-A23.3-94 standards [4] for limiting crack width.

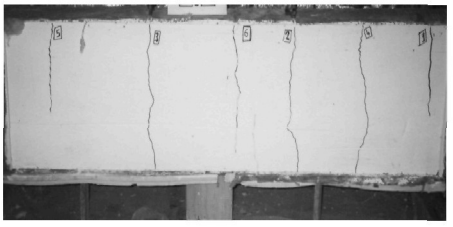


Figure 6. Crack pattern in beam L.8 due to temperature gradient

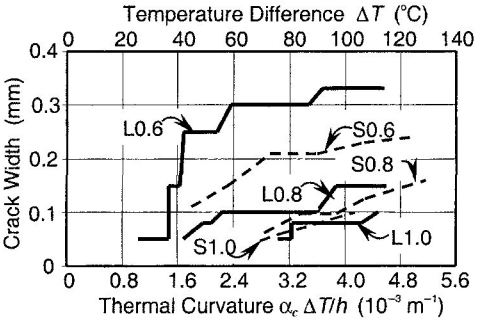



Figure 7. Max. crack width versus $\Delta T$ in beams reinforced with Leadline or steel

## ANALYTICAL PREDICTION OF CRACK FORMATION

### Stresses and Strains due to Difference in Thermal Expansion of Concrete and CFRP

Figure 8a depicts a concrete section reinforced with one layer of CFRP reinforcement and subjected to a linear temperature distribution (Fig. 8b). The CFRP layer has a cross-sectional area $A_f$ and its position is defined by a coordinate $y_f$ from the centroid O of the reinforced concrete section; $y$ is positive downward of O. The temperature, $T_f$ at the level of the CFRP layer is:

$$T_f = T_O + \frac{\Delta T}{h} y_f \qquad \text{or} \qquad T_f = T_{bot} + \Delta T \left( \frac{h - d_f}{h} \right) \tag{1}$$

where $T_O$ and $\Delta T$ are, respectively, the temperature at centroid and the difference in temperature between the top and bottom fibres of the cross-section; $h$ is the height of the concrete section; $T_{bot}$ is the temperature at the bottom fibre; and $d_f$ is the depth of the CFRP layer from the top fibre.

Figure 8c shows the distribution of free strain due to temperature had the concrete section and the CFRP reinforcing layer been free to expand separately. Figure 8d shows the force $N_r$, which if applied on the CFRP layer would restrain its expansion to be equal to $\alpha_c T_f$. The force $N_r$ is:

$$N_r = (\alpha_c - \alpha_{fL}) T_f \; E_f \; A_f \tag{2}$$

where $E_f$ is the elasticity modulus of CFRP. The restraining stress is given by:

$$\sigma_r = (\alpha_c - \alpha_{fL}) T_f \; E_f \tag{3}$$

The restraining force is equivalent to a normal force $N_r$ applied at the centroid O and a moment $M_r = N_r \, y_f$ about an axis $x$-$x$ passing through O. In order to eliminate this artificial restraint, the forces $N_r$ and $M_r$ must be applied in a reversed direction on a transformed section composed of the concrete area plus the area $A_f$ of the CFRP reinforcement multiplied by the modular ratio $n_f = E_f / E_c$ (Fig. 8e). The corresponding strain $\varepsilon_O$ at O and the curvature $\psi$ are:

$$\varepsilon_O = -\frac{1}{E_c A}\left[\left(\alpha_c - \alpha_{fL}\right) T_f E_f A_f\right] \tag{4}$$

$$\psi = -\frac{1}{E_c I}\left[\left(\alpha_c - \alpha_{fL}\right) T_f E_f A_f y_f\right] \tag{5}$$

where $A$ and $I$ are the area of the transformed section and its moment of inertia about an axis through O, respectively, $E_c$ is the modulus of elasticity of concrete. The stresses $\sigma_f$ and $\sigma_c$ in the CFRP layer and the concrete at any fibre at coordinate $y$ are given, respectively, by (Fig. 8f):

$$\sigma_f = E_f\left[\varepsilon_O + \psi\, y_f + \left(\alpha_c - \alpha_f\right) T_f\right] \tag{6}$$

$$\sigma_c = E_c\left(\varepsilon_O + \psi\, y\right) \tag{7}$$

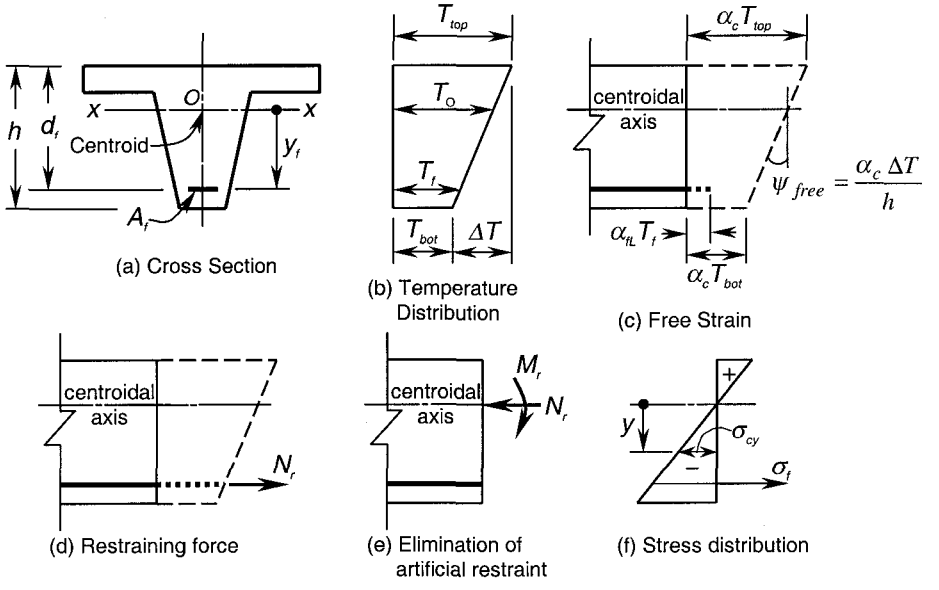



Figure 8. Stresses due to thermal incompatibility of concrete and FRP reinforcement

**Thermal Moments After Cracking**

Consider the concrete beam in Fig. 1 reinforced with CFRP rebars and subjected to temperature rise similar to that of Fig. 8b, with its end rotations restrained. Equations are given below for prediction of the $M$-$\Delta T$ graph (Fig. 9) taking into account the effects of cracking [5].

The first crack occurs at the weakest section when the stress in concrete reaches its tensile strength, $f_{ct1}$. The corresponding end moment is equal to the cracking moment, $M_{cr1}$, and develops at $\Delta T = \Delta T_{cr1}$. With the increase in $\Delta T$, a second crack develops at the next weakest section when the stress reaches a value $f_{ct2}$, which is slightly greater than $f_{ct1}$. Formation of cracks continues with the increase in $\Delta T$ until a so-called *stabilized crack pattern* is developed, when no further cracks can form. The distance between any two cracks cannot be smaller than the crack spacing $s$. The maximum number of cracks, $n$ that can form in a member of length $l$ is equal to the integer part of the quotient ($l/s$). The temperature gradient when cracking reaches the stabilized state is $\Delta T_s$. Further increase of $\Delta T$ beyond $\Delta T_s$ causes widening of the existing cracks.

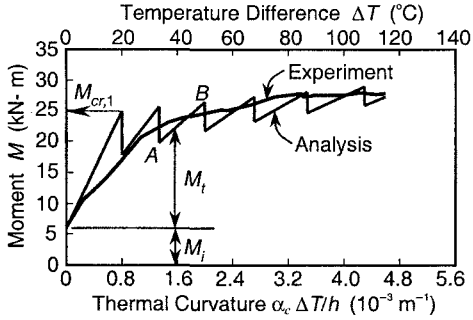



Figure 9. Comparison of analytical and experimental $M$-$\Delta T$ graphs for beam reinforced with 0.8% Leadline

When the member has $m$ cracks it is considered consisting of two parts, a noncracked part of length $(l - ms)$ and moment of inertia $I_1$, and a cracked part of length $ms$ and effective moment of inertia $I_e$. The moment of inertia $I_1$, is about an axis through the centroid of a noncracked transformed section composed of the area of concrete plus the area of the reinforcement multiplied by $E_r/E_c$; where $E_r$ is the elasticity modulus of the reinforcement; here $E_r = E_f$. For the cracked part, the effective moment of inertia, $I_e$ is used to account for the effects of tension stiffening of concrete between cracks; $I_e$ is given by:

$$I_e = \frac{I_1 I_2}{\zeta I_1 + (1-\zeta) I_2} \tag{8}$$

where $I_2$ is the moment of inertia of a transformed fully cracked section composed of the area of concrete in the compression zone plus the area of reinforcement multiplied by $E_r/E_c$; $\zeta$ is an empirical interpolation coefficient given by:

$$\zeta = 1 - 0.5\beta \left( \frac{f_{ct}}{\sigma_{c\,\max}} \right)^2 \tag{9}$$

where $\sigma_{c\,\max}$ is the stress that would exist in the concrete at the extreme tension fibre assuming no cracking; $\beta = 0.5$ assuming non-deformed bars. Thus, at cracking, when $\sigma_{c\,\max} = f_{ct}$, the value of $\zeta$ can be taken as 0.75.

The value of $M$ at which the $m$th crack occurs is given by:

$$M_{cr,\,m} = f_{ct,\,m}\, Z_1 \tag{10}$$

where $Z_1$ is the modulus of the transformed noncracked section, and $f_{ct,\,m}$ is given by [1]:

$$f_{ct,\,m} = f_{ct,\,m-1}\,(1+\gamma) \quad \text{MPa} \tag{11}$$

where $\gamma = 0.02$ is a coefficient giving the increase of tensile strength from one crack to another.

To account for the initial moment, $M_i$, applied prior to the thermal loading test and for the effects of different thermal expansion coefficients of concrete and CFRP, see Eqs. (4) to (7), Eq. (10) must be modified to calculate the thermal moment just before occurrence of the $m$th crack. Thus,

$$M_{cr,\,m} = \left(f_{ct,\,m} - \sigma_{ci} - \sigma_{c\alpha}\right) Z_1 \tag{12}$$

where $\sigma_{ci}$ is the stress at the extreme tension fibre due to the initial moment $M_i$,

$$\sigma_{ci} = \frac{M_i}{Z_1} \tag{13}$$

The value $\sigma_{c\alpha}$ is the stress at the extreme tension fibre due to the effects of difference between $\alpha_{fL}$ and $\alpha_c$; $\sigma_{c\alpha}$ is calculated from Eqs. (4), (5) and (7), substituting $A = A_1$, $I = I_1$ and $y$ = coordinate of the extreme tension fibre from the centroid of the transformed section; $A_1$ and $I_1$ are the area and moment of inertia of the transformed noncracked section, respectively.

Before cracking, i.e. in the range $0 < \Delta T < \Delta T_{cr,1}$, the bending moment due to temperature is:

$$M = \alpha_c E_c I_1 \frac{\Delta T}{h} \tag{14}$$

Solving Eq. (14) with $M = M_{cr,1}$ and $\Delta T = \Delta T_{cr,1}$ gives $\Delta T_{cr,1}$ at which the first crack occurs:

$$\Delta T_{cr,1} = \frac{h}{\alpha_c} \frac{M_{cr,1}}{E_c I_1} \tag{15}$$

or

$$\Delta T_{cr,1} = \frac{h}{\alpha_c} \frac{(f_{ct,1} - \sigma_{ci} - \sigma_{c\alpha}) Z_1}{E_c I_1} \tag{16}$$

After occurrence of the $m$th crack and before formation of the next crack, the value of $M$ is represented by (line $AB$ in Fig. 9):

$$M = \frac{\alpha_c \Delta T}{h} E_c I_1 \left[1 + \frac{m s}{l}\left(\frac{I_1}{I_e} - 1\right)\right]^{-1} \quad (\text{with } \Delta T_{cr,m} \le \Delta T \le \Delta T_{cr,m+1}) \tag{17}$$

Substituting $\Delta T_{cr,m}$ for $\Delta T$ and $m$–1 for $m$, Eq. (17) gives $\Delta T_{cr,m}$ at which the $m$th crack occurs as:

$$M_{cr,m} = \frac{\alpha_c \Delta T_{cr,m}}{h} E_c I_1 \left[1 + \frac{(m-1) s}{l}\left(\frac{I_1}{I_e} - 1\right)\right]^{-1} \tag{18}$$

In deriving the above equations, it was assumed, for simplicity, that the beam does not lose symmetry about the centre of the span as a result of crack formation. This assumption makes the structure statically indeterminate to the first degree, with the indeterminate force being a bending moment $M$ whose magnitude is constant over the span [5].

Equations (12) and (16) give $M_{cr,1}$ and $\Delta T_{cr,1}$. Substituting the value of $\Delta T_{cr,1}$ in Eq. (17) gives the lower ordinate of $M$. Setting $m$ = 2, 3,..., $n$ and solving Eqs. (11), (12) and (18) for $\Delta T_{cr,m}$, then substituting in Eqs. (12) and (17), gives all the values necessary for plotting the graph in Fig. 9. The analytical $M$-$\Delta T$ diagram plotted in Fig. 9 is for beam L.8, reinforced with 0.8% Leadline. The values $s$ = 330 mm and $f_{ct1}$ = 3.5 MPa were used for plotting the $M$-$\Delta T$ diagram. Also plotted in Fig. 9 is the $M$-$\Delta T$ graph obtained from the thermal load test. As can be seen, a reasonable agreement between the analytical and the experimental results is obtained.

## AMOUNT OF REINFORCEMENT TO LIMIT CRACK WIDTH

The crack width, $w$, can be determined from the change in strain, $\Delta\varepsilon_f$, in the CFRP after cracking:

$$w = s\zeta \Delta\varepsilon_f \tag{19}$$

For a cross section subjected to axial force $N$ at the centroid and moment $M$ about an axis through the centroid, the change in CFRP strain, $\Delta\varepsilon_f$, and the corresponding change in stress, $\Delta\sigma_f$,

are calculated for a transformed section ignoring concrete in tension. Thus,

$$\Delta\varepsilon_f = \frac{(M_f / y_{CT}) + N}{E_f A_f} \qquad \text{and} \qquad \Delta\sigma_f = E_f \Delta\varepsilon_f \tag{20}$$

where $y_{CT}$ is the distance from the resultant compression to the resultant tension; $N$ and $M$ are replaced by the statical equivalents, $N$ at the centroid of the CFRP reinforcement and $M_f = N e_f$, where $e_f = (M/N) - y_f$, is the eccentricity of the resultant of $N$ and $M$ from the centroid of CFRP. Equation (20) is used to derive the graph in Fig. 10, which can be used to determine the amount of CFRP reinforcement required for limiting the crack width to a specified value.

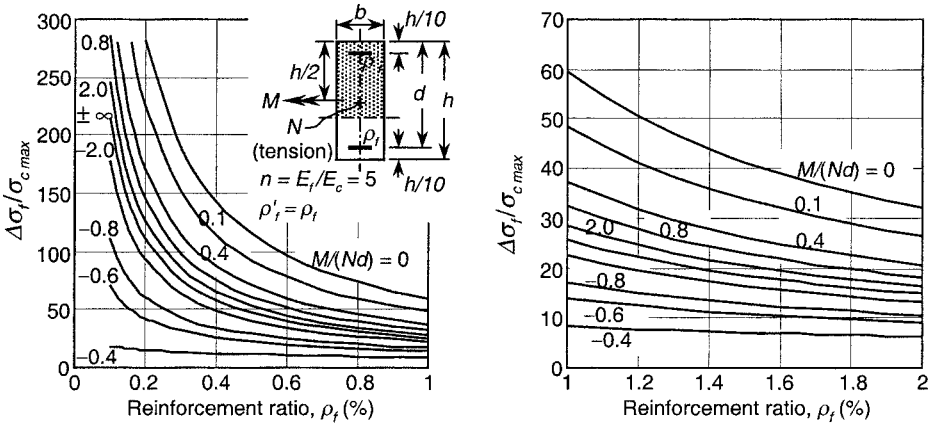



Figure 10. Graphs for determining the minimum amount of CFRP reinforcement

## CONCLUSIONS

The experiments presented confirm that the thermal behaviour of concrete beams reinforced with CFRP (Leadline) rebars is better than that of beams reinforced with steel. The Leadline reinforced beams show higher stiffness than the steel reinforced beams. An analytical model is developed for prediction of the $M$-$\Delta T$ diagrams for thermally cracked concrete beams reinforced with CFRP. The model is verified by comparison with the experimental results. Design charts are presented for determining the minimum amount of CFRP reinforcement necessary for control of cracking due to temperature.

## REFERENCES

[1] Ariyawardena, T., Ghali, A., and Elbadry, M., "Experimental Study on Thermal Cracking in Reinforced Concrete Members," *ACI Structural Journal*, American Concrete Institute, Vol. 94, No. 4, July-Aug. 1997, pp. 432-442.

[2] Mitsubishi Chemical Corporation, *Leadline Carbon Fibre Reinforced Plastic Rods*, Technical Data, Japan, 1995.

[3] Abdalla, H.A., Elbadry, M.M, and Rizkalla, S.H., "Deflection of Concrete Slabs Reinforced with Advanced Composite Materials," Proceedings of the Second International Conference on Advanced Composite Materials in Bridges and Structures, ACMBS-II, Montréal, Québec, August 11-14, 1996, pp. 201-208.

[4] CSA Standard CAN3-A23.3-94, Design of Concrete Structures for Buildings, Canadian Standard Association, Rexdale, December 1994.

[5] Elbadry, M.M. and Ghali, A., "Control of Thermal Cracking of Concrete Structures," *ACI Structural Journal*, American Concrete Institute, Vol. 92, No. 4, July-Aug. 1995, pp. 435-450.

# Author index

*Note*: **Volume 1 – pages 1–582**
**Volume 2 – pages 583–1152**


Abdelrahman, A. 773
Adhikary, B. B. 371
Aiello, M. A. 399
Alkhrdaji, T. 1055
Antonopoulos, C. P. 329
Apinis, R. 1083
Araújo, A. F. 681
Arya, C. 167, 187
Au, S. C. C. 721
Audenaert, K. 517

Bakis, C. E. 689, 927
Balaguru, P. N. 53
Balázs, G. L. 609
Banholzer, B. 1027
Bank, L. C. 389, 497
Bättig, G. 1103
Beeby, A. W. 671
Belarbi, A. 823
Benmokrane, B. 469, 649, 907
Bhat, B. B. 689
Bigaud, D. 271
Blontrock, H. 547
Boothby, T. E. 689, 927
Borosnyói, A. 609
Brameshuber, W. 1019, 1027
Brockmann, J. 1019
Brönnimann, R. 1103
Brostrom, M. 1143
Burden, A. R. 223
Burgoyne, C. J. 711, 731, 875, 939
Burguenono, R. 1143

Campbell, T. I. 741
Campos, C. M. O. 711
Carolin, A. 107
Ceroni, F. 917
Cerqueira, E. C. 97
Chan, C. 281
Chen, G. 197
Chen, J. F. 205, 429
Choi, M. C. 629
Cicerone, S. 1113
Clarke, J. L. 187
Claude, S. 765
Clyde, C. 309
Cole, C. 823
Cosenza, E. 339, 887
Curbach, M. 593
Curtil, L. 45

Debaiky, A. S. 1071
Dejke, V. 505
Dolan, C. W. 585

El-Afandy, T. 773
Elbadry, M. 573, 699
El-Ghandour, A. W. 971
El-Hacha, R. 261, 699
Elzaroug, O. 573
Engel, R. S. 927
Ennaceur, C. 271
Enomoto, T. 639

Fang, Z. 741
Farmer, N. 167
Ferrier, E. 45, 271
Fujii, S. 379
Fujisaki, T. 557
Fukuyama, H. 215, 447, 457, 813
Furuta, T. 215

Galati, N. 399
Gale, L. 629
Garon, R. 53
Gazouli, D. 517
Ghallab, A. 671
Gilbert, R. I. 535, 619
Gossla, U. 1123
Gowripalan, N. 535, 619
Green, M. 261, 1071
Guadagnini, M. 3, 949
Guimarães, G. B. 681, 711

Hamelin, P. 45, 271
Harada, T. 639
Hattori, A. 489
Hegger, J. 1009

Hollaway, L 1133
Holt, G. D. 429
Hope, B. B. 1071
Hosny, A. 773
Huang, P. C. 1033
Hulatt, J. 1133

Ibell, T. J. 629, 721, 959
Ibrahim, M. 45
Ina, T. 63
Ishibashi, K. 567
Ishiyama, S. 897

Jesse, F. 593
Jinno, Y. 299, 981

Kage, T. 63
Kanakubo, T. 215
Karbhari, V. 137, 1113, 1143
Karnes, S. 927
Kato, T. 557
Katz, A. 497
Kay, E. A. 187
Kesse, G. 281
Khin, M. 639
Kimura, H. 639
Kishi, N. 87
Kobayashi, K. 379
Komesu, K. 319
Konno, T. 1063
Kurihashi, Y. 87
Kurosaki, Y. 567

La Rovere, H. 1143
La Tegola, A. 399
Labossière, P. 35
Lacasse, C. 35
Lam, L. 835
Lamanna, A. J. 389
Laoubi, K. 469
Lau, C. P. 309
Lees, J. M. 281
Leung, H. Y. 875
Littwin, R. 1009
Lopez, M. M. 117

Makitani, E. 223
Makitani, T. 223
Maksimovs, R. 527
Manfredi, G. 339, 865, 887, 917
Maruyama, K. 441
Masuda, Y. 63
Masuo, K. 299
Matsuoka, K.G. 87
Matsushita, H. 409
Matsuzaki, Y. 447, 813
Matthys, S. 3, 157
Meier, U. 147, 231, 291
Melo, G. S. 239
Mihashi, H. 897
Mikami, H. 87
Miyagawa, T. 489
Modniks, J. 527, 1083
Molter, M. 1009
Morais, M. 731
Morita, S. 299
Mortazavi, A. A. 855
Munley, E. 585
Murano, Y. 567
Mutsuyoshi, H. 371, 479

Naaman, A. E. 117
Nagato, Y. 239
Nakano, K. 457, 813
Nanni, A. 79, 197, 339, 457, 1033, 1055
Neale, K. W. 35, 765
Neocleous, K. 71
Nicole, J. F. 907
Niitani, K. 1123
Niu, H. 361

Ohnishi, Y. 489
O'Regan, D. P. 187

Pan, X. M. 429
Pannala, S. 927
Pantelides, C. P. 309, 349
Papanicolaou, C. G. 329
Park, S. Y. 117
Patoary, M. K. H. 1043
Pecce, M. 887, 917
Pesic, N. 177
Pilakoutas, K. 3, 71, 177, 855, 949, 971
Pinto, C. T. M. 97
Pinzelli, R. 793
Prota, A. 339
Puterman, M. 497

Qi, W. 223

Realfonzo, R. 865
Reaveley, L. D. 309, 349
Rizkalla, N. S. 741
Rodrigues, C. C. 783
Rößler, G. 1019

Saafi, M. 753
Sagawa, Y. 409
Salles Neto, M. 239
Sato, Y. 127, 989

Satoh, H. 319, 803
Schokker, A. J. 689
Scott, D. W. 389
Seible, F. 137, 1113, 1143
Sekijima, K. 1063
Shahin, H. 773
Shehata, I.A.E.M. 97
Shehata, L. C. D. 97
Sikorsky, C. 137
Silva, M. G. 783
Silva, P. 1033
Smith, S. T. 419
Stöcklin, I. 291
Stratford, T. J. 939
Stubbs, N. 137
Sugiyama, T. 379
Sumida, A. 479, 557
Suter, R. 793

Taerwe, L. 3, 157, 517, 547
Takahashi, Y. 989
Täljsten, B. 107
Tamuzs, V. 527, 1083
Tan, K. H. 249, 661, 997, 1043
Teng, J. G. 205, 419, 835
Tepfers, R. 505, 1083
Terrasi, G. P. 1103
Thériault, M. 765
Thorne, A. 1133
Till, R. D. 117
Tjandra, R. A. 661
Tolman, F. 1093
Ton-That, M.T. 469
Toutanji, H. 53, 753
Triantafillou, T. 157, 329
Tsukagoshi, H. 379, 981
Tsuruta, H. 409
Tumialan, G. 447, 457, 1033

Ueda, T. 127, 441
Ulaga, T. 147
Uomoto, T. 17, 479

Vandevelde, P. 547
Vintzileou, E. 845

Waldron, P. 71, 949, 971
Wang, J. W. 997
Wang, P. 469
Watanabe, H. 299
Watanabe, K. 557
Watanabe, S. 813
Wernli, M. 1113
Whitehead, P. A. 959
Wight, G. 261
Winistoerfer, A. 231
Wu, Z. 361

Yabe, Y. 379, 981
Yamada, K. 897
Yamaguchi, R. 127
Yamakawa, T. 319, 803
Yang, X. 79, 197
Yang, Z. J. 429
Yoshioka, T. 1123

Zhang, A. 803
Zhang, B. 649, 907
Zhao, L. 1143
Zhong, P. 319
Zou, X. W. 619, 535